Passive Acoustic Monitoring Program for the Northern Gulf of Mexico: Project Report

US Department of the Interior
Bureau of Ocean Energy Management
New Orleans Office

BOEM
Bureau of Ocean Energy Management | ESP
ENVIRONMENTAL STUDIES PROGRAM

Passive Acoustic Monitoring Program for the Northern Gulf of Mexico: Project Report

Authors

Jennifer Amaral
Kristen Ampela
Helen Bailey
Robert Bell
Keshab Bhattarai
Mark Deakos
Peter Dugan
Sean Griffin
Adam Frankel
Selene Fregosi
Anwat Khan
Holger Klinck
Ying-Tsong Lin
Naomi Matthew
David Mellinger
James Miller
Dimitri Ponirakis
Gopu Potty
Aaron Rice
Natalia Sidorovskaia
Lora Van Uffelen

DISCLAIMER

Study concept, oversight, and funding were provided by the U.S. Department of the Interior, Bureau of Ocean Energy Management (BOEM), Environmental Studies Program, Washington, DC, under Contract Number M17PC00001, Task Order Nos. M17PD00011 and 140M0119F0001, with HDR (Athens, Alabama). This report has been technically reviewed by BOEM, and it has been approved for publication. The views and conclusions contained in this document are those of the authors and should not be interpreted as representing the opinions or policies of the US government, nor does mention of trade names or commercial products constitute endorsement or recommendation for use.

REPORT AVAILABILITY

To download a PDF file of this report, go to the US Department of the Interior, Bureau of Ocean Energy Management Data and Information Systems webpage (http://www.boem.gov/Environmental-Studies-EnvData/), click on the link for the Environmental Studies Program Information System (ESPIS), and search on 2022-074. The report is also available at the National Technical Reports Library at https://ntrl.ntis.gov/NTRL/.

CITATION

ABOUT THE COVER

ACKNOWLEDGMENTS

Project Delivery Team Member Affiliations	
Jennifer Amaral	Marine Acoustics, Inc.
Kristen Ampela	HDR EOC
Helen Bailey	University of Maryland Center for Environmental Science
Robert Bell	University of Maryland Center for Environmental Science
Keshab Bhattarai	University of Louisiana at Lafayette
Mark Deakos	HDR EOC
Peter Dugan	K. Lisa Yang Center for Conservation Bioacoustics, Cornell Lab of Ornithology, Cornell University
Adam Frankel	Marine Acoustics, Inc.
Selene Fregosi	Oregon State University
Sean Griffin	Proteus Technologies LLC
Anwar Khan	HDR EOC
Holger Klinck	K. Lisa Yang Center for Conservation Bioacoustics, Cornell Lab of Ornithology, Cornell University
Ying-Tsong Lin	Woods Hole Oceanographic Institution
Naomi Mathew	University of Louisiana at Lafayette
James Miller	University of Rhode Island
David Mellinger	Oregon State University
Dimitri Ponirakis	K. Lisa Yang Center for Conservation Bioacoustics, Cornell Lab of Ornithology, Cornell University
Gopu Potty	University of Rhode Island
Aaron Rice	K. Lisa Yang Center for Conservation Bioacoustics, Cornell Lab of Ornithology, Cornell University
Natalia Sidorovskaia	University of Louisiana at Lafayette
Lora Van Uffelen	University of Rhode Island

Contents

List of Figures

List of Photographs (included in Appendix C)

List of Tables

List of Abbreviations and Acronyms

Short form	Long form
3D	three-dimensional
ADEON	Atlantic Deepwater Ecosystem Observatory Network
AIS	Automatic Identification System
BIAS	Baltic Sea Information on the Acoustic Soundscape
BOEM	Bureau of Ocean Energy Management
BSEE	Bureau of Safety and Environmental Enforcement
CF	center frequency
CPA	closest point of approach
CSAC	Chip Scale Atomic Clock
CTD	Conductivity/Temperature/Depth
dB	decibel(s)
dB re 1 μPa	decibels referenced to 1 microPascal
EA	environmental assessment
EARS	Environmental Acoustic Recording System
EEZ	Exclusive Economic Zone
ESA	Endangered Species Act
FFVS	free field voltage sensitivity
FLAC	Free Lossless Audio Codec
ft	foot
GAM	generalized additive models
GB	gigabyte
GOM	Gulf of Mexico
GPS	Global Positioning System
GUI	Graphic User Interface
HF	High-frequency
Hz	Hertz
IF	intermediate frequency
kHz	kilohertz
km	kilometer(s)
LADC	Littoral Acoustic Demonstration Center
LED	light-emitting diode
L_{eq}	equivalent sound level
LF	Low-frequency
LTSA	long-term spectral average
m	meter(s)
MF	Mid-frequency
MMPA	Marine Mammal Protection Act
MP	Monitoring Project
M/V	Motor Vessel
NCEI	National Centers for Environmental Information

Short form	Long form
nm	nautical mile(s)
NMFS	National Marine Fisheries Service
NOAA	National Oceanic and Atmospheric Administration
NUWC	Naval Undersea Warfare Center
PAM	Passive Acoustic Monitoring
PK	Peak Sound Pressure Level
Program	GOM PAM Program
PSD	power spectral density
psi	pounds per square inch
QA/QC	Quality Assurance/Quality Control
RH	Rockhopper
RL	received level
rms	root-mean square
R/V	Research Vessel
SEL_{cum}	Cumulative Sound Exposure Level
SHRU	Several Hydrophone Recording Units
SL	source level
SPL	Sound Pressure Level
TB	terabyte
TL	transmission loss
μPa	microPascal
U.S.	United States
VHF	very high frequency
VLA	vertical line array

Summary

Results from analyses of an approximately 24-month underwater Passive Acoustic Monitoring (PAM) dataset collected from a strategically delineated 100- by 200-kilometer study area in the northern Gulf of Mexico (GOM) are presented and discussed in this report. Recommendations for continuing the two-year monitoring in future years and expanding program objectives to beyond soundscape characterization are also presented.

Underwater acoustic data were collected using a mix of stationary and mobile platforms under Bureau of Ocean Energy Management's (BOEM) GOM PAM Program (Program), the primary objective of which was to design and field test implementation of a large-scale, multi-year, underwater PAM program in the region. The primary purpose of the two-year data collection and analyses was to characterize the existing soundscape (including sounds contributed by both natural and anthropogenic sources) in the GOM. Since the northern GOM is characterized by complex bathymetry, it was important to better understand the influence of prominent geological features such as canyons on the soundscape. Therefore, a site-specific three-dimensional (3D) underwater sound propagation numerical model was setup. Simulation outputs were used to assess sound focusing and defocusing effects caused by 3D variations in underwater bathymetry.

The experimental design targeted collection of underwater acoustic data in the 10 Hertz (Hz) to 96 kilohertz (kHz) frequency range. This frequency range encompassed the most common anthropogenic and natural sounds that contribute to the existing soundscape in the GOM; namely, those related to weather, the oil and gas industry, shipping, marine mammals, and fish. Given the potential for follow-on marine mammal studies, this bandwidth also allows for detection of sounds produced by mysticete whales and most odontocetes, including deep diving whales such as pygmy (*Kogia breviceps*) and dwarf (*Kogia sima*) sperm whales and beaked whales, and lower frequency components of *Kogia* spp.

The study area included portions of the underwater Mississippi and DeSoto Canyons. Both canyons are populated by deep diving marine mammals and exhibit unique acoustic propagation features. Although both canyons were determined to be viable candidates for data collection, the Mississippi Canyon was preferentially selected as the focus area for monitoring primarily because it provided broad industrial source representation, including seismic exploration surveys, oil production platforms, remotely operated vehicle maintenance, and pipeline installation along axis and on both eastern and western slopes.

A systematic random design, which ensured that survey effort was evenly distributed over the study area while avoiding underwater infrastructure, was selected for placement of data recorders. Data were collected at depths ranging from 53 to 2,148 meters (m) within the main habitat types in the region, including the continental shelf (less than 200 m deep), continental slope (200 to 1,600 m deep), and the abyssal plain (greater than 1,600 m deep).

Three different types of stationary moorings equipped with sensors (hydrophones) and recording systems were used, namely Rockhoppers and Environmental Acoustic Recording Systems, both with effective recording bandwidth ranging from 10 Hz to 96 kHz; and Chip Scale Atomic Clock-Several Hydrophone Recording Unit vertical line arrays, with effective recording bandwidth of 10 Hz to 4.5 kHz. Additionally, two separate mobile autonomous platforms (Seaglider™), with an effective recording bandwidth of 10 Hz to 62.5 kHz, were also deployed within selected portions of the study area to collect data in between the stationary moorings within the Mississippi Canyon and to cover selected areas in the DeSoto Canyon. A shipboard playback experiment for measuring sound transmission loss was also conducted to gather data for characterization of underwater sound propagation properties.

Data were analyzed using standardized software packages and acoustic metrics to provide data products consistent with guidelines adopted by the Baltic Sea Information on the Acoustic Soundscape Project as well as the Atlantic Deepwater Ecosystem Observatory Network Project. Results indicated that the key dominant sound sources recorded during this study varied seasonally and primarily consisted of seismic surveys, shipping, storms, and marine mammal calls. Key observations from the data analyses are summarized below:

- There was a noticeable difference in recorded low-frequency (LF) levels (less than 100 Hz) between the recorders deployed at the shelf break versus offshore locations. Low-frequency levels observed at offshore sites were significantly higher and appear to be driven by seismic airgun activities that occurred in closer proximity. Also, high-frequency levels (greater than 1,000 Hz) were higher and more variable during the winter months. This was likely related to higher variability in weather conditions and associated sea states.

- Observed noise levels at the deep-water sites were comparable to those previously reported and are indicative of extensive industry-related sound from oil and gas operations in the northern GOM. Seismic airgun noise contributed to elevated sound levels across multiple years.

- The deep-water monitoring locations exhibited similar sound pressure level distributions in values and frequencies and in general are consistent with the levels previously measured in this region of the GOM.

- In general, deeper locations appeared to have the highest sound pressure levels at the LF bands (below 100 Hz) and the lowest sound pressure levels at the mid-frequency bands (500 to 10,000 Hz).

- On a seasonal basis, levels at frequencies greater than 1,000 Hz were higher and more variable during the winter months. This was likely related to higher variability in weather conditions and associated sea states.

- Though airgun noises were the most dominant anthropogenic sound source in the acoustic environment, other sources, including vessel-related noise, also contributed to the levels below 1 kHz.

- Biological sounds (dolphin whistles, sperm whale (*Physeter macrocephalus*) clicks, Risso's dolphin (*Grampus griseus*) clicks, and beaked whale clicks) were present throughout all deployments.

- As expected, the analyses also revealed a strong relationship between a vessel's closest point of approach and measured LF sound levels, indicating that ship Automatic Identification System (AIS) data is useful for predicting LF noise in the GOM. There was a strong seasonal pattern in vessel activity, with most vessel detections occurring in summer months. Month and year for airgun signal detections had similar patterns to that of vessel detections. Geographic differences in airgun signals were borderline statistically significant, with a dip in the frequency of airgun detections in the middle latitudes and a higher frequency of signal detection in the middle longitudes.

- There were also notable differences between the soundscapes of the Mississippi and DeSoto Canyons, largely as a result of the generally lower anthropogenic activity in the latter.

- The multi-year study spanned from 2018 to 2020, documenting interannual variation and changes in the soundscape that occurred likely as a result of anthropogenic activity restrictions related to the COVID-19 pandemic.

The 3D underwater sound propagation model established by this study provided valuable data for capturing and understanding focusing and defocusing effects due to 3D variations in bathymetry. These

effects can meaningfully intensify or reduce received levels anthropogenic noise, potentially influencing localized impacts to marine mammals. Incorporation of advanced 3D sound propagation modeling is recommended for future Program phases, particularly within complex topographic regions; this would provide valuable data to better understand and account for important acoustic effects. Model simulation output would help answer important questions such as, "How do anthropogenic sounds potentially impact marine mammal habitats?" and "What are the estimated noise exposure levels experienced by marine mammals?"

An important legacy of the GOM PAM Program is the robust, two-year underwater calibrated acoustic dataset that was collected in the field and some of the analytical tools that were developed to further the soundscape characterization data analysis. Approximately 250 terabytes of raw data were collected during the Program, and these were appropriately packaged and submitted to the National Oceanic and Atmospheric Administration's National Centers for Environmental Information (NCEI) for archiving. After NCEI completes archiving of the raw data on its servers, it is anticipated that they will provide public access to the data along with searching and visualization tools.

Since the primary Program objective was to collect data for underwater soundscape characterization, field data collection protocols (especially placement of recorders) were customized to collect data to meet the defined objective. However, if BOEM's overall goal is to generate comprehensive data that will be useful for managing present and future anthropogenic activities in the region, future Program initiatives should be expanded beyond soundscape characterization to also include collecting and analyzing data for the following purposes:

- Evaluation of marine mammal vocalization data for characterizing spatial and temporal distribution of selected mammalian species and modeling spatial and temporal patterns of marine mammal acoustic activity and density estimations for selected species of interest.

- Estimation of impacts of anthropogenic sounds on marine mammals and other species.

- Monitoring long-term trends in soundscapes and marine mammal density.

Conceptual ideas for achieving these additional Program objectives are presented in this report.

The data, results, conclusions, and recommendations presented in this report were generated for BOEM by the HDR Program Team under IDIQ Contract M17PC00001, Task Order Nos. M17PD00011 and 140M0119F0001.

1   Introduction

This report contains results and recommendations from an evaluation of underwater acoustic data that were collected and analyzed under the Bureau of Ocean Energy Management's (BOEM) Passive Acoustic Monitoring (PAM) Program for the northern Gulf of Mexico (GOM). The northern GOM is a highly industrialized environment with multiple anthropogenic sound sources, including shipping, oil and gas activities, and military operations. Noise impacts to protected species (primarily cetaceans) may occur as a result of oil and gas exploration companies undertaking activities (e.g., seismic surveys, platform decommissioning, drilling, vessel noise) licensed by BOEM and the Bureau of Safety and Environmental Enforcement (BSEE). However, characterizing the impacts and trends is difficult without comprehensive baseline data on the noise environment in the GOM.

Also, BOEM and BSEE are required to assess potential impacts on protected species, specifically under the Marine Mammal Protection Act (MMPA), Endangered Species Act (ESA), and National Environmental Policy Act (NEPA) to assist and guide their decision making. The future BOEM MMMPA rulemaking for seismic activities in the GOM will have a monitoring requirement associated with it, including data collection on ambient noise and on noise associated with seismic activities. **In short, there was an urgent need to implement a systematic and comprehensive underwater acoustic data collection effort in the northern GOM. BOEM's GOM PAM Program (Program) was intended to collect and analyze data to meet this need.**

1.1   GOM PAM Program Objectives

The primary objective of the Program was to **design and field test** implementation of a large-scale, multi-year, PAM effort in the northern GOM. The Program was initiated in 2017 and the first two years of data collection (mid-2018, 2019, and mid-2020) and analyses were focused on collecting data primarily for soundscape characterization (including sounds contributed by both natural and anthropogenic sources). This two-year dataset will serve as a reference point for follow-on efforts to characterize changes in the soundscape of the area over time.

Also, the underwater soundscape is significantly influenced at different scales by three-dimensional (3D) sound propagation (Duda et al. 2011; Ballard et al. 2015; Heaney and Campbell 2016; Reilly et al. 2016; Oliveira and Lin 2019; Reeder and Lin 2019; Oliveira et al. 2021). Physical oceanographic and geological conditions associated with continental shelves and shelf break areas can cause horizontal heterogeneity in medium properties, so horizontal reflection/refraction of sound can occur and produce significant 3D sound propagation effects.

Since the northern GOM is characterized by two large canyons (Mississippi and DeSoto), it was important to better understand the influence of these prominent geological features on the soundscape. Therefore, data collected during the first two years were also used to establish a site-specific 3D underwater sound propagation numerical model. Model simulation outputs were used to assess sound focusing and defocusing effects caused by 3D variations in underwater bathymetry.

In the future, besides continuing data collection and analyses for soundscape characterization, Program objectives could be expanded to include collecting and analyzing data for estimating current marine mammal occupancy and (call) density, supporting the estimation of impacts of anthropogenic sounds on marine mammals and other species of concern, and monitoring long-term trends in soundscapes and marine mammal density.

The initial two-year program was implemented as two back-to-back 12-month Monitoring Projects (MP):

- **2018 MP**: Acoustic monitoring was conducted within a 100- by 200-kilometer (km) study area box located in the northern GOM for the 12-month period from May 2018 to April 2019. Two separate deployments were conducted, the first from May to October 2018 (designated as Deployment 1) and the second from November 2018 to April 2019 (Deployment 2). The 2018 MP is also referred to as the Program Pilot Study in other Program documentation.[1]

- **2019 MP**: Monitoring initiated under the 2018 MP was continued for an additional 12 months (May 2019 to April 2020) under this MP.[2] Lessons learned from the 2018 MP were used to guide delineation of the study area boundaries and placement of sensors for the 2019 MP. The study area for this MP was a subset of the 2018 MP study area and measured approximately 100- by 140 km. Two separate deployments were conducted, the first from May to October 2019 (designated as Deployment 3) and the second from November 2019 to April 2020 (Deployment 4).

This report contains results and recommendations from evaluation of the approximately 24 months of data collected under the two MPs.

1.2   2018 and 2019 Monitoring Project Objectives

The experimental data collection and analysis design for both MPs targeted collection of underwater acoustic data in the 10 Hertz (Hz) to 96 kilohertz (kHz) frequency range.[3] This frequency range encompasses the most common anthropogenic and natural sounds that contribute to the existing soundscape in the GOM; namely, those related to weather, the oil and gas industry, shipping, marine mammals, and fish. Given the potential for follow-on marine mammal studies using data collected under the two MPs, this bandwidth also allows for detection of sounds produced by mysticete whales and most odontocetes, including deep diving whales such as pygmy (*Kogia breviceps*) and dwarf (*Kogia sima*) sperm whales and beaked whales, and lower frequency components of *Kogia* spp.

A suite of underwater acoustic sensors and recorders were deployed at strategically selected locations within the delineated study area(s) to collect data for meeting Program objectives. Data were analyzed using standardized software packages to provide data products consistent with guidelines adopted by the Baltic Sea Information on the Acoustic Soundscape (BIAS) Project as well as the Atlantic Deepwater Ecosystem Observatory Network (ADEON) Project (Ainslie et al. 2017). Data analyses were focused on producing outputs to support the primary objective (i.e., soundscape characterization). In future Program phases, data and data products from the two MPs may also be used for other purposes, such as:

- Guide continuation of soundscape characterization data collection and analyses in the northern GOM.

- Expand data collection outside of the study area covered under the two MPs.

---

[1] Implementation of the 2018 MP was covered under BOEM Contract No. M17PC00001, Task Order No. M17PD00011.

[2] Implementation of the 2019 MP was covered under BOEM Contract No. M17PC00001, Task Order No. 140M0119F0001.

[3] Project reports titled: Experimental design for the passive acoustic monitoring pilot study in the northern GOM, by HDR, 2018; and Experimental design for the passive acoustic monitoring pilot study in the northern GOM, by HDR, 2019.

- Develop and test additional approaches for synthesizing and evaluating data collected across different types of PAM platforms (both stationary and mobile).

- Identify strategies to optimize and increase robustness of the data collection and analyses methods during future years of monitoring.

- Characterize spatial variations and contribution to soundscapes in the enclosed and surrounding Mississippi Canyon habitats, including the continental shelf, continental slope, and abyssal plain.

- Characterize variations in soundscapes over multiple temporal scales, including diel, lunar, and seasonal periods.

- Estimate contributions of anthropogenic sounds to the Mississippi Canyon and vicinity soundscape.

- Describe biological sources of sound present in the Mississippi Canyon and vicinity across the frequency spectrum from 10 to 96 kHz.

- Evaluate marine mammal vocalization data.

- Establish how sound propagation influences soundscapes in the various Mississippi Canyon habitats.

1.3 Study Area

The GOM is a semi-enclosed ocean basin that narrowly connects to the Atlantic Ocean through the opening between Cuba and the Yucatán Peninsula and the Florida Straits. The presence of the Loop Current and warm water eddies separated from the Loop Current are dominant oceanographic features of the GOM that considerably influence the GOM ecosystem/seascape. The Western Planning Area lies 17 km (9 nautical miles [nm]) offshore of Texas and extends to the United States (U.S.) Exclusive Economic Zone (EEZ), which is the jurisdictional limit over the continental shelf (**Figure 1**). The EEZ limit is 370 km (200 nm) from the U.S. coast. The Central Planning Area lies offshore of Alabama, Mississippi, and Louisiana from 6 km (3 nm) to the U.S. EEZ. The Eastern Planning Area lies 17 km (9 nm) offshore of the Gulf Coast of Florida and extends to the U.S. EEZ. The water depths in the Western, Eastern, and Central Planning Areas extend up to approximately 3,346 meters (m) (BOEM 2013).

When monitoring the natural environment because of time and resource limitations, it is usually not possible to exhaustively survey the entire area of interest. Therefore, in consultation with BOEM, a representative subset of the northern GOM, which was centered on the underwater Mississippi and DeSoto canyons, was delineated for data collection and analyses. Both shallow and deeper areas within the delineated study area were targeted for data collection.
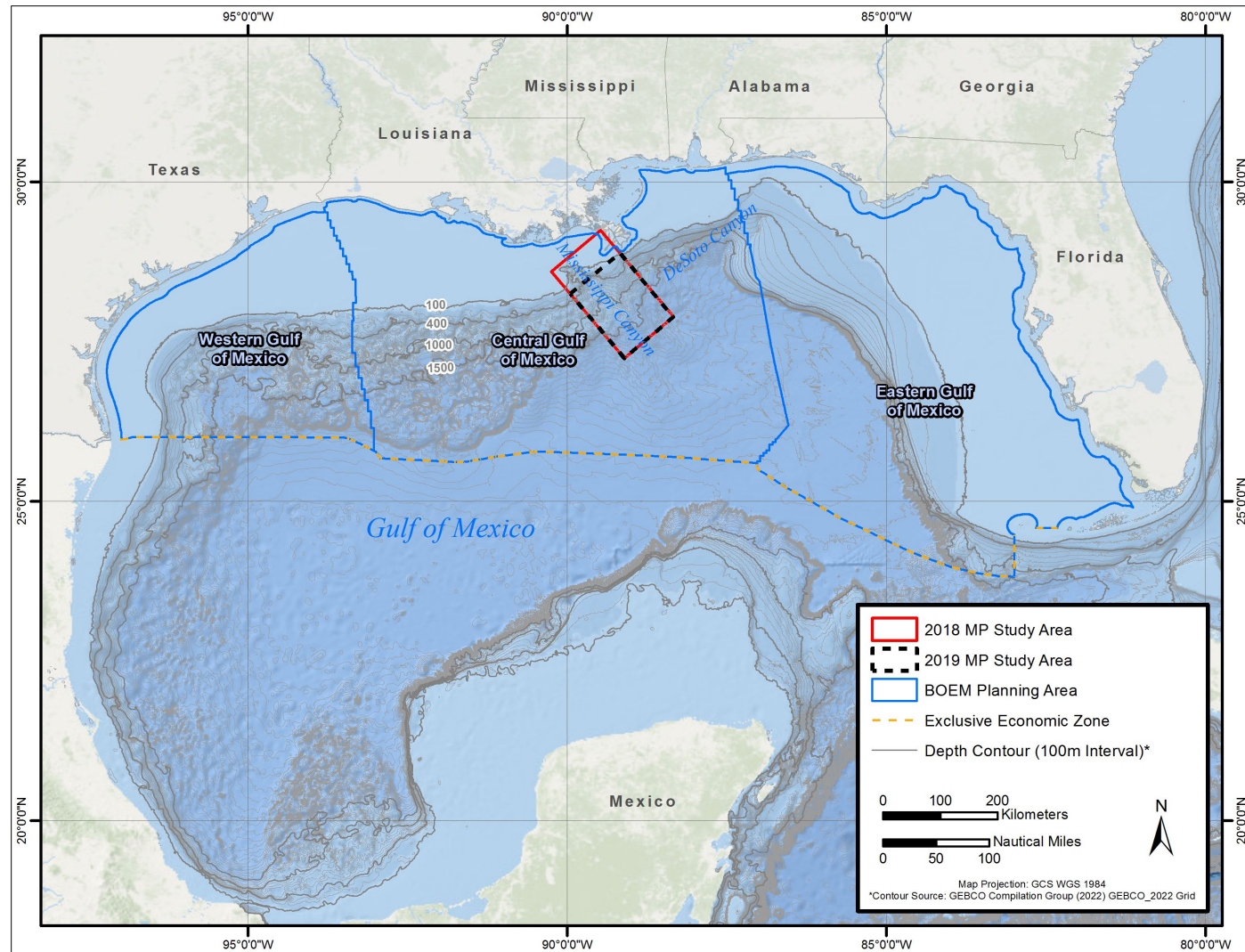
Figure 1. Northern GOM BOEM's Planning Areas and GOM Program 2018 and 2019 MP study areas.

The Mississippi Canyon is located directly south of New Orleans, Louisiana, within BOEM's Central Gulf Planning Area. The DeSoto Canyon, which straddles the Central and Eastern Planning Area boundaries, is located south of Mobile and Pensacola Bays. Both canyons are populated by deep diving marine mammals and exhibit unique acoustic propagation features. Each canyon is characterized by three separate and unique ecosystems, namely the continental shelf (less than 200 m deep), the continental slope (200 to 1,600 m deep), and the abyssal plain (greater than 1,600 m deep).

Though both canyons were determined to be viable candidates for data collection to meet the overall Program and Project objectives, the Mississippi Canyon was preferentially selected as the focus area for both MPs for the following reasons:

- The Mississippi Canyon provides broad industrial source representation, including seismic exploration surveys, oil production platforms, remotely operated vehicle maintenance, and pipeline installation along axis and on both eastern and western slopes. The DeSoto Canyon has some limited industrial activity along its western slope, but almost none towards the center and eastern half.

- PAM has been active in the Mississippi Canyon since 2001 by Cornell University, the Littoral Acoustic Demonstration Center (LADC), the GOM Research Initiative, the National Oceanic and Atmospheric Administration (NOAA), the Sperm Whale Acoustic Monitoring Program, and the Sperm Whale Seismic Study. Availability of these historical multi-decadal datasets was important because they served to validate data collected under the Program.

- The DeSoto Canyon is larger in dimensions than the Mississippi Canyon and would require additional bottom moorings for equivalent planned sensor coverage. The smaller canyon dimension of the Mississippi Canyon also implies a more localized and therefore more targetable concentration of deep-diving whales.

- The Mississippi Canyon experiences a significantly greater exposure to shipping noise than the DeSoto Canyon.

- Given the proximity to elevated anthropogenic noise, the Mississippi Canyon is expected to deliver a more spectrally uniform soundscape. The anthropogenic contribution to the DeSoto Canyon soundscape likely will be dominated by the lower frequencies because of distant source propagation. Mid- (MF) and high-frequency (HF) anthropogenic sources (such as oil platform remotely operated vehicle control/communication) are expected to be less prevalent in the DeSoto Canyon.

- There is an extensive network of meteorological buoys and industrial platforms in the Mississippi Canyon, which can provide corroborative data for analyses and interpretation of weather-related noise trends.

- The Mississippi Canyon experiences a greater influx of fresh water from the Mississippi River. This may play a role in biological soundscapes.

For the 2018 MP, an approximately 100- by 200-km study area box overlapping the Mississippi Canyon was delineated as the 2018 MP study area (**Figure 1**). One of the key lessons learned from analyses of data collected and evaluated under the 2018 MP was that collecting underwater acoustic data using stationary platforms in coastal, shallow-water areas entailed a high risk of expensive monitoring platforms (and accompanying data) being accidently damaged and/or permanently lost due to heavy shipping traffic, including fishing trawlers and/or industrial activities.

In consultation with BOEM, it was therefore decided that for the 2019 MP, shallow-water areas within the 2018 MP study area box less than 100 m would be avoided. The 2019 MP study area was therefore delineated by truncating the shallow-water areas to the north, as shown in **Figure 1**. The 2019 MP study

area box measured approximately 100- by 140-km. The goal was to ensure that, barring unforeseen circumstances and to the extent practicable, a complete data set would be generated for the second 12-month monitoring period.

Marine mammals known to inhabit the study area and its surrounding environment include the Atlantic spotted dolphin (*Stenella frontalis*), bottlenose dolphin (*Tursiops truncatus*), Clymene dolphin (*Stenella clymene*), Fraser's dolphin (*Lagenodelphis hosei*), pantropical spotted dolphin (*Stenella attenuata*), rough-toothed dolphin (*Steno bredanensis*), spinner dolphin (*Stenella longirostris*), striped dolphin (*Stenella coeruleoalba*), false killer whale (*Pseudorca crassidens*), killer whale (*Orcinus orca*), melon-headed whale (*Peponocephala electra*), long- and short-finned pilot whale (*Globicephala melas* and *G. macrorhynchus*), Risso's dolphin (*Grampus griseus*), beaked whales (Ziphiidae), pygmy and dwarf sperm whale, sperm whale (*Physeter macrocephalus*), and fin whale (*Balaenoptera physalus*).

Additionally, the DeSoto Canyon is home to a genetically distinct resident population of Rice's whales (*Balaenoptera ricei*), which appears to have fewer than 100 individuals remaining (NOAA Fisheries 2022). This species was listed as endangered in May 2019 under the ESA (84 *Federal Register* 15446). Because the DeSoto Canyon is a Biologically Important Area for Rice's whales, data collection under the 2018 MP was extended to include selected portions of the DeSoto Canyon.

1.4 Literature Review

Before developing an experimental design for the 2018 MP implementation, a comprehensive literature review was conducted to identify and evaluate available relevant data from previous GOM underwater soundscape characterization efforts (Latusek-Nabholz et al. 2020). The search also included assessment of existing tools and methodologies for acoustic source detection, localization, tracking, and classification. For the literature data review, low, medium, and high underwater noise frequencies were defined as follows:

- **Low-frequency** (**LF**) generally includes sounds in the bandwidths between 10 and 500 Hz. This category is primarily composed of anthropogenic sources, including commercial shipping, followed by seismic sources. However, fish also generate LF sound and can make up a large part of this spectrum for natural ambient noise. The most common way fish produce sounds is by grinding or strumming using musculoskeletal anatomy around the swim bladder. Fish can chorus together and increase the amount of noise in the LF band by as much as 30 decibels (dB) (Hildebrand 2009). Under the right conditions, LF sounds can travel across ocean basins because they propagate over long ranges. Shipping noise has increased more than 12 dB as shipping across the globe has expanded. Over the years, oil exploration and construction has expanded into deeper waters and increased the production of seismic sounds.

- **Mid-frequency** (**MF**) generally includes sounds from 500 Hz to 25 kHz. This category includes natural sources of sound such as sea-surface agitation, including breaking waves, spray, bubble formation and collapse, and rainfall. Heavy precipitation can increase noise levels in this range by as much as 14 dB. Biological sources in the medium-frequency range include snapping shrimp (*Alpheus* spp.). When snapping shrimp are present and actively producing sound, they can also increase the amount of noise by 20 dB. Medium-frequency sounds are more local or regional in nature, as they do not propagate over long distances. Noise associated with military and small vessels also fall in this range.

- **High-frequency** (**HF**) generally includes sounds above 25 kHz and are generally located close to the receiver. Mapping sonars and thermal noise, the result of particles moving close to the hydrophone for instance, are included in this category.

A literature synthesis review was conducted in January 2020 (Latusek-Nabholz et al. 2020). Key findings from the review are summarized below:

- Thirty PAM projects have been conducted in the GOM since 1991. Nine of these studies were specifically designed to gather data on noise in the GOM, while the other 21 studies were designed to gather information on marine mammals. Most data collection efforts focused primarily upon the eastern and central GOM. Additionally, PAM surveys have tended to focus on waters of the continental shelf and slope down to approximately 2,000 m deep; only two surveys covered the abyssal plain, which is also an important biological habitat, extending to approximately 3,200 m.

- The GOM soundscape is characterized by a mix of sounds from both anthropogenic and natural sources. Anthropogenic sounds are primarily associated with navigation, industrial, and military activities. Major sources are categorized logarithmically in **Table 1**. Natural sources include bio-acoustic sounds, earthquakes, wind/waves, rainfall, and thermal agitation of the seawater. Of all the natural sounds, marine mammal calls are of particular interest. Frequency ranges of marine mammal calls in the GOM are shown in **Table 2**. The two different types of sound sources are quantitatively compared in **Figure 2**.

- There are three major anthropogenic contributors to the underwater soundscape in the GOM, namely ship traffic, seismic surveys, and oil drilling activity. Noise from ship traffic is one of the major anthropogenic sources of sound in the GOM, and it includes a variety of sources, including noise related to engines, thrusters, civilian commercial sonar, and other equipment in commercial shipping. Within the delineated study area (**Figure 1**), there are two dominant shipping lanes that form an inverted Y to the north of the Mississippi Canyon. The northeast/southwest-aligned lane runs perpendicular to the shallow northwest canyon origin. The northwest/southeast lane is offset northeast from the canyon and runs nearly parallel to the canyon alignment.

- Seismic surveys are typically conducted using an array of airgun releases that introduce compressed air into the water and create a bubble that generates a pulse of sound sufficiently energetic to penetrate deep beneath the seafloor. A seismic airgun array produces a single, downward-directed, high-energy impulse that is primarily directed downward to map the composition of the seafloor (Gisiner 2016).

- Drilling and production platforms generate a continuous-type sound through transmission of the vibrations of the machinery and drilling equipment such as pumps, compressors, and generators that are operating on the platform. Noise resulting from the drilling operation may include machinery noise, such as that from the drill's drive machinery, including drilling, engine and exhaust, and generator noise. Noise originates from vibration associated with the grinding of rock in the seabed, which can either radiate directly from the drill bit through the rock into the water, or can conduct upwards through the drill shaft, radiating into the surrounding water. Additional noise originates from drill ships and other semi-submersibles that maintain position using dynamically positioned thrusters.

- The Eastern and Central Planning areas within the GOM have been extensively covered by PAM studies; no stationary sensor deployments have been made in the Western Planning Area. Seventeen distinct sites in the Central Planning Area, and more than 50 distinct sites in the Eastern Planning Area, have been covered. Locations of PAM deployments and studies generally have covered the continental shelf and continental slope waters. The majority of PAM studies in the GOM have been conducted in waters between 0 and 1,500 m and only a few have focused on the deeper waters of the GOM, which include the abyssal plain. Additional data gaps were identified concerning differences in sound propagation modeling predictions and field measurements. For instance, academic researchers have theorized that modeling sound propagation from seismic arrays may overestimate propagation losses (Kearns and West 2015).

More information is also needed to address whether there are discrepancies between modeled and actual propagation losses as measured in the field.

Table 1. Anthropogenic sound sources categorized by logarithmic bandwidth

Frequency Range	Representative Acoustic Sources
1–10 Hz	Ship propellers[1]; explosives
10–100 Hz	Shipping activities[1]; explosives; seismic surveying sources[1]; construction activities; industrial activities; naval surveillance sonar systems
100–1,000 Hz	Shipping activities[1]; explosives; seismic surveying sources[1]; construction activities; industrial activities; naval surveillance sonar systems
1,000–10,000 Hz	Nearby shipping activities[1]; seismic airguns[1]; underwater communication; naval tactical sonars; seafloor profilers; depth sounders
10,000–100,000 Hz	Underwater communication; naval tactical sonars; seafloor profilers; depth sounders; mine-hunting sonars; fish finders; some oceanographic systems (e.g., acoustic Doppler current profilers)
Above 100,000 Hz	Mine hunting sonar; fish finders; high-resolution seafloor mapping devices (e.g., side-scan sonars, some depth sounders, some oceanographic sonars, and research sonars for small-scale oceanic features)

Key: Hz = Hertz.
[1] These sources represent the major noise contributors in the GOM.
Sources: NRC 2003 and Hildebrand 2009

Table 2. Frequency range of marine mammal calls in the GOM

Frequency Range	Mammalian Species
1–10 Hz	None known
10–100 Hz	Rice's whale (formerly Bryde's whale) (20), other baleen whales (3, 9, 12, 15, 16, 23)
100–1,000 Hz	Rice's whale (20), other baleen whales (3, 9, 12, 15, 16, 23)
1,000–10,000 Hz	Sperm whale (26), large delphinid whistles and partial (low-end) clicks (4, 8, 13, 14, 18, 21, 24), humpback whale (12), minke whale (15), manatee (29)
10,000–100,000 Hz	Beaked whales (2, 6, 11, 25), sperm whale (26), delphinid whistles and clicks (most energy) (1, 4, 5, 10, 13, 14, 17, 18, 21, 22, 24, 27, 28), partial (low-end) clicks, dwarf and pygmy sperm whales (7, 19)
Above 100,000 Hz	Partial (high-end) delphinid clicks, dwarf and pygmy sperm whales (7, 19)

Sources: Rice et al. 2014a; Širović et al. 2014b; Johnson et al. 2006; NOAA Fisheries 2022; Scripps Whale Acoustics Laboratory 2022; Discovery of Sound in the Sea 2022.
Key: Hz = Hertz.

1. Atlantic spotted dolphin – *Stenella frontalis*
2. Blainville's beaked whale – *Mesoplodon densirostris*
3. Blue whale – *Balaenoptera musculus*
4. Bottlenose dolphin – *Tursiops truncatus*
5. Clymene dolphin – *Stenella clymene*
6. Cuvier's beaked whale – *Ziphius avirostris*
7. Dwarf sperm whale – *Kogia simus*
8. False killer whale – *Pseudorca crassidens*
9. Fin whale – Balaenoptera physalus
10. Fraser's dolphin – *Lagenodelphis hosei*
11. Gervais' beaked whale – *Mesoplodon europaeus*

12. Humpback whale – *Megaptera novaeangliae*
13. Killer whale – *Orcinus orca*
14. Melon-headed whale – *Peponocephala electra*
15. Minke whale – *Balaenoptera acutorostrata*
16. North Atlantic right whale – *Eubalaena glacialis*
17. Pantropical spotted dolphin – *Stenella attenuata*
18. Pygmy killer whale – *Feresa attenuata*
19. Pygmy sperm whale – *Kogia breviceps*
20. Rice's whale – (*Balaenoptera ricei*)
21. Risso's dolphin – *Grampus griseus*
22. Rough-toothed dolphin – *Steno bredanensis*
23. Sei whale – *Balaenoptera borealis*
24. Short-finned pilot whale – *Globicephala macrorhynchus*
25. Sowerby's beaked whale – *Mesoplodon bidens*
26. Sperm whale – *Physeter macrocephalus*
27. Spinner dolphin (long-snouted) – *Stenella longirostris*
28. Striped dolphin – *Stenella coeruleoalba*
29. West Indian manatee – *Trichechus manatus*
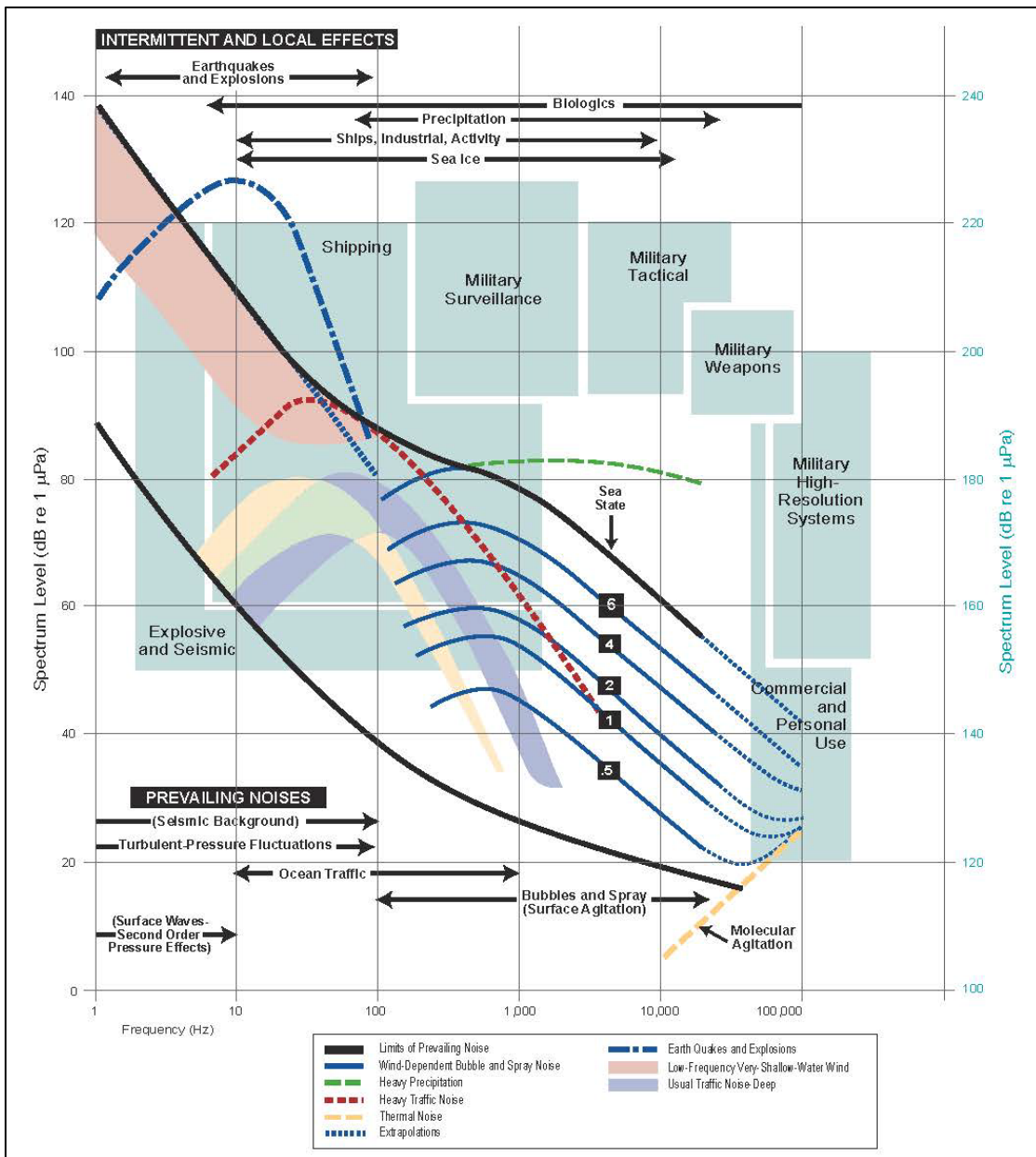
Figure 2. Sources of noise.

Notes: Shipping, military, commercial, and personal uses are shown in blue and use the blue spectrum level values on the right axis. These values are 100 dB greater than the values used on the left axis for intermittent, local effects, and prevailing noises. 100 dB corresponds to five orders of magnitude.

Source: Bradley and Stern 2008 (based on Wenz 1962; reprinted with permission, *Journal of the Acoustical Society of America*)

1.5 Basic Underwater Acoustic Terminology and Key Metrics

A variety of metrics are used to describe sounds, and these different metrics are not directly comparable. The most common term used to define underwater sound is "sound pressure," which in underwater acoustics is expressed as a basic unit in Pascals. Sound pressure is measured by a hydrophone and

recorded using connected electronics. The most common unit used to express sound pressure is the microPascal (μPa).

The pitch of a sound wave is characterized by a frequency content of the wave, which is measured in Hz or kHz. Frequency is often expressed as low (less than 1 kHz), medium (1 to 10 kHz), and high (greater than 10 kHz). Sound levels are often presented as SPL, which can be defined as:

$$dB = 10 \times \log10 \ (Sound\ Pressure^2 / Reference\ Sound\ Pressure^2)$$

It is critical that the value of the reference pressure be specified. This is the "re" in the common unit decibels referenced to 1 microPascal (dB re $1\mu Pa^2$). Sound pressure is often used to characterize continuous sounds in terms of risk of damage to marine animals, such as fish, turtles, and mammals. The root-mean-square (rms) sound pressure and peak sound pressure are the most commonly used sound pressure metrics (Popper et al. 2014). Peak sound pressure is often used to characterize impulsive sounds, is measured as the maximum absolute value of an instantaneous sound pressure during a specific time period and is expressed as dB re 1μPa. The sound exposure level metric is an index of the total energy in a sound received over a chosen time interval and is usually expressed as Sound Pressure Level (SPL) (peak to zero) in dB re 1 μPa^2. This metric can be used to assess risk from exposure to multiple sound sources, as it is an index for accumulated sound energy (Popper et al. 2014).

To assess the exposure of marine mammals to anthropogenic sounds, NOAA's National Marine Fisheries Service (NMFS) recommends specific metrics for establishing acoustic thresholds and predicting impacts of sound sources on marine mammal hearing (NMFS 2016, 2018). NMFS includes both the Cumulative Sound Exposure Level (SEL_{cum}) and Peak Sound Pressure Level (PK) metrics in their recent technical guidance recommendations for determining permanent threshold shift onset acoustic thresholds. The SEL_{cum} metric is typically normalized to a single sound exposure of 1 second and considers both received level (RL) and duration of exposures. This metric is applied to a single source to estimate impacts of exposure to an animal but is not considered appropriate for assessing exposures resulting from multiple activities/sources occurring within the same area or over the same time period (NMFS 2016).

Additionally, the SEL_{cum} metric is not always sufficient for assessing the effects of impulsive sounds (e.g., seismic airguns, impact pile drivers). Therefore, NMFS recommends the concurrent use of the PK metric for impulsive sounds, with PK thresholds. Because NMFS considers dual metric acoustic thresholds for impulsive sounds, the onset of permanent threshold shift is assumed to occur when either the SEL_{cum} or PK metric is exceeded (NMFS 2016). Additional information on frequency weighting and additional metrics is presented in Popper et al. (2014).

All noise measurements performed for this Project, and the metrics and units derived from those measurements, are consistent with, and directly comparable to, guidelines adopted by the BIAS Project and ADEON Project (Ainslie et al. 2017).

2 Underwater Acoustic Data Collection Methods

2.1 Monitoring Instrumentation

During both MPs, acoustic data were collected using a mix of stationary and mobile platforms that were deployed at strategically selected locations within the respective study areas (**Figure 1**). Data were collected at depths ranging from 53 to 2,148 m within the main habitat types in the region, including the continental shelf (less than 200 m deep), continental slope (200 to 1,600 m deep), and the abyssal plain (greater than 1,600 m deep).

Three different types of stationary moorings equipped with sensors (hydrophones) and recording systems were used, namely Rockhoppers (RH) and Environmental Acoustic Recording Systems (EARS), both with effective recording bandwidth ranging from 10 Hz to 96 kHz; and Chip Scale Atomic Clock-Several Hydrophone Recording Unit (CSAC)-Several Hydrophone Recording Units (SHRU) vertical line arrays (VLA), with effective recording bandwidth of 10 Hz to 4.5 kHz. Additionally, two separate mobile autonomous platforms (Seaglider™), with an effective recording bandwidth of 10 Hz to 62.5 kHz, were also deployed within selected portions of the study area to collect data in between the stationary moorings within the Mississippi Canyon and cover selected areas in the DeSoto Canyon.

RHs, EARS, and Seaglider data were primarily used for soundscape characterization. SHRU data collection was geared towards establishment of a 3D sound propagation model and supporting soundscape characterization. **Table 3** contains additional information on the various recording systems used for monitoring.

Table 3. Data recording systems summary

Monitoring System	Number of Units Placed Within the Study Area During Each Deployment	Total Number of Deployments	Servicing and Data Recovery
RH	5	4 (6 months each)	6 months
EARS	5	4 (6 months each)	6 months
CSAC-SHRU	2	2 (6 months each)	No interim servicing
2018 MP Seaglider	1	1 (6 weeks)	No interim servicing
2019 MP Seaglider	1	1 (2 weeks[1])	No interim servicing

Key: CSAC = Chip Scale Atomic Clock; EARS = Environmental Acoustic Recording System; MP = monitoring project; RH = Rockhopper; SHRU = Several Hydrophone Recording Units.
[1] Planned period of data collection; due to adverse weather conditions, data could be collected over two weeks only.

2.1.1 Instrumentation System Specifications

The different data recording systems differed in detail such as depth rating, battery capability, data storage capability, sampling rates, and type of data stored. Between the different systems, there was a trade-off between the schedule, power, and storage under similar conditions. There was also a trade-off between using stationary and mobile data collection platforms. Sensors and data recording systems specifications are summarized in **Table 4**. **Appendix A** presents additional technical specifications and instrument calibration details.

Table 4. Data recording system specifications

Monitoring System	Sample Rate/Bits/ No. of Channels	Monitoring Bandwidth	Duty Cycle	Design Depth (m)
RH	192 kHz 24 bits 1 channel	10 Hz–96 kHz	Continuous	3,500
EARS	192 kHz 16 bits 1 channel	10 Hz–96 kHz	Continuous	6,000
CSAC-SHRU	9.8 kHz 24 bits 4 channels	10 Hz–4.5 kHz	Continuous	500
2018 MP Seaglider	125 kHz	10 Hz–62.5 kHz	Continuous	0–1,000
2019 MP Seaglider	128 kHz 24 bits 1 channel	20 Hz–64 kHz	Continuous	0–1,000

Key: CSAC = Chip Scale Atomic Clock; EARS = Environmental Acoustic Recording System; Hz = Hertz; kHz = kilohertz; m = meter(s); MP = monitoring project; No. = Number; RH = Rockhopper; SHRU = Several Hydrophone Recording Units.

2.2 Monitoring Locations

An in-depth analysis was conducted to develop a defensible strategy for selecting locations within the study area box for data collection.[4] Though a totally random placement of moorings in the survey area would ensure that data were collected within an objective subsample of the study area, selecting a random design also meant that every location in the study area would have a known (typically equal) chance of being selected for monitoring. Adopting a completely random design, on the other hand, could result in placing monitoring points next to one another, while leaving other parts of the study area uncovered (unsurveyed).

One of the key experimental design challenges was the presence of a large number of oil platforms and underwater pipelines in the GOM. Fixed instruments could not be deployed near these structures. Oil platforms typically have a 2-km exclusion zone around them. For pipelines, a 500-m buffer on either side was assumed to be off limits for placing a mooring. Also, moorings could not be placed in close proximity of existing meteorological towers and/or NOAA data collection buoys, because collocation could potentially introduce noise from the non-project anchoring/mooring equipment.

2.2.1.1 2018 MP Stationary Mooring Locations

For the 2018 MP, three alternative design strategies were evaluated for placement of RHs and EARS stationary moorings, namely systematic randomized grid construct, space-filling algorithm grid construct, and stratified grid construct. Additional details and pros and cons about the three different design strategies are discussed in the GOM PAM experimental design report.[5] With input from BOEM, a systematic random design, which ensured that survey effort was evenly distributed over the study area while avoiding the underwater infrastructure, was selected. Final deployment coordinates for RHs and

---

[4] Project reports titled: Experimental design for the passive acoustic monitoring pilot study in the northern GOM, by HDR, 2018; and Experimental design for the passive acoustic monitoring pilot study in the northern GOM, by HDR, 2019.

[5] Project report titled: Experimental design for the passive acoustic monitoring pilot study in the northern GOM, by HDR, 2018.

EARS under the 2018 MP are listed in **Tables 5** and **6** and shown in **Figure 3**. Between the 10 moorings, the 2018 MP covered a depth range of 53 to 1,772 m.

2.2.1.2 2019 MP Stationary Mooring Locations

For placement of EARS and RHs during the 2019 MP, five locations were retained from the 2018 MP, and five new locations were added within the delineated study area (**Tables 7** and **8** and **Figure 4**). Between the ten moorings, the 2019 MP covered a depth range of 440 to 2,148 m.

2.2.2 SHRU Locations

Since SHRU data were intended primarily for establishment of a 3D sound propagation model, a different strategy was adopted to select locations for placement of two custom designed SHRU VLAs. These locations were determined based on analyses of simulation output from a preliminary 3D underwater sound propagation model, which compared acoustic coverage strength at several candidate stations within the Mississippi Canyon and surrounding slopes and plateaus. Additional details regarding the preliminary 3D sound propagation modeling are also discussed in the GOM PAM experimental design report.[6]

The preliminary model simulation showed that locations within the canyon plateau provided better acoustic listening coverage, specifically more uniform and extended. Areas inside the canyon were found to have shadow zones with up to 25 dB variation, and the transmission loss (TL) was stronger. The maximum range considered in the "inside canyon" computation was found to be 30 km. As compared to this, maximum range at areas on the plateaus were estimated at greater than 100 km. Based on this analysis, one station for an "inside the canyon" SHRU (i.e., on the canyon floor) and one station for a Slope SHRU were finalized. The SHRU deployment locations did not change between the two MPs (**Tables 5** through **8** and shown in **Figures 3** and **4)**.

2.2.3 Seaglider Flight Paths

2.2.3.1 2018 MP Seaglider Flight

For the 2018 MP, the Seaglider flight path consisted of three contiguous segments to cover approximately two weeks of data collection in the DeSoto Canyon and two weeks in the Mississippi Canyon (**Table 9** and **Figure 2**). The unit was programmed to cover approximately 20 km per day, during which the unit would record both acoustic and metocean data.

The glider was deployed near the top of DeSoto Canyon on May 10, 2018, from where it transited out of the canyon along its southern slope, diving as deep as possible to follow the seafloor bathymetry. During the second half of the deployment period, the glider traveled westward, reaching the top of the Mississippi Canyon from where it was retrieved on June 18, 2019. During deployment, the flight path was modified as necessary to stay close to the programmed path based on transit speeds and oceanographic currents that were reported back to the pilot via satellite in real time.

---

[6] Project report titled: Experimental design for the passive acoustic monitoring pilot study in the northern GOM, by HDR, 2018.

Table 5. 2018 MP stationary mooring locations, RHs and EARS

Monitoring Station No.	Data Recording System	Monitoring Bandwidth	Deployment 1 (May to October 2018)				Deployment 2 (November 2018 to April 2019)			
			Latitude (deg)	Longitude (deg)	Water Depth (m)	Data Recorded (hours)	Latitude (deg)	Longitude (deg)	Water Depth (m)	Data Recorded (hours)
S1	RH	10 Hz–96 kHz	27.64300	-89.24300	1,413	3,141	27.64300	-89.24300	1,413	4,368
S2	EARS	10 Hz–96 kHz	27.65000	-88.82000	1,772	4179	27.65000	-88.82000	1,772	3,745
S3	RH	10 Hz–96 kHz	28.01100	-89.67500	712	3,106	28.01100	-89.67500	712	4,359
S4	EARS	10 Hz–96 kHz	28.02000	-89.25100	1,280	1,678	27.98713	-89.27067	1,280	3,820
S5	EARS	10 Hz–96 kHz	28.02600	-88.82700	1,672	4,227	27.99418	-88.80950	1,672	3,703
S6	RH	10 Hz–96 kHz	28.38900	-89.68500	685	3,065	28.38900	-89.68500	685	3,052
S7	RH	10 Hz–96 kHz	28.49000	-89.25800	440	3,030	28.49000	-89.25800	440	4,415
S8	EARS	10 Hz–96 kHz	28.40200	-88.83200	1,262	1,332	28.40200	-88.83200	1,262	3,960
S9	RH	10 Hz–96 kHz	28.86100	-89.82400	53	1,108	28.66000	-88.83000	1,067	4,491
S10	EARS	10 Hz–96 kHz	28.77100	-89.26600	131	4,128	28.77180	-89.26640	131	3,808

Key: deg = degree; EARS = Environmental Acoustic Recording Systems; Hz = Hertz; kHz = kilohertz; m = meter(s); No. = Number; RH = Rockhopper; S = Site
Notes:

1. Primary data collection objective was underwater soundscape characterization.
2. RH and EARS were deployed for a total of 24 months (four separate deployments, each lasting six months).
3. During Deployment 1, the RH at Site (S)9 was dragged up by a fishing trawler and therefore the location was moved to deeper waters during Deployment 2.
4. Approximately two weeks into the second deployment, the RH at S3 developed an issue with one of the two 4-terabyte hard drives. The unit successfully switched over to the second hard drive. However, the capacity of the second Solid State Drive alone was not quite enough to store recordings for the entire deployment period. The data storage limit was reached approximately four months after the start of the deployment.

Table 6. 2018 MP stationary mooring locations, SHRU VLAs

Monitoring Station ID	Data Recording System	Monitoring Bandwidth	Latitude (deg)	Longitude (deg)	Water Depth (m)	Data Recorded (hours)
Canyon	SHRU VLA	10 Hz–4.5 kHz	28.40991	-89.78438	4 hydrophones at 175, 200, 250, and 275	3,648
Slope	SHRU VLA	10 Hz–4.5 kHz	28.52531	-89.29874	4 hydrophones at 175, 200, 250, and 275	624

Key: deg = degree; Hz = Hertz; ID = Identification; kHz = kilohertz; m = meter(s); SHRU = Several Hydrophone Recording Units; VLA = vertical line array.
Notes:

1. Primary data collection objective was setting up a 3D underwater sound propagation model.
2. The SHRU VLA data collection period was only six months during each deployment, totaling 12 months over two years.
3. During Deployment 1, the Slope SHRU VLA had an electrical malfunction due to seepage of salt water into the sensor housing, and the recording systems failed after 26 days of data collection.

Table 7. 2019 MP stationary mooring locations, RHs and EARS

Monitoring Station No.	Data Recording System	Monitoring Bandwidth	Deployment 3 (May to October 2019)				Deployment 4 (November 2019 to April 2020)			
			Latitude (deg)	Longitude (deg)	Water Depth (m)	Data Recorded (hours)	Latitude (deg)	Longitude (deg)	Water Depth (m)	Data Recorded (hours)
S1	RH	10 Hz–96 kHz	27.92710	-89.56040	2,148	4,390	27.92710	-89.56040	2,148	Unit lost
S2	EARS	10 Hz–96 kHz	27.64837	-88.82111	1,777	1,048	27.64837	-88.82111	1,777	5,077
S3	RH	10 Hz–96 kHz	27.80900	-89.27890	1,375	4,396	27.80900	-89.27890	1,375	5,096
S4	EARS	10 Hz–96 kHz	27.98871	-89.26963	1,332	5,057	27.98871	-89.26963	1,332	4,682
S5	EARS	10 Hz–96 kHz	27.99373	-88.80897	1,671	5,160	27.99373	-88.80897	1,671	4,371
S6	RH	10 Hz–96 kHz	28.38520	-89.68530	685	4,375	28.38520	-89.68530	685	5,276
S7	RH	10 Hz–96 kHz	28.49160	-89.25810	440	3,973	28.49160	-89.25810	440	2,881
S8	EARS	10 Hz–96 kHz	28.24345	-89.27747	830	5,223	28.24345	-89.27747	830	5,071
S9	RH	10 Hz–96 kHz	28.17980	-88.83490	1,526	4,388	28.17980	-88.83490	1,526	5,171
S10	EARS	10 Hz–96 kHz	27.43412	-89.07278	1,797	5,159	27.43412	-89.07278	1,797	4,680

Key: deg = degree; EARS = Environmental Acoustic Recording Systems; Hz = Hertz; kHz = kilohertz; m = meter(s); No. = Number; RH = Rockhopper; S = Site.
Notes:

1. Primary data collection objective was underwater soundscape characterization.
2. RH and EARS were deployed for a total of 24 months (four separate deployments, each lasting six months).
3. Approximately two weeks into the second deployment, the RH at Site (S)3 developed an issue with one of the two 4-terabyte hard drives. The unit successfully switched over to the second hard drive. However, the capacity of the second Solid State Drive alone was not quite enough to store recordings for the entire deployment period. The data storage limit was reached approximately four months after the start of the deployment.
4. During Deployment 4, the RH at S1 was lost and could not be recovered due to a communication system failure.

Table 8. 2019 MP stationary mooring locations, SHRU VLAs

Monitoring Station ID	Data Recording System	Monitoring Bandwidth	Latitude (deg)	Longitude (deg)	Water Depth (m)	Data Recorded (hours)
Canyon	SHRU VLA	10 Hz–4.5 kHz	28.77150	-89.78500	4 hydrophones at 175, 200, 250, and 275	3,480
Slope	SHRU VLA	10 Hz–4.5 kHz	28.4124	-89.29920	4 hydrophones at 175, 200, 250, and 275	3,480

Key: deg = degree; Hz = Hertz; ID = Identification; kHz = kilohertz; m = meter(s); SHRU = Several Hydrophone Recording Units; VLA = vertical line array.
Notes:

1. Primary data collection objective was setting up a 3D underwater sound propagation model.
2. SHRU VLA data collection period was only six months during each deployment for a total of 12 months over two years.
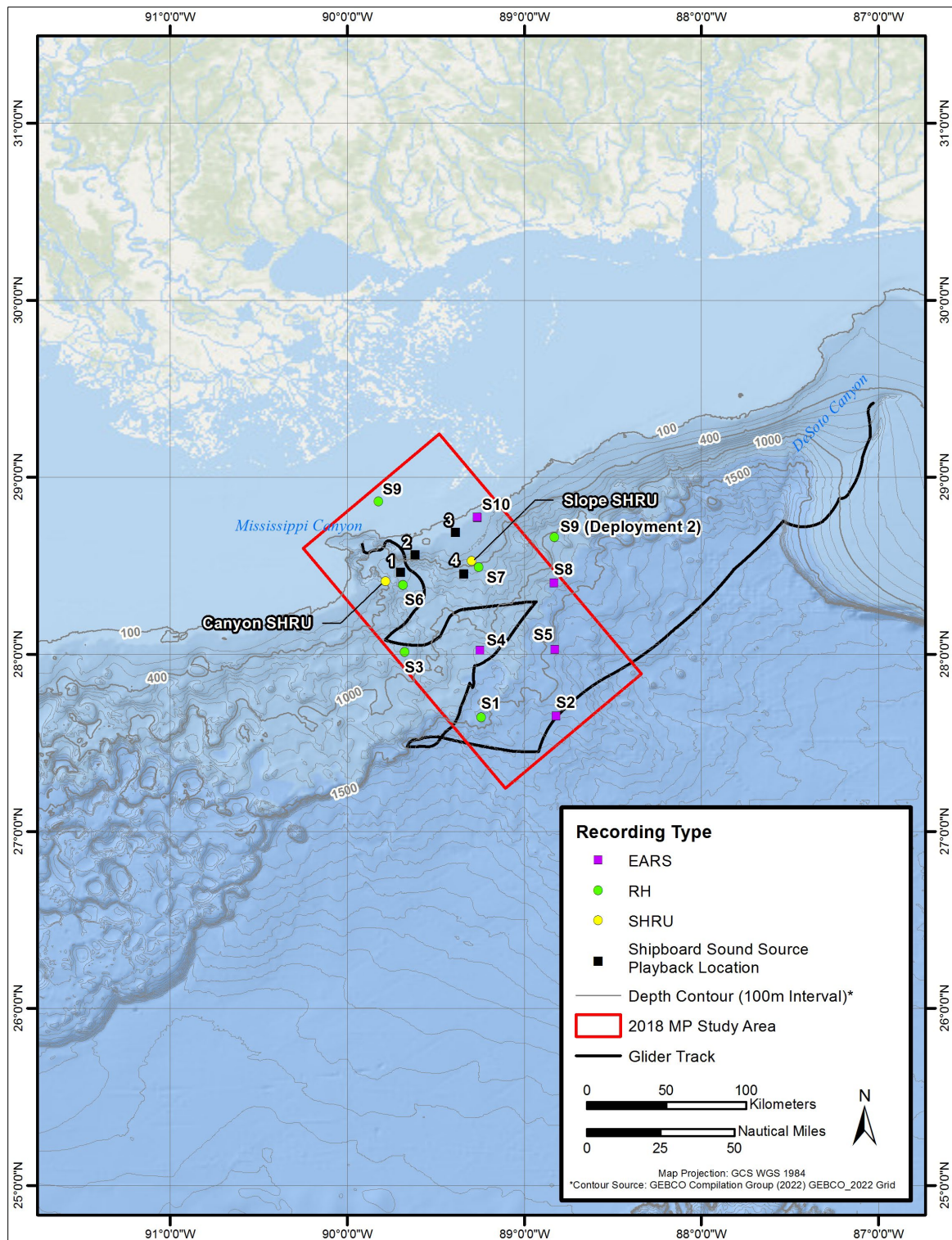
Figure 3. 2018 MP: stationary and mobile platform deployment locations (Deployments 1 and 2).
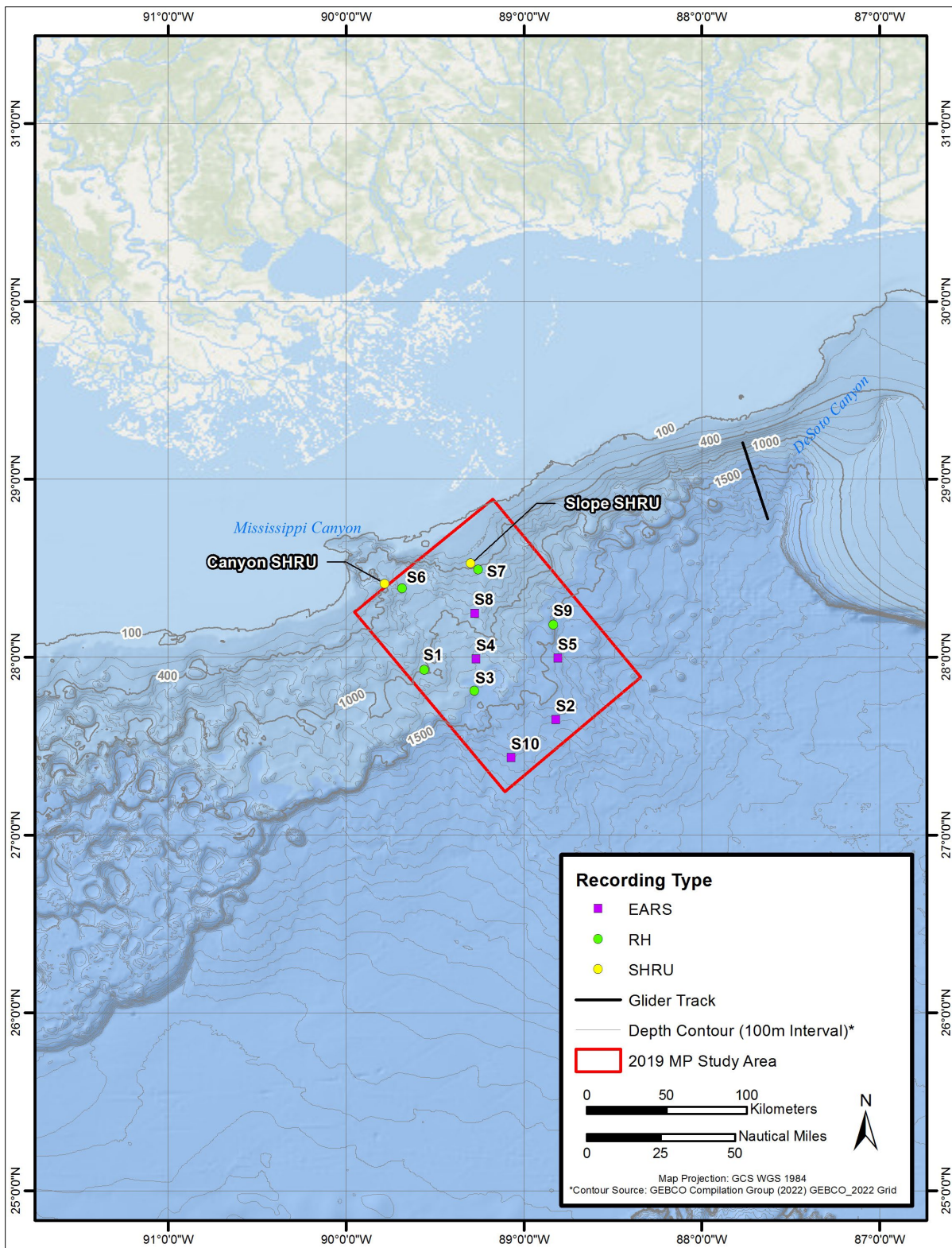
Figure 4. 2019 MP: stationary and mobile platform deployment locations (Deployments 3 and 4).

Table 9. 2018 MP Seaglider flight path segment coordinate

Flight Path Segment No.	Flight Path Segment ID	Data Collection Dates	From		To	
			Latitude (deg)	Longitude (deg)	Latitude (deg)	Longitude (deg)
1	DeSoto Canyon	05/10/2018–5/19/2018	29.419722	-86.995378	28.705587	-87.574675
2	Deep Slope	05/19/2018–05/30/2018	28.676265	-87.601155	27.518300	-89.415167
3	Mississippi Canyon	05/30/2018–06/20/2018	27.519063	-89.415153	28.640717	-89.894550

Key: deg = degree; ID = Identification; No. = Number.

2.2.3.2   2019 MP Seaglider Flight

For the 2019 MP, an initial attempt to launch the Seaglider within the DeSoto Canyon was made on July 23, 2019. The glider was able to complete only four dives and attain a maximum depth of only approximately 10 m, utilizing all the available thrust of the instrument. This was due to prevailing very strong density gradient at the surface, which prevented the glider from attaining deeper depths. These strong density gradients, particularly in the upper 10 m, were caused by a massive influx of freshwater inflow from the Mississippi River due to heavy rains throughout the basin in the prior weeks.

The Seaglider was recovered after four dives and redeployed on July 24, 2019, after modifying the ballast by adding additional lead weight and recalculating flight parameters. The glider was able to achieve approximately 90-m depth, but this utilized the full range of the vehicle's available thrust, and it was unable to penetrate any deeper. Additional weight was added by the Program Field Team, but the additional weight caused the Seaglider to sit low in the water, so the full antenna was not above the water line. The Argos tag, which is the backup method of locating the instrument if communication is lost, was also partially submerged with the additional weight. It was determined that addition of this weight would compromise the ability of the instrument to surface and communicate effectively. The Team corresponded with the manufacturer, Kongsberg Maritime; it was their opinion that the density gradients experienced in this region of the GOM under the current conditions were too extreme for the Seaglider platform to function effectively. During this deployment, the Seaglider instrumentation was functioning properly, and it was able to collect environmental and underwater acoustic data.

During the second attempt in September 2019, the Team was able to deploy the Seaglider successfully. However, after approximately two weeks, the Seaglider reported errors with the internal compact flash, which disabled the unit's ability to read and write mission-critical data, and the Seaglider stopped diving and remained floating on the surface. It did continue to communicate and periodically send position updates, which allowed the Team to recover the unit and download the data collected during the two-week period. Internal inspection of the instrument after recovery revealed that the compact flash card had become dislodged, possibly due to impact of the Seaglider with a hard surface. High quality environmental and acoustic data were collected during the two-week flight path (**Table 10** and **Figure 3**).

Table 10. 2019 MP Seaglider flight path segment coordinate

Flight Path Segment No.	Flight Path Segment ID	Data Collection Dates	From		To	
			Latitude (deg)	Longitude (deg)	Latitude (deg)	Longitude (deg)
1	DeSoto Canyon	09/24/2019–10/05/2019	29.2043882	-87.769433	28.776567	-87.630433

Key: deg = degree; ID = Identification; No. = Number.

2.3 Field Deployments

Each of the four deployments was guided by a BOEM-approved Field Deployment Plan. All field activities were conducted in accordance with a customized, Project-specific Health and Safety Plan, which defined safety and health requirements, designated project safety responsibilities, and described protocols to be followed by the team during field activities. Through careful planning and implementation of corporate and site-specific health and safety protocols, the Project Delivery Team was able to record zero accidents and incidents on this multi-year and challenging project.

2.3.1 Data Collection Timelines

Data were collected during four separate deployments over a 24-month period.

- **Deployment 1**, which extended from May to October 2018, covered data collection during the spring and summer seasons of 2018 (**Table 11** and **Figure 5**). Twelve stationary moorings (five RHs, five EARS, and two SHRU VLAs) were deployed at selected locations within the study area over an eight-day period (**Table 5** and **Figure 3**). This deployment also included data collection using a Seaglider.

- **Deployment 2**, which extended from November 2018 to April 2019, covered data collection during the fall and winter seasons of 2018 and 2019 (**Table 11** and **Figure 5**). Nine of the ten stationary moorings (four RHs and five EARS) were serviced and redeployed at the same locations within the study area (**Table 5** and **Figure 3**). One RH was relocated to deeper waters to avoid shallow, heavy traffic areas.

- **Deployment 3**, which extended from April to October 2019, covered data collection during the spring and summer seasons of 2019 (**Table 12** and **Figure 6**). Twelve stationary moorings (five RHs, five EARS, and two SHRU VLAs) were put in place at the selected locations within the study area over an eight-day period (**Table 6** and **Figure 4**). This deployment also included data collection with a Seaglider.

- **Deployment 4**, which extended from November 2019 to April 2020, covered data collection during the fall and winter seasons of 2019 and 2020 (**Table 12** and **Figure 6**). Ten stationary moorings (five RHs and five EARS) were serviced and redeployed at the same locations within the study area (**Table 6** and **Figure 4**). The final mooring retrieval cruise had to be postponed to June 2019 due to lockdown restrictions imposed by the various state government and partner academic institutions during the COVID-19 pandemic. During the final cruise, nine stationary moorings were successfully retrieved at the end of Deployment 4; the RH deployed at Site 1 could not be recovered during the final recovery cruise due to a malfunction of the acoustic release communication system.

At the end of each deployment, hard drives from each stationary mooring were returned to the laboratory for data extraction, Quality Assurance/Quality Control (QA/QC), pre-processing, and data analyses. Five cruises were undertaken during each MP (**Tables 11** and **12**).

Table 11. 2018 MP sensor deployment timelines

Deployment No.	Cruise No.	Start Date	End Date	Key Activities Completed
1 (May to October 2018)	1	05/10/2018	05/10/2018	• Deployed one Seaglider
	2	05/17/2018	05/24/2018	• Deployed 12 stationary moorings (5 RHs, 5 EARS, and 2 SHRU VLAs)
	3	06/18/2018	06/18/2018	• Seaglider retrieved
2 (November 2018 to April 2019)	4	10/28/2018	11/06/2018	• Retrieved the stationary moorings deployed in May 2018 • Deployed a fresh set of 10 moorings (5 RHs and 5 EARS)
	5	04/04/2019	04/08/2019	• Retrieved stationary moorings deployed in October 2018

Key: EARS = Environmental Acoustic Recording System; No. = Number; RH = Rockhopper; SHRU = Several Hydrophone Recording Units; VLA = vertical line array.

Table 12. 2019 MP sensor deployment timelines

Deployment No.	Cruise No.	Start Date	End Date	Key Activities Completed
3 (April to October 2019)	1	04/04/2019	04/08/2019	• Deployed a fresh set of 10 stationary moorings (5 RHs and 5 EARS)
	2	07/23/2019	07/24/2019	• Attempted to deploy the Seaglider • Deployment was unsuccessful due to ambient buoyancy issue created by heavy influx of freshwater from the Mississippi River
	3	09/24/2019	10/06/ 2019	• Seaglider was retrieved early due performance issues, which could not be addressed on site
	4	11/04/2019	11/11/2019	• Deployed 12 stationary moorings (5 RHs, 5 EARS, and 2 SHRU VLAs)
	5	03/10/2020	03/12/2020	• Retrieved the SHRUs VLAs
4 (November 2019 to April 2020)	6	06/17/2020	June 2020	• Retrieved 9 out of 10 stationary moorings • RH deployed at Site 1 could not be recovered during the final recovery cruise due to a malfunction of the acoustic release communication system

[1] Cruise No.1 of Deployment 3 overlapped with Cruise No. 5 of Deployment 2.
[2] Even though the Deployment 4 data collection ended in April 2020, the moorings could not be recovered until June 2020 due to lockdown restrictions imposed by the various state government and partner academic institutions during the COVID-19 pandemic.
Key: EARS = Environmental Acoustic Recording System; No. = Number; RH = Rockhopper; SHRU = Several Hydrophone Recording Units; VLA = vertical line array.
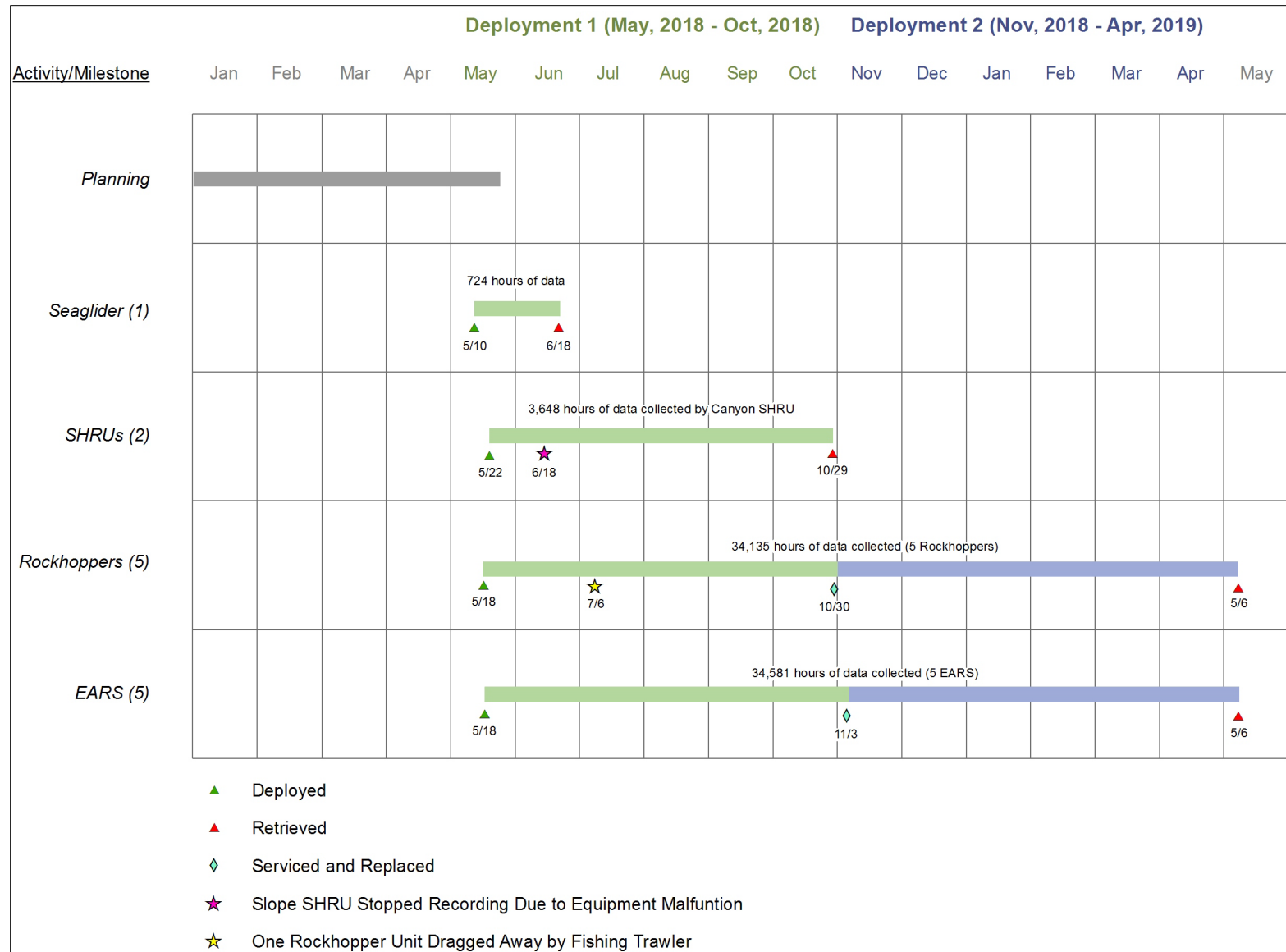
Figure 5. 2018 MP sensor deployment timelines.
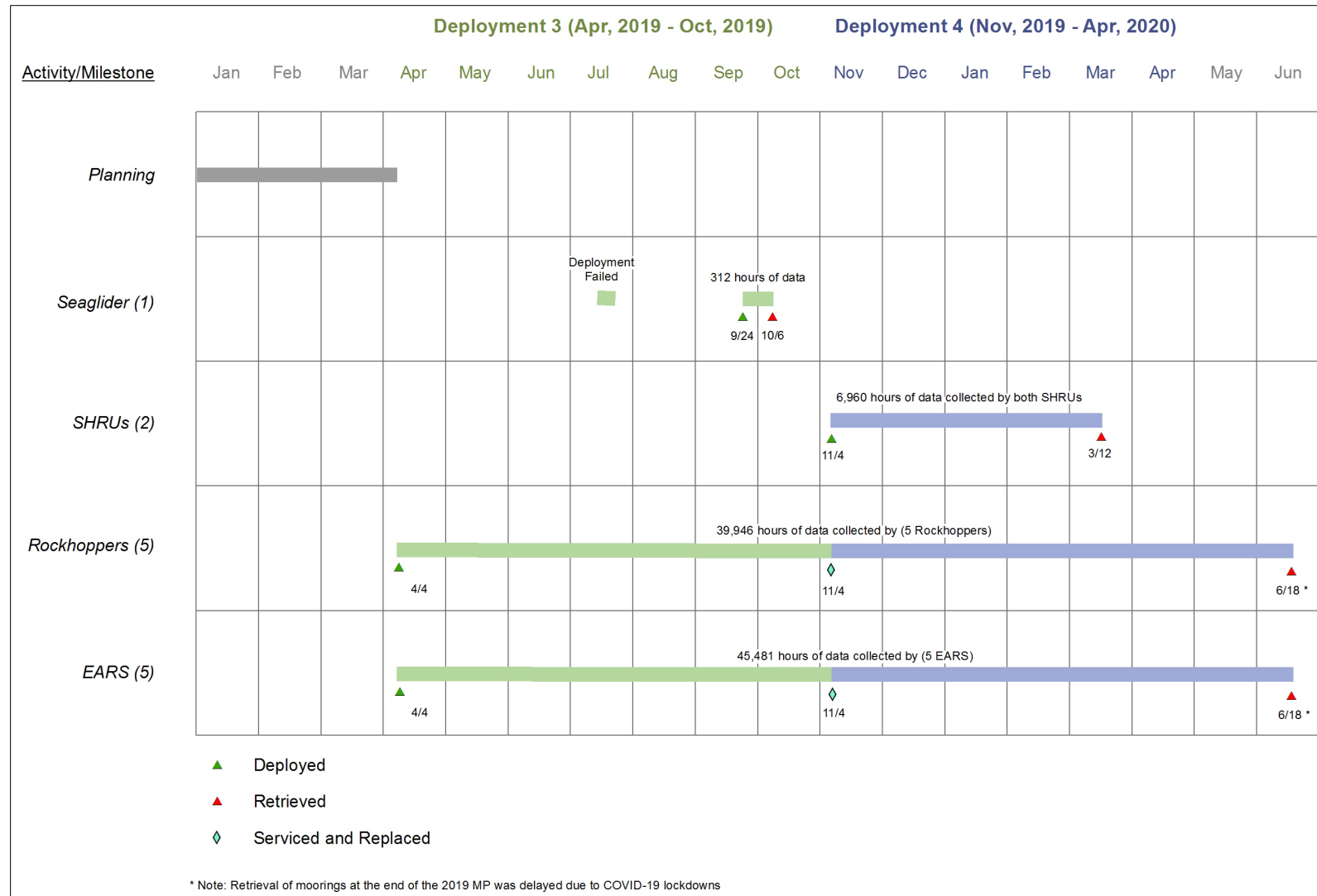
Figure 6. 2019 MP sensor deployment timelines.

2.3.2 Deployment Protocols

Field activities were staged from Cocodrie, Louisiana, a fishing village 31 miles south of Houma on Terrebonne Bay. Located approximately 145 km (78 nm) southwest of New Orleans, this location was convenient to provide support for field data collection efforts in both the Mississippi and DeSoto Canyons.

All stationary moorings were deployed and retrieved from the 116-foot (ft) Research Vessel *(R/V) Pelican*, which was leased from the Louisiana Universities Marine Consortium. The vessel is based at the Louisiana Universities Marine Consortium's DeFelice Marine Center in Cocodrie, Louisiana, and it is equipped to handle a variety of scientific and laboratory operations, including buoy deployment and recovery and hydrographic casts with Conductivity/Temperature/Depth (CTD)-rosette systems. A 30-ft, locally chartered, day vessel was used to deploy and retrieve the mobile platform.

A Field Sampling Plan was developed before each cruise to guide all field activities. The Field Sampling Plan included a customized Health and Safety Plan, which defined safety and health requirements, described onboard safety protocols, and identified safety responsibilities for all field staff. The goal was to ensure that field activities generally complied with applicable federal and state occupational safety and health laws and regulations. **Appendix B** presents specific steps followed during each cruise for deployment and recovery of individual monitoring platforms. **Appendix C** shows a photograph log of field activities.

2.4 Metocean Data Collection

For robust underwater soundscape characterization and interpretation, it was necessary to collect and analyze not only acoustic data but also meteorological and physical oceanography data during each cruise. Conductivity, temperature, and pressure of seawater to support sound speed profiling were collected by CTD casts from the research vessel. Time and weather permitting, expendable bathythermograph sensors were also deployed during selected cruises. Instrumentation onboard the Seaglider collected and transmitted data on temperature, salinity, dissolved oxygen, nutrients, and currents. In addition to metocean data collected by the deployed sensors, additional ancillary data were also obtained from reliable external sources to support data analyses.

2.5 Playback Experiment

During the 2018 MP, a shipboard playback experiment for measuring sound TL was also conducted after the fixed sensors were deployed to gather data for characterization of underwater sound propagation properties. The purpose of the playback experiment was to obtain acoustic TL data for 1) studying propagation of industrial sound sources, 2) ground-truthing the localization abilities within the canyon versus outside the canyon, and 3) validating the underwater sound propagation model.

Two autonomous sound sources were deployed to transmit sound signals at four stations (**Figure 3**). The center frequencies (CF) of these two sources were 550 Hz and 750 Hz, respectively, and the bandwidths for both were 200 Hz. The source level (SL) was 158 dB rms re 1 µPa at 1 m, and the source signal type was a linear frequency modulated chirp. The source system also had monitoring hydrophones. **Table 13** lists playback source signal specifications. **Figure 7** shows the system design and a deployment photograph.

Table 13. Playback experiment source signal specifications

	Signal 1 HF Downchirp	Signal 2 IF Downchirp
Bandwidth	850 to 650 Hz	500 to 650 Hz
Chirp Length	5 sec	6 sec
Source Level	158 dB rms	158 dB rms
Transmission Pattern	At every 0, 10, 20, 30, 40, and 50 sec mark	At every 4, 14, 24, 343, 44, and 54 sec mark

Key: dB = decibel; HF = high-frequency; Hz = Hertz; IF = intermediate frequency; rms = root-mean square; sec = second.
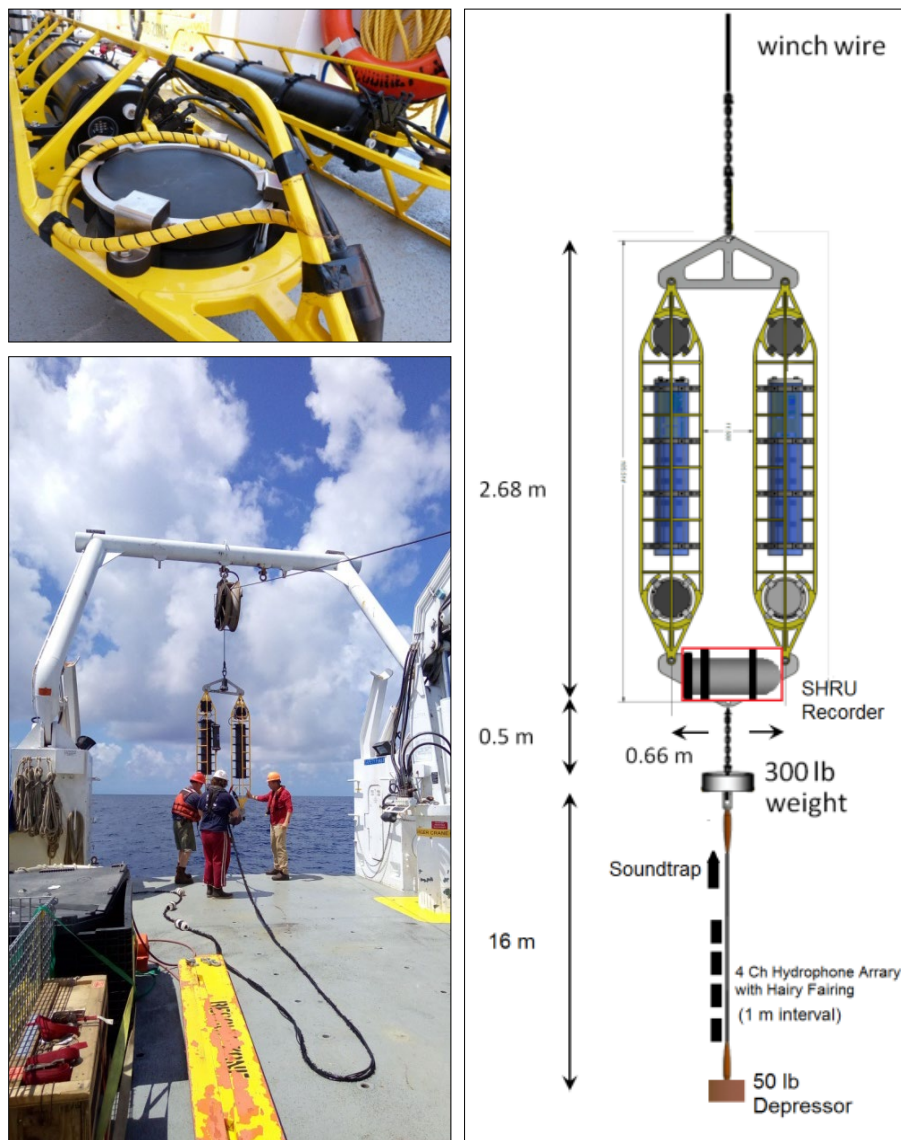
Figure 7. Transmission experiment shipboard source design (right panel) and photographs of the transducer (upper left) and the deployment on site (lower left).

Note: The design and deployment of these sound sources and monitoring hydrophone array were done by the Woods Hole Oceanographic Institution group.

2.6 Field Data Collection Challenges

Deploying unattended, expensive instrumentation underwater in the marine environment, especially over long durations (months), was an inherently risky undertaking. Major risks included equipment and data loss due to damage from collision with ship traffic, industrial activity (such as unmanned vehicles servicing oil and gas infrastructure), equipment dislodging due to trawling, and storm events (hurricanes). Instruments (and data) may also be damaged and lost due to equipment malfunction, the most common cause of which is seawater encroachment into the sealed chambers, which can corrode electrical connections and damage the recording system.

The following preemptive measures were implemented during the MP to minimize potential loss of equipment and data:

- Instruments and systems with a long and successful track record of underwater PAM were selected.

- Hydrophones, recording systems, and power supplies were secured in sealed, watertight compartments, and the entire assembly was coupled with customized, heavy moorings.

- Moorings were deployed underwater by trained and experienced personnel from a large research vessel (*R/V Pelican*) that was properly equipped for these types of deployments.

- Moorings were generally deployed during calm weather to avoid equipment damage due to accidental mishandling because of rough seas.

- Moorings were not placed adjacent to underwater infrastructure to avoid damage from oil and drilling industry service vessels.

- Areas known to be active trawling grounds and designated navigation channels were generally avoided.

- State-of-the-art beacons were installed on the moorings to ensure quick detection, response, and recovery in case the equipment surfaced prematurely:
  - SHRU VLA moorings were equipped with the XEOS KILO location beacons.[7]
  - XEOS Onyx beacons[8] were installed on the RHs.
  - NOVATECH Iridium beacons[9] were fitted on the EARS.
  - The Seaglider was equipped with 1) a primary Iridium satellite connection, 2) a secondary smart position and temperature 6 Argos locating tag from Wildlife Computers,[10] and 3) an acoustic transponder. During each recovery cruise, an acoustic

---

[7] The KILO Subsurface Iridium Satellite Mooring Location Beacon continuously monitors for unplanned or accidental release of subsurface instrument moorings. It makes use of the bi-directional, global, real time Iridium Satellite Short Burst Data network in combination with GPS position location.

[8] The Onyx is an extremely small GPS Satellite tracker that tracks mobile assets with seamless coverage globally. The Iridium satellite constellation with 66 satellites in Low Earth Orbit (LEO) and truly global coverage provide low-latency two-way communication with the Onyx.

[9] The NOVATECH IR-7300 Iridium beacon is a ruggedized incident-alerting system, designed to monitor and protect valuable oceanographic assets. Using the Iridium satellite telemetry system allows users to receive real-time GPS positioning and have bi-directional communication with the beacon.

[10] Argos satellite telemetry is one of the most widely used methods to relay data and track the movements of marine animals. The primary benefits are its global coverage and that locations are calculated in near real time.

deck box was available on the vessel, which would be used to locate the glider if it did not surface as planned.

- RHs were also equipped with an onboard very high frequency (VHF) radio transmitter.
- Both RHs and EARS were equipped with a light-emitting diode (LED) flasher for night recovery, if necessary.

Notwithstanding all the preemptive measures taken, some equipment and data loss were incurred. The following issues were dealt with during Deployment 1:

- One RH (RH402), which was deployed at Site 9 at a relatively shallow depth of 53 m, was apparently trawled and damaged by a shrimping vessel on July 6, 2018. Evaluation of audio recordings form the partially recovered unit and the Global Positioning System (GPS) track of the surfaced equipment indicated that the mooring was brought on board a fishing vessel (most likely the 148-ton shrimper, *Sea Dolphin*); after several hours on deck, it was likely tossed overboard until it was discovered and reported to the Project Team by a sport fisherman a week later. Only the recording unit (glass sphere) was recovered; the acoustic release was missing. For the second deployment, this station was moved to deeper waters (28.660°North, 88.830°West; depth of 1,067 m) to avoid similar loss.

- One of the EARS was also accidently dislodged from its mooring and floated to the surface. Upon receiving an alert from the dislodged unit, a Field Team was immediately dispatched on a search and recover mission. The unit was located and safely retrieved after two days. Apparently, the line had been cut, and it appeared that most likely an oil industry underwater infrastructure servicing robot was responsible for the accident. Data were recovered from the dislodged unit and used in the analyses.

- The Slope SHRU VLA also suffered an equipment malfunction during the first deployment. The power cable manufactured by SubConn, Inc., which connected the second battery housing on the SHRU, failed completely. Post-recovery investigations confirmed that the cause of the malfunction was a defective connector. Apparently, water had intruded into the connector from the base of the pings. Significant corrosion was observed along the connector body, and the plastic protection sleeve had cracked due to pressure of the accumulated water. The water damage shorted the connector, leading to a series of chain effects on the electronics until the recorder stopped working completely at the end of July. This VLA only collected and recorded data for a total of 26 days.

- Also, one of the four hydrophones (SN 238078) on the Slope SHRU VLA, which was deployed at a depth of 250 m, suffered damage during the deployment. The data recorded by this hydrophone showed that the sensitivity was approximately 20 dB lower than the calibrated value. The hydrophone was calibrated and tested before the array assembly, and one likely cause is static electronic damage at some time before the deployment.

At the end of Deployment 4 one RH (Site 10) could not be recovered due to malfunction of the release mechanism.

During the 2019 MP, the first Seaglider deployment, undertaken on July 23, 2019, had to be aborted due to presence of strong density gradients at the surface, which prevented the glider from diving beyond 10 m depths. These strong density gradients, particularly in the upper 10 m, were caused by a massive influx of freshwater sent down the Mississippi River due to heavy rains throughout the basin. The Seaglider was recovered after four dives and redeployed on July 24, 2019, after modifying the ballast by adding additional lead weight and recalculating flight parameters. The instrument was able to achieve approximately 90-m depth, but this utilized the full range of the vehicle's available thrust and it was unable to penetrate any deeper. Additional weight added to the unit caused the Seaglider to sit low in the water, so the full antenna

was not above the water line. The Argos tag, which is the backup method of locating the instrument if communication is lost, was also partially submerged due to the additional weight.

A second successful deployment attempt was made on September 24, 2019. However, within approximately two weeks of being deployed, the unit had to be retrieved due to a malfunction of the internal compact flash card. This malfunction disabled the unit's ability to read and write mission-critical data, and the Seaglider was not able to dive to the programmed depths. A third deployment attempt was planned for spring 2020; however, that could not be undertaken due to COVID-19-pandemic-related lockdowns.

Also, COVID-19 pandemic related lockdowns at various team partner institutions created serious challenges for completing the field work safely and on time and consequently led to a significant delay in conducting data analyses and reporting. Another significant challenge was the delay in acquisition of the AIS data, which is the backbone of the vessel soundscape analysis. The 2018 AIS data were not available until 2020, and the last part of the 2019 AIS data were not available until mid-2021.

3 Data Analyses and Archiving Methods

3.1 Data Analyses

A two-step data analyses approach was adopted, as described in **Sections 3.1.1** (Phase 1) and **3.1.2** (Phase 2).

3.1.1 Phase 1 (Basic) Data Analyses

Data collected under the two MPs by each instrument type were separately processed, analyzed, and reported. RH data were analyzed using the noise analysis tools within the Raven-X toolbox for MATLAB, developed by the Cornell University's Center for Conservation Bioacoustics. A subset of EARS data was analyzed using the EARS MATLAB noise analysis software as a quality control check. The data standards for the analyses were generally consistent with guidelines adopted by the BIAS Project and ADEON Project (Ainslie et al. 2017). The single-hydrophone statistics, as described in the following sections, were generated.

3.1.1.1 Long-term Spectral Average Plots

Long-term spectral average (LTSA) plots were calculated for each site for visualization purposes. The duration of the LTSA can span from hours to months, to show different acoustic events such as ships, storms, seismic surveys, sperm whale click trains, or fish choruses.

3.1.1.2 Equivalent Sound Levels

To examine the variation in sound levels as a function of time, the metric of equivalent continuous SPL, or equivalent sound levels (L_{eq}) (dB re 1 µPa), which represents the average flat frequency-weighting sound pressure of a continuous time-varying signal (ANSI 1994) over specified time intervals, was used. L_{eq} were calculated for one or both sets of the following frequency bands:

- 10 Hz to 1 kHz (LF band), 1 kHz to 10 kHz (mid-frequency [MF] band), and 10 kHz to 96 kHz (HF band): Each of these bands will contain acoustic signatures from a variety of anthropogenic, biological, and geophysical sources. Noise levels in the LF band are expected to be primarily driven by shipping and seismic airguns. The MF band will cover the frequency range of sperm whale echolocation clicks. Signals in the HF band will include vocalizations of a wide variety of delphinids and beaked whales.

- One-third octave frequency bands covering the entire frequency range from 10 Hz to 96 kHz. For sound analysis in a biological context, one-third octave bands are commonly used, since the function of the mammalian ear can be approximated as a set of band-pass filters with a resolution of approximately one-third octave.

3.1.1.3 Cumulative Percentage Distribution

A cumulative percent distribution was computed for each recording site and selected frequency band, which represents the percentage of time that SPLs reached a particular L_{eq}, averaged over 1-second time intervals. The cumulative percent distribution allows for a direct comparison of the statistical noise characteristics of each site within selected frequency bands.

3.1.1.4 Power Spectral Density Levels

To statistically evaluate the SPLs across the entire frequency spectrum at each recording site, power spectral density (PSD) plots were created. The PSD captures long-term variation in ambient noise across the measured frequency domain by representing power spectra (dB re 1 µPa^2/Hz) as a function of frequency using linearly averaged 1-second sound data and a 1 Hz frequency resolution. PSD levels from the entire recording period for each sensor type were represented using the median percentiles of the PSD.

Because the SHRU VLAs have a 100-m depth aperture, two cross-channel statistics, described in the following sections, were also computed using only SHRU data.

3.1.1.5 Cross-spectral Probability Density Plots

Cross-spectral probability density plots illustrating the statistical distribution of PSD levels were generated for each site.

3.1.1.6 Noise Coherence

Coherence of sound data between two channels of a SHRU VLA were computed to identify highly coherent noise sources, such as noise emitted from surface ships passing near the hydrophone array. Coherence is an important soundscape measurement to ensure accuracy of passive acoustic localization.

3.1.1.7 3D Underwater Sound Propagation Model

Data collected by the SHRU VLA under the 2018 MP was used to initiate establishment and testing of an underwater sound propagation model for assessing sound focusing and defocusing effects caused by 3D variations in underwater bathymetry. Model development and validation continued during Phase 2.

3.1.2 Phase 2 (Advanced) Data Analyses

In Phase 2, RH and EARS data collected under the two MPs were combined to create a 24-month dataset for more detailed analyses, which included the following:

- **Power Spectral Density Analysis of Raw Data**: Raw data had been collected using different instruments, each one of which used a different data format. Therefore, a project-customized module of Raven-X was developed and used to generate summary statistics for the raw acoustic data in 1-Hz, 1-second resolution. These Raven-X summary statistics outputs served as inputs for the Phase 2 data analysis. Since the Raven-X outputs are ADEON-guidelines compliant, the Phase 2 outputs are also considered ADEON-guidelines compliant by extension.

- **Detector Band Creation**: Known acoustic sources have specific frequency characteristics. Candidate frequency bands that are likely to be able to indicate the presence of different sources were identified. Some of these frequency bands were determined from the literature, while the remaining bands (defined as empirical bands) were identified through a review of the data. Though these frequency bands were observed, they are not inferred to be associated with any particular source(s).

- **Detection of Acoustic Events in Candidate Bands**: The hourly mean RL in each band is calculated and subtracted from each candidate band to produce a "normalized" band. The detection threshold was taken as the sum of standard deviation of the normalized band plus 3 dB. Any level exceeding this threshold was taken as a detection.

- **AIS Data**: 2018 and 2019 AIS data were obtained[11] and incorporated into the analyses to identify specific acoustic sources.

- **Statistical Analysis**: The bandstats output, the cumulative acoustic power in a 1-hour band in each of the source candidate frequency bands, were analyzed with two predictor variables, namely AIS metrics and windspeed values. The resulting analyses clarified the relative power of these metrics to predict acoustic levels. Graphical representations of the candidate frequency bands were used to identify spatiotemporal patterns.

- **Stationary Mooring and Seaglider Data Comparison**: This comparison was performed to determine how far data from a single stationary buoy could be extrapolated.

During Phase 2, SHRU data were used to advance and validate the 3D sound propagation model that had been initiated under Phase 1. These data were also used to conduct noise coherence and source correlation analyses and soundscape fingerprint analyses. As appropriate and relevant, metocean data collected during the MPs or acquired from external sources were also incorporated into the analyses to support data interpretation.

3.1.2.1 Phase 2 Data Analysis Challenges

COVID-19 pandemic related lockdowns at various team partner institutions created serious challenges for completing the field work safely and on time and consequently led to a significant delay in conducting data analyses and reporting. Another significant challenge was the delay in acquisition of the AIS data, which is the backbone of the vessel soundscape analysis. The 2018 AIS data were not available until 2020, and the last part of the 2019 AIS data were not available until mid-2021.

3.2 Data Archiving

Approximately 250 terabytes (TB) of raw underwater acoustic data were collected during the two MPs over a roughly 24-month period (**Table 14**). These data were appropriately packaged and submitted for archiving to NOAA's National Centers for Environmental Information (NCEI). NCEI is the nation's leading authority for environmental data, and it manages one of the largest archives of atmospheric, coastal, geophysical, and oceanic research in the world. After NCEI completes archiving of the GOM PAM Program's raw data on its servers, it is anticipated that it will provide public access to the data along with searching and visualization tools.

All data submitted to NCEI for archiving are unprocessed to the degree that it is still usable by the public (i.e., formats that do not require proprietary applications to be read). The data are replete with metadata and reports describing collection techniques used by each principal investigator. NCEI will be responsible for backups, data integrity, and standard industry practices for maintaining access to the data objects.

Key steps in the data packaging for archiving consisted of the following:

- Raw acoustic files from each sensor were collated. These files ranged from two minutes to four hours in length. Per NCEI request, small files were concatenated to create files with durations of four hours.

- All files were converted to the Free Lossless Audio Codec (FLAC), providing compression of the acoustic data files without any loss of information. FLAC is an open-source format released by

---

[11] https://marinecadastre.gov/

the Xiph.org Foundation under the BSD license. The libraries used for conversions are libFLAC version 1.3.3 (August 4, 2019).

- After conversion, data were packaged with version 3.1.0 of PassivePacker (NCEI). PassivePacker is an NCEI-provided Python script for packaging acoustic data with metadata and ancillary environmental data in an archive-friendly format. This script also verifies that required NCEI metadata fields were included.

- Where available, additional environmental and ancillary data were also packaged with the acoustic data. For example, Seaglider monitoring data included corresponding temperature, salinity, and dive profiles for each deployment.

- Formatted data were transferred to sets of portable 8 TB hard drives and shipped to NCEI for archiving.

Table 14. Summary of data, sampling rate, and file size for each sensor type

Sensor Type	Original Format	Number of Files (Approximate)	Data Size	Included Ancillary Data
Rockhopper	FLAC	18,520	147.0 TB	
EARS	Proprietary	13,410,066	107.3 TB	
SHRU	WAV	3,114	3.1 TB	
2018 MP Seaglider	FLAC	21,840	891.3 GB	Dive profile, conductivity, temperature, depth
2019 MP Seaglider	FLAC	527	49.5 GB	Dive profile, conductivity, temperature, depth

Key: EARS = Environmental Acoustic Recording System; FLAC = Free Lossless Audio Codec; GB = gigabyte; MP = monitoring project; SHRU = SHRU = Several Hydrophone Recording Units; TB = terabyte; WAV = Waveform Audio.

4 Results

Approximately 250 TB of raw underwater acoustic data were collected during the two MPs over a roughly 24-month period and analyzed per a BOEM-approved Data Analyses Plan. Key results from the analyses are summarized in this section. Information is presented on the different types of analyses conducted and observations made from interpretation of the results, including soundscape characterization, spatial and temporal trends assessment, anthropogenic and biological sound detection, statistical modeling of vessel RLs, fixed and mobile sensor comparison, 3D underwater sound propagation modeling, noise coherence and source correlation analyses, and soundscape fingerprint analysis.

4.1 Soundscape Characterization

4.1.1 Rockhoppers

Between May 2018 and June 2020, a total of 74,081 hours of continuous acoustic data were collected by the RHs during four back-to-back deployments (**Figures 5** and **6**). The units were programmed to collect data continuously at a 197 kHz sampling rate and 24-bit resolution. Data quality was excellent, and no issues (e.g., electronic noise, drop-outs) were detected during the manual QA/QC performed as part of the post-processing.

RH data collected under the two MPs were processed, analyzed, and reported using the noise analysis tools within the Raven-X toolbox for MATLAB developed by the Cornell University's Bioacoustics Research Program package (Dugan et al. 2016). This MATLAB-based package features parallelized data processing capabilities, which enables processing of large audio archives at significantly improved throughput rates. Raven-X features a Noise Analyzer module (Ponirakis et al. 2015), which was used to generate multiple data outputs, including LTSA plots, L_{eq}, cumulative percentage distribution, temporal trends, PSD levels, and spectral probability density plots. The analysis methods and units followed established standards outlined in Ainslie et al. (2017).

Comprehensive results from the RH data analyses were detailed in two separate sensor reports (one per MP).[12] Key results from interpretation of data outputs are:

- Data collected from 2018 through 2020 indicate that the majority of seismic surveys are being conducted further offshore in the GOM. There was a noticeable difference in recorded LF levels (less than 100 Hz) between the two units deployed at the shelf break (Sites 6 and 7) and the offshore sites (Sites 1, 3, and 9).

- There was a noticeable difference in recorded LF levels (less than 100 Hz) between the recorders deployed at the shelf break versus offshore locations. LF levels observed at offshore sites were significantly higher and appear to be driven by seismic airgun activities that occurred in closer proximity (compared to Sites 6 and 7; **Figure 8**). Also, HF levels (greater than 1,000 Hz) were higher and more variable during the winter months. This was likely related to higher variability in weather conditions and associated sea states.

---

[12] Project reports titled: Assessment of ocean ambient sound levels in the northern GOM, May 2018–May 2019, by Klinck H, Ponirakis DW, Dugan PJ, Rice AN, 2019; and Assessment of ocean ambient sound levels in the northern GOM, May 2019–May 2020, by Klinck H, Ponirakis DW, Dugan PJ, Rice AN, 2020.

- Observed noise levels at the deep-water sites were comparable to those previously reported by Estabrook et al. (2016) and Wiggins et al. (2016) and are indicative of extensive industry-related sound from oil and gas operations in the northern GOM (**Figures 9** and **10**). Seismic airgun noise contributed to elevated sound levels across multiple years.

- On a seasonal basis, levels at frequencies greater than 1,000 Hz were higher and more variable during the winter months. This was likely related to higher variability in weather conditions and associated sea states.

- Though airgun noises were the most dominant anthropogenic sound source in the acoustic environment, other sources, including vessel-related noise, also contributed to the levels below 1 kHz.

- During the period of July 11 through 15, 2019, Tropical Storm Barry moved across the hydrophone array. As indicated in **Figure 11**, this corresponded with a significant drop in one-third octave frequency band levels with the CF of 63.1 Hz as all airgun surveys ceased due to hazardous weather conditions. The occurrence of tropical storms seemed to allow measurement of low-frequency levels in the absence of major anthropogenic contributors (i.e., baseline assessment).
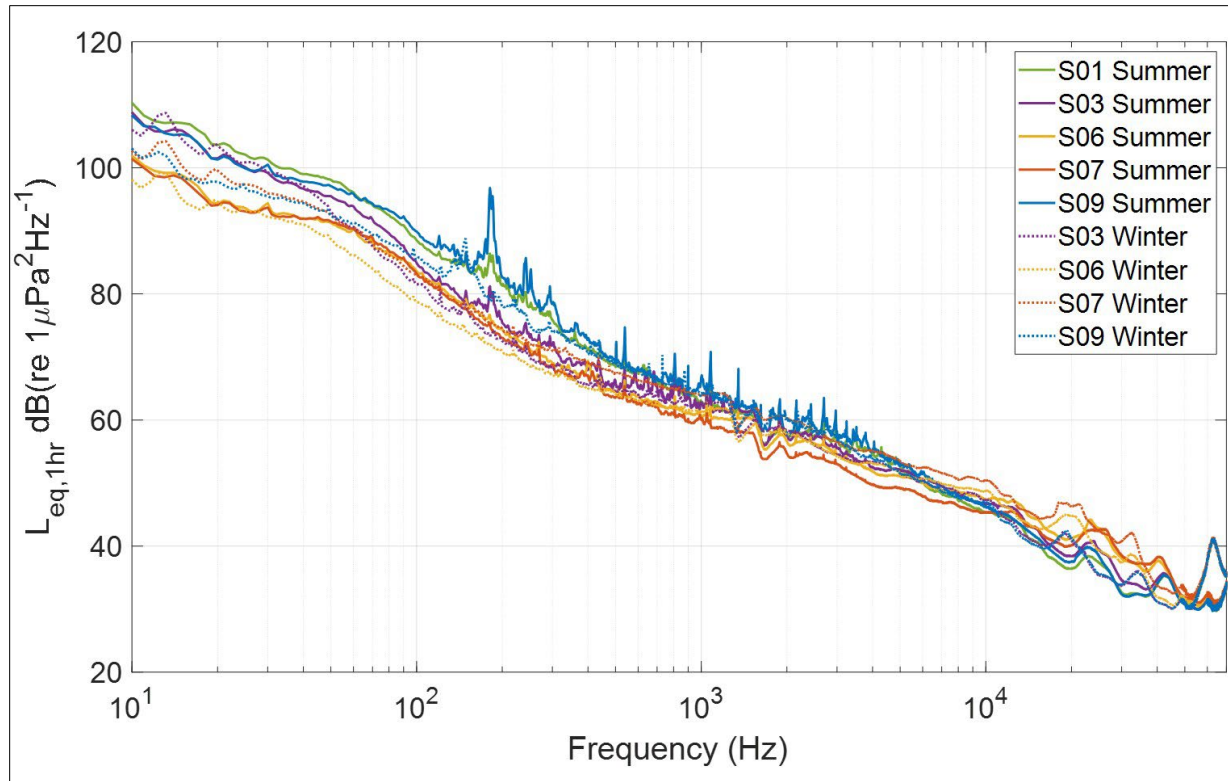
Figure 8. Average PSD levels by site for Deployment 3 (May 2019–November 2019) representing summer months, and Deployment 4 (November 2019–June 2020) representing winter months.
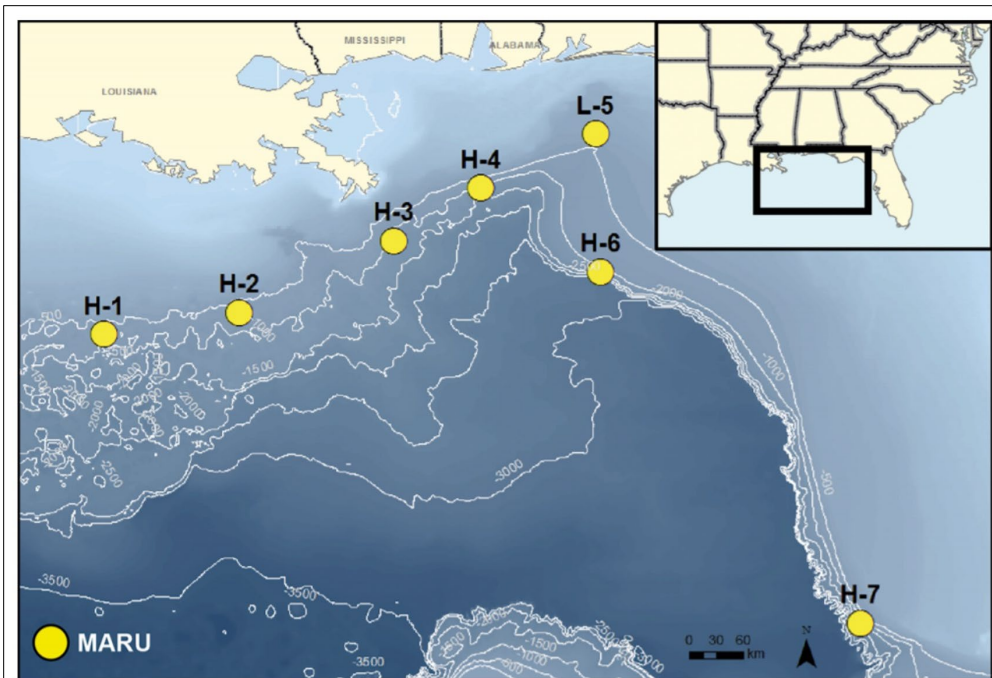
Fig. 1. High-frequency (H) and low-frequency (L) MARU recording sites. Yellow circles: MARU recording locations; white lines: isobaths in 500 m intervals
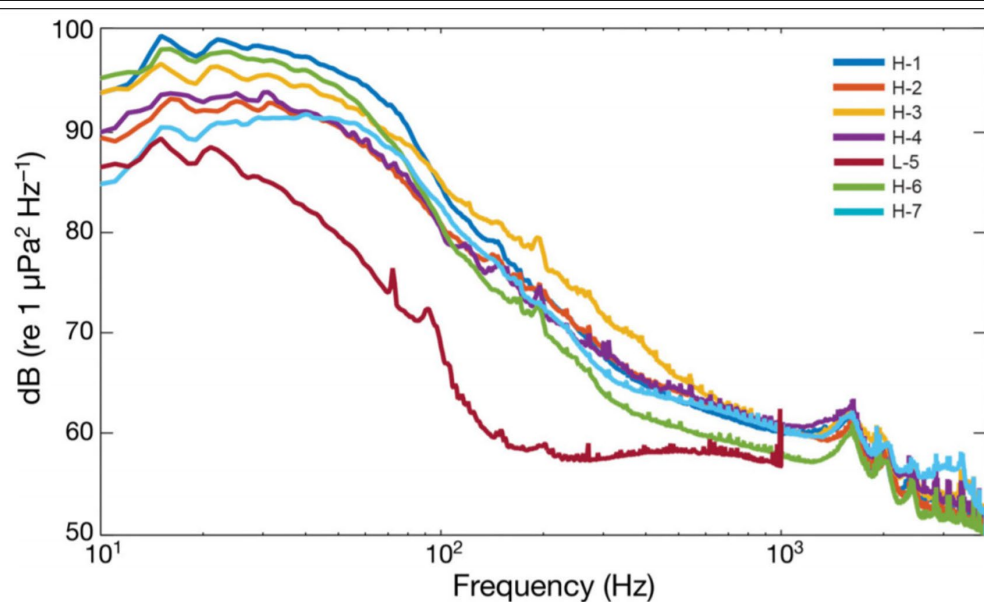
Fig. 5. Power spectral density of sound levels (dB re 1 µPa² Hz⁻¹) of the 50th percentiles for the 7 study sites throughout the recording period averaged over 1 s time intervals

Figure 9. Previous Cornell recorder locations in the GOM (top panel) and corresponding spectrum levels (bottom panel)

Source: Estabrook et al. (2016)

61
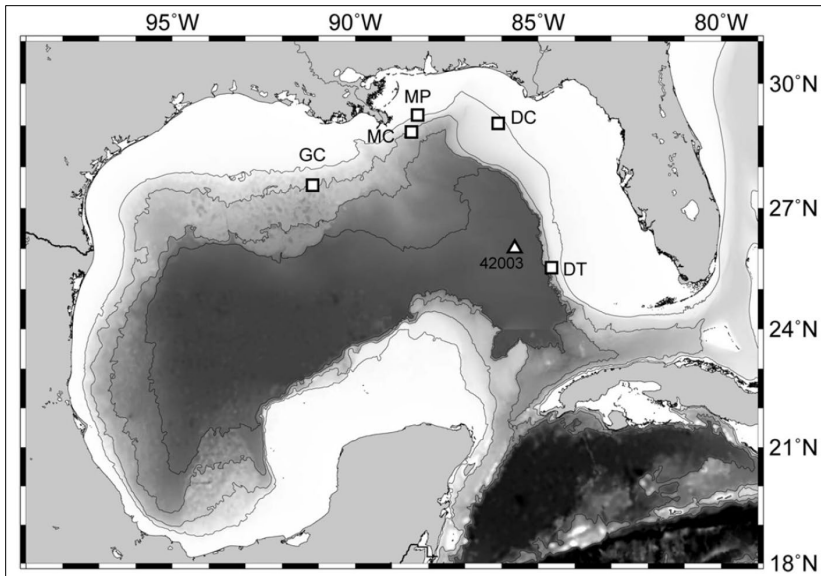
FIG. 1. HARP locations (see Table I) shown as squares with site names. NOAA NDBC weather buoy station 42003 shown as triangle northwest of site DT. GOM bathymetric map with contours at 100, 1000, 2000, and 3000 m depth.
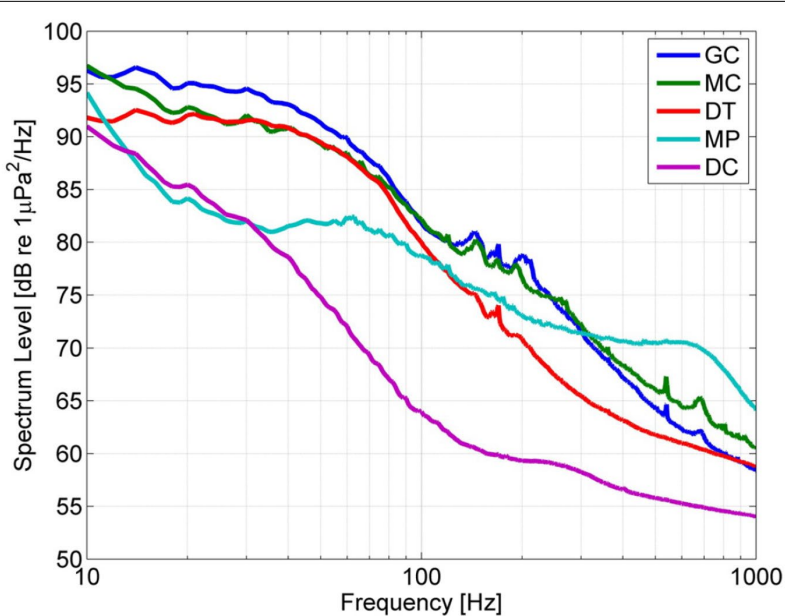
FIG. 3. (Color online) Average sound pressure spectrum levels by site over entire deployment period. See Table I for total number of days used for each average.

Figure 10. Previous Scripps Institution of Oceanography recorder locations in the GOM (top panel) and corresponding spectrum levels (bottom panel)

Source: Wiggins et al. (2016)
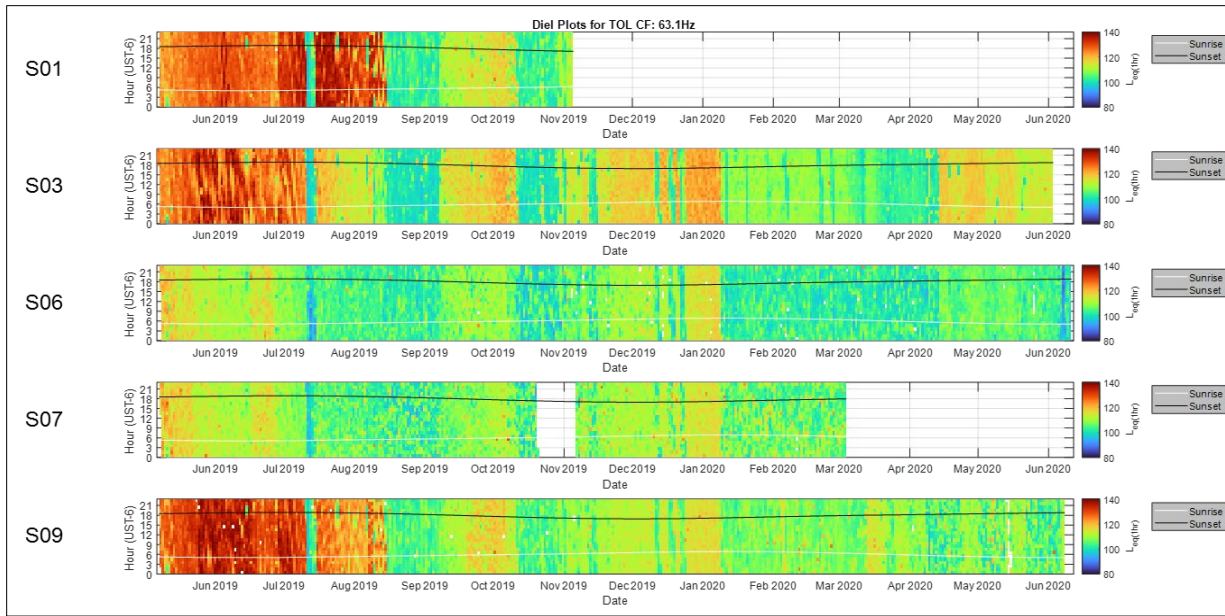
Figure 11. Hourly L_{eq} levels for the on-third octave frequency band with a 63.1 Hz center frequency for each deployment site

Note: Increased levels in this band are indicative of airgun activity

4.1.2 Environmental Acoustic Recording System

Between May 2018 and June 2020, a total of 80,061 hours of continuous acoustic data with a sample rate of 192,000 samples per second were collected by the EARS moorings during the four back-to-back deployments (**Figures 5** and **6**). The units were programmed to collect data continuously at a 192 kHz sampling rate and 24-bit resolution. Data quality was excellent, and no issues (e.g., electronic noise, drop-outs) were detected during the manual QA/QC performed as part of the post-processing.

EARS data collected under the two MPs were processed and analyzed using a noise analysis package developed by the University of Louisiana at Lafayette. The software and data processing workflow are based on the standards developed for previous large-scale ocean ambient noise monitoring projects (Betke et al. 2015; Ainslie et al. 2017). The analyses methods and units followed established standards outlined in Ainslie et al. (2017). Extracted acoustic field characteristics are directly comparable to ones measured in previous and ongoing studies in the Baltic Sea (BIAS Project) and the North Atlantic (ADEON Project). Data analyses outputs included LTSA plots, L_{eq}, cumulative percentage distribution, temporal trends, PSD levels, and spectral probability density plots.

Comprehensive results from the EARS data analyses are presented in four separate sensor reports (two per MP).[13] Key results from interpretation of data outputs are:

---

[13] Project reports titled: Assessment of ocean ambient sound levels in the northern GOM, May-October 2018: autonomous Environmental Acoustic Recording System (EARS) buoys, by Sidorovskaia N, Bhattarai K, 2019; Assessment of ocean ambient sound levels in the northern GOM, October 2018–April 2019: autonomous Environmental Acoustic Recording System (EARS) buoys, by Sidorovskaia N, Bhattarai K, 2019; Assessment of ocean ambient sound levels in the northern GOM, April-November 2019: autonomous Environmental Acoustic Recording System (EARS) buoys, by Sidorovskaia N, Bhattarai K, 2020; and Assessment of ocean ambient sound levels in the northern GOM, November 2019-June 2020: autonomous Environmental Acoustic Recording System (EARS) buoys, by Sidorovskaia N, Griffin S, 2020.

- The measured SPL monitored by the EARS buoys were comparable to levels previously reported in the northern GOM (Wiggins et al. 2016; Sidorovskaia and Li 2016) and were similar to the simultaneously deployed RHs. The 50th percentiles (medians) of one-third octave band SPLs for all sites monitored are shown in **Figures 12** through **14**.

- The LF soundscape was dominated by distant seismic surveys.

- On a seasonal basis, the LF noise curves at deep sites, which are dominated by oil and gas industry activities and service shipping, were lower during the winter months as compared to the summer months. This was an expected finding since the industrial activity in the GOM generally declines during the colder months due to harsh marine weather.

- Biological sounds (dolphin whistles, sperm whale clicks, Risso's dolphin clicks, and beaked whale clicks) were present throughout all deployments.

- The deep-water monitoring locations (Sites 2, 4, 5, and 8) exhibited similar SPL distributions in values and frequency and in general are consistent with the levels previously measured in this region of the GOM.

- In general, deeper locations appeared to have the highest SPLs at the LF bands (below 100 Hz) and the lowest SPLs at the mid frequency (MF) bands (500 to 10,000 Hz).

- The MF band highest SPLs were observed during Deployments 3 and 4 at Site 8 (830 m), which is located at the edge of the study area just outside the Mississippi Canyon.

- There were anthropogenic pauses in the soundscapes due to impacts of the COVID-19 pandemic; exploration surveys and industrial activities were present across all COVID-19-pandemic-impacted months (March through June). However, the decidecade band associated with seismic exploration (63 Hz CF) had the lowest observed levels in April 2020 followed by a quick recovery in the activity levels in May and June 2020.

4.1.3 Comparison of Data from EARS and RH Recorders

Data from each deployment of the RH and EARS recorders were compared against each other (**Figures 15** through **18**). The two datasets were comparable above 100 Hz and a systematic difference in the data below 100 Hz was observed. This deviation appears to begin at 100–200 Hz and increases in magnitude as frequency decreases. At 40 Hz, the difference seems to exceed 10 dB. These differences were seen in the monthly temporal and spatial spectral data.

The experimental design adopted for placement of recorders and data generated under this Project do not readily lend themselves to directly answering the question as to which of these two types of recorders is closer to the "truth". In order to make that determination, a laboratory test will have to be performed under controlled conditions during which representative and comparably calibrated units of the two recorders are tested side-by-side along with a standard reference hydrophone.

4.1.4 Several Hydrophone Recording Unit Vertical Line Arrays

Approximately 11,280 hours of acoustic data were collected by the SHRU VLAs at a sample rate of 9,800 samples per second during two separate, approximately six-month deployments (May to October 2018 and November 2019 to March 2020). The VLAs were placed at the same location (one on the floor of the Mississippi Canyon and the other on the slope) during both deployments (**Tables 3** and **4** and **Figures 6** and **8**) to better capture temporal soundscape variability. Data quality was excellent, and no issues (e.g., electronic noise, drop-outs) were detected during the manual QA/QC performed as part of the post-processing.
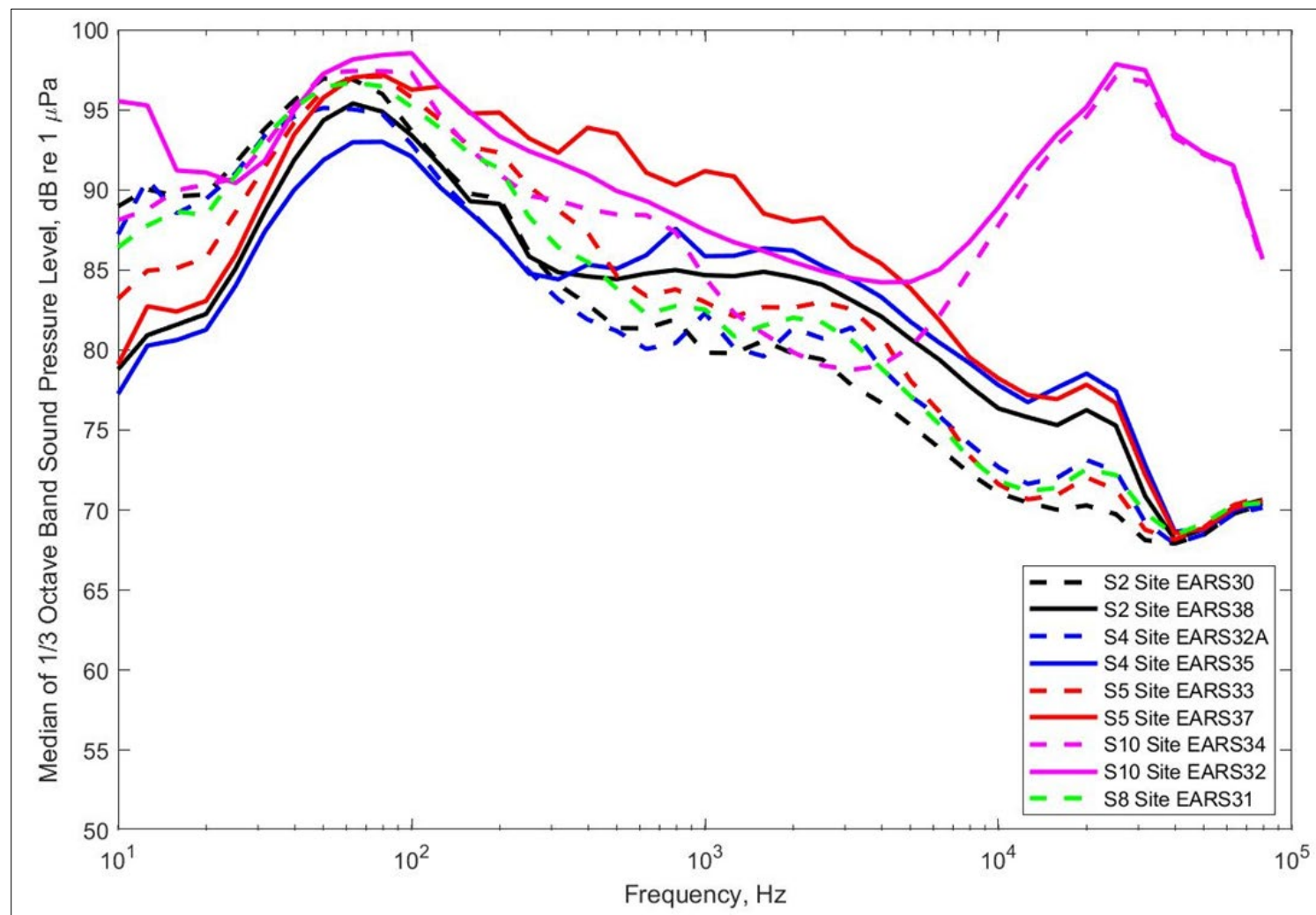
Figure 12. Medians of one-third octave band spectrum (1 second equivalent) for all monitored sites between May 2018 and April 2019 (Deployments 1 and 2) for EARS

Note: The solid lines correspond to the winter deployment, dashed lines correspond to the summer deployment, and colors are associated with deployment sites.
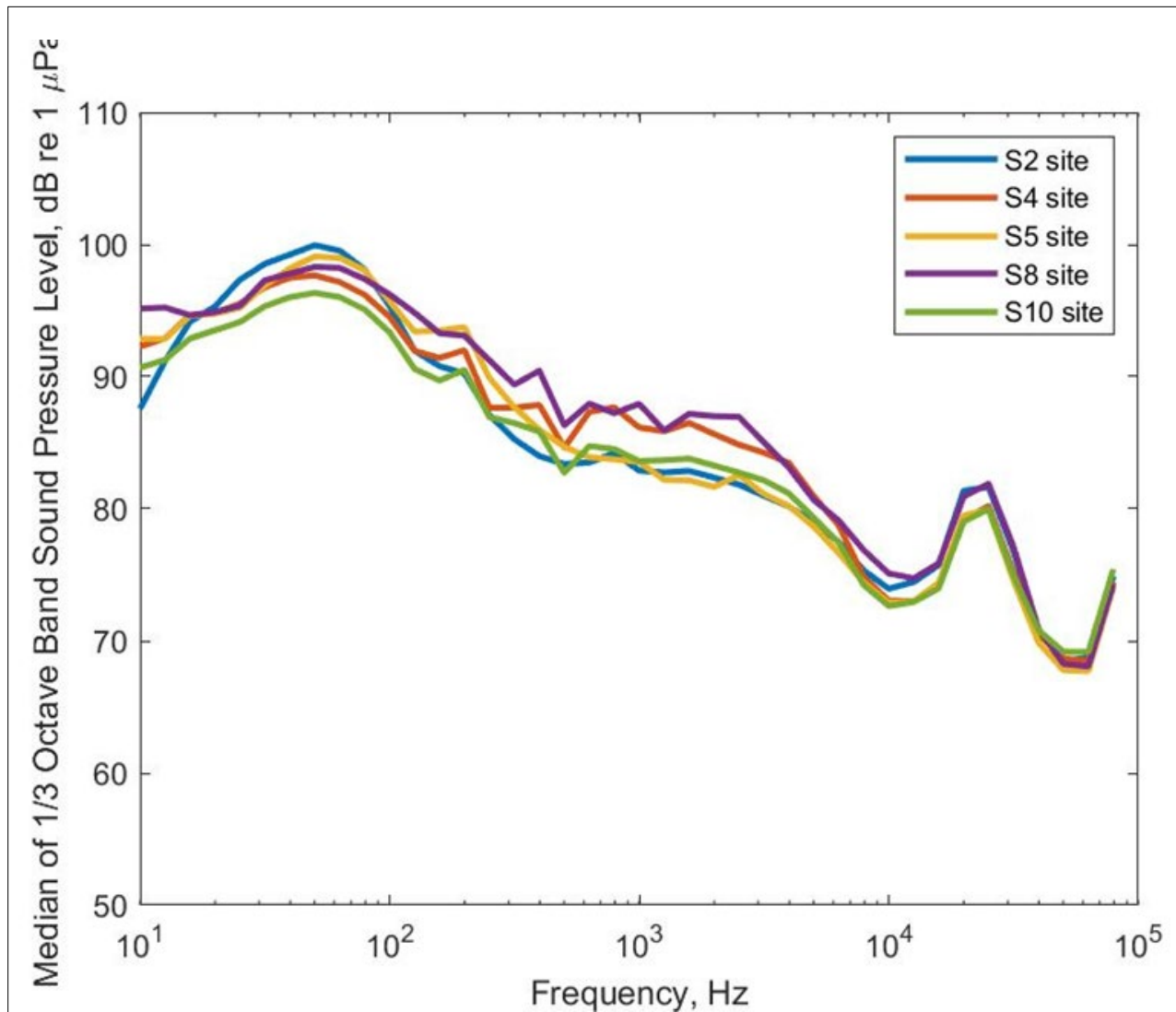
Figure 13. Medians of one-third octave band spectrum (1 second equivalent) for all five monitored sites between April 6 and November 11, 2019 (Deployment 3) for EARS
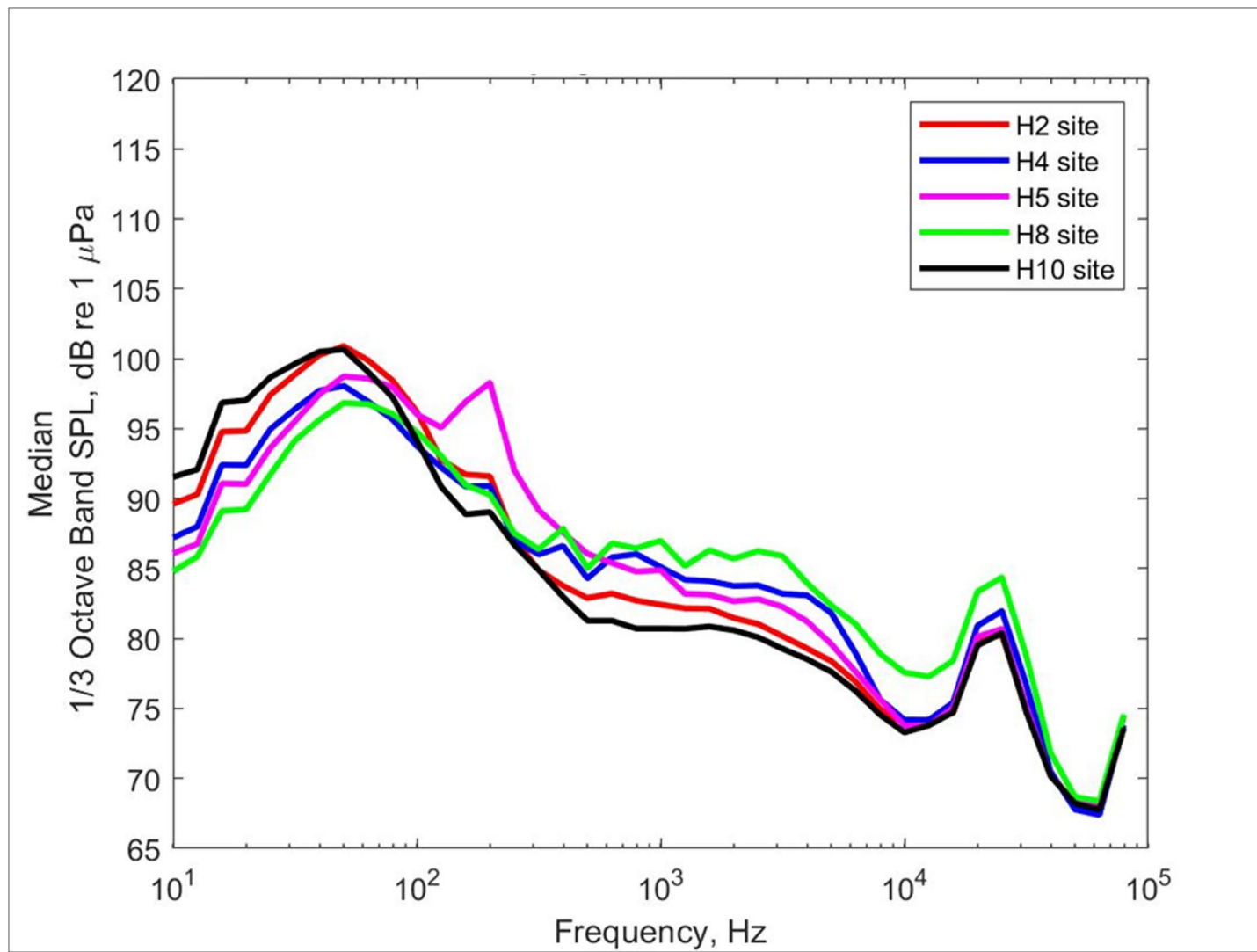
Figure 14. Medians of one-third octave band spectrum (1 second equivalent) for all five monitored sites between November 11, 2019, and June 15, 2020 (Deployment 4) for EARS
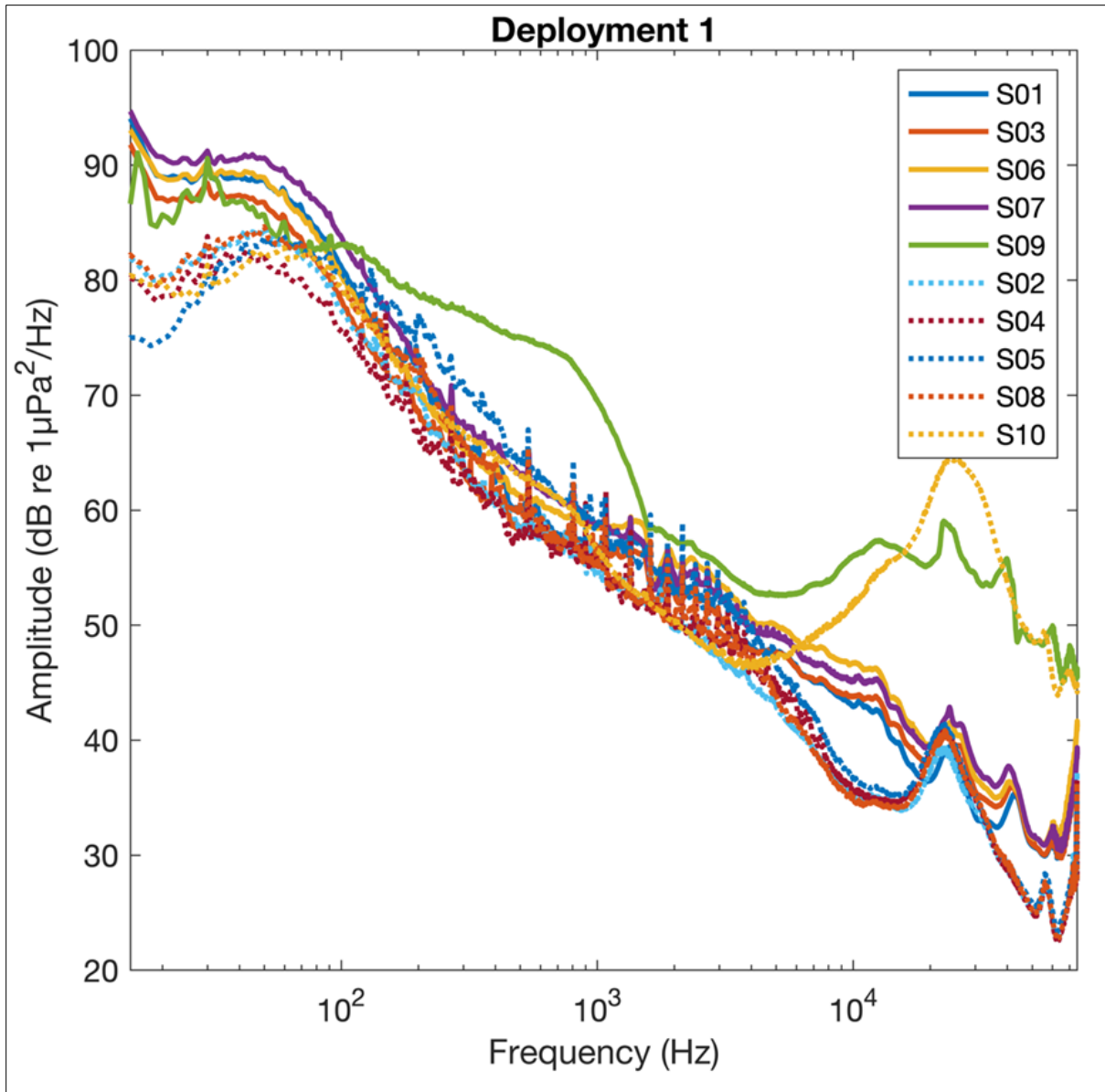
Figure 15. Comparison of RH and EARS median spectra for data collected during Deployment 1.

Note: RH data are shown as solid lines, and EARS are shown as dotted lines. Stations 9 and 10, which were the shallowest water recorder locations, show elevated HF noise.
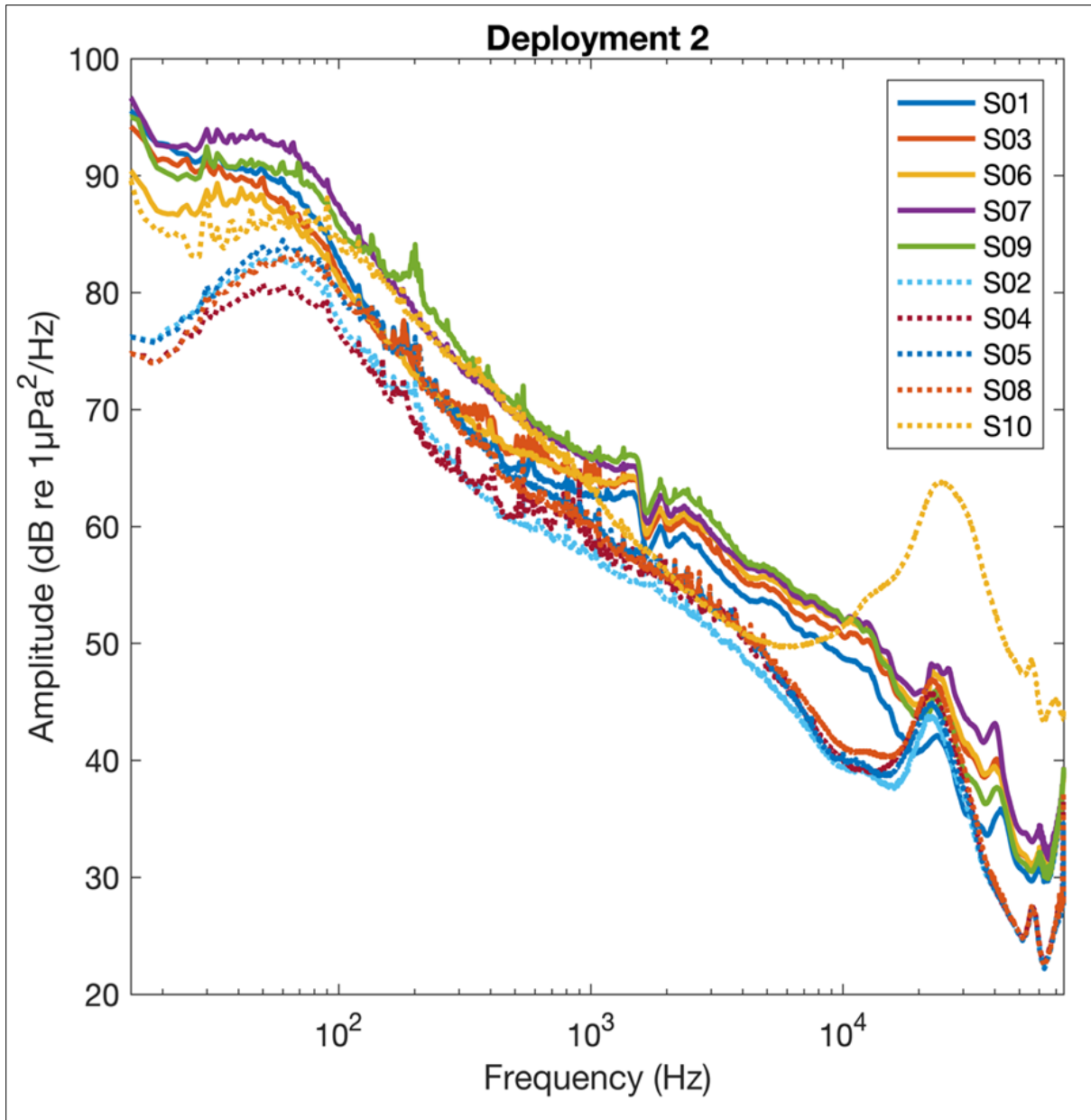
Figure 16. Comparison of RH and EARS median spectra for data collected during Deployment 2.

Note: RH data are shown as solid lines, and EARS are shown as dotted lines.
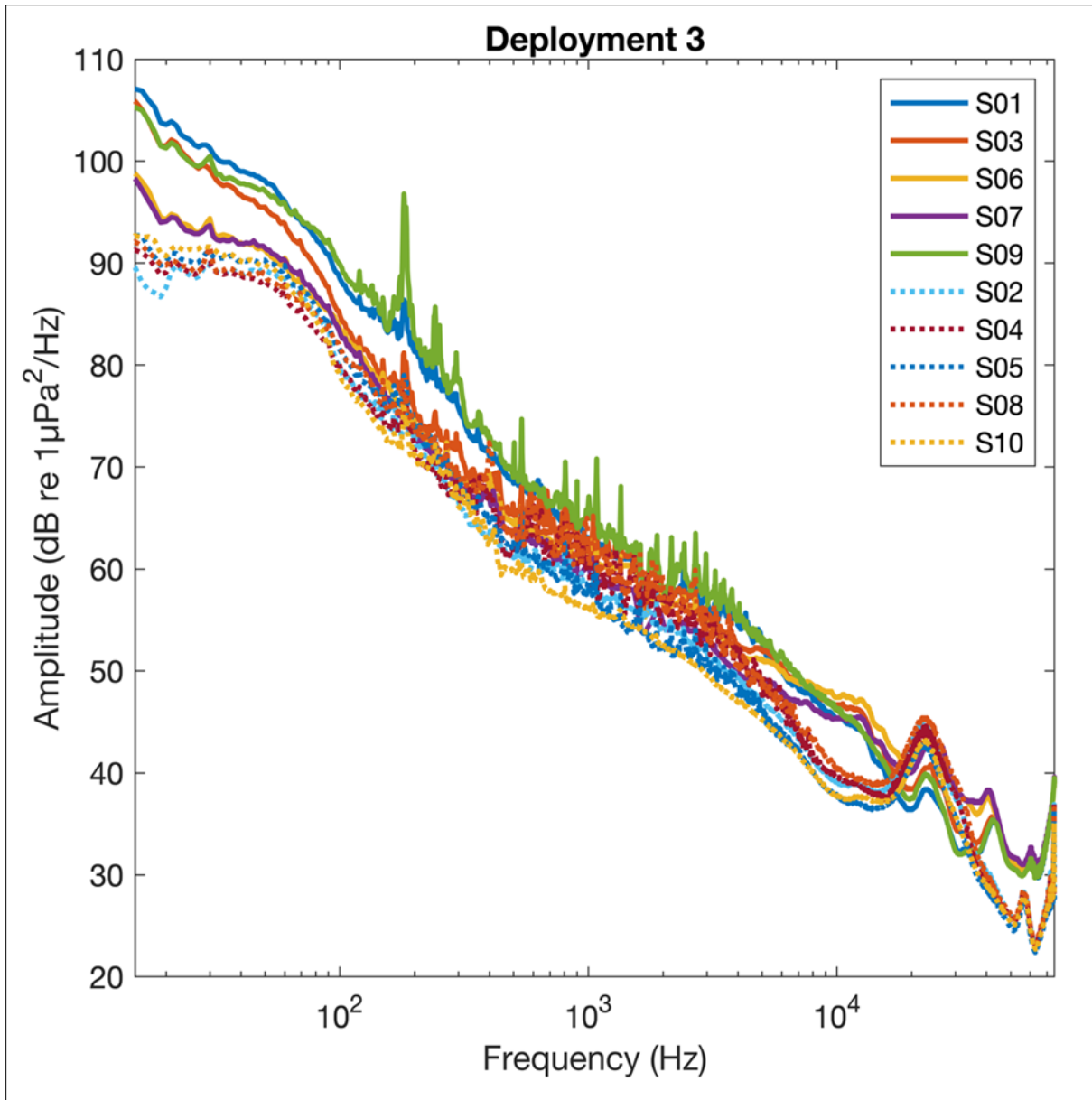
Figure 17. Comparison of RH and EARS median spectra for data collected during Deployment 3.

Note: RH data are shown as solid lines, and EARS are shown as dotted lines.
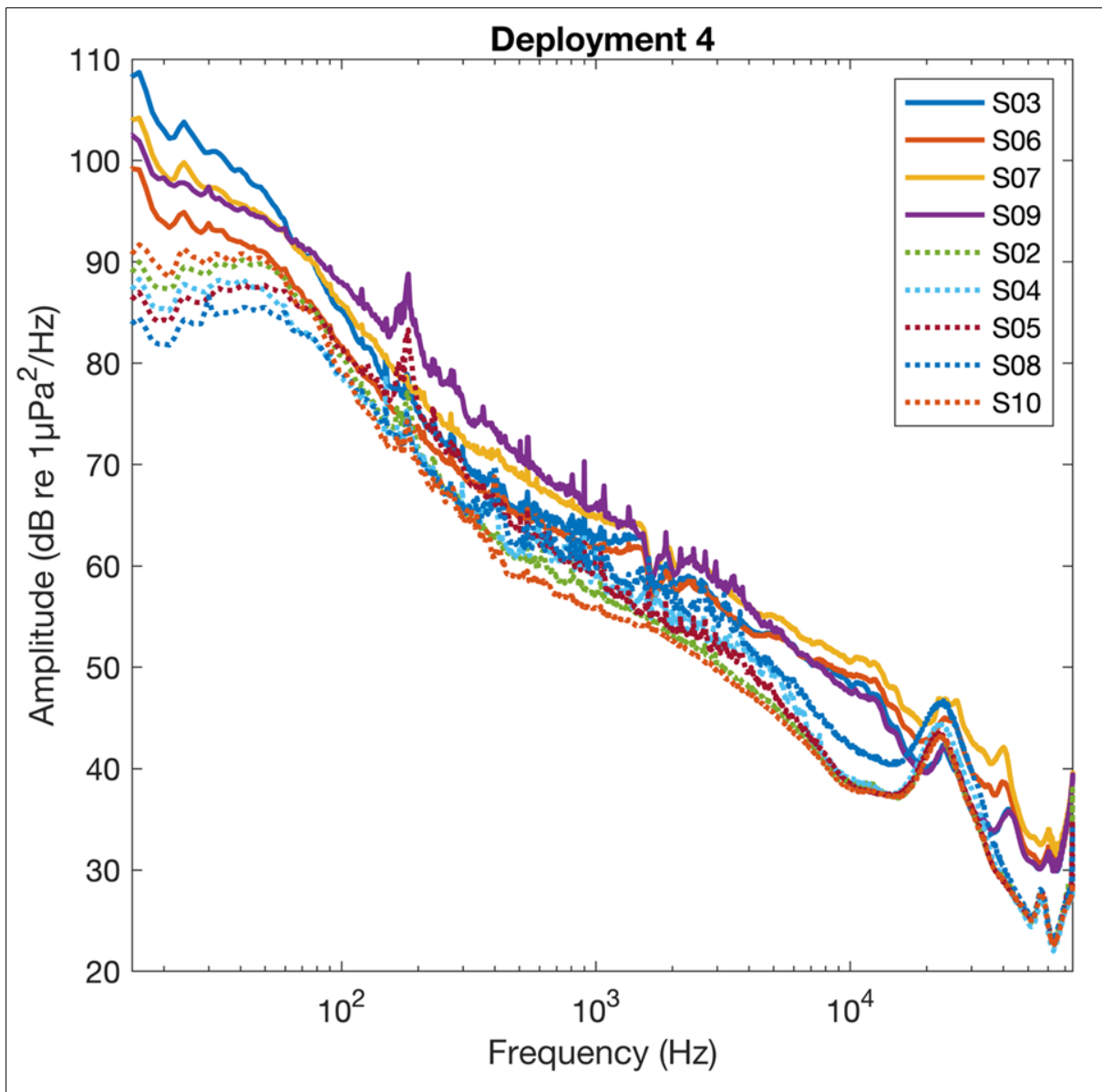
Figure 18. Comparison of RH and EARS median spectra for data collected during Deployment 4.

Note: RH data are shown as solid lines, and EARS are shown as dotted lines.

SHRU VLA data were analyzed using standardized acoustic data analysis protocols following standards outlined in Ainslie et al. (2017) for average sound pressure spectrum levels, L_{eq}, PSD levels, cross-spectral density levels, and noise coherence over the entire deployment period. Site-specific physical oceanography data collected from CTD casts conducted during each cruise and sensors mounted on the VLAs were used to derive sound speed profiles for underwater soundscape characterization and sound propagation modeling. SHRU data were also used for conducting 1) noise coherence and source correlation analyses, and 2) soundscape fingerprint analyses. These analyses are discussed in **Sections 4.8** and **4.10**.

During the 2018 MP, an acoustic playback experiment was conducted to obtain LF broadband acoustic transmission data as a function of distance. These data were used to assess sound propagation from selected anthropogenic sources, ground-truth localization abilities of the SHRU VLA inside and outside a canyon environment and validate the underwater sound propagation model.

Comprehensive results from the SHRU VLA data analyses are presented in individual sensor reports.[14] Key results from these analyses are:

- Overall, observations from soundscape characterization conducted using VLA data were generally consistent with those observed from RHs and EARS data analyses.

- LF soundscapes were dominated by seismic airgun surveys.

- VLA data analyses indicated that the average SPLs measured from 2019 to 2020 were substantially higher than those measured in 2018. This was most probably related to frequent seismic exploration activities conducted during the 2019 deployment period.

- LTSA plots for the Canyon and Slope SHRU based on L_{eq} measured in one-third octave frequency bands are shown in **Figure 19** (May through October 2018) and **Figure 20** (September 2019 through March 2020).

- The acoustic playback experiment was successfully completed. Transmitted and received signals are shown in **Figure 21**.

- Noise coherence results were correlated with a subset of relevant AIS data (see **Section 4.8**). These results demonstrate the utility of collecting PAM data when AIS data are not available.

---

[14] Project reports titled: GOM PAM 2018 program monitoring project SHRU report, by Lin Y-T, 2019; and GOM PAM 2019 program monitoring project SHRU report, by Lin Y-T, 2021.
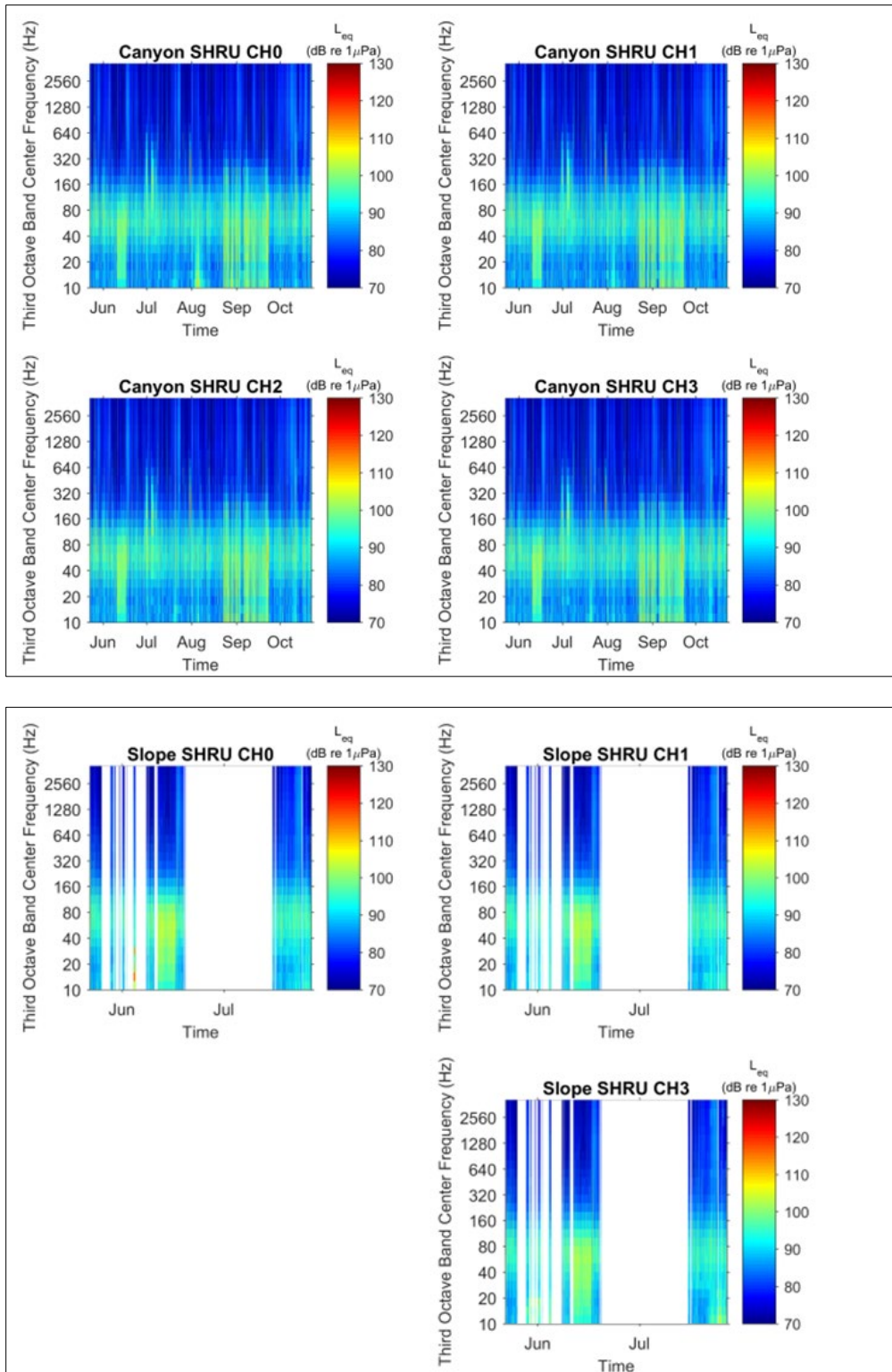
Figure 19. LTSA plots for the Canyon and Slope SHRU based on L_{eq} measured in one-third octave frequency bands.

Note: Data shown are from Deployments 1 and 2 (May to October 2018).
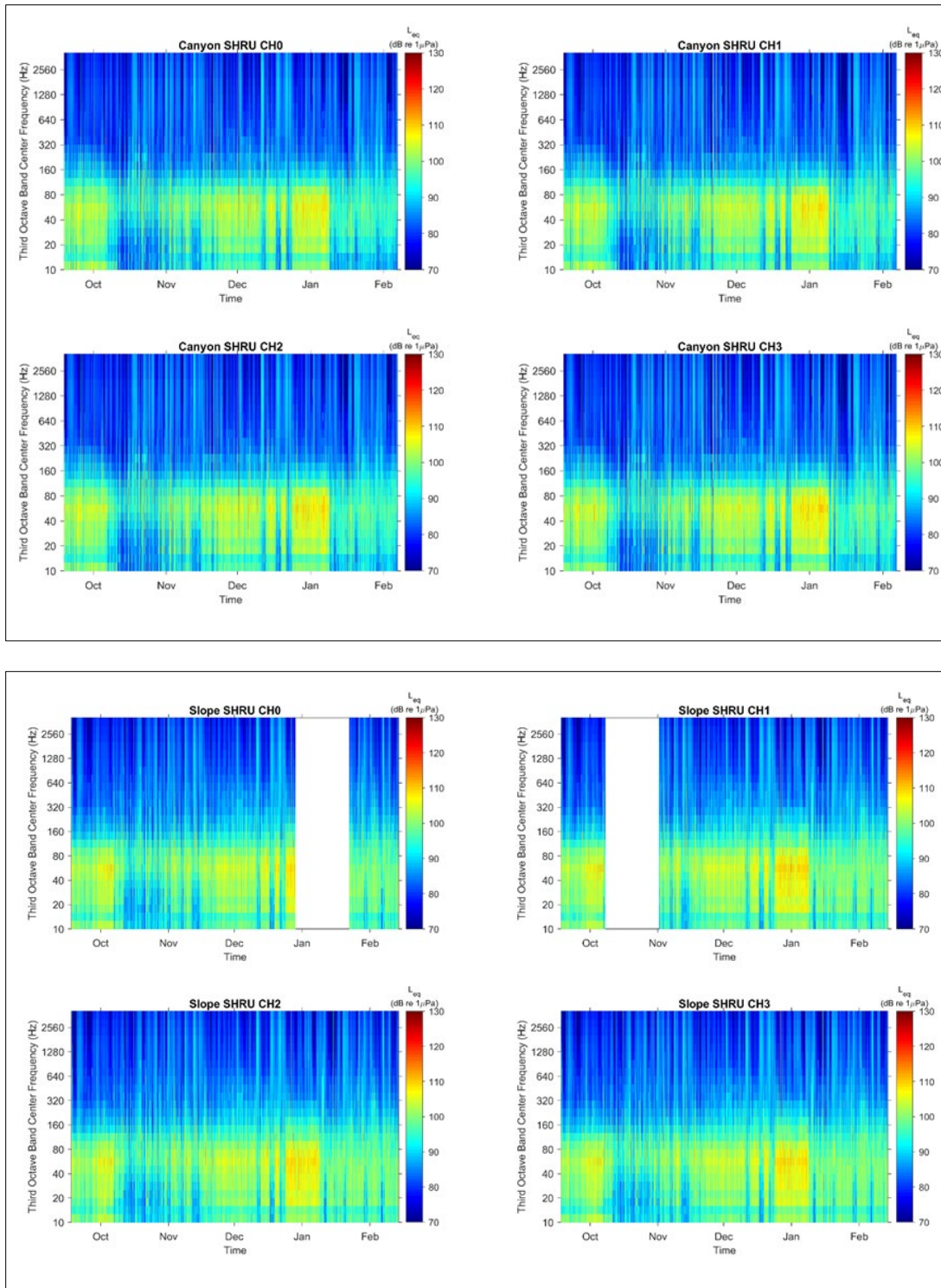
Figure 20. LTSA plots for the Canyon and Slope SHRU based on L_eq measured in one-third octave frequency bands.

Note: Data shown are from Deployments 3 and 4 (September 2019 to March 2020).
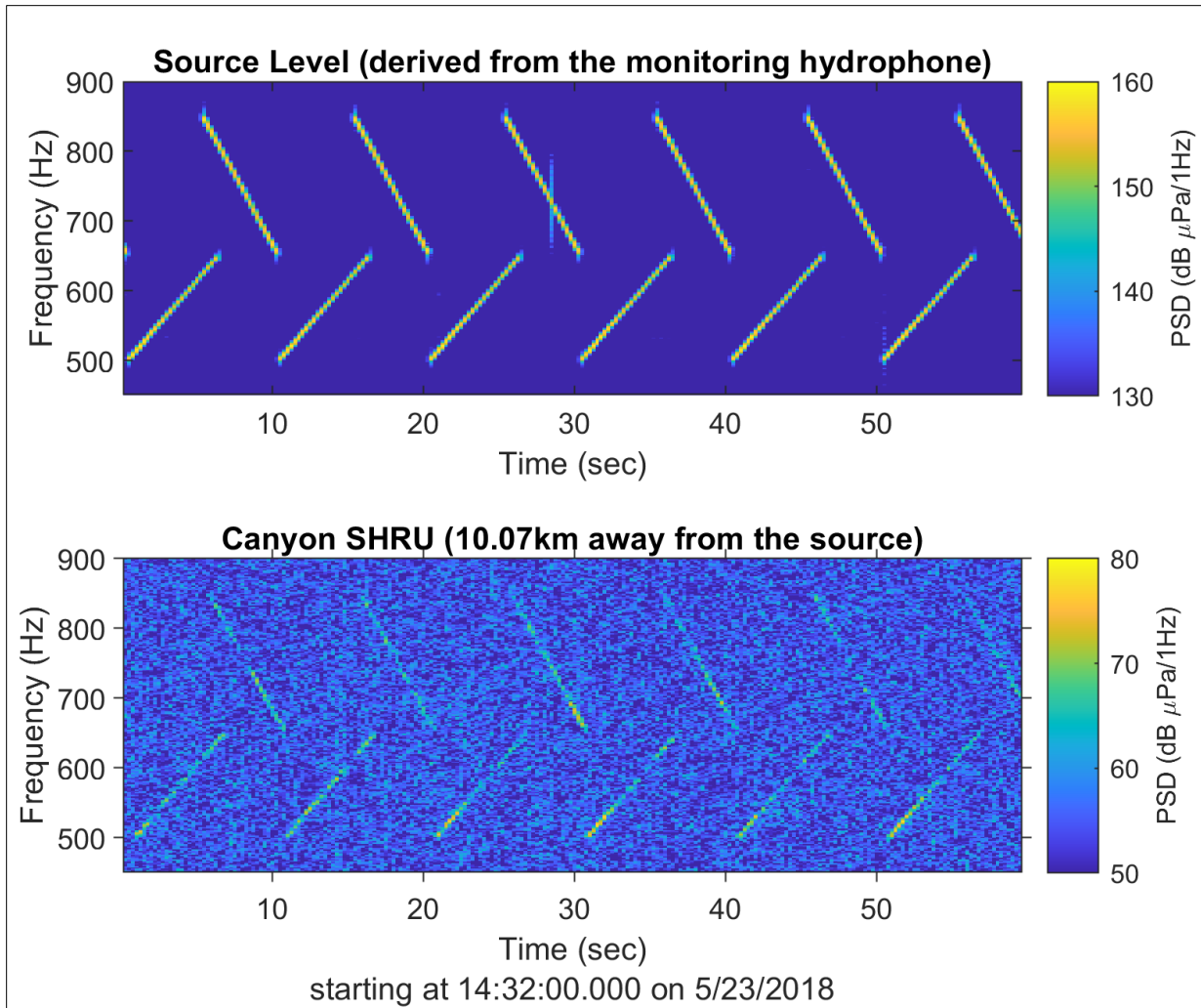
Figure 21. Examples of the playback experiment signals.

Upper panel (A) shows the source level derived from the monitoring hydrophone (~160 dB µPa/1Hz), and bottom panel (B) shows the received signals on the Canyon SHRU 10.07 km from the source.

4.1.5 2018 MP Seaglider

In May through June 2018, the Seaglider collected approximately 724 hours of continuous data at a sample rate of 125,000 samples per second. Data were collected in the DeSoto Canyon area, through a deep-water area near the base of the continental slope, and into the Mississippi Canyon. Data quality was excellent, and no issues (e.g., electronic noise, drop-outs) were detected during the manual QA/QC performed as part of the post-processing.

Data were analyzed using the Raven-X software package (Dugan et al. 2016). The analysis methods and units followed established standards outlined in Ainslie et al. (2017). PSD levels (1 Hz, 1-second resolution) and spectral probability densities (Merchant et al. 2013) were calculated for each region using the 1-hour mean levels. The levels were calibrated and seconds containing glider motor noise detections were removed. Mean hourly PSDs were calculated from the noise-removed data and noise spectra percentiles were calculated from the hourly means.

LTSAs were determined for all three frequency range datasets (full bandwidth, 125 kHz sampling rate, down sampled to 10 kHz, and down sampled to 1 kHz). Noise was removed from each LTSA. Noise spectra percentiles and spectral probability density plots were separately prepared for three flight segments. Additionally, hourly mean PSDs were compared across three glider depth bins (50 to 250 m, 400 to 600 m, and 800 to 1,000 m).

Comprehensive results from the 2018 MP Seaglider data analyses are presented in an individual sensor report.[15] Key results from these analyses are:

- The Seaglider effectively recorded sounds from a greater than or equal to 500-km-long path over a span of approximately six weeks, covering both highly industrialized (Mississippi Canyon) and lightly industrialized (DeSoto Canyon) areas and found large differences (greater than 10 dB) in sound levels between them.

- As measured by the glider, DeSoto Canyon had the lowest surface sound speeds, and Mississippi Canyon had the fastest surface sound speeds, likely due to the influx of warmer waters from the Mississippi River (**Figure 22**). The difference was not large; however, mean sound speed difference between the two areas was only approximately 6 m/second. The significance of the difference in sound speed near the surface, and in the sound speed profile overall, is that sound may propagate differently in the different regions, which is relevant to understanding soundscape differences in the GOM. In this case, the slightly higher sound speed in Mississippi Canyon would cause the shadow zone to occur nearer to a sound source in the surface layer than in De Soto Canyon. What was notably different between the areas was that a mixed layer led to variable sound speeds in the upper 20 m of water in the Mississippi Canyon, with the fastest sound speeds at 20-m depth rather than the surface. This created an intermittent shallow surface duct. This duct has the potential to keep a larger fraction of generated acoustic energy in the upper 20 m of the water column near the surface in the Mississippi Canyon compared to regions without the duct (Urick 1984).

- No evidence of surface sound speed changing with season was detected, but such changes were not expected within a single glider flight.

- Noise levels follow the general pattern of ocean noise elsewhere, with highest levels at low frequencies and a steady decline with increasing frequency to approximately 10 kHz.

---

[15] Project report titled: Assessment of ocean ambient sound levels in the northern GOM, May-June 2018, by Mellinger DK, Fregosi S, 2019.

- Noise levels in regions with the deepest bathymetry (the Deep Slope Region) were higher than glider survey segments with shallower maximum depths. This was possibly due to the ability of sound to propagate further, with less energy lost to the seafloor, in deep water environments compared to shallow ones, and thus allowing for reception of noise from a broader surrounding area (**Figure 23**).

- Noise levels were quietest in DeSoto Canyon, likely due to lower levels of industrialization and shorter sound propagation distances, and conversely loudest in the deep-water areas (**Figure 23**).

- DeSoto Canyon also had the greatest differences in sound levels with depth (**Figure 24**). This was most pronounced at 300 Hz, where the median levels of the shallowest (50- to 250-m) recordings were approximately 8 dB quieter than the mid-depth (400- to 600-m) ones, which in turn were approximately 8 dB quieter than the deepest ones. Differences in median levels with depth were present, though to a lesser extent, from 10 Hz up to 40 kHz, above which the median levels converged. This effect existed for the quieter levels (10th percentile) as well, and was more pronounced for those levels, with nearly a 20 dB difference between the shallowest (50- to 250-m) and deepest (800- to 1,000-m) regions.

- The Deep Slope region had the least differences by depth, with the median 10th and 90th percentile levels showing little difference across the three depth bands measured at most frequencies (**Figure 25**). A difference was observed from approximately 15 to 40 kHz, with the median sound levels at deeper depths (800- to 1,000-m) 2 to 4 dB louder than those at shallower depths (50- to 250-m and 400- to 600-m).

- Mississippi Canyon also had differences in median sound levels with depth, though to a lesser degree (**Figure 26**). Median sound levels at the shallow (50- to 250-m) and middle (400- to 600-m) depths were nearly equal, though the deepest depths (800- to 1,000-m) were approximately 5 dB louder in the 70 to 300 Hz band. At quiet (10th percentile) and loud (90th percentile) sound levels, there were few differences with depth.
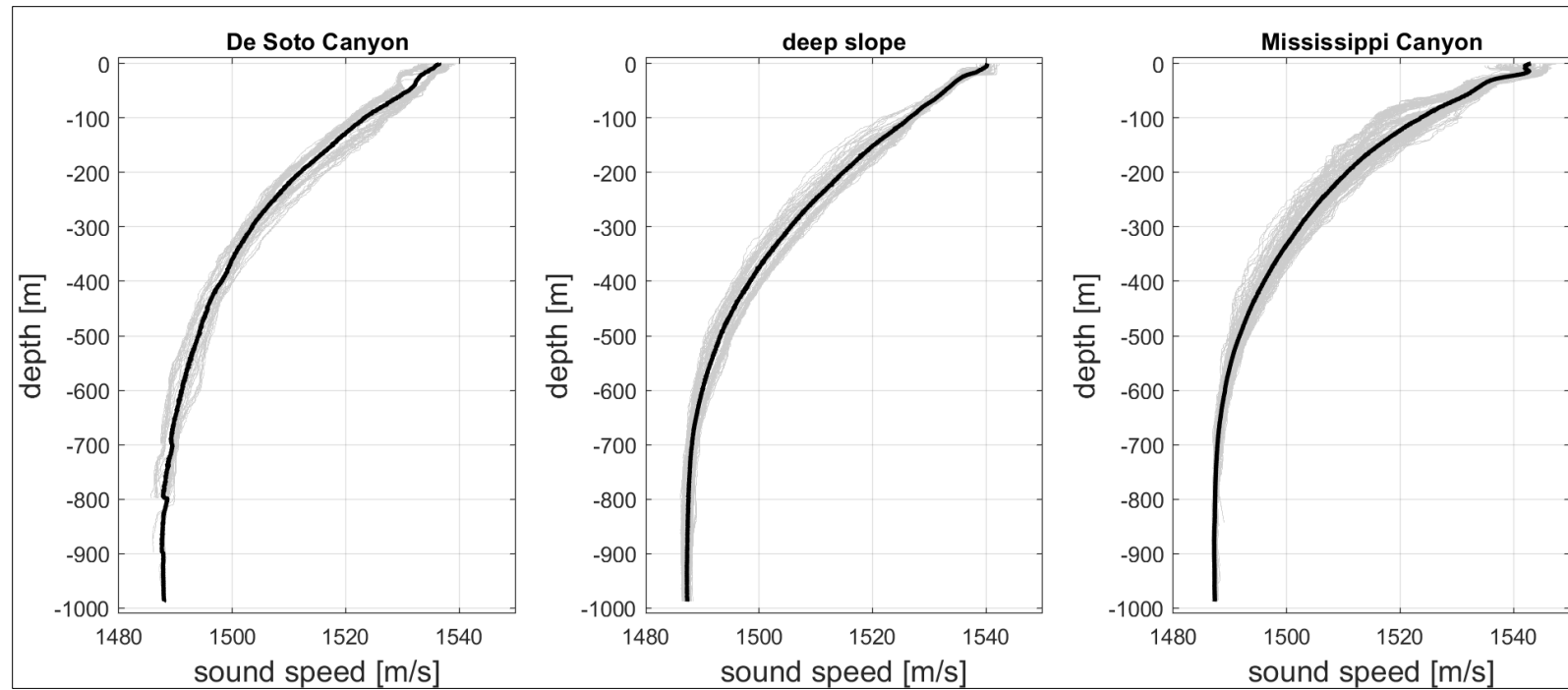
Figure 22. Sound speed profiles for each of the three glider survey regions, as calculated from temperature, depth, and salinity measured in situ by SG639.

Note: Gray lines indicate sound speed for each individual dive, and the thick black line is the mean sound speed across all dives in that region.
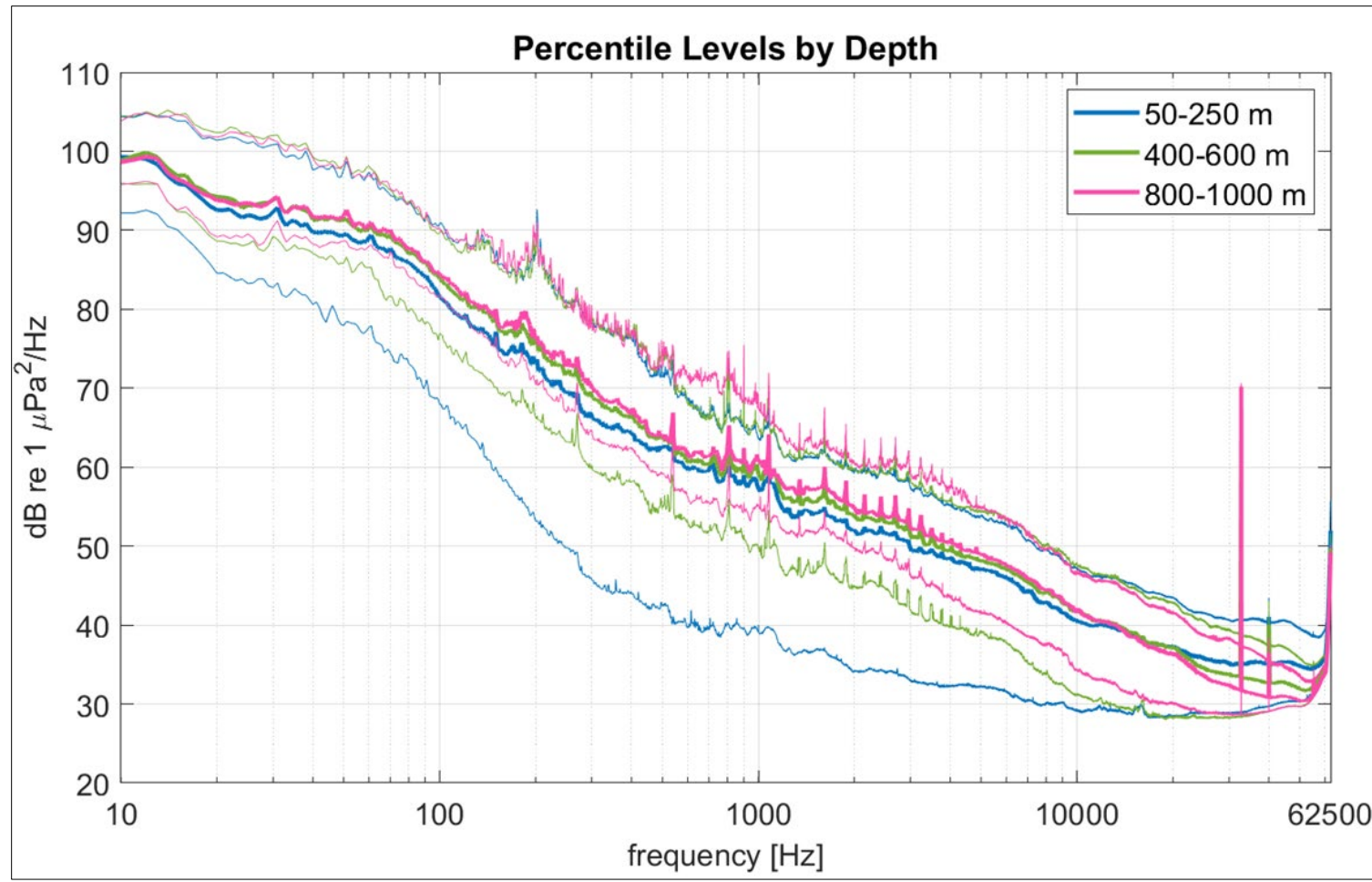
Figure 23. Percentile levels by glider depth, calculated from the hourly mean power spectral densities in three depth bins: 50–250 m (blue), 400–600 m (green), and 800–1000 m (pink).

Note: Thick line is median (50th percentile), upper thin line is 90th percentile, and lower line is 10th percentile.
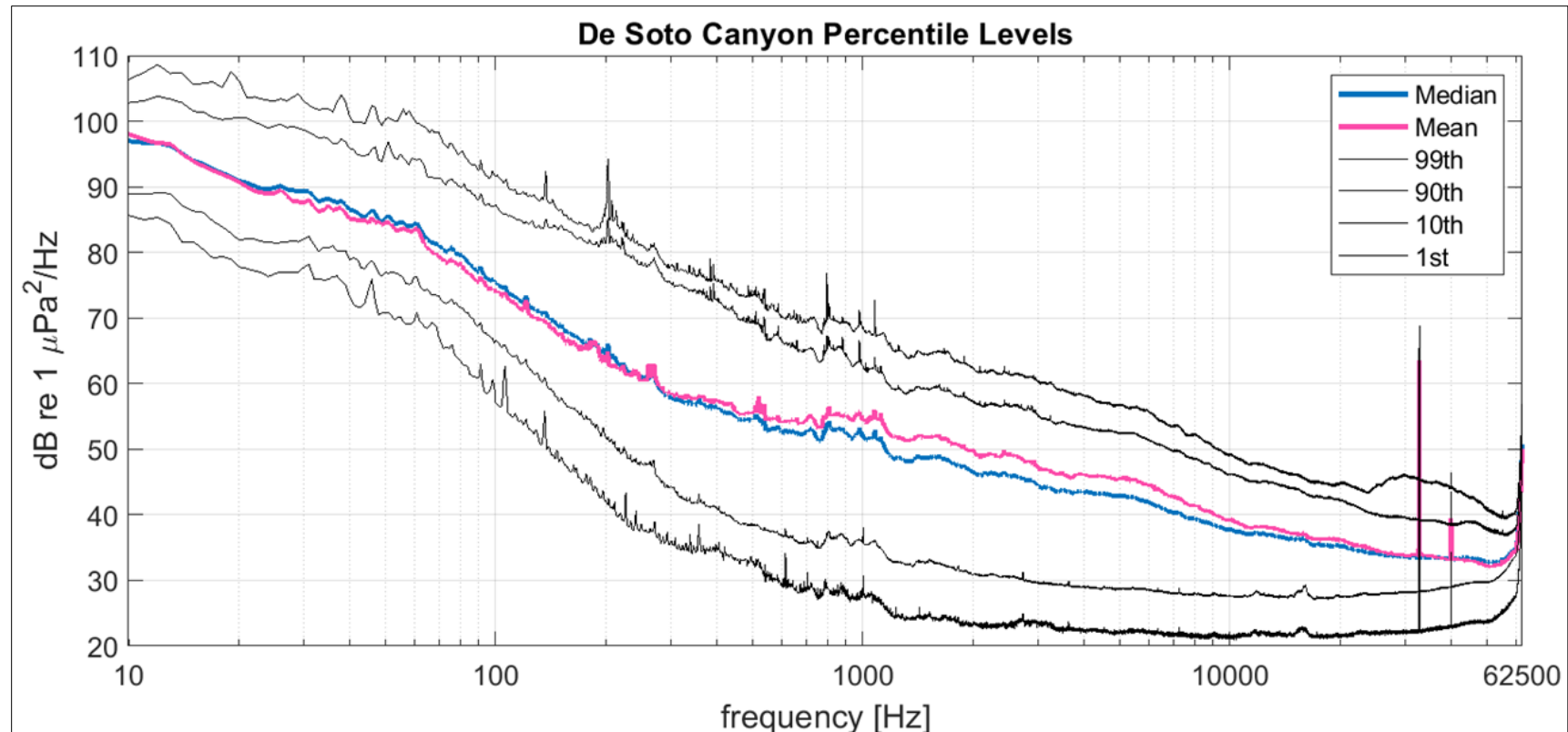
Figure 24. DeSoto Canyon percentile levels.

Note: Noise levels at the 99th, 90th, 50th (blue), 10th, and 1st percentiles for the three segments of the glider track from east to west. The mean is shown in pink. This includes sound recorded at all glider depths between 25 and 1,000 m, unless bathymetry limited the dive depth to shallower than 1,000 m.
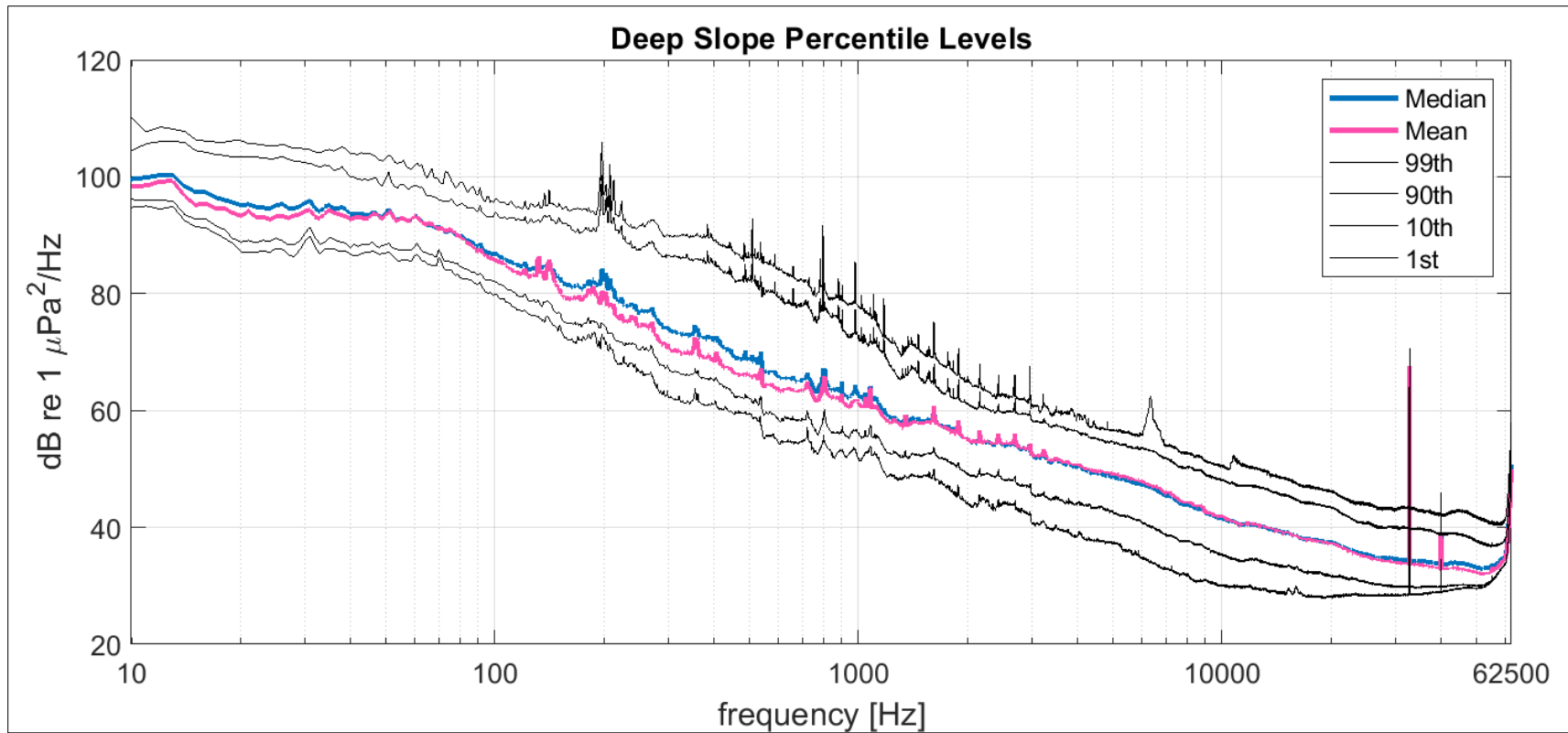
Figure 25. Deep Slope Canyon percentile levels.

Note: Noise levels at the 99th, 90th, 50th (blue), 10th, and 1st percentiles for the three segments of the glider track from east to west. The mean is shown in pink. This includes sound recorded at all glider depths between 25 and 1,000 m, unless bathymetry limited the dive depth to shallower than 1,000 m.
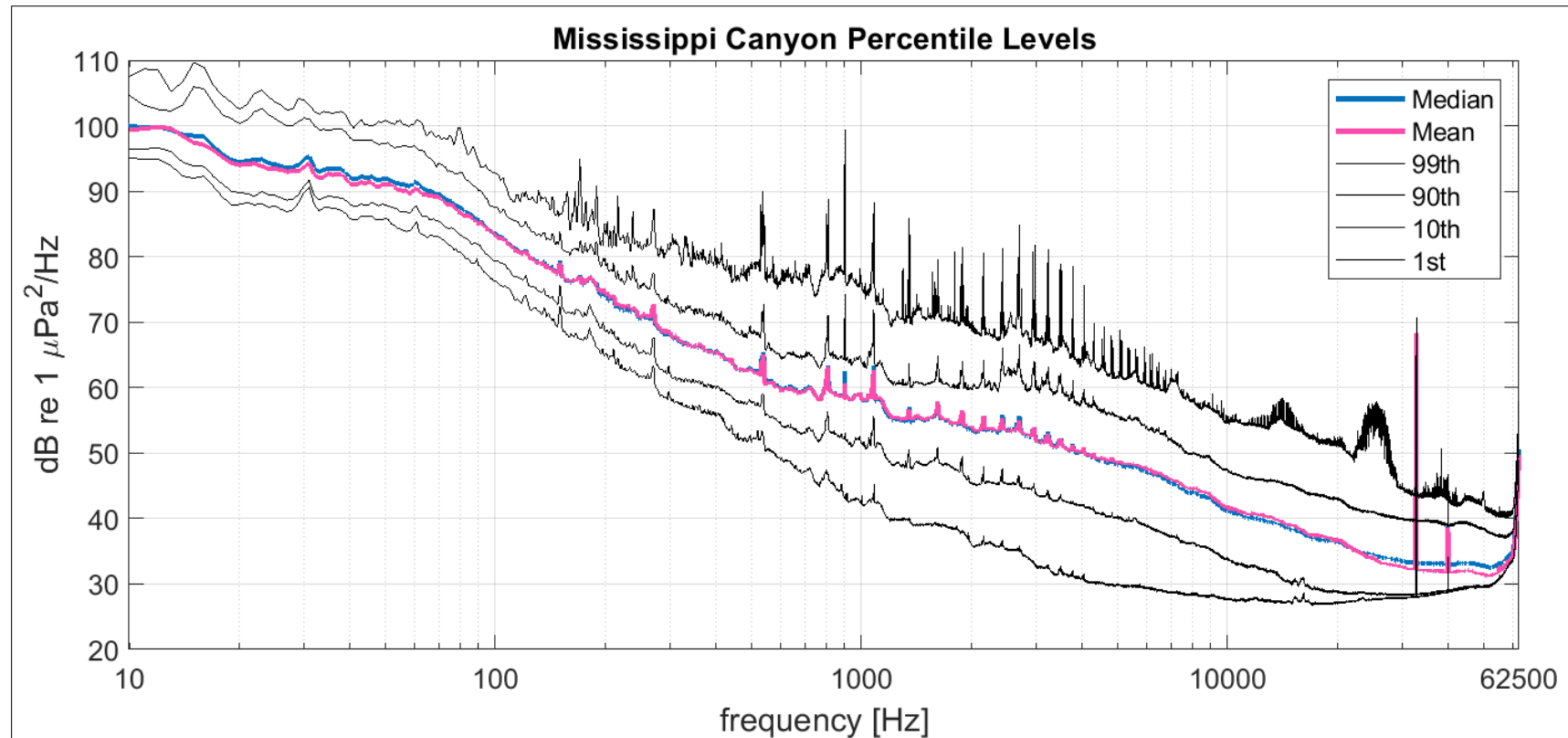
Figure 26. Mississippi Canyon percentile results.

Note: Noise levels at the 99th, 90th, 50th (blue), 10th, and 1st percentiles for the three segments of the glider track from east to west. The mean is shown in pink. This includes sound recorded at all glider depths between 25 and 1,000 m, unless bathymetry limited the dive depth to shallower than 1,000 m.

4.1.6 2019 MP Seaglider

Under the 2019 MP, a Seaglider was deployed on September 24, 2019, near DeSoto Canyon and recovered on October 6, 2019, during which time it completed 63 dives (**Figure 27**).
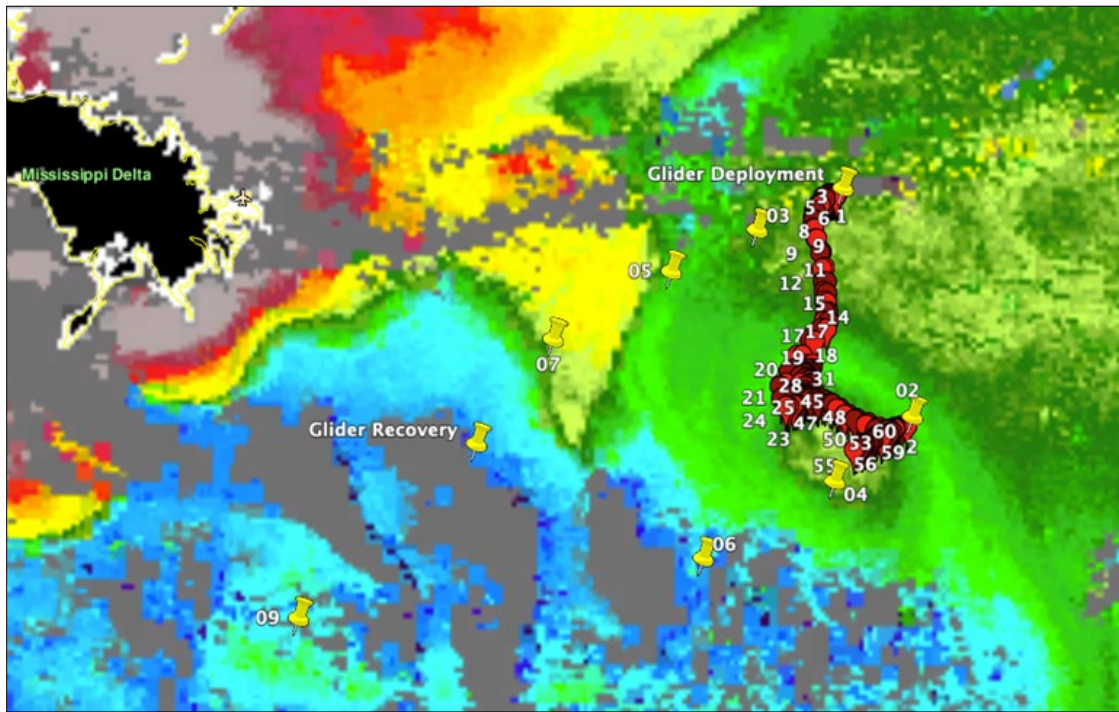
Figure 27. Seaglider track (in red with dive count number) and the mission targets (yellow tacks) overlaid on satellite image of chlorophyll-a index color.

Note: Satellite image courtesy of the Optical Oceanography Laboratory at the University of South Florida.

Passive acoustic data as well as temperature and salinity profiles were collected throughout the deployment. **Figure 28** shows temperature, salinity, and sound speed profile data collected during three different phases of the mission. These data demonstrate that the density difference is primarily due to differences in surface salinity, as the temperature is fairly consistent at the sea surface.

The PAM system recorded continuously during the descent and ascent portions of the Seaglider dives (63 dives) at a sample rate of 128 kHz. PAM data were available for all dive segments except for the descent portions of Dives 36 and 57. Cursory inspection of the acoustic data identified marine mammal vocalizations, particularly dolphin whistles, throughout the mission.

Sample spectrograms (**Figure 29**) show whistles and clicks as well as LF pulses, below 100 Hz, likely attributable to oil and gas activity. A large number of echolocation clicks were visible and audible throughout much of the deployment, notably in the last few acoustic data files of the mission.[16]

---

[16] Project report titled: GOM PAM program 2019 monitoring project Seaglider report, by Uffelen LV, Pomales L, Graupe C, 2019.
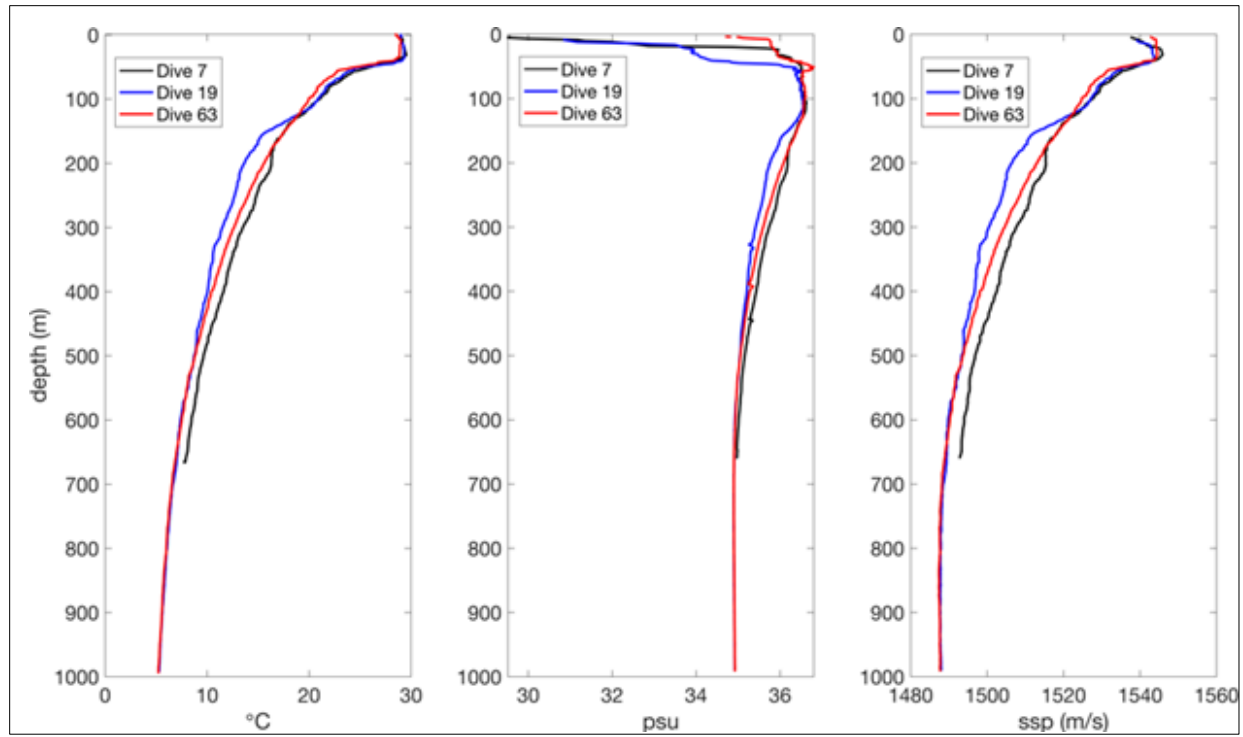
Figure 28. Temperature, salinity, and sound speed profiles observed during three different phases of the September/October 2019 Seaglider mission in the GOM.
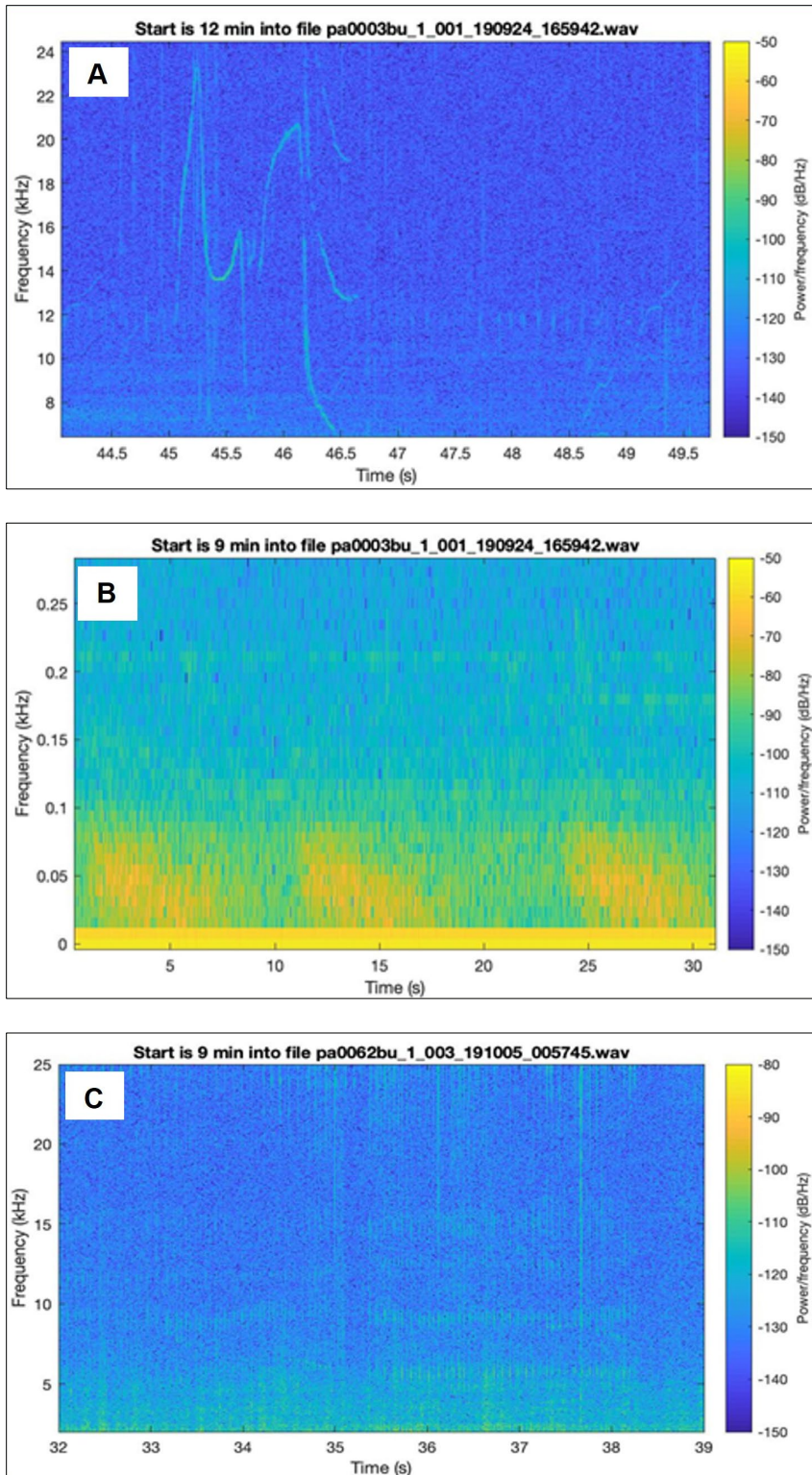
Figure 29. Sample spectrograms from acoustic data collected by the 2019 MP Seaglider deployment showing whistles (a), LF pulses (Dive 3) (b), and clicks (Dive 62) (c).

4.2 Soundscape Spatial and Temporal Trend Analyses

4.2.1 2018 MP Spatial and Temporal Trend Analyses

Spatial and temporal trend analyses were conducted using data collected by the four sensor types during Deployments 1 and 2 under the 2018 MP. For assessment of temporal trends, Wenz curves, which describe average noise levels in deep waters for varying noise sources such as ship traffic, wind waves, and other sources, were used as the basis for the comparison (**Figure 30**) (National Research Council 2003).
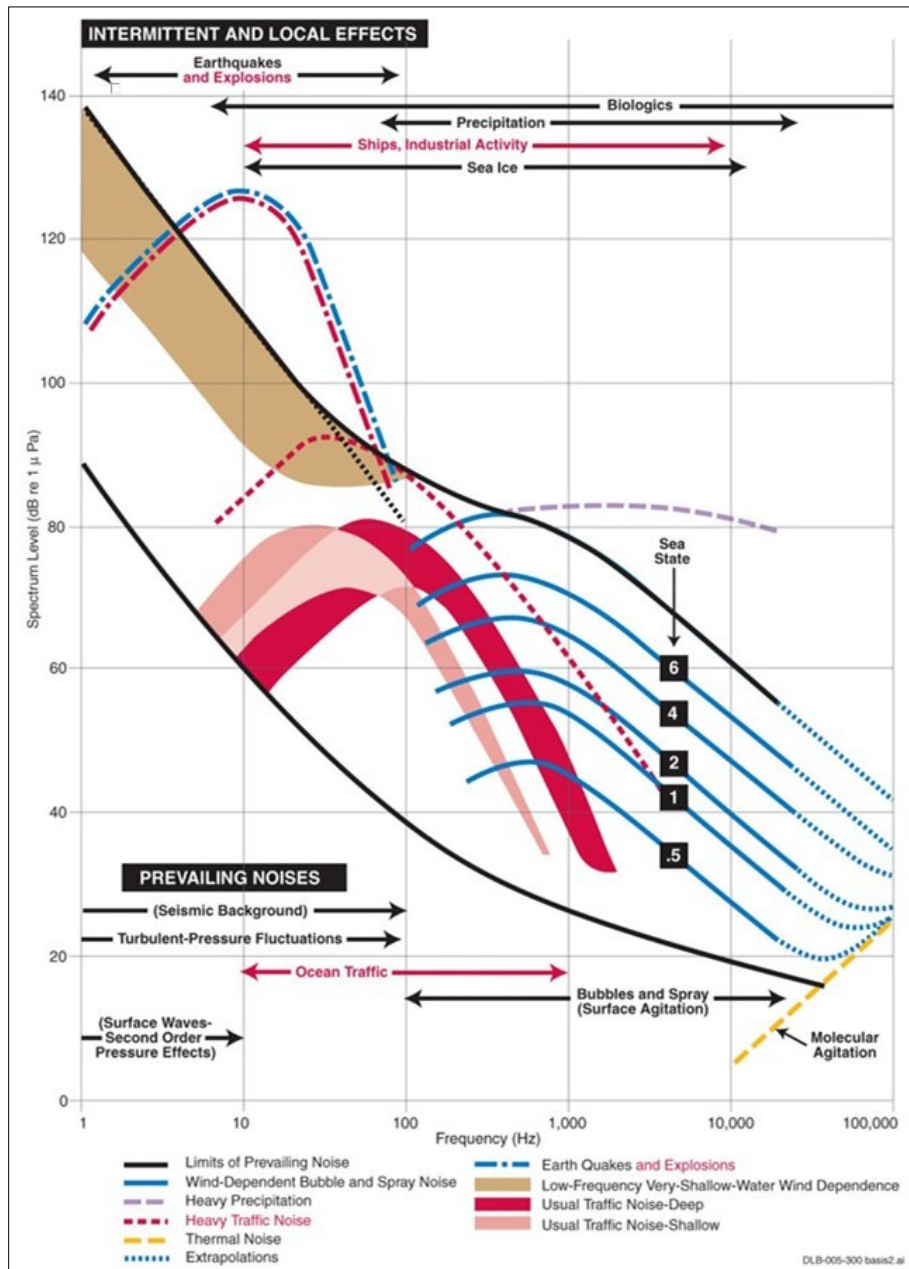
Figure 30. Historical ambient noise Wenz curves.

Note: Plot of Wenz curves abridged from National Research Council (2003)

In **Figure 31,** average noise spectrum levels from data collected by RHs, EARS, SHRU VLAs, and Seaglider over the entire spring and summer 2018 deployment period (Deployment 1) are plotted side-by-side with previously reported Wenz curves of historical typical ambient noises in the marine environment. The average noise spectrum levels are in dB re 1 μPa^2/Hz and shown in 1 Hz wide bands for 10, 100, 1,000, and 10,000 Hz from each of the three systems. Key observations/conclusions from **Figure 31** are:

- The average soundscape characteristics for the study area fall within the Wenz curve bands and are consistent with prior reporting (Latusek-Nabholz et al. 2020).

- In general, the average noise levels were almost centered between the upper and lower noise limit ranges shown in the Wenz curves.

- HF (10 kHz) levels were consistent with lower sea states except for Site 9, in shallow water where the noise was dominated by snapping shrimp. Note that Wenz curves were derived from historical deep-water measurements, and shallow noise is typically higher than deep water for frequencies at or above 1,000 Hz.

- The Mississippi Canyon levels are slightly (but consistently across platforms) quieter than the slope nearby. For example, the SHRU VLAs measured a 1 to 2 dB difference between the canyon and slope. This finding is corroborated by the TL predictions from preliminary simulation runs of the 3D sound propagation model. The model simulations predict a slightly higher transmission loss to similar ranges from the canyon site compared to the slope site. The biological significance of the difference in noise levels between the canyon and slope sites needs further evaluation.

- Measurements recorded by the Seaglider indicate that the noise levels in the DeSoto Canyon are significantly lower than the Mississippi Canyon. This finding is consistent with the known difference in the extent of industrialization of the two canyon areas.

- Seismic exploration dominated measurements recorded by most of the sensors placed in deep waters at frequencies at or below 100 Hz.

- Different sensor systems reported approximately 20 dB or more of variability on a daily basis. In the 1 to 10 kHz band, there was 30 dB of variability. This variability is likely due to a combination of anthropogenic and natural sound sources. Marine mammals, specifically beaked whales, appear to be a significant contributor to the noise field above 30 kHz. The shallow-water site measured with one of the RHs showed the highest levels of noise above 100 Hz and some of the lowest levels at 10 Hz.

- The Seaglider levels are lowest of all the sensors for almost all the bands and are especially low in the DeSoto Canyon. This may be because the Seaglider spent so much time in the shallower water where propagation of natural and anthropogenic sounds received at the sensor may not be as good. Therefore, the average noise levels were lower as compared to the moored sensor systems that recorded at greater depths.
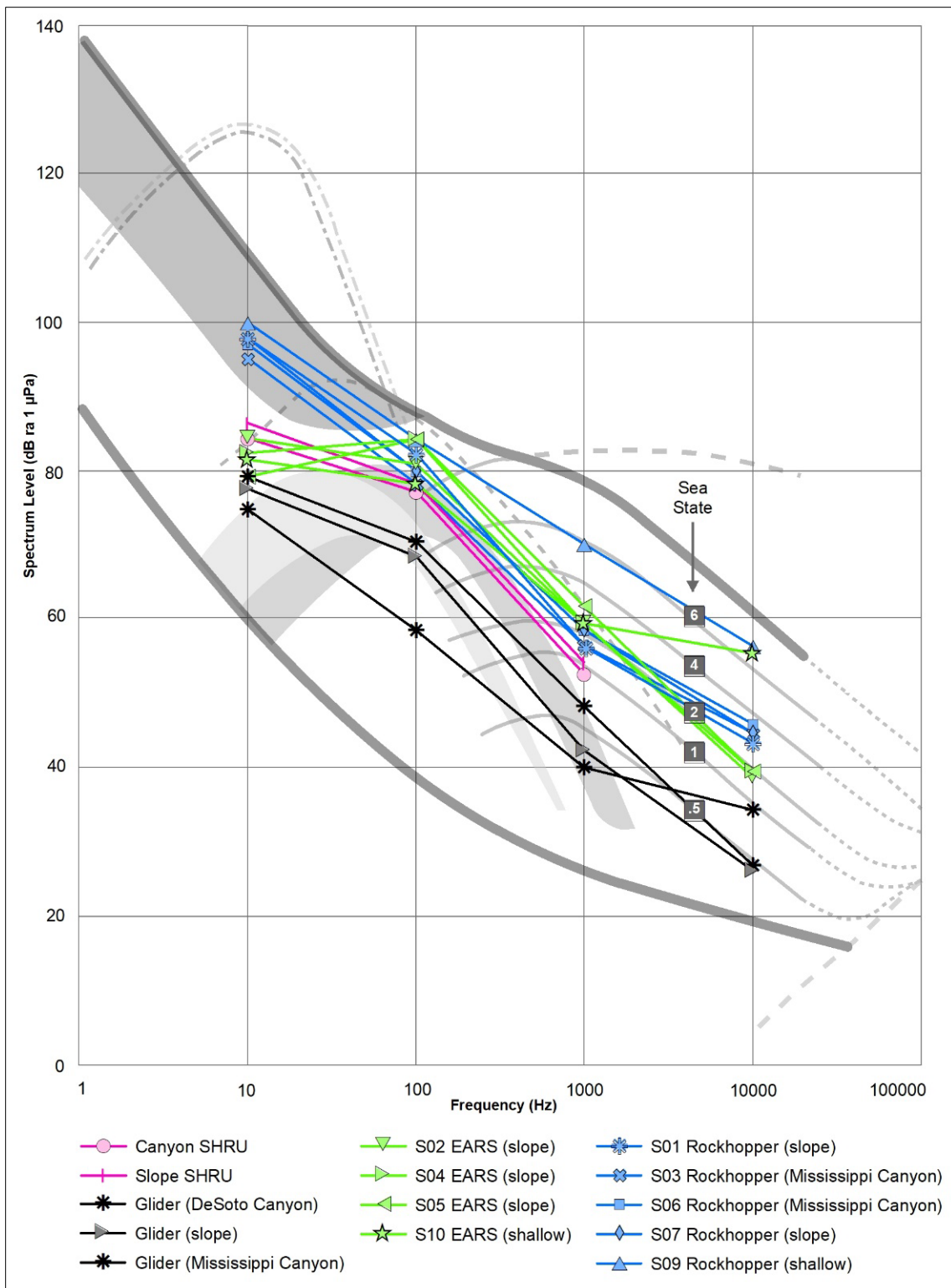
Figure 31. Comparison of the average spectral levels from the four sensor systems deployed under the GOM PAM 2018 MP with historical ambient noise Wenz curves.

Note: Plot of Wenz curves abridged from National Research Council (2003)

In **Figure 32,** average noise spectrum levels from data collected by RHs and EARS over the entire fall 2018 and winter 2019 deployment period (Deployment 2) are plotted side-by-side with previously reported Wenz curves of historical typical ambient noises in the marine environment. The average noise spectrum levels are in dB re 1 μPa^2/Hz and shown in 1-Hz-wide bands (for 10, 100, 1,000, and 10,000 Hz) from each of the three systems. Various factors such as presence of anthropogenic noise sources (e.g., shipping, airgun surveys, oil platforms), weather (e.g., wind, waves, rain, sediment disturbance), propagation regimes (e.g., shallow versus deep water, canyon) appear to have a significant influence in the spatial and temporal variations in the noise characteristics. Key observations/conclusions from **Figure 32** are:
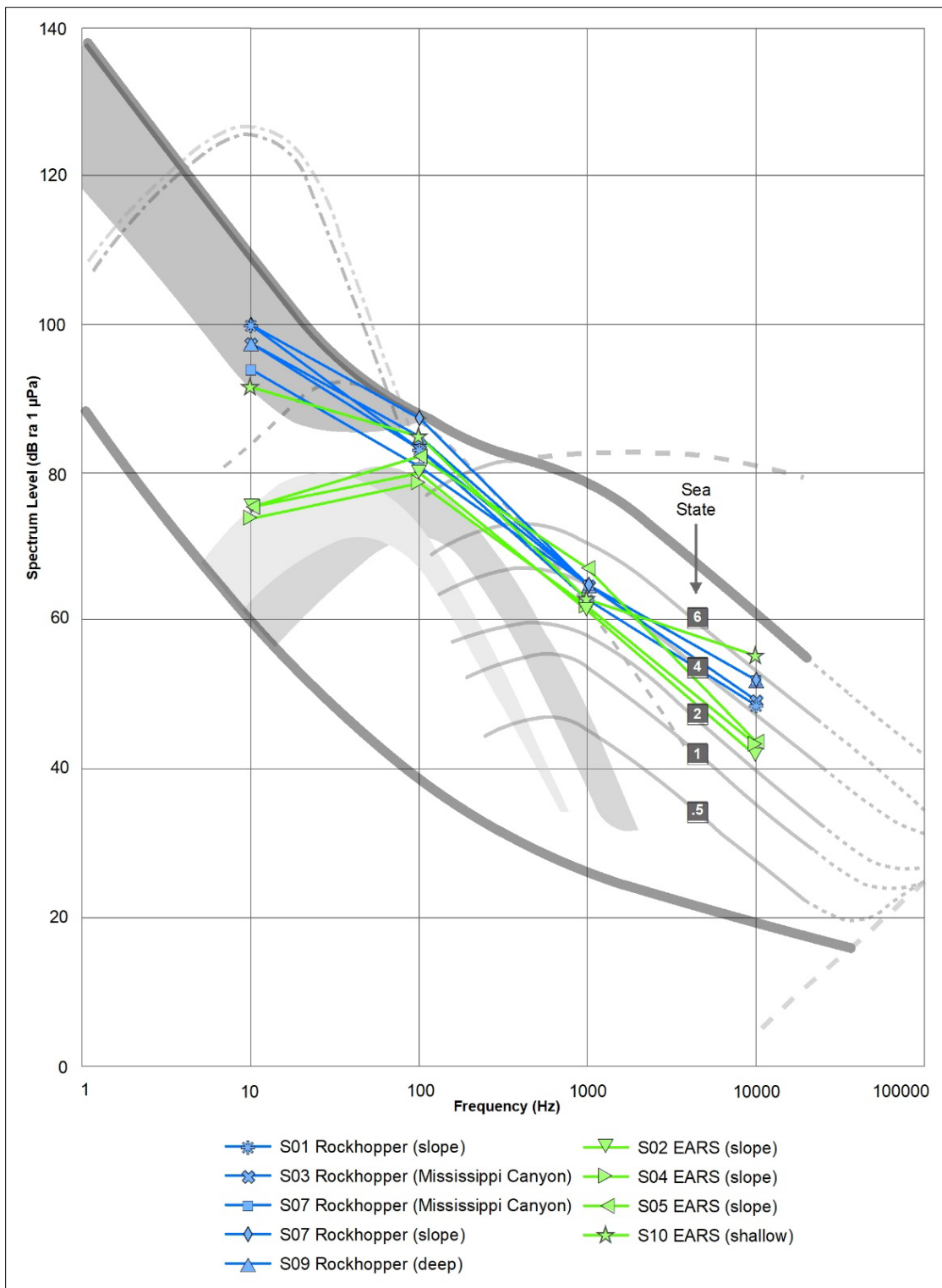
- Average noise spectrum levels from measurements made in fall and winter are louder than measurements from spring and summer, most likely due to seasonal variation in airgun surveys activity. This seasonal variation is evident across all frequency bands.

- Shallow-water noise spectrum levels are quieter at 10 Hz, most likely due to greater interaction with the seafloor as compared to deeper waters.

- Shallow-water levels are louder at 10,000 Hz, most likely due to biological noise sources, specifically snapping shrimp.

- Noise spectrum levels in the Mississippi Canyon are lower than on the slope due to propagation/shielding effects.

Overall, SPLs during the fall and winter months were consistently lower than during the spring and summer months, especially in the LF band below 500 Hz. This is likely correlated to a decline in industrial activities during the colder winter months. Noise levels at higher frequencies (500 Hz to 10 kHz) driven by weather were higher during the winter months. Only during the February to March 2019 period were the LF soundscapes dominated by distant seismic surveys, unlike across the entire deployment period during summer.

To investigate the spatial aspects of the measured noise levels, **Figures 31** through **34** show the noise spectrum levels at each of the measurement sites for data collected during the second deployment under the 2018 MP. These figures correspond to the average spectrum levels from various systems at frequencies of 10, 100, 1,000, and 10,000 Hz, respectively. These figures demonstrate the spatial as well as the frequency structure of the ambient noise spectrum.

In general, shallow-water noise spectrum levels (Sites 9 and 10 in **Figure 31**) are quieter compared to deeper sites at 10 Hz. Shallow-water propagation is highly complex because of modal cut-off effects and boundary interactions, but this most likely could be due to greater interaction with the seafloor as compared to deep waters and the absence of LF noise from distant sources (e.g., shipping, airgun surveys).

It is interesting to note that this trend is reversed for HF (10,000 Hz; **Figure 32**), which indicates nearby sources that may possibly be biological in nature (snapping shrimp). The levels measured by the SHRU VLAs increased by 2 dB (10 Hz and 100 Hz) and by 4.5 dB (1,000 Hz) during the fall and winter seasons compared to the spring and summer seasons. A detailed modeling of canyon propagation is needed to explain whether this increase is driven by weather-related events, biological sources, or waveguide effects.

Figure 32. Comparison of the average spectral levels from EARS and RHs under the GOM PAM 2018 MP.

Note: Deployment 2 measurements plotted side-by-side with historical ambient noise Wenz curves.

4.2.2 2019 MP Spatial and Temporal Trend Analyses

Spatial and temporal trend analyses were conducted using the complete 24-month RH and EARS dataset as part of which monthly spectral levels of the ten RH and EARS recorders were assessed to determine whether any spatial or temporal trends were evident in the data. **Figures D-C1** through **D-C26** in **Appendix D** present the monthly median spectral levels of the ten RHs and EARS recorders over the 24-month data collection duration. In each monthly figure, the top spectrum represents the entire frequency range, while the bottom panel presents the LF band (10 to 1,000 Hz) in more detail. These figures illustrate the temporal variability at each recorder sensor location, as well as an apparent difference in the data recorded by the RH and EARS recorders, particularly below 100 Hz.

4.3 Anthropogenic Sound Detection Analysis

The 24-month RH and EARS dataset were analyzed for detection of the two major anthropogenic contributors to the underwater soundscape in the GOM, namely ship traffic (vessels) and airguns used in seismic surveys. The technical report presented in **Appendix D (Section D.3.2.1)** contains detailed information on these analyses and data outputs; key information from the technical report is summarized and discussed below.

4.3.1.1 Vessel Detection Analysis

Vessels were present within the study area almost every day at every receiver location (**Figure 33**). The effects of spatial and temporal variables on vessel detection rates were explored with a generalized additive model (GAM). Significant patterns by year and month were observed. The number of vessel detections increased from 2018 to 2019 but decreased again in 2020. This may be a side effect of the sampling period and the markedly strong monthly pattern where the number of vessels was highest in the summer months and lower in the winter months. The patterns observed for latitude and water depth were also significant and indicated more contradictory patterns of increased vessel detection rates as latitude and water depth increased (**Figure 34**). The number of vessel detections was greatest in the middle longitudes and decreased strongly to the east, probably related to the location of port facilities (**Figure 35**).
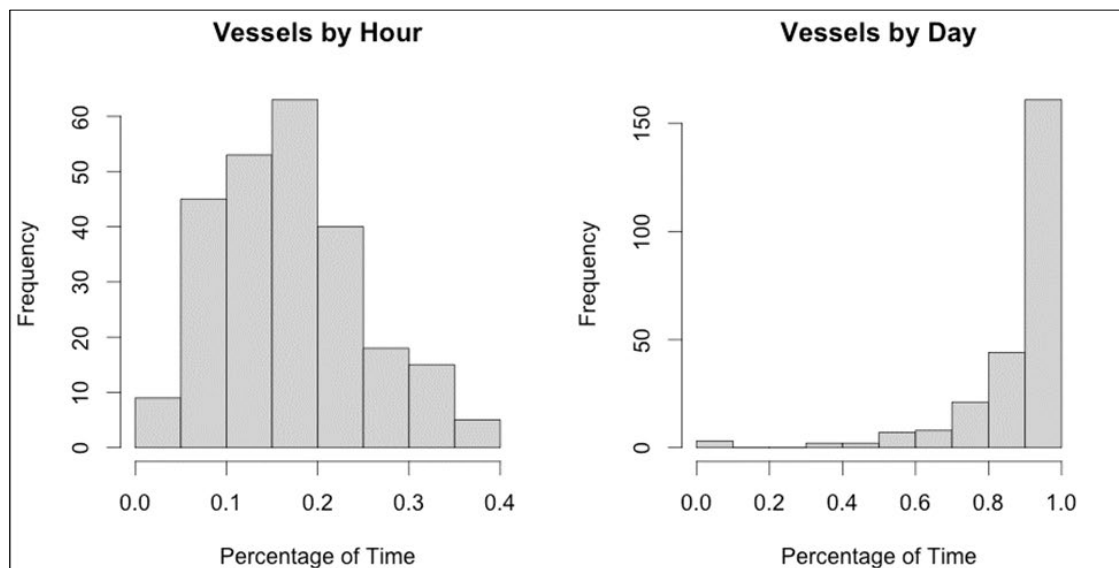
Figure 33. Comparison of monthly values for vessel detection based on hourly inputs (left) and daily inputs (right)..
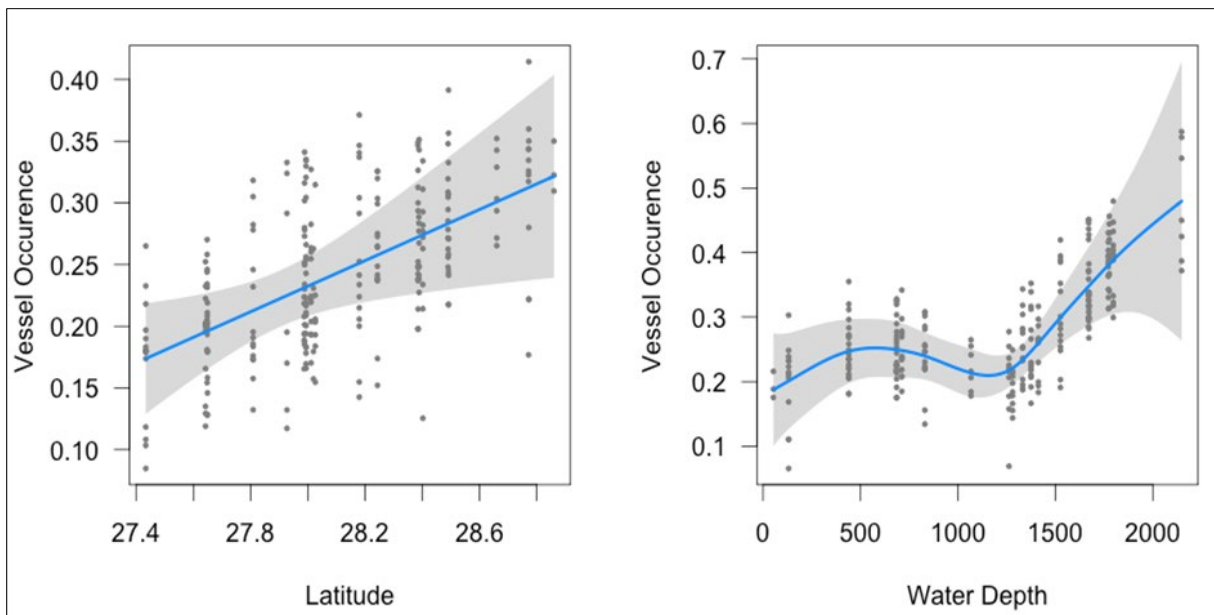
Figure 34. GAM smoothing functions for latitude (left) and water depth (right) effects on vessel detections.
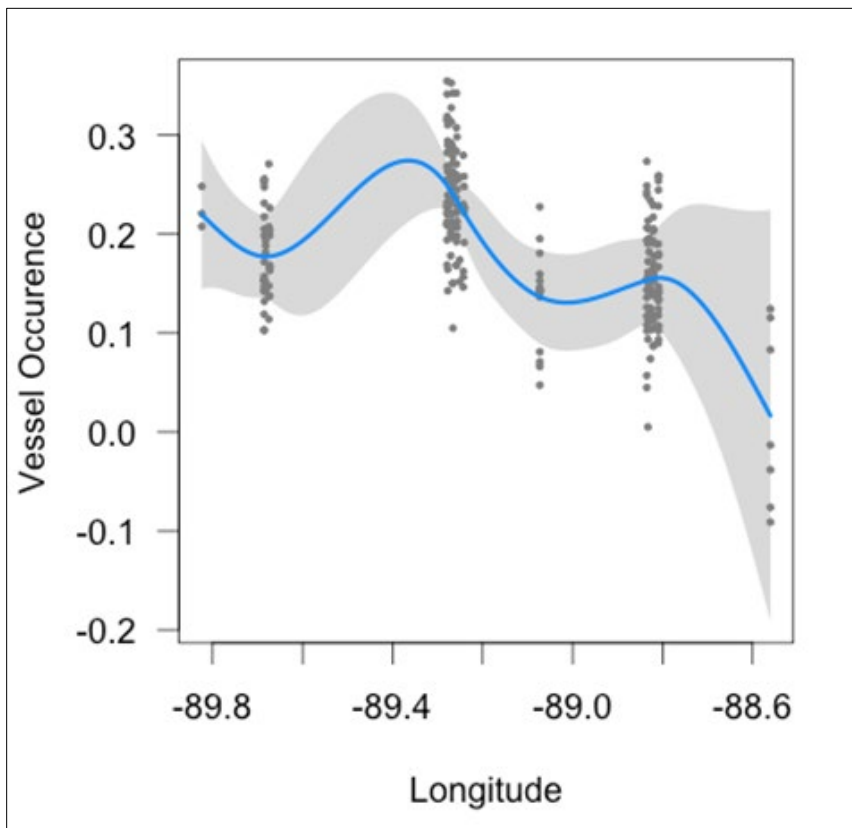
Figure 35. GAM smoothing functions for longitude effects on vessel detections.

4.3.1.2 Airgun Detection Analysis

The approach described in **Section 4.3.1.1** for vessel detection was also adopted airgun signal detections. Month and year for airgun signal detections had similar patterns to that of vessel detections (**Figure 36**). Latitude and longitude effects for airgun signals were borderline statistically significant, with a dip in the frequency of airgun detections in the middle latitudes and a higher frequency of signal detections in the middle longitudes (**Figure 37**).
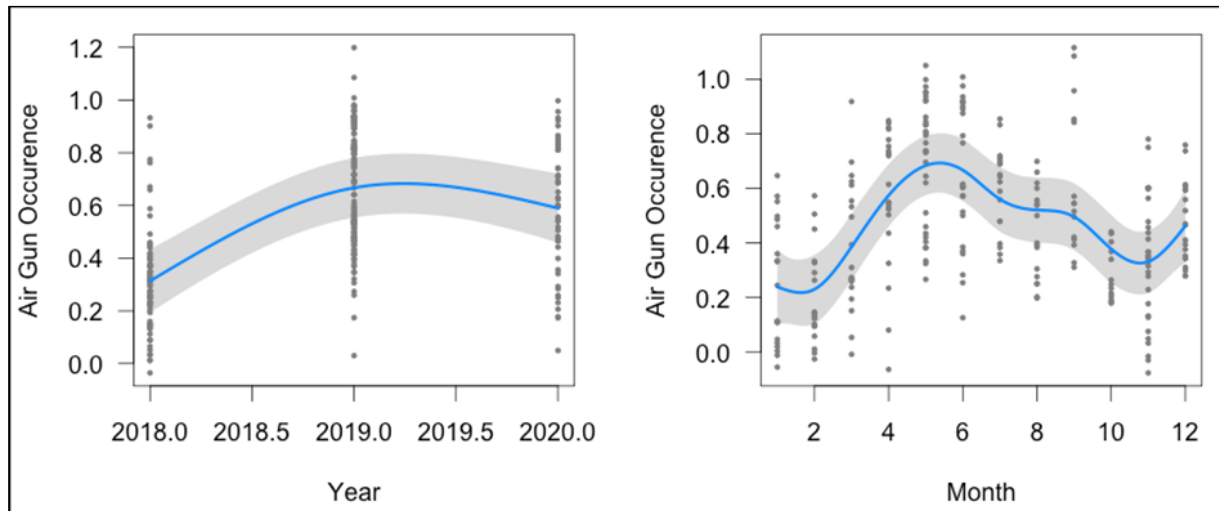
Figure 36. GAM smoothing functions for year (left) and month (right) effects on airgun signal detections.
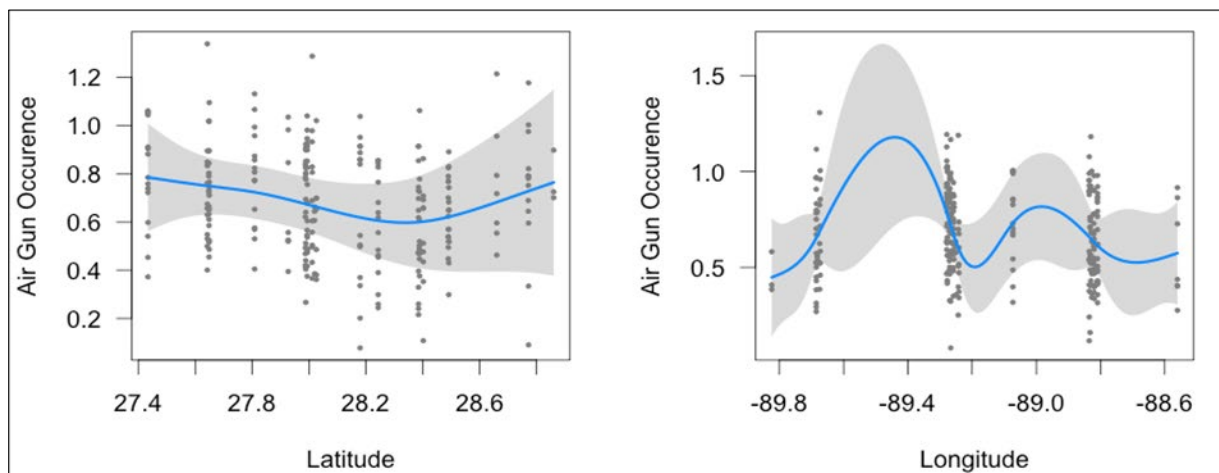
Figure 37. GAM smoothing functions for latitude (left) and longitude (right) effects on airgun signal detections.

4.4   Biological Detection Analysis

To differentiate some of the most common sound-producing marine mammals in the northern GOM that may contribute to the soundscape, frequency bands were identified for the following species/species groups: Rice's whale, beaked whales, and dolphins. The technical report presented in **Appendix D** contains detailed information on these analyses; key information from the technical report is summarized and discussed below.

4.4.1   Rice's Whale Detections

The frequency overlap between the signals of Rice's whales and the prevalent anthropogenic noise made it difficult to reliably detect the calls of Rice's whales using only the spectrally analyzed data. A better approach would be to use a matched-filter detection process that operates on the waveform data.

4.4.2   Dolphin Band Detections: Low-frequency Clicks

Throughout the first deployment, dolphin band detections rose from May until September and then fell precipitously, both in rate and number of detections, in November (**Figure 38**). Detection rates peaked in nearshore shallow waters as well as in offshore water deeper than 1,000 m (**Figure 38**). This may be due to the detection function being triggered by multiple species. Detection rates appeared to increase with latitude. Peak rates were seen in the middle longitudes and decreased to the east and west (**Figure 39**).
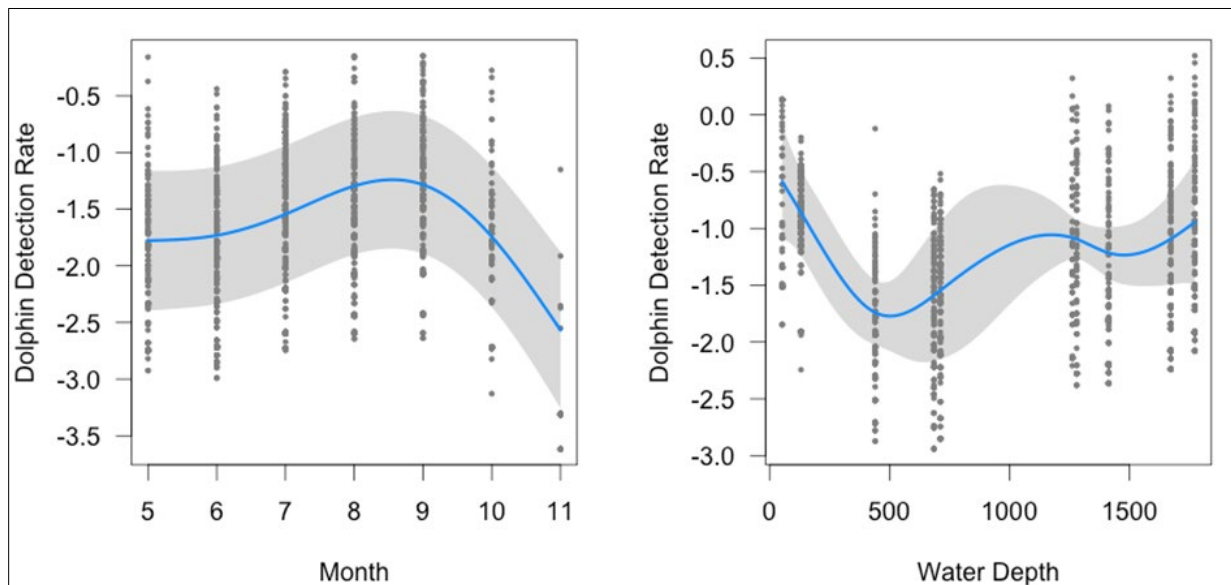
Figure 38. Month (left) and water depth (right) prediction functions for dolphin band detection rates.
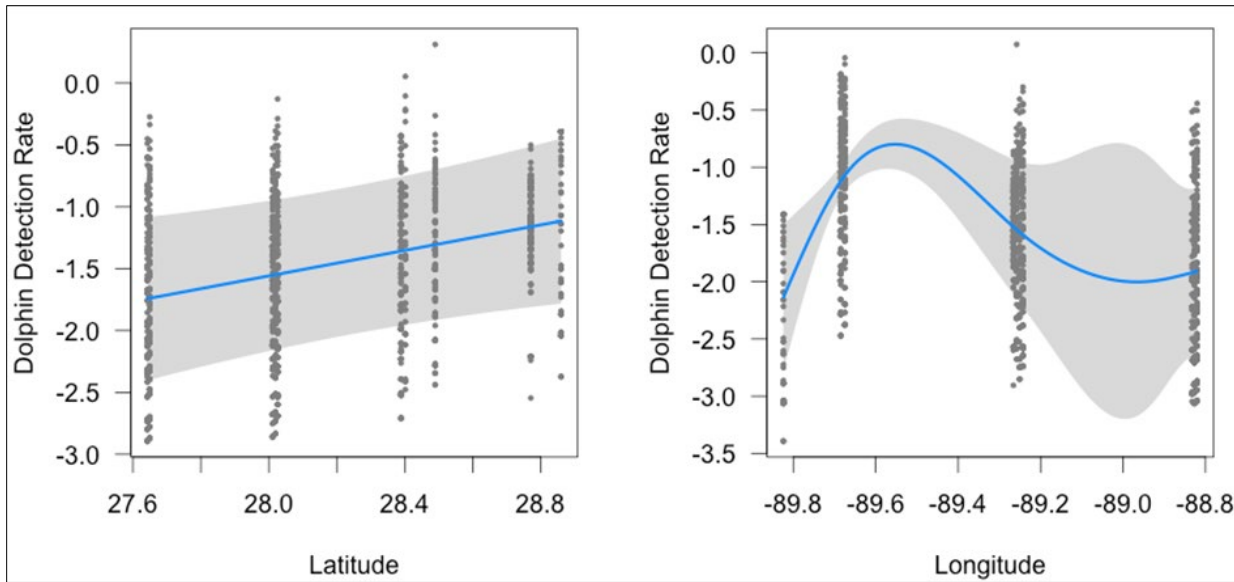
Figure 39. Latitude (left) and longitude (right) prediction functions for dolphin band detection rates.

4.4.3   Beaked Whale Band Detections: Mid-frequency Clicks

Detections in the beaked whale frequency band increased from May through September and then began to decline in October (**Figure 40**). The peak of beaked whale detections appeared to occur at intermediate water depths of 500 to 1,000 m and declined in the very shallow and very deep depths (**Figure 40**), which may indicate a habitat preference for slope environments. Detection rates appeared to be highest in lowest latitudes and decreased as latitude increased. The effect of longitude here appears to be the opposite of that for the dolphin band results, with highest values to the west and east (**Figure 41**).
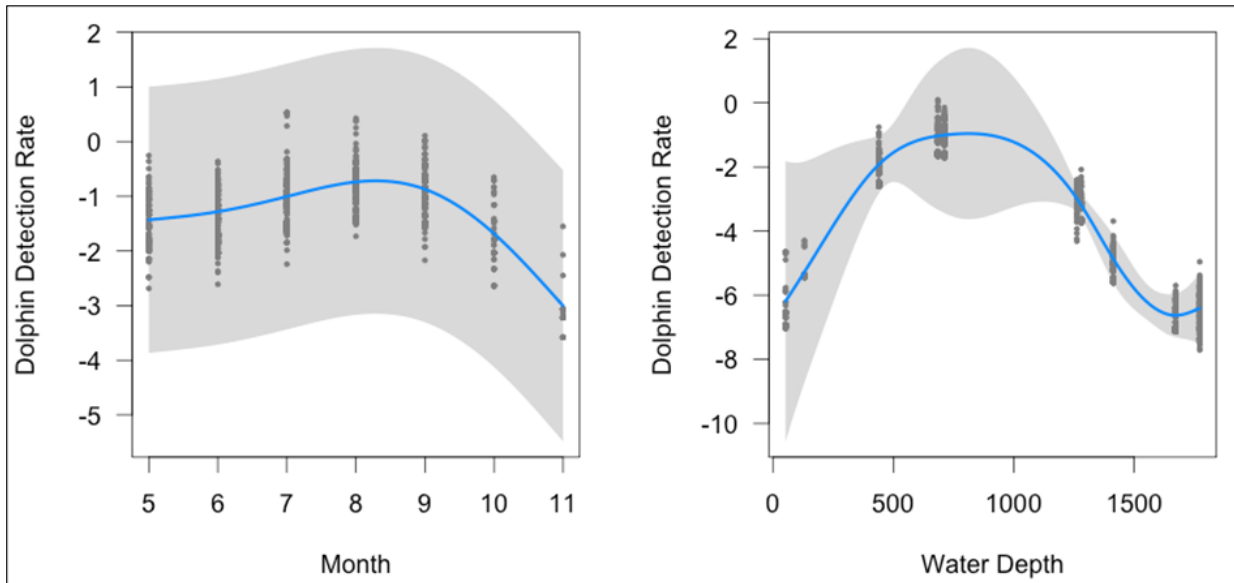
Figure 40. Month (left) and water depth (right) prediction functions for Beaked Whale Band detection rates.

95
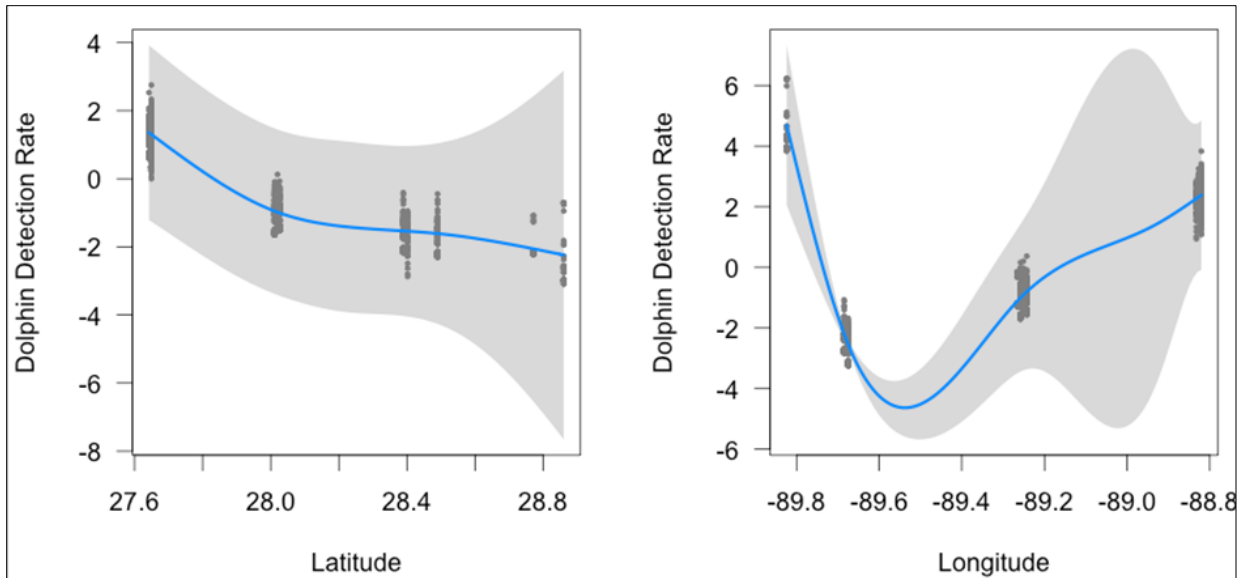
Figure 41. Latitude (left) and longitude (right) prediction functions for beaked whale band detection rates.

4.5 Statistical Modeling of Vessel Received Levels

The individual analyses of the ten receivers produced several common patterns. First the R-squared for most of the analyses was quite high, exceeding 0.5 in some cases. This indicates that a good amount, if not most of the variance in the measured RLs, could be explained by the statistical models. One of the most common patterns in the data was a strong relationship between closest point of approach (CPA) distance and measured LF sound level. In almost all analyses, this relationship was very similar, with a near linear increase in RL as vessels approached within 10 km. This relationship was much stronger than any of the predicted RL values. Based on this finding, it is recommended that future efforts to predict LF noise in the GOM should rely directly upon AIS data as predictor variables.

In most of the receivers, there was also the expected positive relationship between windspeed and wave height with increased measured LF noise. **Sections D.4.4** and **D.4.5** of the technical report presented in **Appendix D** present detailed results and discussion.

Furthermore, the monthly spectra (**Figures D-B1** through **D-B6** in **Appendix D**) showed that in some months, the spectral profiles for individual recorders in deep water were almost identical. However, in other months, the spectral differences exceeded 20 dB. This indicates that the glider-static receiver comparison is not generalizable to the full range and temporal scale of the Project.

4.6 Extrapolation Capability of Acoustic Data: Seaglider/Fixed Sensor Comparison

In order to answer the question "How far can data from a single buoy be extrapolated?", acoustic data from the stationary EARS buoy recorders at Site 2 was compared to data from the 2018 MP Seaglider as it approached, nearly flew over, and departed from that buoy location. Specifically, the Seaglider approached within 1,500 m of the EARS buoy at Site 2 during the first deployment (**Figure 42**).

In evaluating the spectrograms of the 24 hours of data before and after the CPA of the Seaglider to the Site 2 EARS recorder, the expectation was that the acoustic characteristics of the collected data would be

similar at CPA but would diverge as the range between the recorders increased (**Figure 43**). However, the spectrograms from the 2018 MP Seaglider and Site 2 EARS data show minimal similarity at any point.
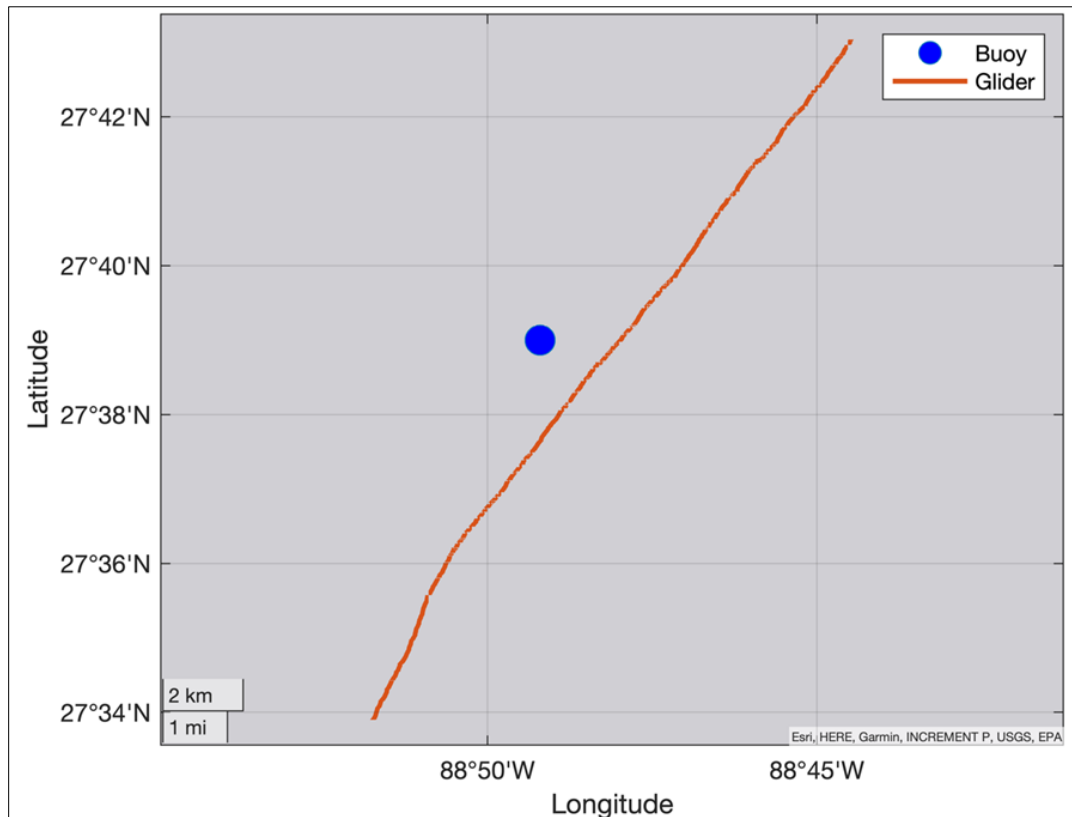
Figure 42. Path of the 2018 MP Seaglider past the Site 2 EARS recorder during Deployment 1.
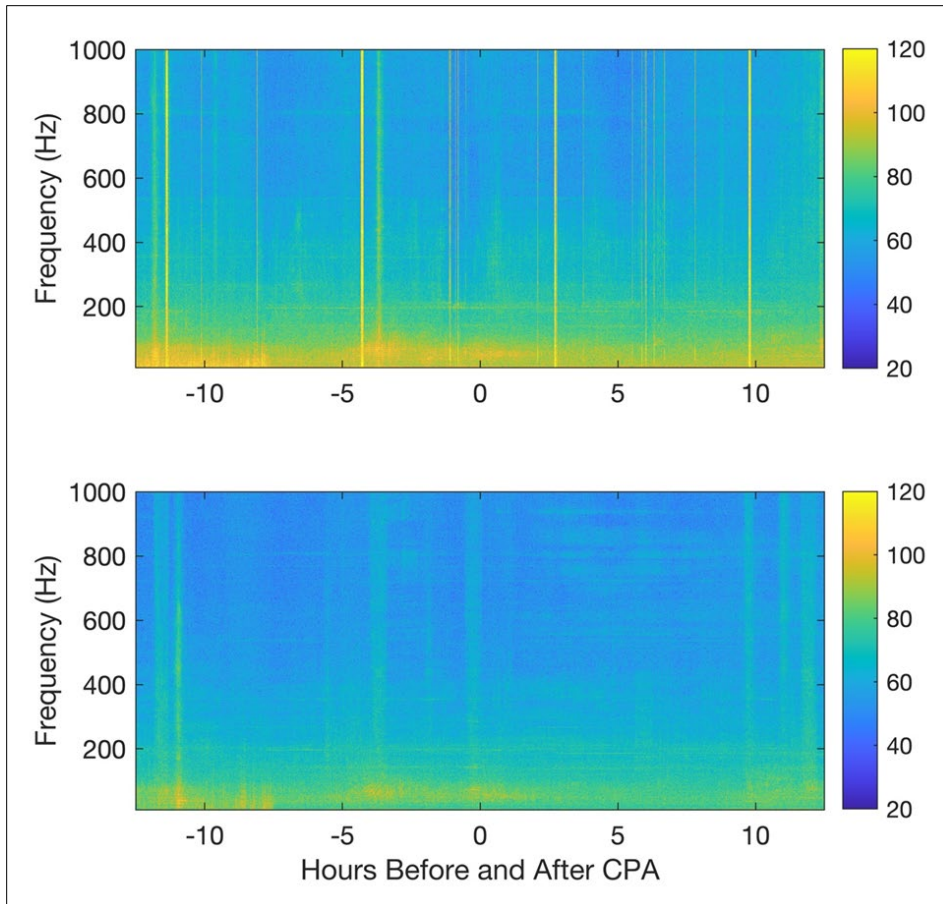
Figure 43. Comparison of spectrograms from the 2018 MP Seaglider (top panel) and the Site 2 EARS recorder (bottom panel) for the 12 hours before and after the Seaglider's CPA.

4.7 3D Underwater Sound Propagation Modeling

The underwater soundscape in the GOM is significantly influenced at different scales by 3D sound propagation (Duda et al. 2011; Ballard et al. 2015; Heaney and Campbell 2016; Reilly et al. 2016; Oliveira and Lin 2019; Reeder and Lin 2019; Oliveira et al. 2021). Physical oceanographic and geological conditions associated with continental shelves and shelf break areas can cause horizontal heterogeneity in medium properties, so horizontal reflection/refraction of sound can occur and produce significant 3D sound propagation effects. Since the northern GOM is characterized by two large canyons (Mississippi and DeSoto), it was important to better understand influence of these prominent geological features on the soundscape.

Accordingly, the SHRU VLA data were used to establish a 3D underwater sound propagation model, which is capable of capturing sound focusing and defocusing effects due to the 3D variation in bathymetry (**Figure 44**). These focusing and defocusing effects can intensify or decrease local ambient noise levels, potentially influencing noise impacts to marine animals.

This model was used to assess 3D propagation of seismic airgun sounds produced during an oil and gas survey conducted by two survey ships on September 29, 2019, the Motor Vessel (*M/V*) *Artemis Angler* and *M/V Artemis Arctic*. The ship positions in the signal analysis time window around 08:57 Coordinated Universal Time on September 29, 2019, are shown in **Figure 45** (panels (a) and (b)), and the mooring

locations of the two vertical hydrophone arrays that recorded the airgun data are shown in **Figure 45** (panels (c) and (d)). The two seismic survey ships were fairly close (5 km) to one another within the time window analyzed, and the distances from them to the two hydrophone arrays were in the range of 135 and 164 km.

Cross-correlation analysis was performed to pair up two sets of airgun pulse arrivals emitted from the two seismic survey ships separately (annotated by yellow and red arrows with sequential numbers in **Figure 45** panels (c) and (d)). The airgun pulses received at the Slope SHRU (**Figure 45** panel c) were up to 7.7 dB stronger than those received at the Canyon SHRU (**Figure 45** panel (d)), even though the Slope SHRU was farther away from the noise source. These differences in RLs were likely caused by horizontal reflection and 3D focusing effects due to canyon and slope bathymetry (**Figure 46**).

Propagation of 50 Hz sound from the seismic survey ships *M/V Artemis Arctic* and *M/V Artemis Angler* were simulated with the 3D sound propagation model. In order to identify 3D propagation effects, Nx2D simulations that constrained sound from propagating across different azimuths were also conducted. The model output from each simulation is shown in **Figure 46**, where panels (a) and (b) are 3D models, and panels (c) and (d) are Nx2D models. To better illustrate horizontal reflection and focusing, depth integrated energy levels are shown.

In future phases of the GOM Program, the 3D model output may be used to address scientific questions such as "Do marine mammals preferentially occupy (in the sense of vocal activity) high TL (low intensity) regions to avoid potential effects from manmade sounds, such as masking?"

Additional details on the 3D sound propagation modeling and simulation data analyses are presented in Lin (2019 and 2021).[17]

---

[17] Project reports titled: GOM PAM 2018 program monitoring project SHRU report, by Lin Y-T, 2019; and GOM PAM 2019 program monitoring project SHRU report, by Lin Y-T, 2021.
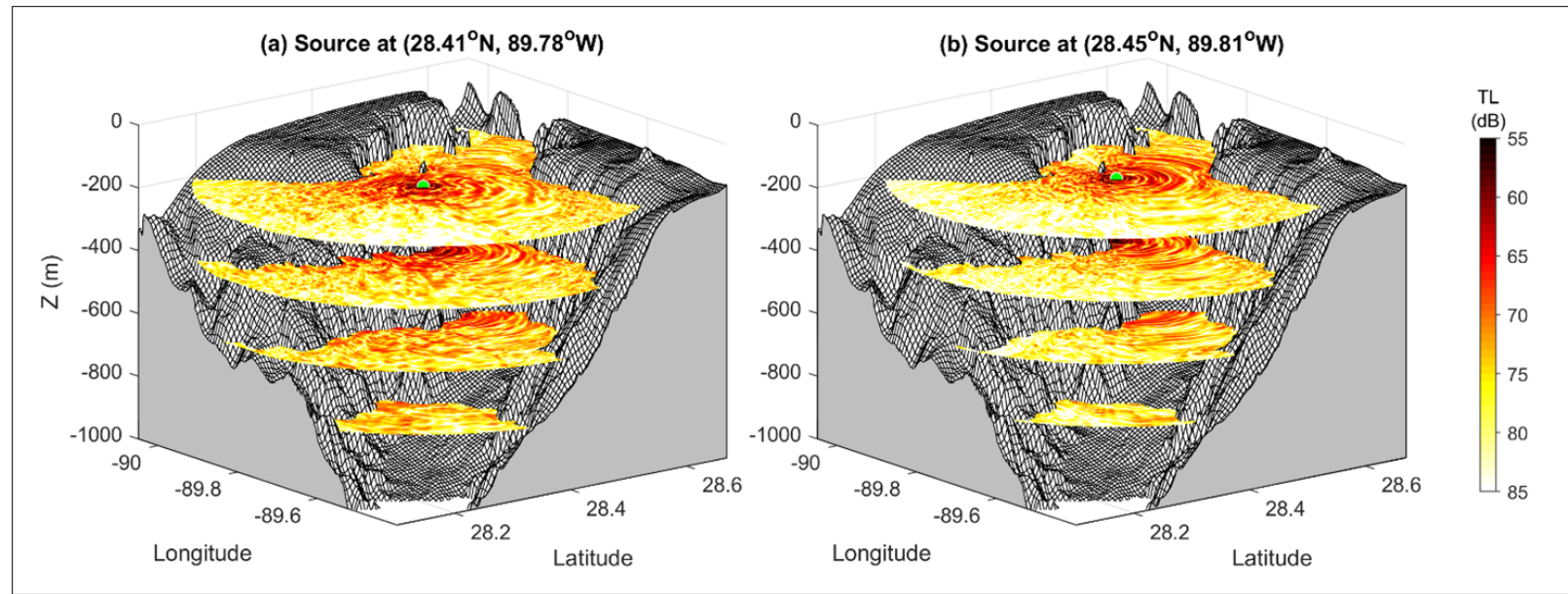
Figure 44. TL output of the 3D underwater soundscape model in the Mississippi Canyon.
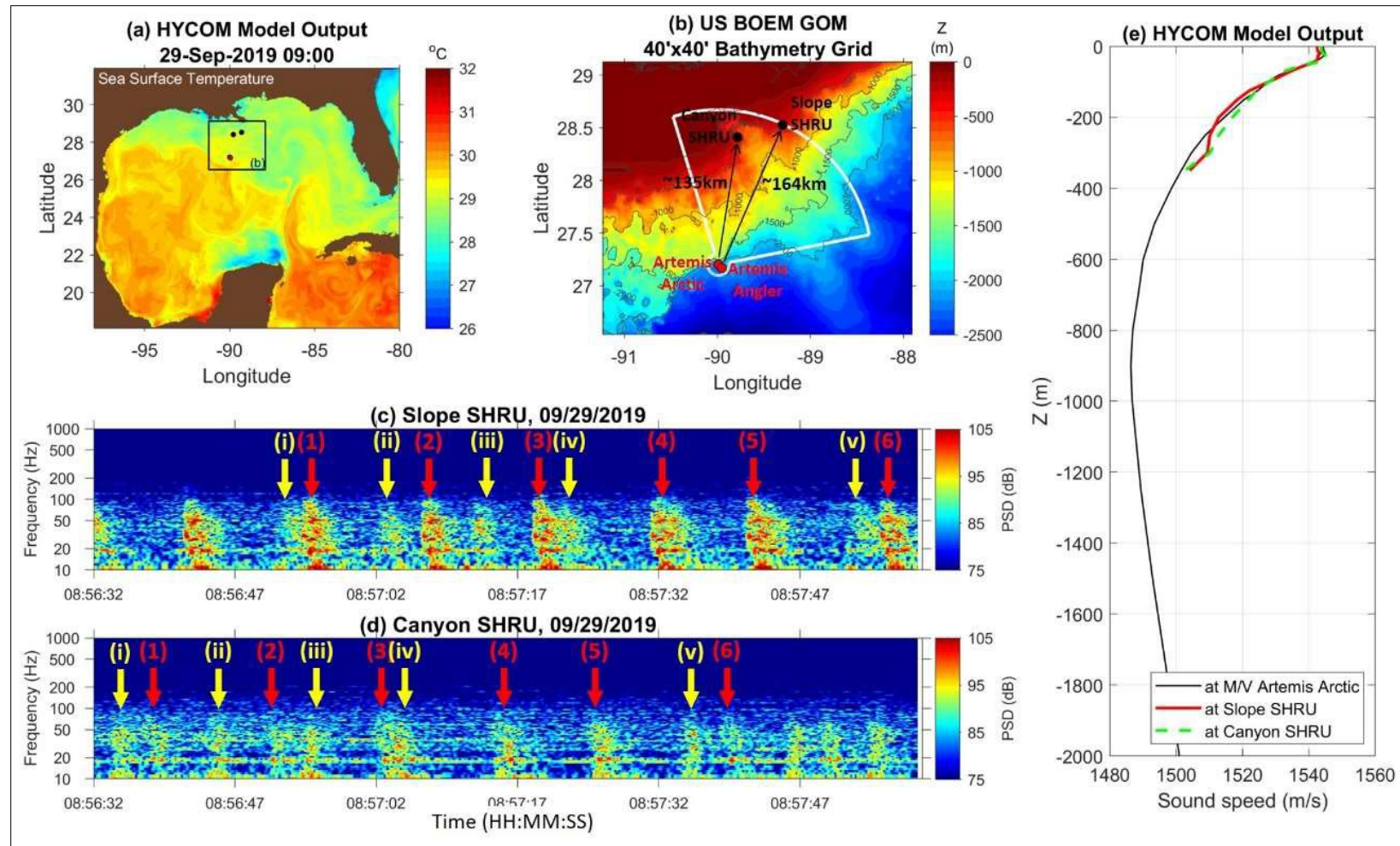
Figure 45. (a) HYCOM sea surface temperature (SST) output in the GOM.

Note: The 3D propagation model area is indicated by the box around the Mississippi Canyon. (b) A high-resolution bathymetry map in which the ship and hydrophone array locations are marked. (c) and (d) Spectrograms of received airgun pulses on the two hydrophone arrays. The airgun pulses emitted from each of the two survey ships are annotated by yellow and red arrows, respectively. (e) Sound speed profiles calculated using the HYCOM temperature and salinity output.
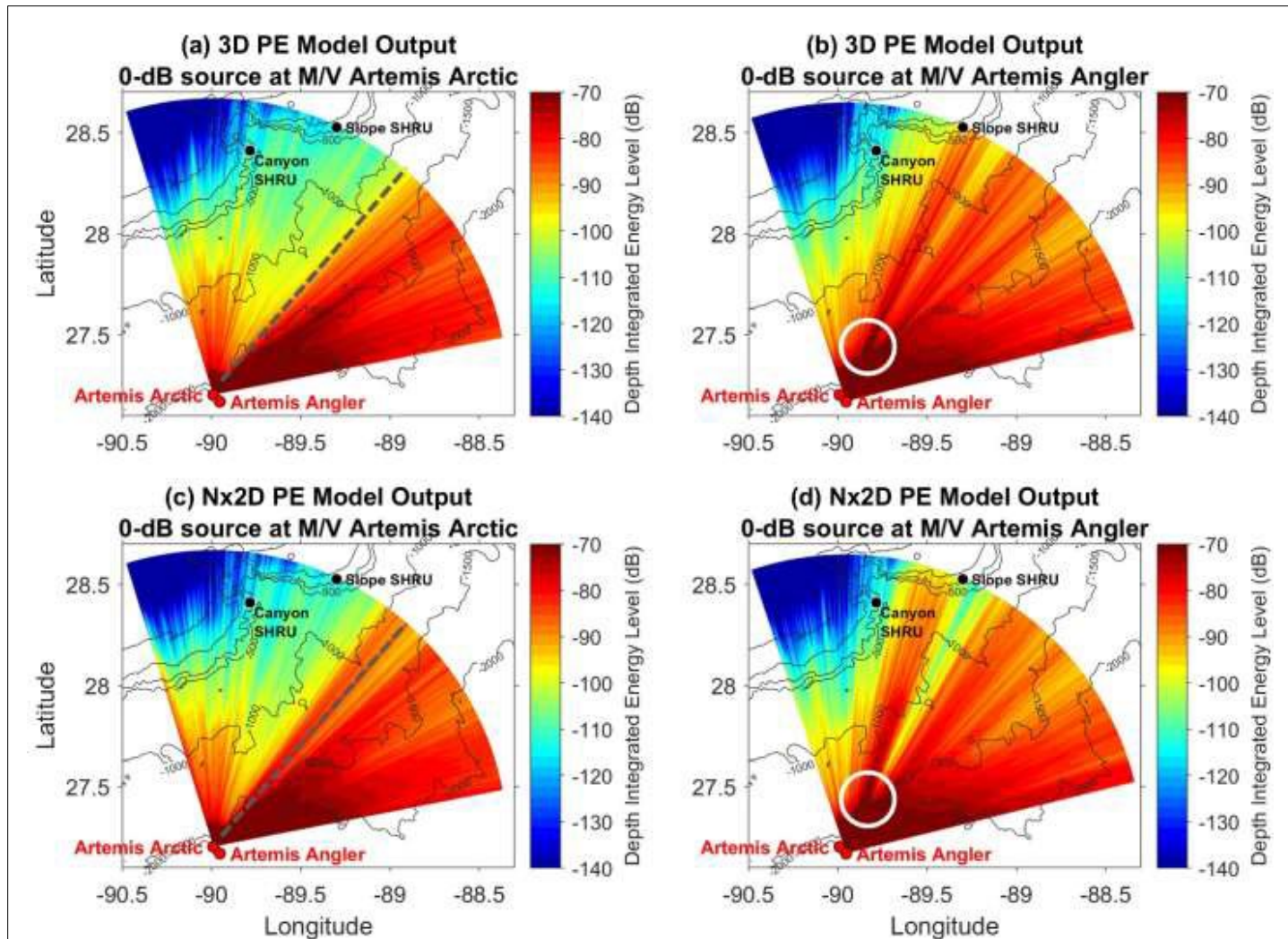
Figure 46. (a) and (b) 3D and (c) and (d) Nx2D sound propagation (50 Hz) model output for the airgun pulse propagation study.

4.8 Noise Coherence and Source Correlation Analyses

Noise source correlation with available marine traffic data was conducted using the SHRU VLA data, which, among the four sensor types, is the only dataset that lends itself to this type of analyses. AIS data overlapping with the period of SHRU VLA deployment were obtained from a commercial vendor. **Figure 47** shows an example of correlation between soundscape statistics and AIS data. This example clearly shows the potential of using passive acoustic data, especially noise coherence, for monitoring marine traffic when AIS data are not available. Additional information on these analyses and results are presented in Lin (2021).[18]
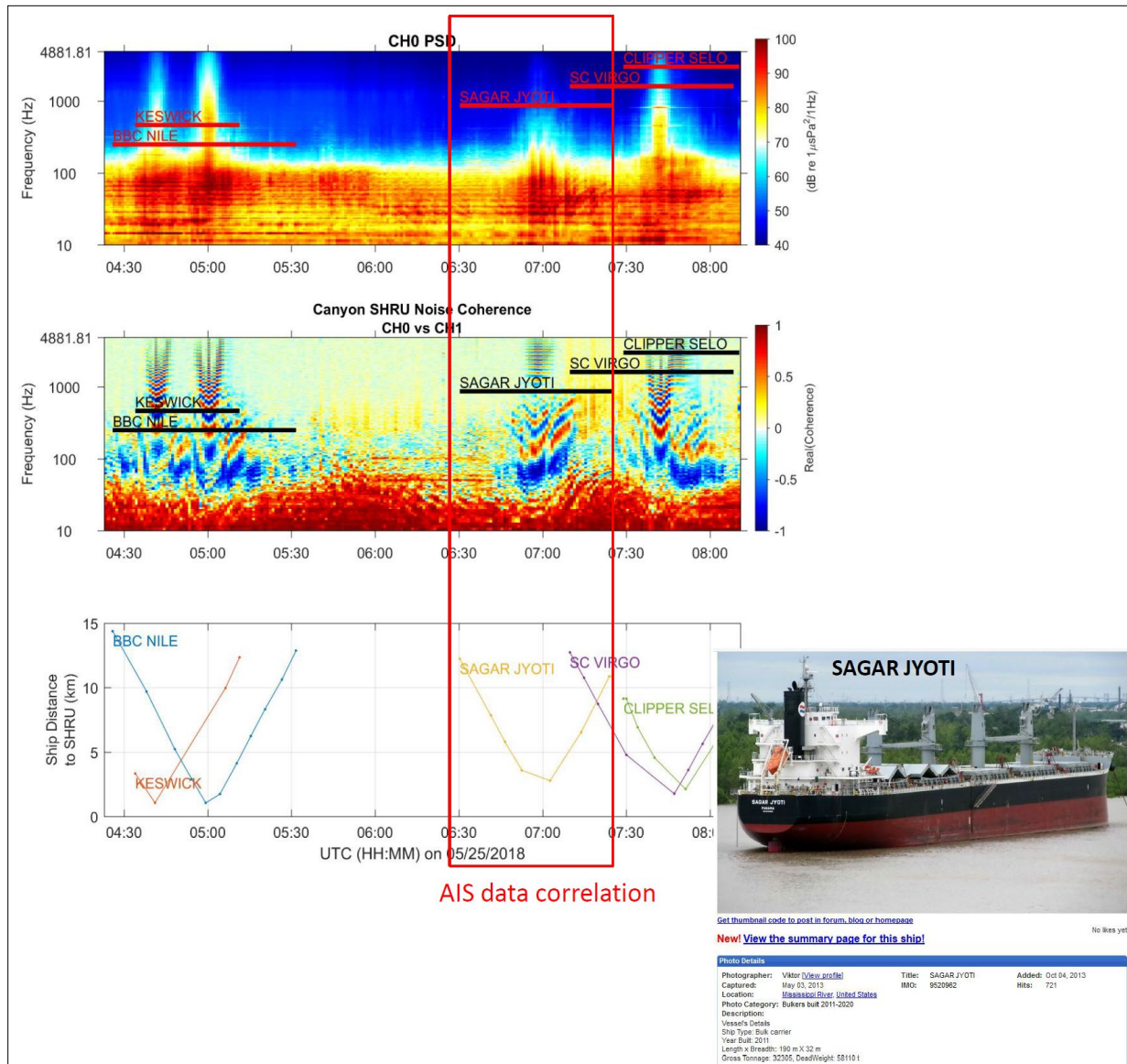
Figure 47. An example of correlation between soundscape statistics and AIS data.

---

[18] Project report titled: GOM PAM 2019 program monitoring project SHRU report, by Lin Y-T, 2021.

4.9 Mississippi Canyon Soundscape Characterization Analyses Using SHRU VLA Data

4.9.1 SPL Time Series Comparison

As part of the soundscape characterization, in addition to the six standard soundscape statistics, a time series of 12-hour average SPLs in the LF (10 to 1,000 Hz) and MF (1,000 to 4,883 Hz) bands at the Canyon SHRU array location were also computed with the SHRU VLA data. The outputs from these analyses are shown in **Figure 48**. The measurement shows that +/- 5 dB average pressure changes are seen in the LF band, while the MF band has larger deviation (up to +/- 10 dB).
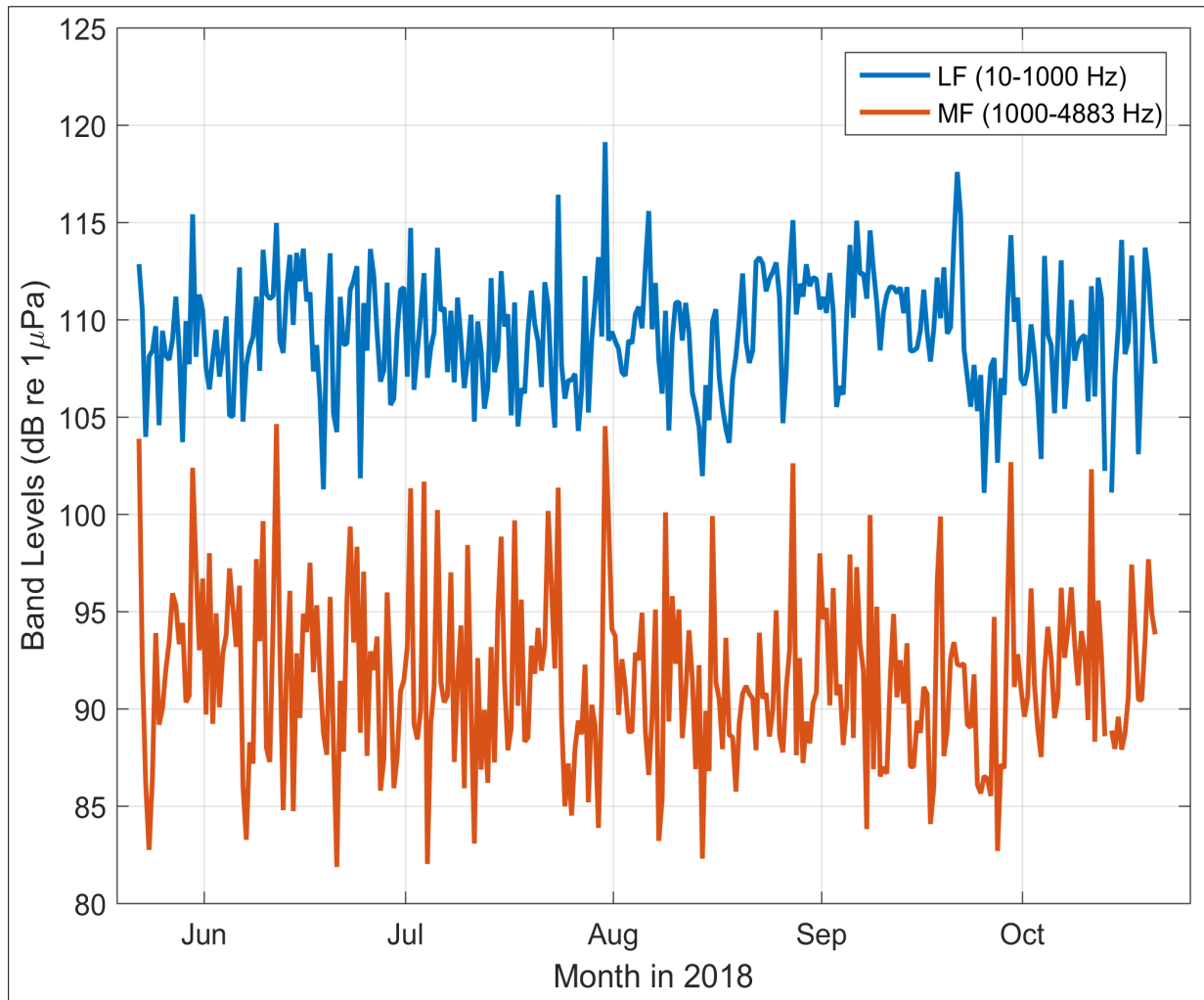
Figure 48. Time series of 12-hour average SPLs in the LF (10–1,000 Hz) and MF (1,000–4,883 Hz) bands at the Canyon SHRU array.

4.9.2 Soundscape Differences Between the Mississippi Canyon Floor and Slope

Soundscape statistics computed for the SHRU VLA data showed significant differences between the Mississippi Canyon floor and slope based on comparison of long-term percentile levels (**Figure 49**) and average PSD levels (**Figure 50**). In the next phase, these outputs will be compared to outputs from similar analyses performed with the 2019 MP SHRU VLA data to determine if the statistical difference between the canyon floor and slope are consistent over time.
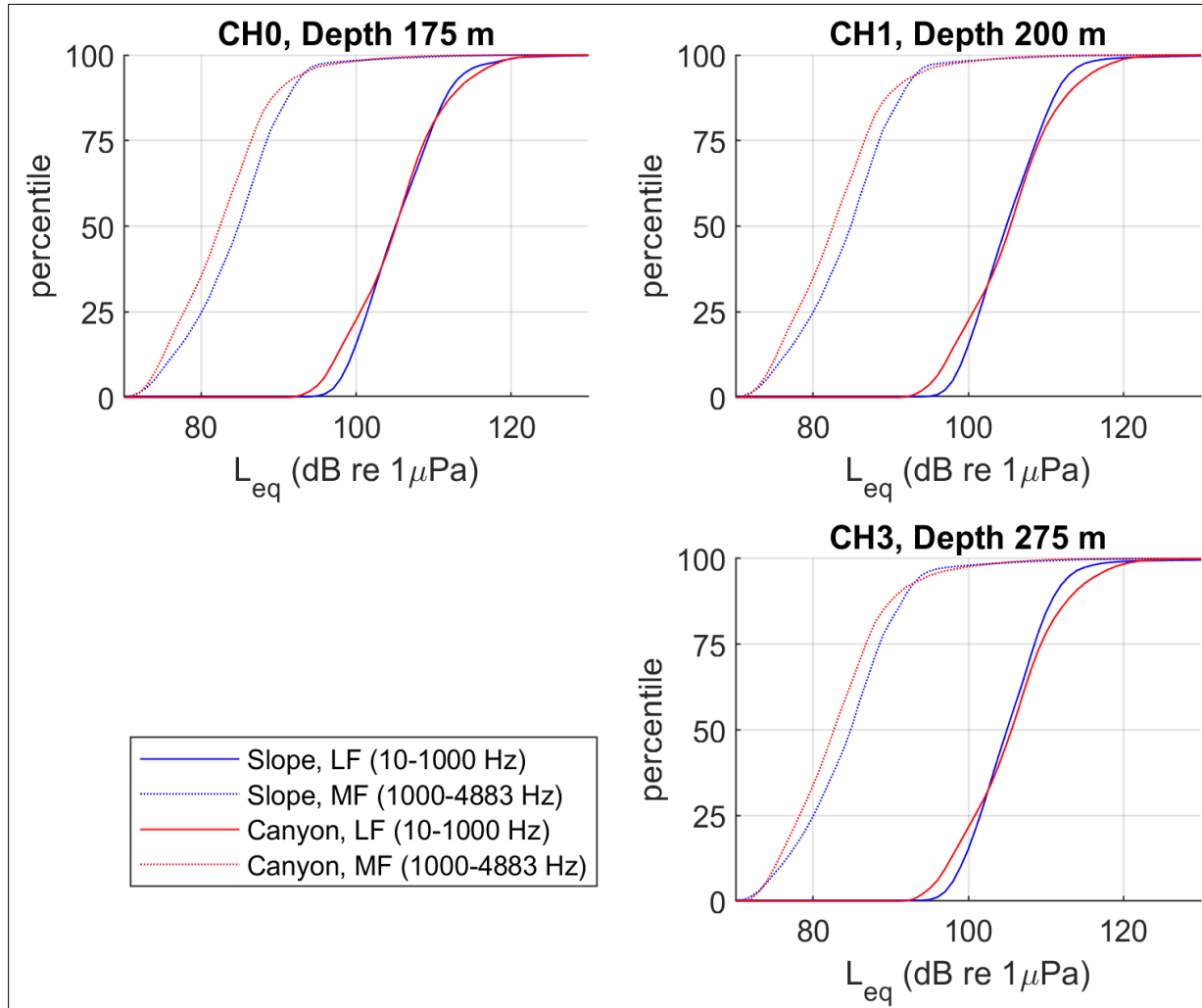
Figure 49. Comparisons of long-term percentile levels measured at the Slope (blue curves) and Canyon (red curves) SHRU sites.
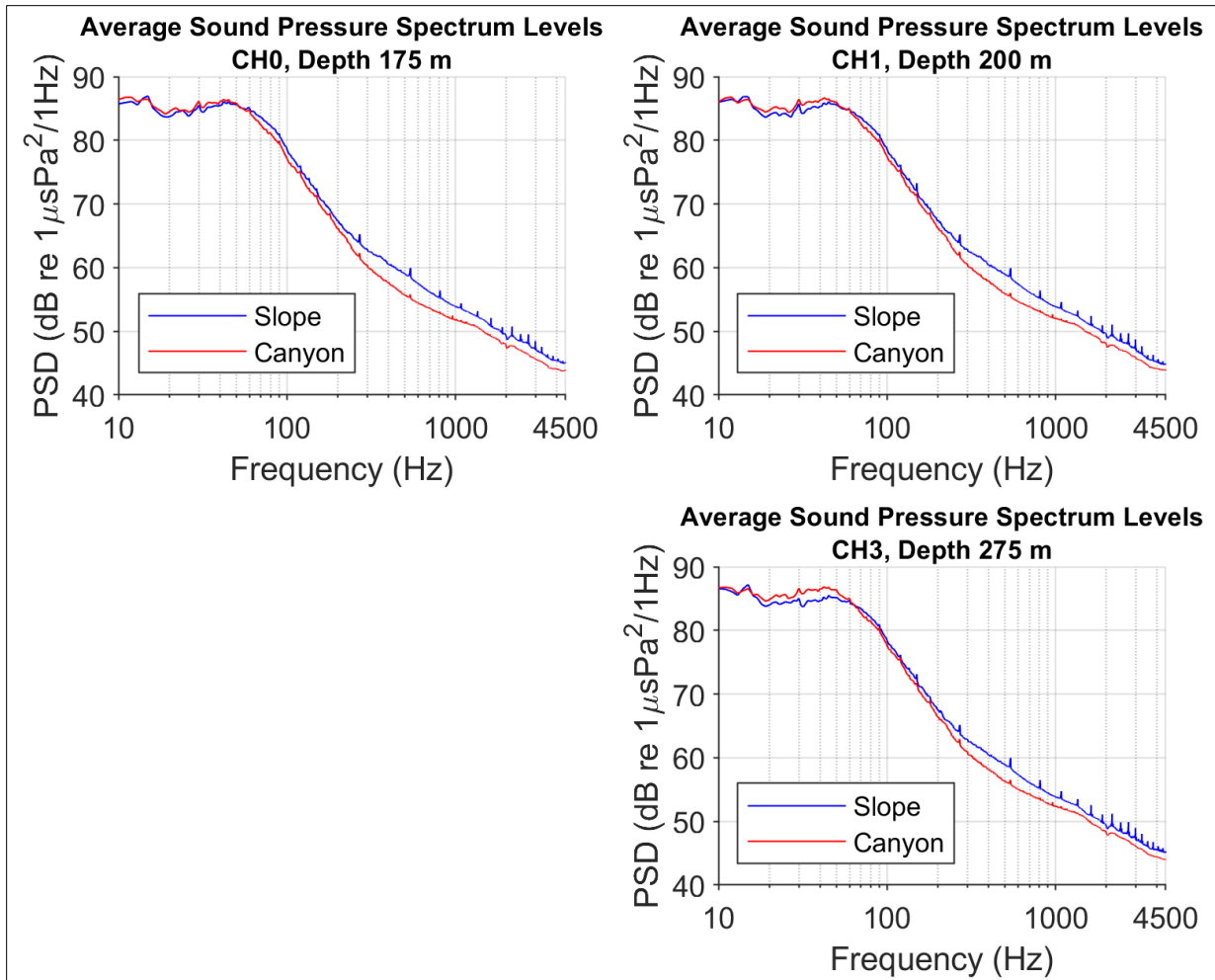
Figure 50. Comparisons of average PSDL measured on the Mississippi Canyon slope (blue curves) and floor (red curves).

4.9.3 Annual Soundscape Variability between the Mississippi Canyon Floor and Slope

To better understand the annual soundscape variability between the Mississippi Canyon floor and its slope, SPLs computed from the 2018 MP SHRU VLA data were compared with SPLs computed with the 2019 MP data. **Figure 51** shows comparison of the average SPL measured on the floor of the Mississippi Canyon during 2018 and 2019.
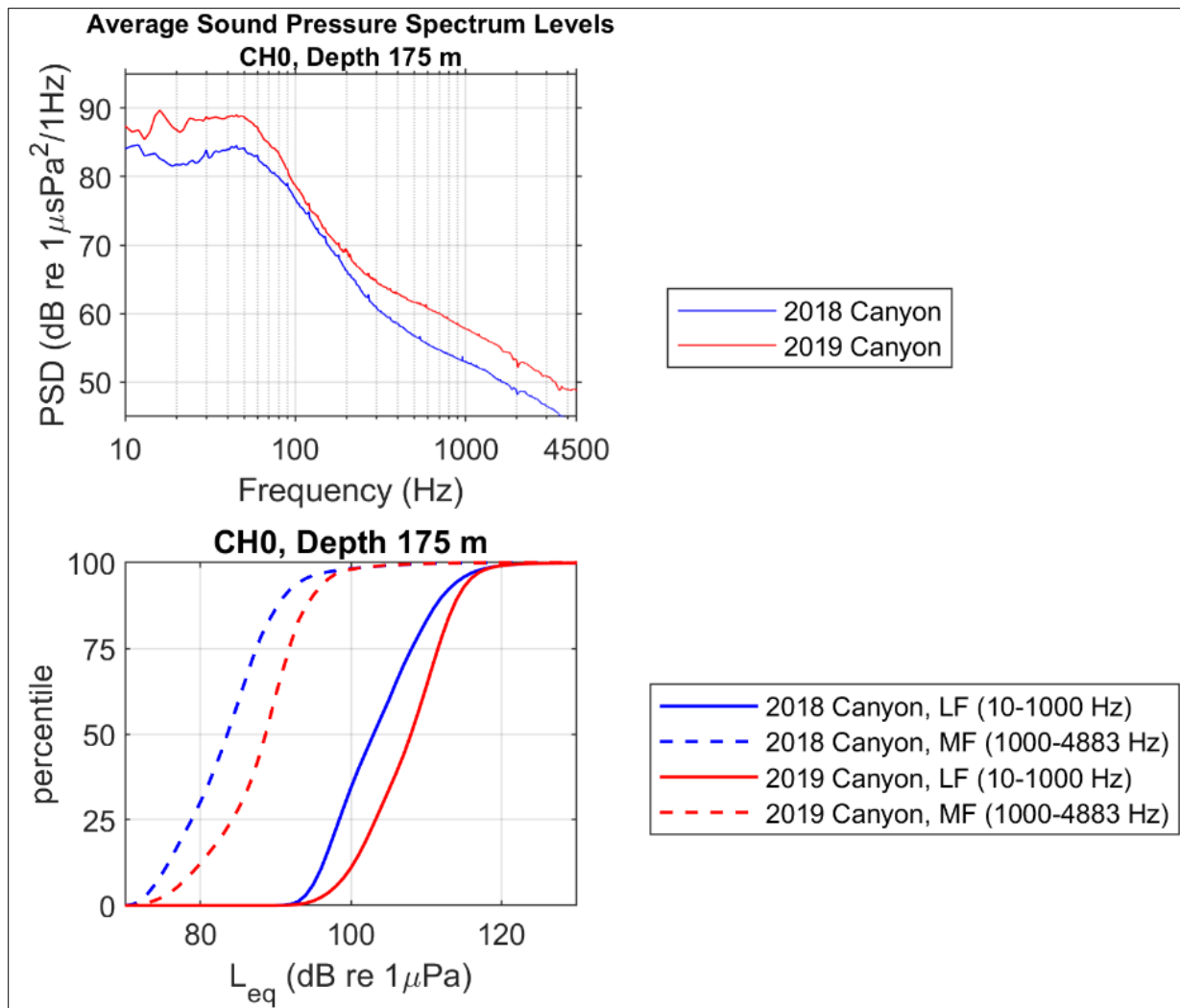
Figure 51. Comparison of average SPL measured in 2018 and 2019 on the Mississippi Canyon floor.

4.10 Soundscape Fingerprint Analysis

The noise coherence and source correlation analysis presented in **Section 4.8**. was further developed to generate a "soundscape fingerprint" by computing ship noise coherence across discrete frequency bands. A 3D model adopting realistic ocean environmental data in the Mississippi Canyon was used to simulate spatial noise coherence distributions across the canyon area. Because the coherence distribution highlights the acoustic influence of bathymetric features that can be unique at different locations, the distribution is referred to as a "soundscape fingerprint." In fact, the pattern of the coherence distribution resembles the impression of a human fingerprint (**Figure 52**).
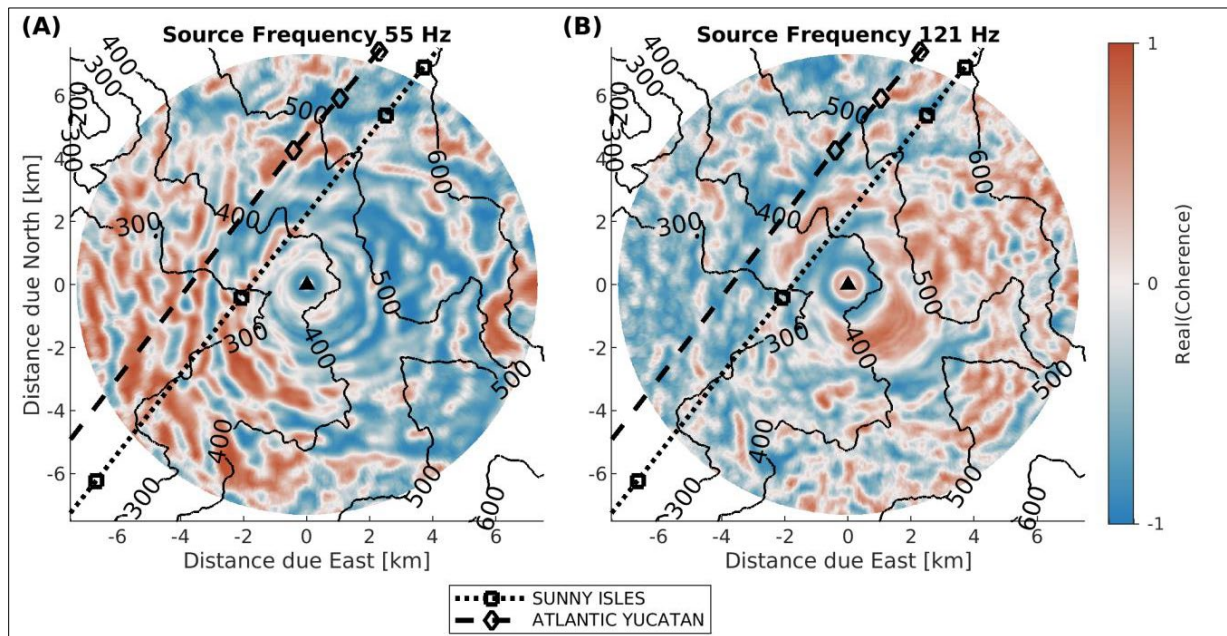
Figure 52. Acoustic fingerprint for the Canyon SHRU at 55 Hz and 121 Hz

Note: Black contours 224 are constant bathymetry depths at 100-meter intervals and labeled in meters. Estimated ship tracks 225 are denoted by dotted (SUN) or dashed (ATL) lines connecting open squares (SUN) or open 226 diamonds (ATL). Squares and diamonds in the ship tracks denote known AIS locations. (A) The 227 range-variable bathymetry forces a positive (red) coherence at 55 Hz west of the SHRU and negative 228 (blue) to the east. (B) At 121 Hz the coherence sign is flipped to negative (blue) to the west and 229 positive (red) to the east.

Ship noise recorded by the Canyon SHRU array was shown to contain the acoustic influence of bathymetric features, and noise coherence was demonstrated to be an effective metric for identifying ship traffic in recorded data. Comparison of the data and the model showed a promising agreement for lower frequencies which are less susceptible to temporal environmental changes, suggesting an avenue for source localization efforts in strongly range-dependent environments. Furthermore, seasonal variability in the soundscape fingerprint was examined, with models suggesting a strong influence of seasonal changes to near-surface ocean properties (**Figures 53** and **54**).
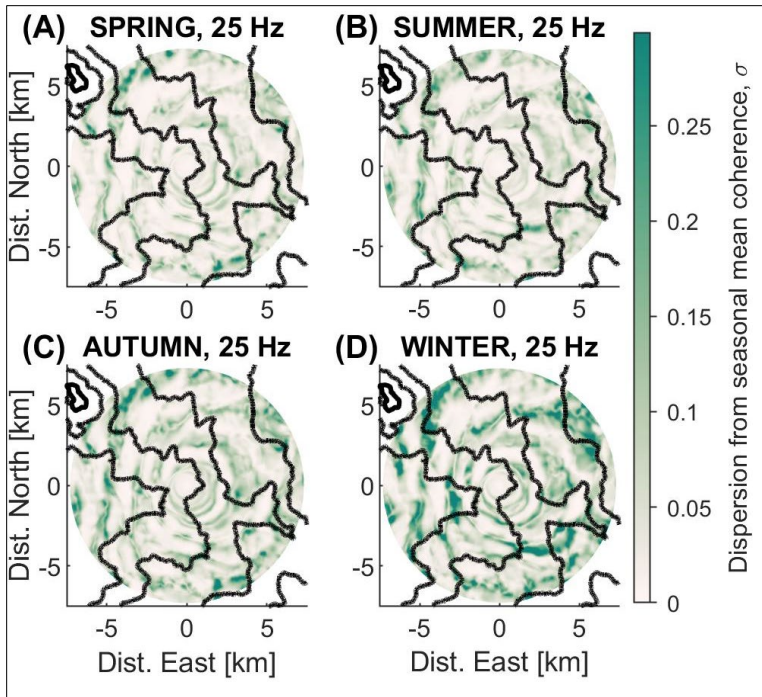
Figure 53. Dispersion of soundscape fingerprints from seasonal means, represented by one standard 296 deviation across seasonal samples. Source frequency 25 Hz.
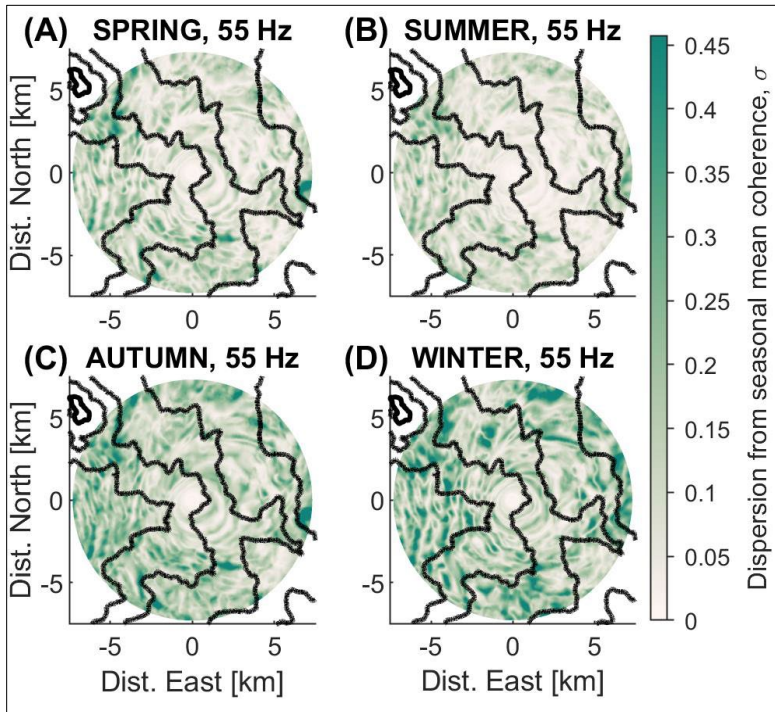
Figure 54. Dispersion of soundscape fingerprints from seasonal means, represented by one standard 299 deviation across seasonal samples. Source frequency 55 Hz.

5 Discussion

Soundscapes are created from the interaction of the spatial-temporal patterning of natural and anthropogenic sounds in the environment (Pijanowski et al. 2011). The northern GOM is a productive subtropical region that supports a variety of vocally active species, including fish and marine mammals (Wall et al. 2013; Roberts et al. 2016; Boyd et al. 2021). It is also a major area for oil and gas exploration and extraction, military operations, fishing, and tourism. The GOM PAM Program study area was focused on the central portion of the northern GOM where the flow of freshwater from the Mississippi River creates strong ecological gradients. The underwater soundscape described in this study provides valuable information on the current environment that can be used to inform assessments of future changes in ambient sound caused by restoration and human activities (such as increased shipping, future renewable energy development), species occurrence and density, and potential impacts of elevated noise to protected species.

5.1 Ambient Sound Levels

The northern GOM has very high average ambient sound levels at 10 to 100 Hz and moderately high levels at frequencies up to 1 kHz and above, relative to other locations around the world (Dahl et al. 2007). SPLs recorded under the GOM PAM Program were similar to those previously recorded in this region in 2010 to 2013 (Estabrook et al. 2016; Wiggins et al. 2016), indicating persistently high levels of LF noise over the decade. Human-caused sound (anthrophony) has been increasing globally because of shipping, resource exploration and exploitation, and infrastructure development (Duarte et al. 2021). The northern GOM is one of the most industrialized parts of the ocean; therefore, this ecosystem has experienced long-term, chronic exposure to LF noise pollution.

In addition to these anthropogenic sources of sound, wind, and storm events (geophony) periodically elevate ambient sound levels at higher frequencies (500 Hz and above). Wind speeds from storms have been found to be correlated with SPLs at 900 Hz in the GOM (Wiggins et al. 2016). During this study, Tropical Storm Barry moved through the study area in mid-July 2019. Although this storm created underwater sound, there was a reduction in the one-third octave frequency band levels, with the CF of 63.1 Hz as seismic surveys and shipping transits ceased due to the adverse weather conditions. This reduction in LF sound (less than 100 Hz) was similarly found during Hurricane Isaac in August 2012 (Wiggins et al. 2016) and Tropical Storm Barry in 2001 (Newcomb et al. 2002).

5.2 Detection of Anthropogenic Sounds

As in 2010 to 2013 (Estabrook et al. 2016; Wiggins et al. 2016), monitoring conducted under the GOM PAM Program from 2018 to 2020, found that the LF soundscape was dominated by distant seismic survey and ship traffic sounds. Seismic surveys produce loud, LF sounds created by airguns. In this LF range (below 100 Hz), elevated sound levels occurred nearly continuously during the summer months. Although the activity creates an impulsive sound, the multiple paths it propagates not necessarily in deep water means the duration of the sound increases with distance to form a nearly continuous signal (Greene and Richardson 1988; Guerra et al. 2011).

Airgun occurrence had strong annual and monthly patterns. Latitude and longitude predictors were both only marginally significant, and water depth had no statistically significant effect. This likely reflects the greater distance over which airgun operations could be detected. The same temporal pattern of airgun activity was seen on many of the recorders.

Despite seismic surveys not occurring in proximity to the recorder locations in this study, the sounds were detected, and SPLs elevated for months. A similar elevation of LF (10 to 100 Hz) ambient sound levels

was found in the polar waters of the North Atlantic (Klinck et al. 2012) and the Chukchi Sea (Roth et al. 2012), where seismic surveys occurred. Airguns in the Chukchi and Beaufort Seas elevated average sound levels by 2 to 8 dB re 1 μPa^2/Hz at 20 to 50 Hz, depending on distance from the source (Roth et al. 2012). Along the Mid-Atlantic Ridge, airgun sounds were detected on hydrophones at a depth of approximately 900 m in the Deep Sound Channel up to 4,000 km away during at least nine months per year at all 12 recording locations (Nieukirk et al. 2012). The main sources of these airgun sounds were Newfoundland, northeastern Brazil, and Senegal and Mauritania in West Africa, which personified the LF soundscape in the Atlantic Ocean almost year-round (Nieukirk et al. 2012).

The northern GOM is well-positioned to support a transition to a renewable energy future, as much of the infrastructure already exists to support offshore wind development in the region. As part of the current administration's goal of permitting 30 gigawatts of offshore wind power development by 2030, BOEM recently announced that it is preparing a draft environmental assessment (EA) to consider the impacts of potential offshore wind leasing in federal waters of the GOM. The area that will be reviewed in the EA includes almost 30 million acres just west of the Mississippi River to the Texas/Mexico border. This is the same area for which BOEM recently requested public input in a Call for Information and Nominations. BOEM plans to narrow the area that is advanced for Wind Energy Area delineation, which are offshore locations that appear most suitable for wind energy development, based on stakeholder and ocean user input received as through this call.

Though the GOM PAM Program study area lies to the east of the area that the EA will consider, findings and recommendations from the GOM PAM Program monitoring are relevant to guiding future offshore wind energy development in this region. For example, impulsive sounds from pile-driving of turbine foundations have their main energy below 2 kHz, with the peak generally at 100 to 500 Hz (Bailey et al. 2010; Amaral et al. 2020). Impact pile driving usually occurs in waters up to approximately 50-m depth (Bailey et al. 2014), with greater TL and lower corresponding received sound levels at greater ranges (10 km from source) than seismic surveys occurring in deeper water. Although similar, these two different sound sources are expected to have different contributions to the soundscape, and their classification as impulsive or non-impulsive sounds for EAs will depend on the range and bathymetry (Hastie et al. 2019). If seismic surveys ceased, and even if offshore wind energy development moved forward, a reduction in the average LF ambient sound levels would be expected because of the shorter time period and shallower water location of the activity.

5.3 Vessel Sound Levels

The second major source of anthropogenic noise detected in the northern GOM was vessel traffic, which is prevalent in this region. In contrast to seismic survey sounds that were persistent in time, vessel passages were more transitory. Received sound levels tend to depend on the proximity and size of the vessel (Bassett et al. 2012). Daily detections of vessel activity, reported for close passbys to the receivers (i.e., close enough to create a Lloyd mirror interference pattern), varied from below 10 percent to near constant or daily occurrences. There was a strong seasonal pattern, with most vessel detections occurring in the summer months (May to June). The annual pattern indicated an increase in vessel traffic from 2018 to 2019, and a subsequent decrease in 2020. However, the sampling within the first and last year only covered a portion of the years 2018 and 2020. Monitoring in 2018 began in late May, and most recording was completed by May 2020. Therefore, these partial years may have missed a portion of the peak in vessel traffic. Another possibility is that the decline in vessel numbers in 2020 may reflect reduced vessel traffic due to the COVID-19 pandemic.

The effects of latitude and longitude on the distribution of vessel detections were both statistically significant. Vessel detection rates increased with both water depth and latitude. However, the magnitudes of these effects were not equivalent. Water depth appeared to be the stronger predictor, and this may

reflect better acoustic propagation in deeper waters, or all these effects could reflect the prominent shipping routes into the Port of New Orleans.

Program data showed vessel noise contributed to the underwater sound levels below 1 kHz year-round almost every day at all the recorder locations. High vessel traffic off the U.S. coast in the northeast Pacific (McDonald et al. 2006) and western Atlantic (Rice et al. 2014) similarly caused increased ambient sound levels. Off California, ambient sound levels were higher by 10 to 12 dB re 1 μPa^2/Hz at 30 to 50 Hz in 2003 to 2004 compared to 1964 to 1966, which is thought to have been caused by an increase in commercial shipping (McDonald et al. 2006). Off the U.S. East Coast, the Mid-Atlantic coastal areas had the highest ambient sound levels, and these were mainly attributable to vessel noise in proximity to high-use shipping ports (Rice et al. 2014). New Jersey had the most hours above 120 dB re 1 μPa within the 71 to 224 Hz frequency band in the region spanning the Gulf of Maine to off the coast of Georgia (Rice et al. 2014), but these levels were still generally lower than recorded in the northern GOM study area.

Statistical analysis of Received Vessel Band noise focused on predicting the actual RL at the recorders. This involved 1) measurement of distance from each vessel to the recorder, 2) estimation of the SL of the vessel, and 3) prediction of the TL between the two. Modeled vessel noise level was most often a good predictor of measured levels. However, on occasion these functions curiously showed a negative relationship with measured noise levels. Such an occurrence may be due to overprediction of noise levels at this location.

The most important vessel predictor for measured sound level was the CPA. This variable is relatively easy and quick to calculate when AIS data are available. A significant challenge in the analysis was the delay in acquisition of the AIS data, which is the backbone of the vessel soundscape analysis. The 2018 AIS data were not available until 2020, and the last part of the 2019 AIS data were not available until 2021. In the future, analysis of collected and archived data should consider focusing on the AIS metrics. This is particularly the case where studies are focusing on large, commercial vessels, and the analysis is occurring more than 12 months after data collection. However, if propagation predictions are needed, then 3D modeling should be conducted along with a comparison of simpler propagation models. Additionally, if a future study involves near real-time data and analyses or aims to include sound emissions from smaller, recreational vessels that may not be using AIS, then propagation modeling is beneficial.

5.4 Detection of Biological Sounds

The main source of biological sounds (biophony) detected were marine mammal calls. More than 20 species of marine mammals occur in the waters of the northern GOM, with species of dolphins, including the bottlenose dolphin, predominantly populating continental shelf waters, and deeper diving species such as beaked whales and the sperm whale inhabiting offshore waters (Fulling et al. 2003). One baleen whale, the newly named Rice's whale, is a year-round resident of northeastern GOM waters, with a very small population (50 to 100 whales) listed as endangered under the ESA (84 FR 15446; Hayes et al. 2021).

To differentiate some of the most common sound-producing marine mammals that may contribute to the ambient soundscape, frequency bands for the known vocalizations of five marine mammal species or species groups (Rice's whale, beaked whales, and dolphins) were identified. The recorded acoustic data were assessed to determine which characteristics informed the spatial and temporal patterns of these marine mammal species or groups.

The frequency overlap between the signals of Rice's whales and the prevalent anthropogenic sound environment made reliably detecting the calls of Rice's whales difficult using only the spectrally analyzed data. A potentially better approach to test in the future would be a matched-filter detection process that operates on the waveform data.

The detection rate results from the "dolphin" and "beaked whale" frequency bands had similar temporal patterns. Detection rates increased from May to September and began to decline in October. November rates were generally lower. Note data from November 2018 (under Deployment 1) were sparse, as some recorders had stopped recording early due to either recording system failures, severed moorings, trawled recorders, or data compression issues.[19] All these issues were addressed in subsequent deployments.

The effect of water depth on detection rates had the opposite effects for the two frequency bands. In the dolphin band, peaks were seen in both shallow and deep waters, while the values from approximately 400 to 700 m were lower. This pattern is perhaps most easily explained by multiple species being detected with differing habitat preferences (Roberts et al. 2016). The peak of beaked whale band detections appeared to occur at intermediate water depths of 500 to 1,000 m and then declined in the very shallow and very deep depths. This may indicate a habitat preference for slope environments.

Latitude also had contrasting effects between the two frequency band results. For the dolphin band, the detection rates were lowest in the southernmost waters and increased over the more northerly recorders. For beaked whale band detections, the rates were highest in the south and decreased to the north. Finally, longitude also had opposite trends for these two bands. The highest dolphin band detection rates were found in the central longitudes, while the highest beaked whale band detection rates were found to the far west and east of the study area.

5.5 Use of Multiple Sensor Platforms

A variety of stationary and mobile sensor types and platforms were deployed in this study that allowed a broad characterization of the ambient soundscape as well as detailed modeling of the temporal and spatial patterns of the anthrophony and biophony. It is recognized that it may not be feasible to deploy such a comprehensive suite of sensors in all future studies. Selection of the most appropriate type of monitoring platform will depend on the stated goals and objectives of the data collection and analyses. Benefits and potential applications of single and multiple stationary arrays of acoustic recorders and mobile platforms are summarized in **Table 15** to guide future study planning.

---

[19] Project reports titled: Assessment of ocean ambient sound levels in the northern GOM, May 2018–May 2019, by Klinck H, Ponirakis DW, Dugan PJ, Rice AN, 2019; Assessment of ocean ambient sound levels in the northern GOM, May-October 2018: autonomous Environmental Acoustic Recording System (EARS) buoys, by Sidorovskaia N, Bhattarai K, 2019; and Assessment of ocean ambient sound levels in the northern GOM, October 2018–April 2019: autonomous Environmental Acoustic Recording System (EARS) buoys, by Sidorovskaia N, Bhattarai K, 2019.

Table 15. Summary of sensor platforms, benefits, and potential applications for future monitoring

Platform	Example Benefits	Potential Applications
Stationary: Single Depth	• Long-term (several months to a year) recordings at a specific location • Compare sound levels and characteristics over time	• Further characterize the soundscape in DeSoto Canyon, which had lower sound levels recorded in the present study • Long-term baseline recordings within potential lease areas for offshore wind energy in the western GOM
Stationary: Multiple Depths in a Vertical Line	• Mid-term (weeks to months) recordings at multiple depths • Compare sound levels over time and between depths	• Localization ability for sound sources, such as vessel traffic • Validate sound propagation models and received sound levels within areas of interest
Mobile	• Potentially large spatial coverage over short-term (weeks) periods • Recordings throughout the water column and derived sound speed profiles	• Sample the soundscape within the western GOM, particularly within the call area for offshore wind energy, where there is currently a lack of data

Key: GOM = Gulf of Mexico.

6 Recommendations

Recommendations for continuing the monitoring in future years; expanding data collection, analyses, and interpretation beyond soundscape characterization; and advancing data analyses using the existing two-year dataset are presented in this section for BOEM's consideration.

6.1 Future Monitoring in the Northern Gulf of Mexico

Key lessons learned and recommendations from the monitoring and data analyses conducted under the GOM PAM Program are listed below; these could serve to guide planning for future monitoring and data analyses that may be conducted under this Program:

- The primary objective of the two-year data collection and monitoring was to characterize the existing soundscape (including sounds contributed by both natural and anthropogenic sources) in the GOM:
  - This two-year dataset will serve as an important reference point for similar monitoring conducted in the future. In future years, the Program could be expanded to cover other important objectives such as estimating marine mammal occupancy and (call) density, supporting estimation of impacts of anthropogenic sounds on marine mammals and other species of concern, and monitoring long-term trends in soundscapes and marine mammal density.

- The data collection and analysis experimental design provided an effective approach and framework for collecting and analyzing a robust dataset for soundscape characterization in the northern GOM:
  - The experimental design adopted for the two MPs can be used to guide continuation of monitoring in future years.

- A variety of stationary and mobile sensor types and platforms were deployed in this study that allowed a broad characterization of the ambient soundscape as well as detailed modeling of the temporal and spatial patterns of the anthrophony and biophony. The selected mix of monitoring platforms and sensors (RHs, EARS, SHRU, Seaglider) was well suited for collecting data to support the overall GOM PAM Program objectives:
  - It is recognized that it may not be feasible to deploy such a comprehensive suite of sensors in all future studies. Selection of the most appropriate type of monitoring platform will depend on the stated goals and objectives of the data collection and analyses. Benefits and potential applications of single and multiple stationary arrays of acoustic recorders and mobile platforms were summarized in **Table 15** to guide future study planning.

- An important legacy of this Program is the robust, two-year underwater acoustic dataset that was collected in the field within the delineated study areas:
  - For future years of monitoring, it is recommended that data collection be focused on the western portion of the northern GOM, and within the proposed offshore wind energy call area as a first priority and the DeSoto Canyon as a second priority.

- The multi-hydrophone SHRU VLAs provided a unique dataset that allows for analyses of parameters that cannot be evaluated using data from single hydrophone moorings. Because of schedule and resource constraints, only two stations could be monitored using the SHRU VLAs during each monitoring year of this study:

- o For future years of monitoring, additional locations should be considered for placement of SHRU VLA monitors.

- Use of a mobile platform was effective in ensuring that data were also collected between the stationary moorings, allowing for the soundscape in the entire study area to be adequately characterized:

  - o Use of one or more mobile platforms are recommended in future years in which sampling over a large area is of interest. Use of a multiple glider fleet could also be considered in future years to provide a large coverage area and data redundancy.

- The effective frequency range of the monitoring instrumentation (10 Hz to 96 kHz) was appropriate to encompass the most common anthropogenic and natural sounds likely to be encountered in the GOM:

  - o For future years of monitoring, it is recommended that a similar frequency range is used to encompass low- to high-frequency sounds for robust and useful comparison of spatial and temporal trends in the soundscape over the years.

- Monitoring under both MPs began in early summer (late April to early May). The power packs for the instrumentation used in the monitoring last approximately six months; therefore, the equipment needed to be serviced in late fall/early winter (around November), by which time weather and sea conditions had deteriorated in the GOM. Handling of heavy moorings, even from large vessels, is not recommended during rough seas to ensure personnel health and safety and to minimize equipment damage:

  - o For future years of monitoring, it is recommended that monitoring start no later than late March to early April so the six-month servicing can be completed before the end of October.

- To ensure personnel health and safety, mobile platforms are best deployed and retrieved from smaller fishing vessels. Typically, deployment and retrievals take no more than a one-day cruise:

  - o For future years, monitoring with mobile platforms should be avoided during the November to March timeframe, when conditions in the GOM are not conducive to operating at far offshore locations from smaller vessels.

- Notwithstanding all the preemptive measures that were implemented to avoid equipment and data loss, a few stationary platforms were either damaged or lost during the deployments. One SHRU VLA also suffered some data loss due to seawater seepage into the recorder casing:

  - o Mitigation plans, such as satellite trackers on sensors, together with redundancy (multiple units) should be used, when possible, to reduce the impact of any equipment or data loss on the project outcomes.

- Very little relevant data are currently available about ocean sound levels in the deeper waters of the central GOM and in the western portion of the northern GOM:

  - o Acoustic data collection in the ultra-deep areas of the northern GOM is strongly recommended for future years, especially as the industry is now operating farther offshore (e.g., Shell Oil's Stone Project). Once this area is commercially developed, the opportunity for measuring and determining a true natural acoustic baseline will be lost. Another priority area is the western GOM offshore of Texas and Louisiana, within the call area (and future lease areas) for offshore wind, to provide a baseline before construction.

- The northern GOM shallow-water soundscapes are extremely complex in nature and poorly understood. There is an urgent need to collect and analyze data in the shallow waters of the

GOM. However, expensive monitoring equipment cannot be deployed in shallow-water areas because these areas carry a high-risk for losing moorings due to heavy industrial, shipping, and fishing activities:

- o Risk-benefit analysis should be conducted if long-term monitoring of the shallow-water areas is a priority. Commercial, off-the-shelf, trawl-resistant housings are available. These could be outfitted with low-cost acoustic recorders (e.g., sound traps) for shallow water recording systems.

- Both MPs were focused on collecting and analyzing data to meet the stated Program objective, which was ambient soundscape characterization. Data analyses results indicated that the region is biologically active, and numerous marine mammal vocalizations also were recorded:

  - o During future phases of the GOM PAM Program, data from the two MPs may be further analyzed in detail to support other Program objectives such as estimating current marine mammal occupancy and (call) density in the study area; projecting potential impacts of anthropogenic sounds on marine mammals, fish, and other protected species; and developing long-term trends in the soundscape and marine mammal occurrence/density.

- Due to resource and field time limitations, a playback experiment could be conducted only under the 2018 MP, and it included transmitting signals at only four stations. Additionally, the SL had to be minimized so it could be considered de minimis to satisfy environmental compliance:

  - o During future program phases, more detailed and longer-duration playback experiments should be considered to determine sensor detection ranges and sound propagation, and to assist with localization of sounds. Use of a calibrated source can also assist in improving understanding of differences in levels recorded across different platforms.

- The 3D underwater sound propagation model was used during the planning phase to optimize selection of SHRU VLA stations by maximizing the hydrophone listening coverage. Results of the data analyses showed that presence of a 3D undersea environment (canyons and slopes) makes the acoustic propagation complex and challenging. To dissect the soundscape components for extracting environmental information or monitoring anthropogenic noise, sound propagation effects in the soundscape measurements must be removed. Without doing this, noise source signatures cannot be clearly observed, and the true soundscape environment information or anthropogenic noise level may be deviated by sound propagation effects, including multipath arrivals, focusing and defocusing, scattering, and sound signal phase dispersion:

  - o Incorporation of advanced 3D sound propagation modeling is recommended for future data analyses phases, particularly within complex topographic regions; this would provide valuable data to better understand and account for important acoustic effects. Model simulation output would help answer important questions such as "Do marine mammals preferentially occupy (in the sense of vocal activity) high TL (low intensity) regions to avoid potential anthropogenic sounds, such as masking?"

- Sensors often store data in different formats, some open and some proprietary. This may create some challenges in creating a cohesive public database for future researchers:

  - o Establishing a common, open format (e.g., FLAC) for all data submissions will make large data collections more accessible in the future.

- The magnitude of data collected during this Program required significant effort to prepare and format for archiving at NOAA's NCEI:

  - o In the future, incremental formatting and archiving of collected acoustic data with a repository, such as NCEI, would help to reduce some of the challenges associated with processing large volumes of data. This should be detailed within a Data Management

Plan, including required formats and methods of data transfer, although the challenge should be recognized that archiving practices and requirements for passive acoustic data continue to evolve over time. Assigning a Program Data Manager early in the process for multi-sensor and multi-institutional projects could also assist with data conformity and sharing.

6.2 Expanding Program Objectives

Since the primary Program objective was to collect data for underwater soundscape characterization, field data collection protocols (especially placement of recorders) were customized to collect data to meet the defined objective. However, if BOEM's overall goal is to generate comprehensive data that will be useful for managing present and future anthropogenic activities in the region, future Program initiatives should be expanded beyond soundscape characterization to also include collecting and analyzing data for the following purposes:

1. Evaluation of marine mammal vocalization data for characterizing spatial and temporal distribution of selected mammalian species and modeling spatial and temporal patterns of marine mammal acoustic activity and density estimations for selected species of interest.

2. Estimation of impacts of anthropogenic sounds on marine mammals and other species.

3. Monitoring long-term trends in soundscapes and marine mammal density.

Conceptual ideas for achieving these additional Program objectives are discussed below.

6.2.1 Program Objective 1: Characterize the spatial and temporal distribution (including density) of select marine mammal species

Marine mammals are common in the GOM and occupy a range of habitats, from shallow coastal waters to the deep abyssal plain. They also have a high potential for being negatively impacted by anthropogenic noise. Under this objective, the spatial and temporal distribution of marine mammals in the GOM will be further investigated in order to provide information about ecological areas of importance for these animals, and also to serve as a baseline metric to better understand potential changes in marine mammal distribution over time.

To address this objective, acoustic data previously collected under the 2018 and 2019 MPs could be further analyzed to characterize occurrence and distribution of select marine mammal species similar to previous acoustic studies conducted in the area (Li et al 2020, 2021). This could be accomplished by applying available automated species detection algorithms to the data where possible, as well as performing manual data processing and review where needed. Because of the potential influence of high levels of anthropogenic noise (e.g., vessel traffic) and biological masking noise (e.g., snapping shrimp), it is possible that conventional automated detectors for marine mammals will be ineffective or perform poorly on data obtained from shelf waters. In these cases, a manual approach will be necessary to identify periods of marine mammal presence. This manual analysis approach would involve trained analysts processing multi-band, long-term spectral averages and/or examine recordings individually, annotating the presence of all cetacean calls encountered.

The resulting detections would be plotted over multiple temporal scales (diel, lunar, seasonal) to characterize the existing trends in bio-acoustic activity at each monitored location. Information provided by these analyses would include, but is not limited to, time and date of detection, spatial location of the sensor that recorded the animal vocalization, identification of species/species groups where possible, and relative frequency of detections by species/species group and sensor location. Because of the

experimental design adopted for the 2018 and 2019 data collection efforts, these analyses would likely not provide precise animal locations or abundance/density of calling animals.

Suggested target species/species groups and associated sampling rates are as follows:

- Rice's whale (would require a 2 kHz sampling rate)
- Sperm whales (would require >20 kHz sampling rate)
- Pygmy and dwarf sperm whales (would require 384 kHz sampling rate)
- Beaked whales (>100 kHz sampling rate)
- Other large and small delphinids (>32 kHz sampling rate)
- Vocalizing fish species (would require a 2 kHz sampling rate)

Some delphinid species produce individually identifiable calls, known as signature whistles (Janik and Sayigh 2013; Bebus and Herzing 2015; Fearey et al. 2019). These can be used to determine the minimum number of individuals present and track those individuals through the time series of detections (Bailey et al. 2021). Such information can be valuable to identify how frequently individuals are detected as an indication of how resident or transient the animals are. It can also be used to determine expected exposure levels for individuals given how frequently they occur in an area and whether it is the exposed animals that return after a disturbance event, or whether it is naïve animals entering from outside the area affected.

In order to determine the actual locations of vocalizing marine mammals, and derive estimates of animal density (number of animals per unit area), the following sub-objectives could potentially be pursued as part of the follow-on monitoring program:

- Develop estimates of species-specific detection probabilities (as a function of range) for occupancy and call density estimation. Call density estimation is based on the detection of animal calls, not individual animals, because animals can be present but not calling.
- Describe spatial and temporal trends in occupancy and call density.
- Develop estimates of call production rates1 necessary to convert call density into animal density and abundance.
- Construct species-specific spatio-temporal habitat models that explain patterns in species density as a function of environmental covariates.
- Develop empirical or model-based spatial maps of animal densities for different areas of the northern GOM.
- Combine call density measurements with call production rates to calculate species-specific density and abundance estimates.

Regarding survey design, it will be necessary to specify the spatial and temporal resolution at which abundance and density estimates are required before a design can be finalized. For example, fixed sensors will be preferable if the main objective is to assess temporal trends, although mobile sensors might be ideal if spatial coverage is key. An ideal design might in fact be comprised of a combination of sensors. Finally, drifting sensors are also a possibility.

If there is a desire to obtain spatially explicit density surface models for some species, then the best option may be a network of sensors spaced over the entire area of interest in a systematic manner. Many aspects will have to be considered, in particular the spatial coverage of a given sensor, which influences the probability of detection of a sound by a sensor. As noted above, if some sensors provide the ability to locate animals this task is considerably simplified using distance sampling methods or their

modifications; if not, methods that by-pass location might be considered (e.g., spatially explicit capture-recapture, SECR).

It is unlikely that a single design will allow collection of reliable data in an optimal way for multiple species. Hence hybrid designs, in which different nodes might occur at different scale grids, should be considered. In particular, a sensible multi-purpose design might be achieved essentially with overlapping designs, where a small number of sensors, perhaps more expensive but capable of providing localization of close-range sounds, are placed within a network of coarser but cheaper sensors which essentially collect information on spatial distribution (**Figure 55**). Additionally, these could potentially allow for matching of sounds which can travel larger distances, allowing the estimation of animal density using SECR approaches (e.g., Martin et al. 2012). Smaller scale experiments might be conducted using additional sensors and gliders/drifting buoys.

6.2.2 Program Objective 2: Support the Estimation of Impacts of Anthropogenic Sounds on Marine Mammal and Other Species

Determining the effects of anthropogenic sounds on marine mammals is a complex task requiring multifaceted information about the occurrence, distribution, ecology, behavior, and hearing sensitivities of target species, as well as knowledge about the anthropogenic sounds involved, how the sound propagates through the environment, and the RLs. It is important at the outset to identify the time scales of interest, i.e., long-term changes in population densities, medium-term changes in local densities associated with sounds over the period of days, associated with animals leaving an area, or short-term acoustic or other behavioral response over the period of seconds or minutes. It is also important to distinguish between inferences that can be obtained from controlled experimental and observational studies. Broadly, observational studies can identify correlation, but not causation.

With these challenges in mind, data collected under the GOM PAM Program could be used to inform studies of behavioral impacts on marine mammals. For example, the GOM PAM Program effort will produce data that will be used to build time series and 3D sound propagation models, which could help inform anticipated predictive studies of anthropogenic impacts on marine mammals. The 3D variation in bathymetry creates focusing and defocusing regions, which can correlate with animal behavior.
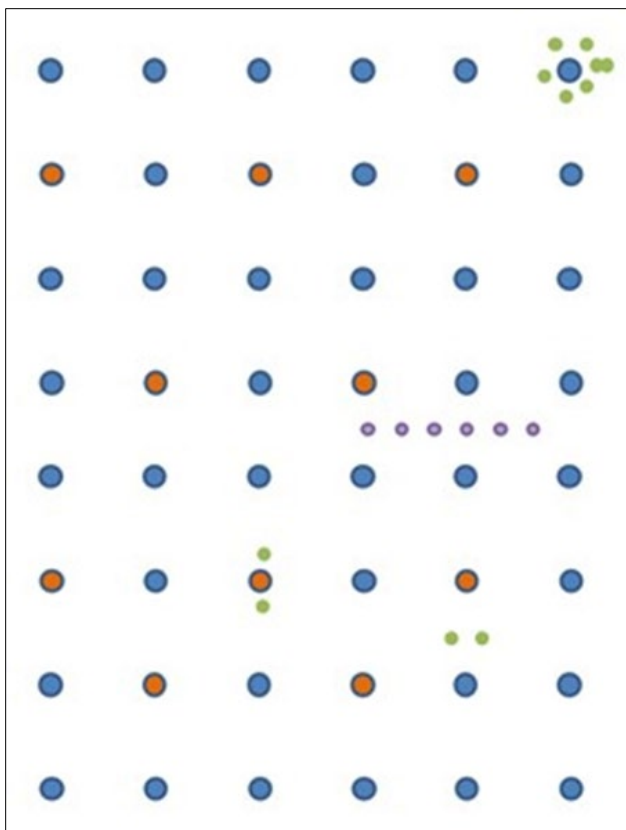
Figure 55. An example of a hybrid design with different sensor types.

Note: Hypothetically, blue sensors would be standard sensor nodes, orange would represent ranging capable sensors, while green sensors might be redundant or dedicated to small scale studies/experiments, and purple sensors might be involved in specific sound propagation experiments/calibrations.

The collected information on ambient sound levels is also important for determining when a sound source will no longer be distinguishable above the background noise level as this will occur at shorter ranges when the ambient levels are inherently noisy.

Future studies could focus on collecting data on specific variables of interest in impact studies (e.g., sound intensity in a band of interest, or occurrence of target species, or density), as well as leveraging previously collected data where possible. Regarding study design, large-scale observational studies of population change could leverage existing designs that capture both sound levels of potential stressors and animal acoustic activity. Another approach would be to design dedicated smaller scale experiments aimed to answer questions about animals' reactions to specific sound sources, such as seismic surveys.

6.2.3 Program Objective 3: Monitor Long-term Trends in Soundscapes and Marine Mammal Density

Objective 3 focuses on characterizing long-term (multi-year) temporal trends in the phenomena being studied, namely soundscape and animal density. To meet this objective, information obtained through Objectives 1 and 2 can be integrated to develop an advanced understanding of how changes in marine mammal density correlate with changes in the anthropogenic sound field they experience. Data will be collected over a multi-year time frame, possibly adjusting spatial and or temporal coverage depending on the spatial and temporal precision required in trend estimation. Specific sub-objectives may include the following:

- Statistically evaluate the feasibility of reducing the number of sensors required for continued monitoring in follow-on years to capture changes in soundscape and marine mammal density.

- Statistically evaluate whether natural temporal variations in soundscapes and marine mammal occurrence in the GOM will permit intermittent monitoring efforts to capture long-term trends, and if so, at what interval (e.g., 3, 5, 10 years?).

- Implement an adjusted sampling plan for long-term monitoring of soundscapes and marine mammal trends based on guidance from the findings of the first two sub-objectives.

- Estimate long-term trends in soundscape and marine mammal occurrence and density and how these vary over space.

It should be noted that the evaluation of trends over time is slightly more complex than joining a set of points in time, because there are different ways in which such point joining exercise could take place. The spatial-temporal models of variables of interest (be it soundscape, e.g., sound intensity in a band of interest, or occurrence of species, or density), will likely be an intrinsically statistical problem. An optimal survey design for obtaining a density in each time point might not be optimal to evaluate trend in said density over a longer time period. As an example, if evaluating trend over multiple years is key, then a fixed network of sensors over years would be preferable, but to get a mean density in each year, a rotating set of sensors providing wide spatial coverage might be optimal. With conflicting objectives, a design that represents a compromise between these might be required (e.g., a set of fixed locations for trend over time, and some rotating sensors / moving platforms to provide ample spatial coverage.

A wide variety of soundscape metrics have been developed, mostly for terrestrial systems, that provide information on the spatiotemporal patterns of biodiversity and environmental sounds (Pieretti and Danovaro 2020). These metrics have the advantage that they can provide a holistic and time efficient approach to synthesizing large acoustic data sets and providing a measure of biodiversity and anthropogenic activity that will complement ongoing species-specific detection studies. Metrics that identify the contribution of different components of the soundscape are also highly beneficial for ecosystem-based management. Depending on the environment, pre-processing of recordings and the application of some metrics, or weighted combinations of metrics, have proved more useful for indicating biological patterns and ecosystem changes (Parks et al. 2014; Towsey et al. 2014). These metrics could be applied and further refined to the collected acoustic data to determine if they perform better with adaptations that take into account the GOM's unique ambient soundscape.

6.3   Advancing the Modeling and Data Analyses

A robust dataset is now available from the two MPs. Due to time and resource constraints, only selected analyses were conducted under this study. Several different aspects of the soundscape could be further evaluated and explored using the available dataset, preferably supplemented with collection of some limited additional field data. For example, measurements and modeling of the GOM 3D soundscape could be advanced further as discussed below.

One of the distinct features revealed by the 3D acoustic propagation modeling study conducted under this Program is the non-negligible seasonal variability of the 3D soundscape. This outcome warrants further assessment for the purpose of generating a soundscape metric that can be referenced to characterize ambient sound signatures and their temporal variability. Advanced modeling study and data analyses are suggested, along with inter-seasonal sound transmission experiments.

A necessary feature of a regional environment soundscape metric is a relative stability over some specified time interval. Stability in the soundscape can be represented by a constraint on the allowed noise coherence variability. This is a desirable trait as it allows a single metric to be used over a longer period

of time, reducing the need to continuously update 3D acoustic propagation models, and locking in ambient sound signatures that can be further ping-pointed, investigated, and explored to characterize the surrounding environments for shipping density, oil and gas exploration and extraction activities, marine mammal habitats, and other activities. To demonstrate the seasonal variability of the GOM soundscape, a seasonal mean of the noise coherence model at 25 and 55 Hz is displayed in **Figures 56** and **57**, respectively.

The noise coherence can range from -1 to +1, so a seasonal dispersion of 0.25, as apparent in **Figure 56** panel (D) during winter at 25 Hz, is significant, and the dispersion displayed at 55 Hz (**Figure 57**) is even more so. Of importance is that the LF displays smaller dispersion when compared to the HF. This suggests that the temporal variability of the soundscape is frequency-dependent, with LFs remaining stable over longer time frames. Additionally, the range of dispersion over the computational environment suggests that certain spatial locations are "acoustic hot spots," which are also sensitive to source frequency and require more frequent updates to the underlying soundscape metric.

Further development of the modeling effort could be supported by more ocean temperature and salinity data, which would allow a finer handling of the temporal variability study of the soundscape metric. Besides that, the collected PAM data under this Program can be further analyzed to study variability in different time scales shorter than seasons and most importantly to reconstruct the 3D soundscape "fingerprint." It is also suggested to use playback transmission experiments with controlled sources to validate 3D sound propagation models and PAM techniques for environmental characterization, especially passive acoustic localization of marine mammals.

To summarize, three main pathways to improvement of the 3D soundscape study in the GOM are immediately identifiable:

- **Advanced data analyses and modeling study of identifying time intervals of soundscape stability at varying source frequencies:** Currently, it is evident that a season defined by roughly three calendar months is too long to capture a stable soundscape. It is also evident that the duration of soundscape stability varies with source frequency. Additionally, it is recommended to increase environmental data resolution for the acoustic modeling. Currently, a single vertical mean sound speed profile is translated horizontally across the entire computational domain, therefore placing all range variability in the bathymetry.

- **Identification of ship signatures in the PAM data by cross-referencing AIS data to create a library of ship signatures:** This library would map ship signals with known ship locations and would provide the opportunity to incorporate machine learning techniques to train a system for identifying ship location from new signals. This method will benefit greatly from the first bullet above, which can provide appropriate constraints to apply on selecting proper training data to avoid identification errors due to the time-dependent nature of the ocean state and consequently any received ship noise.

Playback transmission experiments with controlled sources: A short playback experiment was conducted during the 2018 MP, which provided critical TL data for the 3D modeling. Additional playback experiments could be conducted to generate high-resolution TL maps, complementing the soundscape coherence maps. Four playback experiments per year (one in each season) are recommended to capture seasonal as well as annual variability. To capture temporal variability in a shorter time scale, each of these four playback experiments should last for a few weeks.
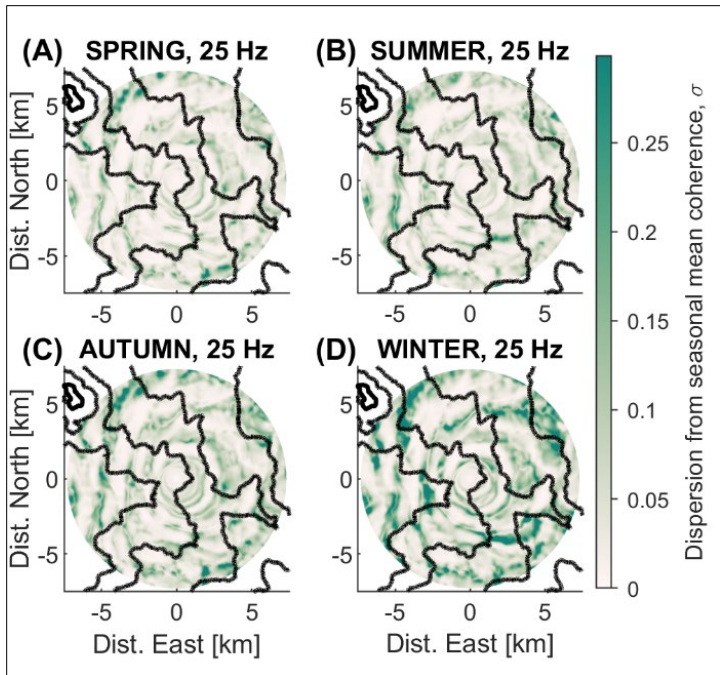
Figure 56: Seasonal variability at 25 Hz.

Note: The standard deviation of the noise coherence at each spatial location is plotted for four 3-month periods.
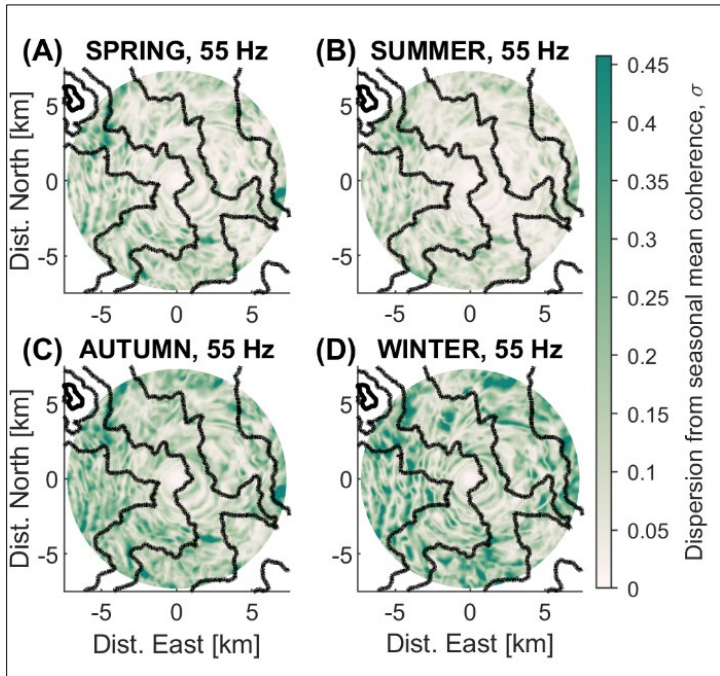
Figure 57: Seasonal variability at 55 Hz.

Note: The standard deviation of the noise coherence at each spatial location is plotted for four 3-month periods.

7 References

Ackleh AS, Ioup GE, Ioup JW, Ma B, Newcomb JJ, Pal N, Sidorosvkaia N, Tiemann C. 2012. Assessing the Deepwater Horizon oil spill impact on marine mammal population through acoustics: endangered sperm whales. J Acoust Soc Am. 131(3):2306–2314. doi: 10.1121/1.3682042.

Ainslie MA, Miksis-Olds JL, Martin B, Heaney K, de Jong CAF, von Benda-Beckman AM, Lyons AP. 2017. ADEON soundscape and modelling metadata standard. Version 2.0 DRAFT. Durham (NH): University of New Hampshire. 41 p. Technical report by TNO for ADEON Prime Contract No. M16PC00003.

Amaral J, Vigness-Raposa K, Miller JH, Potty GR, Newhall A, Lin Y-T. 2020. The underwater sound from offshore wind farms. Acoust Today. 16:13–21.

[ANSI] American National Standards, Inc. 1994. Procedures for outdoor measurement of sound pressure level. New York (NY): Acoustical Society of America. 34 p. ANSI S12.18:1994.

Ballard MS, Goldsberry BM, Isakson MJ. 2015. Normal mode analysis of three-dimensional propagation over a small-slope cosine shaped hill. J Comput Acoust. 23:1550005. doi: 10.1142/s0218396x15500058.

Bailey H, Senior B, Simmons D, Rusin J, Picken G, Thompson PM. 2010. Assessing underwater noise levels during pile-driving at an offshore windfarm and its potential impact on marine mammals. Mar Pollut Bull. 60:888–897.

Bailey H, Brookes KL, Thompson PM. 2014. Assessing environmental impacts of offshore wind farms: lessons learned and recommendations for the future. Aquat Biosyst. 10:8.

Bailey H, Fandel AD, Silva K, Gryzb E, McDonald E, Hoover AL, Ogburn MB, Rice AN. 2021. Identifying and predicting occurrence and abundance of a vocal animal species based on individually specific calls. Ecosphere 12:e03685.

Bassett C, Polagye B, Holt MM, Thomson J. 2012. A vessel noise budget for Admiralty Inlet, Puget Sound, Washington (USA). J Acoust Soc Am. 132(6):3706–3719.

Bebus, SE, Herzing, DL. 2015. Mother-offspring signature whistle similarity and patterns of association in Atlantic spotted dolphins (*Stenella frontalis*). Anim Behav Cognit. 2:71–87.

Betke K, Folegot T, Matuschek R, Pajala J, Persson L, Tegowski J, Tougaard J, Wahlberg M. 2015. BIAS standards for signal processing: aims, processes and recommendations. Amended version. 2015. Verfuß, UK, Sigray P, Editors. Sweden: Baltic Sea Information on the Acoustic Soundscape. 28 p. accessed July 2017.

[BOEM] Bureau of Ocean Energy Management. 2013. GOM OCS oil and gas lease sales: 2014 and 2016; eastern planning area lease sales 225 and 226—final environmental impact statement. Volume I: chapters 1–8. New Orleans (LA): Bureau of Ocean Energy Management, GOM Region. 710 p. OCS EIS/EA BOEM 2013-200. https://www.boem.gov/sites/default/files/boem-newsroom/Library/Publications/2013/BOEM-2013-200-v1.pdf.

Boyd AD, Gowans S, Mann DA, Simard P. 2021. Tropical storm Debby: soundscape and fish sound production in Tampa Bay and the Gulf of Mexico. PLOS ONE 16:e0254614.

Bradley DL, Stern R. 2008. Underwater sound and the marine mammal acoustic environment: A guide to fundamental principles. Bethesda (MD): Marine Mammal Commission.

Calupca TA, Fristrup KM, Clark CW. 2000. A compact digital recording system for autonomous bioacoustic monitoring. J Acoust Soc Am. 108(5):2582. doi: 10.1121/1.474359.

Christensen MG, Jakobsson A. 2009. Multi-pitch estimation. In: Juang BH, editor. Synthesis lectures on speech and audio processing. https://doi.org/10.2200/s00178ed1v01y200903sap005.

Dahl PH, Miller JH, Cato DH, Andrew RK. 2007. Underwater ambient noise. Acoust Today 3:23–33.

DeCourcy BY, Lin Y-T. Data Forthcoming. Spatial and temporal variation of three-dimensional ship noise coherence in a submarine canyon. J Acoust Soc Am.

Discovery of the Sound in the Sea. 2022. Manatee. Discovery of the Sound in the Sea (DOSITS) [accessed 28 January 2022]. https://dosits.org/galleries/audio-gallery/marine-mammals/sirenians/manatee/.

Duarte CM, Chapuis L, Collin SP, Costa DP, Devassy RP, Eguiluz VM, Juanes F. 2021. The soundscape of the Anthropocene ocean. Science 371(6529). doi: 10.1126/science.aba4658.

Duda TF, Lin Y-T, Reeder DB. 2011. Observationally constrained modelling of sound in curved ocean internal waves: examination of deep ducting and surface ducting at short range. J Acoust Soc Am. 130(3):1173–1187. doi: 10.1121/1.3605565.

Dugan, PJ, Klinck, H, Roche, MA, Helble, TA. 2016. RAVEN X High Performance Data Mining Toolbox for Bioacoustic Data Analysis. rXiv preprint arXiv:1610.03772

Estabrook BJ, Ponirakis, DW, Clark, CW, Rice, AN. 2016. Widespread spatial and temporal extent of anthropogenic noise across the northeastern GOM shelf ecosystem. Endanger Species Res. 30:267–282. doi:10.3354/esr00743.

Fearey J, Elwen SH, James BS, Gridley T. 2019. Identification of potential signature whistles from free-ranging common dolphins (*Delphinus delphis*) in South Africa. Anim Cognit. 22:777–789.

Fulling GL, Mullin KD, Hubard CW. 2003. Abundance and distribution of cetaceans in outer continental shelf waters of the U.S. Gulf of Mexico. Fish Bull. 101:923–932.

Gisiner RC. 2016. Sound and marine seismic surveys. Acoust Today. 12:10–18.

Greene CR, Richardson WJ. 1988. Characteristics of marine seismic survey sounds in the Beaufort Sea. J Acoust Soc Am. 83:2246.

Guerra M, Thode AM, Blackwell SB, Macrander AM. 2011. Quantifying seismic survey reverberation off the Alaskan North Slope. J Acoust Soc Am. 130(5):3046–3058.

Hastie G, Merchant ND, Götz T, Russell DJF, Thompson P, Janik VM. 2019. Effects of impulsive noise on marine mammals: investigating range-dependent risk. Ecol Appl. 29:e01906.

Hayes SA, Josephson E, Maze-Foley K, Rosel PE, Turek J. 2021. U.S. Atlantic and Gulf of Mexico marine mammal stock assessments - 2020. Washington DC: U.S. Department of Commerce. 403 p. NOAA Tech Memo NMFS-NE 271.

Heaney KD, Campbell RL. 2016. Three-dimensional parabolic equation modelling of mesoscale eddy deflection. J Acoust Soc Am. 139(2):918–926. doi: 10.1121/1.4942112.

Hildebrand JA. 2009. Anthropogenic and natural sources of ambient noise in the ocean. Mar Ecol Prog Ser. 395:5–20.

Janik VM, Sayigh LS. 2013. Communication in bottlenose dolphins: 50 years of signature whistle research. J Compar Physiol A. 199:479–489.

Johnson M, Madsen PT, Zimmer WMX, Aguilar de Soto N, Tyack PL. 2006. Foraging Blainville's beaked whales (*Mesoplodon densirostris*) produce distinct click types matched to different phases of echolocation. J Exp Biol. 209(Pt 24):5038–5050.

Klinck H, Nieukirk SL, Mellinger DK, Klinck K, Matsumoto H, Dziak RP. 2012. Seasonal presence of cetaceans and ambient noise levels in polar waters of the North Atlantic. J Acoust Soc Am. 132(3):EL176.

Kearns & West. 2015. Synthesis report: stakeholder webinars to inform development of a monitoring plan for marine mammals in the Gulf of Mexico. Washington (DC): Bureau of Ocean Energy Management (BOEM). 24 p. https://www.boem.gov/Synthesis-Report-Stakeholder-Webinars/.

Li K, Sidorovskaia NA, Guilment T, Tiemann CO. 2021. Decadal assessment of sperm whale site-specific abundance trends in the Northern Gulf of Mexico using passive acoustic data. J Mar Sci Eng. 9(5):454. https://doi.org.10.3390/jmse9050454.

Li K, Sidorovskaia NA, Guilment T, Tiemann CO. 2020. Model-based unsupervised clustering for distinguishing Cuvier's and Gervais' beaked whales in acoustic data. Ecol Inf. 58:101094. https://doi.org.10.1016/jecoinf.2020.101094. Accessed May 2019.

Latusek-Nabholz JN, Whitt AD, Fertl D, Gallien DR, Ampela K, Khan AA, Sidorovskaia N. 2020. Literature synthesis on passive acoustic monitoring projects and sound sources in the Gulf of Mexico. New Orleans (LA): US Department of the Interior, Bureau of Ocean Energy Management. Contract No.: M17PC00001. OCS Study BOEM 2020-009. 99 p.

McDonald MA, Hildebrand JA, Wiggins SM. 2006. Increases in deep ocean ambient noise in the Northeast Pacific west of San Nicholas Island, California. J Acoust Soc Am. 120(2):711–718.

National Research Council. 2003. Wenz curves describing pressure spectral density levels of marine ambient noise from weather, wind, geologic activity, and commercial shipping in ocean noise and marine mammals. In: Ocean noise and marine mammals: committee on potential impacts of ambient noise in the ocean on marine mammals. Washington (DC): The National Academies Press. p. 195. https://doi.org/10.17226/10564

Newcomb J, Fisher R, Field R, Rayborn G, Kuczaj S, Ioup G, Ioup J, Turgut A. 2002. Measurements of ambient noise and sperm whale vocalizations in the northern Gulf of Mexico using near bottom hydrophones. OCEANS'02 MTS/IEEE 3:1365–1371.

Merchant ND, Barton TR, Thompson PM, Pirotta E, Dakin DT, Dorocicz J. 2013. Spectral probability density as a tool for marine ambient noise analysis. Proc Meetings Acoust. 19:010049. doi:10.1121/1.4799210.

Nieukirk SL, Mellinger DK, Moore SE, Klinck K, Dziak RP, Goslin J. 2012. Sounds from airguns and fin whales recorded in the mid-Atlantic Ocean, 1999–2009. J Acoust Soc Am. 131(2):1102–1112.

[NMFS] National Marine Fisheries Service. 2016. Technical guidance for assessing the effects of anthropogenic sound on marine mammal hearing: underwater acoustic thresholds for onset of permanent and temporary threshold shifts. Silver Spring (MD): National Marine Fisheries Service, Office of Protected Resources. 189 p. NOAA Tech Memo NMFS-OPR-55.

[NMFS] National Marine Fisheries Service. 2018. 2018 revisions to: Technical guidance for assessing the effects of anthropogenic sound on marine mammal hearing (Version 2.0): underwater thresholds for onset of permanent and temporary threshold shifts. Silver Spring (MD): National Marine Fisheries Service. 167 pp. NOAA Tech Memo NMFS-OPR-59.

[NOAA Fisheries] National Oceanic and Atmospheric Administration Fisheries. 2022. Rice's whales. https://www.fisheries.noaa.gov/species/rices-whale. Accessed February 2022.

Oliveira TCA, Lin Y-T. 2019. Three-dimensional global scale underwater sound modelling: the T-phase wave propagation of a Southern Mid-Atlantic Ridge earthquake. J Acoust Soc Am. 146(3):2124–2135. doi: 10.1121/1.5126010.

Oliveira TCA, Lin Y-T, Porter MB. 2021. Underwater sound propagation modelling in a complex shallow water environment. Front Mar Sci. 8:751327. doi: 10.3389/fmars.2021.751327.

Parks SE, Miksis-Olds JL, Denes SL. 2014. Assessing marine ecosystem acoustic diversity across ocean basins. Ecol Inf. 21:81–88.

Pijanowski BC, Villanueva-Rivera LJ, Dumyahn SL, Farina A, Krause BL, Napoletano BM, Gage SH, Pieretti N. 2011. Soundscape ecology: the science of sound in the landscape. BioScience 61(3):203–216.

Pieretti N., Danovaro R. 2020. Acoustic indexes for marine biodiversity trends and ecosystem health. Philos Trans R Soc B 375:20190447.

Ponirakis DW, Dugan PJ, Zollweg JA, Porter MB, Clark CW. 2015. A Matlab based HPC toolset for noise analysis of large acoustic datasets. In: Proceedings of the 7th International Conference on Detection, Classification, Localization, and Density Estimation of Marine Mammals using Passive Acoustics, 2015 July 13–16, La Jolla, CA. San Diego (CA): Scripps Institution of Oceanography. page 85.

Popper A, Hawkins A, Fay R, Mann D, Bartol S, Carlson T, Coombs S, Ellison W, Gentry R, Halvorsen M, Løkkeborg S, Rogers P, Southall B, Zeddies D, Tavolga W. 2014. Sound exposure guidelines. In: Popper A, editor. Sound exposure guidelines for fishes and sea turtles: a technical report prepared by ANSI-accredited Standards Committee S3/Sc1 and registered with ANSI. New York (NY): Springer. p. 33-51. doi:10.1007/978-3-319-06659-2_7.

Reeder DB, Lin Y-T. 2019. 3D acoustic propagation through an estuarine salt wedge at low-to-mid-frequencies: modelling and measurement. J Acoust Soc Am. 146(3):1888–1902. doi: 10.1121/1.5125258.

Reilly SM, Potty GR, Thibaudeau D. 2016. Investigation of horizontal refraction on Florida Straits continental shelf using a three-dimensional Gaussian ray bundling model. J Acoust Soc Am. 140(3):EL269–EL273.

Rice AN, Tielens JT, Estabrook BJ, Muirhead CA, Rahaman A, Guerra M, Clark CW. 2014. Variation of ocean acoustic environments along the Western North Atlantic Coast: a case study in context of the right whale migration route. Ecol Inf. 21:89–99.

Rice AN, Palmer KJ, Tielens JT, Muirhead CA, Clark CW. 2014. Potential Bryde's whale (*Balaenoptera edeni*) calls recorded in the northern GOM. J Acoust Soc Am. 135(5):3066–3076.

Roberts JJ, Best BD, Mannocci L, Fujioka E, Halpin PN, Palka DL, Garrison LP, Mullin KD, Cole TVN, Khan CB, McLellan WA, Pabst DA, Lockhart GG. 2016. Habitat-based cetacean density models for the U.S. Atlantic and Gulf of Mexico. Sci Rep. 6:22615.

Roth EH, Hildebrand JA, Wiggins SM, Ross D. 2012. Underwater ambient noise on the Chukchi Sea continental slope from 2006–2009. J Acoust Soc Am. 131(1):104–110.

Scripps Whale Acoustic Laboratory. 2022. Scripps whale acoustic lab. San Diego (CA): Scripps Institute of Oceanography [accessed 28 January 2022]. https://www.cetus.ucsd.edu/.

Sidorovskaia NA, Li K. 2016. Decadal evolution of the northern GOM soundscapes. Proc Meet Acoust. 27(1):040014, doi: 10.1121/2.0000382.

Širović A, Bassett HR, Johnson SC, Wiggins SM, Hilderbrand JA. 2014. Bryde's whale calls recorded in the Gulf of Mexico. Mar Mamm Sci. 30(1):399–409.

Towsey M, Wimmer J, Williamson I, Roe P. 2014. The use of acoustic indices to determine avian species richness in audio-recordings of the environment. Ecol Inf. 21:110–119.

Urick RJ. 1984. Ambient noise in the sea. Washington (DC): Naval Sea Systems Command. 194 p.

Wall CC, Simard P, Lembke C, Mann DA. 2013. Large-scale passive acoustic monitoring of fish sound production on the West Florida Shelf. Mar Ecol Prog Ser. 484:173–188.

Warren VE, Marques TA, Harris D, Thomas L, Tyack PL, Aguilar de Soto N, Hickmott L, Johnson MP. 2017. Spatio-temporal variation in click production rates of beaked whales: Implications for passive acoustic density estimation. J Acoust Soc Am. 141(3):1962–1974.

Wenz GM. 1962. Acoustic ambient noise in the ocean: spectra and sources. J Acoust Soc Am. 34:1936–1956. doi: 10.1121/1.1909155

Wiggins SM, Hall JM, Thayre BJ, Hildebrand JA. 2016. GOM low-frequency ocean soundscape impacted by airguns. J Acoust Soc Am. 140(1):176–183. doi:10.1121/1.4955300.

Appendix A: Monitoring Instrument Specifications

Three different types of stationary moorings equipped with sensors (hydrophones) and recording systems were used for data collection, namely RHs, EARS, and SHRU VLAs. Additionally, two separate mobile autonomous platforms (Seaglider™) were also deployed within selected portions of the study area to collect data in between the stationary moorings. The different data recording systems differed in detail such as depth rating, battery capability, data storage capability, sampling rates and type of data stored. Between the different systems there is a trade-off between the schedule, power, and storage under similar conditions. There is also a trade-off between using stationary and mobile data collection platforms. Additional specifications for each instrument type are presented below.

A.1 Rockhoppers

RHs are a newer version of the bottom-mounted marine autonomous recording buoys developed in the late 1990s by the Center for Conservation Bioacoustics at the Cornell Laboratory of Ornithology (Calupca et al. 2000) (**Figure A-1**). The RHs deployed under the GOM PAM MPs are small and compact versions that are encased in a 17-inch glass sphere. They are capable of recording with a sampling rate as high as 384 kHz with 24-bit resolution, are depth rated to 3,500 m, and can be deployed from a research vessel with only a few people to handle equipment for each deployment.

The RHs had an effective recording bandwidth of 10 Hz to 75 kHz; the bandwidth was optimized for recording cetacean species that occur in the survey area. They were programmed to collect data continuously at a 197-kHz sampling rate and 24-bit resolution. The lower sampling rate also reduced battery power demand, therefore extending the deployment duration. The true dynamic range of the system at the 197-kHz sampling rate is approximately 17.5 bits (107 dB). The analog system sensitivity is shown in **Figure A-2**. The clipping level of the analog-to-digital converter is ± 5 Volts.

The electronic noise floor is illustrated in **Figure A-2**. All units were fully characterized before deployment. One representative RH hydrophone was sent to the Naval Undersea Warfare Center (NUWC), Rhode Island, for characterization at 3 degrees Celsius and 1,000 pounds per square inch (psi) pressure. The sensitivity curve provided by NUWC for this hydrophone was universally applied to all units (see **Section 2.6** for additional details on the calibration process).

The RHs were deployed on a short (approximately 10-m) mooring, which makes deployment and recovery easy. The hydrophone sits approximately 11 m above the seafloor and is separated from the glass sphere by approximately 20 centimeters to minimize acoustic interference. The overall buoyancy of the system is approximately +5 kilograms, which results (depending on oceanographic conditions) in ascent rates of approximately 1 m/second during recovery. Each RH is equipped with a pressure switch-enabled recovery system featuring a GPS/Iridium transmitter, a VHF radio transmitter, and a LED-flasher.
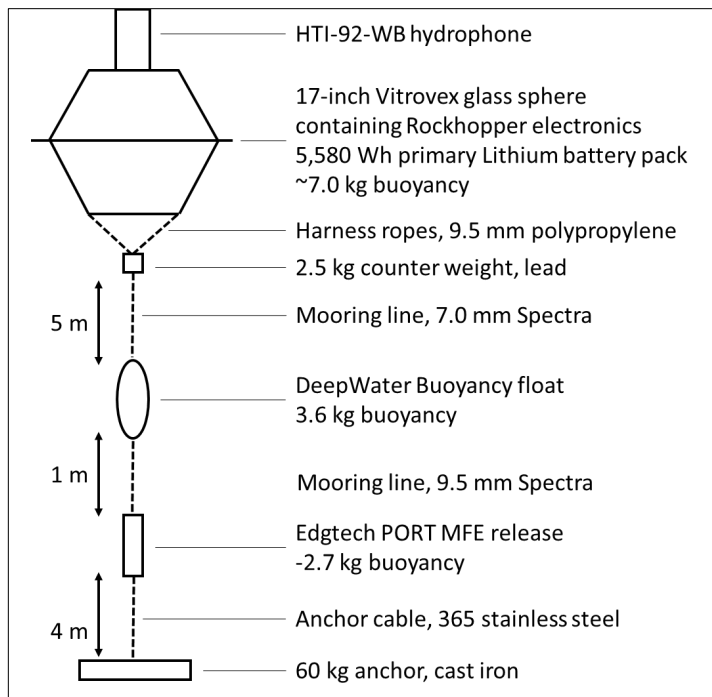
Figure A-1. RH mooring design and system components.

Note: Not to scale; all components are rated to 3,500 depth.

Key: kg=kilogram(s); mm=millimeter(s)
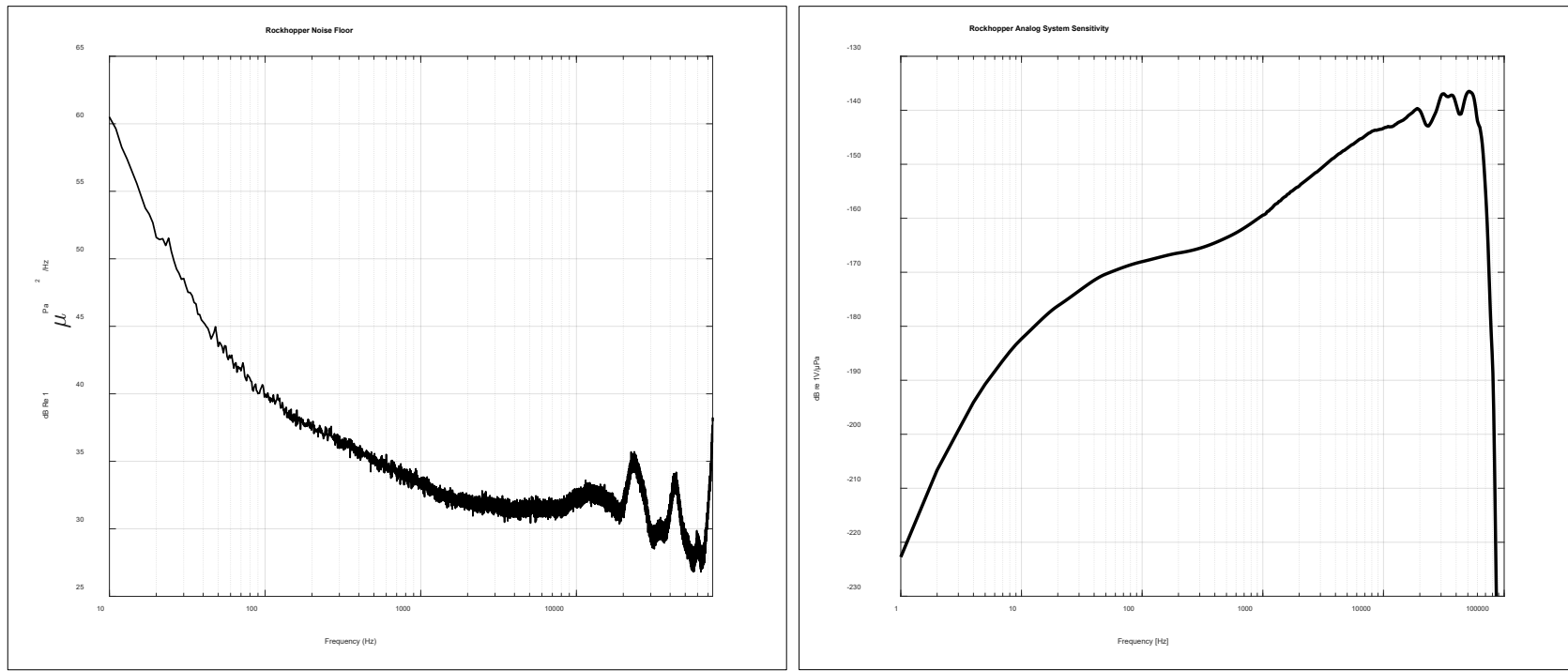
Figure A-2. Rockhopper (A) system noise floor (left) and (B) analog system sensitivity (right).

Note: At a sampling rate of 197 kHz, the corner frequency of the anti-aliasing filter is approximately 65 kHz resulting in a practical system sensitivity up to approximately 75 kHz.

A.2   EARS

EARS were developed by the U.S. Naval Oceanographic Office for ambient water column noise measurements. Past EARS deployments in the GOM (2001, 2002, 2007, 2010, 2015, and 2017) targeted monitoring of ambient noise soundscapes and deep-diving marine mammals (sperm whales, beaked whales, and deep-water dolphins) (Ackleh et al. 2012). They have also been used extensively by the Gulf Ecological Monitoring and Modeling Project, which the LADC has been implementing in the northern GOM between the Mississippi and DeSoto Canyons since 2015. The LADC is a consortium of research faculties that includes GOM PAM Program Team member University of Louisiana at Lafayette.

EARS are bottom-moored, recording systems (**Figure A-3**) and are depth-rated for use up to 6,000 m. All electronics and batteries are contained in an 8-inch-diameter by 24-inch-long pressure vessel. The battery pack consists of 124 alkaline D cells, which are preferred because of transportation safety issues and ease of disposal. The electronics are a low-power design (average power under 70 megawatts), providing extended recording durations with minimal battery requirements. Four 2.5-inch disk drives provide the recording capacity for the EARS. Recording is continuous, and all data are stored to magnetic disks for post-mission analysis. Use of four 2-TB disks allows continuous recording for up to eight months. Similar to the RHs, the EARS also have an effective recording bandwidth of 10 Hz to 96 kHz (192 kHz, 16-bit sampling) in a one-channel configuration.

The versions deployed under the 2018 MP consist of electronics and hydrophones mounted between a 500-kilogram anchor and 10 to 12 glass ball floats (**Figure A-3**). This configuration allows for the positioning of the recording system in free field to minimize unwanted interference from acoustic signals scattered from the mooring parts and bottom. An additional battery pack ensures six months of uninterrupted data recordings. Data are continuously recorded at a 192-kHz sampling rate. The data are stored as 16-bit integers in proprietary binary format. The recovery uses acoustic releases that detach from the anchor weight when a special acoustic message is received from a release communication transducer. The recording package then floats to the surface for recovery.

Before deployment, each EARS buoy was subjected to electronics and hard drive tests and internal clock synchronization with the GPS onboard the deployment vessel. The frequency response function of each EARS buoy was measured before deployment by inputting the set of sinusoidal signals of pre-defined frequencies (**Figure A-4**) into the recording system. The frequency response function is interpolated to a resolution of 1 Hz and used to calibrate the recorded signals during the data processing stage. As with RHs, one representative hydrophone was calibrated at the NUWC Rhode Island at 3 degrees Celsius and 1,000 psi pressure. The sensitivity curve provided by NUWC for this hydrophone was universally applied to all units. The calibration adjustments were made, and selective datasets were reprocessed (see **Section 2.6** for additional details on the calibration process).
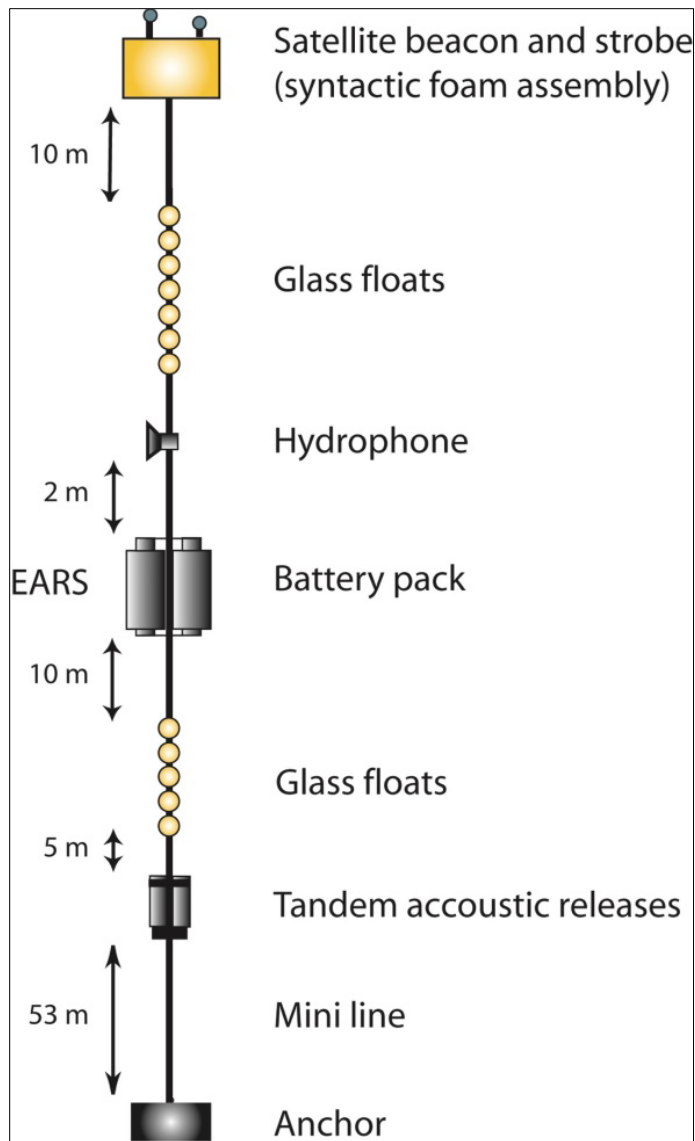
Figure A-3. EARS mooring design and system components.
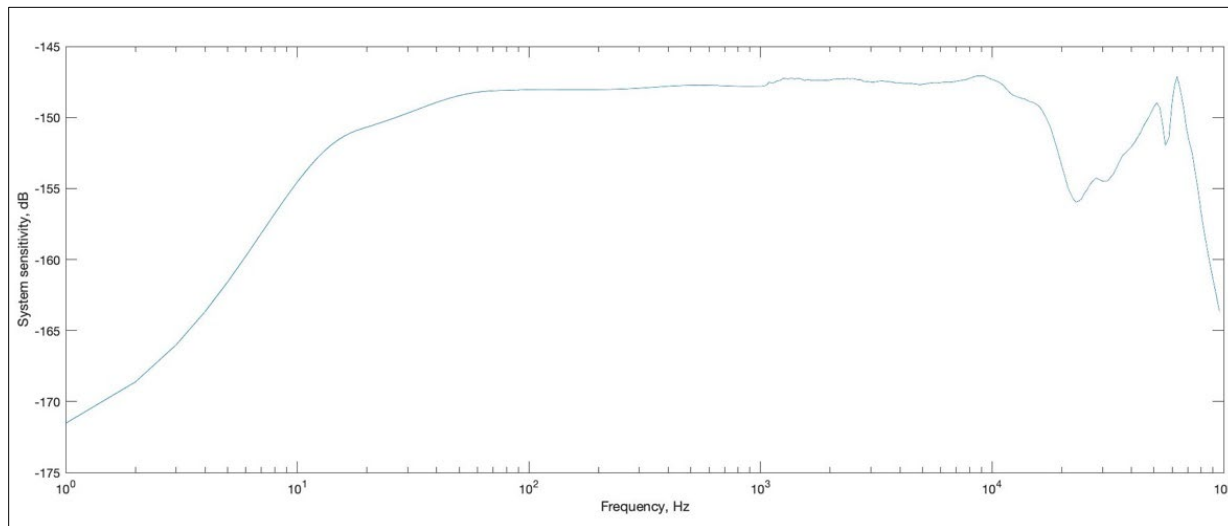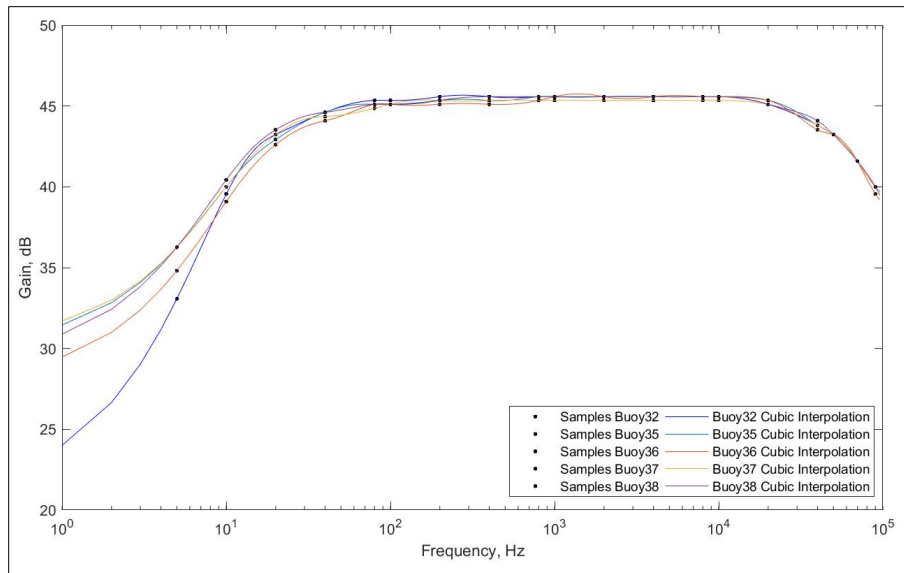
Figure A-4. An example of the EARS sensitivity curve used in the analysis.

Note: Black dots are measured data; the five curves are interpolated to 1-Hz resolution.

A.3   SHRU VLAs

SHRU VLAs have been developed by the Woods Hole Oceanographic Institution and have been successfully used for PAM at many different locations. These systems have unique, state-of-the-art technologic features to ensure the most robust and accurate passive acoustic measurements. First, the electronics utilize a CSAC for extreme timing precision, and the hydrophone mount uses a robust aluminum cage with flow shield and hairy fairing wire to minimize flow and strumming noise (**Figure A 5**).

For the 2018 MP, each SHRU VLA was equipped with four hydrophones, had a continuous duty cycle, and had a sampling rate of 9.8 kHz with 24-bit resolution. The monitoring band width was 10 Hz to 4.5 kHz. The four-element hydrophone array provided directional passive acoustic data as a function of arrival angles in vertical dimension. Two slightly differing mooring configurations were deployed: one on the Mississippi Canyon floor and the other on the slope (**Figures A-6 and A-7**). To improve the mooring stability within the canyon due to anticipated strong currents, the SHRU mooring was equipped with a large fluid-dynamic design buoy (StableMoor® Buoy) (**Figure A-8**). The hydrophone mounting design for both SHRU was intended to minimize flow and strumming noise. Besides hydrophones, the SHRU also recorded data from water temperature and pressure sensors.

After deployment, the SHRU VLA positions were surveyed to improve position accuracy using an acoustic triangulation method based on in-situ sound speed profile measurements and sound propagation modeling (**Figure A-9**). An acoustic transducer was deployed off the ship with a known position derived from the ship's GPS position. The transducer transmitted 12-kHz signals to communicate with the acoustic release at the bottom of the hydrophone moorings.

Figure A-5. A) CSAC-SHRU electronic board (A) and (B) Hydrophone cage with flow shield and hairy fairing wire (B).

Canyon Mooring M1

Gulf of Mexico Mooring As Deloyed

150 m Depth — Stable Moor with XEOS Kilo → Table A
(B) (H) — 2 m 1/2" Mooring Chain
— 3 m 1/2" Mooring Chain
(S)(B)(B) — 3 ton Swivel
— 20 m 1/4" Jac. Nil. Wirerope with Hairy Fairing
175 m (CTH) — Hydrophone Cage (s/n 238079) with Flow Shield → Table A
(CTH) — 24.5 m 1/4" Jac. Nil. Wirerope with Hairy Fairing
200 m (CTH) — Hydrophone Cage (s/n 238081) with Flow Shield → Table A
(CTH) — 24.5 m 1/4" Jac. Nil. Wirerope with Hairy Fairing
(CTH) —
225 m — Double SHRU on Strongback → Table A
(CTH) — 24.5 m 1/4" Jac. Nil. Wirerope with Hairy Fairing
250 m (CTH) — Hydrophone Cage (s/n 238084) with Flow Shield → Table A
(CTH) — 24.5 m 1/4" Jac. Nil. Wirerope with Hairy Fairing
275 m (CTH) — Hydrophone Cage (s/n 238077) with Flow Shield → Table A
(CTH) — 20 m 1/4" Jac. Nil. Wirerope with Hairy Fairing
(A) — 20 m 1/4" Jac. Nil. Wirerope with Hairy Fairing
(A) — 10 m 1/4" Jac. Nil. Wirerope with Hairy Fairing
(A) — 5 m 1/4" Jac. Nil. Wirerope with Hairy Fairing
(A) (A) (A) — 2 Sets of (4) 17" Glass Balls on 3/8" Mooring Chain
— 2 m 3/8" Mooring Chain
(B) — EdgeTech 8242 Acoustic Release → Table A
(B) — 3 m 3/8" Mooring Chain
(J) —
345 m Depth — 3000 lb Ww Mace Anchor

Table A
Instrument Depth and Marking

Instrument	Serial No.	Mount at
SBE-39	3120	150 m (Stablemoor)
Tpod	2297	150 m (Stablemoor)
SBE-39	3076	175 m (Cage)
Tpod	2298	200 m (Cage)
SBE-39	3124	225 m (Shru)
Tpod	2049	250 m (Cage)
SBE-39	3077	275 m (Cage)
Tpod	2085	345 m (Rlse)

(CTH) Clevis Fastener Hardware	Total Count
(1) 3/4"-10 x 3.5" Hex Head Bolt	(10)
(2) 3/4" Flat Washer	(20)
(1) 3/4" Lock Washer	(10)
(1) 3/4" 16 Hex Nut	(10)
(4) 5/8" Shackle Bushing	(40)

Hardware Designation

(A)	(2) 1/2" SH, (1) 5/8" SL
(B)	(1) 1/2" SH, (1) 5/8" SL, (1) 5/8" SH
(H)	(2) 5/8" SL, (1) 5/8" SH
(J)	(1) 1/2" SH, (1) 5/8" SL, (1) 7/8" SH
(S)	Swivel

Hardware Required
(per mooring without spares)

(18)	1/2" Anchor Shackle (SH)
(5)	5/8" Anchor Shackle (SH)
(1)	7/8" Anchor Shackle (SH)
(12)	5/8" Sling Link (SL)
(1)	3-Ton Swivel with Anode

Woods Hole Oceanographic Institution
designed by John Kemp, drawn by Jim Ryder
file: Gulf of Mexico   date: 03/15/2018

Figure A-6. Canyon SHRU mooring design (with StableMoor® buoy).

150 m Depth

48" Steel Sphere ← Table A

2 m 3/8" Mooring Chain

3 ton Swivel

20 m 1/4" Jac. Nil. Wirerope with Hairy Fairing

175 m

Hydrophone Cage (s/n 238082) with Flow Shield ← Table A

24.5 m 1/4" Jac. Nil. Wirerope with Hairy Fairing

200 m

Hydrophone Cage (s/n 238085) with Flow Shield ← Table A

24.5 m 1/4" Jac. Nil. Wirerope with Hairy Fairing

225 m

Double SHRU on Strongback ← Table A

24.5 m 1/4" Jac. Nil. Wirerope with Hairy Fairing

250 m

Hydrophone Cage (s/n 238078) with Flow Shield ← Table A

24.5 m 1/4" Jac. Nil. Wirerope with Hairy Fairing

275 m

Hydrophone Cage (s/n 238076) with Flow Shield ← Table A

20 m 1/4" Jac. Nil. Wirerope with Hairy Fairing

20 m 1/4" Jac. Nil. Wirerope with Hairy Fairing

18.2 m 1/4" Jac. Nil. Wirerope with Hairy Fairing

2 Sets of (4) 17" Glass Balls on 3/8" Mooring Chain

2 m 3/8" Mooring Chain

EdgeTech 8242 Acoustic Release ← Table A

2 m 3/8" Mooring Chain

3 m 3/8" Mooring Chain

350 m Depth

3000 lb Ww Mace Anchor

Gulf of Mexico Mooring
As Deployed

Slope Mooring M2

Table A		
Instrument Depth and Marking		
Instrument	Serial No.	Mount at
Tpod	2300	150 m (Sphere)
SBE-39	3078	175 m (Cage)
Tpod	2301	200 m (Cage)
SBE-39	3128	225 m (Shru)
Tpod	2302	250 m (Cage)
SBE-39	3123	275 m (Cage)
Tpod	2304	345 m (Rlse)

(CTH) Clevis Fastener Hardware	Total Count
(1) 3/4"-10 x 3.5" Hex Head Bolt	(10)
(2) 3/4" Flat Washer	(20)
(1) 3/4" Lock Washer	(10)
(1) 3/4" 16 Hex Nut	(10)
(4) 5/8" Shackle Bushing	(40)

Hardware Designation	
(A)	(2) 1/2" SH, (1) 5/8" SL
(B)	(1) 1/2" SH, (1) 5/8" SL, (1) 5/8" SH
(J)	(1) 1/2" SH, (1) 5/8" SL, (1) 7/8" SH
(S)	Swivel

Hardware Required (per mooring without spares)	
(18)	1/2" Anchor Shackle (SH)
(5)	5/8" Anchor Shackle (SH)
(1)	7/8" Anchor Shackle (SH)
(12)	5/8" Sling Link (SL)
(1)	3-Ton Swivel with Anode

Woods Hole Oceanographic Institution
designed by John Kemp, drawn by Jim Ryder
file: Gulf of Mexico   date: 03/15/2018

Figure A-7. Slope SHRU mooring design.

Figure A-8. Canyon SHRU StableMoor® buoy.

Figure A-9. Surveyed (triangulated) Canyon (left) and Slope (right) SHRU mooring positions.

A.4   Seaglider

The Seaglider is a mobile Autonomous Underwater Vehicle (**Figure A-10**) that moves through the water in a saw-tooth like pattern and surfaces every few hours. Navigation is accomplished using a combination of GPS fixes while on the surface, and internal sensors that monitor the vehicle heading, depth, and attitude during dives. Rather than an electrically driven propeller, the vehicle uses small changes in buoyancy and wings to achieve forward motion. The glider can travel approximately 20 km/day, and dive to 1,000 m. The unit also collects physical oceanographic data throughout the water column during each dive.
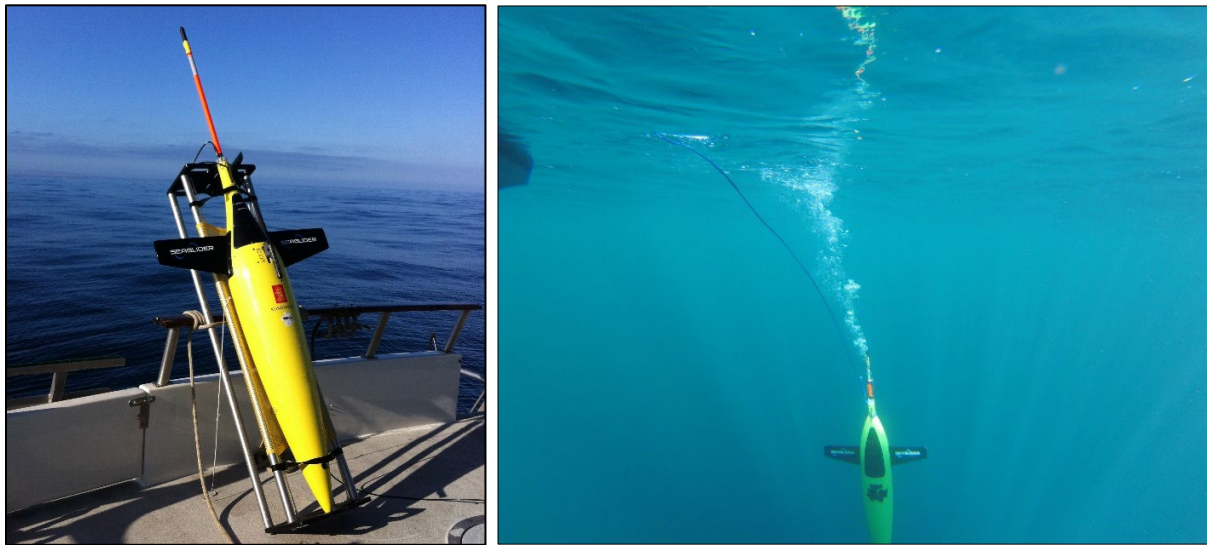
Figure A-10. Seaglider autonomous underwater vehicle.

A.4.1   2018 MP Seaglider

For the 2018 MP, a glider (SG639) was deployed in selected portions of the study area by the Cooperative Institute for Marine Resources Studies, Oregon State University. The unit is commercially available from Huntington Ingalls Industries/Technical Solutions, Lynnwood, Washington. It was outfitted with an acoustic recording system (Wideband Intelligent Signal Processor and Recorder available from Embedded Ocean Systems, Seattle, Washington), which was programmed to record sound continuously at all depths below 25 m, at a sampling rate of 125 kHz and a resolution of 16 bits, with sounds compressed for storage using the FLAC.

The recording system includes a "pre-whitening" filter to effectively capture ocean sounds without either clipping or hitting the noise floor (Christensen and Jakobsson 2009). Self-noise from glider operations that may be caused by pumping of the buoyancy bladder, movement of the ballast to steer and orient the glider, and so on, was removed using a table of all glider roll, pitch, and buoyancy operations. Recordings that occurred within 10 seconds of any of these actions were removed before further processing of the acoustic data.

The system's pitch and roll are controlled using an adjustable ballast (the vehicle battery). Because the glider travels slowly, it does not generate much flow noise. This is especially important at low frequencies, where this noise is most prevalent and can be problematic.

A.4.2   2019 MP Seaglider

For the 2019 MP, another Seaglider was deployed in selected portions of the study area by the Ocean Engineering Department of the University of Rhode Island. The unit is commercially available from Huntington Ingalls Industries/Technical Solutions, Lynnwood, Washington. In addition to the standard conductivity, temperature and pressure sensors, it was equipped with the PAM MK II Observer System. The Observer is a mature stand-alone acoustic recording package developed by JASCO Applied Sciences and was adapted to integrate with the Seaglider platform. The Observer was programed to record sound continuously at a sampling rate of 128 kHz and resolution of 24 bits. The system boasts 4 terabytes of data storage, and data were stored at full resolution in 30-minute .WAV files onboard. Files were also later converted to FLAC.

A.5   Instrument Calibration

A.5.1   RHs and EARS Hydrophones

Using representative calibration data for testing and verifying functionality of hydrophones to be deployed in the field is a standard approach for underwater PAM projects. This approach also was adopted for the 2018 MP. It was assumed that all hydrophones acquired for data collection using the RH and EARS moorings would have the same or similar sensitivity curves. Therefore, one representative RH hydrophone (HTI-92WB) and one representative EARS hydrophone (HTI 97) were selected for calibration at NUWC in Newport, Rhode Island. The NUWC's Underwater Sound Reference Division serves as the equivalent to the National Institute of Standards and Technology in underwater acoustics. It provides the U.S. with a wide variety of underwater transducer standards just as the National Institute of Standards and Technology provides for other types of measurements.

Typical curves of receive sensitivity up to the first resonance and a beam pattern at a lower frequency for one plane for the HTI-92WB as well as beam patterns for both planes up to 23 kHz for the HTI-97 were provided by the hydrophone manufacturer. A few additional calibration steps were taken to ensure data quality. The rationale for these additional steps is described below.

Since the Program measures sound in three dimensions and requires accurate sensitivity measurements for the class of hydrophones being used over a wider range of frequencies (much wider than specified by the manufacturer), the Program Team needed to do a representative calibration supply for the unknown information. The manufacturer provides a sensitivity measurement (free field voltage sensitivity [FFVS]) that defines the sensitivity along the hydrophone's primary axis at a frequency below the first resonance peak. Hydrophone sensitivity is nearly flat over frequencies below the first resonance point. Generally, the hydrophone variation is less than +/- 1 dB from the manufacturer's listed sensitivity and is better.

Additionally, there are no hydrophones that are highly sensitive, omni-directional, and flat across the bandwidths desired and used recorded by RHs and EARS. The FFVS curves also provide information regarding how the hydrophone sensitivity rolls off at and well above resonance. Without knowledge of the direction from which sound arrives, the sensitivity of the hydrophone is only accurate up to the frequency where the beam pattern is omni-directional in three dimensions.

Calibration methods typically make measurements in two planes (X-Y and X-Z) to provide a general description of the beam patterns. Each planar measurement is done at a single frequency. Multiple beam pattern measurements are made at different frequencies to gain a better understanding of where omni-directionality begins to degrade. Hydrophone beam patterns are a function of geometry and construction. Theoretically, only the geometry matters but realistically, the construction degrades the performance. Typically, where the wires enter the hydrophone mold will be the first place the beam pattern starts to

degrade from omni-directional. Beam pattern measurements are limited by costs since they take significant time to make.

Additionally, hydrophones are affected as pressure is increased. Well-designed hydrophones like the HTI 92WB and HTI-97DA minimize these effects up to their rated pressures. As part of the additional calibration steps, EARS and RH hydrophones were also tested down to 1,000 psi to determine if there are any significant changes in sensitivity for these designs.

The following steps were undertaken as part of the calibration process:

1. Hydrophone sensitivity (FFVS) typically ranges from 3 Hz to 90 kHz (unamplified version of the hydrophone) at ambient pressure and 20 degrees Celsius. The hydrophone manufacturer had provided NUWC FFVS runs from 2 Hz to 25 kHz. During the calibration process, additional FFVS runs were conducted from 3 Hz to 90 kHz and up to 1,000 psi pressure (approximately 675-m depth).

2. For the HTI-97, X-Z and X-Y plane beam patterns—which included frequencies of 4 kHz, 8 kHz, 10 kHz, 15 kHz, and 23 kHz—were provided by the hydrophone manufacturer based on NUWC testing. Similar testing for the 40-, 60-, and 80-kHz frequencies were performed at the Naval Surface Warfare Center's Panama City calibration facility.

3. No beam pattern measurements were provided by the manufacturer for the HTI-92WB, and that testing could not be performed for all frequencies due to resource limitations. Therefore, X-Z plane measurements were performed at NUWC for the 5-, 10-, and 50-kHz frequencies, and X-Y beam pattern measurements were conducted for the 5- and 10-kHz frequencies.

Except for some military applications, it is standard practice in acoustic monitoring to use representative calibration data to calibrate sensors to be deployed in the field. Representative calibration curves were used to calibrate the hydrophone mounted on the deployed RHs and EARS moorings. Before each deployment of RHs, air tests were conducted in the laboratory to compare the outputs of hydrophones intended for deployment against the calibrated reference hydrophones to ensure that the sensitivities were close. For EARS, a tap test was performed in air to validate that the hydrophone and wiring were functional.

The EARS hydrophones also undergo a more elaborate QA/QC procedure that is performed every three to five years. Key steps in this process are summarized below:

1. Electronic noise analysis

a. A spectral noise analysis is performed in the laboratory using the standard EARS Graphic User Interface (GUI) program. The EARS assembly is powered on the bench using a battery, and the front-end of EARS is terminated with an equivalent impedance to the transducer. The EARS GUI provides the PSD of the resultant data sampled by the EARS electronics (**Figure A-11**).

b. The front-end preamp is terminated with an equivalent capacitance and sample data for approximately 10 to 20 minutes. The amplitude per square Hz is determined as the square root of the calculated PSD.
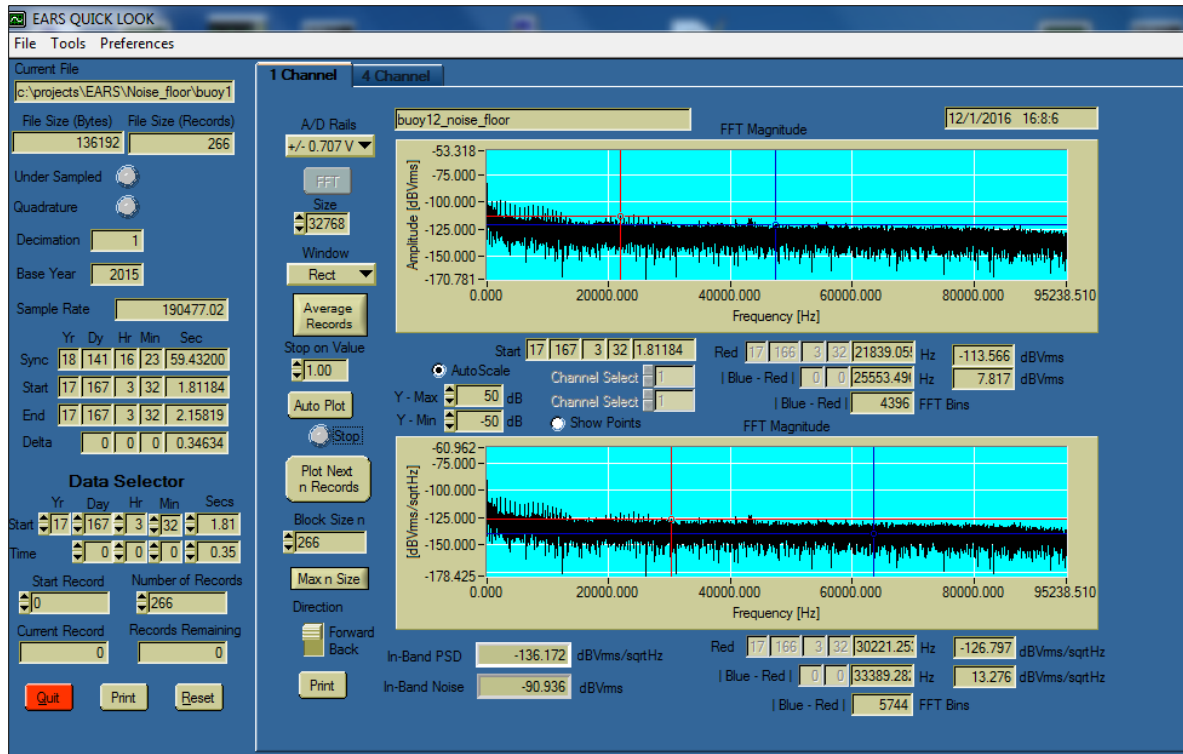
Figure A-11. EARS PSD plot from Bench Noise Test Buoy 12.

2. EARS Electronic Gain Measurement

A function generator is used to output a known amplitude tone (20 millivolts peak to peakmVp-p) at various frequencies (**Table A-1**). The EARS sampled amplitude is obtained using the EARS GUI program. The gain is computed from the ratio of the output to the input signal levels. Gain spot checks are run at select frequencies on all units before deployment to ensure gains are reasonable.

Table A-1. Amplitude tones and frequencies used for EARS electronic gain measurement

Frequency (Hz)	Output (mVp-p)	dB
5	800	32.04
10	1,800	39.08
20	2,800	42.92
40	3,500	44.86
80	3,700	45.34
100	3,700	45.34
200	3,800	45.34
400	3,800	45.58
800	3,800	45.58
1,000	3,800	45.58
2,000	3,800	45.58
4,000	3,800	45.58
8,000	3,700	45.34
10,000	3,700	45.34

144

Frequency (Hz)	Output (mVp-p)	dB
20,000	3,600	45.11
40,000	3,100	43.81
50,000	2,800	42.92
70,000	2,400	41.58
90,000	2,000	40.00

Key: dB = decibel(s); Hz = Hertz; mVp-p = millivolts peak to peak

3. **EARS Electronic Gain Measurement**

Hydrophone sensitivity is an important factor in the accuracy of SPLs. A hydrophone's sensitivity curve relates the measured SPL to the output voltage across the hydrophone's leads. The hydrophone's manufacturer will provide these measurements for the rated bandwidth of the hydrophone, which is generally the sensitivity of the hydrophone up to the maximum frequency that the hydrophone is omni-directional (near equal sensitivity from sound received from any direction).
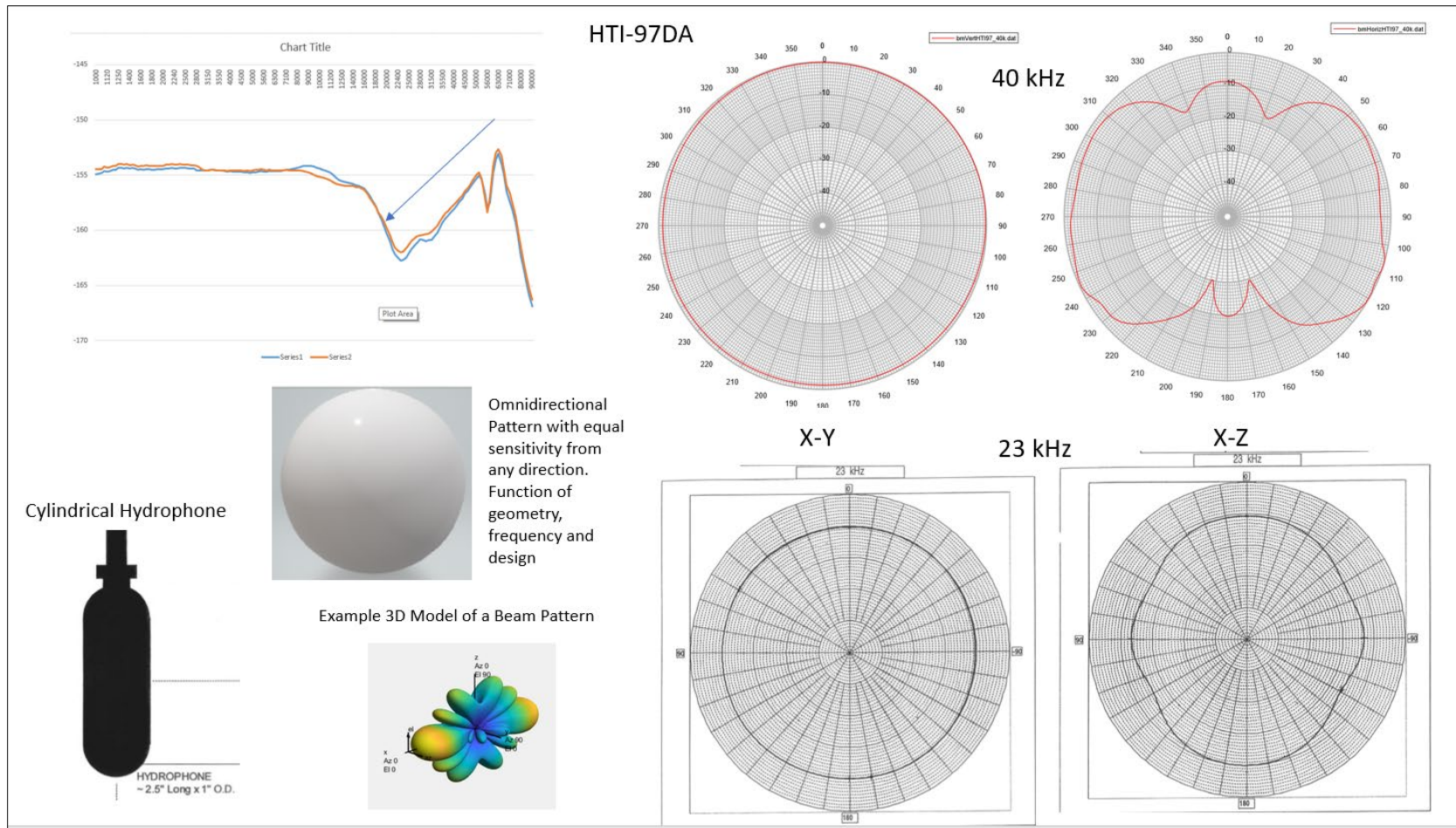
The omni-directionality of a hydrophone is a function of the hydrophone's geometry (e.g., cylindrical, spherical, circular), source wavelength (1/frequency) and to some extent the hydrophone construction. Manufacturers provide a hydrophone's sensitivity when purchased and generally have at least a sensitivity curve of a representative hydrophone. The single value of sensitivity provided by the manufacturer is the sensitivity of that hydrophone in the LF region (left side of the sensitivity curve).

Hydrophones typically have flat sensitivity curves in this region. As the wavelength of a sound wave approaches the geometric size (e.g., length, diameter, ceramic thickness) of the hydrophone's shape, the hydrophone beam pattern will begin to degrade from omni-directional. Once this happens, to report accurate sensitivities, the direction sound is received in relation to the hydrophone's orientation must be known. This requires a 3D array of hydrophones. A very small hydrophone will maintain omni-directionality over a broad bandwidth but will have very low sensitivity.

Selection of a hydrophone for an application is a tradeoff between bandwidth and sensitivity. The HTI-97DA was used for EARS for the soundscape work as it has reasonably good bandwidth and sensitivity. It was also rated for depths up to the required field measurements. It is omni-directional up to approximately 20 kHz (**Figure A-12**).

A calibration of sensitivity and beam pattern over a wide range of frequencies was performed to understand the hydrophone's performance. The manufacturer's measured sensitivities for each hydrophone used in the soundscape work all fell within a +/- 0.5 dB range of the manufacturer's quoted sensitivity (-193 dB re 1V/uPa). The sensitivity curve shown in **Figure A-12** (upper left corner) was the result of a representative HTI-97DA calibration at high (1,000 psi) and low pressure (50 psi). A 40-dB gain preamp was used in the calibration work.

The sensitivity of some hydrophones will change with pressure, and this sensitivity measurement was performed to ensure that the sensitivities of the HTI-97DA design did not change significantly with pressure since the field measurements were made up to approximately 1,200 m. The Program's calibration measurement was limited to 1,000 psi due to financial constraints. EARS uses the performance of the representative hydrophone for its performance measurements since it is too costly to perform detailed calibrations on all hydrophones used during the soundscape work.

Figure A-12. HTI-97A sensitivity and beam pattern.

A.5.2   SHRU

New hydrophones were acquired for SHRU VLAs from High Tech Inc.[20] Calibration specifications were provided by the manufacturer for the listening frequency range from 10 to 5,000 Hz for these sensors.

A.5.3   Seagliders

Calibration data for the hydrophone used on the Seagliders were also provided by the hydrophone manufacturer, High Tech Inc. Data were provided on hydrophone sensitivity (-164.5 dB re 1 V/μPa) and included a spectral sensitivity curve. Calibration data for the recorder system were provided by the manufacturer EOS, Inc. These data included specified pre-amplifier gain and spectrum and analong-to-digital sensitivity.

---

[20] http://www.hightechincusa.com/products/hydrophones/hti92wb.html

Appendix B: Monitoring Platform Deployment and Recovery Protocols

B.1 Field Deployment and Retrieval Protocols for Stationary Moorings

B.1.1 RHs and EARS Deployment

A similar process was followed for deployment of RHs and EARS. The EARS moorings are preassembled on deck (**Figure B-1**), which is staged with gear and sensors deployed from starboard to port, or right to left. All loads are secured and orderly handled over the side as they are deployed. No personnel are allowed to position themselves in the bight (anywhere inside the starboard glass balls and the anchor attached to the crane) as the potential exists to be snagged and pulled overboard.

Figure B-1. Shipboard deck set up for deployment of EARs.

The first "load" sent over the side is a series of glass balls, which are part of the top flotation device, until the tag point on the last yellow strap of the top set of glass balls. The top float is pushed over manually by a technician, and the remaining floats are helped along while one person operates the tag line. As the floats are deployed, the vessel is instructed to move forward at 2 knots via radio communications with the bridge. Note, on the R/V Pelican, the captain has the capability to steer the ship from the aft deck controls.

Once the top floats are in the water, the mooring's recording package is sent over the side, while a third person operates a second tag line on it. Once the mooring is tagged, the first tag line is released, and the assembly is allowed to slide (pulled by drag from the top floats in the water) into the water and is controlled by the second tag line.

The technician responsible for the first tag line moves to the third tag line at the rear end of the bottom float chain, and once secured, the second tag line is released. A fourth tag line is attached to the acoustic

releases, and the bottom floats are allowed to slide slowly into the water. Once tension is applied to the fourth tag line, the third tag line is released. The technician responsible for the fourth tag line then allows the releases to slide into the water.

A smaller line is wound onto the sea winch, and the load on the fourth tag line is transferred to the ship's sea winch. Once the sea winch has the tension, the ship is instructed to increase speed to 4 to 5 knots, and the ship's crew pays out line using the winch. It is critical to maintain tension on the mini line since slack may be sucked into the ship's propeller.

Once all the mini line is deployed, the load is transferred to the anchor, which is secured to the crane. The anchor chain is shackled to the mini line. The load from the sea winch is transferred to the crane (via the quick release), and the sea winch's wire line shackle is removed as tension is released. The crane then moves the weight overboard, and the quick release is used to drop the anchor.

B.1.2   RHs Retrieval

The RH unit, as retrieved, is composed of a glass sphere instrument housing and tether attached to an Edgetech acoustic release (Figure C-2). The total mass of the package is approximately 50 kilograms. The general process is as follows: arrive at station, interrogate, wait for signal/sighting, locate, and retrieve. The following stepwise process will be followed at each station:

- Upon reaching the station, the field technician is informed by the captain that the ship is on station and over the gear; permission to deploy transducer is obtained by the field technician.

- The Edgetech transducer is lowered into the water, and the captain is informed that gear is in the water.

- The RH mooring is interrogated by the Edgetech deck-box, confirming its presence and functionality.

- The Edgetech acoustic release command is sent, and time of response is recorded.

- The Edgetech transducer is removed from the water, and the captain is informed that all gear is out of the water.

- The ship remains on station while the requisite time is spent awaiting surfacing of the RH. Early estimates for time to surface at the deployed depth is 45 minutes.

- A visual, radio, and satellite/GPS watch is maintained during the recovery period.

- When the RH unit surfaces, a VHF radio signal at 154.585 megahertz is sent, a strobe is activated, and notification of its GPS location is transmitted via satellite.

- When a valid location, VHF signal, or visual sighting of the RH is obtained, the captain is informed and is directed by the field technician to the location of the surfaced equipment.

- The RH position is approached, and the ship is positioned alongside the unit, which is secured by a gaff and lifted aboard by the crew.

- The RH is then powered down for shipment back to Ithaca.

- No data manipulation, collection, or analysis is performed in situ.

Figure B-2. Left panel: RH in water (left) and Right panel: RH on deck (right).

B.1.3   EARS Retrieval

Recovery of the EARS moorings begins with establishing an initial vessel position based on wind and currents in the area to ensure the mooring does not rise up under the vessel. The Team generally stays up current of the mooring. In 2,000 m of water, the EARS mooring requires approximately ten minutes to break the surface and can move hundreds of meters during its ascent after release from the bottom. Once in position, communication is established with the mooring releases.

Before a release command, all hands will be on deck for visual location of the mooring when it surfaces. The release is only performed during daylight hours to ensure the mooring can be visually located even though there is a satellite location beacon and a strobe on the mooring. In addition, the Team maintains acoustic release ranging to monitor the mooring ascent to obtain an approximate range as the mooring nears the surface. Once the mooring is located, the ship transits close to the mooring from the downwind side (the ship moves faster than the mooring in wind) and backs towards the mooring.

The captain uses the aft vessel controls to easily and safely position the vessel close to the mooring. When close, a grapple is used to snag the mooring and pull it close to the vessel while the vessel secures the aft propellers. A line is then attached to one of the float straps, allowing the crane to lift the mooring onto the aft deck. This usually requires three lifts with the crane per mooring due to the length of the mooring. Once on-board, the EARS data recorder is removed from the mooring and safely secured for transportation. Typically, no data manipulation, collection, or analysis is performed *in-situ*. A refurbished recorder (tested and repowered) will then be inserted into the recovered mooring. The mooring is inspected, and all suspect components replaced to prepare the mooring for redeployment.

B.1.4   SHRU VLA Deployment

The SHRU mooring design includes vertical array moorings with a 3,000-pound anchor, acoustic release, and subsurface StableMoor® buoy (for the Canyon SHRU) or a 41-ft steel sphere (for the Slope SHRU) for flotation. The deployment protocol for the Canyon and Slope SHRU VLAs are similar with the subsurface steel ball first deployed off the aft of the research vessel as the vessel moves ahead at 1–2 knots.

The mooring is slowly paid out and various mooring attachments such as temperature sensors are strapped on. When the research vessel reaches the specified location for the mooring, the 3,000-pound anchor is lifted by the A-frame over the fantail. The anchor is held by the winch and a quick release. The captain notifies the deck that the position has been reached, the anchor is lowered until reaching the water surface, and the lead mooring technician activates the quick release. The anchor falls to the bottom and pulls the mooring to the bottom upright.

B.1.5   SHRU VLA Recovery

Upon arriving at the site, the team interrogates the acoustic release on the mooring, then maneuvers the vessel 300 m away from the mooring location and releases the mooring. The StableMoor® buoy on the Canyon SHRU or the 48-inch steel sphere on the Slope SHRU rises to the sea surface first, and the team waits until the bottom four glass ball floats come up to the sea surface before retrieving the mooring and all components (except the 3,000-pound anchor).

For the Canyon SHRU mooring, the StableMoor® buoy is recovered first using the ship's crane from the port side. For the Slope SHRU, the 48-inch steel sphere is recovered with the A-frame. After the StableMoor® or steel sphere is placed in the cradle and secured, the mooring load is transferred to the ship's small deck winch to recover the mooring in segments. Each SHRU VLA mooring consists of a total of five segments, which are necessary to recover the hydrophone cages and the electronic packages. During the recovery, the ship is held stationary.

After each mooring is recovered, the team checks the SHRU clocks against the GPS time to record the total clock drift during the deployment. The data disks are recovered, and the data files are immediately copied to a backup disk. Data processing typically begins after the units are returned to the laboratory.

Appendix C: Field Cruise Photograph Log

Photo C-1. *R/V* Pelican docked at Cocodrie, Louisiana.

Photo C-2. The 2018 MP field deployment team with the *R/V* Pelican crew.

From left to right: Derek Jaskula (Cornell University), Brad Lingsch (Proteus Technologies LLC), Kenny (R/V Pelican intern), Matthew Firneno (University of New Orleans graduate student), Natalia Sidorovskaia (University of Louisiana at Lafayette), Evan Wellmeyer (University of New Orleans graduate student), Jerome Hamilton (cook), John Lacross (R/V Pelican marine technician), Fred Channell (Cornell University), Tad Berkey (R/V Pelican captain), Sean Griffin (Proteus Technologies LLC, Chief Scientist), Dirk Wacker (R/V Pelican deckhand), Elliot (R/V Pelican crew)

Photo C-3. RHs ready for deployment.
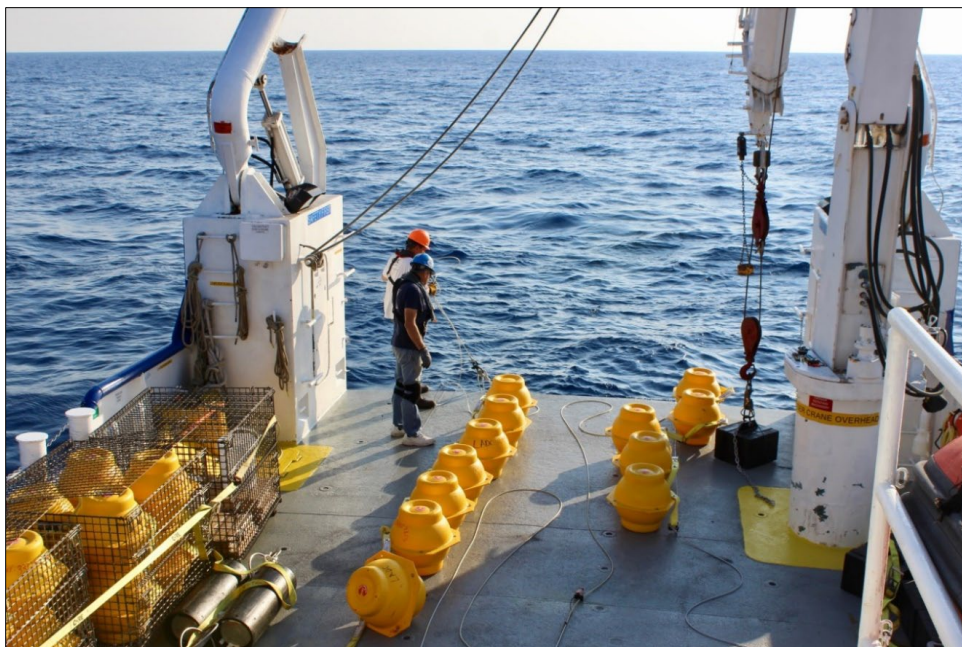
Photo C-4. EARS mooring ready for deployment.
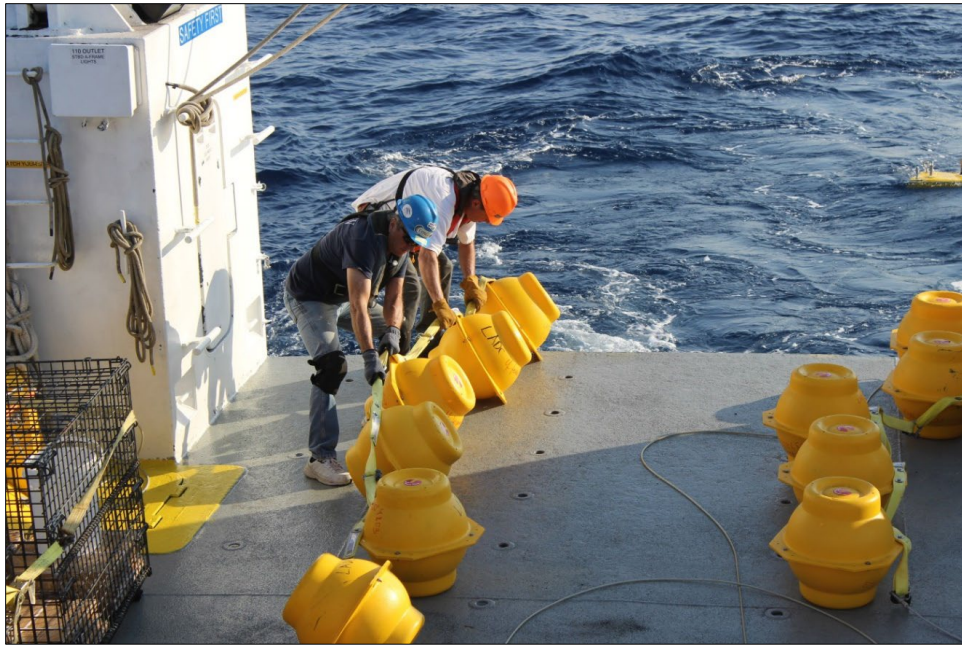
Photo C-5. EARS mooring deployment, satellite beacon in the water.

Photo C-6. EARS mooring deployment, top floats in the water.
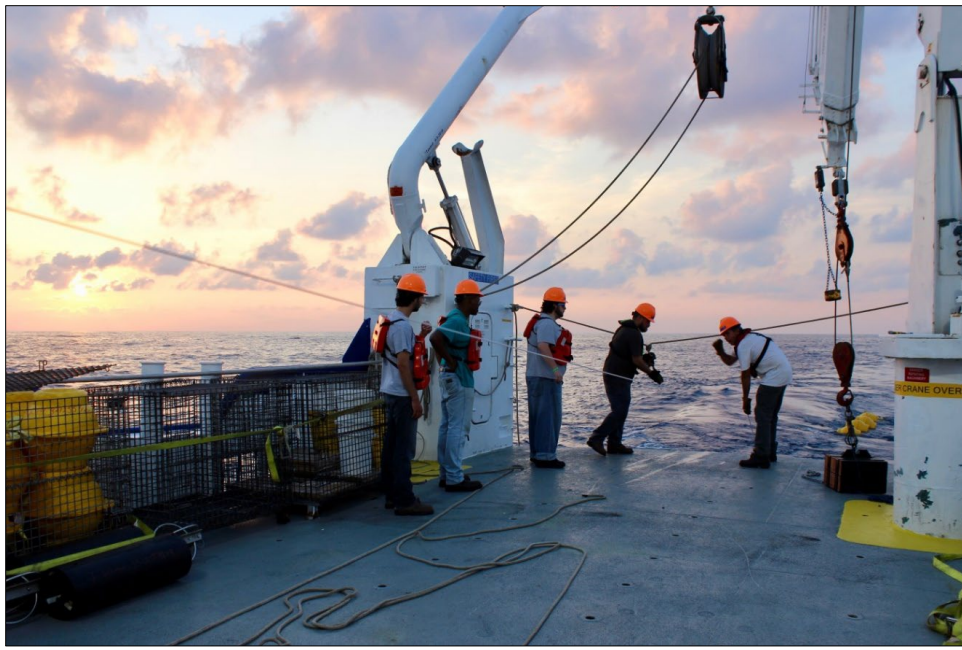
Photo C-7. EARS mooring deployment, final stage (anchor release preparation).

Photo C-8. Preparing the RH mooring for deployment.
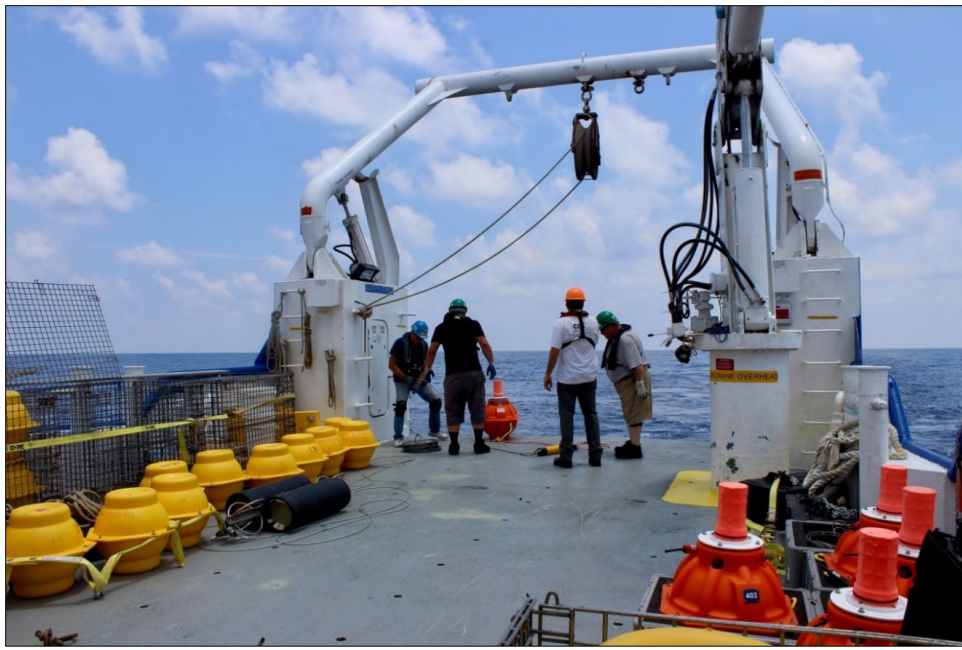
Photo C-9. RH mooring deployment.

Photo C-10. CTD unit deployment for collection of oceanographic data.
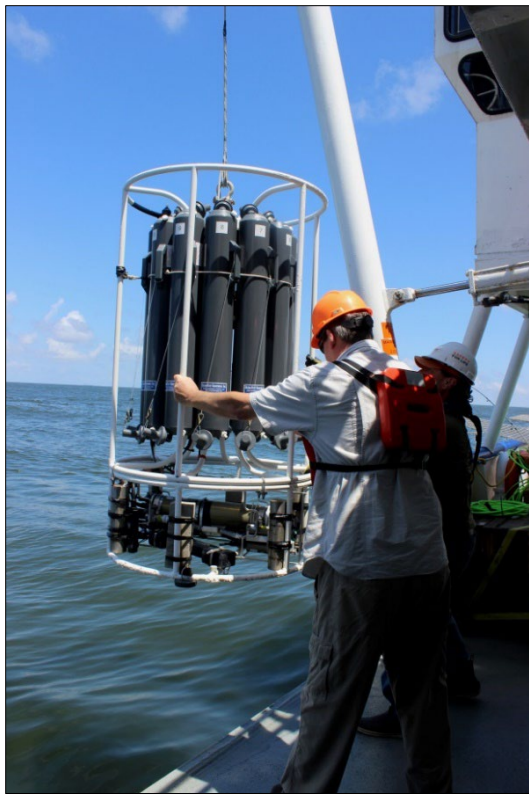
Photo C-11. Deployment of the CTD unit.

Photo C-12. StableMoor® buoy for the Canyon SHRU VLA.

Photo C-13. SHRU VLA hydrophone cage.

Photo C-14. Principal Investigator Dave Mellinger setting up the glider, dockside at Venice, Louisiana.

Photo C-15. Seaglider system check.

Photo C-16. Glider hydrophone check.

Photo C-17. Turning the Seaglider using a magnetic key.
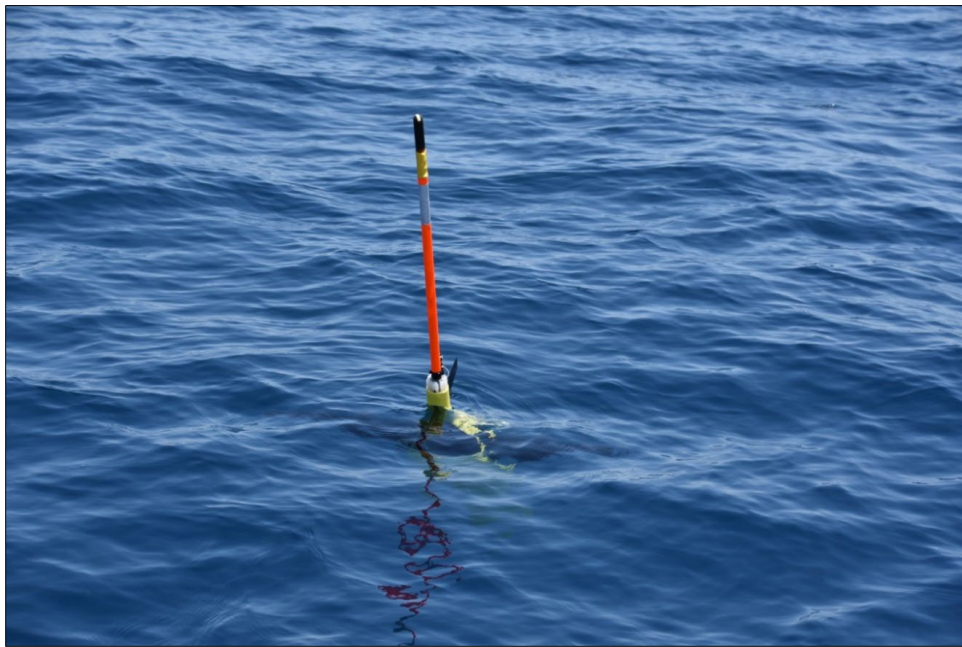
Photo C-18. Seaglider in the water, immediately before making its first dive.

Appendix D: GOM PAM Program Advanced Data Synthesis and Analysis Report

Prepared Under:
BOEM IDIQ Contract No. M17PC00001, Task Order No. 140M0119F0001, Task 7 (Data Analysis, Synthesis, and Annual and Final Reports)

by:

Marine Acoustics, Inc.

MAI
MARINE ACOUSTICS, INC.

In Collaboration with:

HDR

300 N. Madison Street
Athens, AL 35611

Table of Contents

List of Figures

164

165

167

List of Tables

List of Acronyms and Abbreviations

Short form	Long form
ACF	autocorrelation function plots
AR	autoregressive
ADEON	Atlantic Deepwater Ecosystem Observatory Network
AIS	Automatic Identification System
AUV	autonomous underwater vehicle(s)
BB	broadband
BIAS	Baltic Sea Information on the Acoustic Soundscape
BOEM	Bureau of Ocean Energy Management
BSEE	Bureau of Safety and Environmental Enforcement
CCB	Cornell Conservation Bioacoustics program
COVID	corona virus disease
CPA	closest point of approach
CSAC-SHRU	Chip Scale Atomic Clock-Several Hydrophone Recording Units
dB	decibel(s)
dB re 1µPa2	decibel(s) referenced to 1 microPascal squared
EARS	Environmental Acoustic Recording System
edf	empirical distribution function (statistics)
ESA	Endangered Species Act
F-value	value on the F distribution calculated by dividing two mean squares
GAMs	generalized additive model(s)
GAMMs	generalized additive mixed model(s)
GDEM	Global Digital Elevation Model
GOM	Gulf of Mexico
HF	high frequency
HP	hydrophone(s)
Hz	Hertz
ID	identification
kHz	kiloHertz
km	kilometer(s)
LF	low frequency
m	meter(s)
MF	mid frequency
MAI	Marine Acoustics, Inc.
MATLAB®	MATrix LABoratory
MMPA	Marine Mammal Protection Act
MMSI	Maritime Mobile Service Identity
MP	Monitoring Project
N/A	not applicable
NASA	National Aeronautics and Space Administration
NEPA	National Environmental Policy Act

Short form	Long form
NOAA	National Oceanic and Atmospheric Administration
OSCAR	Ocean Surface Current Analysis Real-time
OSU	Oregon State University
P-value	level of marginal significance within a statistical hypothesis test, representing the probability of the occurrence of a given event
PAM	Passive Acoustic Monitoring
Program	Gulf of Mexico Passive Acoustic Monitoring Program
Ref.df	reference degrees of freedom (statistics)
RH	Rockhopper(s)
RL	received level
R-squared	measure of how much of the variance is in the dependent variable (statistics)
s	scaled
SA2	simple or second statistical approach
SHRU	Several Hydrophone Recording Units
SL	source level
SLBB	broadband source level
SNR	signal-to-noise ratio
SOG	speed over ground
SPL	sound pressure level
Std. Error	Standard Error
STW	speed through the water
SVP	sound velocity profile(s)
TL	transmission loss
TOB	third-octave band
VLA	vertical line array(s)
WHOI	Woods Hole Oceanographic Institution

Glossary of Acoustic Terminology

Amplitude. The magnitude of the signal. Amplitude is perceived as loudness and typically reported using a decibel unit.

Decibel (dB): Defined as 10 x log10(Io/Iref), where Io is the measured intensity and Iref is the reference intensity. In underwater acoustics, the reference intensity is typically 1 µPa.

Frequency: Frequency is defined as the number of cycles of sound occur within a second. Frequency is perceived as pitch and typically reported with units of Hertz (Hz) or kilohertz (kHz).

Hertz (Hz): The number of cycles per second of a sound wave.

Received Level (RL): This refers to the amplitude at any receiver at any arbitrary distance. It is also known as Sound Pressure Level (SPL). The unit for continuous sources are dB re 1µPa2.

Signal To Noise Ratio (SNR): Literally the comparison of the amplitude of a sound signal and the (typically background) noise level. In intensity terms, it is signal intensity divided by noise level intensity. Alternatively, it can be derived as subtracting the noise level in dB from the signal level in dB.

Source Level (SL): This value describes the amplitude of a source. It is traditionally presented as the value that occurs at a distance 1 meter from the source. The proper unit for a SL is dB re 1µPa2-m2. Historically, it was often used with a unit of dB re 1µPa at 1m.

Spectral Level: The amount of sound intensity in a 1-Hz-wide frequency band. The proper unit is dB re 1µPa2/Hz.

Third-Octave band: The amount of sound intensity in a one-third octave wide frequency band. The proper unit is dB re 1µPa2.

Transmission (Propagation) Loss (TL or PL): The amount of sound intensity lost between the sound source and the sound receiver.

D.1 Introduction

D.1.1 Background

The northern Gulf of Mexico (GOM) is a highly industrialized environment with multiple anthropogenic sound sources, including shipping, oil and gas activities, and military operations. Noise impacts to protected species (e.g., cetaceans) may occur as a result of activities associated with oil and gas exploration licensed by Bureau of Ocean Energy Management (BOEM) and the Bureau of Safety and Environmental Enforcement (BSEE). These activities may include seismic surveys, platform decommissioning, drilling, and resulting increases in vessel traffic. However, characterizing the acoustic impacts and trends associated with such activities is difficult without comprehensive baseline data on the ambient noise environment in the GOM.

Also, BOEM and BSEE are required to assess potential impacts on protected species, specifically under the Marine Mammal Protection Act (MMPA), Endangered Species Act (ESA), and the National Environmental Policy Act (NEPA) to assist and guide their decision making. Future BOEM MMPA rulemaking for seismic activities in the GOM will have a monitoring requirement associated with it, including collection of ambient noise data and noise data associated with seismic activities. In short, there was an urgent need to implement a systematic and comprehensive acoustic data collection effort in the GOM. BOEM's Passive Acoustic Monitoring (PAM) Program in the northern GOM was intended to collect and analyze data to meet this need.

Before developing an experimental design for the data collection program, a comprehensive literature review was conducted to identify and evaluate available relevant data from previous GOM underwater soundscape characterization efforts (Latusek-Nabholz et al. 2020).

D.1.1.1 Key Literature Findings

Low-frequency (LF) noise generally includes sounds in the bandwidths between 10 and 500 Hertz (Hz). This frequency range of underwater sound is primarily produced by anthropogenic sound sources, including commercial shipping and seismic surveys. Medium-frequency (MF) noise includes sounds from 500 Hz to 25 kiloHertz (kHz), and this range is dominated by natural sources of sound, such as sea-surface agitation, including break waves, spray, bubble formation and collapse, and rainfall. Heavy precipitation can increase noise levels in this range by as much as 20 decibels (dB). Sound generated by military and small vessels are also included in the medium-frequency range. Overall, medium-frequency sounds are more local or regional in nature, as they do not propagate over long distances. High-frequency (HF) sound generally ranges above 25 kHz and is generally located close to the receiver. Thermal noise, the result of particles moving close to the hydrophone for example, as well as mapping sonars, are included in this category.

The literature review conducted for the Gulf of Mexico Passive Acoustic Monitoring Program (Program) showed that the northern GOM soundscapes are characterized by a mix of industrial and natural sound sources across the 200 to 40,000 Hz band (Sidorovskaia and Li 2016). Shipping activity and seismic surveys are the major noise contributors in the GOM (Estabrook et al. 2016; Wiggins et al. 2016; Sidorovskaia and Li 2016). Analysis of long-term (i.e., multi-year) sound recordings reveal pervasive activity from seismic surveys (Estabrook et al. 2016; Sidorovskaia and Li 2016; Wiggins et al. 2016), often detected across broad expanses of the GOM and ranges extending to at least 700 kilometers (km) (378 nautical miles) (Rice et al. 2015; Estabrook et al. 2016). Estabrook et al. (2016) noted that sound levels from shipping activity were not nearly as pronounced as those from seismic surveys, which for the latter, in many cases, persisted for months at a time.

In a review of multi-year GOM Environmental Acoustic Recording Systems (EARS) data, scientists found no indication of an increasing baseline level of ambient noise (Sidorovskaia and Li 2016) below 1,000 Hz. However, Sidorovskaia and Li (2016) noted that high-frequency spectral levels showed an increase in more recent years (2010 and 2015) in the ambient soundscape of the northern GOM. This increase in the ambient soundscape may be attributed to anthropogenic activities, including the increasing use of unmanned devices (e.g., sonars, autonomous underwater vehicles [AUV]), which use high-frequency bands for communication and exploration for seismic exploration.

Seasonal variations in ambient noise levels due to industrial exploration are evident in various studies conducted in the GOM (Snyder 2007; Estabrook et al. 2016; Wiggins et al. 2016; Sidorovskaia and Li 2016). Anthropogenic noise sources showed considerable seasonal variability, with the highest levels measured during the summer months (Sidorovskaia and Li 2016). There is also documented evidence of regional variations in anthropogenic noise in the GOM (Wiggins et al. 2016).

D.1.2 Advanced Data Synthesis and Analysis

The primary objective of the Program was to design and field test implementation of a large-scale, multi-year, passive underwater acoustic monitoring effort in the northern GOM. Data collected under the first two years of the Program (2018 and 2019) were analyzed in two separate phases to generate outputs for characterization of the existing underwater soundscape (including sounds contributed by both natural and anthropogenic sources) in the northern GOM. Under Phase 1, *basic* data analyses were separately performed on data collected in each year. *Advanced* data analyses were performed on the combined two-year data set under Phase 2. Results and recommendations from these advanced analyses are presented in this report.

The Program was initiated and implemented as two distinct 12-month Monitoring Projects (MP):

- 2018 MP (**Figure D-1**): Acoustic monitoring was conducted within a 100- by 200-km study area box located in the northern GOM for the 12-month period from May 2018 to April 2019. Two separate deployments were conducted, the first from May to October 2018 (designated as Deployment 1) and the second from November 2018 to April 2019 (Deployment 2).

- 2019 MP (**Figure D-1**): Monitoring initiated under the 2018 MP was continued for an additional 12 months (May 2019 to April 2020). Lessons learned from the 2018 MP were used to guide delineation of the study area boundaries and placement of sensors for the 2019 MP. The 2019 MP study area box measured approximately 100 by 140 km. Two separate deployments were conducted, the first from May to October 2019 (designated as Deployment 3) and the second from November 2019 to April 2020 (Deployment 4).
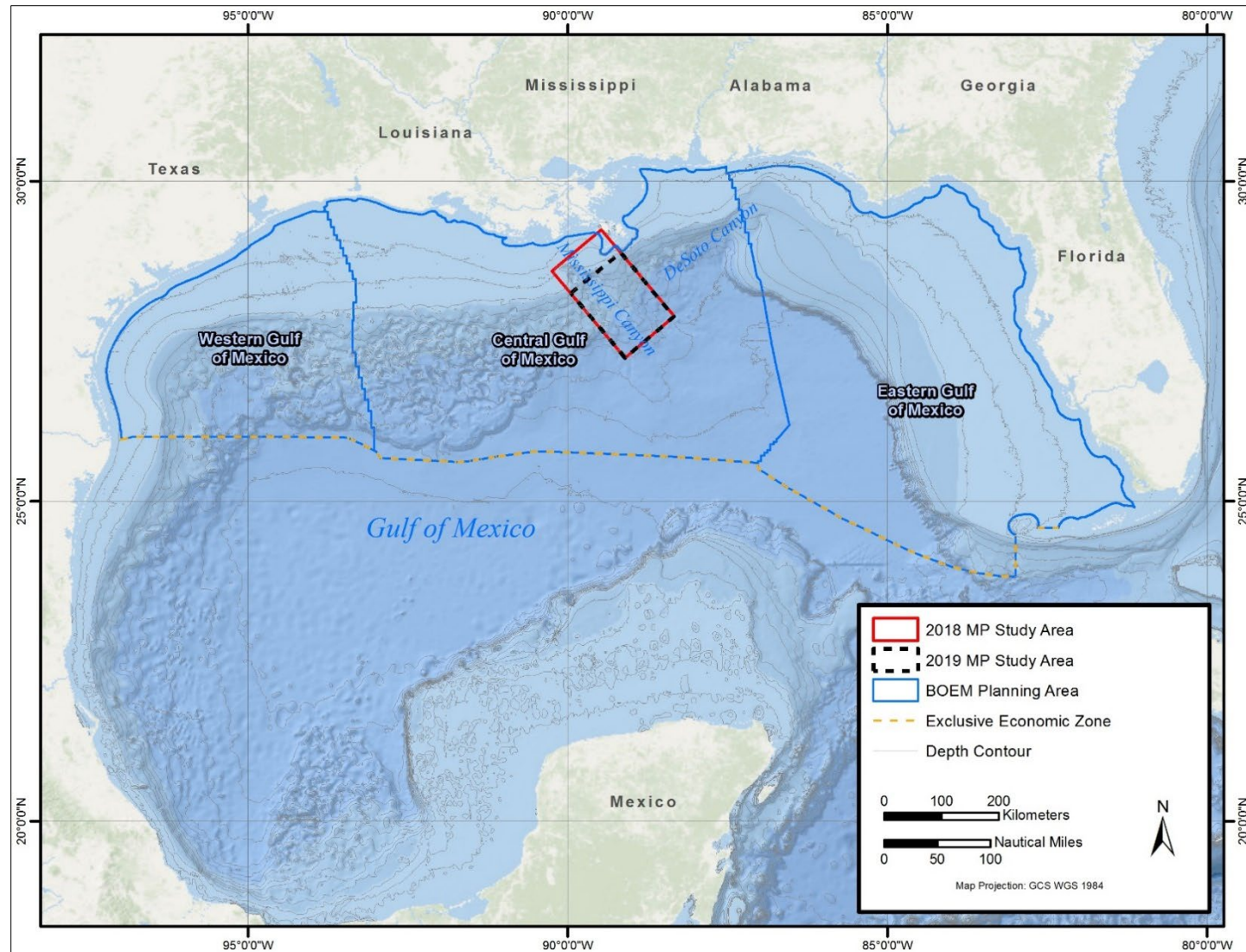
Figure D-1. Northern GOM BOEM planning areas and GOM Program 2018 and 2019 MP study areas.

D.1.3 Monitoring Instrumentation

During both MPs, underwater acoustic data were collected using a mix of stationary and mobile platforms that were deployed at selected locations within the respective study areas (**Figures D-2** and **D-3**). Data were collected at depths ranging from 53 to 2,148 meters (m) within the main habitat types in the region, including the continental shelf (less than 200 m deep), continental slope (200 to 1,600 m deep), and the abyssal plain (more than 1,600 m deep).

Three different types of stationary moorings equipped with sensors (hydrophones) and recording systems were used, namely Rockhoppers (RH) and EARS, both with effective recording bandwidth ranging from 10 Hz to 96 kHz; and Chip Scale Atomic Clock-Several Hydrophone Recording Unit (CSAC-SHRU) vertical line arrays (VLA), with effective recording bandwidth of 10 Hz to 4.5 kHz. Additionally, two separate mobile autonomous underwater platforms (Seagliders), with an effective recording bandwidth of 10 Hz to 62.5 kHz, were also deployed within selected portions of the study area to collect data from the areas between the stationary moorings within the Mississippi Canyon and to cover selected areas in the DeSoto Canyon.

D.1.4 Monitoring Locations

Under both the 2018 and 2019 MPs, 12 stationary moorings (5 RH, 5 EARS, and 2 CSAC-SHRU) were deployed (**Table D-1** and **Figure D-2,** and **Table D-2** and **Figure D-3**, respectively). Between the 12 moorings, the 2018 MP covered a depth range of 53 to 1,672 m. In the 2019 MP, for placement of EARS and RH, five locations were retained from the 2018 MP and five new locations were added within the delineated study area. The CSAC-SHRU locations remain unchanged from 2018. Between the 12 moorings, the 2019 MP covered a depth range of 356 to 2,170 m.

D.1.4.1 Seaglider Flight Paths

For the 2018 MP, the Seaglider path consisted of three contiguous segments to cover approximately two weeks of data collection in the DeSoto Canyon and two weeks in the Mississippi Canyon (**Table D-3** and **Figure D-2**). For the 2019 MP, very limited underwater acoustic and environmental data were collected with the Seaglider due to operational and weather constraints (**Table D-4** and **Figure D-3**).

D.1.5 Data Analysis Approach

A two-step data analysis approach was adopted:

- **Phase 1 (Basic Data Analyses):** Data collected under the 2018 MP by each instrument type were separately processed, analyzed, and reported. RH and Seaglider data were analyzed using the noise analysis tools within the Raven-X toolbox for MATrix LABoratory (MATLAB®) developed by the Cornell University Center for Conservation Bioacoustics. EARS data were analyzed using the EARS MATLAB noise analysis software; as a quality control check both analyses toolboxes were tested on the same data subset to ensure identical outputs. SHRU VLA data were analyzed using standardized acoustic data analyses protocols.

  Phase 1 data analyses outputs included long-term spectral average plots, equivalent sound levels, cumulative percentage distribution, temporal trends, power spectral density levels, and spectral probability density plots. The data standards for the analyses generally were consistent with guidelines adopted by the Baltic Sea Information on the Acoustic Soundscape (BIAS) project as well as the Atlantic Deepwater Ecosystem Observatory Network (ADEON) project (Ainslie et al. 2017).
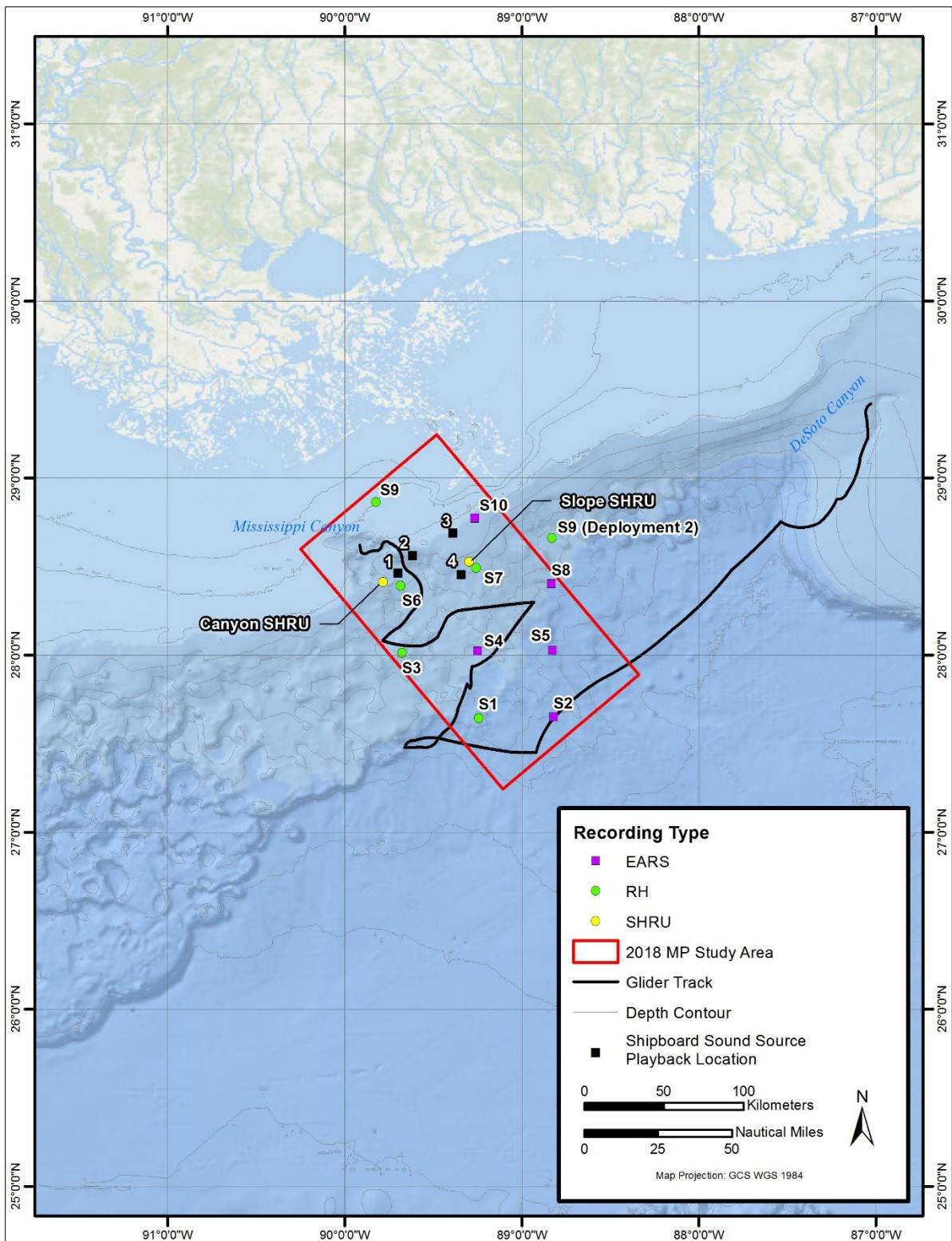
Figure D-2. Locations of stationary and mobile platform deployments (Deployments 1 and 2) under the 2018 MP.
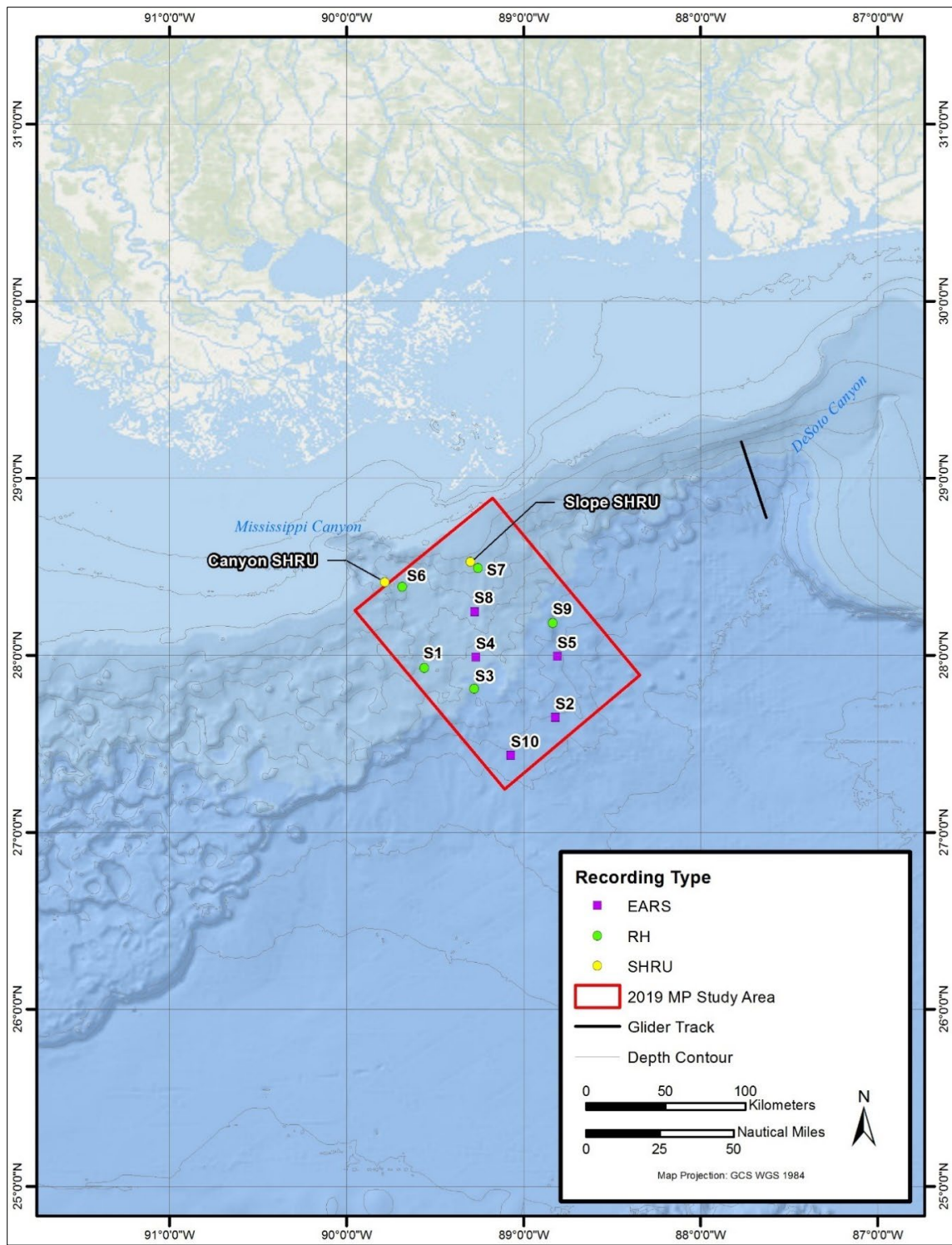
Figure D-3. Locations of stationary and mobile platform deployments (Deployments 3 and 4) under the 2019 MP.

Table D-1. Stationary mooring locations under the 2018 MP

Monitoring Station No.	Data Recording System	Monitoring Bandwidth	Deployment 1 (May to October 2018)				Deployment 2 (November 2018 to April 2019)			
			Latitude (°)	Longitude (°)	Water Depth (m)#	Duration Data Recorded (hours)	Latitude (°)	Longitude (°)	Water Depth (m)	Duration Data Recorded (hours)
S1	RH	10 Hz–96 kHz	27.64300	-89.24300	1,413	3,141	same as Deployment 1			4,368
S2	EARS	10 Hz–96 kHz	27.65000	-88.82000	1,772	4,179	same as Deployment 1			3,745
S3	RH	10 Hz–96 kHz	28.01100	-89.67500	712	3,106	same as Deployment 1			4,359
S4	EARS	10 Hz–96 kHz	28.02000	-89.25100	1,280	1,678	27.98713	-89.27067	1,280	3,820
S5	EARS	10 Hz–96 kHz	28.02600	-88.82700	1,672	4,227	27.99418	-88.80950	1,672	3,703
S6	RH	10 Hz–96 kHz	28.38900	-89.68500	685	3,065	same as Deployment 1			3,052
S7	RH	10 Hz–96 kHz	28.49000	-89.25800	440	3,030	same as Deployment 1			4,415
S8	EARS	10 Hz–96 kHz	28.40200	-88.83200	1,262	1,332	same as Deployment 1			3,960
S9	RH	10 Hz–96 kHz	28.86100	-89.82400	53	1,108	28.66000	-88.83000	1,067	4,491
S10	EARS	10 Hz–96 kHz	28.77100	-89.26600	131	4,128	28.77180	-89.26640	131	3,808
Canyon SHRU	SHRU	10 Hz–4.5 kHz	28.40991	-89.78438	4 HP[a]: 175, 200, 250, 275	3,648	N/A			
Slope SHRU	SHRU	10 Hz–4.5 kHz	28.52531	-89.29874	4 HP[a]: 175, 200, 250, 275	624	N/A			

Key: RH=Rockhopper; EARS=Environmental Acoustic Recording Systems; N/A=not applicable; SHRU=Several Hydrophone Recording Units

[a] # HP=hydrophones

Notes:

1. RHs and EARS were deployed for a total of 24 months (four separate deployments each lasting six months).

2. SHRU data collection period was only six months during each deployment, for a total of 12 months over two years.

3. During Deployment 1, the RH at Site 9 was dragged up by a fishing trawler; as a result, the Site 9 location was moved to deeper waters during Deployment 2.

4. During Deployment 1, the Slope SHRU had an electrical malfunction due to seepage of salt water into the sensor housing, resulting in the recording systems failing after 26 days of data collection.

5. Approximately two weeks into the second deployment, the RH at Site 3 developed an issue with one of the two 4-terabyte hard drives. The unit successfully switched over to the second hard drive. However, the capacity of the second solid state drive (hard drive) alone was not quite sufficient to store recordings for the entire deployment period. The data storage limit was reached approximately four months after the start of the deployment.

Table D-2. Stationary mooring locations under 2019 MP

Monitoring Station No.	Data Recording System	Monitoring Bandwidth	Deployment 3 (May 2019 to October 2019)				Deployment 4 (November 2019 to June 2020)			
			Latitude (°)	Longitude (°)	Water Depth (m)#	Duration Data Recorded (hours)	Latitude (°)	Longitude (°)	Water Depth (m)	Duration Data Recorded (hours)
S1	RH	10 Hz–96 kHz	27.92710	-88.56040	2,148	4,390	same as Deployment 3			Unit lost
S2	EARS	10 Hz–96 kHz	27.64837	-88.82111	1,777	1,048	same as Deployment 3			5,077
S3	RH	10 Hz–96 kHz	27.80900	-89.27890	1,375	4,396	same as Deployment 3			5,096
S4	EARS	10 Hz–96 kHz	27.98871	-89.26963	1,332	5,057	same as Deployment 3			4,682
S5	EARS	10 Hz–96 kHz	27.99373	-88.80897	1,671	5,160	same as Deployment 3			4,371
S6	RH	10 Hz–96 kHz	28.38520	-89.68530	685	4,375	same as Deployment 3			5,276
S7	RH	10 Hz–96 kHz	28.49160	-89.25810	440	3,973	same as Deployment 3			2,881
S8	EARS	10 Hz–96 kHz	28.24345	-89.27747	830	5,223	same as Deployment 3			5,071
S9	RH	10 Hz–96 kHz	28.17980	-88.83490	1,526	4,388	same as Deployment 3			5,171
S10	EARS	10 Hz–96 kHz	27.43412	-89.07278	1,797	5,159	same as Deployment 3			4,680
Canyon SHRU	SHRU	10 Hz–4.5 kHz	28.77150	-89.78500	4 HPª at 175, 200, 250, 275	3,480	N/A			
Slope SHRU	SHRU	10 Hz–4.5 kHz	28.4124	-89.29920	4 HPª at 175, 200, 250, 275	3,480	N/A			

Key: RH=Rockhopper; EARS=Environmental Acoustic Recording Systems; N/A=not applicable; SHRU=Several Hydrophone Recording Units
ª # HP=hydrophones
Notes:
1. RH and EARS were deployed for a total of 24 months (four separate deployments each lasting six months).
2. SHRU data collection period was only six months during each deployment, for a total of 12 months over two years.
3. During Deployment 4, the RH at Site 1 was lost and could not be recovered due to a communication system failure.

Table D-3. Segment and coordinates of 2018 MP Seaglider flight path

Flight Path Segment Number	Flight Path Segment ID	Data Collection Dates	To		From	
			Latitude (°)	Longitude (°)	Latitude (°)	Longitude (°)
1	DeSoto Canyon	05/10/2018–5/19/2018	29.419722	-86.995378	28.705587	-87.574675
2	Deep Slope	05/19/2018–05/30/2018	28.676265	-87.601155	27.518300	-89.415167
3	Mississippi Canyon	05/30/2018–06/20/2018	27.519063	-89.415153	28.640717	-89.894550

Table D-4. Segment and coordinates of 2019 MP Seaglider flight path

Flight Path Segment Number	Flight Path Segment ID	Data Collection Dates	From		To	
			Latitude (°)	Longitude (°)	Latitude (°)	Longitude (°)
1	DeSoto Canyon	09/24/2019–10/05/2019	29.2043882	-87.769433	28.776567	-87.630433

- **Phase 2 (Advanced Data Analyses):** In Phase 2, acoustic data collected under the two MPs were combined to create a 24-month dataset for detailed analyses and soundscape characterization. Based on guidance provided by BOEM, Phase 2 analyses were to include anthropogenic noise source identification and characterization (e.g., received level, spectrum, duration, and, if possible, localization, tracking, and estimation of source levels). *Due to schedule, resources, or logistical constraints, representative datasets were used for some of the analyses.* The results of the data analyses also were used to identify data and information gaps. Key steps in Phase 2 analyses included the following:

  o **Raw Data Power Spectral Density Analysis**: Raw data were collected using different instruments, each of which uses a different data format. A project-customized module of Raven-X was used to generate summary statistics for the raw acoustic data in 1-Hz, 1-second resolution. The Raven-X outputs, which served as inputs for the Phase 2 analyses, are compliant with ADEON-guidelines. Therefore, by extension, the Phase 2 outputs are also ADEON-guidelines compliant.

  o **Detector Band Creation**: Known acoustic sources have specific frequency characteristics. Candidate frequency bands that are likely to be able to indicate the presence of different sources were identified. Some of these frequency bands were determined from the literature, while the remaining bands (defined as empirical bands) were identified through a review of the data. While these frequency bands were observed, they were not associated *a priori* with any particular source(s).

  o **Detection of Acoustic Events in Candidate Bands**: The hourly mean received level (RL) in each band was calculated and subtracted from each "candidate" band to produce a "normalized" band. The detection threshold is taken as the sum of standard deviation of the normalized band plus 3 dB. A subset of the data was hand scored for vessel and airgun presence. The 3 dB threshold was established based on comparison of detection rates at different thresholds and hand-scored values. Any level exceeding this threshold was taken as a detection.

- o **Automatic Identification System (AIS) Data**: AIS data for 2018 and 2019 were obtained from BOEM and the National Oceanic and Atmospheric Administration (NOAA)-sponsored website (https://marinecadastre.gov/) and incorporated into the analyses to identify specific acoustic sources.
- o **Statistical Analysis**: The "bandstats" output, the cumulative acoustic power in a 1-hour band in each of the source candidate frequency bands, were analyzed with a suite of predictor variables. These variables include the AIS metrics and the windspeed values. The resulting analyses clarifies the relative power of these metrics to predict acoustic levels. Graphical representations of the candidate frequency bands were used to identify spatiotemporal patterns.

In Phase 2, data collected by the mobile platforms were evaluated independently of data collected by stationary platforms because of the differences in spatial and temporal extent and coverage of different areas with potentially different species assemblages and soundscape drivers. To the extent practicable, data analysis protocols for stationary and mobile platforms were made consistent to ensure compatibility of results. As appropriate and relevant, meteorological/oceanographic data collected during the MPs or acquired from external sources were also incorporated into the analyses to support data interpretation.

D.2 Data Analysis Challenges

COVID-19 pandemic related lockdowns at various team partner institutions created serious challenges for completing the field work safely and on time and consequently led to a significant delay in conducting data analyses and reporting. Another significant challenge was the delay in acquisition of the AIS data, which is the backbone of the vessel soundscape analysis. The 2018 AIS data were not available until 2020, and the last part of the 2019 AIS data were not available until mid-2021.

D.3 Methods

Phase 2 analysis were conducted in accordance with a BOEM-approved Advanced Data Analyses Plan and the primary objective of these analysis was to advance basic soundscape characterization conducted under Phase 1. In both phases, stationary and mobile platform data were evaluated separately since they were collected in somewhat different areas and therefore likely to consist of different species mix. To the extent practicable, the analysis protocols for stationary and mobile platforms were made consistent to ensure compatibility of results.

Since the overall objective of the Phase 2 analysis was to support underwater soundscape characterization, the following specific types of assessments were performed:

- a) Define and create source-specific frequency bands for 10 EARS/RHs. These bands were based on published reports of the characteristics of sources known to occur in the study area, including some biological sources.
- b) Perform detection operations on the EARS/RH frequency bands. The detections of signals in these bands would reflect the presence of the sources nominally associated with each band.
- c) Perform vessel and airgun detection operations. This discrimination detection effort focused on the presence of vessels and airgun activity, using an approach derived to create additional frequency bands that represented the presence of airguns and vessel passings.
- d) Statistical analyses of the vessel noise band RLs. This effort determined how much of the variability in sound RLs at each buoy can be explained by independent predictors of windspeed, wave height, and vessel presence (i.e., AIS data).
- e) Consideration of the "extrapability" of results. Initial analysis was based upon a comparison of the glider that overflew a static receiver. The expectation was that during the close approach, the

two receivers would record similar data and the similarity would decrease with increasing distance.

D.3.1 Comparison of RH and EARS datasets

Before combining the RH and EARS datasets for use in the statistical analyses, a comparison of the spectral properties of the five RH and five EARS recorders was performed using data from all four deployments. The same instrument type was deployed at each site regardless of the deployment number. For example, for Deployments 1 through 4, a RH recorder was always deployed at site S1 (**Table D-5**).

Table D-5. Recorder type deployed at each site for all deployments

Site	Recorder Type
S1	RH
S2	EARS
S3	RH
S4	EARS
S5	EARS
S6	RH
S7	RH
S8	EARS
S9	RH
S10	EARS
Key: RH=Rockhopper; EARS= Environmental Acoustic Recording Systems	

D.3.2 Frequency Band Detection Analyses

D.3.2.1 Creation of Defined Frequency Bands

Predefined sound frequency bands were compiled to identify the sources of sound in the data recordings as they were assessed. The underlying assumption of this process is that the presence of sound in a defined frequency band indicates the potential presence of that sound source in the Program environment. For example, sounds in the frequency band from 2,000 to 4,000 Hz may be indicative of the presence of sperm whales (**Table D-6**).

These predefined frequency bands were derived from published descriptions of biological and anthropogenic sounds or from collected data (**Table D-6**). The "Empirical" frequency bands were defined after manual examination of the recorded acoustic data. However, several of the identified frequency bands have overlapping frequency ranges.

The selection of the frequency bands for the biological sources was based on the species of marine mammals and other sound-producing marine taxa potentially occurring in the Program area. Similarly, the selection of the possible sound-producing anthropogenic sources was based on the types of human activities that occur in the Program study area and the types of sound sources employed during the execution of those activities. For example, various sonar and subsea imaging sources (**Table D-6**, rows 13 to 18) may be used during scientific research, fishing, or geophysical exploration in the GOM.

Table D-6. Sound sources, frequency ranges, and references for the pre-defined frequency bands

Band Number	Band Name	Frequency Range (Hz)		Reference
		Low	High	
1	Bottlenose Dolphin Whistles	2,000	12,500	Frankel et al. 2014
2	Rice's Whale (formerly GOM Bryde's Whale)	70	160	Rice et al. 2014
3	Cuvier's Beaked Whale	29,000	43,000	Erbe et al. 2017
4	Short-finned Pilot Whale	3,000	6,000	Baron et al. 2008
5	Sperm Whale	2,000	4,000	Thode et al. 2002
6	Fish	25	2,000	Staaterman et al. 2014
7	Snapping Shrimp	2,000	10,000	Staaterman et al. 2014
8	Vessels, Airgun, Piles	10	40	McPherson et al. 2016
9	Vessels	200	2,500	Sidorovskaia and Li 2016
10	Airguns, Piles	200	1,000	Hildebrand 2009; Sidorovskaia and Li 2016
11	Weather	200	10,000	Sidorovskaia and Li 2016
12	Chirp Sonar	1,000	15,000	Schock 2004
13	Deep Side Scan	11,500	12,500	Hildebrand 2009
14	Sub-bottom profiler	3,000	7,000	Hildebrand 2009
15	Edgetech 424	8,000	15,000	Crocker and Fratantonio 2016
16	Knudsen TR-1075	3,500	5,500	Crocker and Fratantonio 2016
17	Edgetech 4200 EMI	60,000	70,000	Crocker and Fratantonio 2016
18	Empirical Band 2	10,000	20,000	Observed in Data
19	Empirical Band 3	20,000	30,000	Observed in Data
20	Empirical Band 5	40,000	50,000	Observed in Data
21	Empirical Band 6	50,000	60,000	Observed in Data
22	Empirical Dolphins	5,000	15,000	Observed in Data
23	Empirical Chirp Sonar	49,000	51,000	Observed in Data
24	Empirical 500–1000 pulses	500	1,000	Observed in Data

D.3.2.2 Anthropogenic Sound (Vessel and Airgun) Detection Analysis

Band-limited energy detectors were developed for vessel and airgun signals, the two most prominent sources of anthropogenic sound in the northern GOM. The airgun detector calculated the energy in the 10 to 100 Hz band on an hourly basis and then subtracted the value from the 25 to 63 kHz reference band to produce the airgun detection index. Detections occurred when this index was greater 12 dB above the 10th percentile level of the index.

The vessel detection algorithm was similar. It was based on a vessel detection index calculated as the hourly signal to noise ratio of the 250 to 2,500 Hz band relative to the same 25 to 63 kHz reference band. This detector was tuned for the broadband Lloyd mirror interference patterns that accompany a close passage of a vessel moving past the recorder. A daily moving mean of the vessel detection index was calculated, and detections occurred when the index was 3 dB greater than the moving mean.

The acoustic record of the 2018 MP Seaglider was also examined for the presence of vessels and airgun activity. The noise characteristics of the glider acoustic record were different from that of the moored autonomous recorders. Therefore, the glider recordings were "hand scored" for the presence of vessels and airguns rather than tuned to a detection algorithm.

D.3.2.3 Biological Sound Detection Analysis

To attempt to document or investigate the presence of marine animals in the Program area, several frequency band metrics were added to the analysis suite. These included frequency bands for the known vocalizations of the following marine mammal species and groups: Rice's whale (*Balaenoptera ricei*), beaked whales, and dolphins. Detection efforts for *Kogia* species were not attempted due to bandwidth limitations caused by the anti-aliasing filters on the recorders (Klinck, pers. comm.).

Since the data provided was for only summary energy metrics and did not include the waveforms, only simple energy detectors could be used for nominal marine mammal species assessed. As such, these results should be considered preliminary at best. It would be desirable for future dedicated biological analyses to be conducted using the waveform data and more sophisticated detection methods.

The energy detection method used was based on Clark et al. (in prep.). This method computes the signal-to-noise ratio (SNR) of a frequency band of the signal of interest with a frequency band in which the signal does not occur. When an animal vocalizes, there is energy in the signal band but no additional energy in the reference band. Therefore, the ratio of the two (i.e., the SNR) increases. For beaked whales, the possibility of adjacent frequency bands both above and below the beaked whale band existed (**Figure D-4**). A SNR for the beaked whale band was generated that spanned 29 to 43 kHz, relative to the 20 to 30 kHz and 40 to 50 kHz bands. In this case, the two SNR metrics were multiplied in an element-wise fashion, and the product of the two was taken as the beaked whale index (**Figure D-5**). Strong positive values of this index (greater than 10 dB) were taken as potential indicators of beaked whale presence.
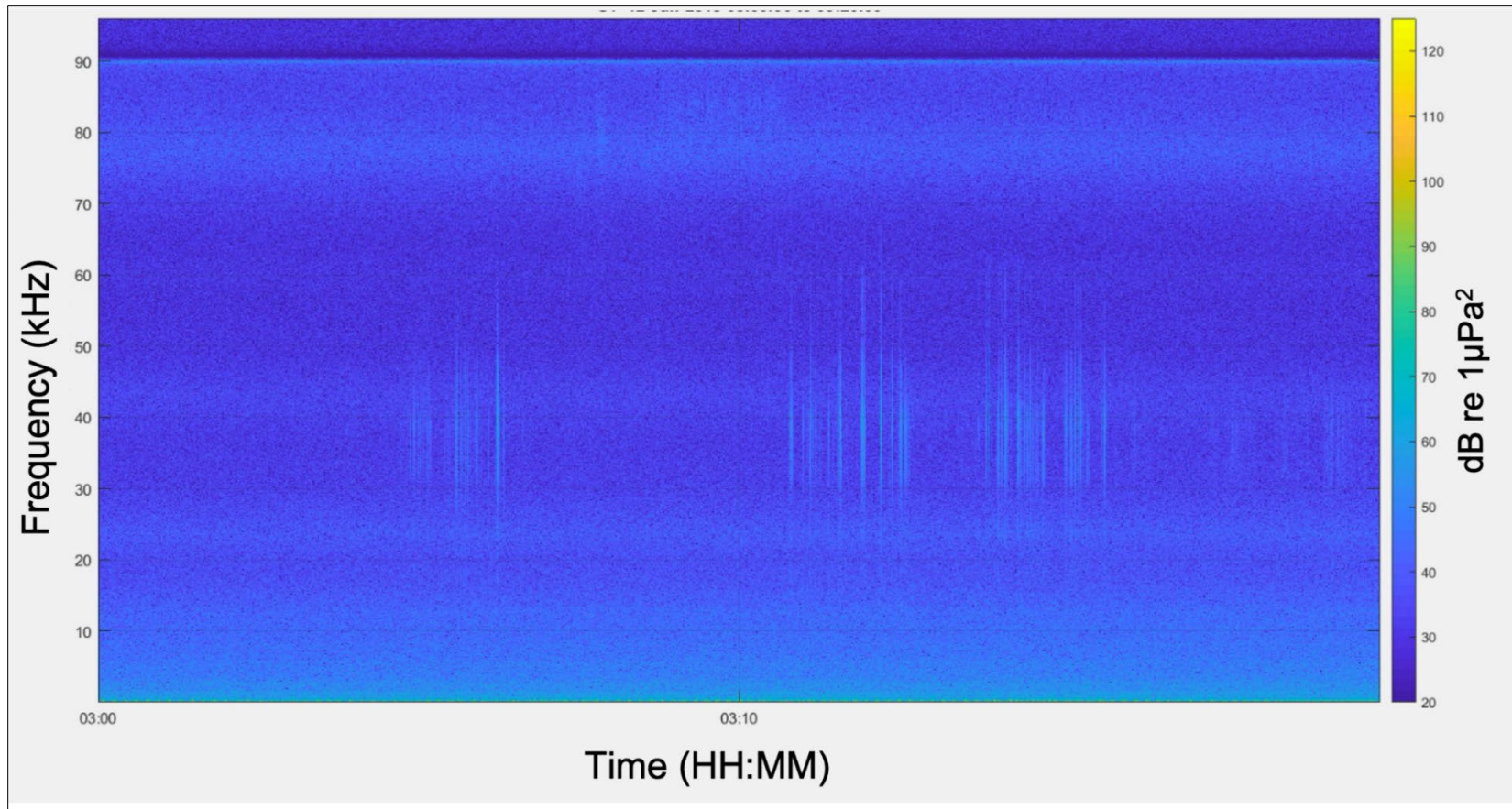
Figure D-4. Sample nominal beaked whale band (mid-frequency clicks) spectrogram.
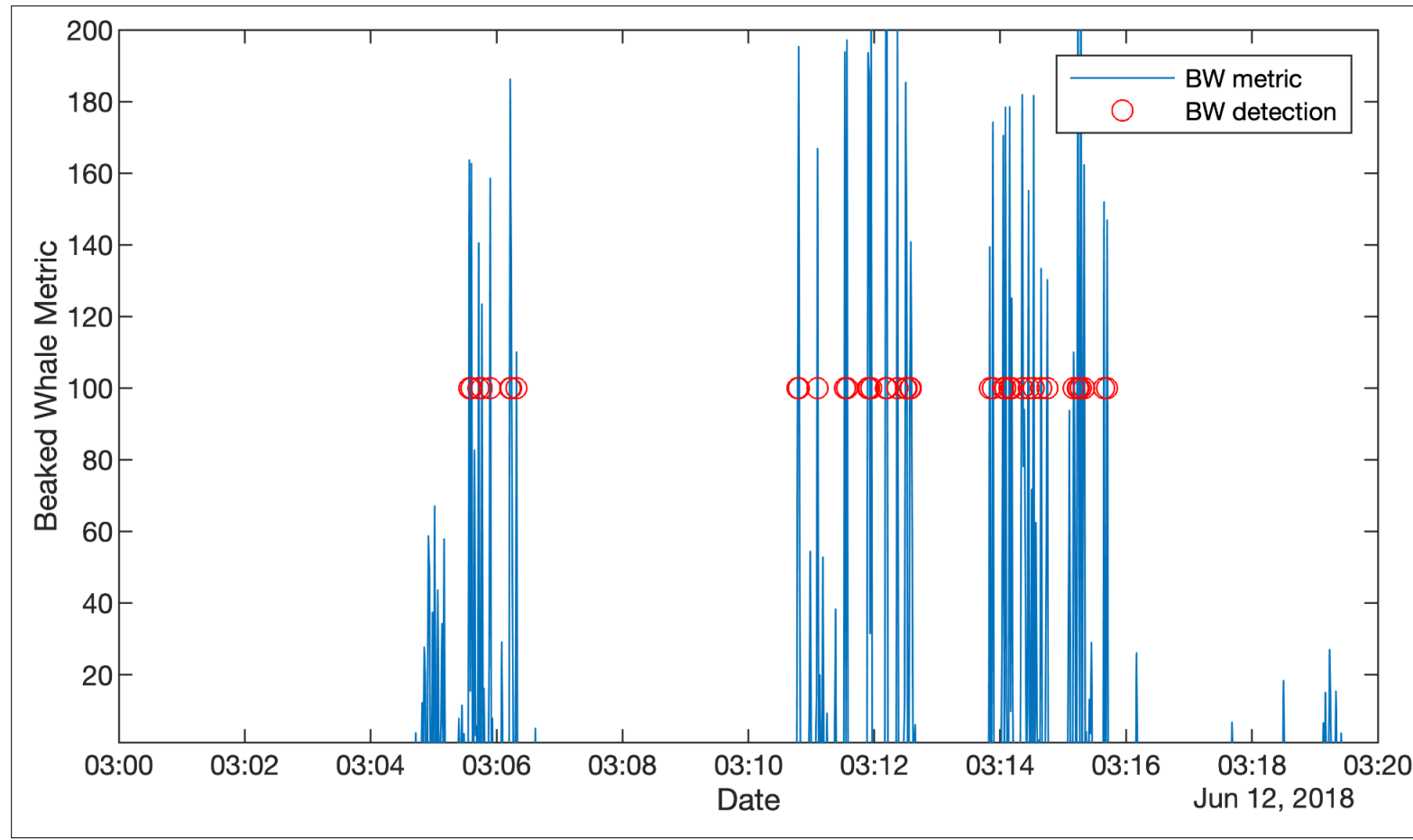
Figure D-5. Sample nominal beaked whale band (mid-frequency click) detection, with the blue lines representing the second-by-second beaked whale index, while the red circles represent signal exceedances or potential detections of beaked whales.

D.3.3 Statistical Analysis of Measured Vessel Received Levels

One approach to characterizing the sources of ambient noise was to predict how much of the variability in the recorded sound levels at each receiver could be explained by environmental conditions and independently available vessel descriptors.

D.3.3.1 Automatic Identification System Data

The AIS was developed with the intent to increase vessel safety (Tetreault 2005). An AIS-equipped ship continuously broadcasts its location, speed, course, identity, and additional information. Other vessels use this information to increase their situational awareness of surrounding vessel traffic. Shore-based receivers began archiving AIS data for management and research purposes. Among the AIS data fields transmitted are the Maritime Mobile Service Identity (MMSI) number, which provides a unique identification for each vessel. The MMSI number can be used to extract descriptive characteristics from a vessel database (e.g., IHS4 Markit). Processed AIS data (MarineCadestre.gov n.d.) were downloaded as datasets became available over time.

D.3.3.2 Source Level Models

A shipping noise model that can produce dynamic and static noise maps of broadband (BB) vessel noise was created (Frankel et al. 2017). The overall model is based on vessel speed and other descriptors as provided in the AIS tracks and IHS Markit database. These empirical data were viewed as an excellent complement to existing vessel source level models (e.g., Ross 1976). Additional vessel source-level information was discovered in the publications of McKenna et al. (2013) and Veirs et al. (2016). The authors of these two studies were contacted and agreed to provide copies of their measurements to be used as inputs into modeling and analyses for this project.

McKenna et al. (2013) collected and published 944 source level (SL) estimates for 570 different vessels transiting the Santa Barbara Channel. Some vessels were measured more than once. They used a simple $20 \log_{10}(\text{range})$ transmission loss (TL) model to calculate SLs. This simple spherical spreading approach presents a possible source of bias in their published values. Nevertheless, these data are the first large modern measurement set of vessel SLs. The authors also reported the speed through the water (STW) for the vessels. STW was obtained by subtracting the effect of surface currents from the measured speed over ground (SOG).

Veirs et al. (2016) also reported 2,182 SL estimates of 1,582 different vessels that passed by a calibrated hydrophone. The authors used both spherical spreading and an empirical TL measurement to produce multiple SL estimates. This dataset also included AIS-derived SOG. MAI converted their SOG speeds to STW.

The need to calculate STW from SOG values requires a surface current measurement or estimate. Regional current models were used for the vessels in the source level measurements. However, for the creation of the larger AIS-based noise model, a single worldwide current speed database was preferred. The Ocean Surface Current Analysis Real-time (OSCAR) database funded by the National Aeronautics and Space Administration (NASA) (ESR 2009) was selected for this purpose. OSCAR has monthly temporal and 1/3° latitude and longitude spatial resolutions.

The details of the SL measurements from McKenna et al. (2013) and Veirs et al. (2016) can be found in their respective papers; both papers used a similar methodology. Acoustic recordings were made of vessels as they passed by calibrated hydrophones, which allowed for measurement of the absolute received sound pressure level (SPL). The range from the receiver to the vessels was determined using AIS data. TL was estimated and added to the RL to produce the estimated vessel SLs.

Veirs et al. (2016) reported SLs in four forms representing two TL models, both with and without frequency absorption terms. The first model was based on simple spherical spreading, which was also used by McKenna et al (2013). The second model was empirically based on a single TL experiment conducted in March 2014 that produced a TL estimate of $18.6 \times \log_{10}$(range).

McKenna et al. (2013) provided SL data for 570 vessels, and their data set included both broadband (20 to 1,000 Hz) and one-third octave band SLs. The mean and standard deviation for each of these band levels were calculated **(Figure D-6)**.
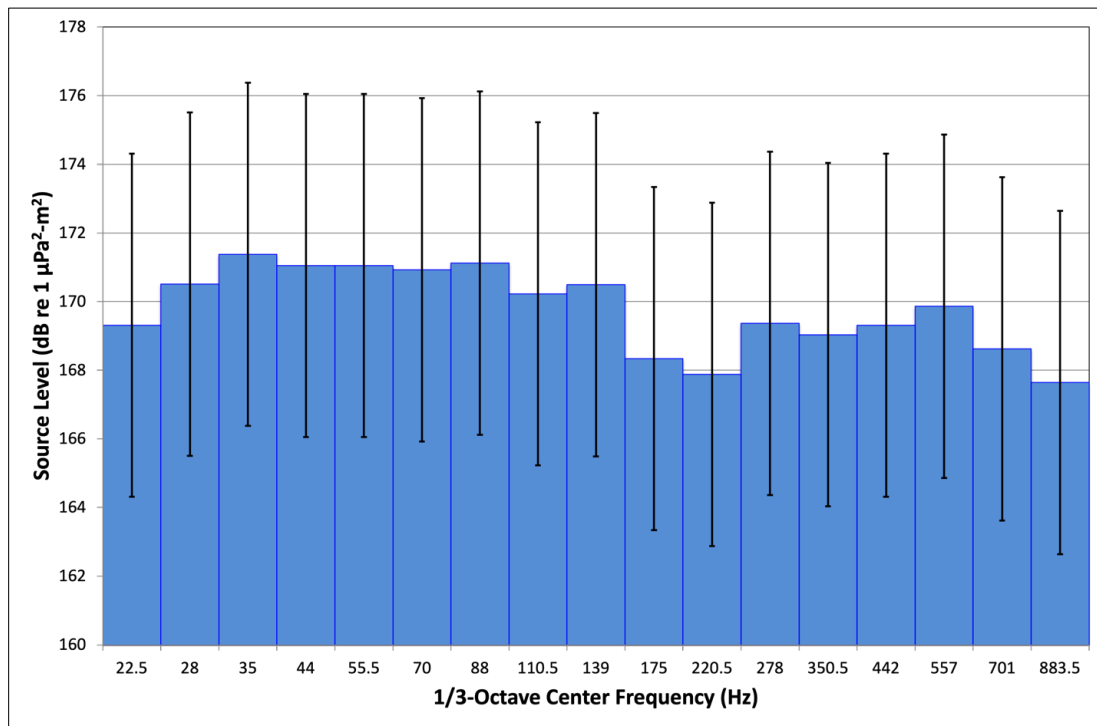
Figure D-6. Mean vessel spectrum as reported in McKenna et al. (2013).

Veirs et al. (2016) provided broadband source level data for 1,595 separate vessels that were measured between 1 and 23 times during their study. A total of 2,182 measurements were made. The broadband source level (SLBB) values provided by both Veirs et al. (2016) and McKenna et al. (2013) were used as inputs to the SL model.

The identity and speed of the vessel during the measurement was determined from AIS data. McKenna et al. (2013) adjusted the AIS SOG to STW using a local current model for Southern California (Interdisciplinary Oceanography Group 2017). Veirs et al. (2016) reported the AIS SOG value. Part of the analysis for this project was converting the McKenna et al. (2013) and Veirs et al. (2016) speed values to STW values using the Haro Strait model (NOAA 2016). Simard et al. (2016) also produced a vessel SL model that reports one-third-octave band levels. SLs for each vessel were calculated for the bands centered on 50 and 200 Hz.

D.3.3.3 Transmission Loss Model

The three-dimensional (3d) underwater sound propagation model, which was developed under the GOM Program, was used to predict the TL between vessels and the stationary recorders.[21] The principle of reciprocity was used as the models were run from each recorder location. Seasonal sound velocity profiles (SVP) were selected to reduce computational load and were extracted from the Global Digital Elevation Model (GDEM) database (Carnes 2009), which has a spatial resolution of 0.25° in latitude and longitude. The nearest node (location) in the database to each actual recorder position was selected. A grid of nine positions, spanning 0.5° by 0.5° and centered on the selected position, was averaged over space. The resulting monthly mean SVP profiles were plotted and grouped by season (**Figure D-7**). Winter included January, February, and March; spring consisted of April, May, and June; summer included July, August, and September; and fall consisted of October, November, and December. The mean SVP profile of each three-month period for each site were exported and used to calculate the TL fields.
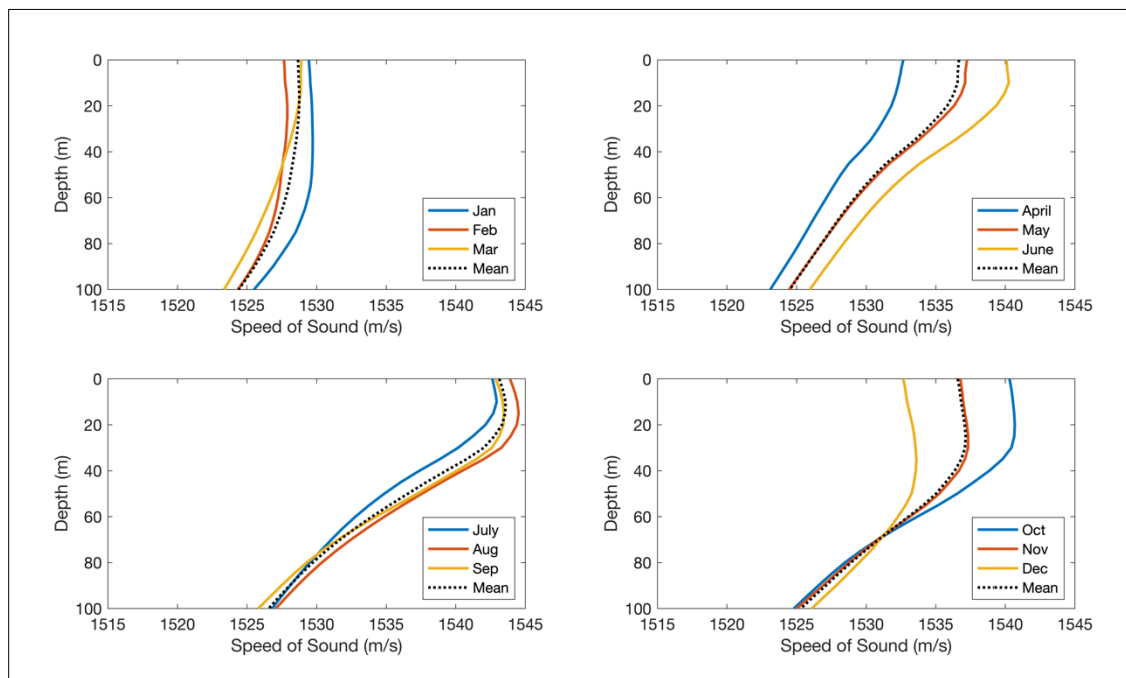
Figure D-7. Seasonal mean sound velocity profiles extracted from the GDEM database (Carnes 2009) for Site 10 during Deployment 1.

The propagation models were run for 50 and 200 Hz, as these frequencies are found within the main energy distribution of vessel and airgun noise. TLs were reported for three water depths (5, 10, and 20 m), which covered the nominal depth range of vessel propellers.

D.3.3.4 Received Sound Pressure Levels

Predicted received SPLs at each recorder were calculated by subtracting the TL from the broadband SL estimates and the one-third-octave estimates. Two broadband estimates were produced using the 50 Hz TL predictions (BB1) and the 200 Hz TL predictions (BB2). The one-third-octave SLs used their respective TL predictions to generate the predicted the third-octave band (TOB) RLs (Hz50 and Hz200).

---

[21] Project reports titled: GOM PAM 2018 program monitoring project SHRU report, by Lin Y-T, 2019; and GOM PAM program 2019 monitoring project SHRU report, by Lin Y-T, 2021.

D.3.3.5 Statistical Modeling

The goal of the statistical modeling was the prediction of the variance amount in the measured SPLs with independently derived predictor variables. These variables include the distance of the vessel from the recorder as well as the predicted received sound level at the recorder. Additional metrics of windspeed and wave height were included since these environmental conditions are known to influence the level of LF sound.

Statistical analyses were run using generalized additive mixed models (GAMMs), although the initial analyses used simple generalized additive models (GAMs). GAMs and GAMMs both fit smoothed weighting curves to the dependent and predictor variables. These curve fits are then tested to see whether they are statistically significant. The values of the dependent variables may be adjusted during the modeling process by the additional predictor variables. Therefore, these curve fits show the general form of the relationship (e.g., **Figures D-8** and **D-9**). In these examples, the y-axis values of these smoothed plots differ from the original data because these curves are fit to adjusted modeled values that include the influence of the other predictor variables. The shape of the curve is the important component in illustrating the relationship between two variables.

GAM analyses were used to explore the relationship between the variables and determine the appropriate statistical distribution and link function. A gamma distribution with a log link function was used. These initial analyses also examined evidence of autocorrelation in the data. The existence of autocorrelation was anticipated given that the SLs at time 't' are very much related to the final SLs at time 't +10'.

Autocorrelation function plots (ACF) showed strong evidence of autocorrelation within the data. The method chosen to address this issue was to move to a GAMM model using autoregressive (AR) 1 correlation structure. The GAMM was first run without the AR1 correlation structure, and the value of the first lag of the autocorrelation function was used as the predicted value for the AR1 correction factor in the subsequent GAMM.
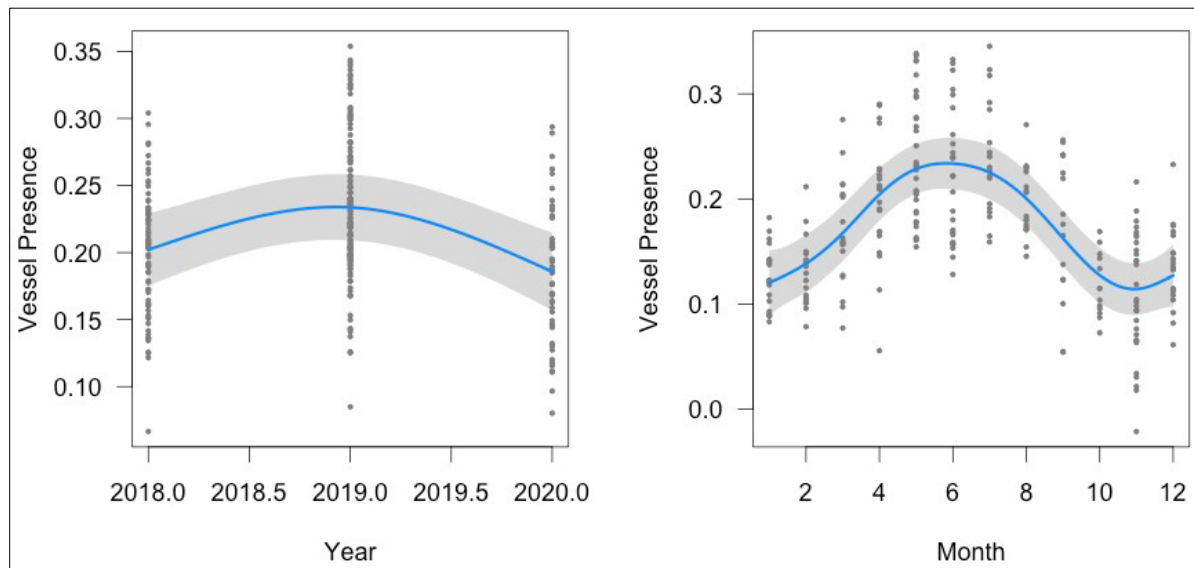
Figure D-8: GAM smoothing functions for Year and Month effects on vessel detections.

Note: The Vessel Presence metric represents the monthly mean of hourly detections. The temporal patterns of vessel detection rates are explored as a function of year and month.
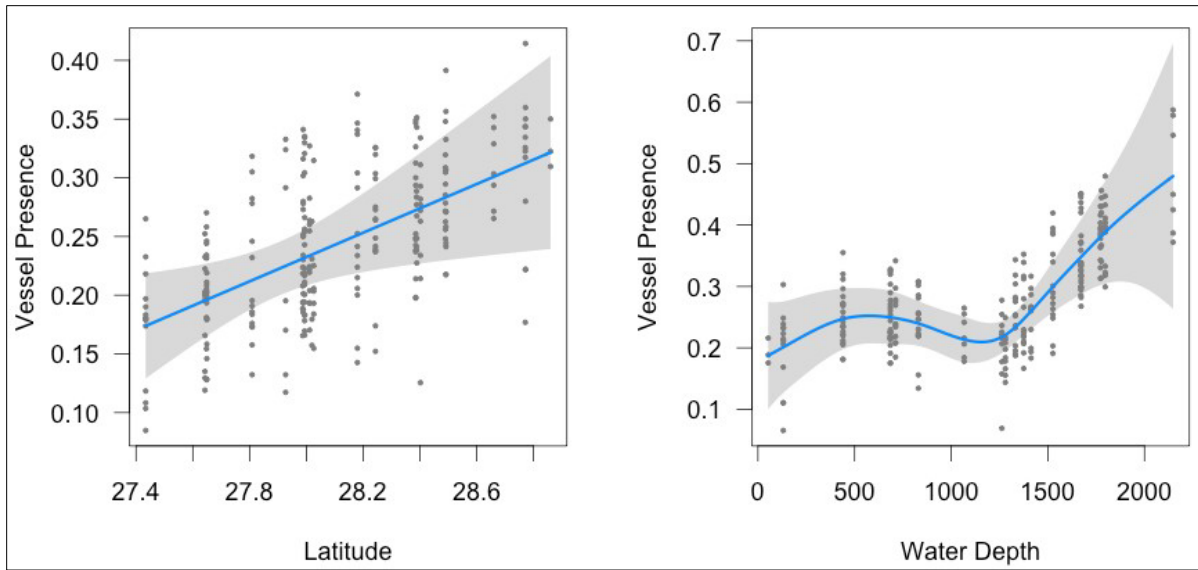
Figure D-9: GAM smoothing functions for Latitude and Water Depth effects on vessel detections.

Note: The Vessel Presence metric represents the monthly mean of hourly detections. The temporal patterns of vessel detection rates are explored as a function of year and month.

D.3.3.6   Revised Simplified Statistical Analysis of Measured Vessel Received Levels

Deployment 1 RL data were assessed using the full predicted RL model statistical approach previously outlined herein. However, based on the Deployment 1 results, it was apparent that a different statistical approach was needed. The predicted RL variables in the original GAMM analysis did not result in a strong predictive power and were frequently outperformed by the weather and AIS-derived statistical variables.

Therefore, a second, more simple statistical approach was implemented to characterize the sources of ambient noise from vessel RLs and predict or identify the sources of variability at each of the 10 EARS and RH receivers. The simplified statistical analysis approach was based on the 1-hour, 1-Hz resolution data and used only weather and AIS-derived predictor variables for the GAMM analysis. The same Vessel Band acoustic measure was calculated for each hour, and the minimum closest point of approach (CPA) for each vessel in that hour was determined. The minimum CPA and the number of vessels passing from 0 to 2 km, 2 to 4 km, and 4 to 10 km were tabulated and input into the statistical model. The simplified model used the form: Gamma Family with the log Link Function. The following is the formula for the simplified model:

VesselBand ~ s(sDate, k = 50, bs = "ts") + s(WaveHeight) + s(Windspeed) + s(CPAmin) + (km2) + (km4) + (km10)

Where:

   VesselBand is measured SPL in the band from AA to BB Hz.

   sDate is the "normalized date", which spans from -365 to 365 representing the date range of the project. This transformation of date values is done to improve the performance of the statistical model.

   WaveHeight is the wave height in meters reported by the weather buoys.

   Windspeed is the wind speed reported by the weather buoys in (check units).

CPAmin is the minimum CPA of any vessel in the 1-hour time period determined by analysis of the AIS data.

Km2 represents the number of vessels that approached within 2 km of the recording buoys during the hour.

Km4 represents the number of vessels than approached between 2 and 4 km of the recorder.
Km10 represents the number of vessels that approached between 4 and 10 km of the recorder.

D.4 Results

D.4.1 Comparison of Data from EARS and RH Recorders

A comparison of data from each deployment of the RH and EARS recorders was conducted to obtain the median spectra for each recorder and deployment (**Figures D-10** to **D-13**). There appears to be a consistent difference between the two recording systems below 100 Hz, which is also evident in the monthly temporal and spatial spectral data.
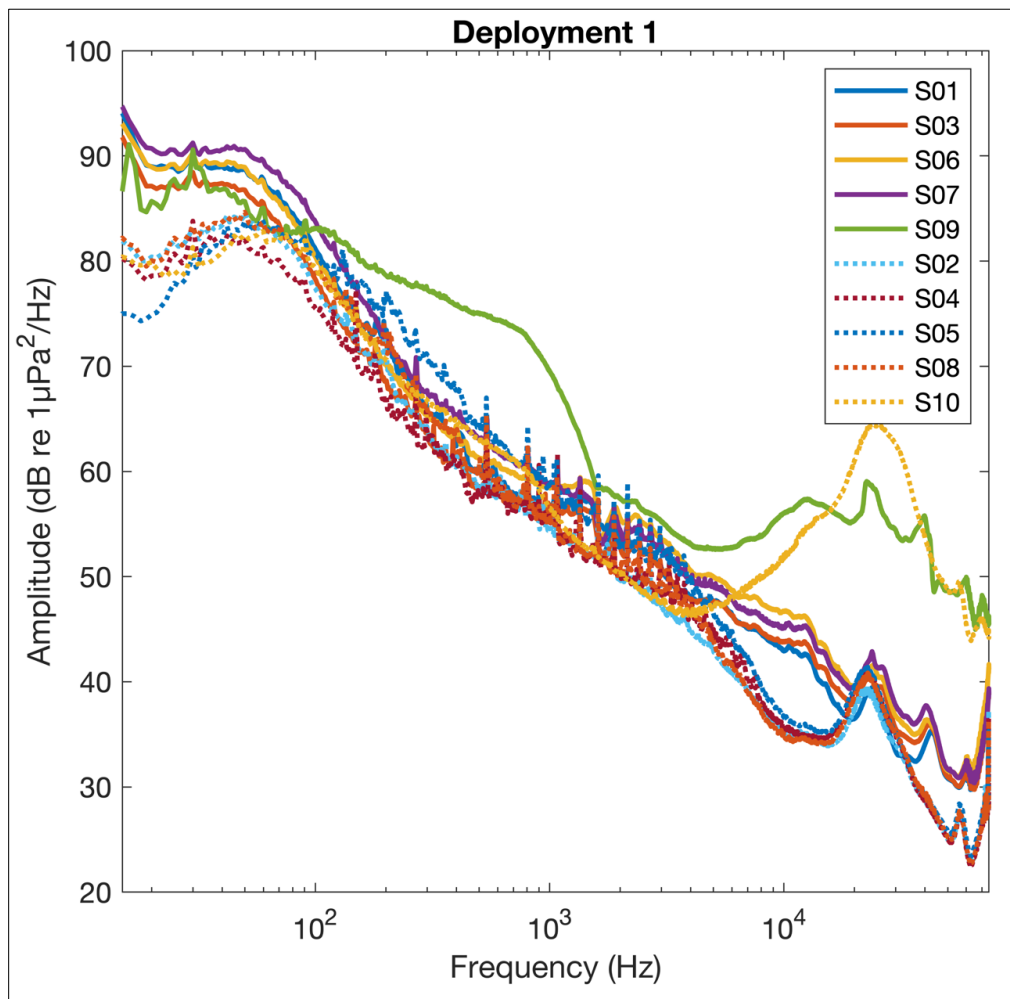
Figure D-10. Median spectra for all 10 EARS and RH recorders during Deployment 1.

Note: Data recorded by the RHs are shown as solid lines, and data from EARS are shown as dotted lines. Stations 9 and 10, which were the shallowest water recorder locations, show an elevation in high frequency noise.

194
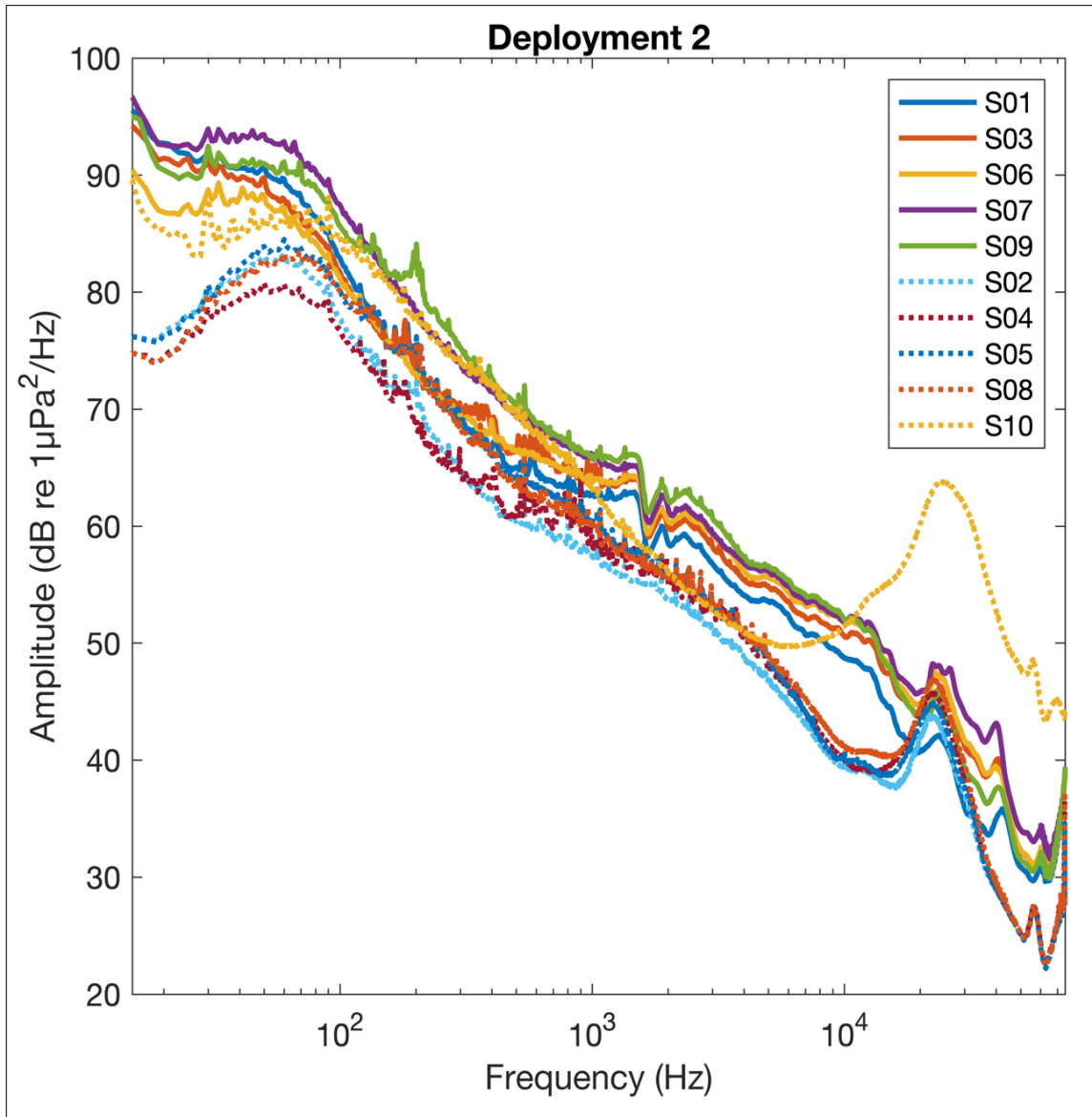
Figure D-11. Median spectra for all 10 EARS and RH recorders during Deployment 2.

Note: Data recorded by the RHs are shown as solid lines, while data from EARS are shown as dotted lines.
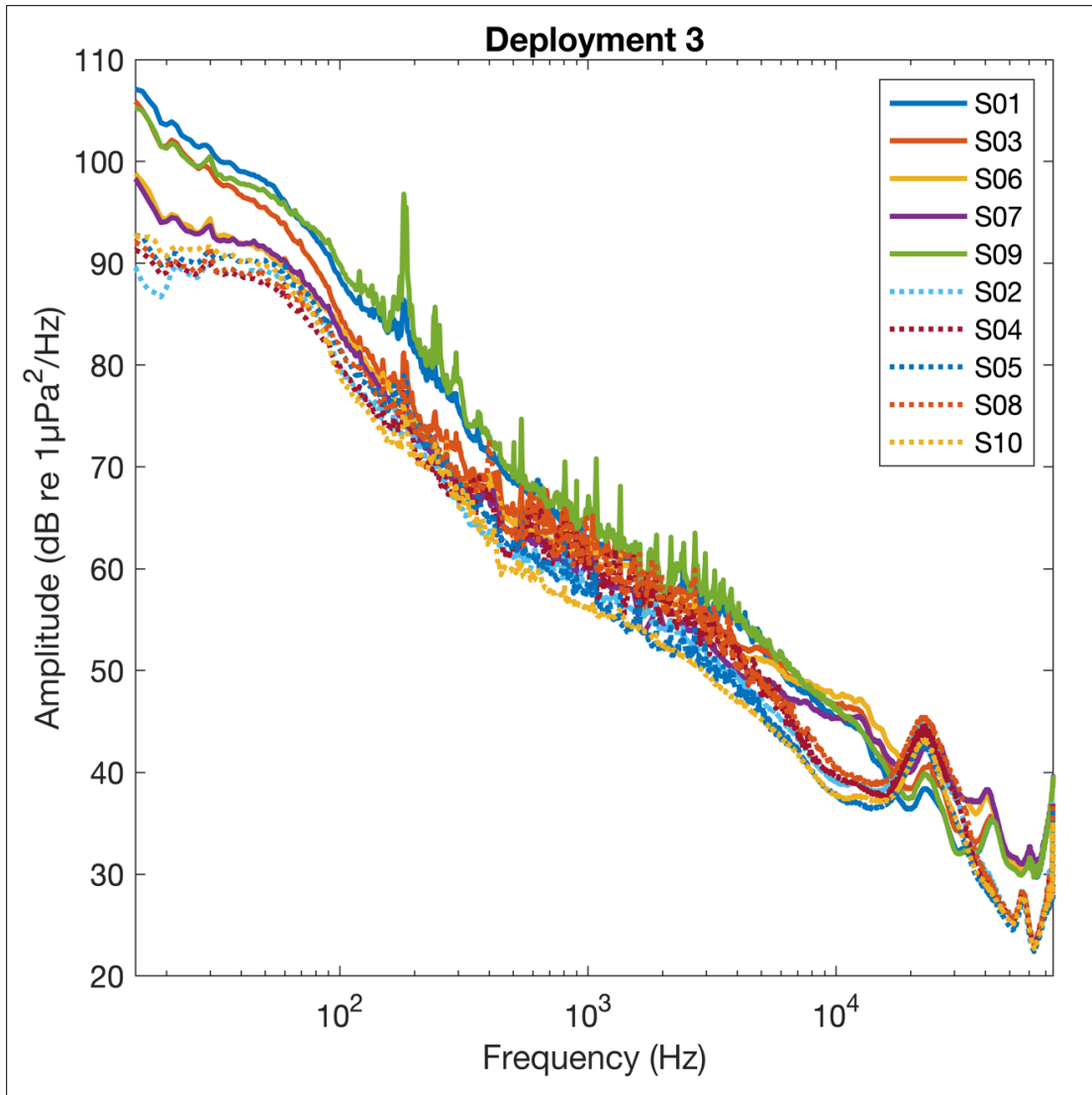
Figure D-12. Median spectra for all 10 EARS and RH recorders during Deployment 3.

Note: Data recorded by the RHs are shown as solid lines, while data from EARS are shown as dotted lines.
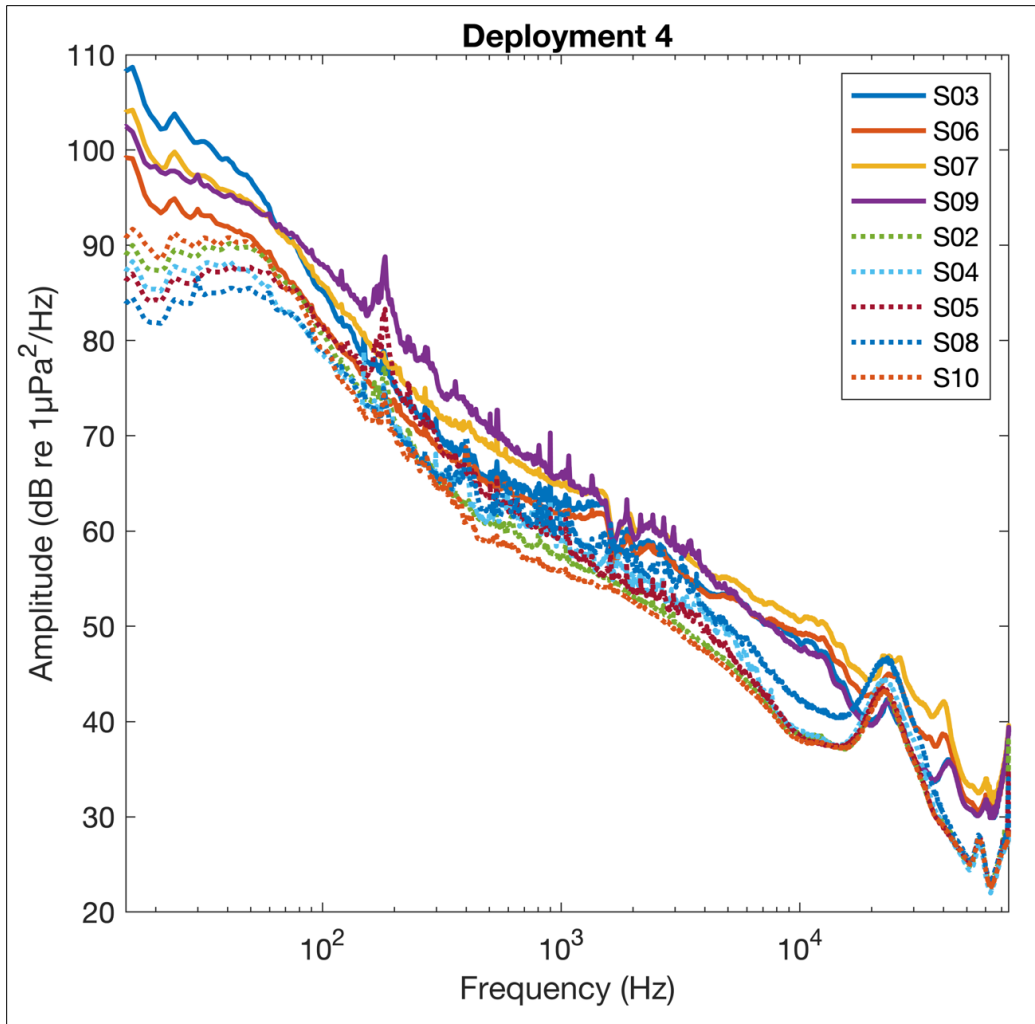
Figure D-13. Median spectra for all 10 EARS and RH recorders during Deployment 4.

Note: Data recorded by the RHs are shown as solid lines, while data from EARS are shown as dotted lines.

D.4.2   Anthropogenic (Vessel and Seismic Airgun) Sound Detection Analysis

The primary goal of this analysis was to characterize the anthropogenic input into the soundscape of the northern GOM (**Figure D-1**), an area characterized by a large amount of vessel traffic. Furthermore, seismic exploration using airguns is a common input into the northern GOM soundscape.

Exploratory detection analyses investigated the performance of band limited energy detectors over a variety of integration times using data from Deployment 1. The best detection performance was found to occur with a 1-hour integration time. This allowed the use of the summarized 1-hour, third octave band (TOB) datasets, which accelerated the detection analysis process.

D.4.2.1   Vessel Detection Analysis

Vessel detections were made on an hourly basis, which were then converted to daily estimates of vessel presence. If a vessel was detected for at least 1 hour, a vessel was associated with that day. Finally, monthly values were taken as the mean of hourly and daily estimates of vessel presence (**Figure D-14**). The metric based on hourly inputs ranges from 0 to 0.4 and has a quasi-normal distribution. The metric based on daily

input ranges from 0 to 1.0 and is highly skewed to the maximum value; this shows that vessels were present almost every day at every receiver location. The difference in the hourly and daily based airgun metrics was less since airgun operations tend to be more persistent in time than transitory vessel passages.
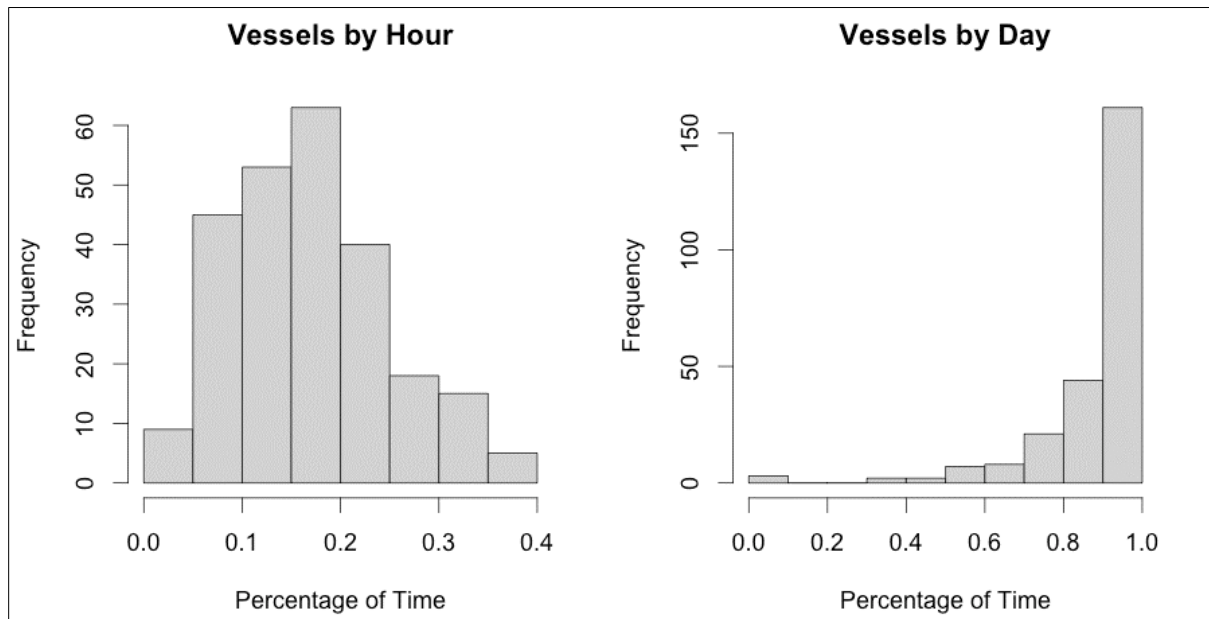
Figure D-14. Comparison of monthly values for vessel detection based on hourly inputs (left) and daily inputs (right).

The effects of spatial and temporal variables on vessel detection rates were explored with a GAM. Significant patterns by year and month were observed. Numbers of vessel detection increased from 2018 to 2019 but decreased again in 2020. This may be a side effect of the sampling period and the markedly strong monthly pattern, where the number of vessels was highest in summer and lower in winter months (**Table D-7** and **Figure D-8**). The patterns seen for latitude and water depth were also significant and indicated more contradictory patterns of increased vessel detection rates as latitude and water depth increased (**Figure D-9**).

Table D-7. GAM details for vessel detections

A. Parametric Coefficients	Estimate	Std. Error	t-value	p-value
(Intercept)	0.1687	0.0034	49.9252	< 0.0001
B. Smoothing Terms	**edf**	**Ref.df**	**F-value**	**p-value**
s(Year)	1.9697	1.9988	16.3144	< 0.0001
s(Month)	5.5831	6.7431	27.1694	< 0.0001
s(Lat)	1.0000	1.0000	6.0799	0.0144
s(Lon)	5.4112	5.9740	5.8301	< 0.0001
s(WaterDepth)	4.7717	5.4302	9.4967	< 0.0001
Key: edf=empirical distribution function; F-value=value on the F distribution calculated by dividing two mean squares; Lat=latitude; Lon=longitude; p-value= level of marginal significance within a statistical hypothesis test, representing the probability of the occurrence of a given event; Ref.df=reference degrees of freedom; s=scaled; Std. Error=Standard Error				

The number of vessel detection was greatest in the middle longitudes and decreased strongly to the east, probably related to the location of port facilities (**Figure D-15**).
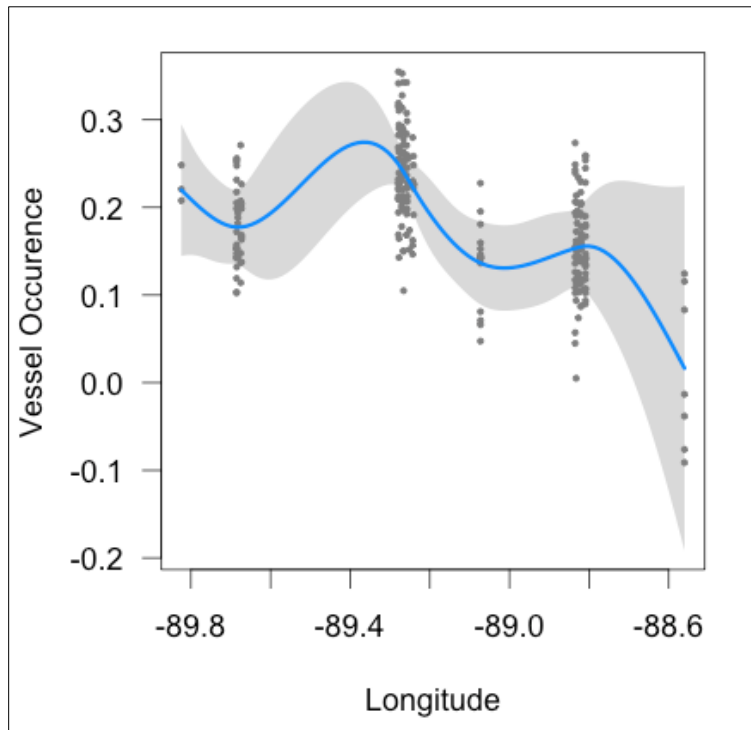
Figure D-15. GAM smoothing functions for Longitude effects on vessel detections.

D.4.2.2 Airgun Detection Analysis

A similar detection analysis was conducted for airgun signal detections (**Table D-8**). Month and year for airgun signal detections had similar patterns to that of vessel detections (**Figure D-16**). Latitude and longitude effects for airgun signals were borderline statistically significant, with a dip in the frequency of airgun detections in the middle latitudes and, again, a higher frequency of signal detection in the middle longitudes (**Figure D-17**).

Table D-8. GAM details for airgun detections

A. Parametric Coefficients	Estimate	Std. Error	t-value	p-value
(Intercept)	0.3668	0.0144	25.5239	< 0.0001
B. Smooth Terms	**edf**	**Ref.df**	**F-value**	**p-value**
s(Year)	1.9816	1.9995	39.2143	< 0.0001
s(Month)	7.0302	8.0963	13.5408	< 0.0001
s(Lat)	2.7219	3.2705	2.9462	0.0428
s(Lon)	6.4339	6.9885	2.0527	0.0436
s(WaterDepth)	1.0000	1.0000	0.0878	0.7673
Key: edf=empirical distribution function; F-value=value on the F distribution calculated by dividing two mean squares; Lat=latitude; Lon=longitude; p-value= level of marginal significance within a statistical hypothesis test, representing the probability of the occurrence of a given event; Ref.df=reference degrees of freedom; s=scaled; Std. Error=Standard Error				
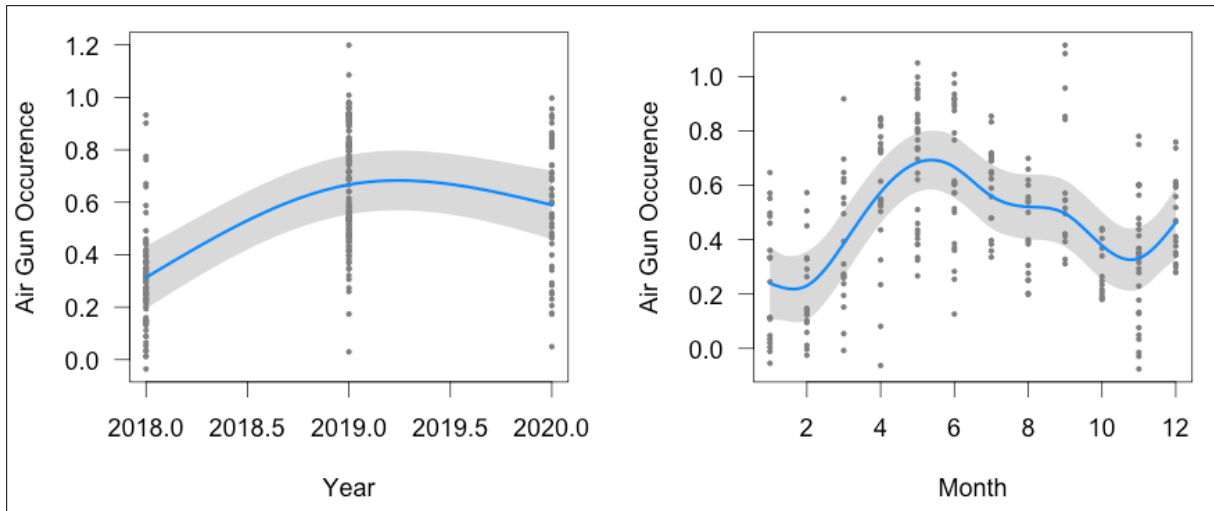
Figure D-16. GAM smoothing functions for Year and Month effects on air gun signal detections.
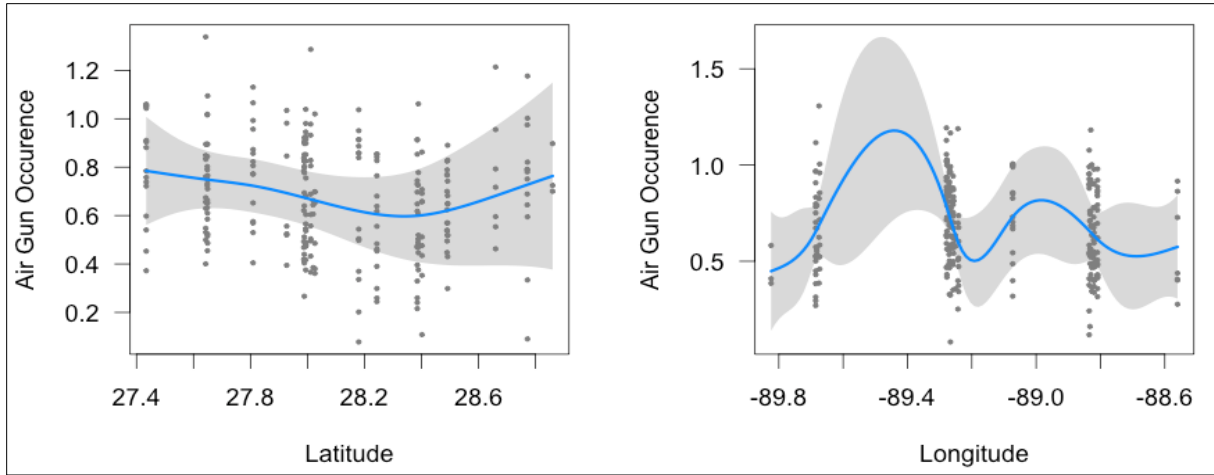
Figure D-17. GAM smoothing functions for Latitude and Longitude effects on air gun signal detections.

D.4.2.3   Vessel and Airgun Detection Patterns

The spatial and temporal patterns of the vessel and airgun detections can be found in **Appendix D-A**. For each month and buoy location, the percentage of vessel and airgun detections is shown as the pie charts (**Appendix D-A, Figures D-A1 to D-A26**). At a given time, it is possible for both an airgun and a vessel to be detected. Therefore, a pie chart filled to 50 percent with green would indicate continuous airgun presence. Airguns were detected operating continuously during some months (e.g., May and June 2019 and April and May 2020).

D.4.2.4   Seaglider Vessel and Airgun Detection Analysis

The hand-scored glider acoustic records produced 65 hours with vessel detections and only 8 hours with airgun detections. The distribution of vessel detections was examined as a function of latitude, longitude, and glider depth using a GAMM with an autocorrelation correction (**Table D-9**). The model was significant with an adjusted R-square of 0.26 (N=750). The curve fit functions show an increased number of vessel detections at higher latitudes and western longitudes (**Figure D-18**).

Table D-9. GAMM details for Seaglider vessel detections

A. Parametric Coefficients	Estimate	Std. Error	t-value	p-value
(Intercept)	-3.0497	0.2133	-14.2976	< 0.0001
B. Smooth Terms	**edf**	**Ref.df**	**F-value**	**p-value**
s(Lat)	1.0000	1.0000	40.4632	< 0.0001
s(abs(Lon))	3.8768	3.8768	25.1599	< 0.0001
s(Depth)	1.0000	1.0000	0.5670	0.4517
Key: edf=empirical distribution function; F-value=value on the F distribution calculated by dividing two mean squares; Lat=latitude; Lon=longitude; p-value= level of marginal significance within a statistical hypothesis test, representing the probability of the occurrence of a given event; Ref.df=reference degrees of freedom; s=scaled; Std. Error=Standard Error				
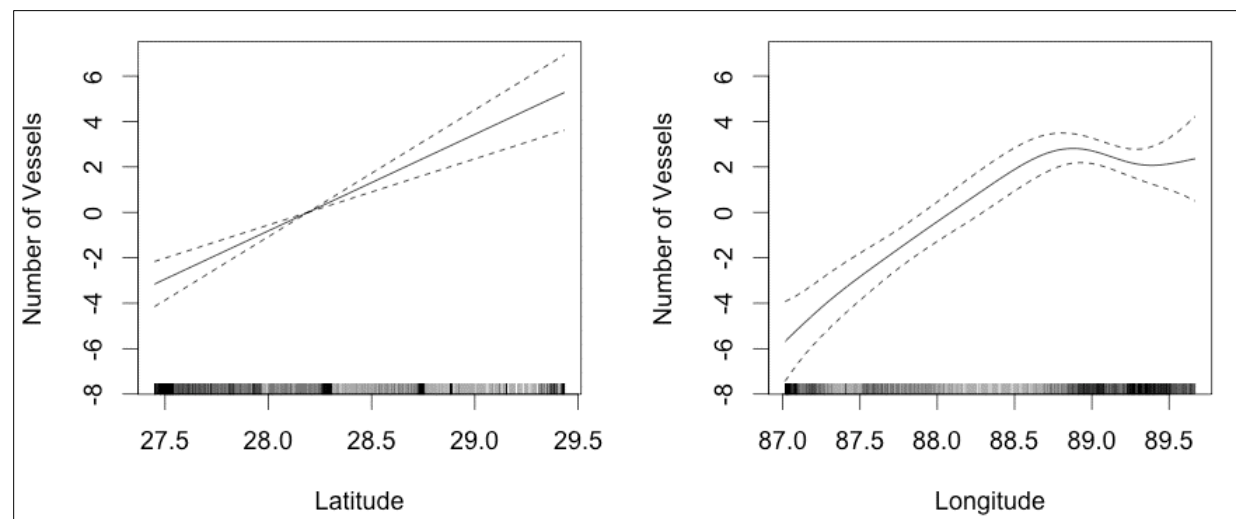
Figure D-18. GAM smoothing functions for Latitude and Longitude effects on vessel detections from the Seaglider.

D.4.3 Biological Detection Analysis

D.4.3.1 Rice's Whale (*Balaenoptera ricei*) Detections

The frequency overlap between the signals of Rice's whales and the prevalent anthropogenic noise made it difficult to reliably detect the calls of Rice's whales using only the spectrally analyzed data. A better approach would be to use a matched-filter detection process that operates on the waveform data.

D.4.3.2 Dolphin Band Detections: Low-frequency Clicks

Hourly detection rates were converted to binary yes/no values. The daily mean of these values was calculated and analyzed as a function of month, latitude, longitude, and water depth to examine for spatial and temporal patterns. All predictors for the dolphin band detections were statistically significant (**Table D-10**). The overall model had an adjusted R-square of 0.257. Throughout the first deployment, dolphin band detections rose from May until September and then fell precipitously, both in rate and number of detections, in November (**Figure D-19**). Detection rates peaked in nearshore shallow waters as well as in offshore water deeper than 1,000 m. This may be due to the detection function being triggered by multiple species. Detection rates appeared to increase with latitude. Peak rates were seen in the middle longitudes and decreased to the east and west (**Figure D-20**).

Table D-10. GAM output of dolphin band detection rates

A. Parametric Coefficients	Estimate	Std. Error	t-value	p-value
(Intercept)	-1.1931	0.0244	-48.9009	< 0.0001
B. Smooth Terms	**edf**	**Ref.df**	**F-value**	**p-value**
s(Month)	2.9484	2.9979	30.0646	< 0.0001
te(Lat)	1.0003	1.0004	4.4688	0.0347
te(Lon)	2.7912	2.8335	4.9775	0.0017
s(WaterDepth)	4.2630	4.6721	7.7719	< 0.0001
Key: edf=empirical distribution function; F-value=value on the F distribution calculated by dividing two mean squares; Lat=latitude; Lon=longitude; p-value= level of marginal significance within a statistical hypothesis test, representing the probability of the occurrence of a given event; Ref.df=reference degrees of freedom; s=scaled; Std. Error=Standard Error				
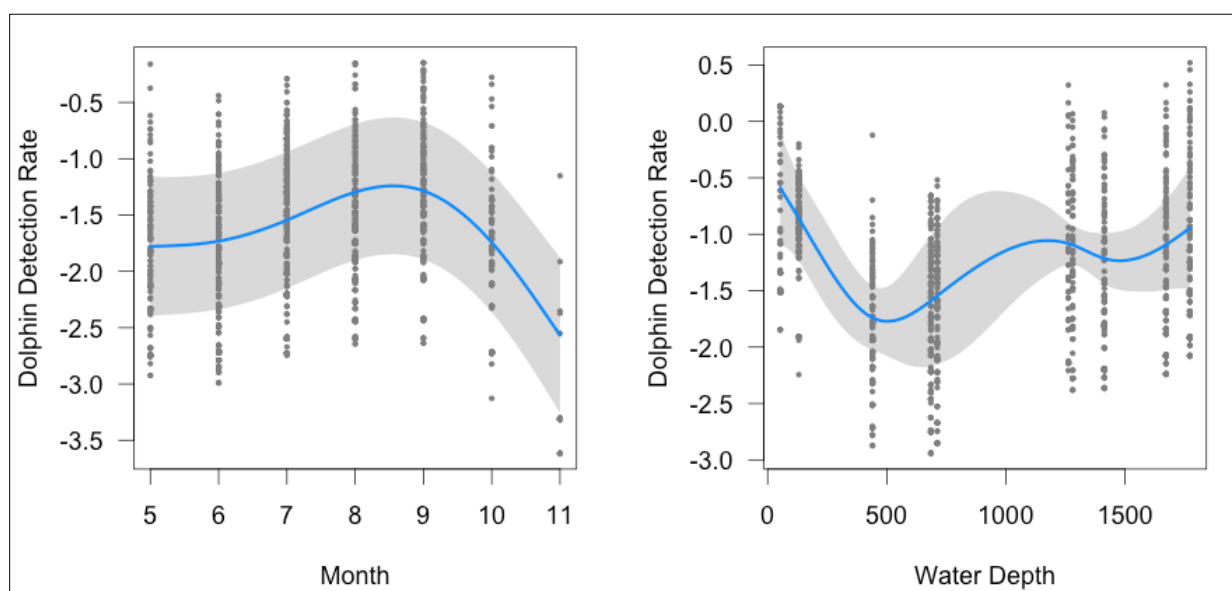
Figure D-19. Month and Water Depth prediction functions for dolphin band detection rates.
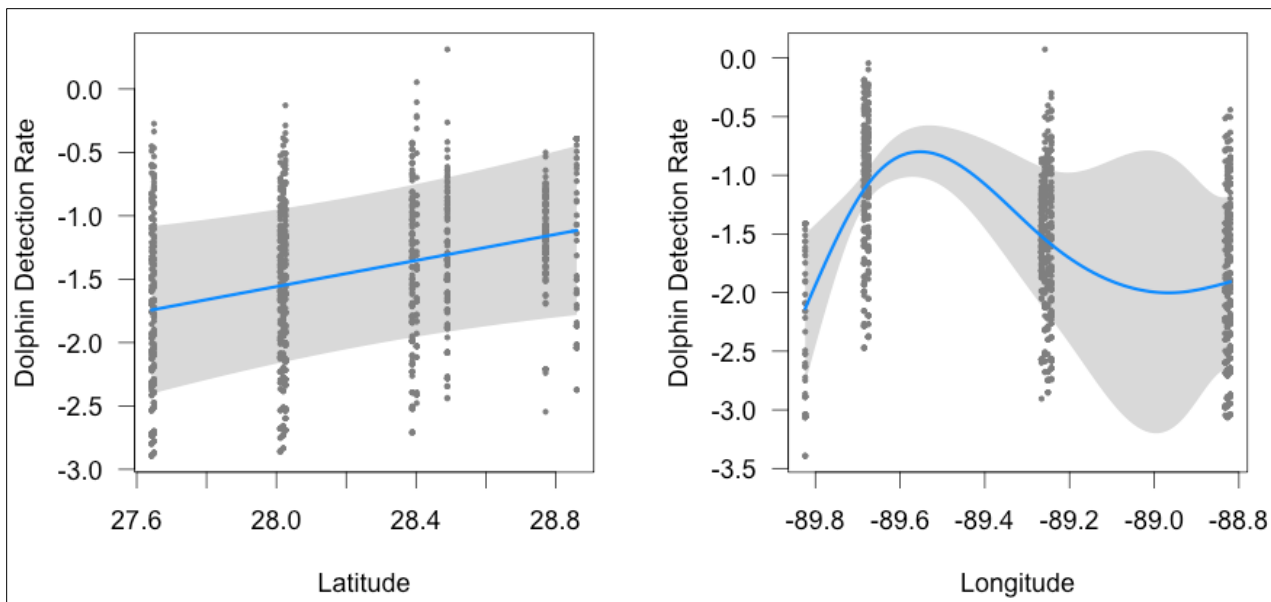
Figure D-20. Latitude and Longitude prediction functions for dolphin band detection rates.

D.4.3.3. Beaked Whale Band Detections: Mid-frequency Clicks

Hourly "beaked whale band" detection rates were converted to binary yes/no values. The daily means of these values were calculated and analyzed as a function of month, latitude, longitude, and water depth to examine for spatial and temporal patterns (**Table D-11**). All predictors for the beaked whale band detections were statistically significant. The overall model had a remarkably high adjusted R-square value of 0.594. Detection rates appear to increase from May through September and then begin to decline in October (**Figure D-21**). The peak of beaked whale detections appeared to occur at intermediate water depths of 500 to 1,000 m and decline in the very shallow and very deep depths, which may indicate a habitat preference for slope environments.

Table D-11. GAM output for Beaked Whale band detection rates.

A. Parametric Coefficients	Estimate	Std. Error	t-value	p-value
(Intercept)	-2.9421	0.0646	-45.5107	< 0.0001
B. Smooth Terms	**edf**	**Ref.df**	**F-value**	**p-value**
s(Month)	2.9527	2.9982	35.2393	< 0.0001
te(Lat)	2.0576	2.0690	24.2420	< 0.0001
te(Lon)	2.9340	2.9506	27.4816	< 0.0001
s(WaterDepth)	3.9361	3.9784	10.3034	< 0.0001
Key: edf=empirical distribution function; F-value=value on the F distribution calculated by dividing two mean squares; Lat=latitude; Lon=longitude; p-value= level of marginal significance within a statistical hypothesis test, representing the probability of the occurrence of a given event; Ref.df=reference degrees of freedom; s=scaled; Std. Error=Standard Error				
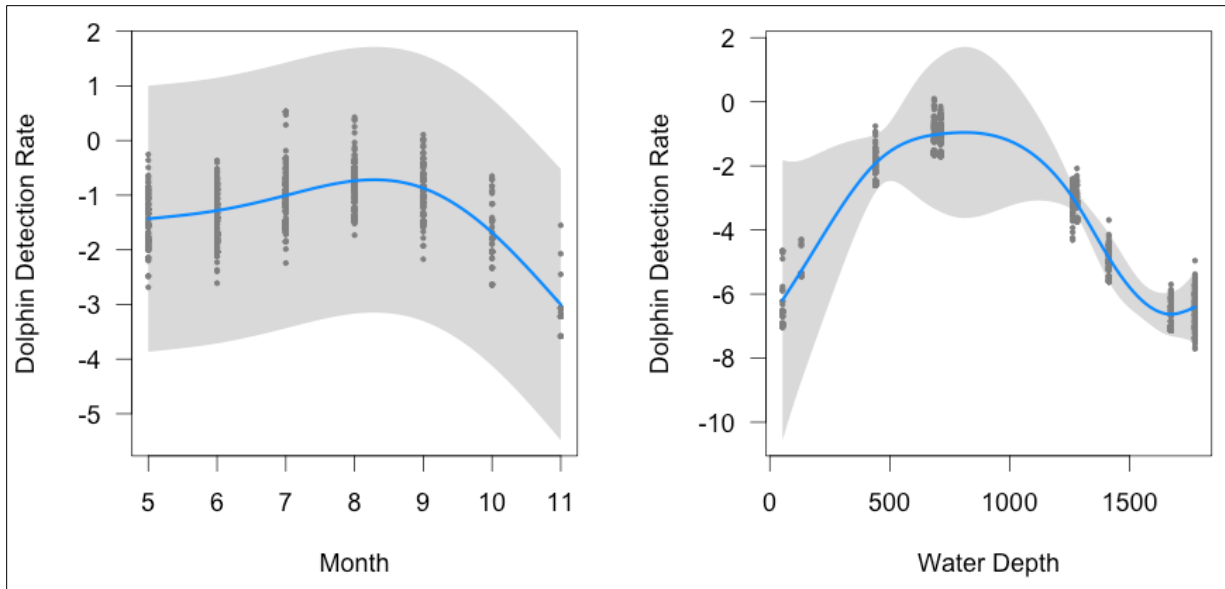
Figure D-21. Month and Water Depth prediction functions for beaked whale band detection rates.

Detection rates appear to be highest in lowest latitudes and decrease as latitude increases. The effect of longitude here appears to be the opposite of that for the dolphin band results, with highest values to the west and east (**Figure D-22**).
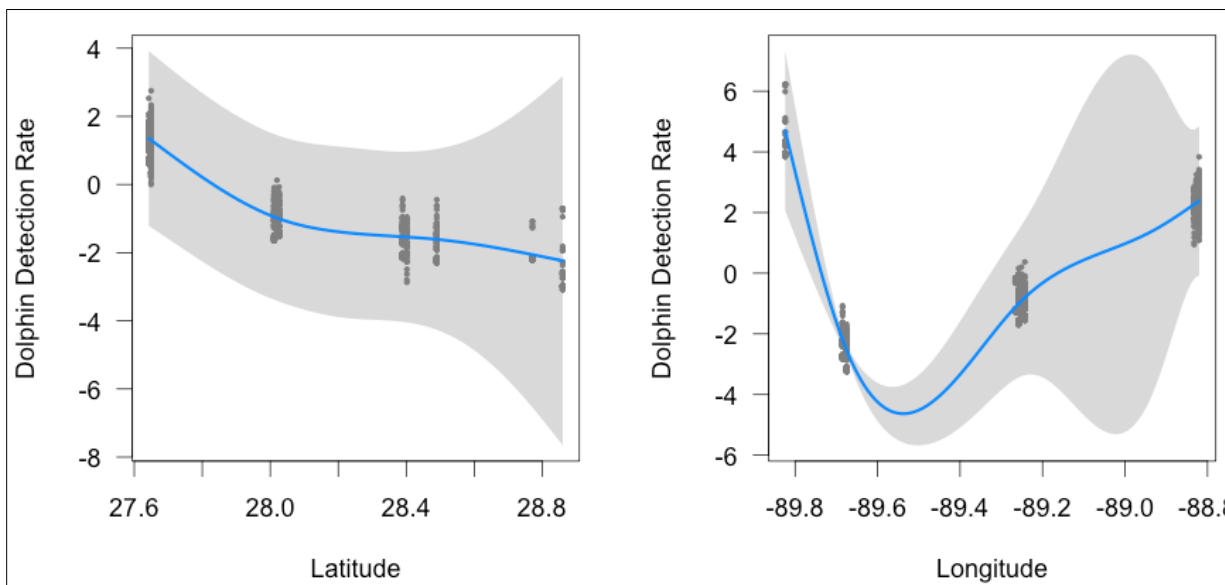
Figure D-22. Latitude and Longitude prediction functions for beaked whale band detection rates.

D.4.4 Statistical Analysis of Vessel Received Levels

This analysis was undertaken to determine the contribution of vessel noise to the overall soundscape. An added benefit is that it offers a method to predict or model vessel noise contributions in unmonitored areas. The northern GOM is a highly industrialized area, and noise from vessels and airgun operations are the major anthropogenic contribution to the ambient soundscape (Estabrook et al. 2016; Wiggins et al. 2016). Accordingly, the predicted contribution of vessels to the measured RLs in the 200 to 2,500 Hz

band at each receiver was analyzed. Additional predictive variables include the windspeed, wave height, CPA between each vessel, and receiver.

The AIS-based modeling to predict vessel RLs was conducted in several bands. Hz50 and Hz200 represent the predicted spectral levels at 50 Hz and 200 Hz. Note that in each of these analyses, the date values were "scaled" so the "sDate" values only spanned the two-year period of the experiment (from -1 to 1). The R-squared (i.e., measure of how much of the variance is in the dependent variable) for each analysis is also reported. R-squared is a measure of how much of the variance is in the dependent variable (i.e., the 200 to 2,500 Hz vessel band sound level is explained by the independent or predictor variables).

Results from statistical analyses of vessel received levels using Deployment 1 data are presented and discussed below

D.4.4.1 Deployment 1, Receiver 1

The significant predictors for Receiver 1 included scaled date, windspeed, CPA, and predicted BB level (**Table D-12**; **Figures D-23** and **D-24**). The R-squared value was 0.483. The date function is complex and may reflect the contribution of airgun signals to the measured levels.

The windspeed function shows a simple increase in LF noise as windspeed increases. The CPA function shows a clean and marked increase in Vessel Band noise level as vessels approach closer to the receiver. The predicted BB function was borderline significant, and its curve fit shows little relationship between the two variables.

Table D-12. GAM output for Deployment 1, Receiver 1

A. Parametric Coefficients	Estimate	Std. Error	t-value	p-value
(Intercept)	4.5799	0.0007	6428.4166	< 0.0001
B. Smooth Terms	**edf**	**Ref.df**	**F-value**	**p-value**
s(sDate)	36.7457	49.0000	25.3114	< 0.0001
s(WaveHeight)	1.0001	1.0001	2.9124	0.0879
s(Windspeed)	1.0000	1.0000	49.2164	< 0.0001
s(CPA)	8.9311	8.9311	166.1668	< 0.0001
s(Hz200) -200 Hz TOB RL	1.0000	1.0000	0.0528	0.8182
s(BB1) BB RL (w 50 Hz TL)	3.9427	3.9427	3.0960	0.0220
s(BB2) BB RL (w/200 Hz TL)	1.0000	1.0000	0.0538	0.8166

Key: BB=broadband; CPA= closest point of approach; edf=empirical distribution function; F-value=value on the F distribution calculated by dividing two mean squares; Hz=Hertz; Lat=latitude; Lon=longitude; p-value= level of marginal significance within a statistical hypothesis test, representing the probability of the occurrence of a given event; Ref.df=reference degrees of freedom; RL=received level; s=scaled; Std. Error=Standard Error; TL=transmission loss; TOB=third-octave band
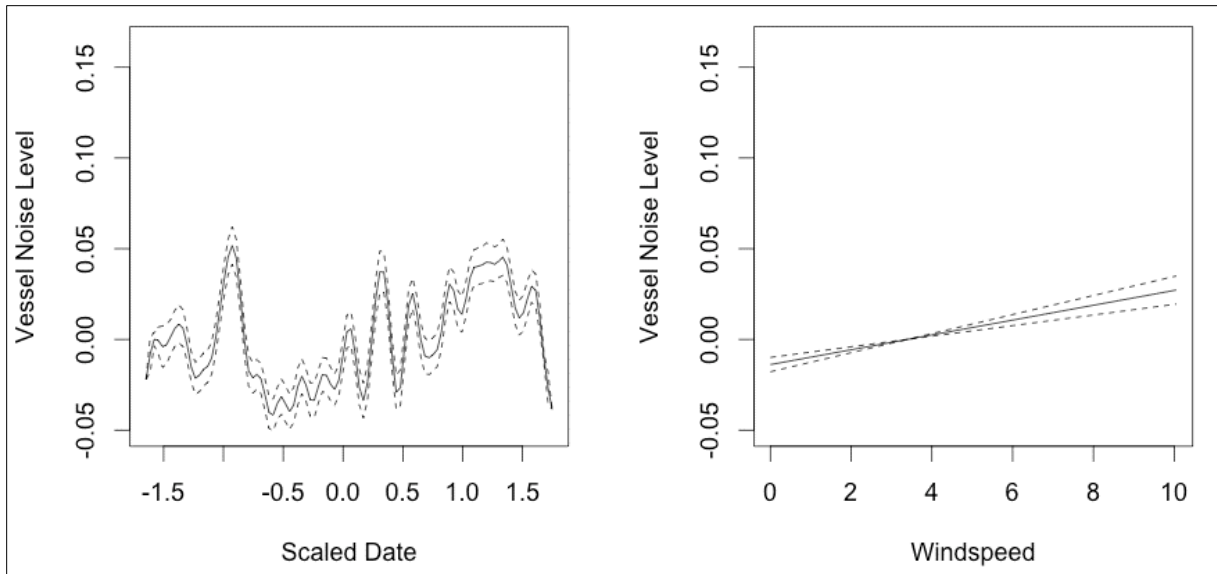
Figure D-23. Smoothing functions for Measured Vessel Band Noise as a function of Scaled Date and Windspeed for Receiver 1.
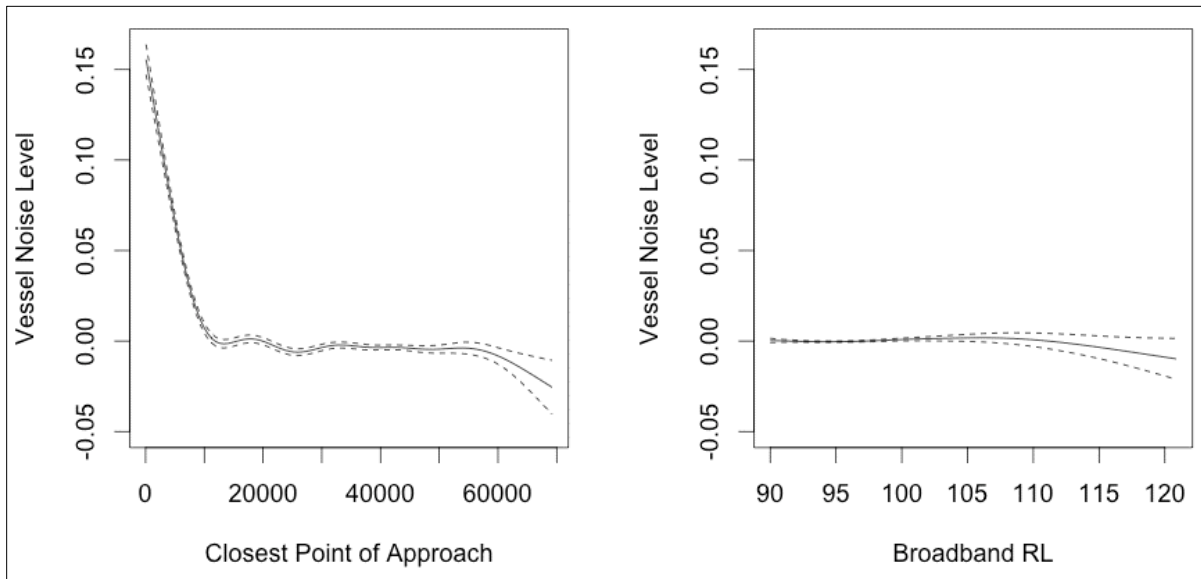
Figure D-24. Smoothing functions for Measured Vessel Band Noise as a function of CPA and predicted RL for Receiver 1, Deployment 1.

D.4.4.2   Deployment 1, Receiver 2

The significant predictors for Receiver 2 included scaled date, CPA, and predicted BB level (**Table D-13**; **Figure D-25**). The R-squared value was 0.500. The date function is complex and may reflect the contribution of airgun signals to the measured levels. The CPA function shows a clear increase in Vessel band noise level as vessels approach the receiver. This effect becomes apparent at a range of approximately 10 km.

Table D-13. GAM output for Deployment 1, Receiver 2

A. Parametric Coefficients	Estimate	Std. Error	t-value	p-value
(Intercept)	4.4876	0.0008	5299.3872	< 0.0001
B. Smooth Terms	**edf**	**Ref.df**	**F-value**	**p-value**
s(sDate)	40.1935	49.0000	29.5363	< 0.0001
s(WaveHeight)	1.0000	1.0000	2.5937	0.1073
s(Windspeed)	1.6665	1.6665	1.1491	0.1999
s(CPA)	8.8453	8.8453	289.9161	< 0.0001
s(Hz200) -200 Hz TOB RL	3.0302	3.0302	2.0410	0.0949
s(BB1) BB RL (w 50 Hz TL)	1.0000	1.0000	0.1162	0.7332
s(BB2) BB RL (w/200 Hz TL)	1.0006	1.0006	2.5905	0.1075
Key: BB=broadband; CPA= closest point of approach; edf=empirical distribution function; F-value=value on the F distribution calculated by dividing two mean squares; Hz=Hertz; Lat=latitude; Lon=longitude; p-value= level of marginal significance within a statistical hypothesis test, representing the probability of the occurrence of a given event; Ref.df=reference degrees of freedom; RL=received level; s=scaled; Std. Error=Standard Error; TL=transmission loss; TOB=third-octave band				
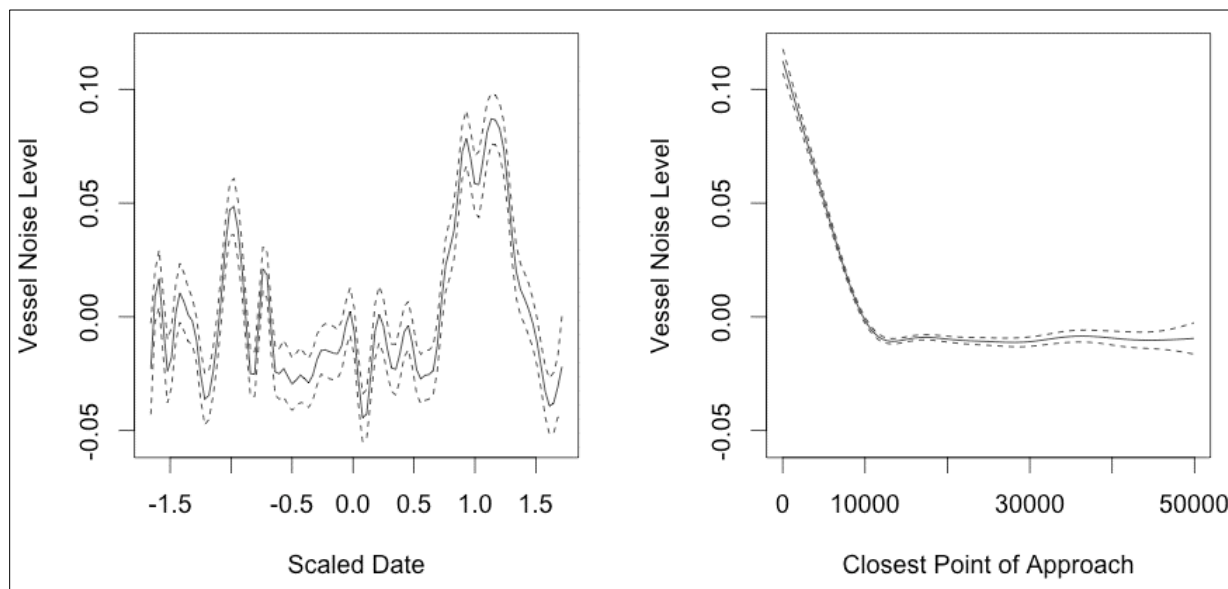
Figure D-25. Smoothing functions for Measured Vessel Band Noise as a function of Wave Height and Windspeed for Receiver 2, Deployment 1.

D.4.4.3   Deployment 1, Receiver 3

The significant predictors for Receiver 3 included scaled date, windspeed, wave height, CPA, and predicted BB level (**Table D-14**; **Figures D-26**, **D-27**, and **D-28**). The R-squared value was 0.283.

The scaled date function for this receiver is simple and shows a slight increase in LF noise across the entire recording period. The wave height function shows a simple increase in LF noise as wave height increases up to approximately 2 m. There are a few measurements of wave height more than 6 m that complicate the shape of the smoothing function. The windspeed function shows a simple increase in LF noise as windspeed increases. The CPA function shows increases in measured LF noise as vessels

approach within 10 km of the recorder. As the predicted RLs increased above 100 decibels referenced to 1 microPascal squared (dB re $1\mu Pa^2$), the predicted RL shows an increase in the measured RL.

Table D-14. GAM output for Deployment 1, Receiver 3

A. Parametric Coefficients	Estimate	Std. Error	t-value	p-value
(Intercept)	4.5639	0.0012	3727.8837	< 0.0001
B. Smooth Terms	**edf**	**Ref.df**	**F-value**	**p-value**
s(sDate)	0.9175	49.0000	0.1689	0.0023
s(WaveHeight)	3.9106	3.9106	17.3975	< 0.0001
s(Windspeed)	1.0000	1.0000	33.0425	< 0.0001
s(CPA)	8.8051	8.8051	99.7800	< 0.0001
s(Hz200) -200 Hz TOB RL	1.0000	1.0000	0.4744	0.4910
s(BB1) BB RL (w 50 Hz TL)	1.0000	1.0000	1.5468	0.2137
s(BB2) BB RL (w/200 Hz TL)	3.0172	3.0172	4.0763	0.0067

Key: BB=broadband; CPA= closest point of approach; edf=empirical distribution function; F-value=value on the F distribution calculated by dividing two mean squares; Hz=Hertz; Lat=latitude; Lon=longitude; p-value= level of marginal significance within a statistical hypothesis test, representing the probability of the occurrence of a given event; Ref.df=reference degrees of freedom; RL=received level; s=scaled; Std. Error=Standard Error; TL=transmission loss; TOB=third-octave band
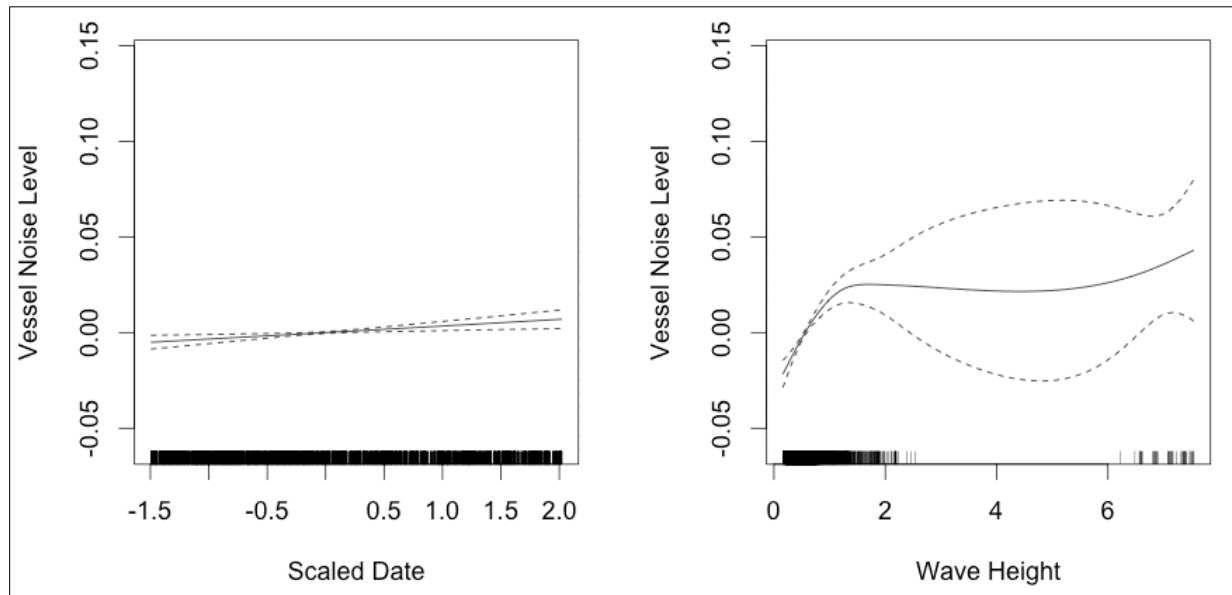
Figure D-26. Smoothing functions for Measured Vessel Band Noise as a function of Scaled Date and Wave Height for Receiver 3, Deployment 1.
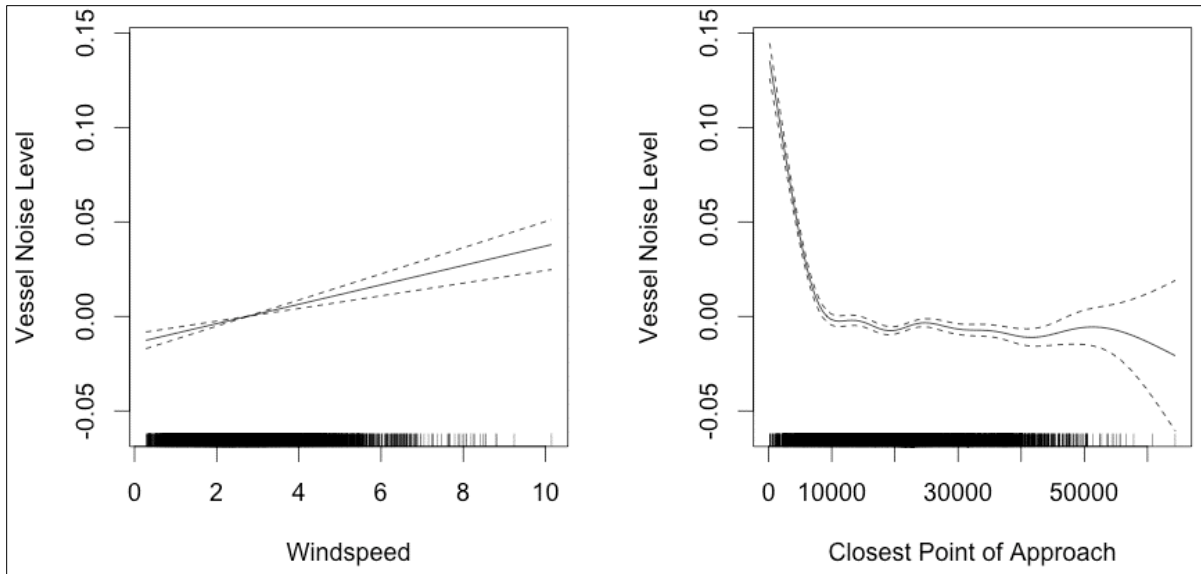
Figure D-27. Smoothing functions for Measured Vessel Band Noise as a function of Windspeed and CPA for Receiver 3.
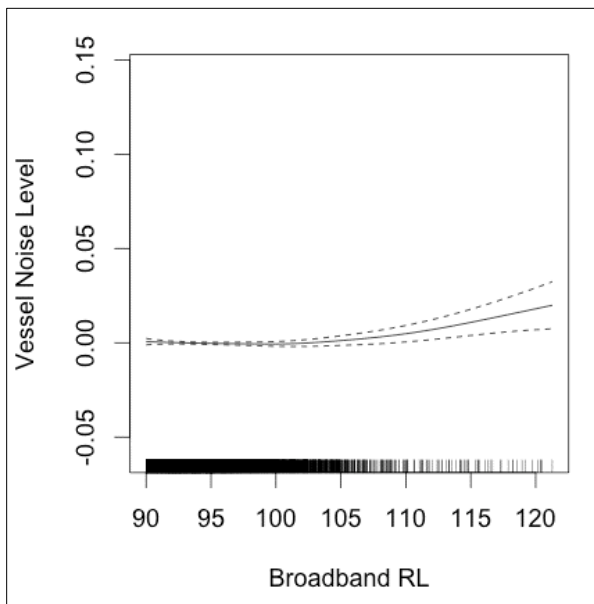
Figure D-28. Smoothing functions for Measured Vessel Band Noise as a function of predicted BB RL for Receiver 3, Deployment 1.

D.4.4.4 Deployment 1, Receiver 4

The significant predictors for Receiver 4 included scaled date, wave height, windspeed, and CPA (**Table D-15**; **Figures D-29**, and **D-30**). The R-squared value was 0.516. The data function is complex and likely reflects the contribution of airgun signals to the measured data. The wave height function reflects an increase in measured LF noise as wave height increases to 2.5 m. The windspeed function shows a simple increase in LF noise as windspeed increases. The CPA function shows that LF noise increases as vessels approach within 10 km of the recorder (**Figure D-30**).

Table D-15. GAM output for Deployment 1, Receiver 4

A. Parametric Coefficients	Estimate	Std. Error	t-value	p-value
(Intercept)	4.4781	0.0009	5070.0197	< 0.0001
B. Smooth Terms	**edf**	**Ref.df**	**F-value**	**p-value**
s(sDate)	43.7241	49.0000	24.4023	< 0.0001
s(WaveHeight)	1.0000	1.0000	5.1574	0.0232
s(Windspeed)	1.0000	1.0000	17.3588	< 0.0001
s(CPA)	8.6951	8.6951	128.5288	< 0.0001
s(Hz200) -200 Hz TOB RL	1.0000	1.0000	0.2316	0.6303
s(BB1) BB RL (w 50 Hz TL)	1.0000	1.0000	0.9053	0.3414
s(BB2) BB RL (w/200 Hz TL)	1.0000	1.0000	3.5316	0.0602
Key: BB=broadband; CPA= closest point of approach; edf=empirical distribution function; F-value=value on the F distribution calculated by dividing two mean squares; Hz=Hertz; Lat=latitude; Lon=longitude; p-value= level of marginal significance within a statistical hypothesis test, representing the probability of the occurrence of a given event; Ref.df=reference degrees of freedom; RL=received level; s=scaled; Std. Error=Standard Error; TL=transmission loss; TOB=third-octave band				
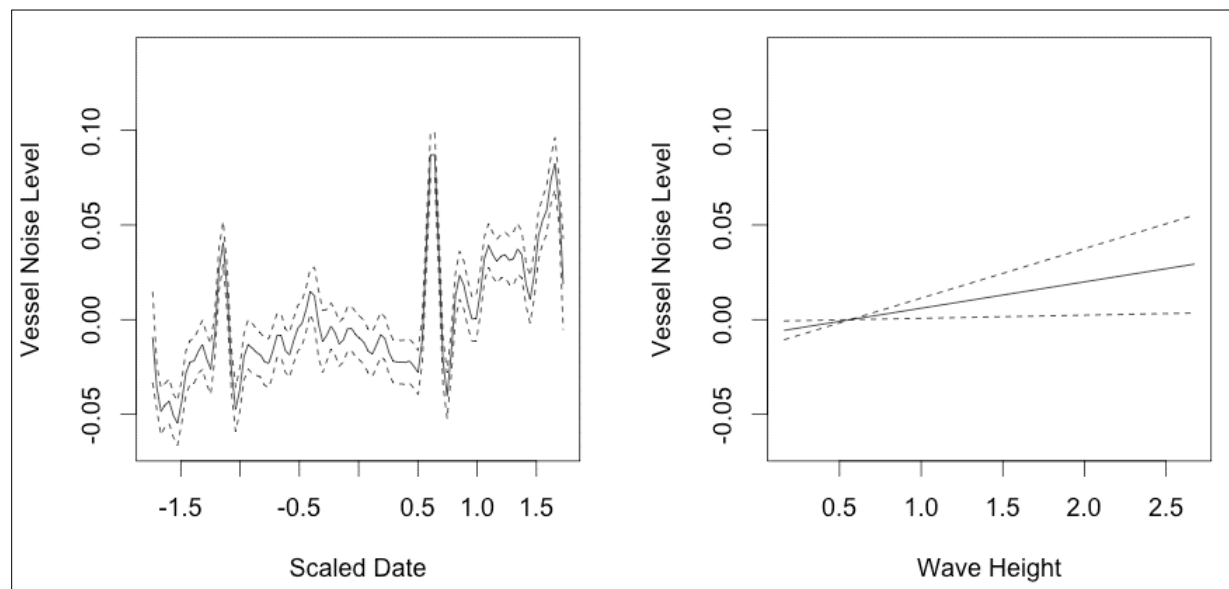
Figure D-29. Smoothing functions for Measured Vessel Band Noise as a function of Scaled Date and Wave Height for Receiver 4, Deployment 1.
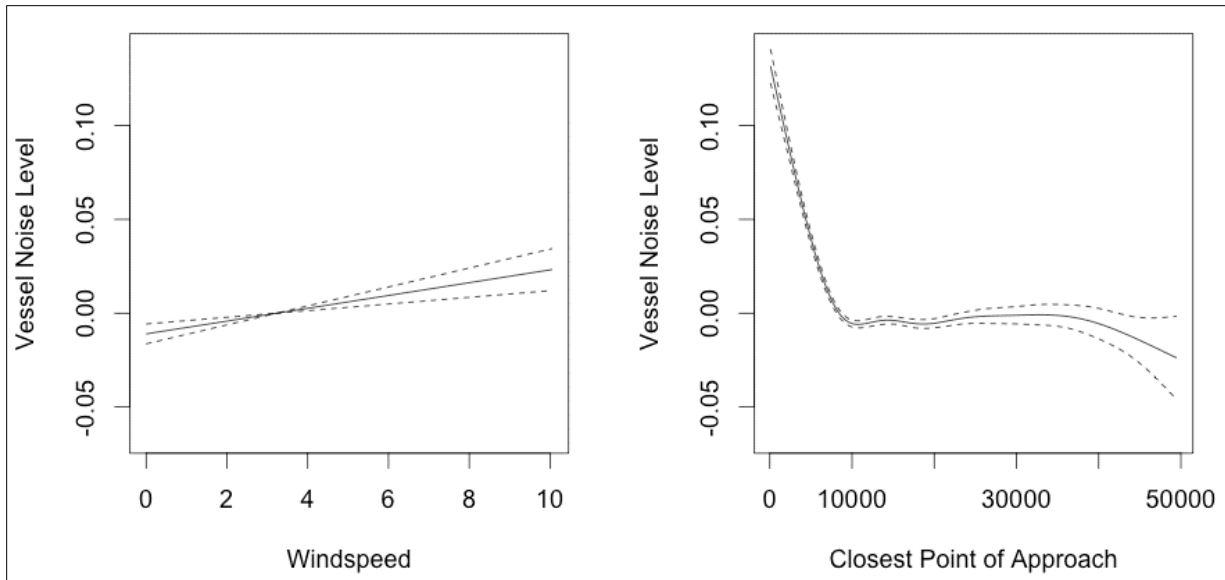
Figure D-30. Smoothing functions for Measured Vessel Band Noise as a function of Windspeed and CPA for Receiver 4, Deployment 1.

D.4.4.5 Deployment 1, Receiver 5

The significant predictors for Receiver 5 included scaled date, wave height, windspeed, and CPA (**Table D-16; Figures D-31 and D-32**). The R-squared value was 0.612. The data function is complex and likely reflects the contribution of airgun signals to the measured data. The wave height function paradoxically predicts a decrease in measured LF noise as wave height increases to 6 m. This may be the result of inclusion of a handful of very high measured wave heights. The windspeed function shows a simple increase in LF noise as windspeed increases. The CPA function shows that LF noise increases as vessels approach within 10 km of the recorder.

Table D-16. GAM output for Deployment 1, Receiver 5

| A. Parametric Coefficients	Estimate	Std. Error	t-value	p-value
(Intercept)	4.5578	0.0008	5603.2702	< 0.0001
B. Smooth Terms	**edf**	**Ref.df**	**F-value**	**p-value**
s(sDate)	40.7308	49.0000	56.8832	< 0.0001
s(WaveHeight)	1.0000	1.0000	4.5267	0.0334
s(Windspeed)	1.0000	1.0000	11.5082	0.0007
s(CPA)	8.5924	8.5924	216.3535	< 0.0001
s(Hz200) -200 Hz TOB RL	1.0000	1.0000	0.1717	0.6786
s(BB1) BB RL (w 50 Hz TL)	1.0000	1.0000	2.7581	0.0968
s(BB2) BB RL (w/200 Hz TL)	1.0000	1.0000	0.0012	0.9723
Key: BB=broadband; CPA= closest point of approach; edf=empirical distribution function; F-value=value on the F distribution calculated by dividing two mean squares; Hz=Hertz; Lat=latitude; Lon=longitude; p-value= level of marginal significance within a statistical hypothesis test, representing the probability of the occurrence of a given event; Ref.df=reference degrees of freedom; RL=received level; s=scaled; Std. Error=Standard Error; TL=transmission loss; TOB=third-octave band
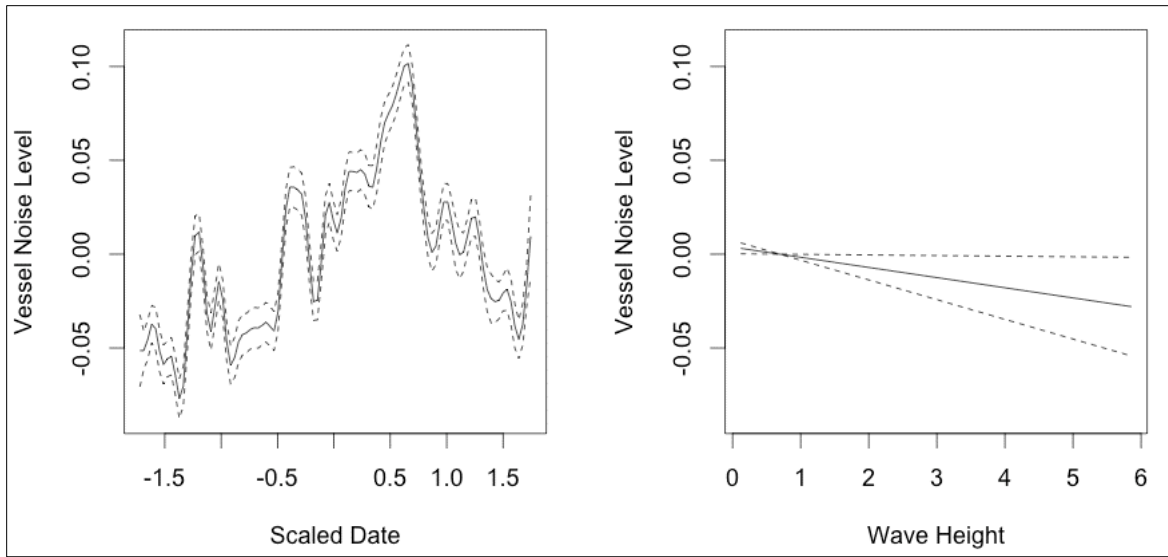
Figure D-31. Smoothing functions for Measured Vessel Band Noise as a function of Wave Height and Windspeed for Receiver 5, Deployment 1.
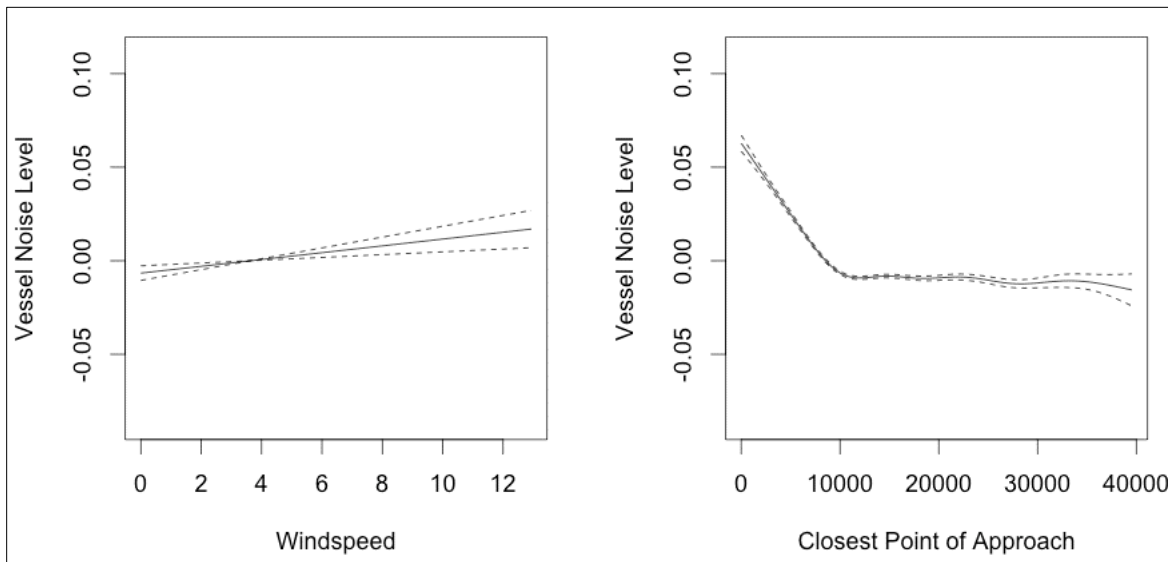
Figure D-32. Smoothing functions for Measured Vessel Band Noise as a function of Wave Height and Windspeed for Receiver 5, Deployment 1.

D.4.4.6   Deployment 1, Receiver 6

The significant predictors for Receiver 6 included scaled date, windspeed, and CPA (**Table D-17; Figures D-33 and D-34**). The R-squared value was 0.349. The scaled Date function is complex and hard to interpret. The windspeed functions shows a clear increase in LF noise as windspeed increases. The function clearly shows the increase in received levels as vessel approach the receiver within 10 km.

212

Table D-17. GAM output for Deployment 1, Receiver 6

A. Parametric Coefficients	Estimate	Std. Error	t-value	p-value
(Intercept)	4.5834	0.0012	3669.6195	< 0.0001
B. Smooth Terms	**edf**	**Ref.df**	**F-value**	**p-value**
s(sDate)	28.1260	49.0000	8.6928	< 0.0001
s(WaveHeight)	0.9999	0.9999	1.2730	0.2592
s(Windspeed)	1.0000	1.0000	48.0183	< 0.0001
s(CPA)	8.9244	8.9244	189.6414	< 0.0001
s(Hz200) -200 Hz TOB RL	1.0000	1.0000	0.0234	0.8785
s(BB1) BB RL (w 50 Hz TL)	1.0000	1.0000	1.7653	0.1840
s(BB2) BB RL (w/200 Hz TL)	1.0000	1.0000	0.4031	0.5255
Key: BB=broadband; CPA= closest point of approach; edf=empirical distribution function; F-value=value on the F distribution calculated by dividing two mean squares; Hz=Hertz; Lat=latitude; Lon=longitude; p-value= level of marginal significance within a statistical hypothesis test, representing the probability of the occurrence of a given event; Ref.df=reference degrees of freedom; RL=received level; s=scaled; Std. Error=Standard Error; TL=transmission loss; TOB=third-octave band				
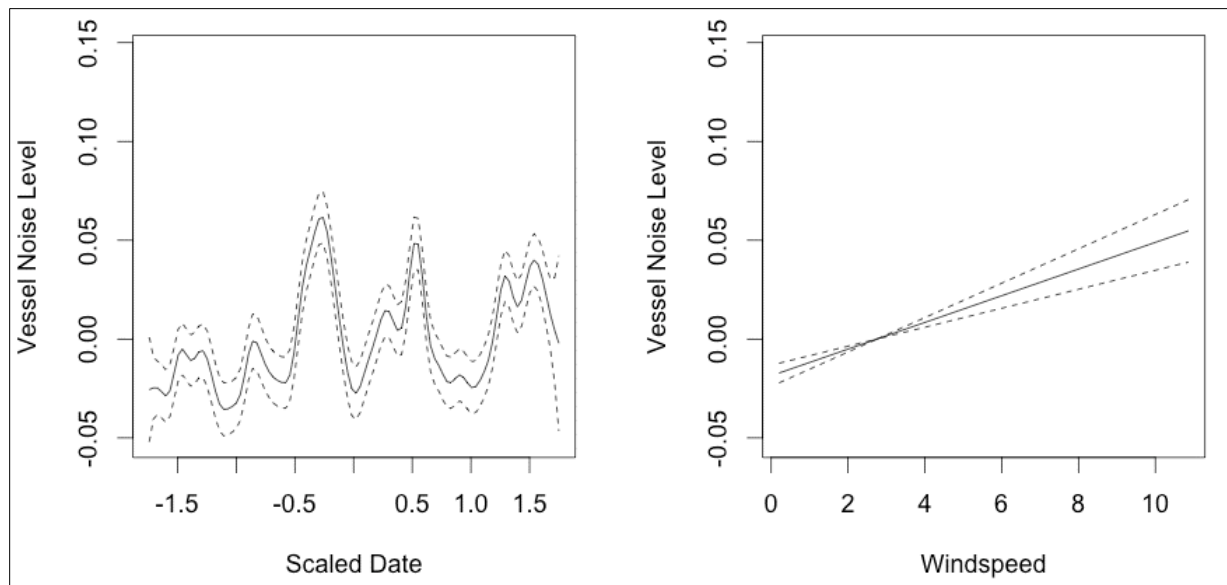
Figure D-33. Smoothing functions for Measured Vessel Band Noise as a function of Scaled Date and Windspeed for Receiver 6, Deployment 1.

213
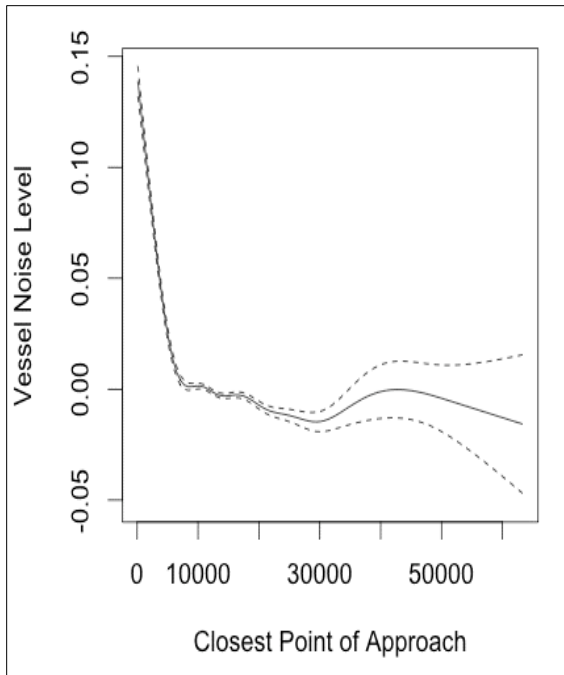
**Figure D-34. Smoothing functions for Measured Vessel Band Noise as a function of CPA for Receiver 6, Deployment 1.**

D.4.4.7   Deployment 1, Receiver 7

The significant predictors for Receiver 7 included scaled date, wave height, windspeed, CPA, and predicted BB RL (**Table D-18**; **Figures D-35**, **D-36**, and **D-37**). The R-squared value was 0.486. The Scaled Date function shows a slight increase in RL throughout the first deployment. The wave height function oscillates at higher wave heights but shows the increase in received noise level from 0 to 2 m as seen in other receivers. The most consistent trends are seen with increased Vessel band noise level as windspeed increases and CPA decreases. These functions curiously show a negative relationship with measured noise levels, which may be due to overprediction of noise levels at this location.

Table D-18. GAM output for Deployment 1, Receiver 7

A. Parametric Coefficients	Estimate	Std. Error	t-value	p-value
(Intercept)	4.5900	0.0009	5331.6673	< 0.0001
B. Smooth Terms	**edf**	**Ref.df**	**F-value**	**p-value**
s(sDate)	0.9997	49.0000	0.3482	< 0.0001
s(WaveHeight)	6.9005	6.9005	7.2718	< 0.0001
s(Windspeed)	1.9177	1.9177	51.6145	< 0.0001
s(CPA)	8.9762	8.9762	868.9379	< 0.0001
s(Hz200) -200 Hz TOB RL	3.8095	3.8095	1.1637	0.2073
s(BB1) BB RL (w 50 Hz TL)	6.3829	6.3829	25.1998	< 0.0001
s(BB2) BB RL (w/200 Hz TL)	3.4084	3.4084	2.8563	0.0195
Key: BB=broadband; CPA= closest point of approach; edf=empirical distribution function; F-value=value on the F distribution calculated by dividing two mean squares; Hz=Hertz; Lat=latitude; Lon=longitude; p-value= level of marginal significance within a statistical hypothesis test, representing the probability of the occurrence of a given event; Ref.df=reference degrees of freedom; RL=received level; s=scaled; Std. Error=Standard Error; TL=transmission loss; TOB=third-octave band				
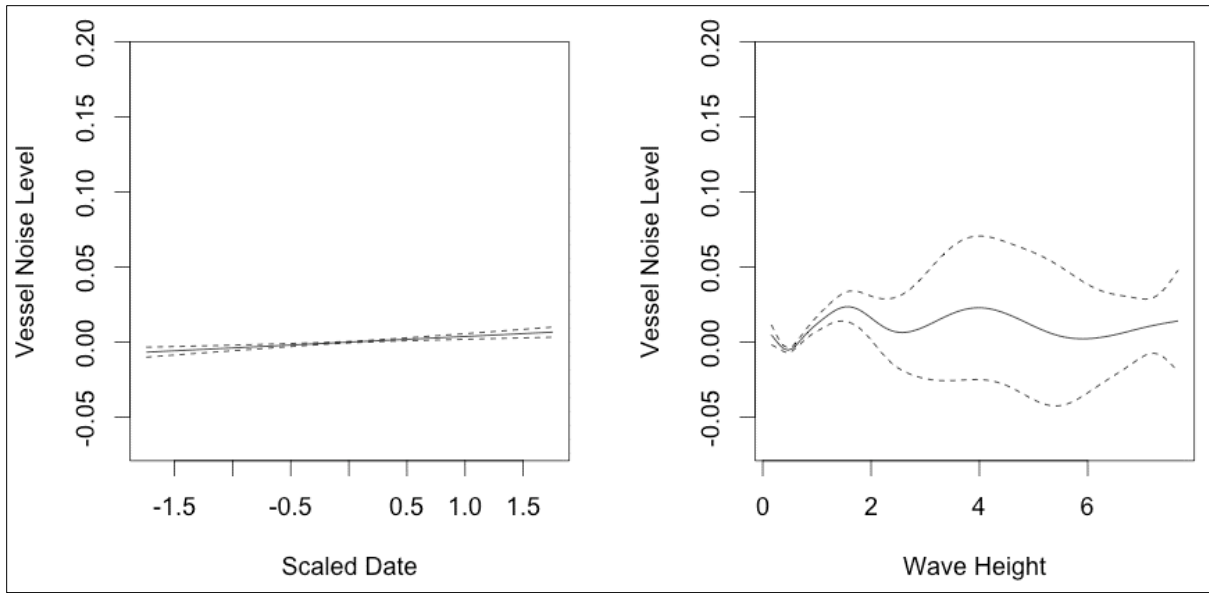
Figure D-35. Smoothing functions for Measured Vessel Band Noise as a function of Scaled Date and Wave Height for Receiver 7, Deployment 1.
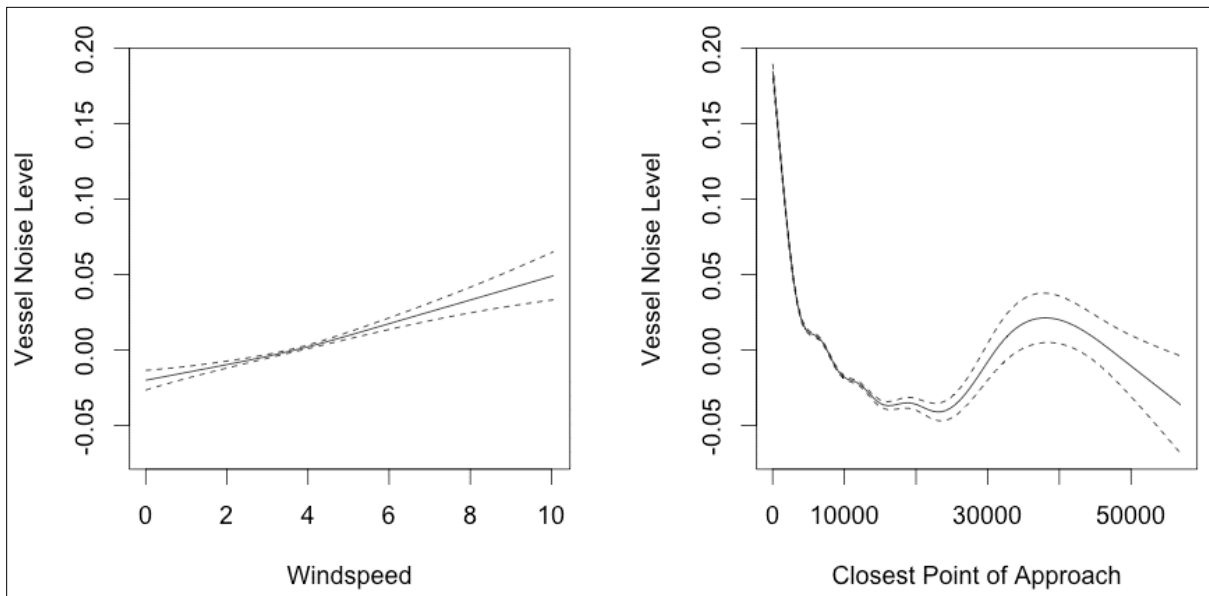
Figure D-36. Smoothing functions for Measured Vessel Band Noise as a function of Windspeed and CPA for Receiver 7, Deployment 1.
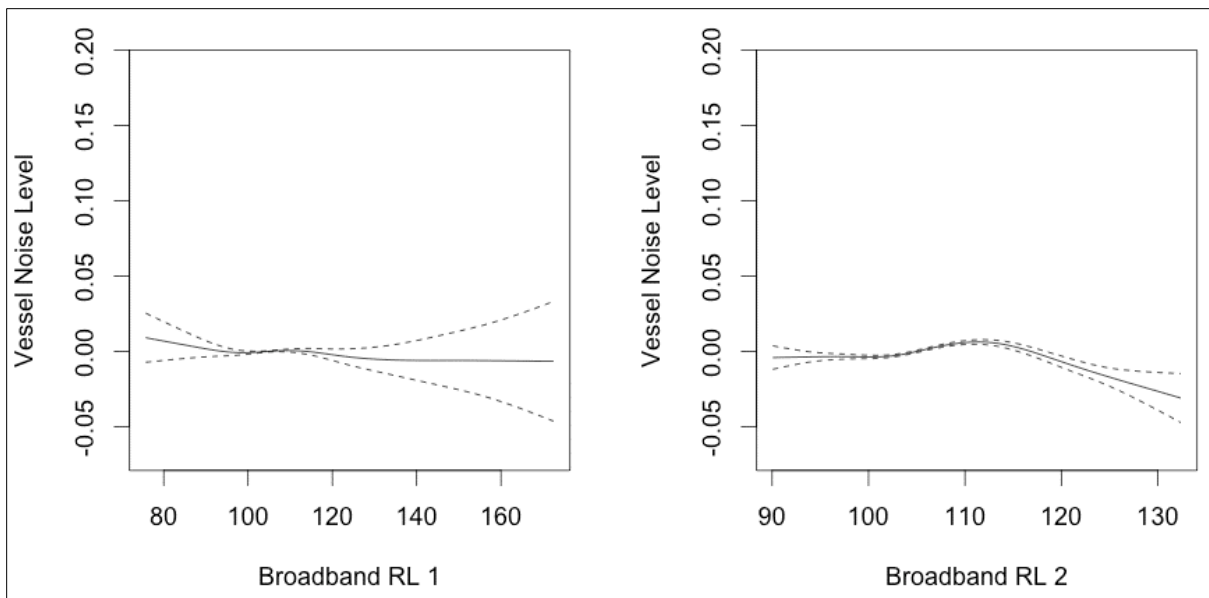
Figure D-37. Smoothing functions for Measured Vessel Band Noise as a function of Predicted BB Levels for Receiver 7, Deployment 1.

D.4.4.8 Deployment 1, Receiver 8

The significant predictors for Receiver 8 included windspeed, CPA, and predicted BB RL (**Table D-19**; **Figures D-38** and **D-39**). The R-squared value was only 0.115. The windspeed functions show a clear increase in LF noise as windspeed increases. The CPA function shows a clear increase in measured LF noise as vessels approach within approximately 7 km of the receiver. Paradoxically, the modeled BB RL predicts a decrease in measured LF noise at higher noise levels. This could be the result of an error in source level estimation or TL predictions for this location.

Table D-19. GAM output for Deployment 1, Receiver 8

A. Parametric Coefficients	Estimate	Std. Error	t-value	p-value
(Intercept)	4.5067	0.0027	1650.9840	< 0.0001
B. Smooth Terms	**edf**	**Ref.df**	**F-value**	**p-value**
s(sDate)	0.5701	49.0000	0.0259	0.1347
s(WaveHeight)	1.0000	1.0000	0.1520	0.6966
s(Windspeed)	3.3137	3.3137	4.1362	0.0054
s(CPA)	8.6430	8.6430	129.7145	< 0.0001
s(Hz200) -200 Hz TOB RL	1.0000	1.0000	2.6352	0.1046
s(BB1) BB RL (w 50 Hz TL)	3.7221	3.7221	4.9365	0.0016
s(BB2) BB RL (w/200 Hz TL)	2.3834	2.3834	1.5937	0.1242
Key: BB=broadband; CPA= closest point of approach; edf=empirical distribution function; F-value=value on the F distribution calculated by dividing two mean squares; Hz=Hertz; Lat=latitude; Lon=longitude; p-value= level of marginal significance within a statistical hypothesis test, representing the probability of the occurrence of a given event; Ref.df=reference degrees of freedom; RL=received level; s=scaled; Std. Error=Standard Error; TL=transmission loss; TOB=third-octave band				

216
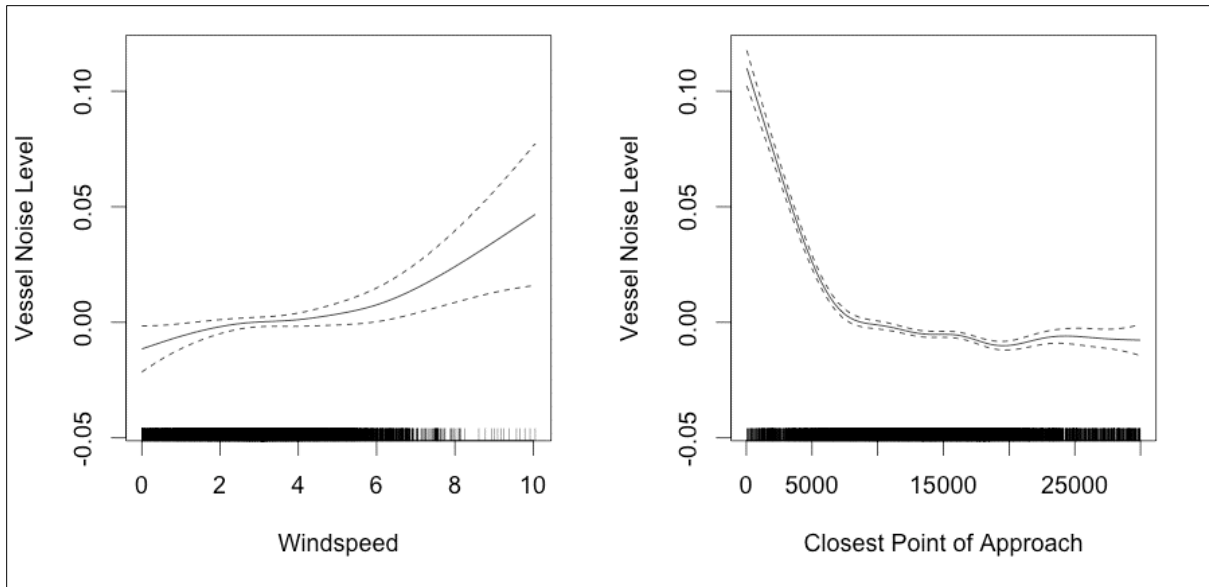
Figure D-38. Smoothing functions for Measured Vessel Band Noise as a function of Wave Height and Windspeed for Receiver 8, Deployment 1.
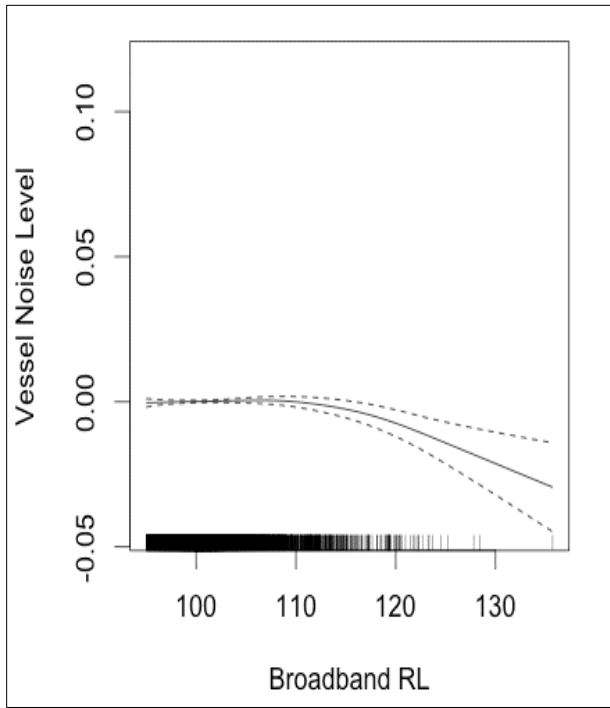
Figure D-39. Smoothing Functions for Measured Vessel Band Noise as a function of CPA for Receiver 8, Deployment 1.

D.4.4.9   Deployment 1, Receiver 9

The significant predictors for Receiver 9 included wave height, windspeed, and CPA (**Table D-20**; **Figures D-40** and **D-41**). The R-squared value was only 0.100. Paradoxically, the wave height function shows a decrease in LF noise as wave height increases to 2.5 m, while increases in windspeed predicted

increased Vessel band noise levels. CPAs within approximately 5 km predicted strong increases in received vessel band noise levels.

Table D-20. GAM output for Deployment 1, Receiver 9

A. Parametric Coefficients	Estimate	Std. Error	t-value	p-value
(Intercept)	4.7060	0.0031	1511.0153	< 0.0001
B. Smooth Terms	**edf**	**Ref.df**	**F-value**	**p-value**
s(sDate)	0.0000	49.0000	0.0000	0.7788
s(WaveHeight)	1.0000	1.0000	7.6108	0.0058
s(Windspeed)	1.0000	1.0000	5.2447	0.0220
s(CPA)	8.8484	8.8484	209.0272	< 0.0001
s(Hz200) -200 Hz TOB RL	1.0000	1.0000	2.1859	0.1393
s(BB1) BB RL (w 50 Hz TL)	1.0000	1.0000	0.4827	0.4872
s(BB2) BB RL (w/200 Hz TL)	1.0000	1.0000	0.0926	0.7609

Key: BB=broadband; CPA= closest point of approach; edf=empirical distribution function; F-value=value on the F distribution calculated by dividing two mean squares; Hz=Hertz; Lat=latitude; Lon=longitude; p-value= level of marginal significance within a statistical hypothesis test, representing the probability of the occurrence of a given event; Ref.df=reference degrees of freedom; RL=received level; s=scaled; Std. Error=Standard Error; TL=transmission loss; TOB=third-octave band
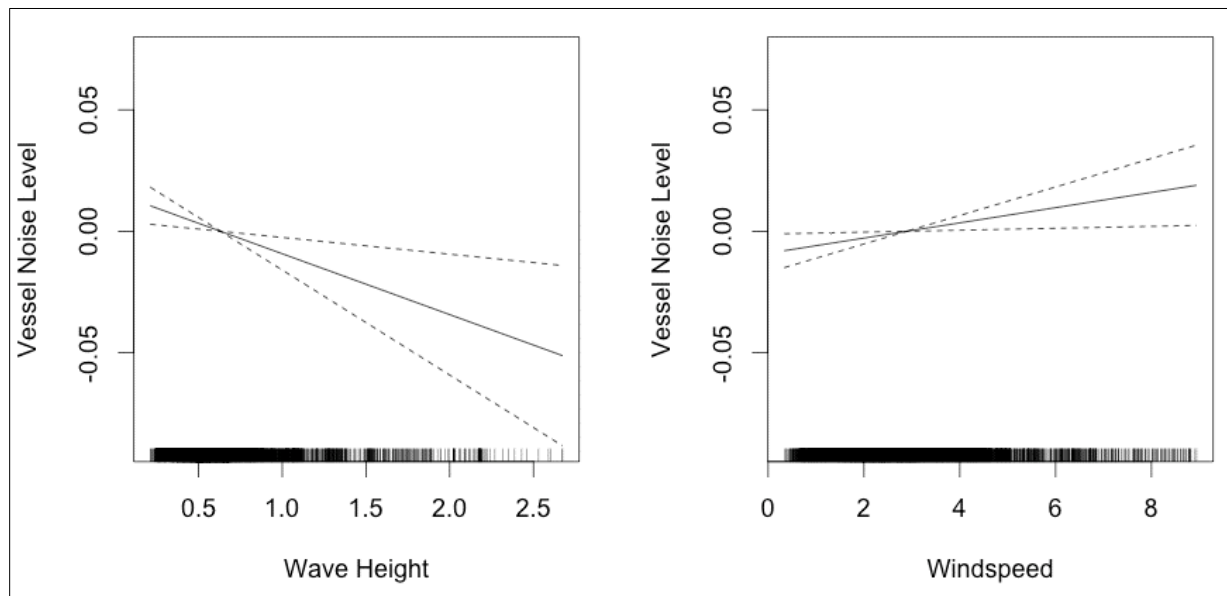
Figure D-40. Smoothing functions for Measured Vessel Band Noise as a function of Wave Height and Windspeed for Receiver 9, Deployment 1.
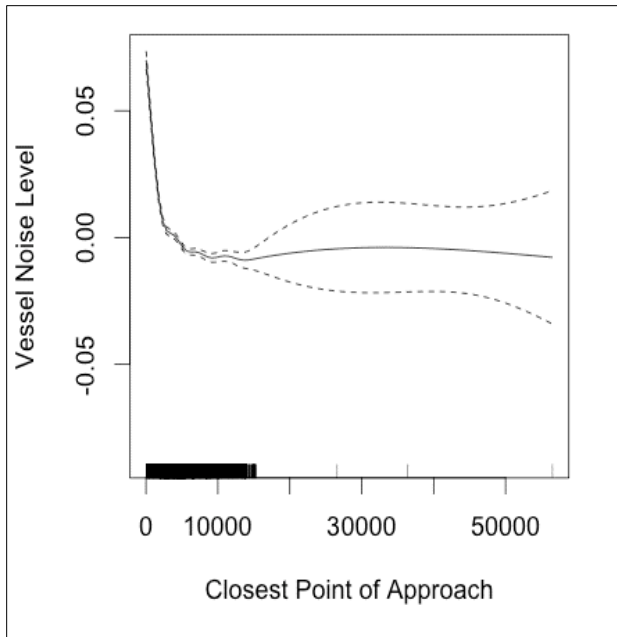
**Figure D-41. Smoothing functions for Measured Vessel Band Noise as a function of CPA for Receiver 9, Deployment 1.**

D.4.4.10 Deployment 1, Receiver 10

The significant predictors for Receiver 10 included scaled date, wave height, windspeed, CPA, and all three predicted RL metrics (**Table D-21**; **Figures D-42**, **D-43**, and **D-44**). The R-squared value was 0.421. The scaled Date function is complex and likely reflects the airgun activity late in the recording period. The wave height function for Receiver 10 is complex, unusual, and hard to interpret. The windspeed functions shows a clear increase in LF noise as windspeed increases. The CPA function shows an increase in measured LF noise as vessels approached within 10 km of the recorder. The 200 Hz RL function and the BB RL function both show a positive near-linear relationship between predicted and measured RL. However, the 200 Hz function shows a stronger relationship.

Table D-21. GAM output for Deployment 1, Receiver 10

A. Parametric Coefficients	Estimate	Std. Error	t-value	p-value
(Intercept)	4.5273	0.0012	3752.5849	< 0.0001
B. Smooth Terms	**edf**	**Ref.df**	**F-value**	**p-value**
s(sDate)	36.4854	49.0000	18.3865	< 0.0001
s(WaveHeight)	6.8869	6.8869	7.4095	< 0.0001
s(Windspeed)	4.2631	4.2631	6.3593	< 0.0001
s(CPA)	8.9509	8.9509	665.2577	< 0.0001
s(Hz200) -200 Hz TOB RL	1.0000	1.0000	18.6362	< 0.0001
s(BB1) BB RL (w 50 Hz TL)	5.2608	5.2608	12.7145	< 0.0001
s(BB2) BB RL (w/200 Hz TL)	5.0689	5.0689	5.8241	< 0.0001
Key: BB=broadband; CPA= closest point of approach; edf=empirical distribution function; F-value=value on the F distribution calculated by dividing two mean squares; Hz=Hertz; Lat=latitude; Lon=longitude; p-value= level of marginal significance within a statistical hypothesis test, representing the probability of the occurrence of a given event; Ref.df=reference degrees of freedom; RL=received level; s=scaled; Std. Error=Standard Error; TL=transmission loss; TOB=third-octave band				
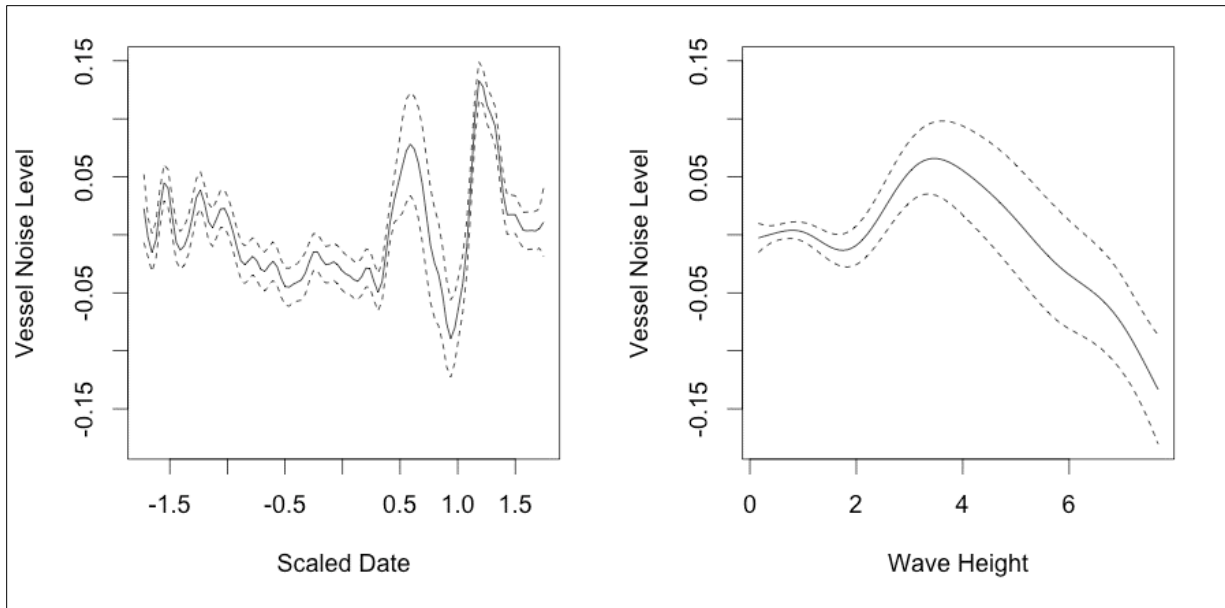
Figure D-42. Smoothing functions for Measured Vessel Band Noise as a function of Scaled Date and Wave Height for Receiver 10, Deployment 1.
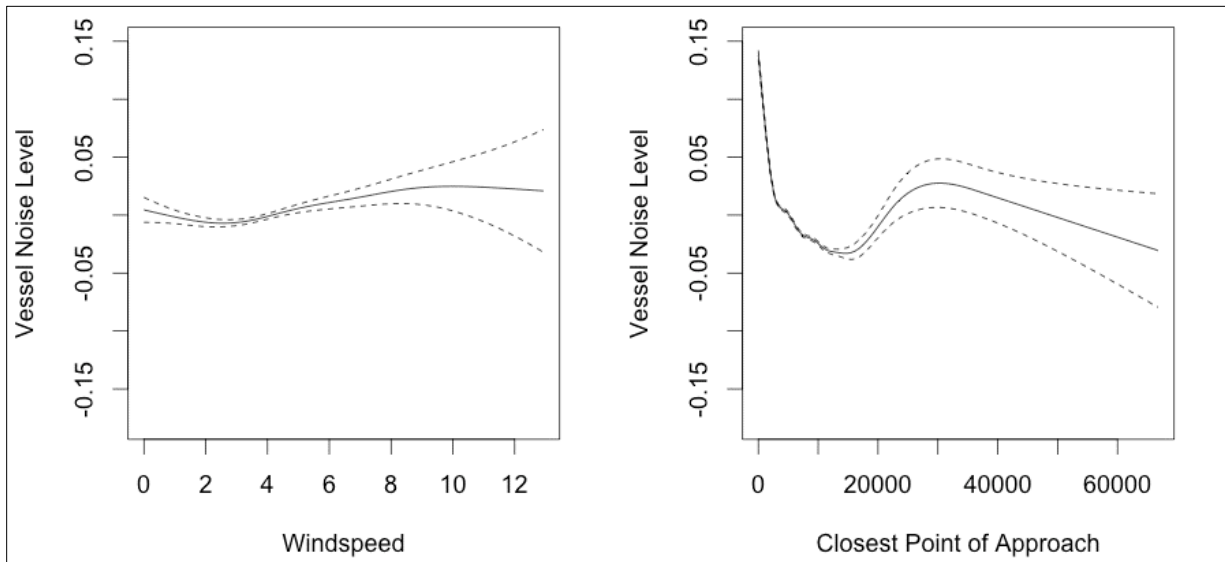
Figure D-43. Smoothing functions for Measured Vessel Band Noise as a function of Windspeed and CPA for Receiver 10, Deployment 1
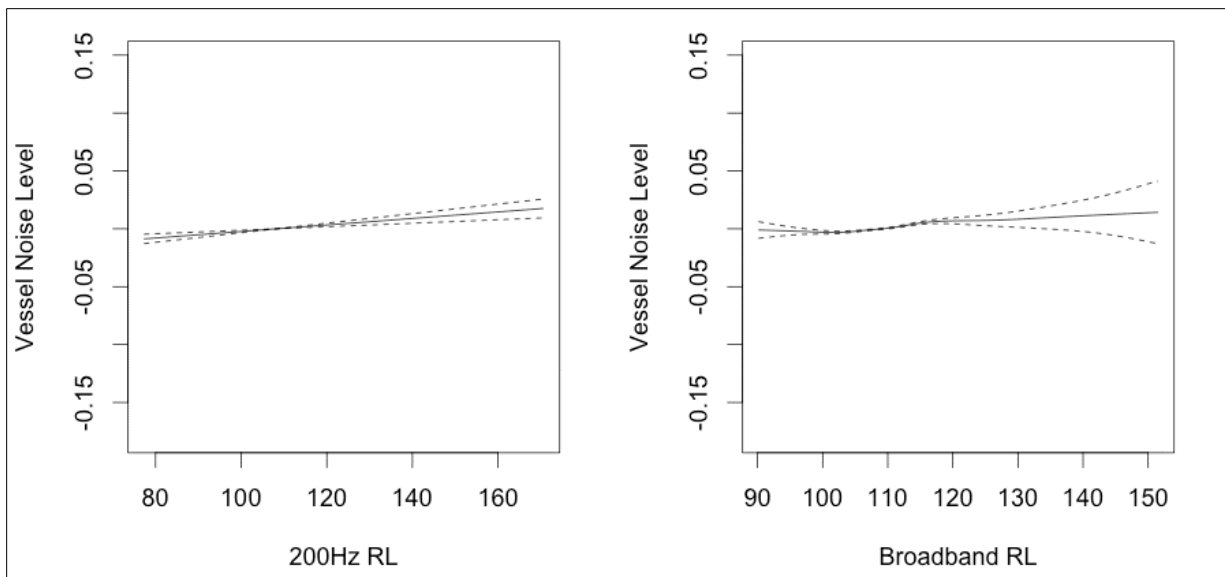
Figure D-44. Smoothing functions for Measured Vessel Band Noise as a function of 200 Hz RL and BB RL for Receiver 10, Deployment 1.

D.4.5 Revised Simplified Statistical Modeling Results of Vessel Received Levels

The model and analysis results of a second, simpler statistical approach that was implemented to assess vessel RLs for all ten EAR and RH sensors for all four deployments resulted in higher R-square values (i.e., or a better model fit) for the vessel data. Accordingly, all sensor data for all four deployments was assessed using the simpler statistical approach. To provide a comparison for the data presented and discussed in **Section D.4.4**, results from the simplified statistical modeling for the ten sensors for Deployment 1 are presented and discussed below. Similar results for Deployments 2 through 4 are presented in **Appendix D-B**. To differentiate the figure and table modeling results resulting from the Simple Statistical Analysis from those of the full statistical modeling, the designation SA2 is given in the caption.

D.4.5.1 Deployment 1, Receiver 1 (Statistical Approach 2)

The simplified statistical analysis resulted in a greater R-square (0.671) than resulted from the full statistical predicted RL analysis (**Table D-22**). Both approaches resulted in a significant and complex smooth fit to the scaled date, and both results reported increased vessel band noise levels with increasing windspeed (**Figure D-45**). The smooth fit to minimum CPA had a similar shape, with the inflection point at approximately 10 km in both analyses.

Table D-22. GAM SA2 output for Deployment 1, Receiver 1

A. Parametric Coefficients	Estimate	Std. Error	t-value	p-value
(Intercept)	4.7106	0.0008	5583.3855	< 0.0001
km2	0.0392	0.0051	7.6588	< 0.0001
km4	0.0203	0.0036	5.6526	< 0.0001
km10	0.0205	0.0023	8.7221	< 0.0001
B. Smooth Terms	edf	Ref.df	F-value	p-value
s(sDate)	44.0524	49.0000	147.6610	< 0.0001
s(WaveHeight)	6.2418	6.2418	9.3809	< 0.0001

s(Windspeed)	1.0000	1.0000	10.5758	0.0012
s(CPAmin)	1.0000	1.0000	36.7337	< 0.0001

Key: CPA= closest point of approach; edf=empirical distribution function; F-value=value on the F distribution calculated by dividing two mean squares; km=kilometer; min=minimum; p-value= level of marginal significance within a statistical hypothesis test, representing the probability of the occurrence of a given event; Ref.df=reference degrees of freedom; s=scaled; Std. Error=Standard Error

D.4.5.2 Deployment 1, Receiver 2 (Statistical Approach 2)

The simplified analysis had a larger R-square (0.515 [vice 0.500 for statistical approach 1) than the predicted RL analysis (**Table D-23**). Scaled date and minimum CPA were significant in both models. However, windspeed was significant in the simplified analysis and was not in the predicted RL analysis (**Figure D-46**).

Table D-23. GAM SA2 output for Deployment 1, Receiver 2

A. Parametric Coefficients	Estimate	Std. Error	t-value	p-value
(Intercept)	4.4932	0.0012	3625.2581	< 0.0001
km2	-0.0059	0.0085	-0.6876	0.4917
km4	-0.0063	0.0049	-1.2989	0.1941
km10	0.0039	0.0019	2.0298	0.0425
B. Smooth Terms	edf	Ref.df	F-value	p-value
s(sDate)	43.7402	49.0000	52.5753	< 0.0001
s(WaveHeight)	1.0000	1.0000	0.0027	0.9583
s(Windspeed)	1.0000	1.0000	6.2093	0.0128
s(CPAmin)	7.7553	7.7553	19.5051	< 0.0001

Key: CPA= closest point of approach; edf=empirical distribution function; F-value=value on the F distribution calculated by dividing two mean squares; km=kilometer; min=minimum; p-value= level of marginal significance within a statistical hypothesis test, representing the probability of the occurrence of a given event; Ref.df=reference degrees of freedom; s=scaled; Std. Error=Standard Error

D.4.5.3 Deployment 1, Receiver 3 (Statistical Approach 2)

For Receiver 3, both statistical analyses showed that scaled date, wave height, wind speed, and minimum CPA were all significant predictors (**Table D-24**), with an R-square value of 0.491. The shape of the smooth fits for these variables in both analyses were similar (**Figure D-47**).

Table D-24. GAM SA2 output for Deployment 1, Receiver 3

A. Parametric Coefficients	Estimate	Std. Error	t-value	p-value
(Intercept)	4.5561	0.0010	4566.3883	< 0.0001
km2	0.0151	0.0120	1.2571	0.2088
km4	-0.0021	0.0080	-0.2560	0.7979
km10	-0.0127	0.0042	-2.9962	0.0028
B. Smooth Terms	edf	Ref.df	F-value	p-value
s(sDate)	39.8317	49.0000	34.9559	< 0.0001
s(WaveHeight)	6.4432	6.4432	8.6504	< 0.0001
s(Windspeed)	1.0000	1.0000	85.4003	< 0.0001

| **s(CPAmin)** | 6.2801 | 6.2801 | 12.4484 | < 0.0001 |

Key: CPA= closest point of approach; edf=empirical distribution function; F-value=value on the F distribution calculated by dividing two mean squares; km=kilometer; min=minimum; p-value= level of marginal significance within a statistical hypothesis test, representing the probability of the occurrence of a given event; Ref.df=reference degrees of freedom; s=scaled; Std. Error=Standard Error
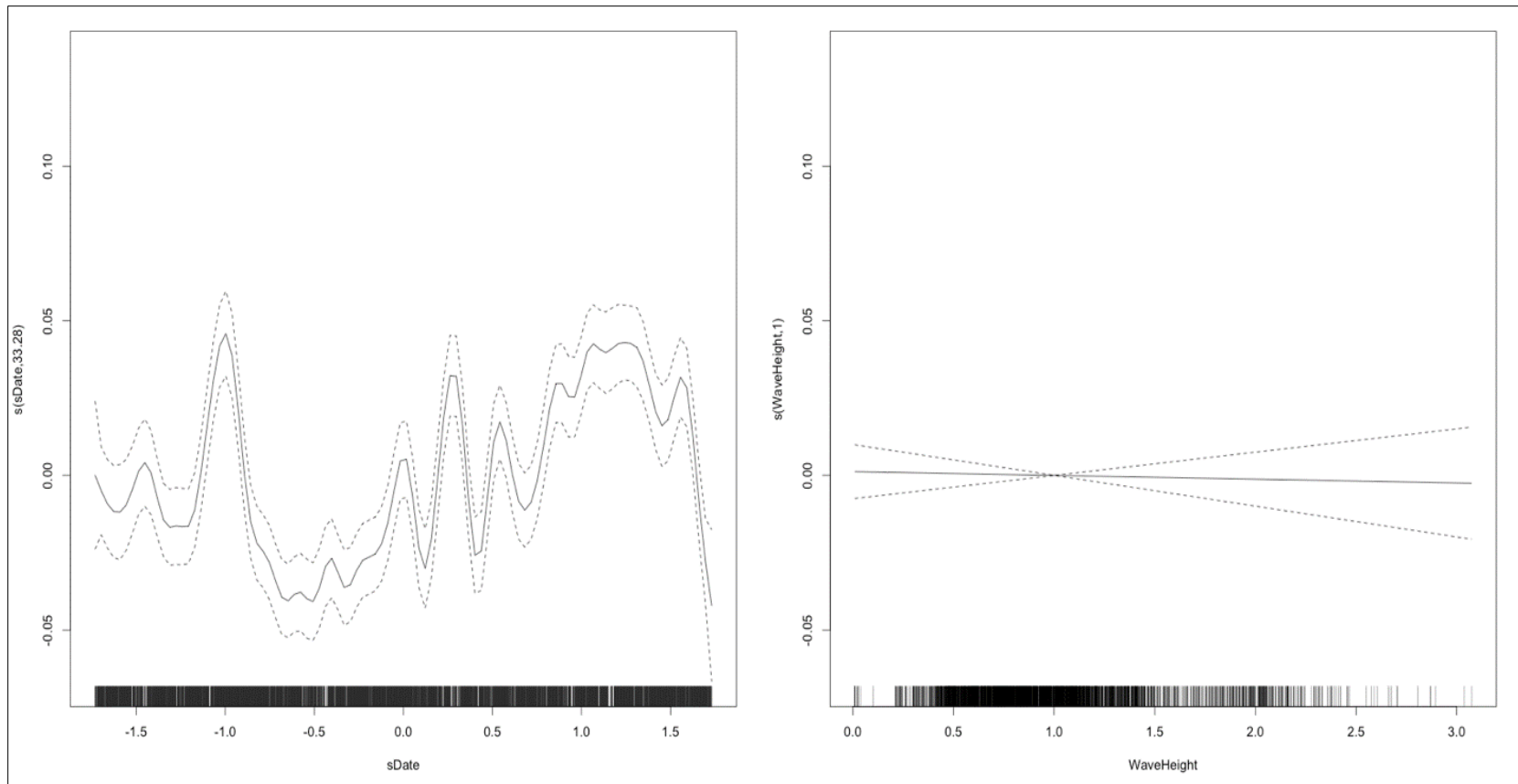
Figure D-45a. SA2 smoothing functions for Measured Vessel Band Noise as a function of Date, Wave Height, Windspeed, and CPA for Receiver 1, Deployment 1.
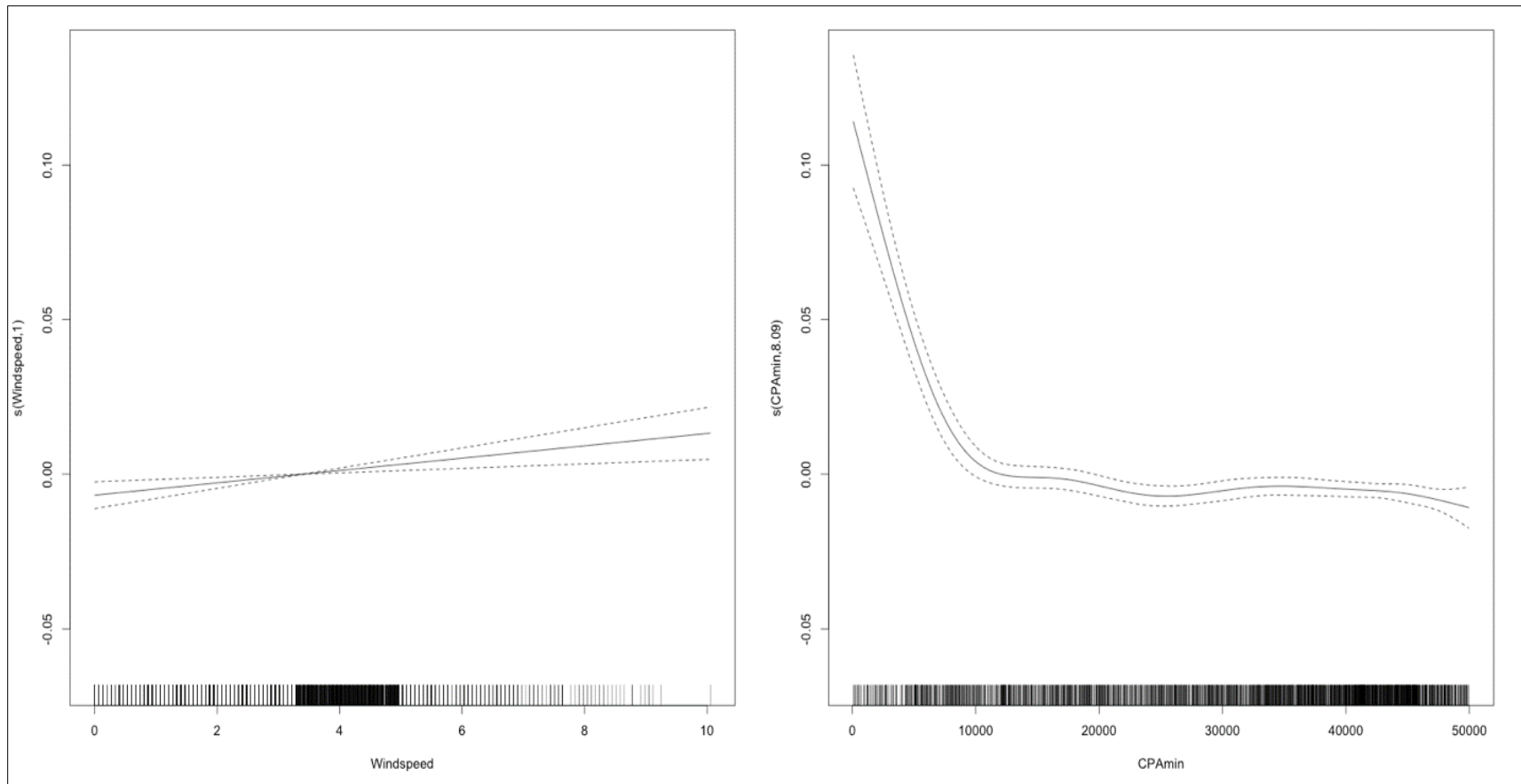
Figure D-45b. SA2 smoothing functions for Measured Vessel Band Noise as a function of Date, Wave Height, Windspeed, and CPA for Receiver 1, Deployment 1.
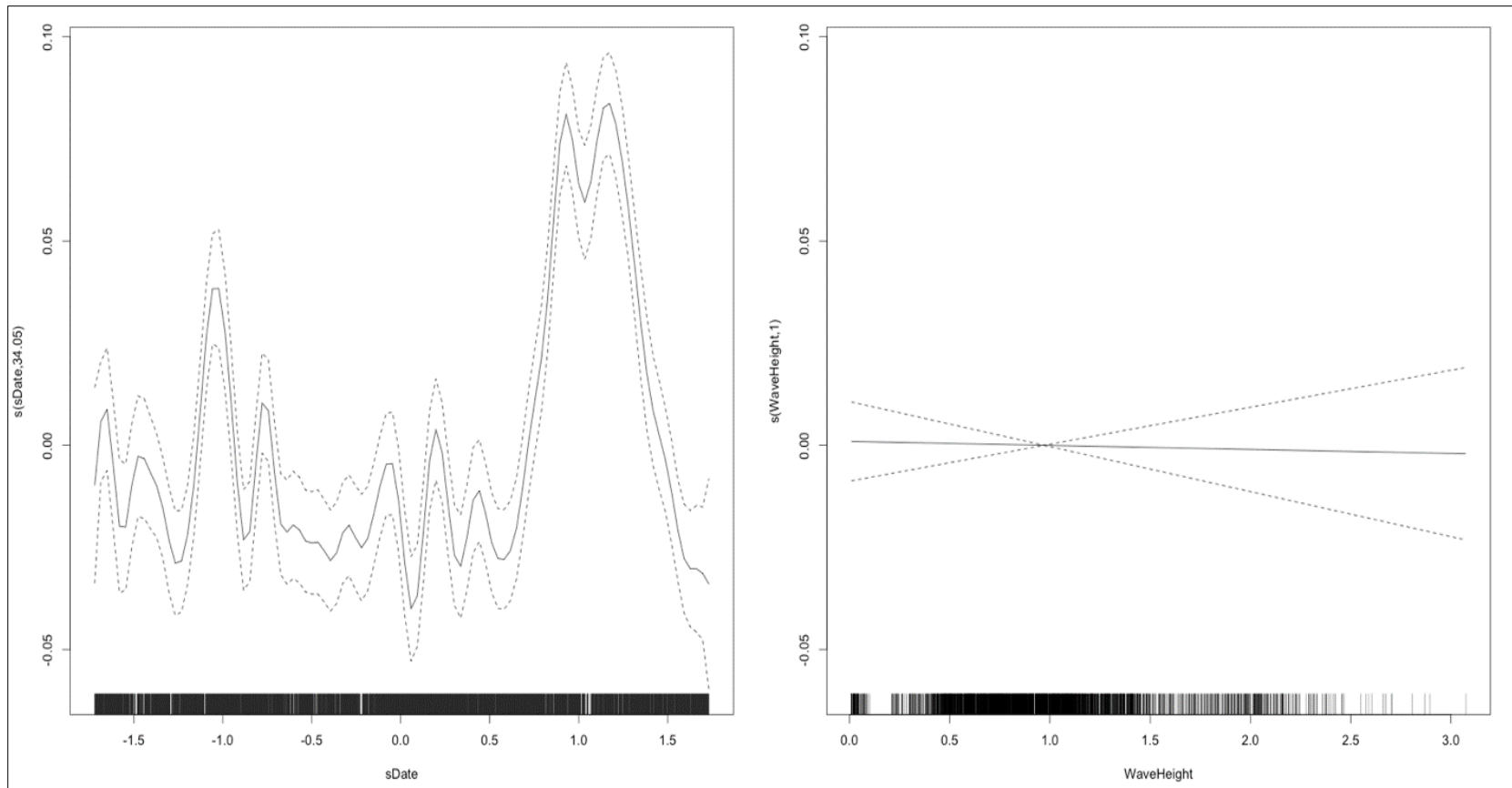
Figure D-46a. SA2 smoothing functions for Measured Vessel Band Noise as a function of Date, Wave Height, Windspeed, and CPA for Receiver 2, Deployment 1.
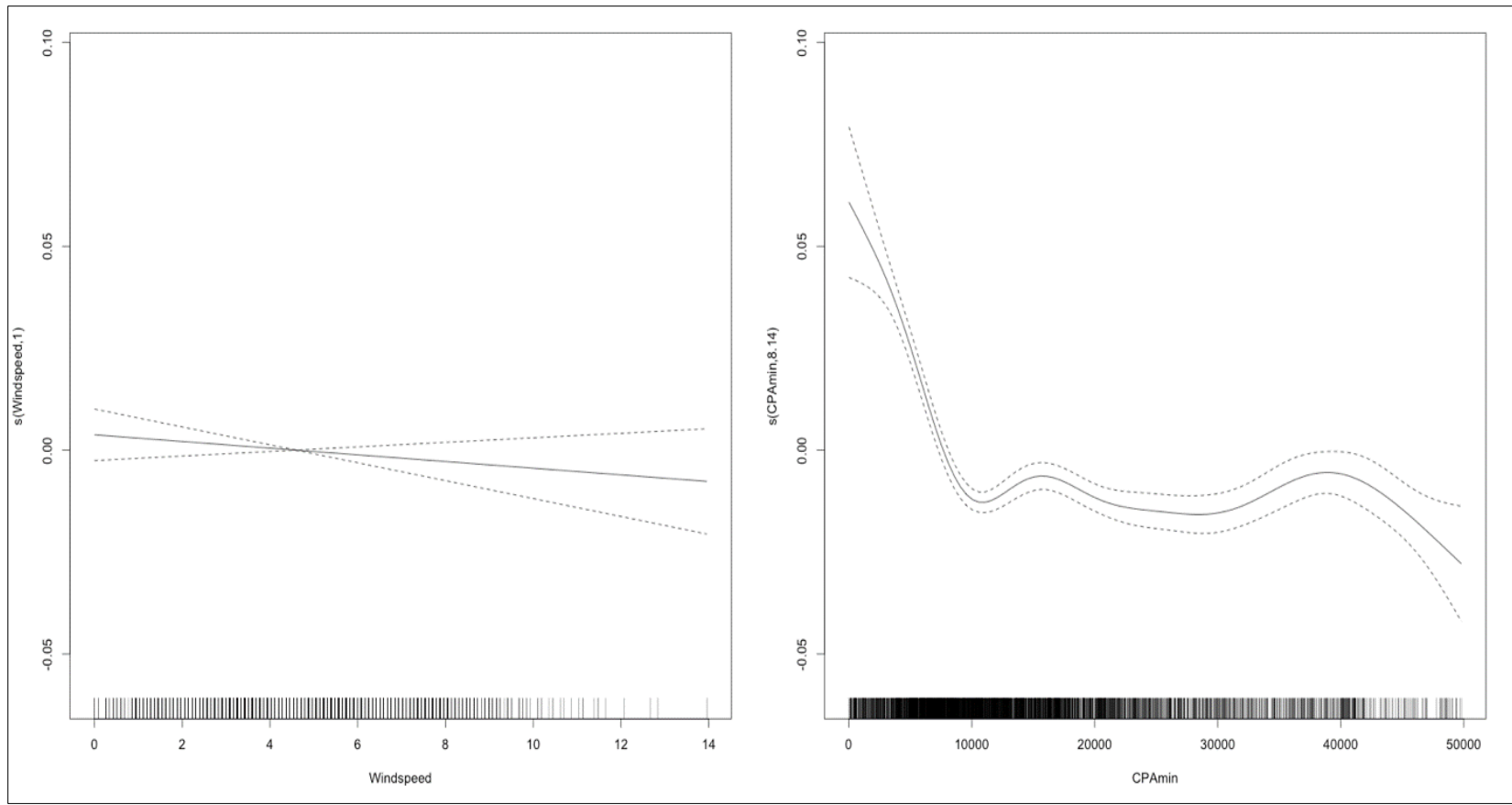
Figure D-46b. SA2 smoothing functions for Measured Vessel Band Noise as a function of Date, Wave Height, Windspeed, and CPA for Receiver 2, Deployment 1.
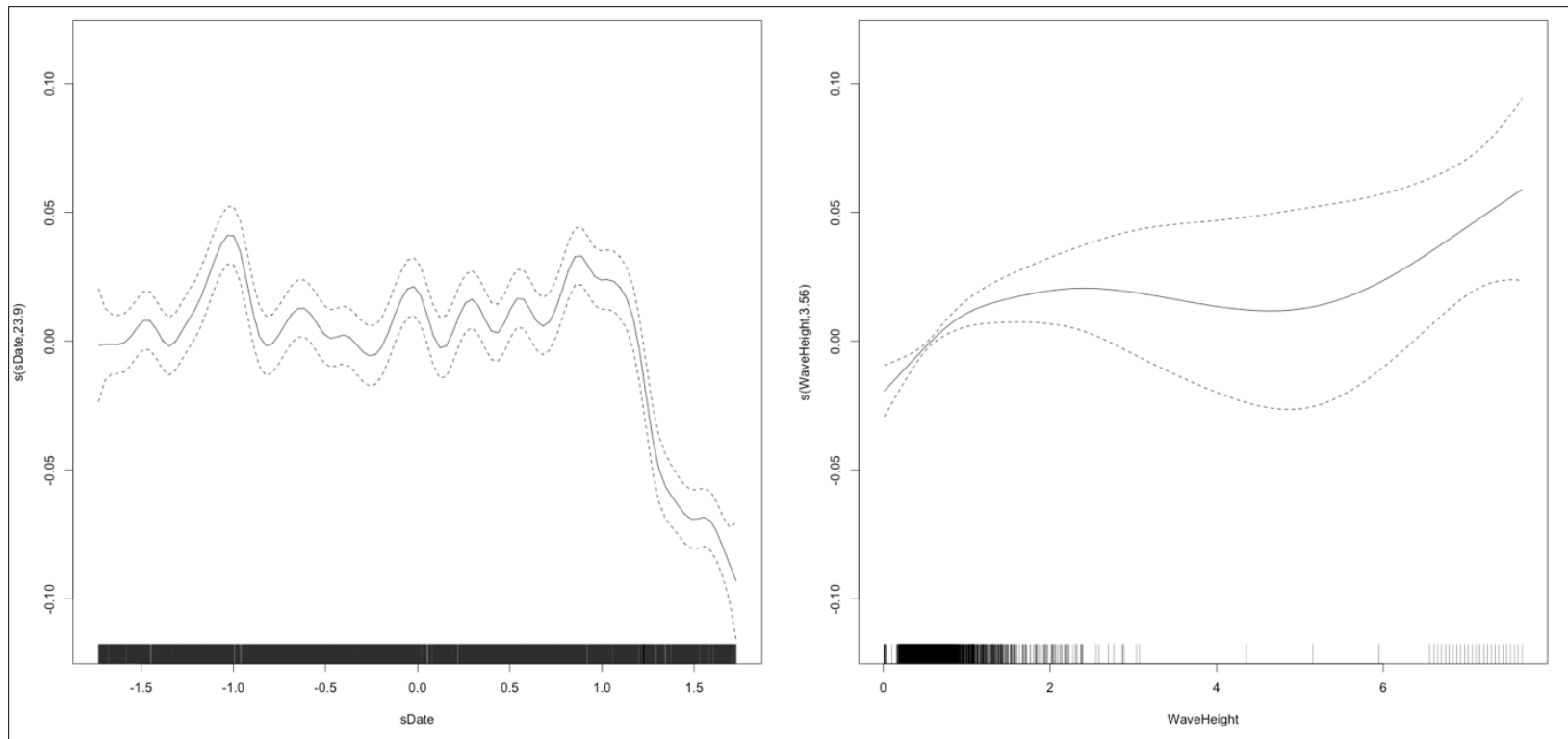
Figure D-47a. SA2 smoothing functions for Measured Vessel Band Noise as a function of Date, Wave Height, Windspeed, and CPA for Receiver 3, Deployment 1.
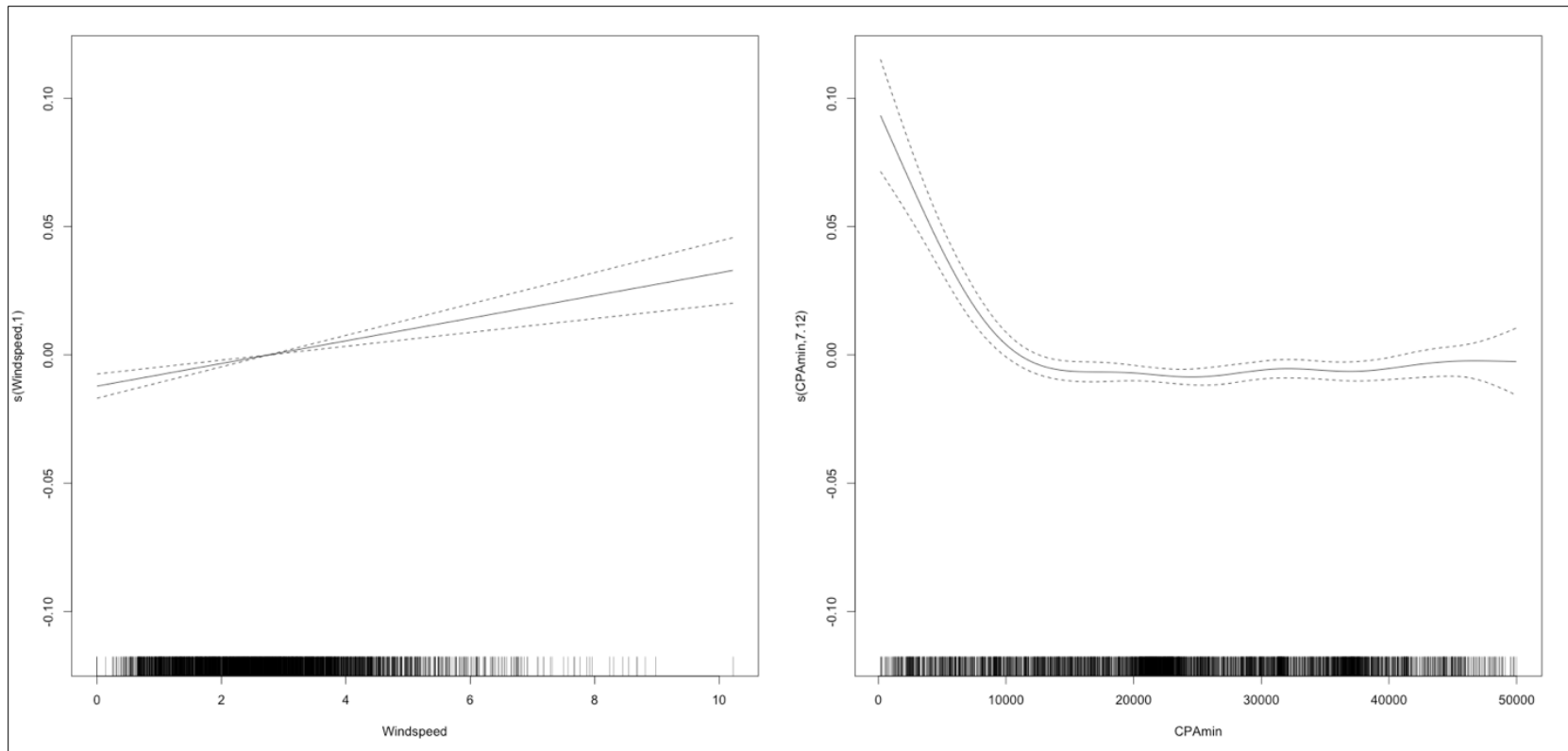
Figure D-47b. SA2 smoothing functions for Measured Vessel Band Noise as a function of Date, Wave Height, Windspeed, and CPA for Receiver 3, Deployment 1.

D.4.5.4 Deployment 1, Receiver 4 (Statistical Approach 2)

Both statistical analyses for Receiver 4, Deployment 1 resulted in scaled date, wave height, wind speed, and minimum CPA as all significant predictors (**Table D-25**). The R-square for the shape of the smooth fits for these variables in both analyses were similar (**Figure D-48**).

Table D-25. GAM SA2 output for Deployment 1, Receiver 4

| A. Parametric Coefficients	Estimate	Std. Error	t-value	p-value
(Intercept)	4.4815	0.0016	2785.4192	< 0.0001
km2	0.0280	0.0109	2.5765	0.0101
km4	0.0184	0.0075	2.4420	0.0147
km10	0.0009	0.0025	0.3719	0.7100
B. Smooth Terms	edf	Ref.df	F-value	p-value
s(sDate)	44.0743	49.0000	29.0284	< 0.0001
s(WaveHeight)	1.0000	1.0000	5.6692	0.0174
s(Windspeed)	1.0000	1.0000	17.5270	< 0.0001
s(CPAmin)	5.3380	5.3380	5.4207	< 0.0001
Key: CPA= closest point of approach; edf=empirical distribution function; F-value=value on the F distribution calculated by dividing two mean squares; km=kilometer; min=minimum; p-value= level of marginal significance within a statistical hypothesis test, representing the probability of the occurrence of a given event; Ref.df=reference degrees of freedom; s=scaled; Std. Error=Standard Error				

D.4.5.5 Deployment 1, Receiver 5 (Statistical Approach 2)

For Receiver 5, both statistical analyses resulted in the scaled date, wave height, wind speed, and minimum CPA all being significant predictors (**Table D-26**). The R-square value is 0.674. The shape of the smooth fits for these variables in both analyses were similar (**Figure D-49**).

**Table D-26. GAM SA2 output for Deployment 1, Receiver 5**

A. Parametric Coefficients	Estimate	Std. Error	t-value	p-value
(Intercept)	4.5559	0.0010	4626.2543	< 0.0001
km2	0.0093	0.0052	1.7946	0.0728
km4	0.0022	0.0028	0.7945	0.4269
km10	0.0029	0.0009	3.2223	0.0013
B. Smooth Terms	edf	Ref.df	F-value	p-value
s(sDate)	45.8967	49.0000	149.1195	< 0.0001
s(WaveHeight)	5.9244	5.9244	8.5030	< 0.0001
s(Windspeed)	1.0000	1.0000	24.3613	< 0.0001
s(CPAmin)	5.9998	5.9998	19.1413	< 0.0001
Key: CPA= closest point of approach; edf=empirical distribution function; F-value=value on the F distribution calculated by dividing two mean squares; km=kilometer; min=minimum; p-value= level of marginal significance within a statistical hypothesis test, representing the probability of the occurrence of a given event; Ref.df=reference degrees of freedom; s=scaled; Std. Error=Standard Error				
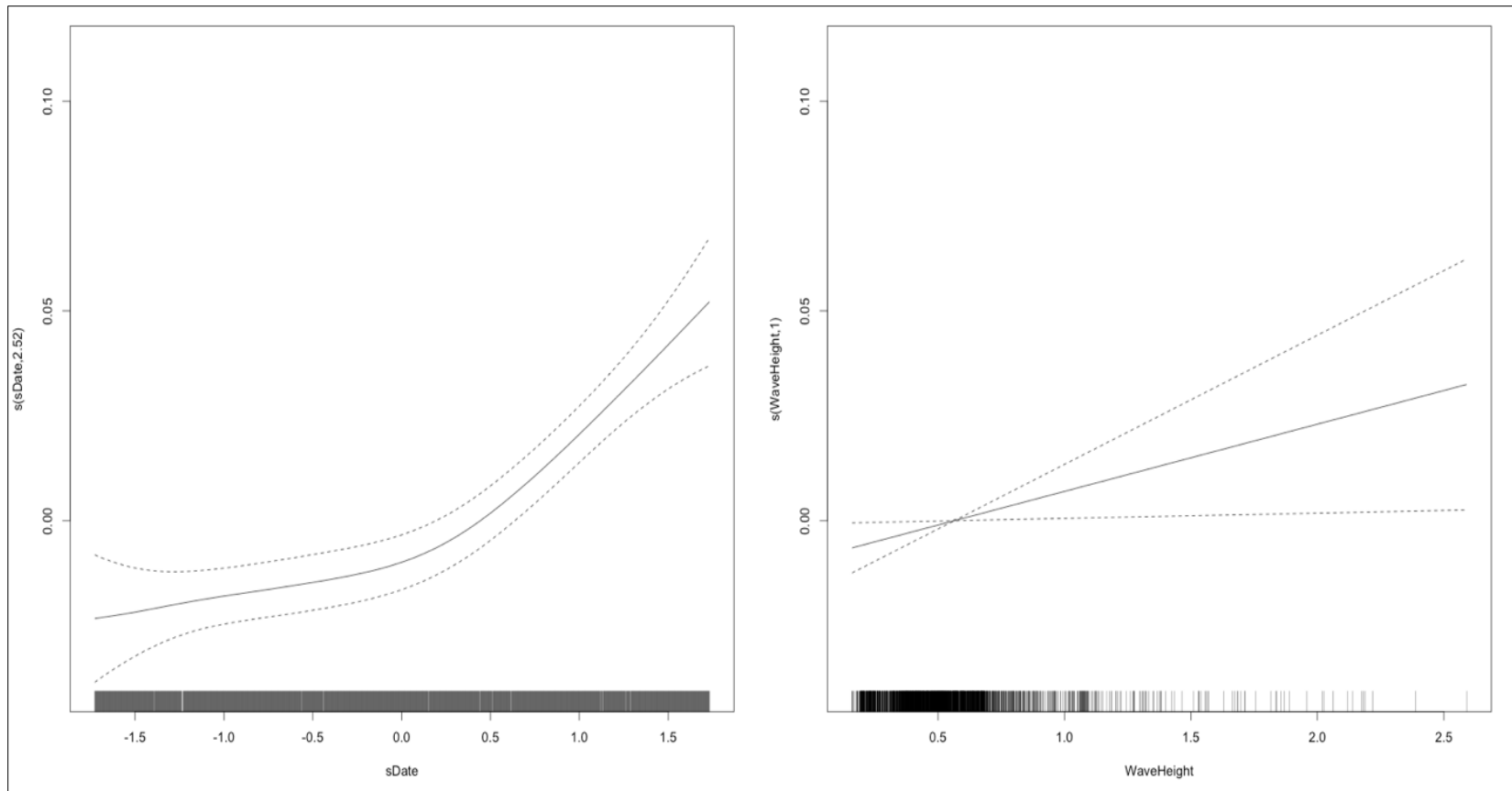
Figure D-48a. SA2 smoothing functions for Measured Vessel Band Noise as a function of Date, Wave Height, Windspeed, and CPA for Receiver 4, Deployment 1.
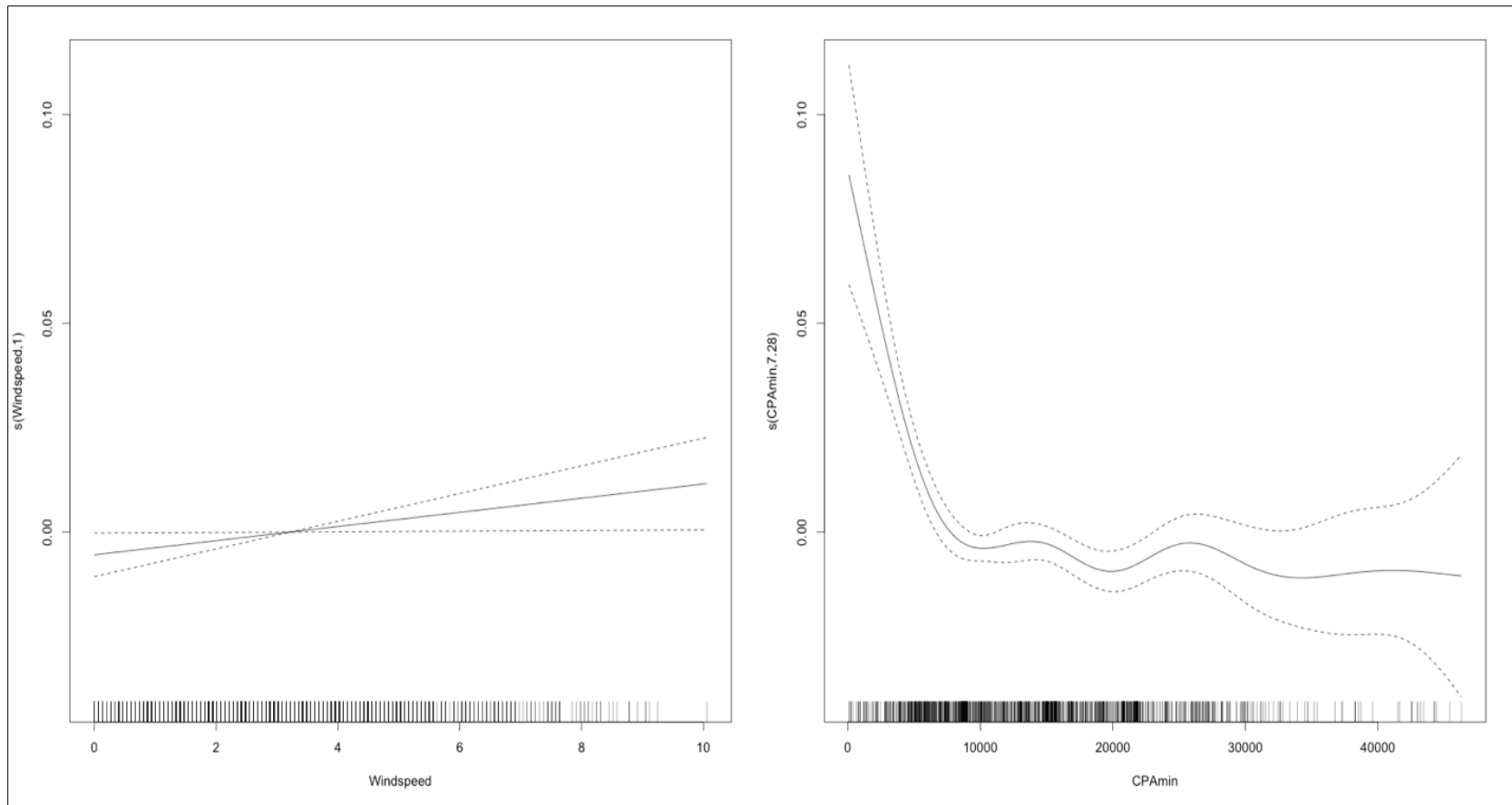
Figure D-48b. SA2 smoothing functions for Measured Vessel Band Noise as a function of Date, Wave Height, Windspeed, and CPA for Receiver 4, Deployment 1.
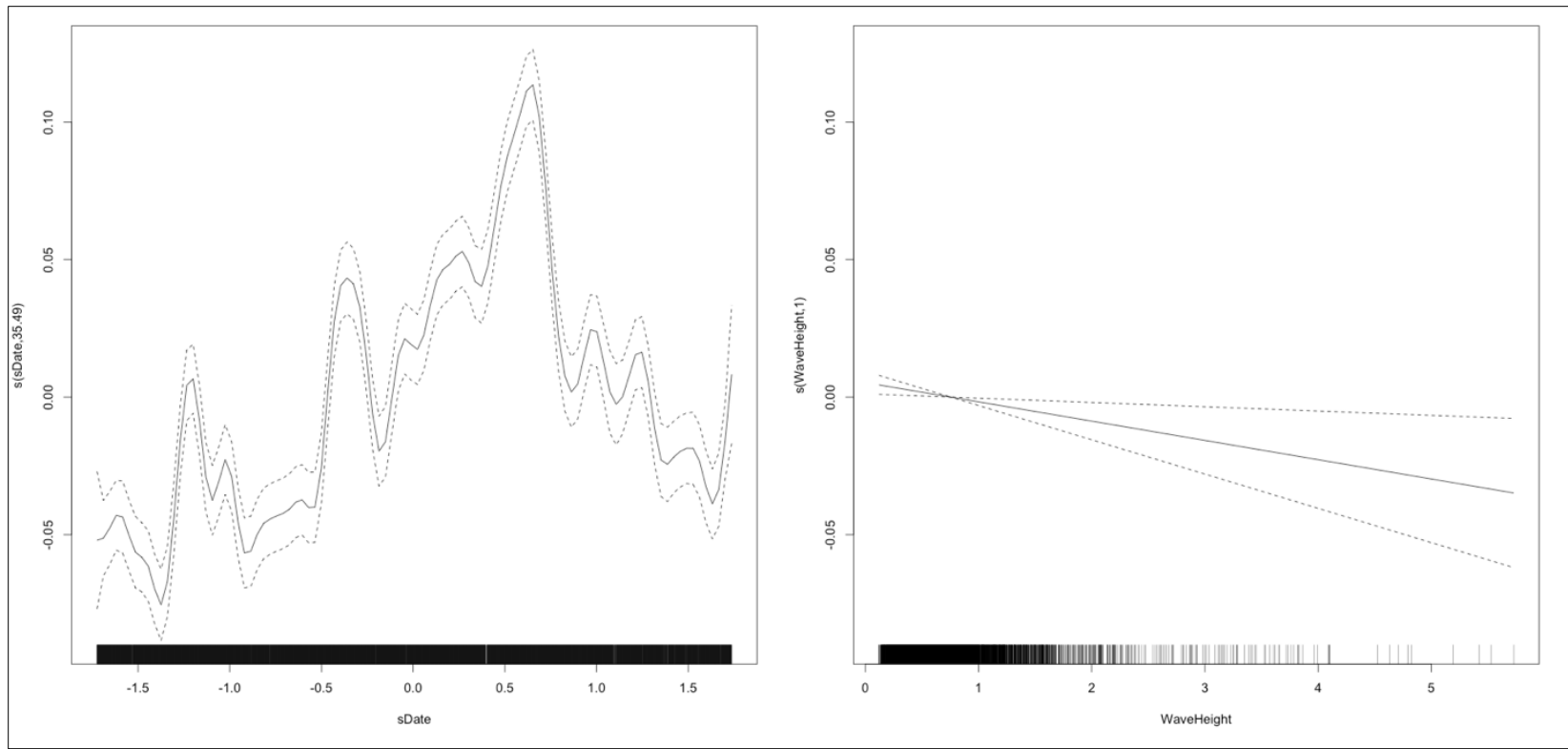
Figure D-49a. SA2 smoothing functions for Measured Vessel Band Noise as a function of Date, Wave Height, Windspeed, and CPA for Receiver 5, Deployment 1.
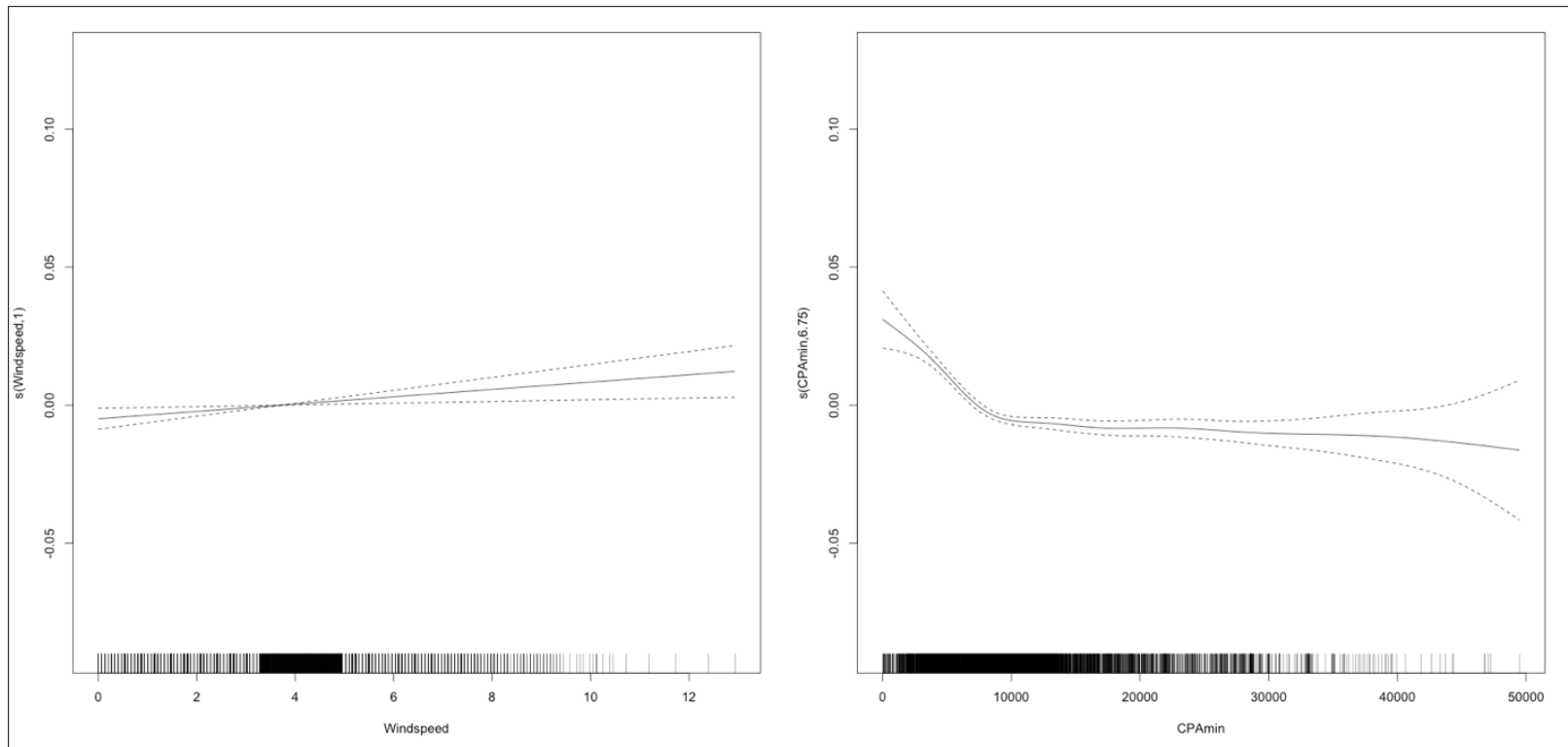
Figure D-49b. SA2 smoothing functions for Measured Vessel Band Noise as a function of Date, Wave Height, Windspeed, and CPA for Receiver 5, Deployment 1.

D.4.5.6 Deployment 1, Receiver 6 (Statistical Approach 2)

Both statistical analyses for Receiver 6 showed that scaled date, wind speed, and minimum CPA were all significant predictors (**Table D-27**). The R-square was 0.407. The simplified analysis also found that wave height predicted increased LF noise levels (**Figure D-50**). The shape of the smooth fit to the scaled date, wind speed, wave height, and minimum CPA variables in both analyses were similar, except for minimum CPA. The simplified analysis curve showed increased LF noise as the minimum CPA decreased, but the shape of the curve did not have the notable inflection point seen in all previous sensors.

Table D-27. GAM SA2 output for Deployment 1, Receiver 6

A. Parametric Coefficients	Estimate	Std. Error	t-value	p-value
(Intercept)	4.5861	0.0012	3935.9757	< 0.0001
km2	0.0800	0.0056	14.2991	< 0.0001
km4	0.0313	0.0044	7.0286	< 0.0001
km10	0.0043	0.0016	2.6848	0.0073
B. Smooth Terms	edf	Ref.df	F-value	p-value
s(sDate)	40.7142	49.0000	19.2240	< 0.0001
s(WaveHeight)	4.6228	4.6228	2.8579	0.0265
s(Windspeed)	1.0000	1.0000	66.8009	< 0.0001
s(CPAmin)	1.0000	1.0000	37.4071	< 0.0001
Key: CPA= closest point of approach; edf=empirical distribution function; F-value=value on the F distribution calculated by dividing two mean squares; km=kilometer; min=minimum; p-value= level of marginal significance within a statistical hypothesis test, representing the probability of the occurrence of a given event; Ref.df=reference degrees of freedom; s=scaled; Std. Error=Standard Error				

D.4.5.7 Deployment 1, Receiver 7 (Statistical Approach 2)

Both analyses resulted in the scaled date, wave height, wind speed, and minimum CPA variables being all significant predictors for Receiver 7 in Deployment 1 (**Table D-28**). The shape of the smooth fits for these variables in both analyses were similar (**Figure D-51**). The adjusted R-square value for the simplified analysis was also higher, 0.552 versus 0.486 resulting from statistical approach 1.

Table D-28. GAM SA2 output for Deployment 1, Receiver 7

A. Parametric Coefficients	Estimate	Std. Error	t-value	p-value
(Intercept)	4.5957	0.0019	2421.2043	< 0.0001
km2	0.0094	0.0049	1.9053	0.0568
km4	0.0059	0.0018	3.1865	0.0015
km10	0.0062	0.0008	7.8988	< 0.0001
B. Smooth Terms	edf	Ref.df	F-value	p-value
s(sDate)	1.0091	49.0000	0.3969	< 0.0001
s(WaveHeight)	1.8954	1.8954	4.2832	0.0118
s(Windspeed)	3.9156	3.9156	26.8821	< 0.0001
s(CPAmin)	7.7710	7.7710	51.1244	< 0.0001
Key: CPA= closest point of approach; edf=empirical distribution function; F-value=value on the F distribution calculated by dividing two mean squares; km=kilometer; min=minimum; p-value= level of marginal significance within a statistical hypothesis test, representing the probability of the occurrence of a given event; Ref.df=reference degrees of freedom; s=scaled; Std. Error=Standard Error				
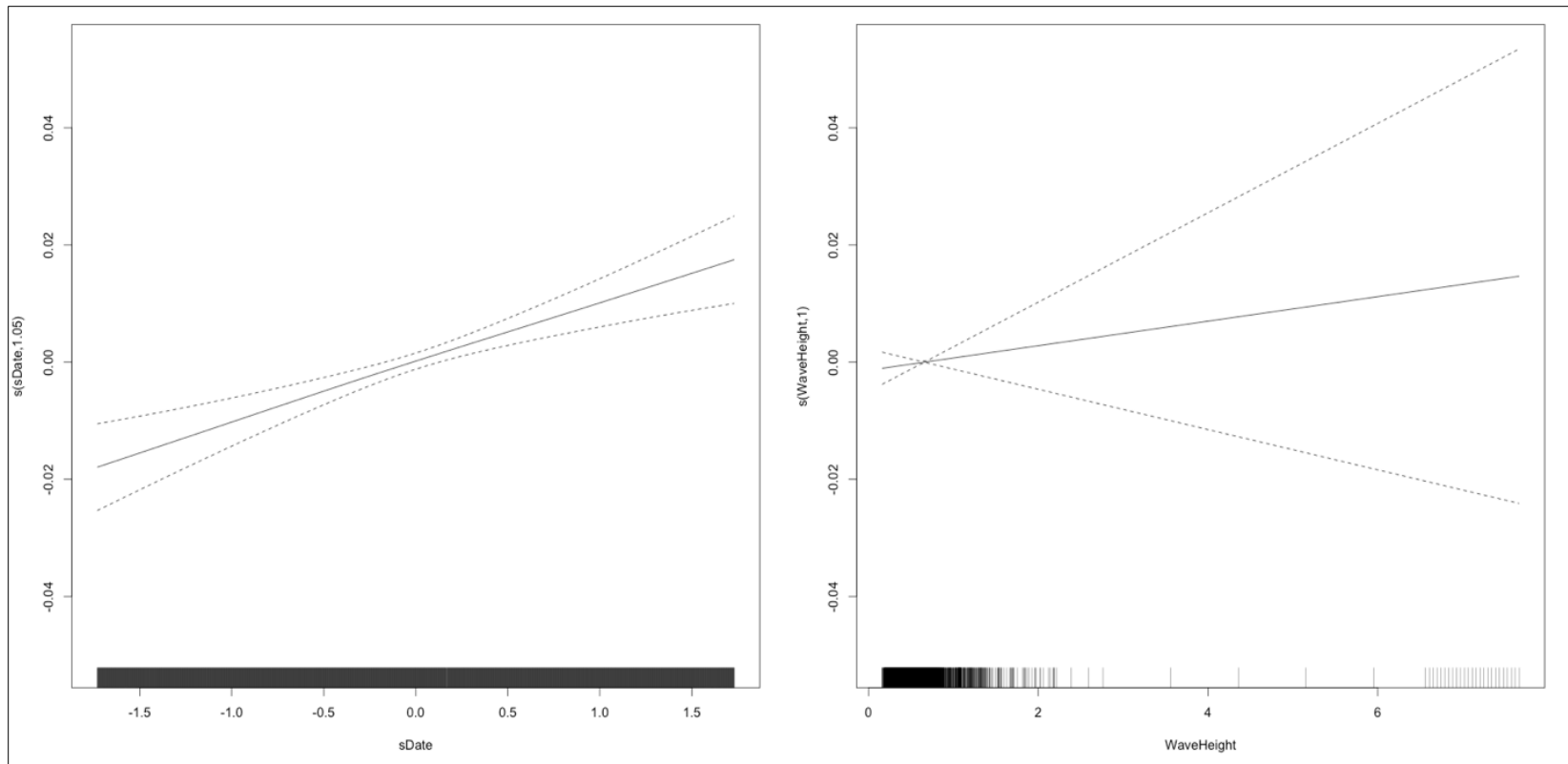
Figure D-50a. SA2 smoothing functions for Measured Vessel Band Noise as a function of Date, Wave Height, Windspeed, and CPA for Receiver 6, Deployment 1.
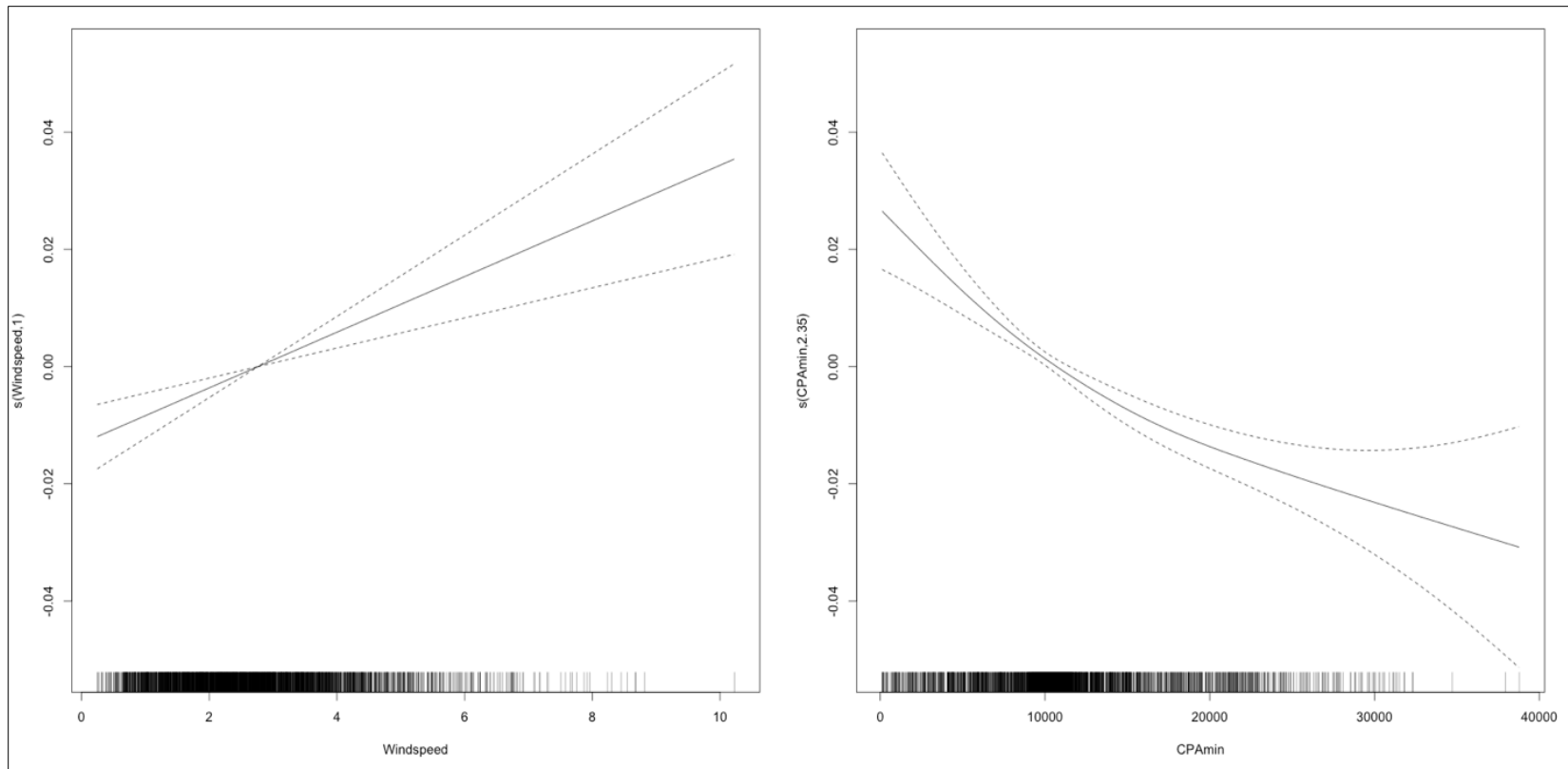
Figure D-50b. SA2 smoothing functions for Measured Vessel Band Noise as a function of Date, Wave Height, Windspeed, and CPA for Receiver 6, Deployment 1.
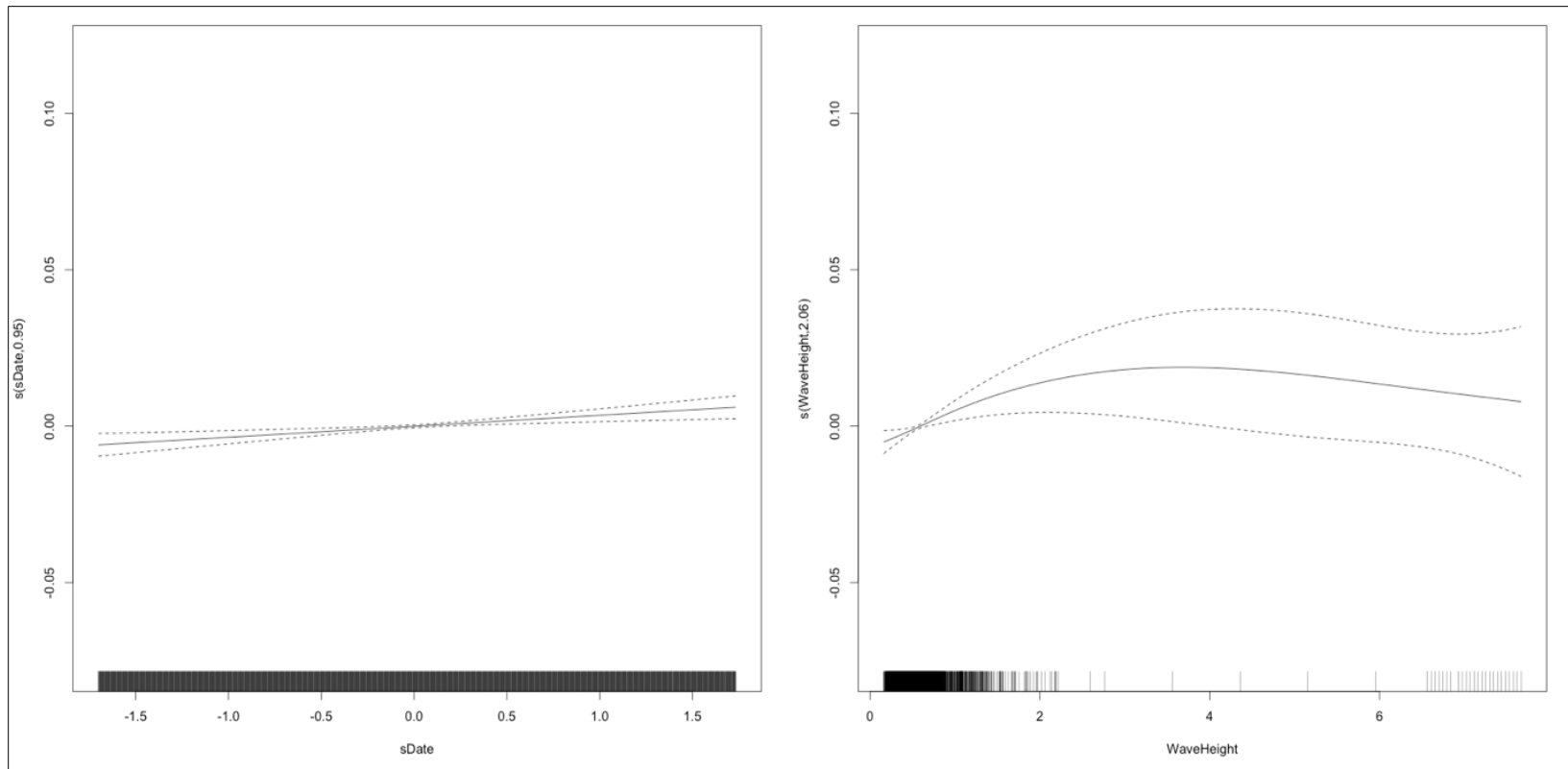
Figure D-51a. SA2 smoothing functions for Measured Vessel Band Noise as a function of Date, Wave Height, Windspeed, and CPA for Receiver 7, Deployment 1.
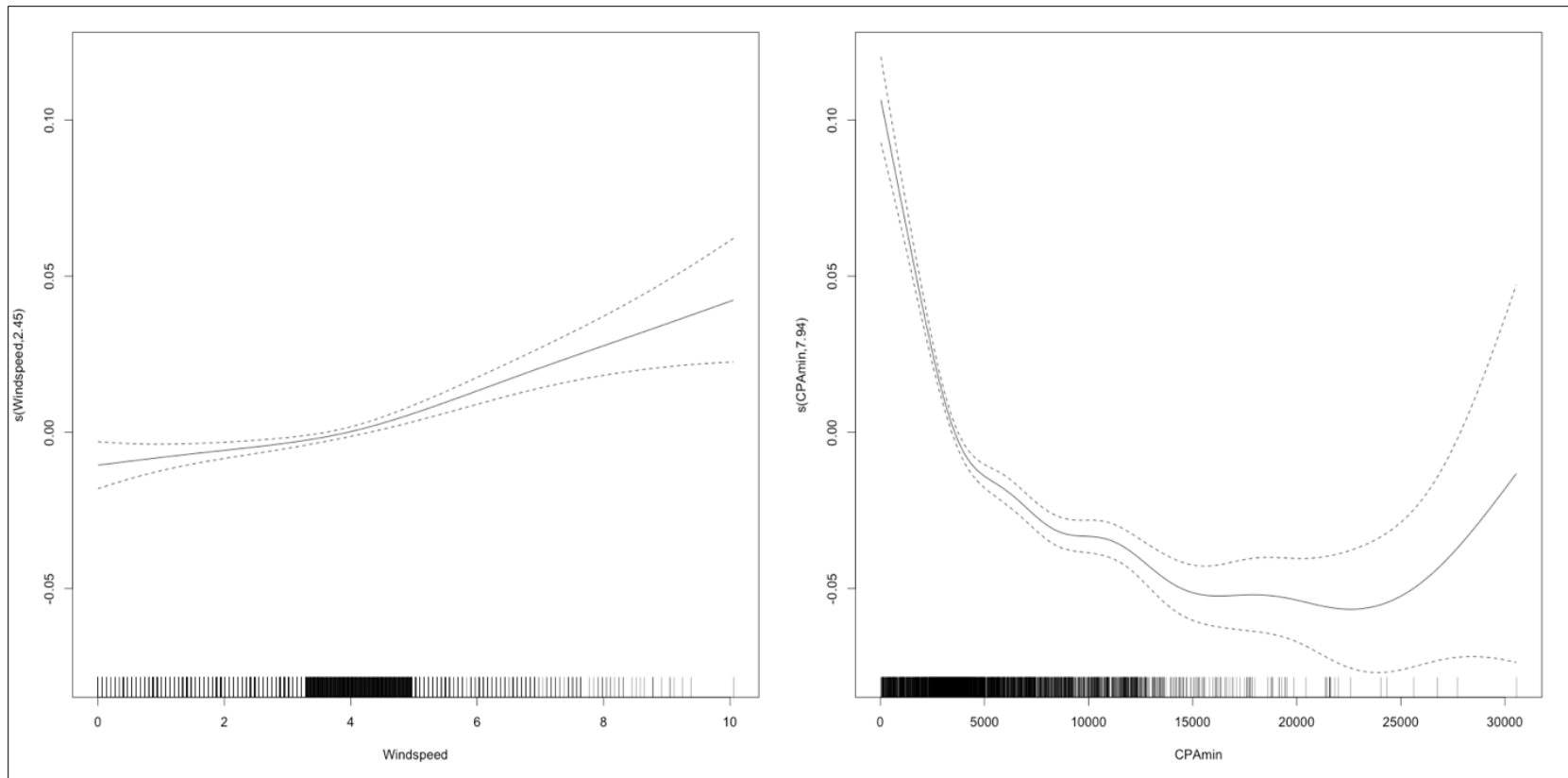
Figure D-51b. SA2 smoothing functions for Measured Vessel Band Noise as a function of Date, Wave Height, Windspeed, and CPA for Receiver 7, Deployment 1.

D.4.5.8 Deployment 1, Receiver 8 (Statistical Approach 2)

The result of the original statistical predicted RL analysis for Receiver 8 was that only windspeed and minimum CPA were significant predictors. However, only date and minimum CPA were significant predictors as the result of the simplified statistical analysis (**Table D-29**). The R-square value for the SA2 was 0.633. The shape of the minimum CPA curve fit was similar in both analyses (**Figure D-52**). The relatively small sample size for this Receiver during Deployment 1 may be partially responsible for the uncertainty in predictor variables other than minimum CPA.

Table D-29. GAM SA2 output for Deployment 1, Receiver 8

A. Parametric Coefficients	Estimate	Std. Error	t-value	p-value
(Intercept)	4.5051	0.0015	3010.2755	< 0.0001
km2	0.0286	0.0108	2.6514	0.0081
km4	0.0125	0.0062	2.0138	0.0442
km10	0.0069	0.0025	2.7816	0.0055
B. Smooth Terms	edf	Ref.df	F-value	p-value
s(sDate)	40.6895	49.0000	35.9378	< 0.0001
s(WaveHeight)	1.7724	1.7724	1.4944	0.2996
s(Windspeed)	1.0000	1.0000	1.6056	0.2053
s(CPAmin)	6.3320	6.3320	4.5896	0.0001

Key: CPA= closest point of approach; edf=empirical distribution function; F-value=value on the F distribution calculated by dividing two mean squares; km=kilometer; min=minimum; p-value= level of marginal significance within a statistical hypothesis test, representing the probability of the occurrence of a given event; Ref.df=reference degrees of freedom; s=scaled; Std. Error=Standard Error

D.4.5.9 Deployment 1, Receiver 9 (Statistical Approach 2)

The smallest sample size (N=1108) and lowest R-square value compared to all other sensors were the result of the SA2 (**Table D-30**) for Receiver 9. The Receiver 9 R-square value was 0.100 for the original predicted RL analysis, while the SA2 resulted in a R-square value of 0.253. The shapes of the smooth fit curves for all variables were similar from both analyses (**Figure D-53**).

Table D-30. GAM SA2 output for Deployment 1, Receiver 9

A. Parametric Coefficients	Estimate	Std. Error	t-value	p-value
(Intercept)	4.7045	0.0035	1344.1693	< 0.0001
km2	0.0043	0.0043	1.0030	0.3161
km4	0.0033	0.0020	1.6111	0.1074
km10	0.0006	0.0008	0.7182	0.4728
B. Smooth Terms	edf	Ref.df	F-value	p-value
s(sDate)	17.8830	49.0000	3.0201	< 0.0001
s(WaveHeight)	4.2038	4.2038	5.2304	0.0003
s(Windspeed)	1.0000	1.0000	5.0738	0.0245
s(CPAmin)	5.7121	5.7121	5.1273	0.0001

Key: CPA= closest point of approach; edf=empirical distribution function; F-value=value on the F distribution calculated by dividing two mean squares; km=kilometer; min=minimum; p-value= level of marginal significance within a statistical hypothesis test, representing the probability of the occurrence of a given event; Ref.df=reference degrees of freedom; s=scaled; Std. Error=Standard Error
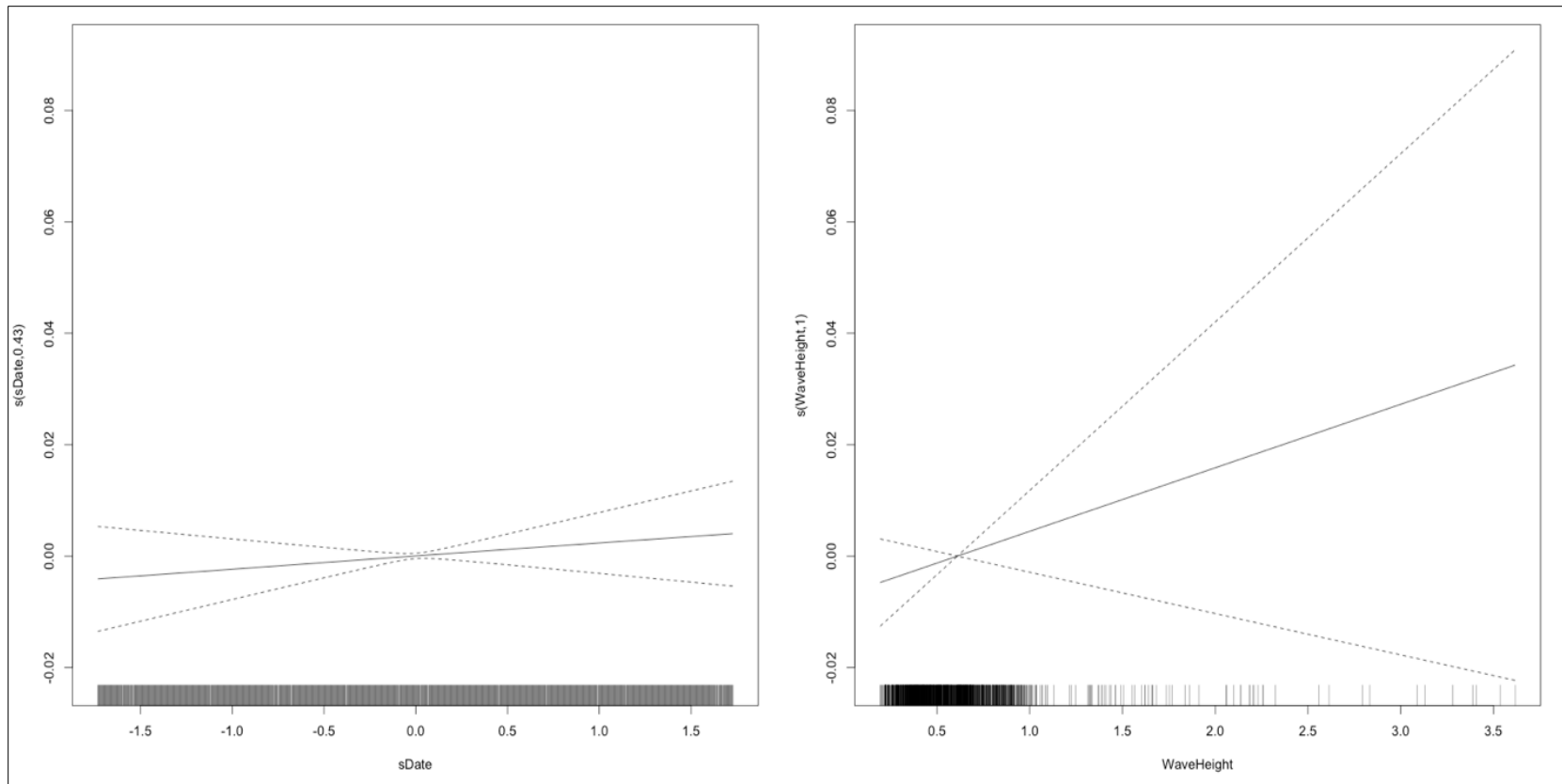
Figure D-52a. SA2 smoothing functions for Measured Vessel Band Noise as a function of Date, Wave Height, Windspeed, and CPA for Receiver 8, Deployment 1.
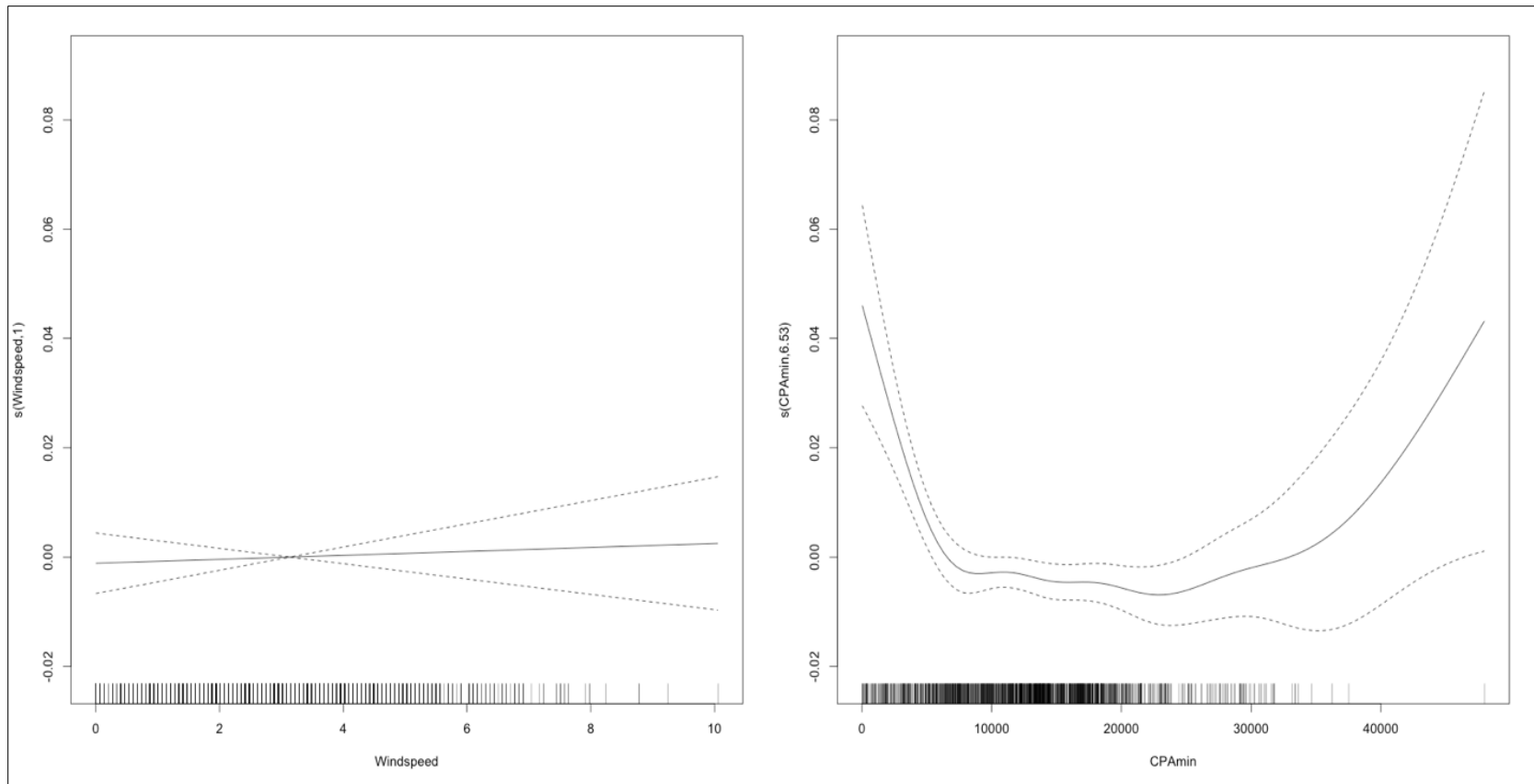
Figure D-52b. SA2 smoothing functions for Measured Vessel Band Noise as a function of Date, Wave Height, Windspeed, and CPA for Receiver 8, Deployment 1.
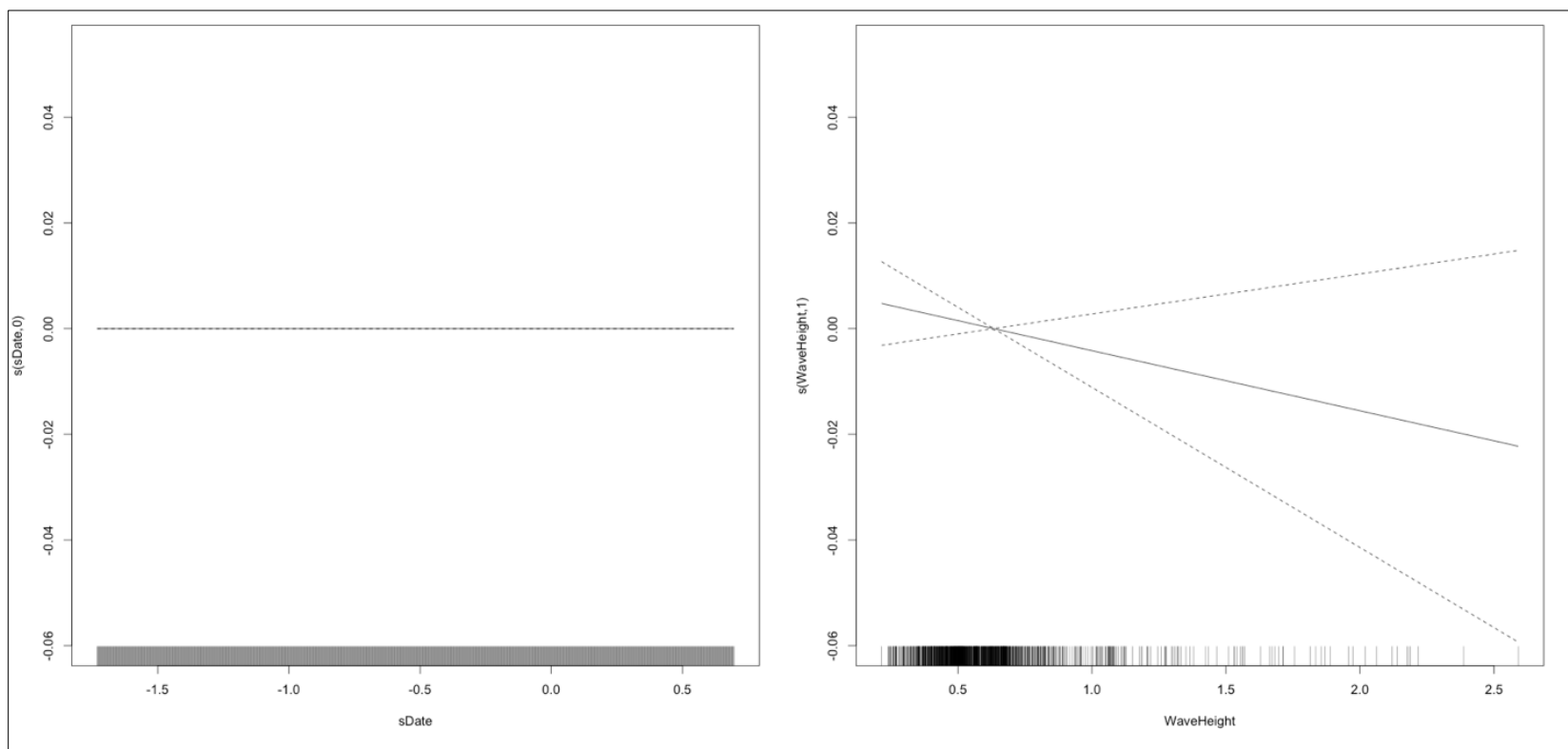
Figure D-53a. SA2 smoothing functions for Measured Vessel Band Noise as a function of Date, Wave Height, Windspeed, and CPA for Receiver 9, Deployment 1.
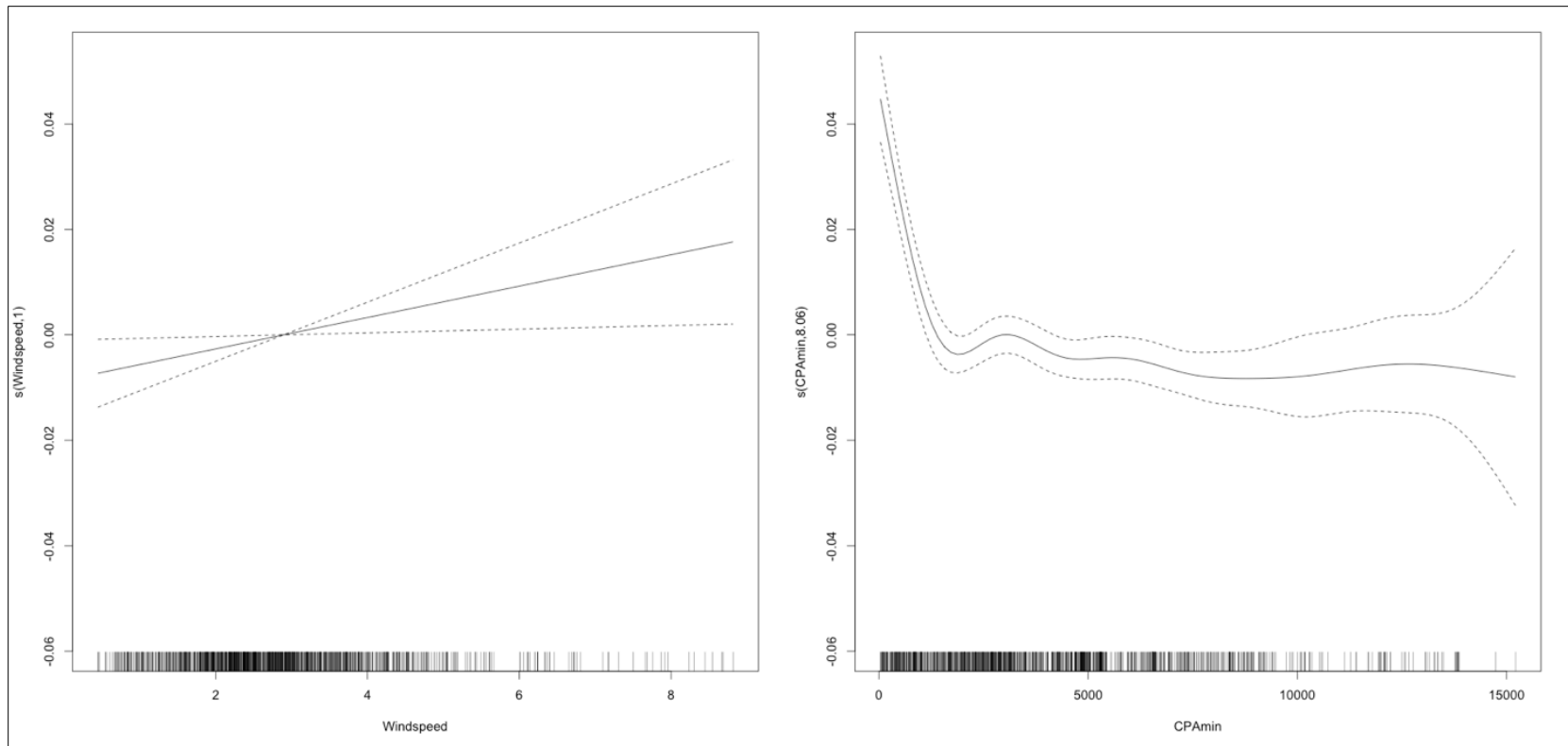
Figure D-53b. SA2 smoothing functions for Measured Vessel Band Noise as a function of Date, Wave Height, Windspeed, and CPA for Receiver 9, Deployment 1.

D.4.5.10 Deployment 1, Receiver 10 (Statistical Approach 2)

Both statistical analyses for Receiver 10, Deployment 1 resulted in significant predictors of scaled date, wave height, windspeed, and minimum CPA (**Table D-31**). The shapes of the smoothed fitted curves were similar in both analyses (**Figure D-54**). The R-squared value was somewhat higher in the simplified analysis versus the original statistical analysis (0.492 versus 0.421).

Table D-31. GAM SA2 output for Deployment 1, Receiver 10

| A. Parametric Coefficients	Estimate	Std. Error	t-value	p-value
(Intercept)	4.5200	0.0020	2280.8793	< 0.0001
km2	0.0182	0.0039	4.7058	< 0.0001
km4	0.0150	0.0017	8.9266	< 0.0001
km10	0.0045	0.0007	6.5022	< 0.0001
B. Smooth Terms	**edf**	**Ref.df**	**F-value**	**p-value**
s(sDate)	43.4332	49.0000	38.4445	< 0.0001
s(WaveHeight)	8.0524	8.0524	14.7354	< 0.0001
s(Windspeed)	5.7822	5.7822	8.2390	< 0.0001
s(CPAmin)	8.2372	8.2372	33.4353	< 0.0001
Key: CPA= closest point of approach; edf=empirical distribution function; F-value=value on the F distribution calculated by dividing two mean squares; km=kilometer; min=minimum; p-value= level of marginal significance within a statistical hypothesis test, representing the probability of the occurrence of a given event; Ref.df=reference degrees of freedom; s=scaled; Std. Error=Standard Error				
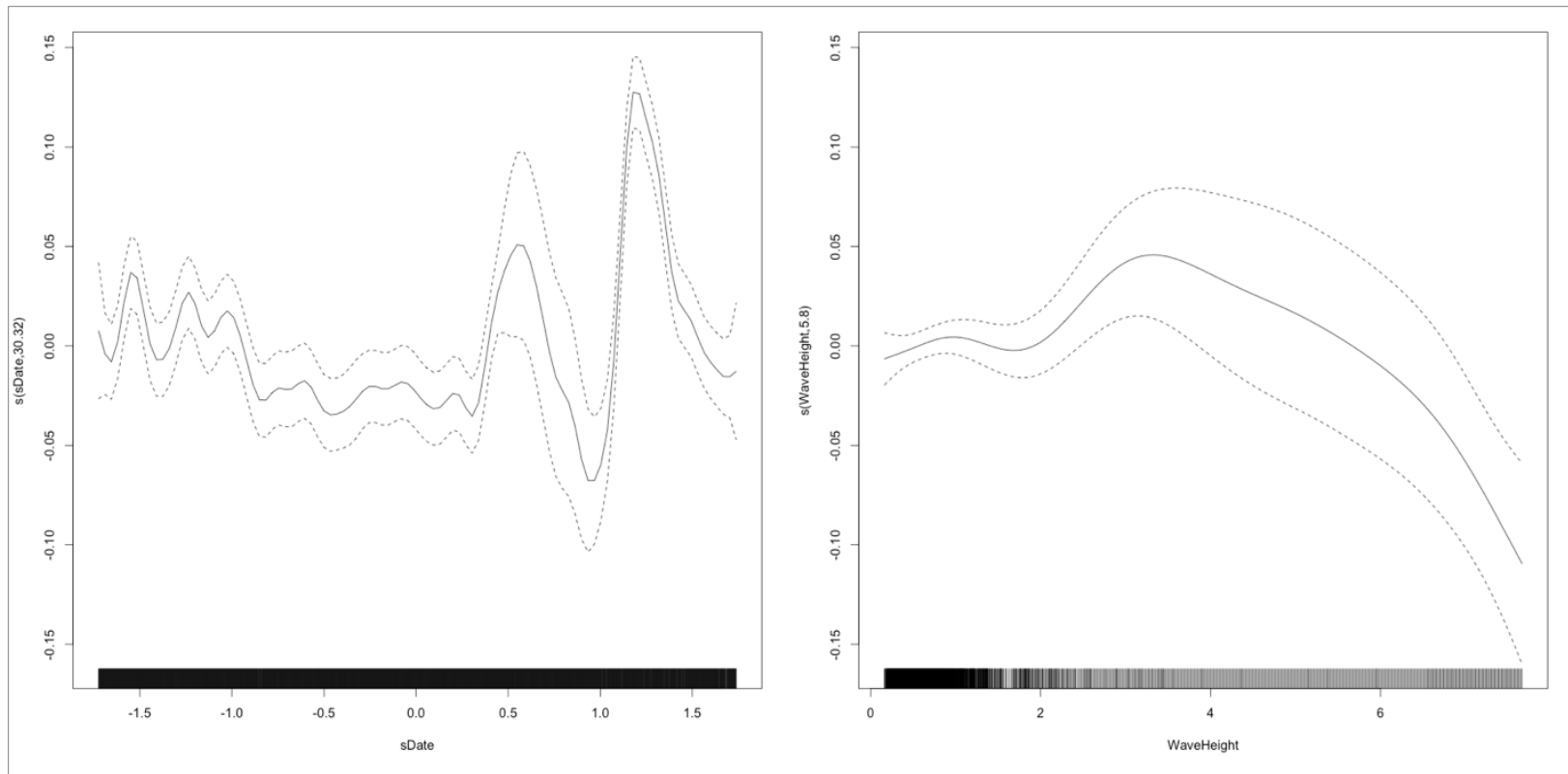
Figure D-54a. SA2 smoothing functions for Measured Vessel Band Noise as a function of Date, Wave Height, Windspeed, and CPA for Receiver 10, Deployment 1.
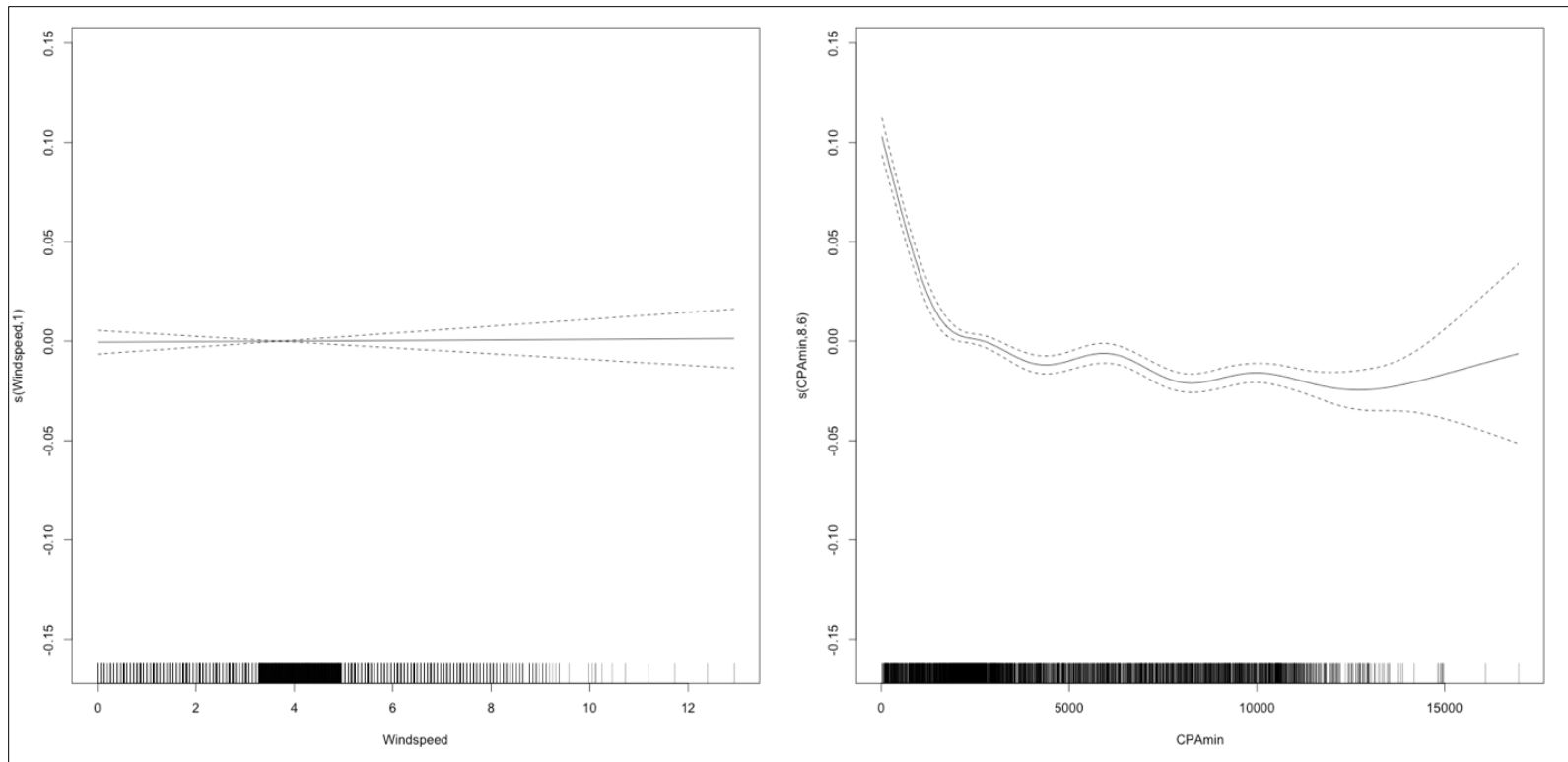
Figure D-54b. SA2 smoothing functions for Measured Vessel Band Noise as a function of Date, Wave Height, Windspeed, and CPA for Receiver 10, Deployment 1.

D.4.6 Summary of Statistical Modeling of Vessel Received Levels

The individual analyses of the 10 receivers produced several common patterns. First the R-squared for most of the analyses was quite high, exceeding 0.5 in some cases. This indicates that a goodly amount, if not most, of the variance in the measured RL could be explained by the statistical models. One of the most common patterns in the data was a strong relationship between CPA distance and measured LF sound level. In almost all analyses, this relationship was very similar, with a near linear increase in RL as vessels approached within 10 km. This relationship was much stronger than any of the predicted RL values. Based on this finding, it is recommended that future efforts to predict LF noise in the GOM should rely directly upon AIS data as predictor variables. In most of the receivers, there was also the expected positive relationship between windspeed and wave height with increased measured LF noise.

### D.4.7 Temporal/Spatial Trends of Recorder Data

The monthly spectral levels of the ten RH and EARS recorders were assessed to determine whether any spatial or temporal trends were evident in the data. The monthly median spectral levels of the ten RH and EARS recorders over the duration of the Program are presented in **Appendix D-C**. In each monthly figure, the top spectrum represents the entire frequency range, while the bottom panel presents the LF band (10 to 1,000 Hz) in more detail. These figures illustrate the temporal variability at each recorder sensor. In all **Appendix D-C** figures, there is an apparent difference in the data recorded by the RH and EARS recorders.

D.4.8 Extrapolation Capability of Acoustic Data: Glider/Fixed Sensor Comparison

This analysis was intended to answer the question: How far can data from a single buoy be extrapolated? To answer this question acoustic data from the 2018 MP Deployment 1 Seaglider flight as it approached, nearly flew over, and then departed from one of the stationary recorders (EARS buoy at Site 2) were compared. The Seaglider approached within 1,500 m of the EARS buoy at this site (**Table D-1**) during Deployment 1 (**Figure D-55**).

In evaluating the spectrograms of the 24 hours of data before and after the CPA of the OSU glider to the Site 2 EARS recorder, the expectation was that the acoustic characteristics of the collected data would be similar at CPA but would diverge as the range between the recorders increased (**Figure D-56**). However, the spectrograms from the Seaglider and Site 2 EARS data show minimal similarity at any point. Furthermore, the monthly spectra (**Appendix D-B, Figures D-B1 to D-B6**) show that in some months, the spectral profiles for individual recorders in deep water are almost identical. However, in other months, the spectral differences can exceed 20 dB. This indicates that the glider-static receiver comparison is not generalizable to the full range and temporal scale of the project. Instead, a statistical analysis of RL as a function of latitude, longitude, and water depth would be a more promising avenue to pursue, similar to the analysis results in **Section D.4.4** of this report.
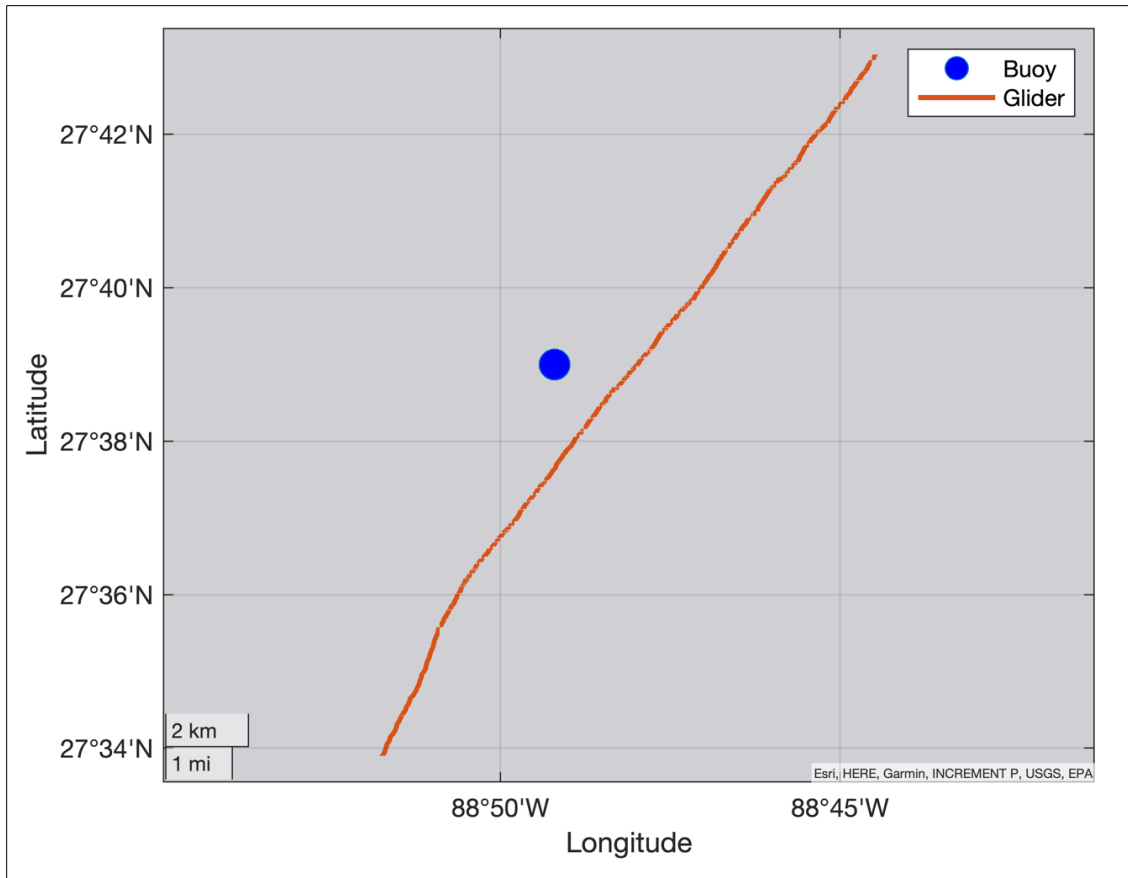
Figure D-55. Path of the 2018 MP Seaglider past the Site 2 EARS recorder during Deployment 1.
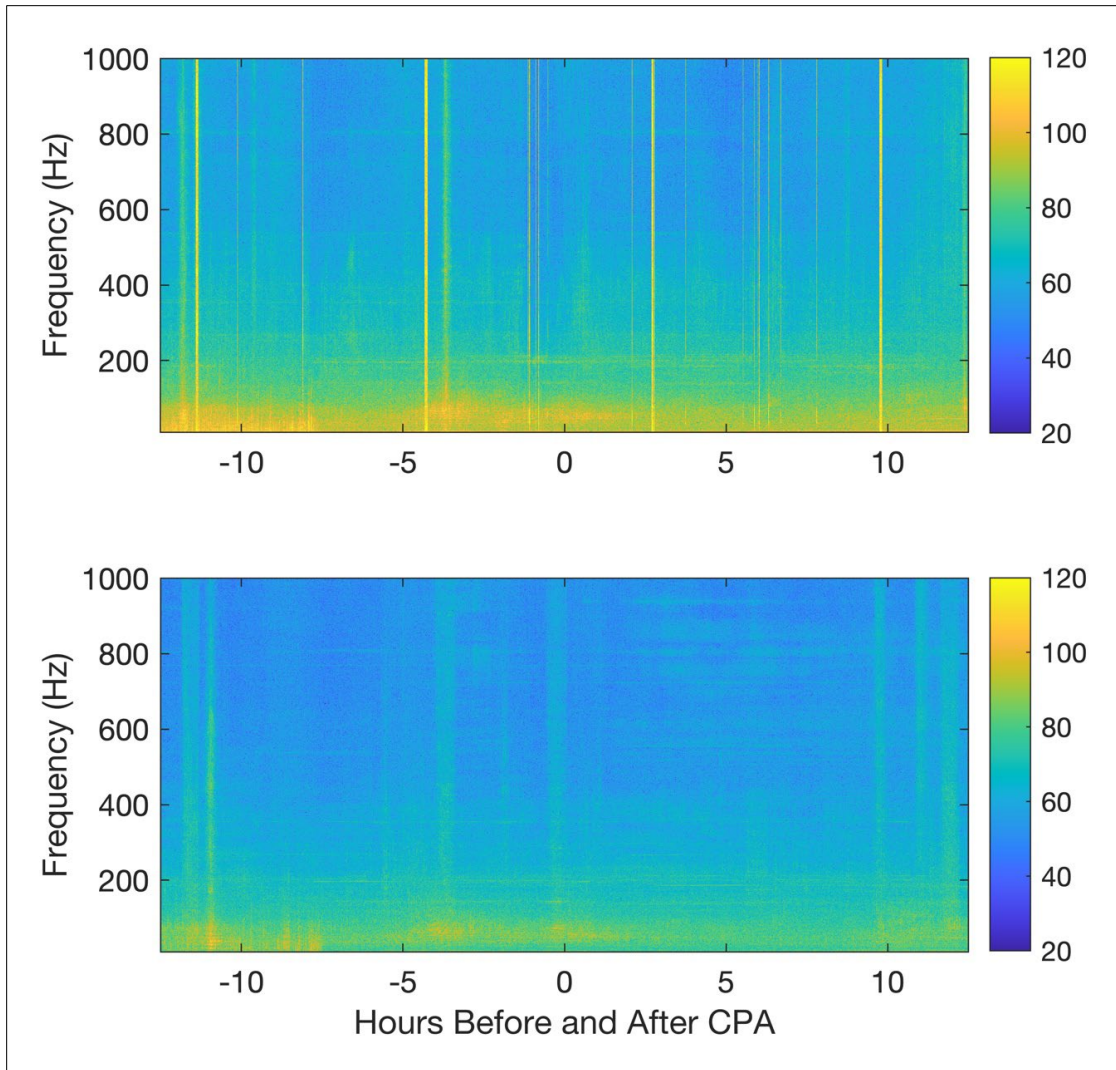
Figure D-56. Comparison of spectrograms from the 2018 MP Seaglider (top panel) and the Site 2 EARS recorder (bottom panel) for the 12 hours before and after the CPA (color bar units are dB re 1μPa^2).

D.5   Discussion

The marine environment of the northern GOM is highly industrialized with anthropogenic sound sources such as shipping, oil and gas activities, military operations, and scientific research contributing to the GOM's ambient soundscape. Noise impacts to protected marine species (e.g., marine mammals) may occur in association with oil and gas exploration and development activities, which include seismic surveys, platform decommissioning, drilling, construction, and the resulting increases in vessel traffic. The purpose of the GOM PAM Program was to establish a baseline of the ambient soundscape in the northern GOM and characterize one of the dominant noise inputs from vessel traffic.

A substantial portion of the work in this Program has been in the development of new analysis tools that are based on the spectral analysis output provided by the Cornell Conservation Bioacoustics program (CCB). These tools are available for continued analysis of additional data as well as providing a springboard for derivative analytical procedures.

D.5.1   Anthropogenic Detection

Daily detections of vessel activity, reported for close passbys to the receivers (i.e., close enough to create a Lloyd mirror interference pattern), varied from below 10 percent to near constant or daily occurrences. There was a strong seasonal pattern, with most vessel detections occurring in summer months (May to June). The annual pattern indicated an increase in vessel traffic from 2018 to 2019 and a subsequent decrease in 2020. However, the sampling within the first and last year only covered a portion of the years 2018 and 2020. Monitoring in 2018 began in late May, and most recording was completed by May 2020. Therefore, these partial years may have missed a portion of the peak in vessel traffic. Another possibility is that the decline in vessel numbers in 2020 may reflect reduced vessel traffic due to the corona virus disease (COVID)-19 pandemic.

The effects of latitude and longitude on the distribution of vessel detections were both statistically significant, but the patterns were not particularly informative. Vessel detection rates increased with both water depth and latitude. However, the magnitudes of these effects were not equivalent (**Table D-7; Figure D-14**). Water depth appears to be the stronger predictor, and this may reflect better acoustic propagation in deeper waters, or all these effects could reflect the prominent shipping routes into the Port of New Orleans.

Airgun occurrence had similar strong annual and monthly patterns. Latitude and longitude predictors were both borderline significant, and water depth had no significant effect. This likely reflects the greater distance over which airgun operations could be detected. The same temporal pattern of airgun activity was seen on many of the recorders.

D.5.2   Biological Detection

More than 20 species of marine mammals occur in the waters of the northern GOM, with species of dolphins, including the bottlenose dolphin, predominantly populating continental shelf waters, and deeper diving species such as beaked whales and the sperm whale inhabiting offshore waters (Fulling et al. 2003). One baleen whale, the newly named Rice's whale (formerly GOM Bryde's whale), is a year-round resident of northeastern GOM waters, with a very small population (50 to 100 whales) that is listed as endangered under the ESA (Hayes et al. 2021; SMM 2021).

To differentiate some of the most common sound-producing marine mammals in the northern GOM that may contribute to the ambient soundscape, frequency bands for the known vocalizations of five marine mammal species or species groups (Rice's whale, beaked whales, and dolphins) were identified. The

recorded acoustic data were assessed to determine which characteristics informed the spatial and temporal patterns of these marine mammal species or groups.

The frequency overlap between the signals of Rice's whales and the prevalent anthropogenic noise environment made reliably detecting the calls of Rice's whales difficult using only the spectrally analyzed data. A better approach would be to use a matched-filter detection process that operates on the waveform data.

The detection rate results from the "dolphin" and "beaked whale" frequency bands had similar temporal patterns. Detection rates increased from May to September and began to decline in October. November rates were lower still, but the data from November 2018 were sparse, as some recorders stopped recording early due to internal faults in the recorders, severed moorings, trawled recorders, and data compression issues.[22] All these issues were addressed in subsequent deployments.

The effect of water depth on detection rates had opposite effects for these two bands. In the dolphin band, peaks were seen in both shallow and deep waters, while the values from approximately 400 to 700 m were lower. This pattern is perhaps most easily explained by multiple species being detected. The peak of beaked whale band detections appeared to occur at intermediate water depths of 500 to 1,000 m and then declined in the very shallow and very deep depths. This may indicate a habitat preference for slope environments.

Latitude also had opposite effects between the two detection band results. For the dolphin band, the detection rates were lowest in the southernmost waters and increased over the more northerly recorders. For beaked whale band detections, the rates were highest in the south and decreased to the north. Finally, longitude also had opposite trends for these two bands. The highest dolphin band detection rates were found in the central longitudes, while the highest beaked whale band detection rates were found to the far west and east of the Program area.

D.5.3 Statistical Analysis of Measured Vessel Noise Levels

The statistical analysis of Received Vessel Band noise focused on predicting the actual RL at the receivers. This involved 1) measurement of distance from each vessel to the receiver, 2) estimation of the SL of the vessel, and 3) prediction of the TL between the two. Modeled vessel noise level was most often a good predictor of measured levels. However, on occasion these functions curiously showed a negative relationship with measured noise levels. Such an occurrence may be due to overprediction of noise levels at this location.

However, the analyses shown in **Section D.4.4** show that the most important vessel predictor for measured sound level was CPA. This variable is relatively easy and quick to calculate. Future analyses should consider focusing on the AIS metrics and omit the time-consuming three-dimensional propagation modeling. Furthermore, if propagation predictions are needed, then three-dimensional modeling should be conducted along with a comparison of simpler propagation models.

---

[22] Preliminary project reports titled: Assessment of ocean ambient sound levels in the northern GOM, May 2018–May 2019 by Klinck H, Ponirakis DW, Dugan PJ, and Rice AN, 2019; Assessment of ocean ambient sound levels in the northern GOM, May-October 2018: autonomous Environmental Acoustic Recording System (EARS) buoys by Sidorovskaia N, Bhattarai K, 2019; and Assessment of ocean ambient sound levels in the northern GOM, October 2018–April 2019: autonomous Environmental Acoustic Recording System (EARS) buoys by Sidorovskaia N, Bhattarai K, 2019.

D.6   Recommendations

The analysis effort completed required compilation and understanding of numerous different datasets collected by multiple institutions. The quality and duration of the data allowed for different types of analyses that yielded valuable insight into the soundscape of the Program study area. Lessons learned from this analysis effort resulted in the following recommendations for future efforts:

1. Approximately 250 terabytes of raw data were collected during the Program by six different types of recorders, each one of which stored raw data in a different format. Using six differently formatted, very large raw datasets for Phase 2 analyses would therefore have been extremely time consuming and involve an inordinate amount of manual labor. In consultation with BOEM, it was therefore decided to pre-process the raw data before using it as an input for Phase 2 analyses. In future Program phases, if time and resource constraints are not a significant issue, then it is recommended that advanced data analyses be conducted using raw data as this would allow for use of standard analytical tools and outputs (instead of instead of development and application of custom analysis tools).

2. Also, for future analysis, if pre-processed data are used, it is recommended that hybrid millidecade data representations (Martin et al. 2021) be considered. This is because use of one second, one Hz resolution data, while appealing, result in very large data files, which are difficult to exchange, manipulate, and analyze.

3. It is recommended that future efforts that involve detection and classification of signals begin with actual waveforms. Without waveform data it is much more difficult to correctly assign sources to received signals and to ground-truth automated detection efforts.

4. Based on the results of the statistical analysis, it is recommended that future analyses of vessel noise levels should consider focusing on the AIS metrics and omit the time-consuming three-dimensional propagation modeling. If propagation predictions are needed, then 3D modeling should be conducted along with a comparison of simpler propagation models to determine if simpler models can be used instead to save time.

5. Also based on the statistical analysis results, it is recommended that future efforts to predict LF noise in the GOM should rely directly upon AIS data as predictor variables.

6. The cause of the differences in LF data reported by EARS and RH should be investigated further.

7. A better approach for detecting the frequency bands of the Rice's whale would be to use a matched-filter detection process that operates on the waveform data.

D.7   Acknowledgements

D.8   Literature Cited

Ainslie MA, de Jong CAF, Martin B, Miksis-Olds JL, Warren JD, Heaney KD. 2017. Project dictionary (terminology standard). DRAFT. Durham (NH): University of New Hampshire. Technical report by TNO for ADEON Prime Contract No. M16PC00003.

Baron SC, Martinez A, Garrison LP, and Keith EO. 2008. Differences in acoustic signals from delphinids in the western North Atlantic and northern Gulf of Mexico. Mar Mammal Sci. 24:42–56.

Carnes MR. 2009. Description and evaluation of GDEM-V 3.0. Stennis Space Center (MS): Naval Research Laboratory. 24 p.

Clark CW, Gagnon GC, Stevenson D, Frankel AS, and Vigness-Raposa K. (in prep.). Demonstration of ocean basin scale passive acoustic tracking of marine mammals and response to anthropogenic noise sources.

Crocker SE, Fratantonio FD. 2016. Characteristics of sounds emitted during high-resolution marine geophysical surveys. Newport (RI): Naval Undersea Warfare Center Division. 266 p. Report No.: OCS Study 2016-044.

[ESR] Earth and Space Research. 2009. OSCAR third degree resolution ocean surface currents. Ver. 1. Pasadena (CA): NASA Jet Propulsion Laboratory.

Erbe C, Dunlop R, Jenner KCS, Jenner MNM, McCauley RD, Parnum I, Parsons M, Rogers T, Salgado-Kent C. 2017. Review of underwater and in-air sounds emitted by Australian and Antarctic marine mammals. Acoust Aust. 45(3):1-63.

Estabrook BJ, Ponirakis DW, Clark CW, and Rice AN. 2016. Widespread spatial and temporal extent of anthropogenic noise across the northeastern Gulf of Mexico shelf ecosystem. Endanger Species Res. 30:267–282.

Frankel AS, Amaral JL, Ellison WT. 2017. NOAA shipping noise mapping pilot project final report. Middleton (RI): Marine Acoustics, Inc. Report No. TN-17-017.

Frankel AS, Zeddies D, Simard P, Mann D. 2014. Whistle source levels of free-ranging bottlenose dolphins and Atlantic spotted dolphins in the Gulf of Mexico. J Acoust Soc Am. 135:1624–1631.

Fulling GL, Mullin KD, Hubard CW. 2003. Abundance and distribution of cetaceans in outer continental shelf waters of the U.S. Gulf of Mexico. Fish Bull. 101:923–932.

Hayes SA, Josephson E, Maze-Foley K, Rosel PE, Turek J. (Eds.). 2021. US Atlantic and Gulf of Mexico marine mammal stock assessments 2020. Woods Hole (MA): Northeast Fisheries Science Center, National Marine Fisheries Service. 403 p. NOAA Technical Memorandum NMFS-NE-271

Hildebrand JA. 2009. Anthropogenic and natural sources of ambient noise in the ocean. Mar Ecol Prog Ser. 395:5–20.

Interdisciplinary Oceanography Group. 2017. UCSB ocean surface currents mapping project – real time data.

Latusek-Nabholz JN, Whitt AD, Fertl D, Gallien DR, Ampela K, Khan AA, Sidorovskaia N. 2020. Literature synthesis on passive acoustic monitoring projects and sound sources in the Gulf of Mexico. New Orleans (LA): US Department of the Interior, Bureau of Ocean Energy Management. Contract No.: M17PC00001. OCS Study BOEM 2020-009. 99 p.

Lin YT. 2021. Three-dimensional propagation of seismic airgun signals in the Mississippi Canyon area of the Gulf of Mexico. JASA Express Letters 1. https://doi.org/10.1121/10.0003451.

MarineCadestre.gov. No Date. Vessel traffic data. Bureau of Ocean Energy Management (BOEM) and National Oceanic and Atmospheric Administration (NOAA). marinecadastre.gov/data.

Martin SB, Gaudet BJ, Klinck H, Dugan PJ, Miksis-Olds JL, Mellinger DK, Mann DA, Boebel O, Wilson CC, Ponirakis DW, Moors-Murphy H. 2021. Hybrid millidecade spectra: A practical format for exchange of long-term ambient sound data. JASA Express Letters 1. https://doi.org/10.1121/10.0003324.

McKenna MF, Wiggins SM, Hildebrand JA. 2013. Relationship between container ship underwater noise levels and ship design, operational and oceanographic conditions. Sci Rep. 3:1–10.

McPherson C, Martin B, MacDonnell J, Whitt C. 2016. Examining the value of the Acoustic Variability Index in the characterisation of Australian marine soundscapes. In: Proceedings of Acoustics 2016, 2016 November 9–11, Brisbane, Australia. Brisbane (AU): Australian Acoustical Society.

[NOAA] National Oceanic and Atmospheric Administration. 2016. Tides and currents model. https://tidesandcurrents.noaa.gov/. Accessed January 2016.

Rice AN, Palmer KJ, Tielens JT, Muirhead CA, and Clark CW. 2014. Potential Bryde's whale (*Balaenoptera edeni*) calls recorded in the northern Gulf of Mexico. J Acoust Soc Am. 135:3066–3076.

Ross D. 1976. Mechanics of underwater noise. New York (NY): Pergamon Press.

Schock SG. 2004. A method for estimating the physical and acoustic properties of the sea bed using chirp sonar data. IEEE J Oceanic Engineering. 29(4):1200–1217.

Sidorovskaia NA, Li K. 2016. Decadal evolution of the northern Gulf of Mexico soundscapes. Proc Meetings Acoust. 27(1): 040014. https://doi.org/10.1121/2.0000382.

Simard YR, Roy N, Gervaise C, Giard, S. 2016. Analysis and modeling of 255 source levels of merchant ships from an acoustic observatory along St. Lawrence Seaway. J Acoust Soc Am. 140:2002–2018. doi: 10.1121/1.4962557.

[SMM] Society for Marine Mammalogy. 2021. List of marine mammal species and subspecies. Committee on Taxonomy, Society for Marine Mammalogy. [accessed November 2021]. https://marinemammalscience.org/science-and-publications/list-marine-mammal-species-subspecies/.

Staaterman E, Paris CB, DeFerrari HA, Mann DA, Rice AN, and D'Alessandro EK. 2014. Celestial patterns in marine soundscapes. Mar Ecol Prog Ser. 508:17–32.

Tetreault BJ. 2005. Use of the automatic identification system (AIS) for maritime domain awareness (MDA). IEEE Oceans 2005. 2:1590–1594. doi: 10.1109/OCEANS.2005.1639983

Thode A, Mellinger DK, Stienessen S, Martinez A, Mullin K. 2002. Depth-dependent acoustic features of diving sperm whales (*Physeter macrocephalus*) in the Gulf of Mexico. J Acoust Soc Am. 112:308–321.

Veirs S, Veirs V, Wood JD. 2016. Ship noise extends to frequencies used for echolocation by endangered killer whales. PeeerJ 4:e1657. https://doi.org/10.7717/peerj.1657.

Wiggins SM, Hall JM, Thayre BJ, Hildebrand JA. 2016. Gulf of Mexico low-frequency ocean soundscape impacted by airguns. J Acoust Soc Am. 140:176–183.

Appendix D-A: Spatial and Temporal Patterns of the Detection of Vessels and Airguns
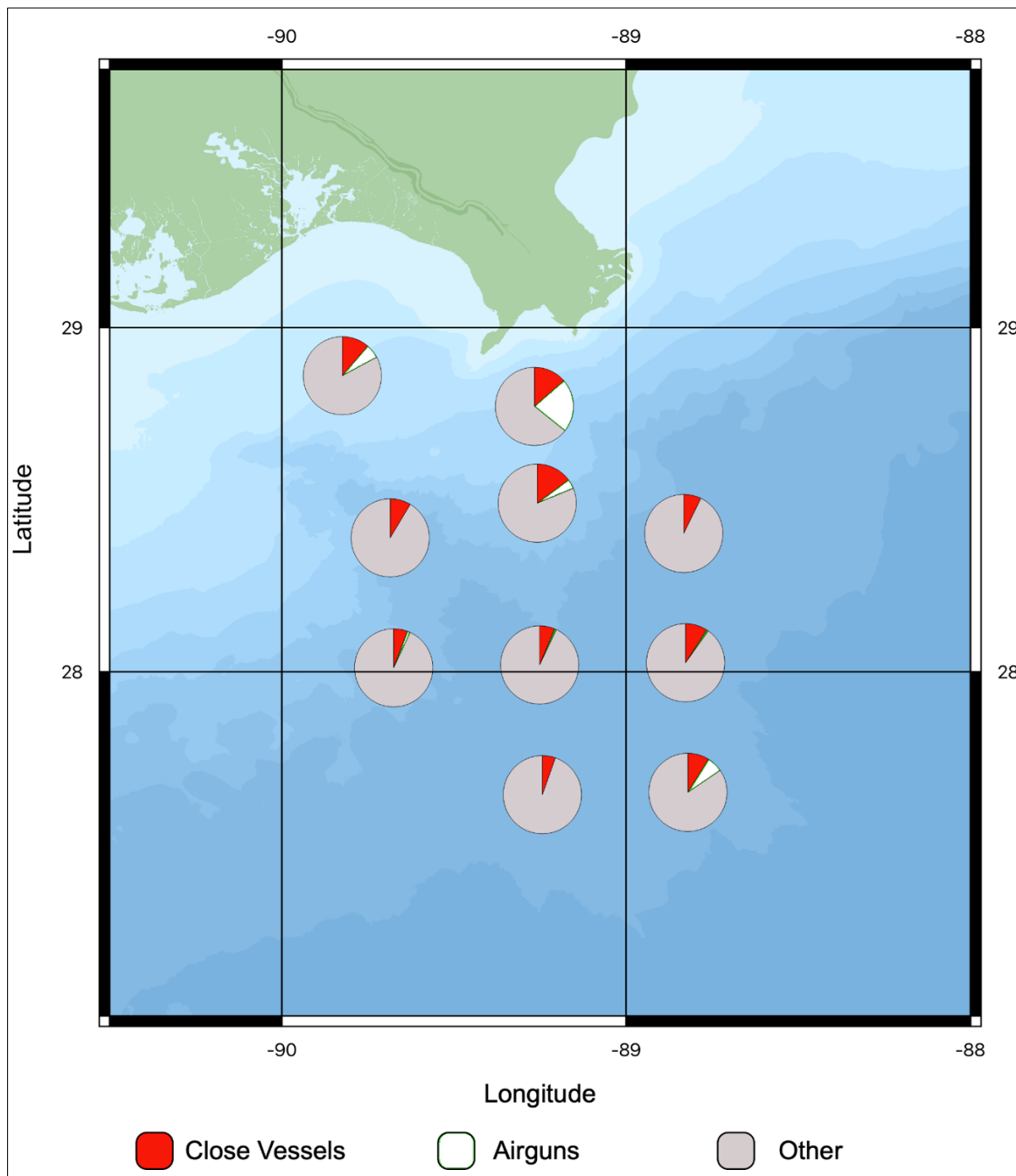
**Figure D-A1. Vessel and airgun detections for May 2018.**
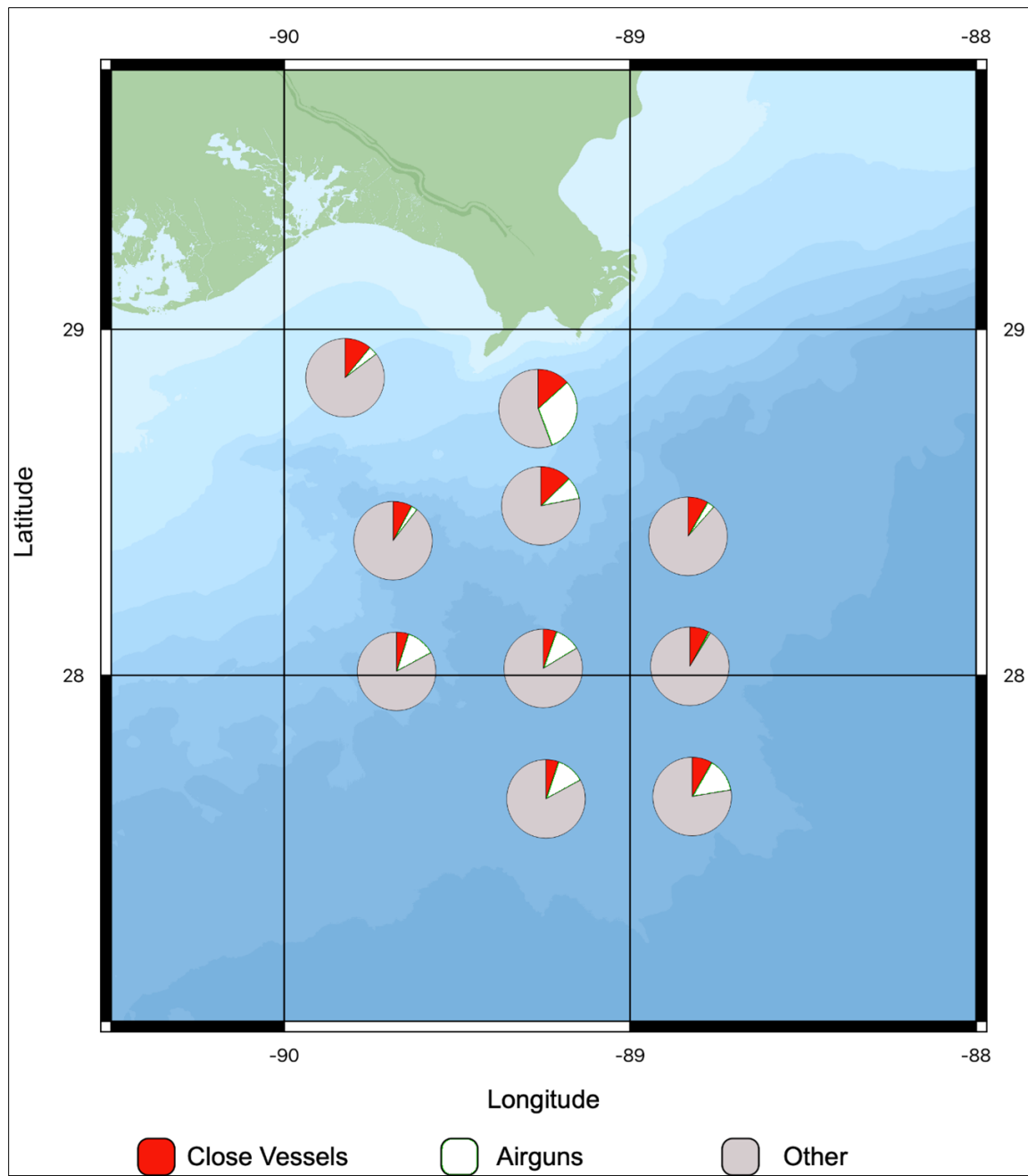
Figure D-A2. Vessel and airgun detections for June 2018.
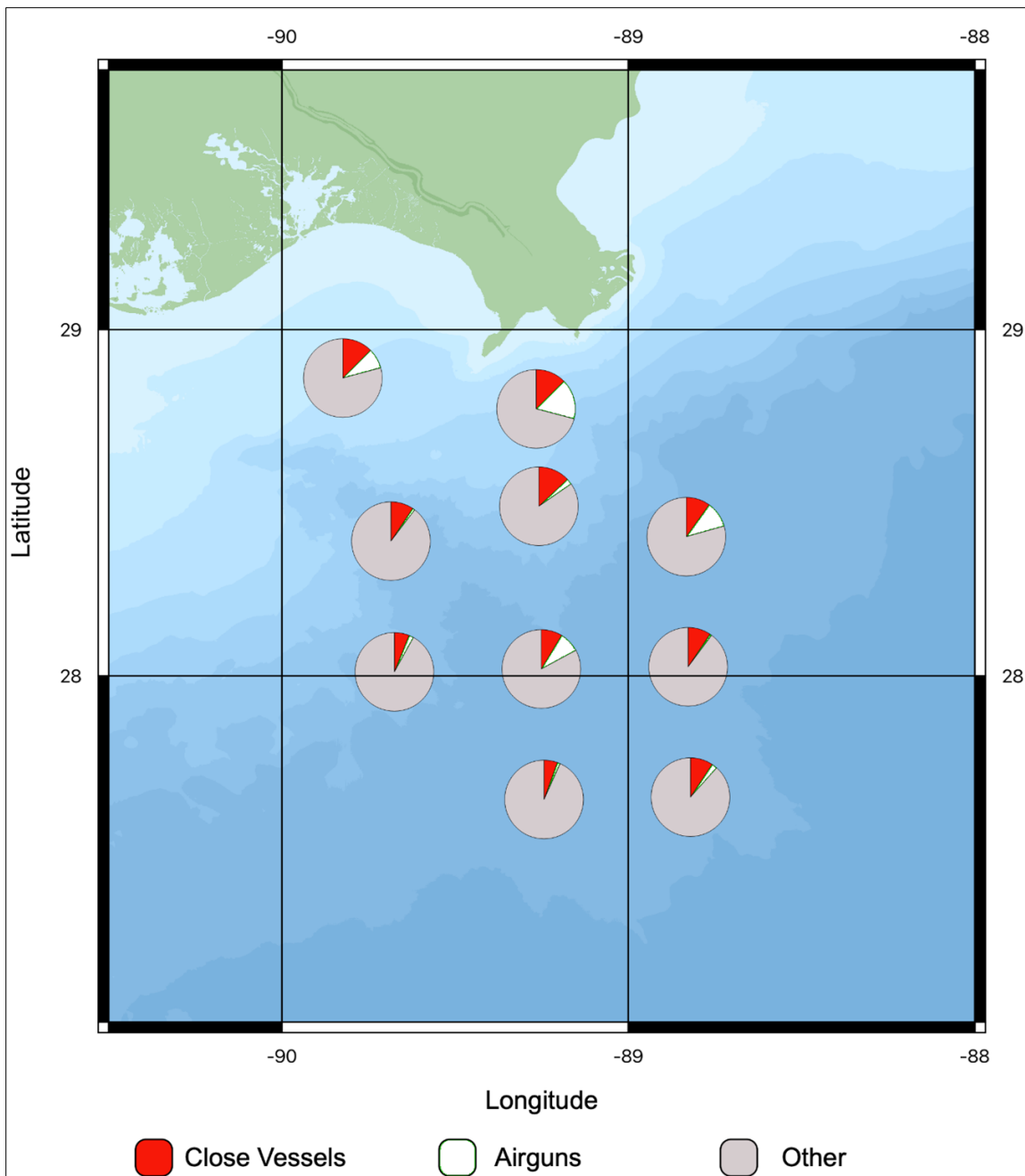
**Figure D-A3. Vessel and airgun detections for July 2018.**
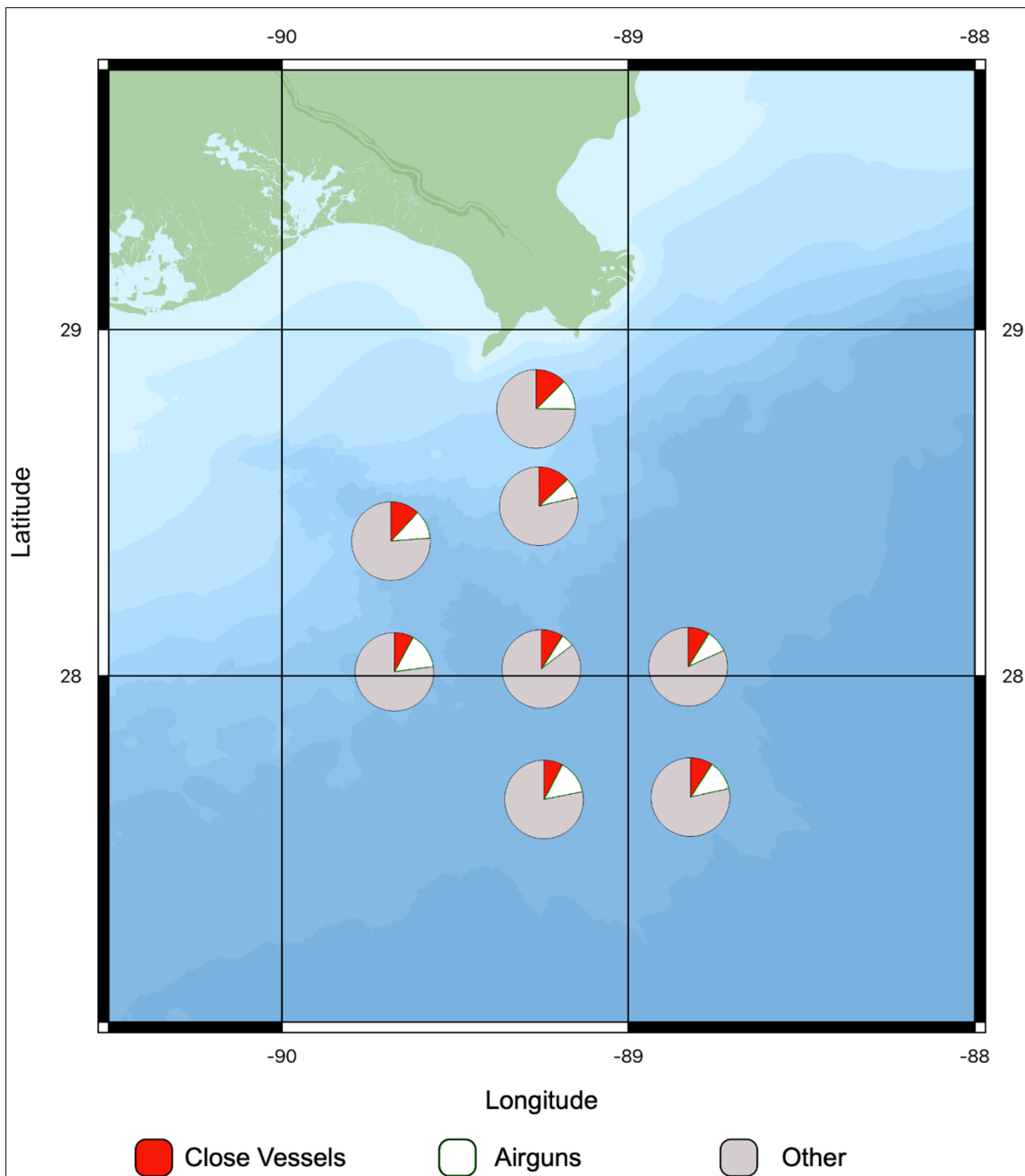
Figure D-A4. Vessel and airgun detections for August 2018.
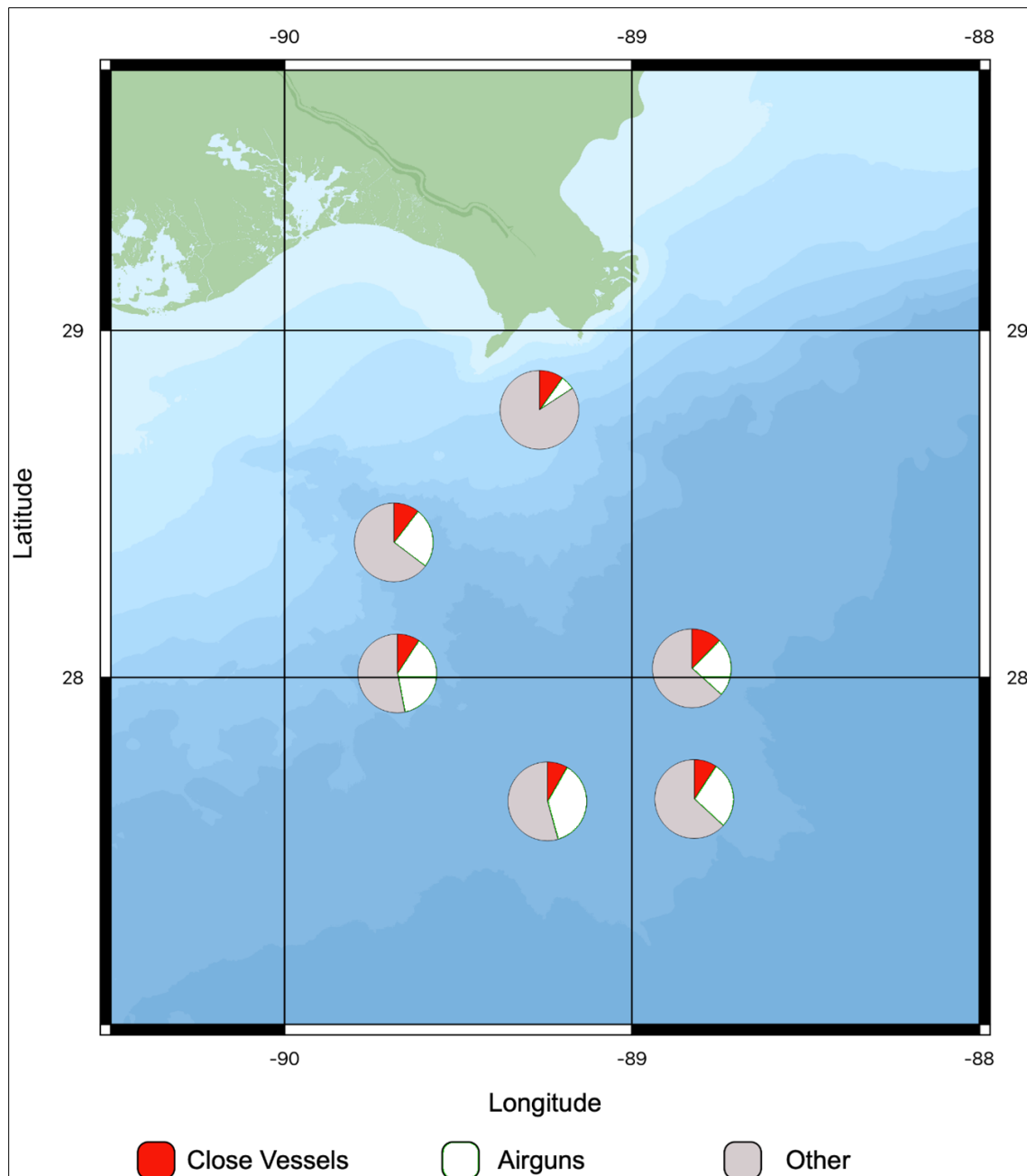
Figure D-A5. Vessel and airgun detections for September 2018.
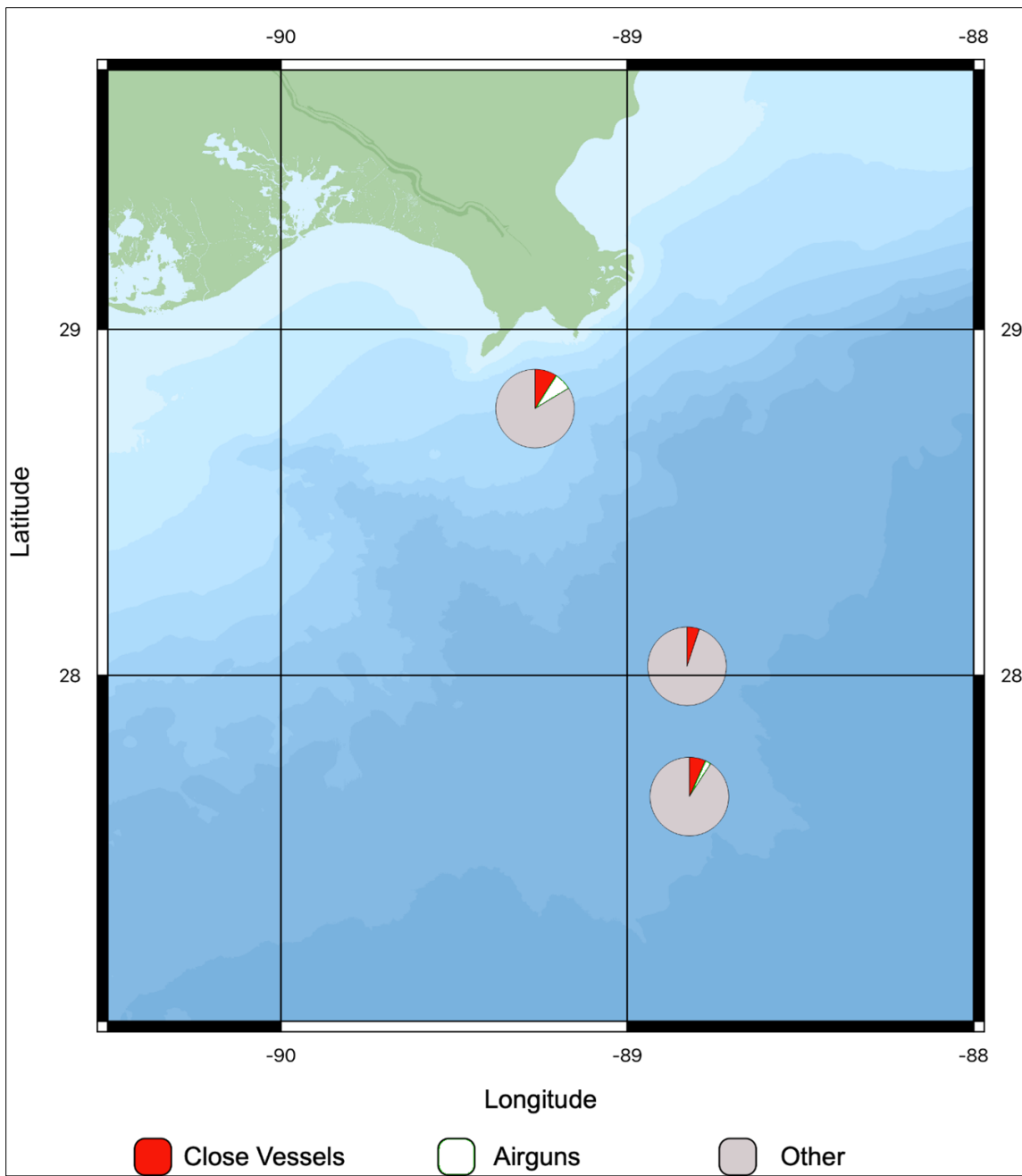
Figure D-A6. Vessel and airgun detections for October 2018.
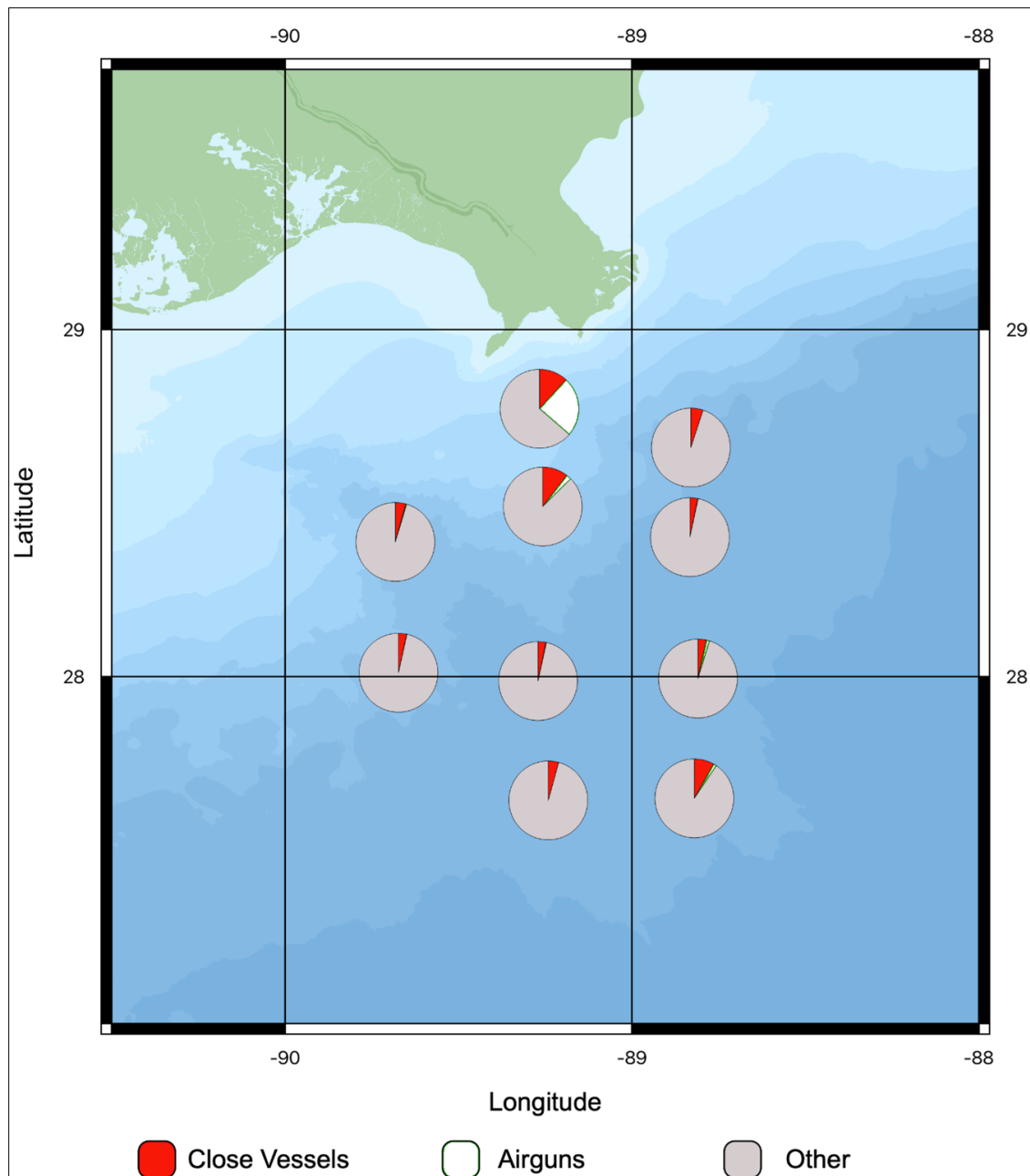
Figure D-A7. Vessel and airgun detections for November 2018.
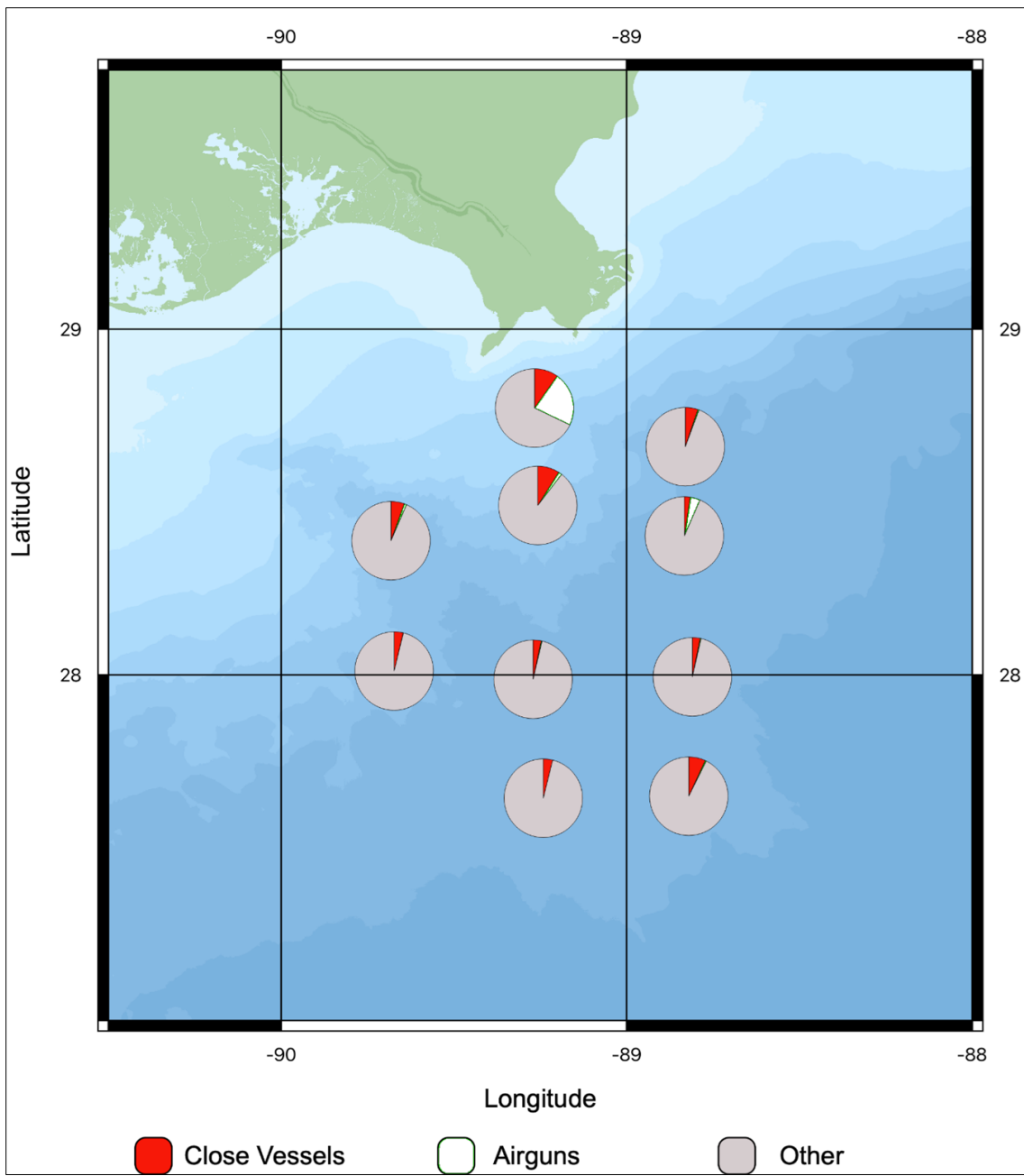
Figure D-A8. Vessel and airgun detections for December 2018.
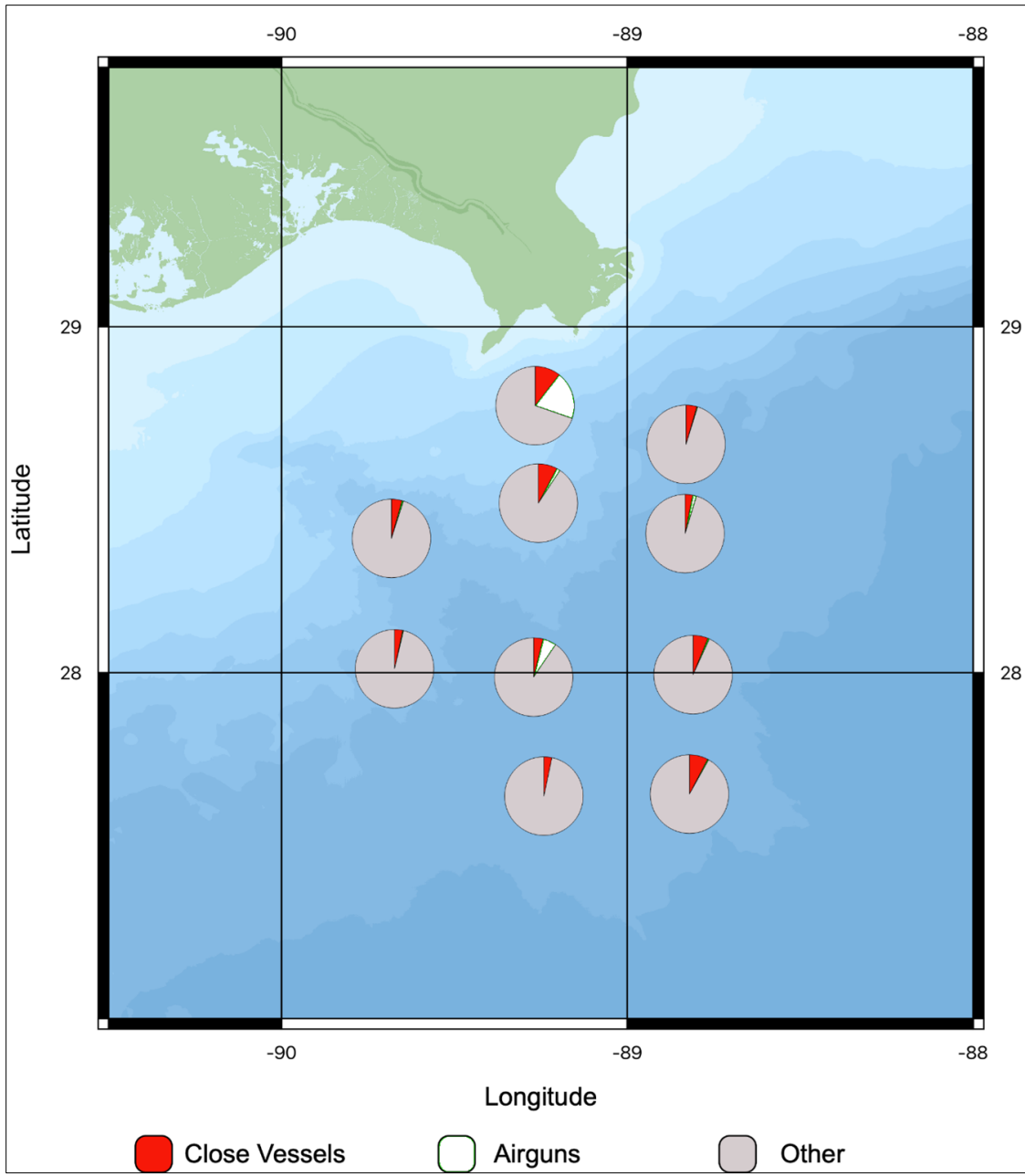
Figure D-A9. Vessel and airgun detections for January 2019.
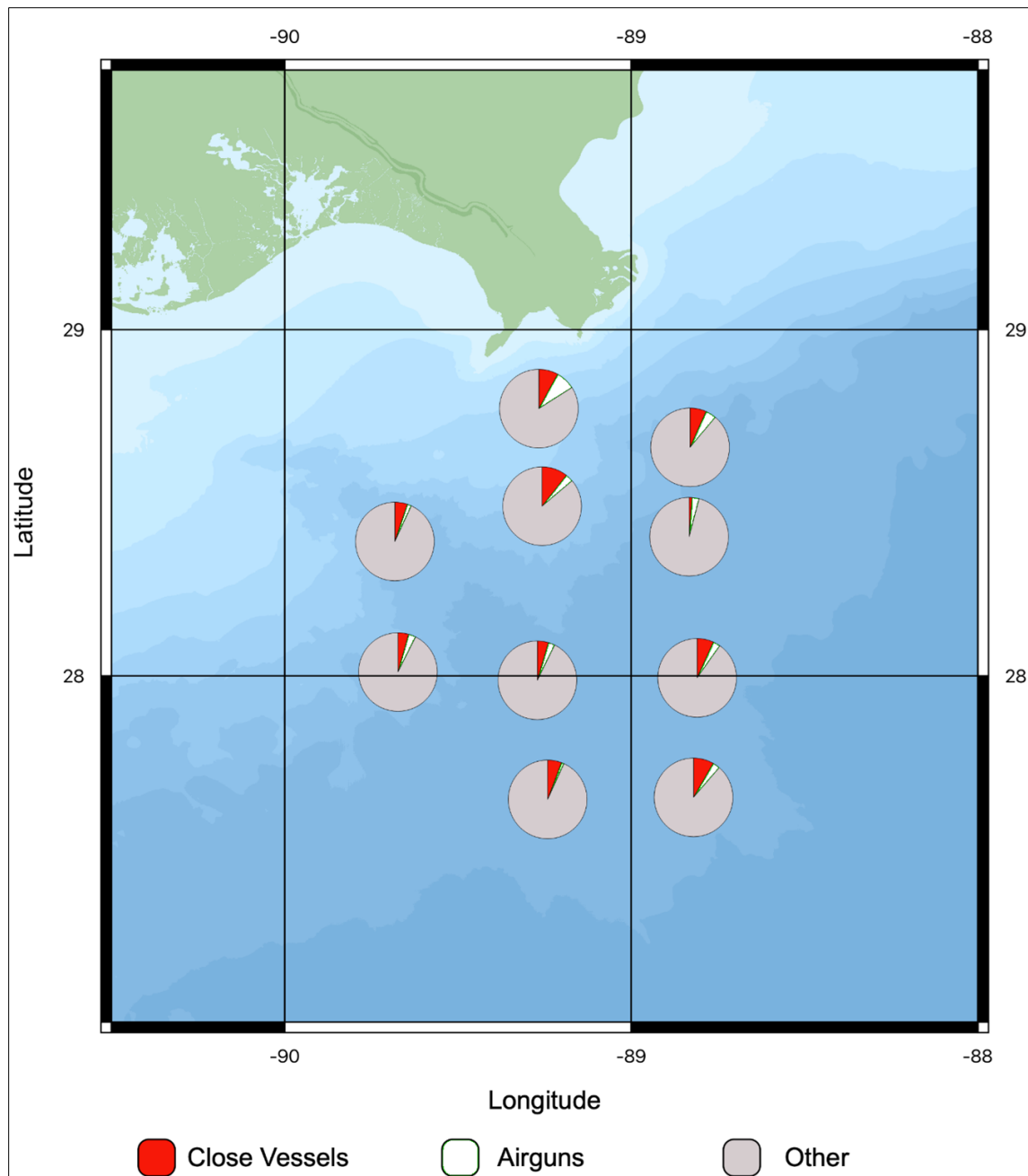
Figure D-A10. Vessel and airgun detections for February 2019.
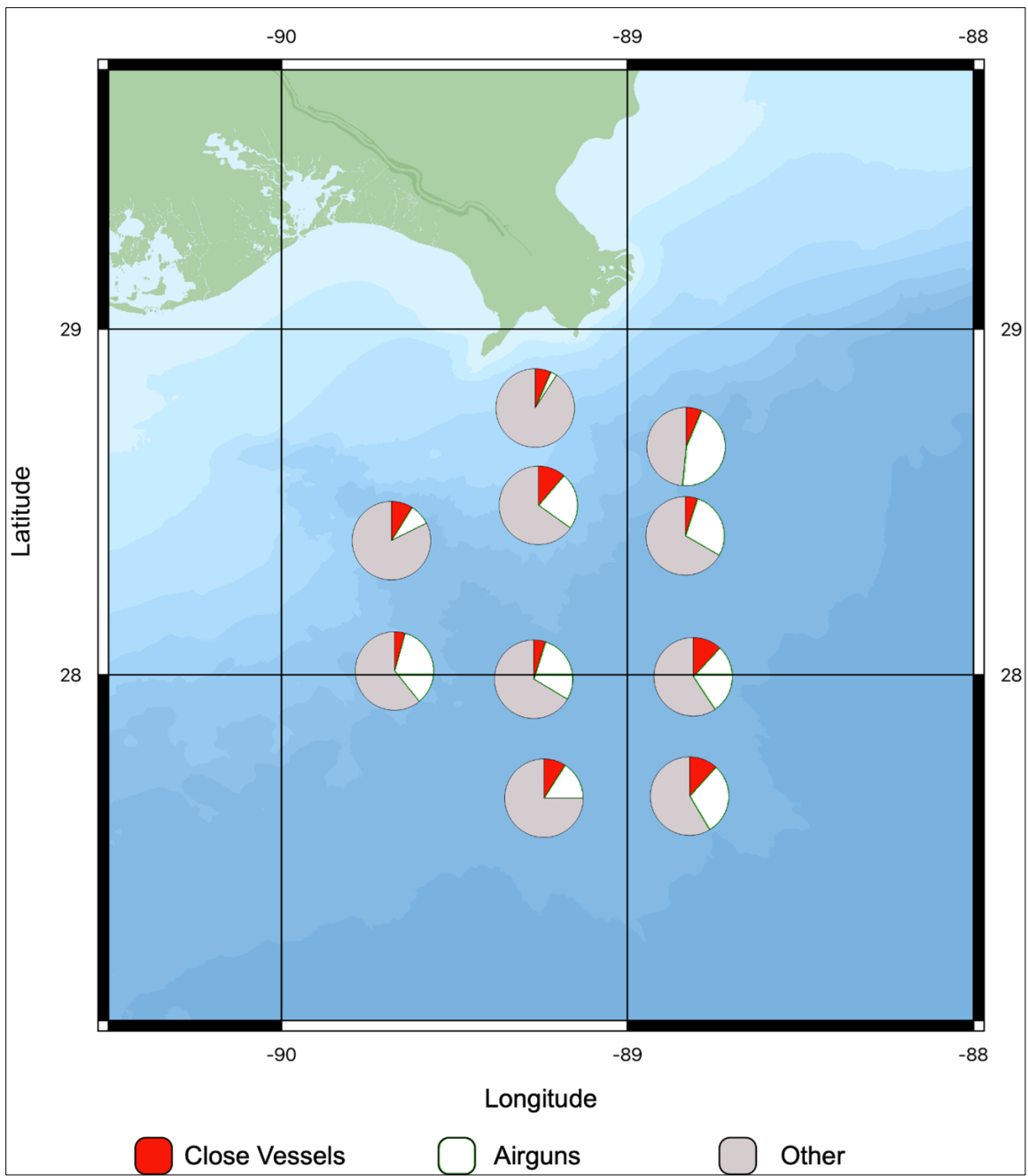
**Figure D-A11. Vessel and airgun detections for March 2019.**
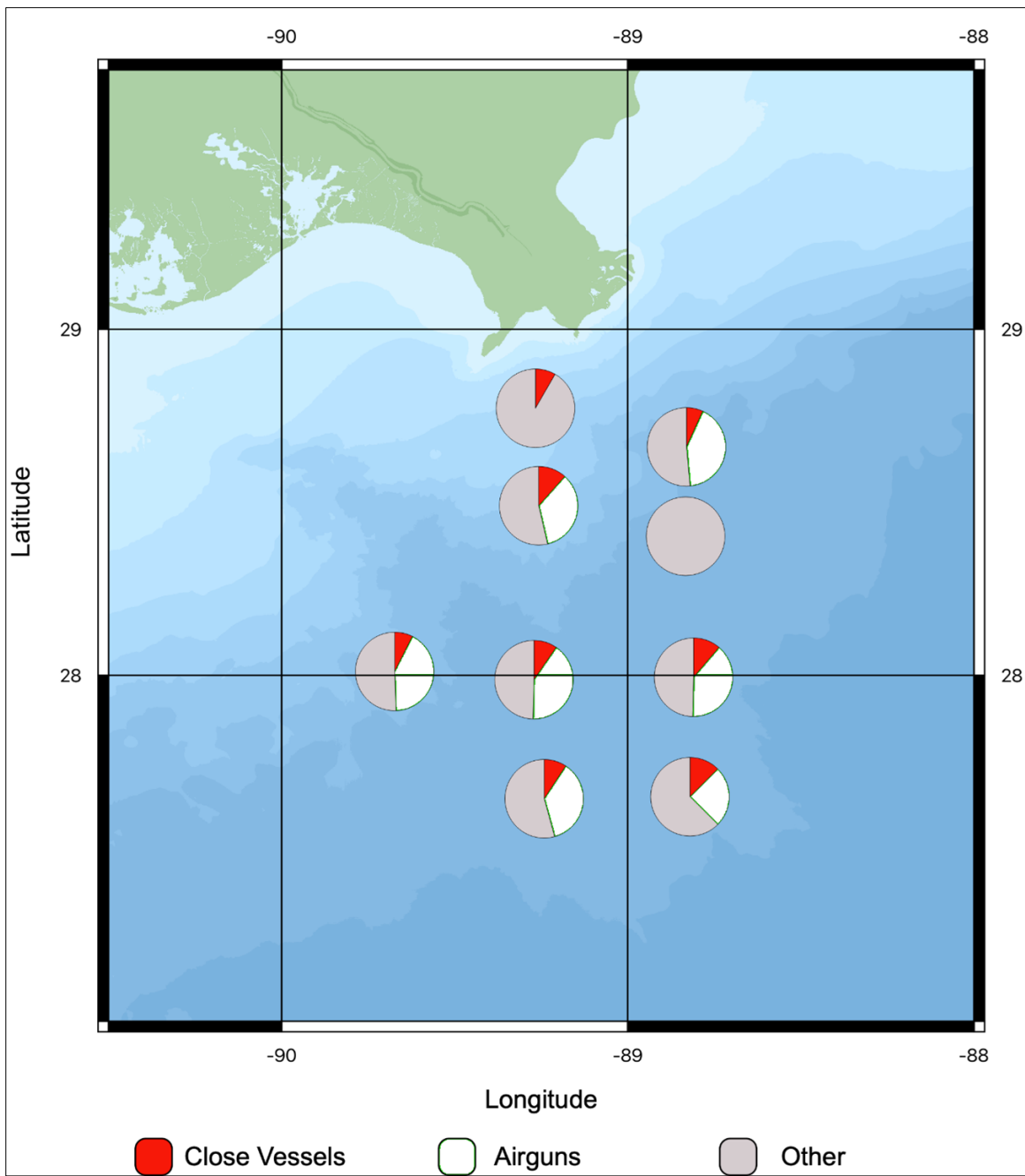
Figure D-A12. Vessel and airgun detections for April 2019.
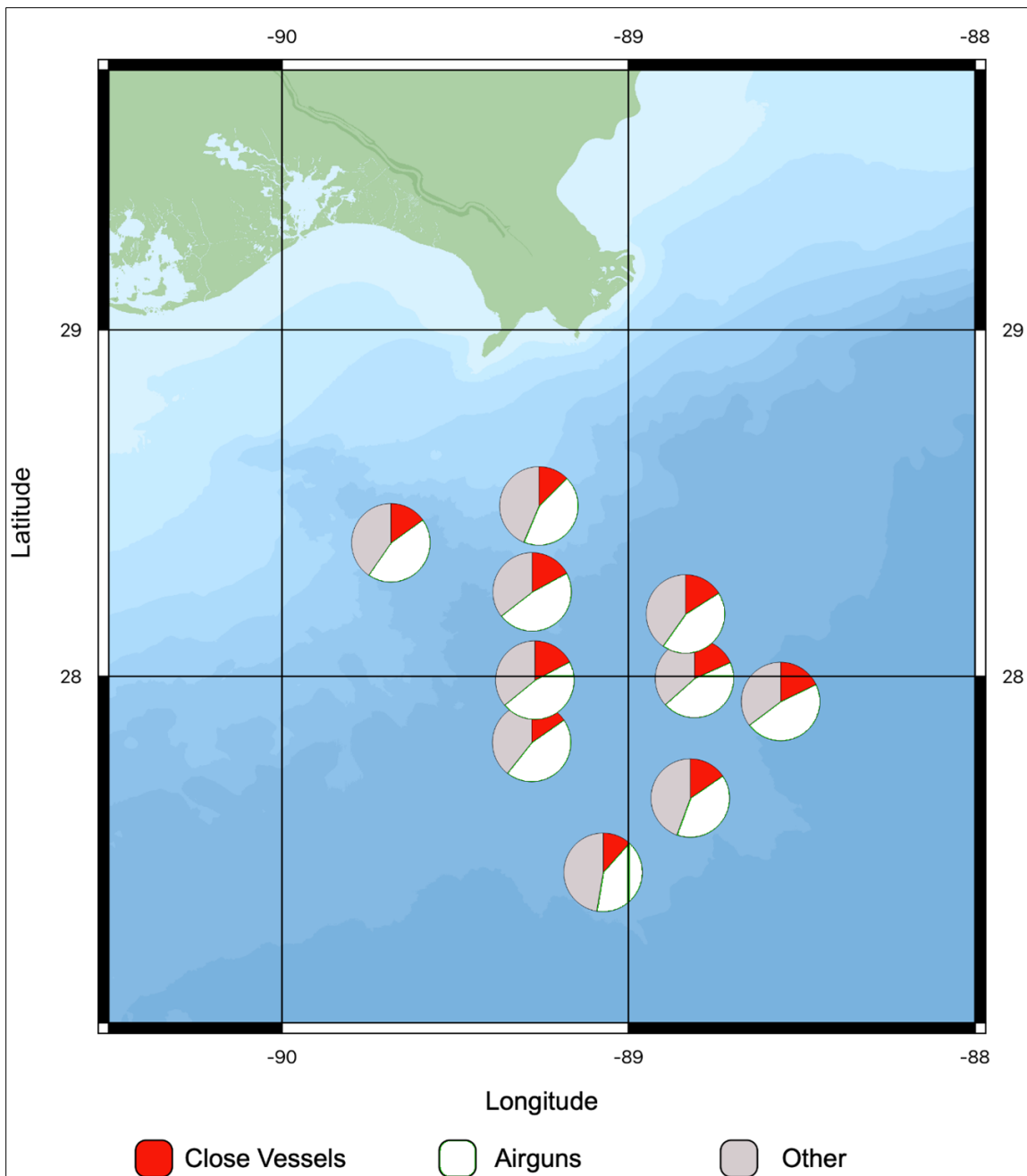
Figure D-A13. Vessel and airgun detections for May 2019.
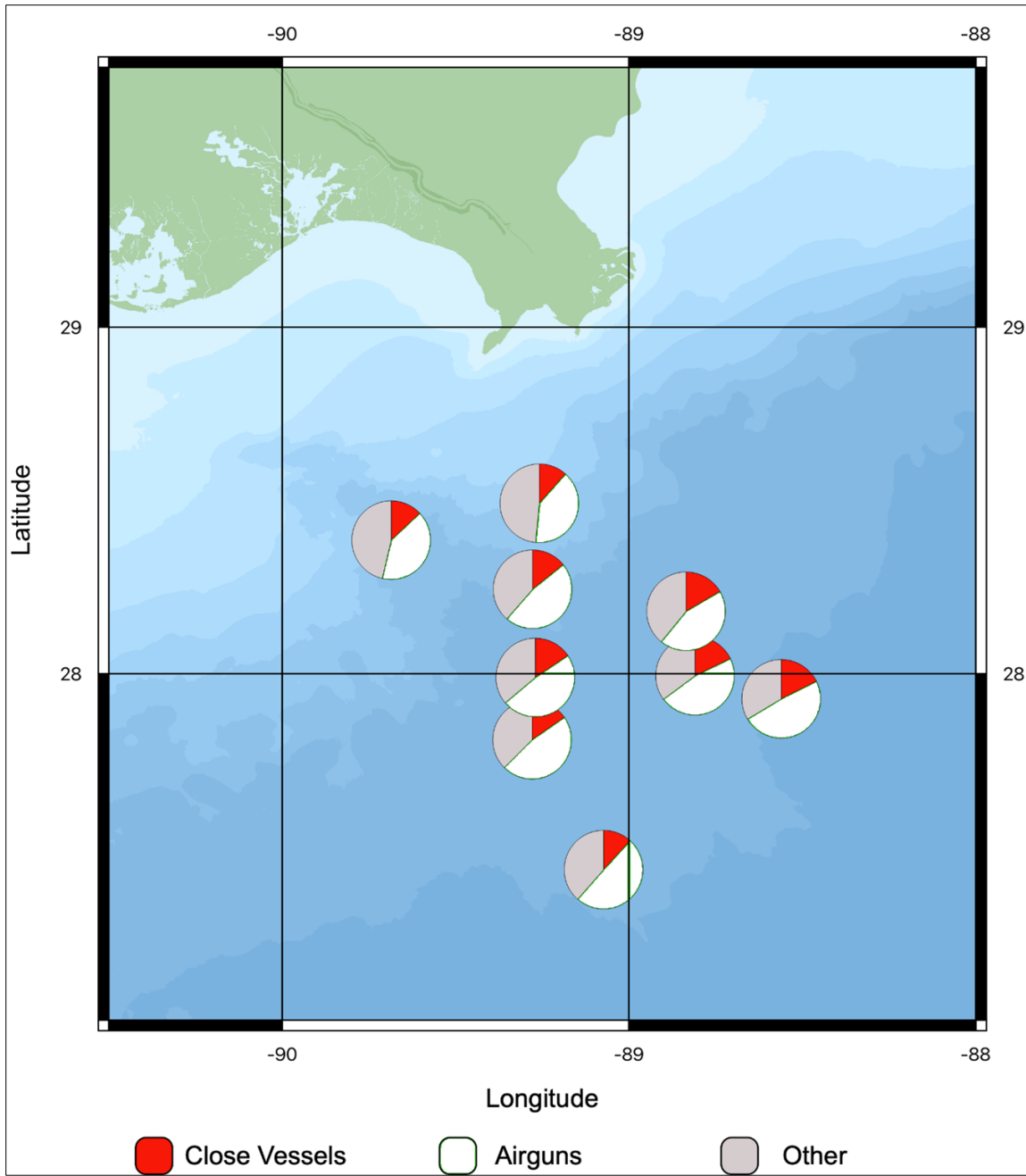
**Figure D-A14. Vessel and airgun detections for June 2019.**
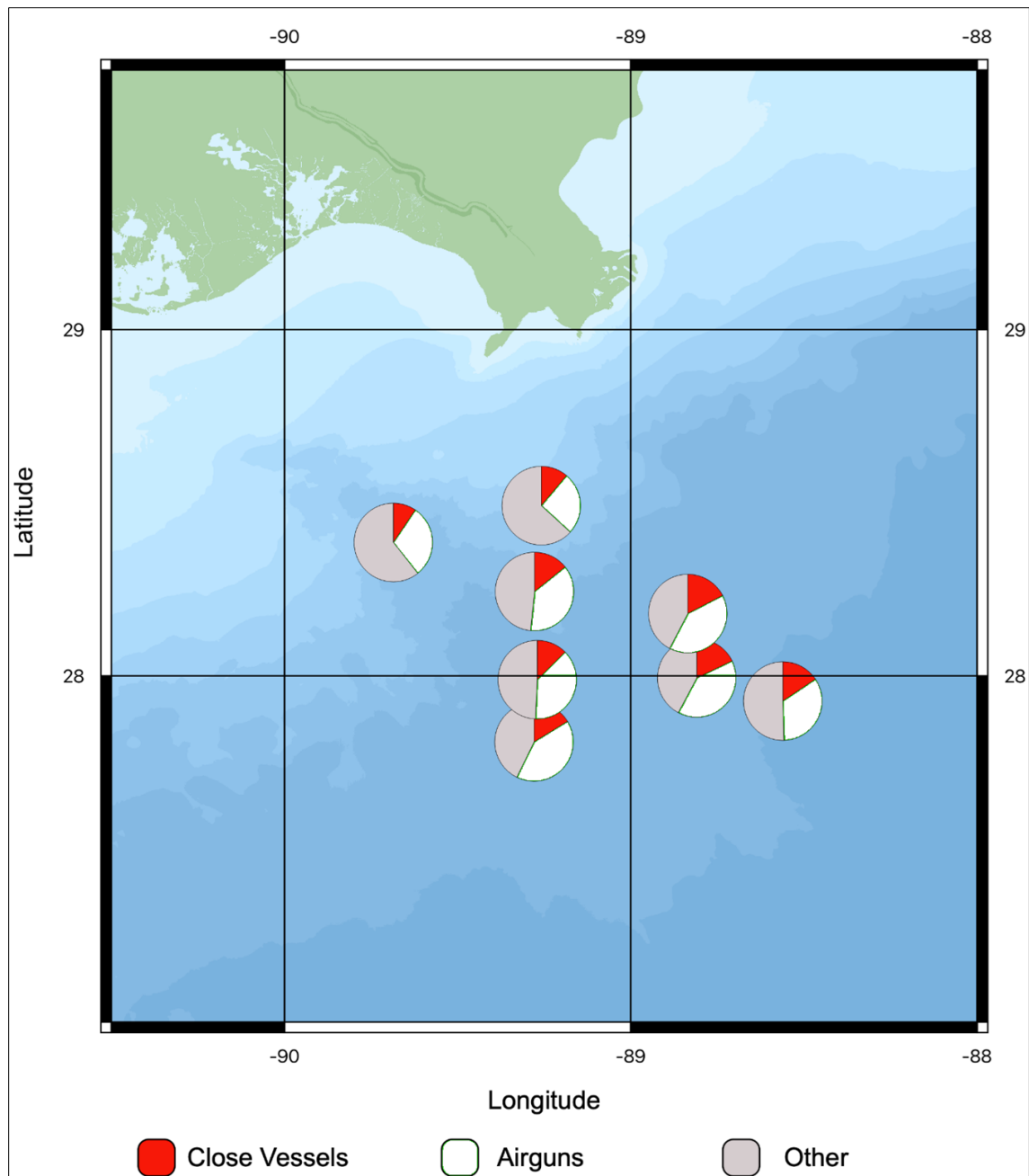
Figure D-A15. Vessel and airgun detections for July 2019.
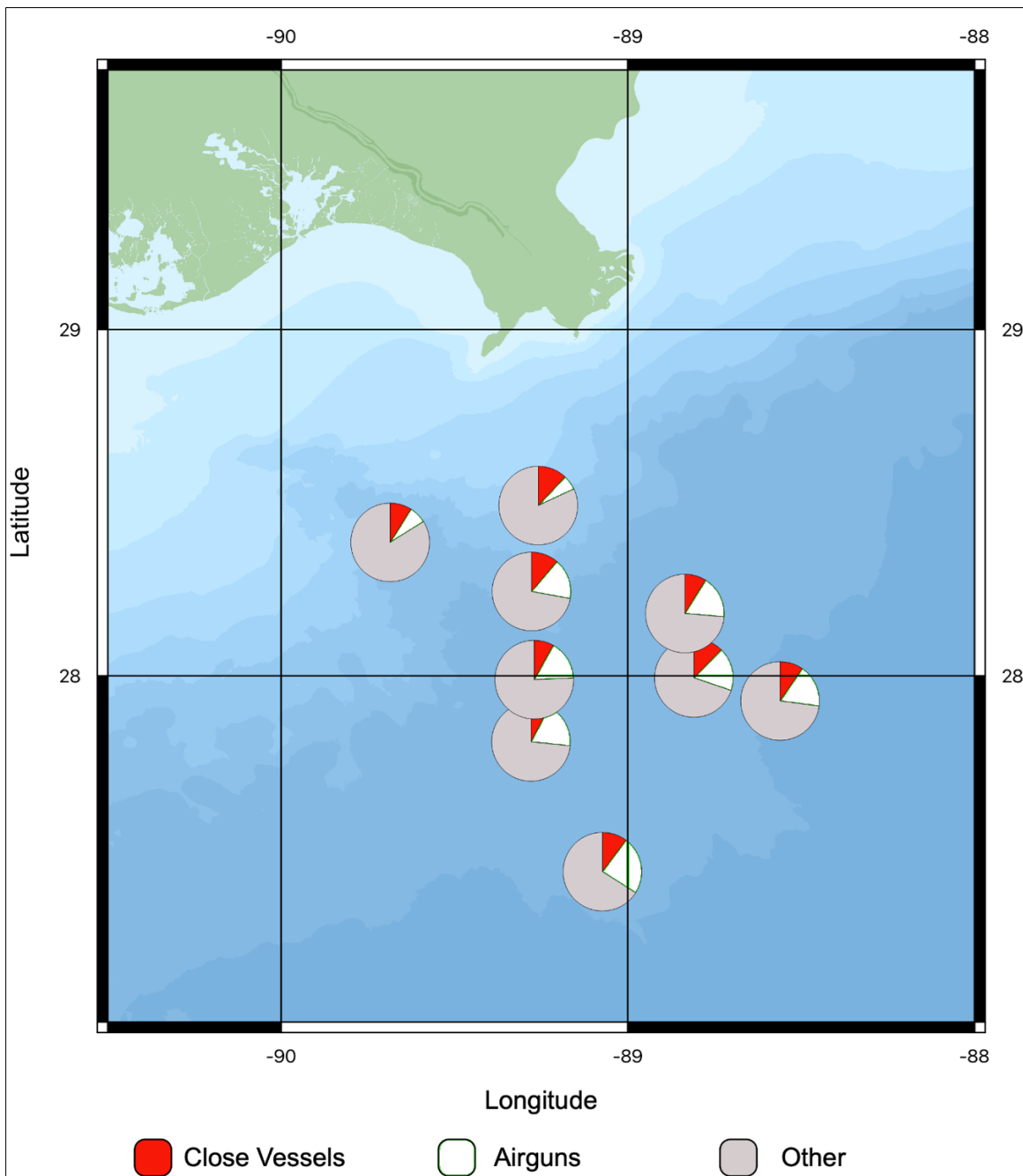
Figure D-A16. Vessel and airgun detections for August 2019.
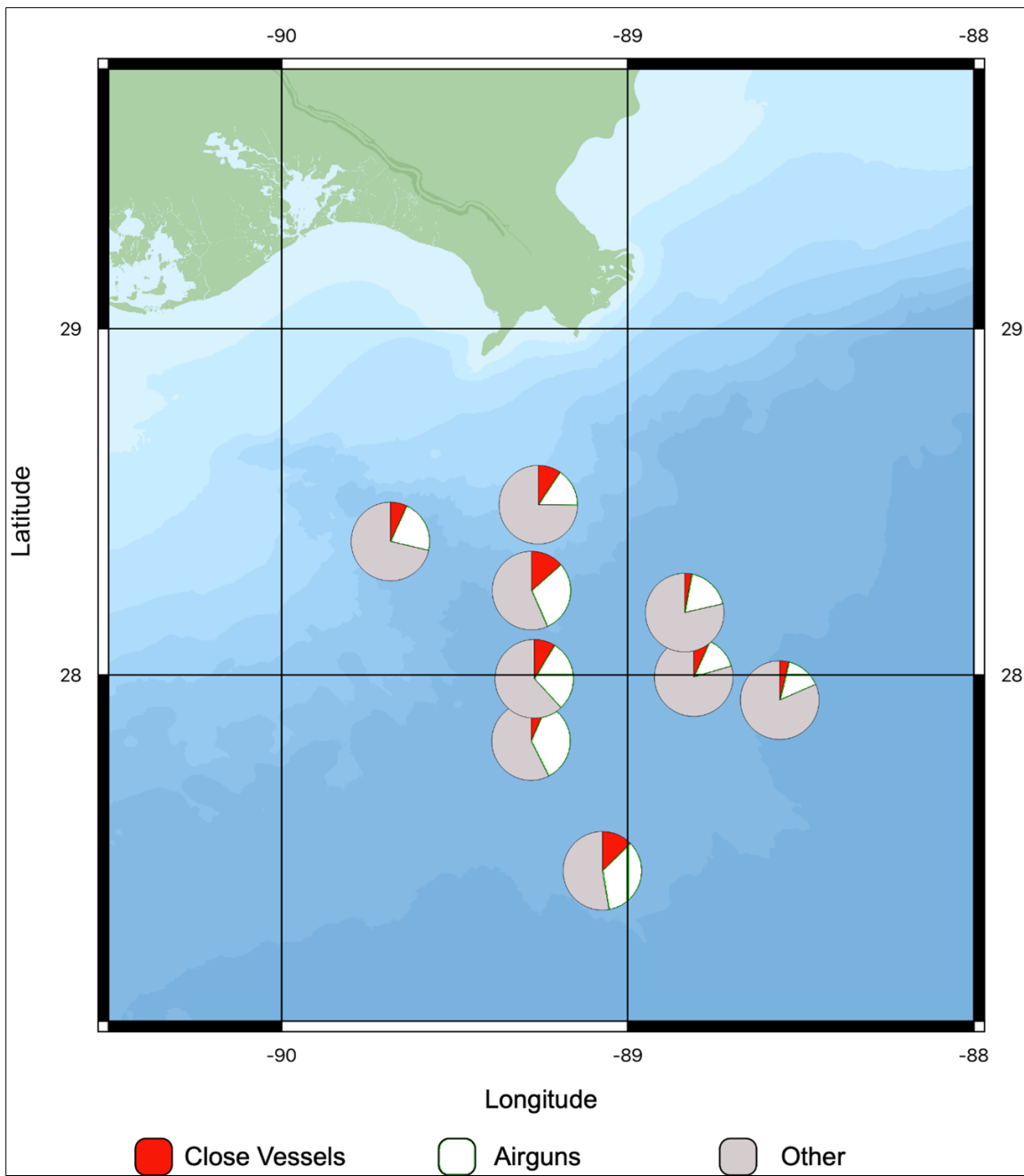
Figure D-A17. Vessel and airgun detections for September 2019.
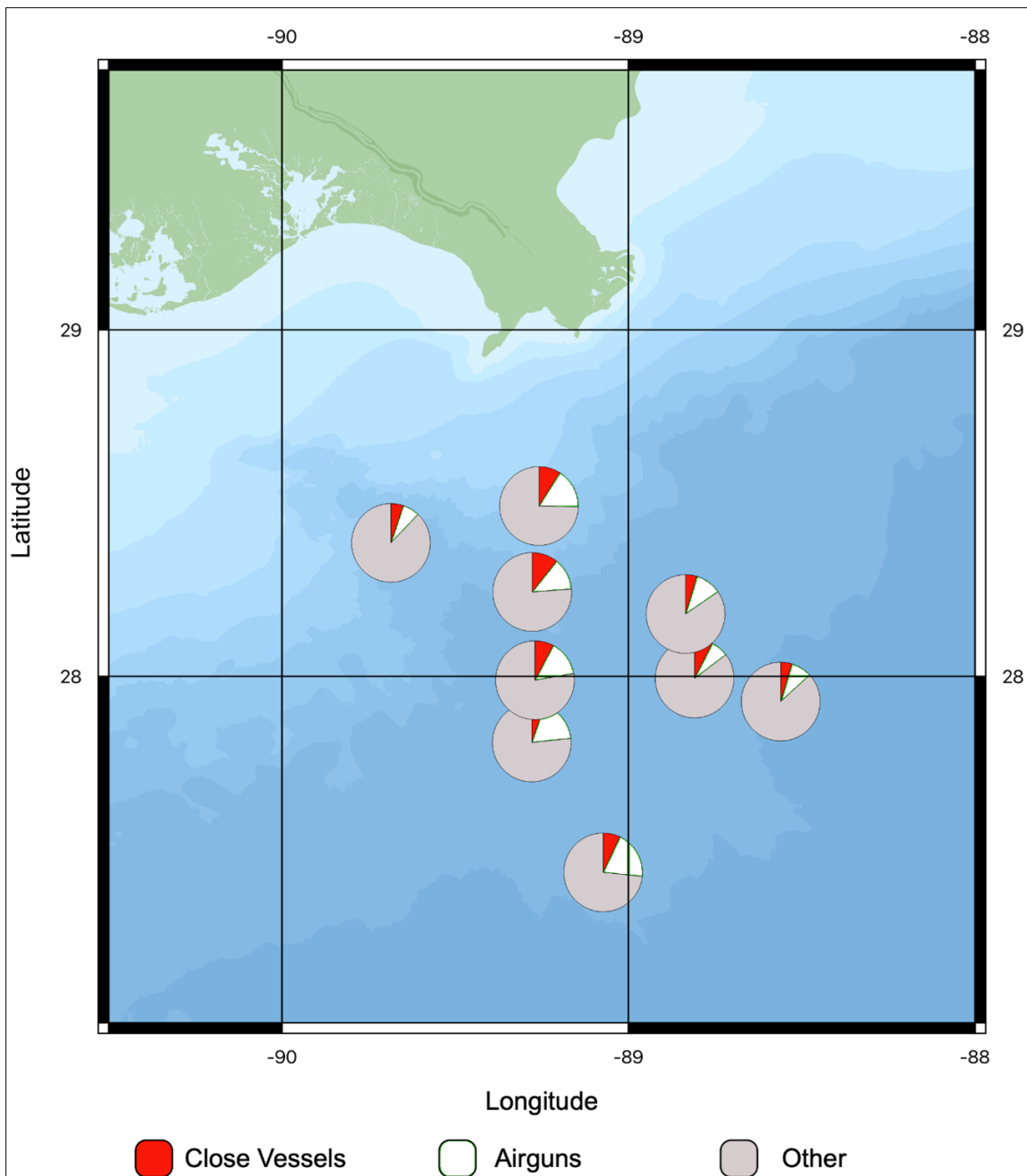
**Figure D-A18. Vessel and airgun detections for October 2019.**
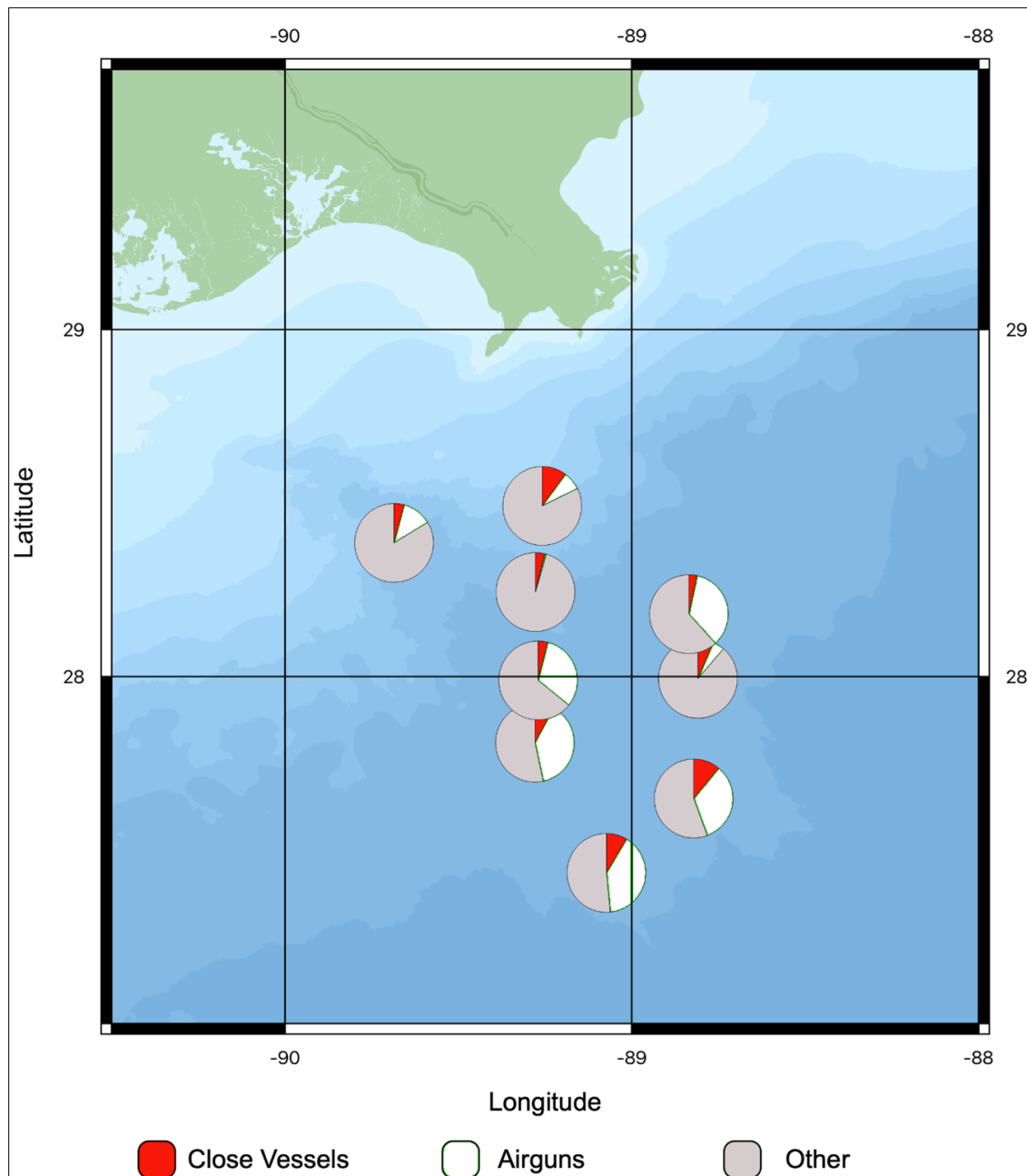
**Figure D-A19. Vessel and airgun detections for November 2019.**
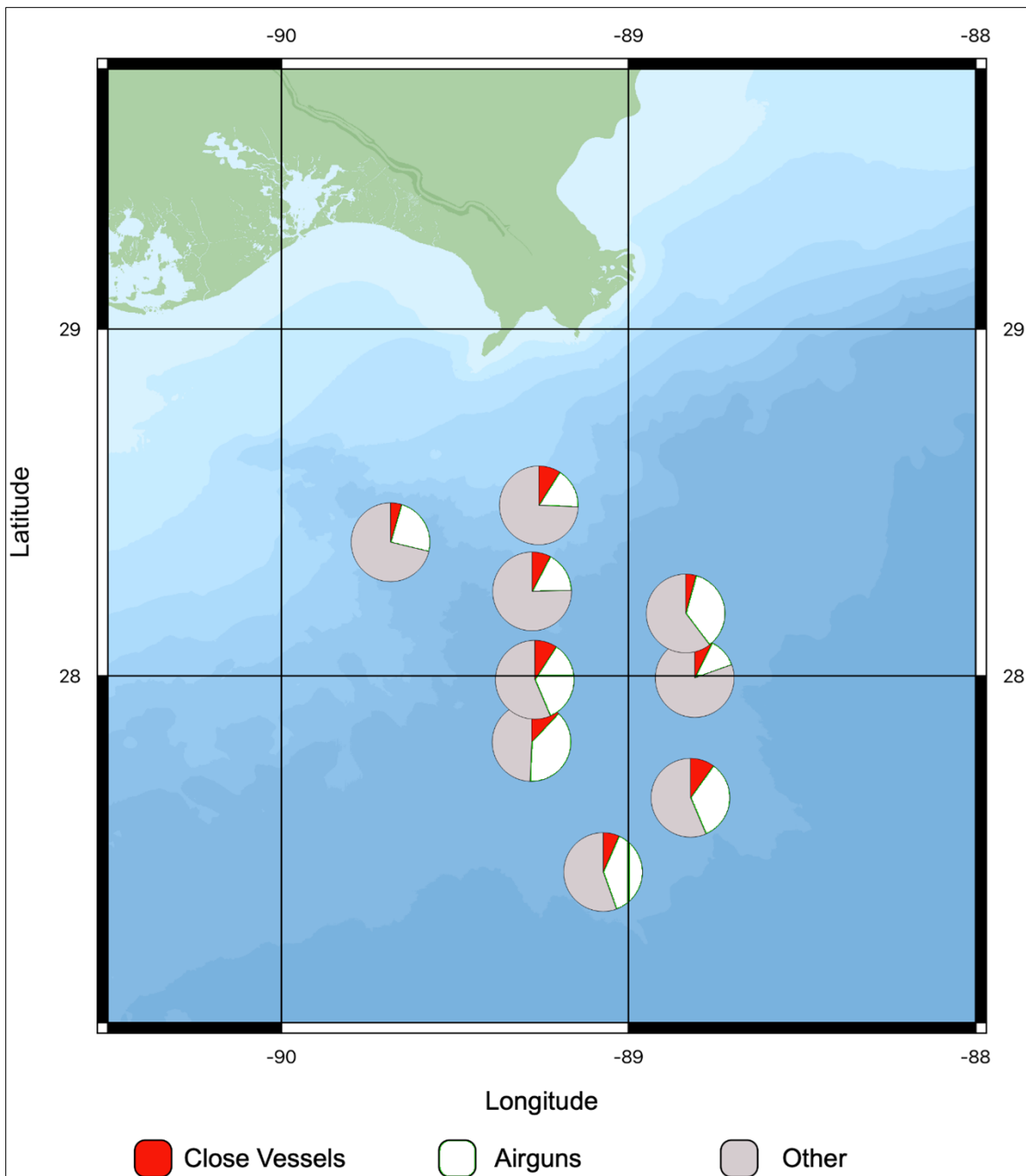
Figure D-A20. Vessel and airgun detections for December 2019.
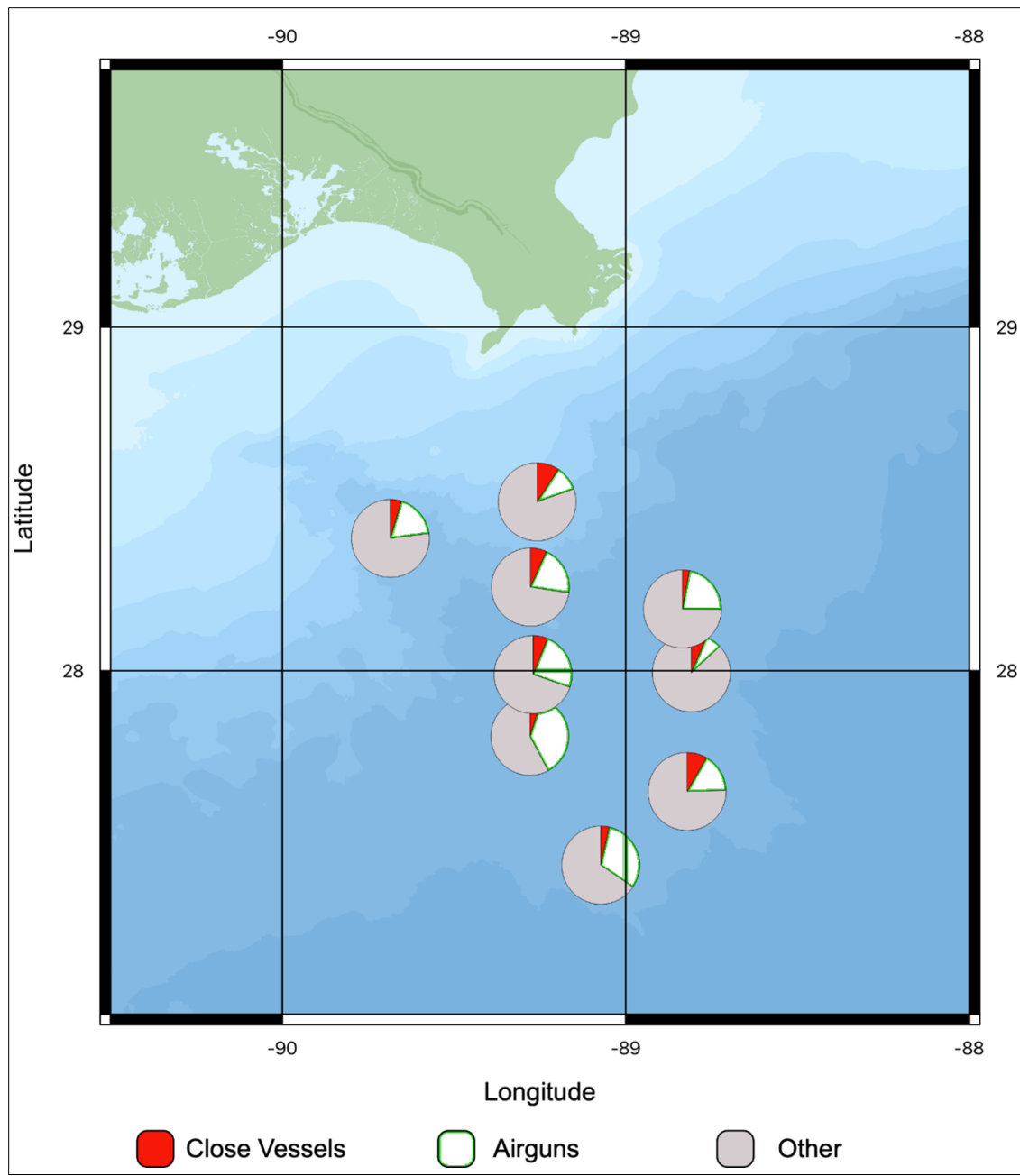
Figure D-A21. Vessel and airgun detections for January 2020.
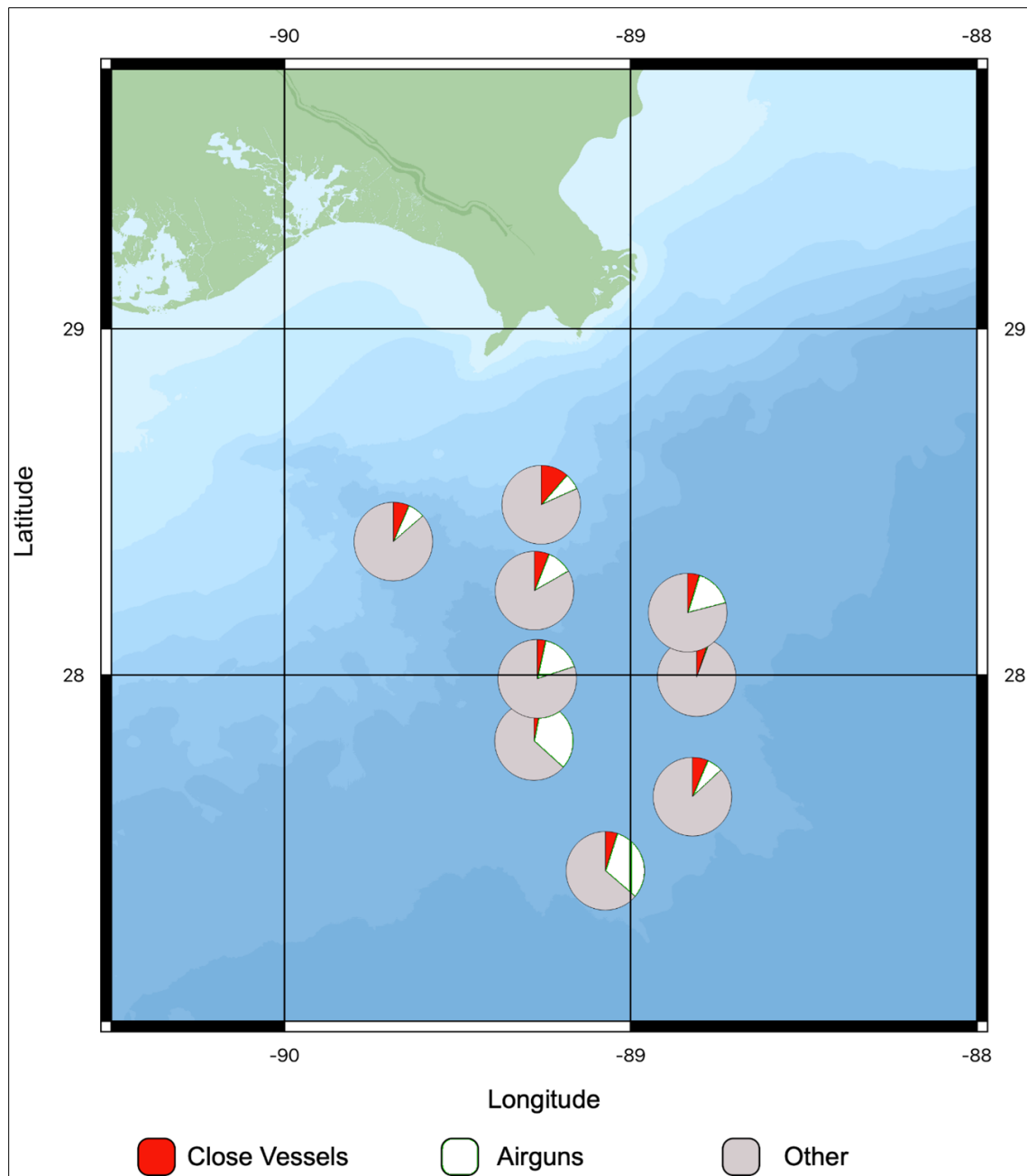
Figure D-A22. Vessel and airgun detections for February 2020.
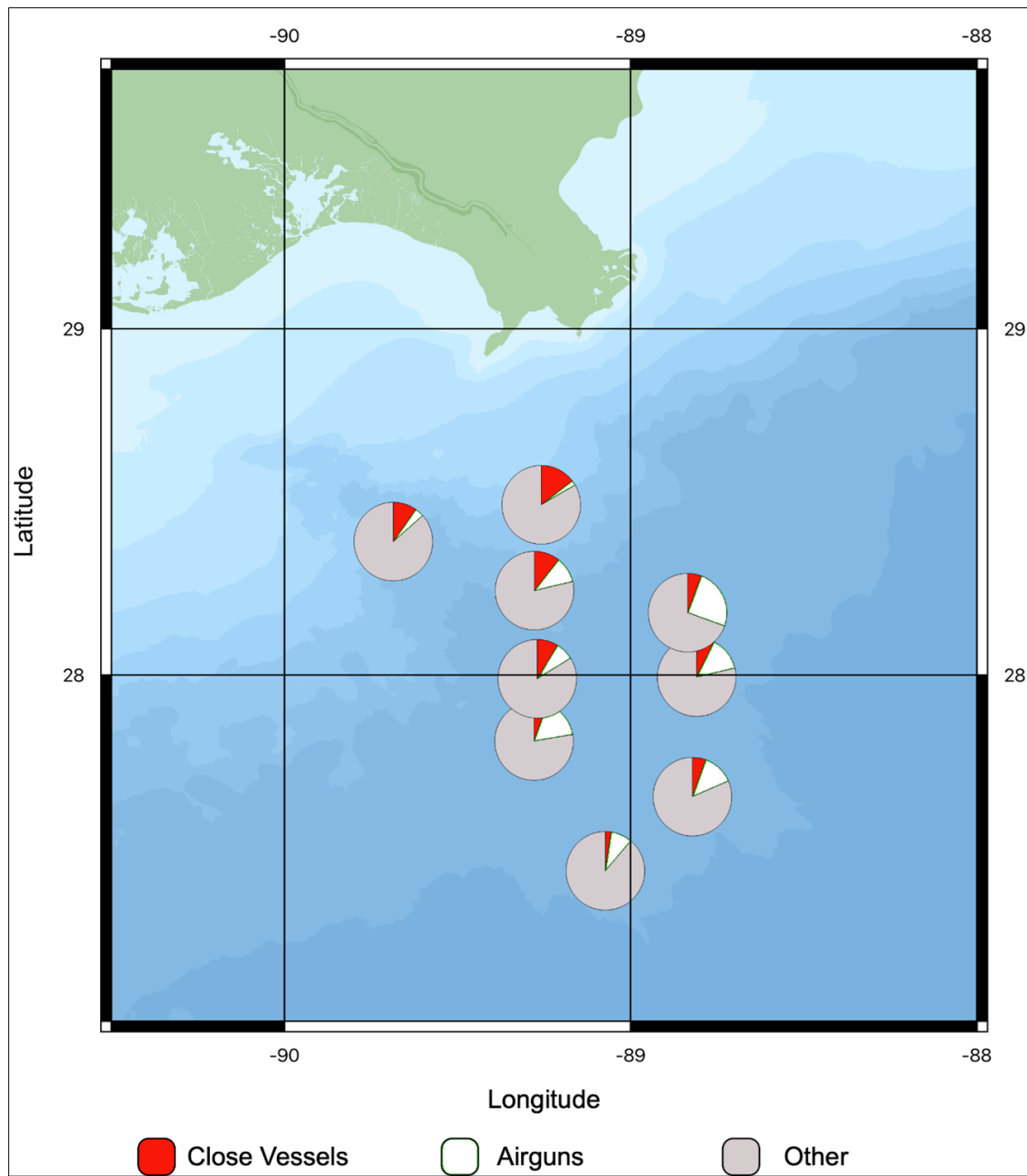
Figure D-A23. Vessel and airgun detections for March 2020.
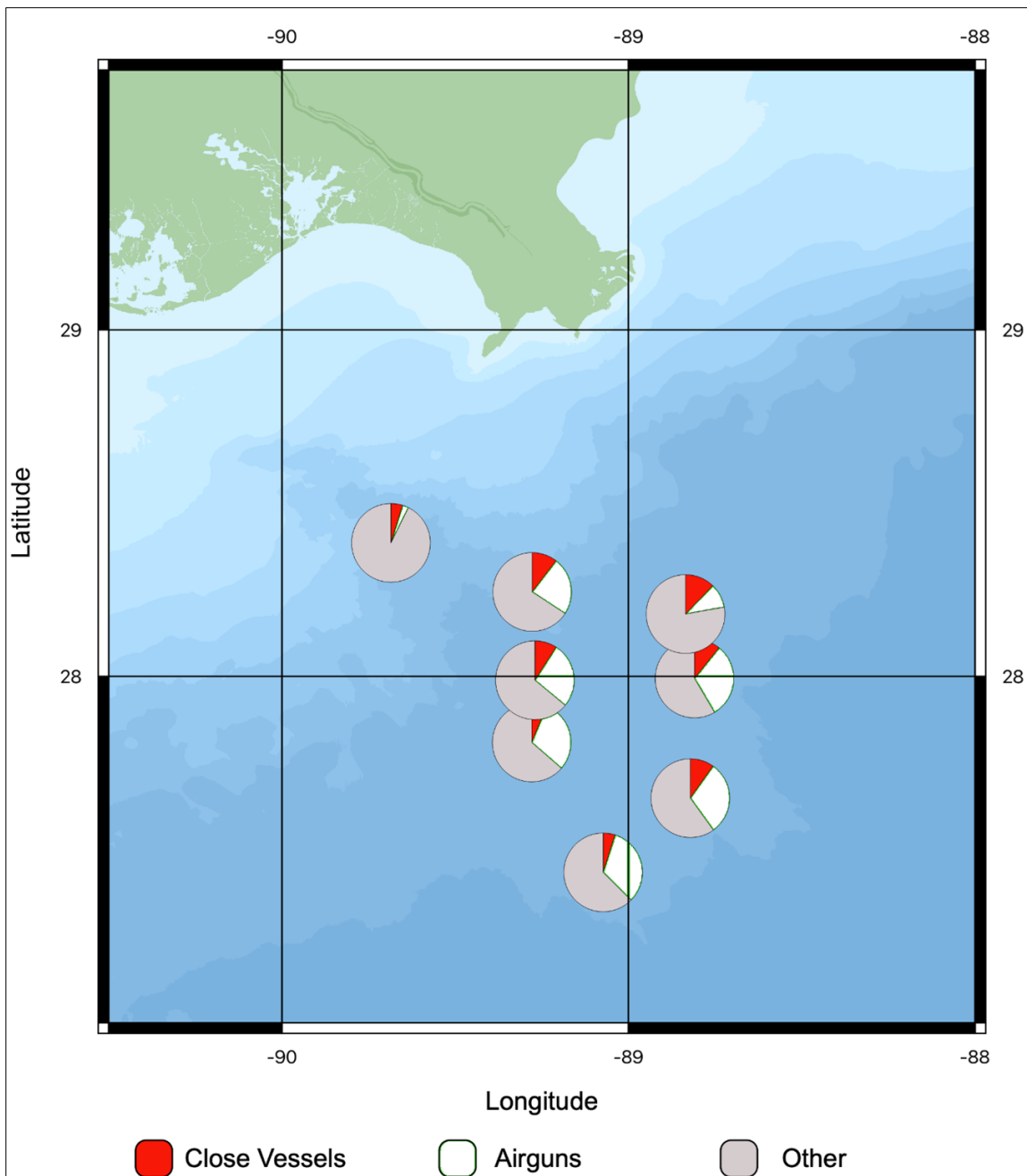
**Figure D-A24. Vessel and airgun detections for April 2020.**
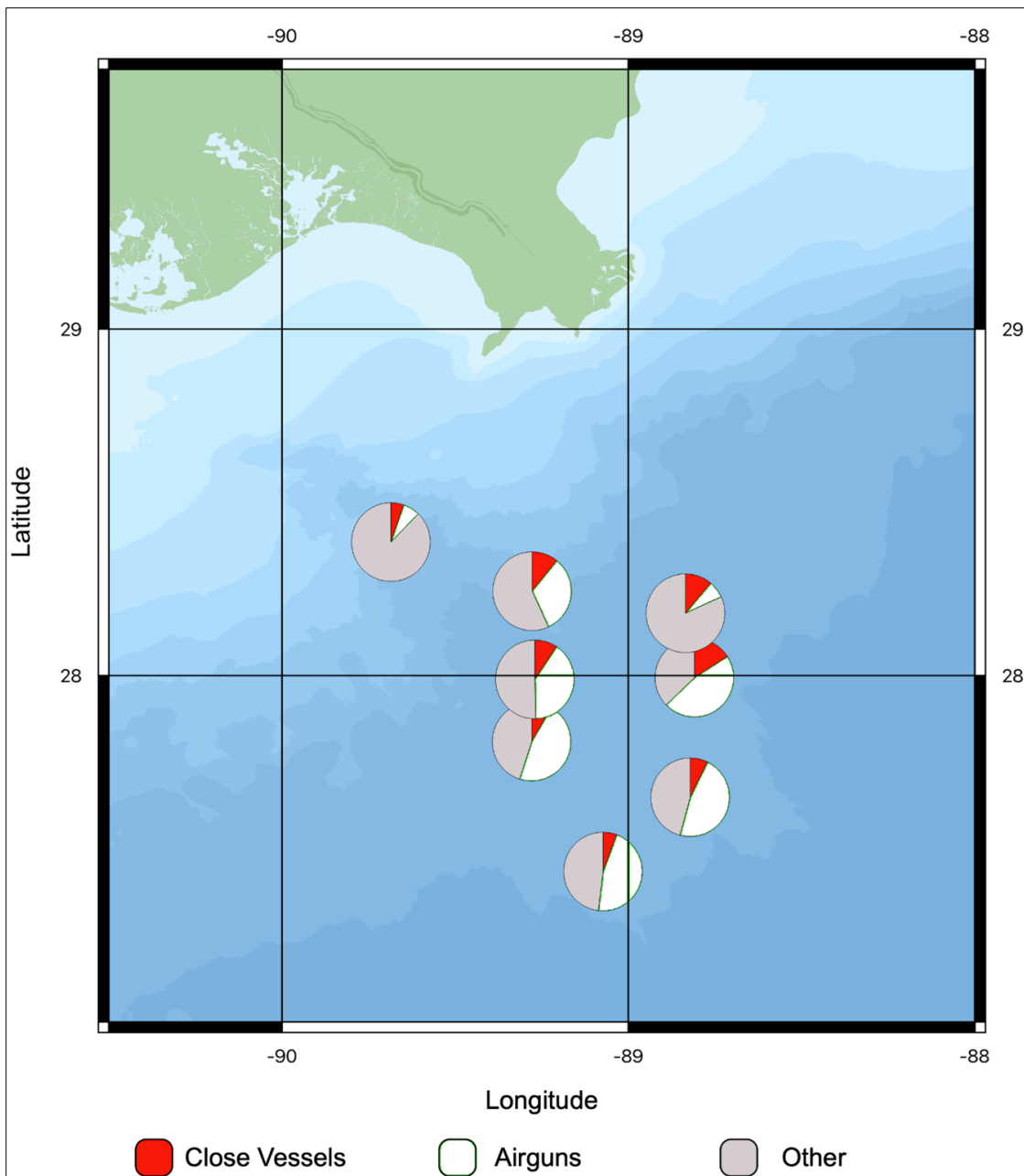
Figure D-A25. Vessel and airgun detections for May 2020.
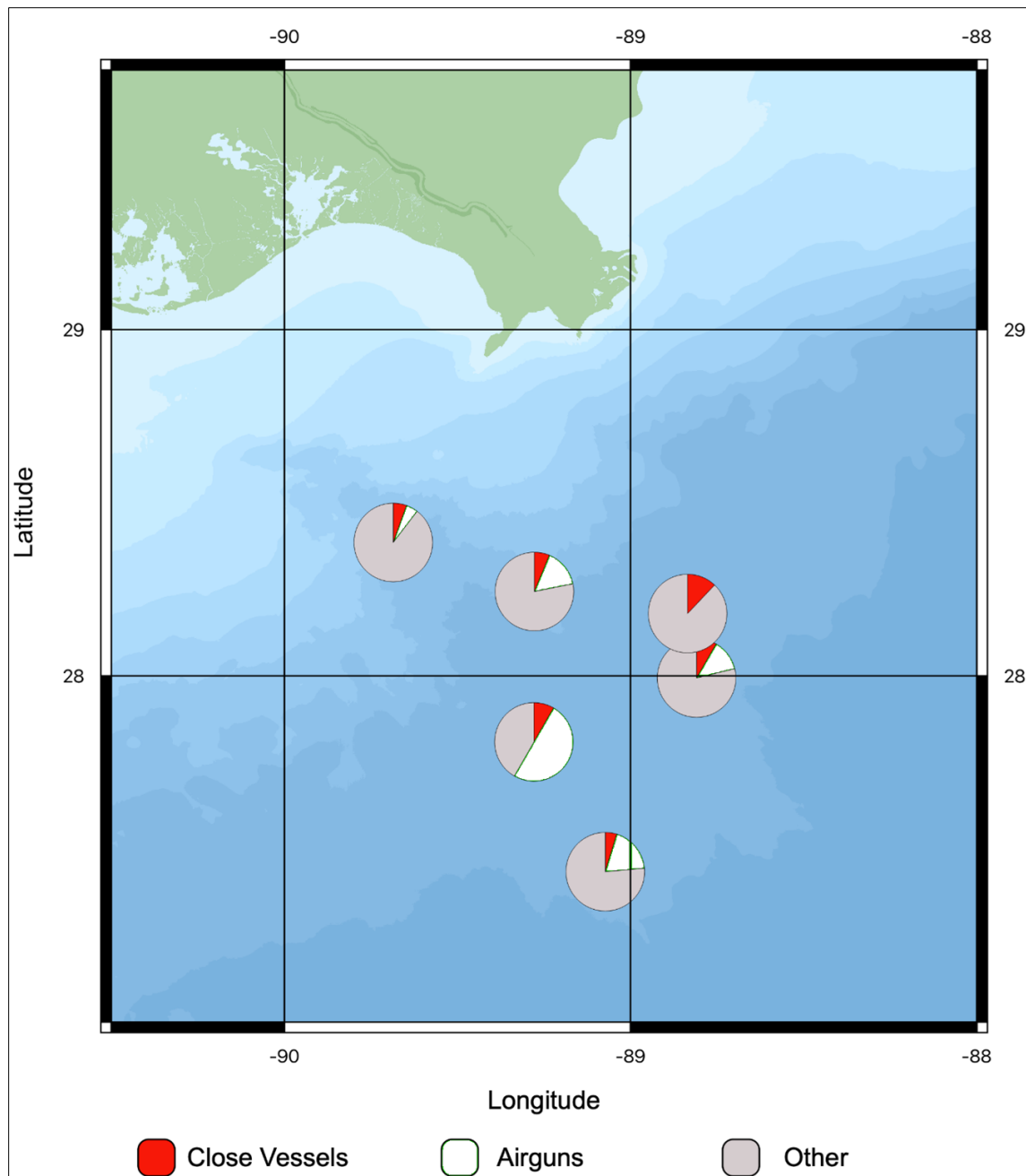
Figure D-A26. Vessel and airgun detections for June 2020.

Appendix D-B: Simplified Statistical Approach Results of Deployments 2 through 4 Vessel Received Levels

DEPLOYMENT 2

Table D-B1. GAM output for Deployment 2, Receiver 1

| A. parametric coefficients	Estimate	Std. Error	t-value	p-value
(Intercept)	4.6169	0.0007	6385.6556	< 0.0001
km2	0.0097	0.0107	0.9098	0.3630
km4	-0.0023	0.0078	-0.2989	0.7650
km10	-0.0007	0.0038	-0.1840	0.8540
B. smooth terms	edf	Ref.df	F-value	p-value
s(sDate)	42.7750	49.0000	71.5179	< 0.0001
s(WaveHeight)	3.9348	3.9348	20.5096	< 0.0001
s(Windspeed)	3.6754	3.6754	29.6019	< 0.0001
s(CPAmin)	6.7332	6.7332	7.8383	< 0.0001
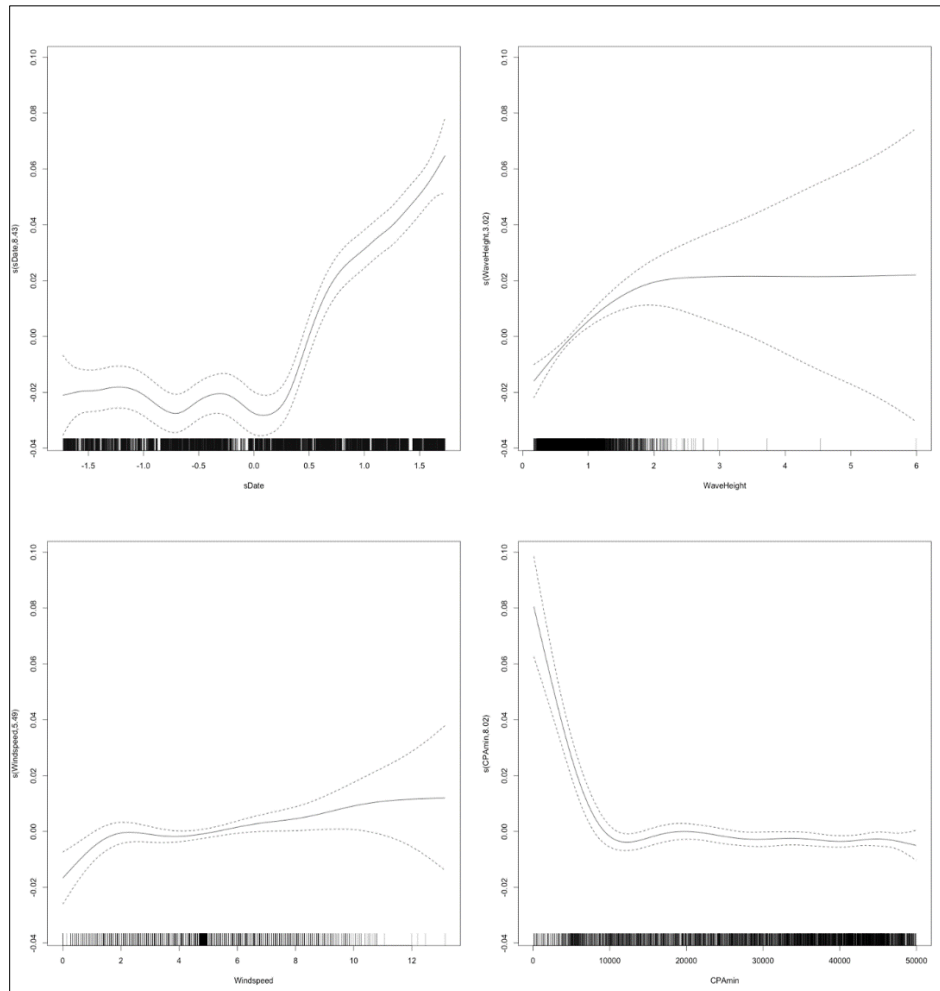
Figure D-B1. SA2 smoothing functions for Measured Vessel Band Noise as a function of Date, Wave Height, Windspeed, and CPA for Receiver 1, Deployment 2.

Table D-B2. GAM output for Deployment 2, Receiver 2

| A. parametric coefficients	Estimate	Std. Error	t-value	p-value
(Intercept)	4.5136	0.0012	3899.8731	< 0.0001
km2	0.0293	0.0048	6.0980	< 0.0001
km4	0.0201	0.0037	5.3839	< 0.0001
km10	0.0085	0.0017	5.0327	< 0.0001
B. smooth terms	edf	Ref.df	F-value	p-value
s(sDate)	38.8337	49.0000	117.6090	< 0.0001
s(WaveHeight)	1.0000	1.0000	24.6496	< 0.0001
s(Windspeed)	1.0000	1.0000	17.8622	< 0.0001
s(CPAmin)	3.2779	3.2779	9.3601	< 0.0001
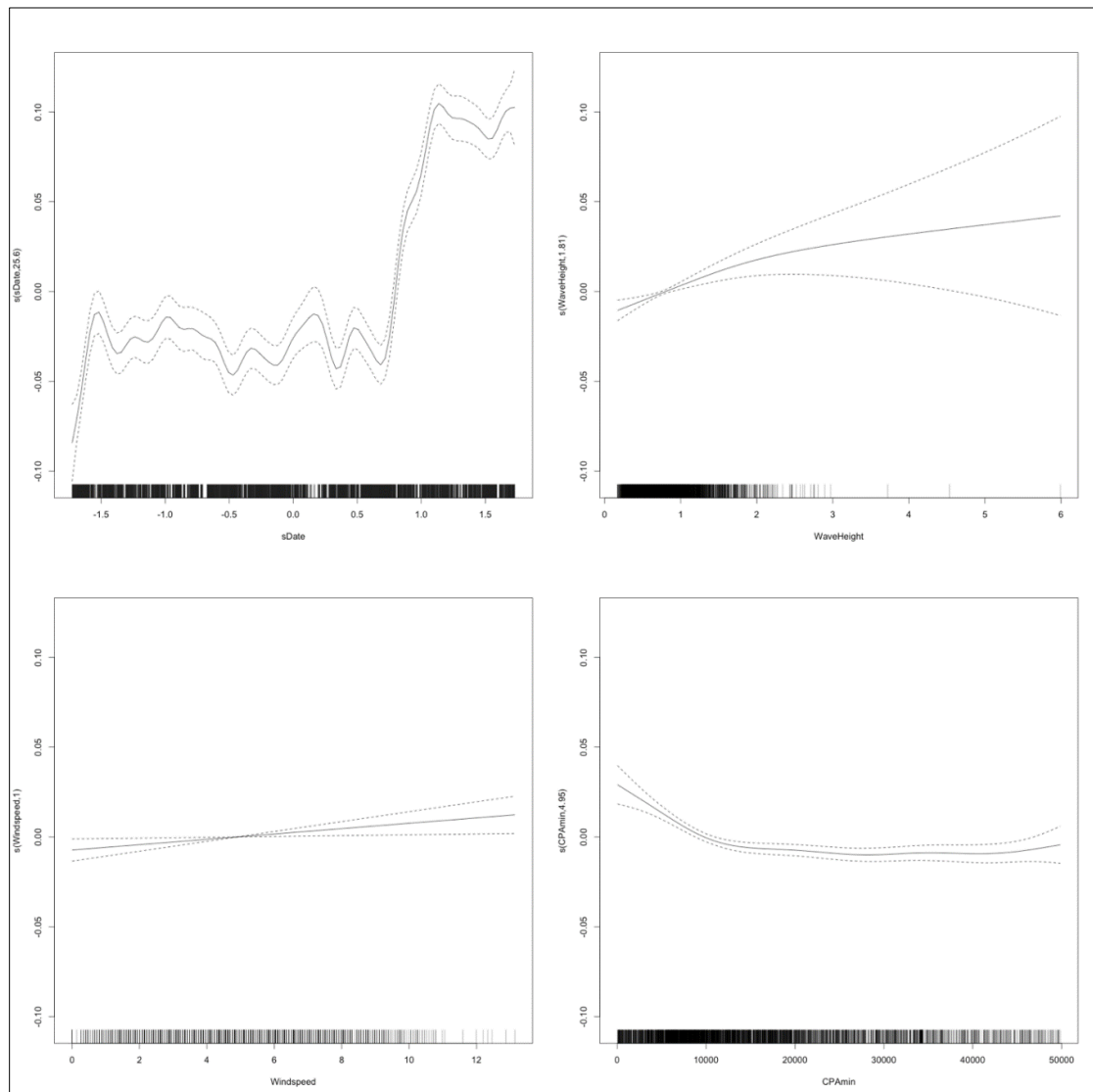
Figure D-B2. SA2 smoothing functions for Measured Vessel Band Noise as a function of Date, Wave Height, Windspeed, and CPA for Receiver 2, Deployment 2.

**Table D-B3. GAM output for Deployment 2, Receiver 3**

A. parametric coefficients	Estimate	Std. Error	t-value	p-value
(Intercept)	4.6174	0.0006	8156.1005	< 0.0001
km2	0.0530	0.0066	8.0384	< 0.0001
km4	0.0346	0.0045	7.7606	< 0.0001
km10	0.0110	0.0020	5.4315	< 0.0001
B. smooth terms	edf	Ref.df	F-value	p-value
s(sDate)	43.1319	49.0000	58.0407	< 0.0001
s(WaveHeight)	3.4464	3.4464	71.1011	< 0.0001
s(Windspeed)	1.0000	1.0000	163.6694	< 0.0001
s(CPAmin)	3.2739	3.2739	4.8104	0.0013
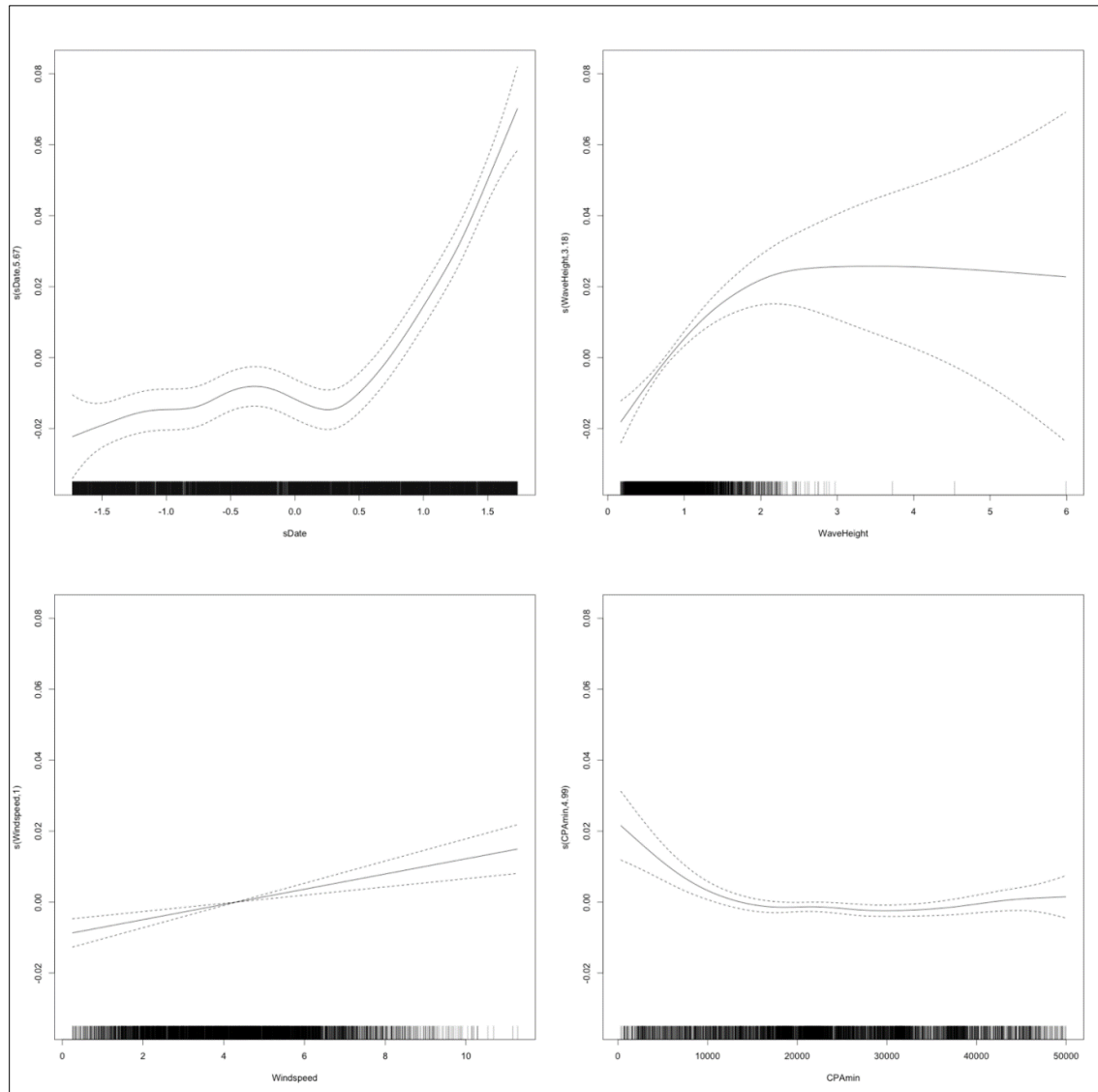
Figure D-B3. SA2 smoothing functions for Measured Vessel Band Noise as a function of Date, Wave Height, Windspeed, and CPA for Receiver 3, Deployment 2.

**Table D-B4. GAM output for Deployment 2, Receiver 4**

A. parametric coefficients	Estimate	Std. Error	t-value	p-value
(Intercept)	4.5015	0.0006	7062.4300	< 0.0001
km2	0.0044	0.0086	0.5146	0.6068
km4	0.0165	0.0059	2.8079	0.0050
km10	0.0026	0.0023	1.1468	0.2515
B. smooth terms	edf	Ref.df	F-value	p-value
s(sDate)	41.7865	49.0000	60.9431	< 0.0001
s(WaveHeight)	4.9438	4.9438	29.6807	< 0.0001
s(Windspeed)	3.9395	3.9395	31.6058	< 0.0001
s(CPAmin)	7.3711	7.3711	9.2162	< 0.0001
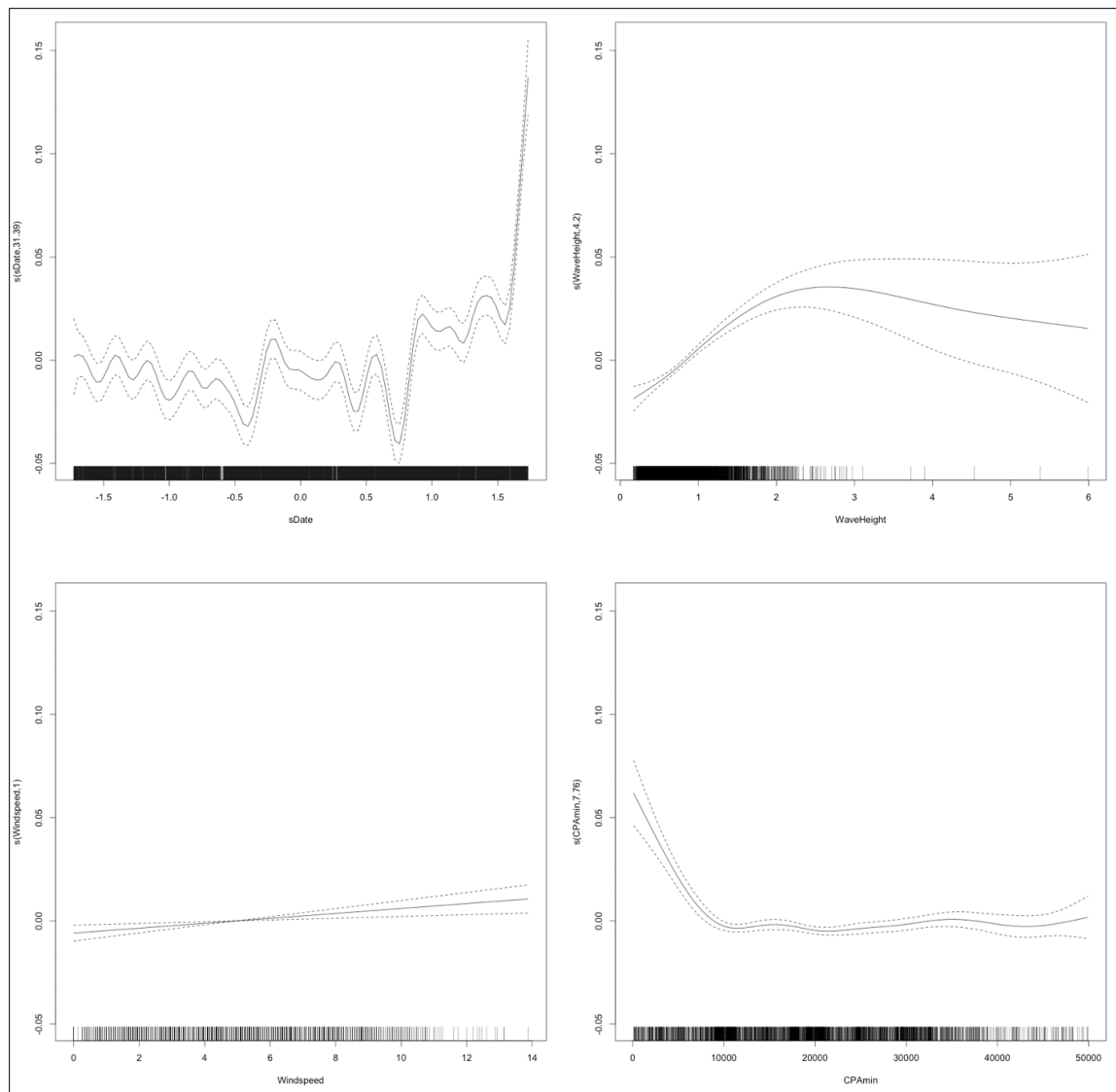
Figure D-B4. SA2 smoothing functions for Measured Vessel Band Noise as a function of Date, Wave Height, Windspeed, and CPA for Receiver 4, Deployment 2.

**Table D-B5. GAM output for Deployment 2, Receiver 5**

A. parametric coefficients	Estimate	Std. Error	t-value	p-value
(Intercept)	4.5500	0.0007	6105.8569	< 0.0001
km2	0.0328	0.0029	11.2034	< 0.0001
km4	0.0146	0.0021	6.8469	< 0.0001
km10	0.0076	0.0008	9.1069	< 0.0001
B. smooth terms	edf	Ref.df	F-value	p-value
s(sDate)	39.5263	49.0000	108.5052	< 0.0001
s(WaveHeight)	1.0000	1.0000	29.2715	< 0.0001
s(Windspeed)	3.3844	3.3844	20.2612	< 0.0001
s(CPAmin)	1.0000	1.0000	0.0776	0.7806
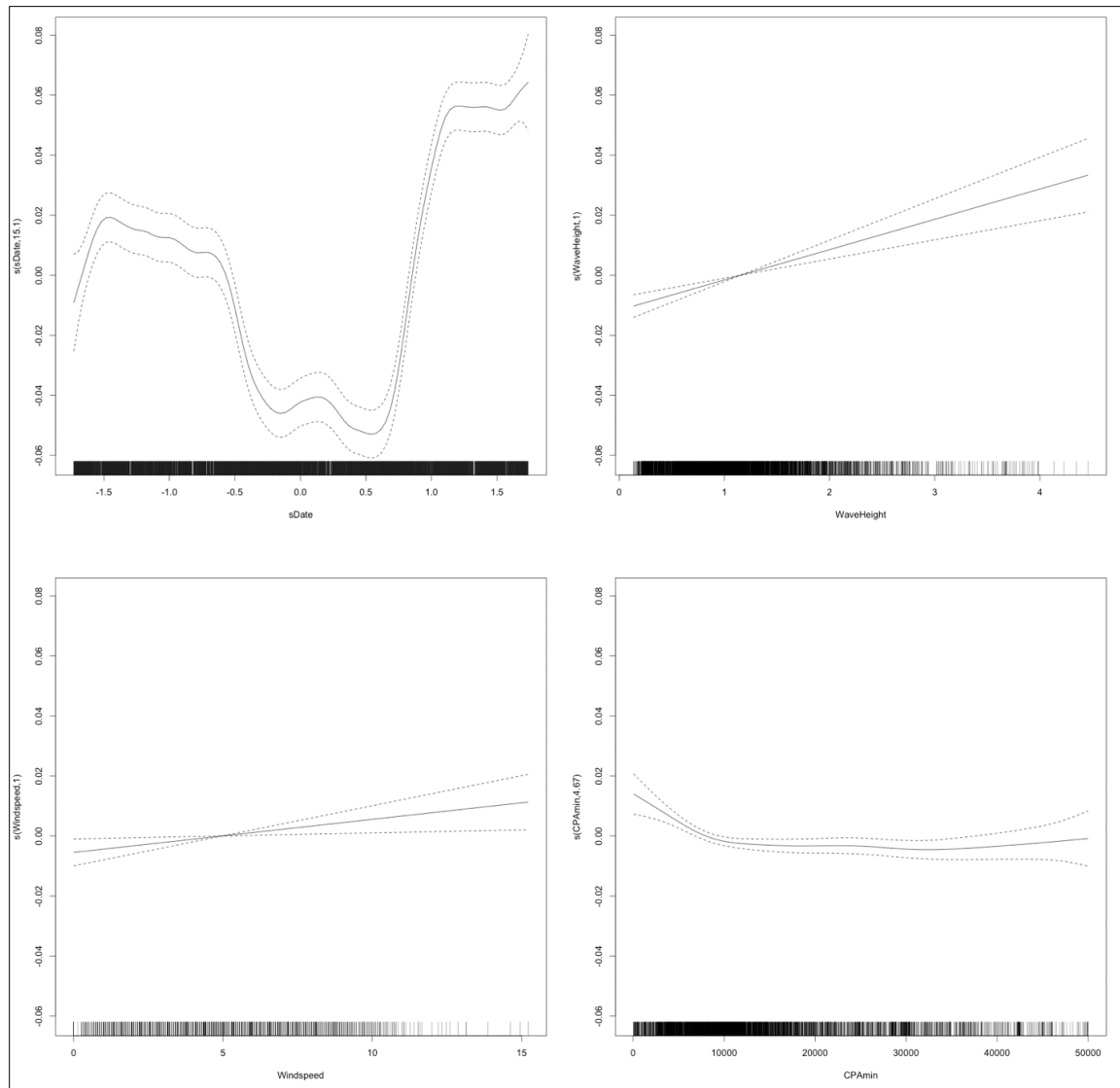
Figure D-B5. SA2 smoothing functions for Measured Vessel Band Noise as a function of Date, Wave Height, Windspeed, and CPA for Receiver 5, Deployment 2.

Table D-B6. GAM output for Deployment 2, Receiver 6

| A. parametric coefficients	Estimate	Std. Error	t-value	p-value
(Intercept)	4.6034	0.0008	5967.1622	< 0.0001
km2	0.0523	0.0046	11.3207	< 0.0001
km4	0.0120	0.0032	3.7479	0.0002
km10	0.0034	0.0013	2.6437	0.0082
B. smooth terms	edf	Ref.df	F-value	p-value
s(sDate)	42.6212	49.0000	44.2084	< 0.0001
s(WaveHeight)	3.8132	3.8132	36.4942	< 0.0001
s(Windspeed)	4.4370	4.4370	57.6110	< 0.0001
s(CPAmin)	3.0912	3.0912	20.6640	< 0.0001
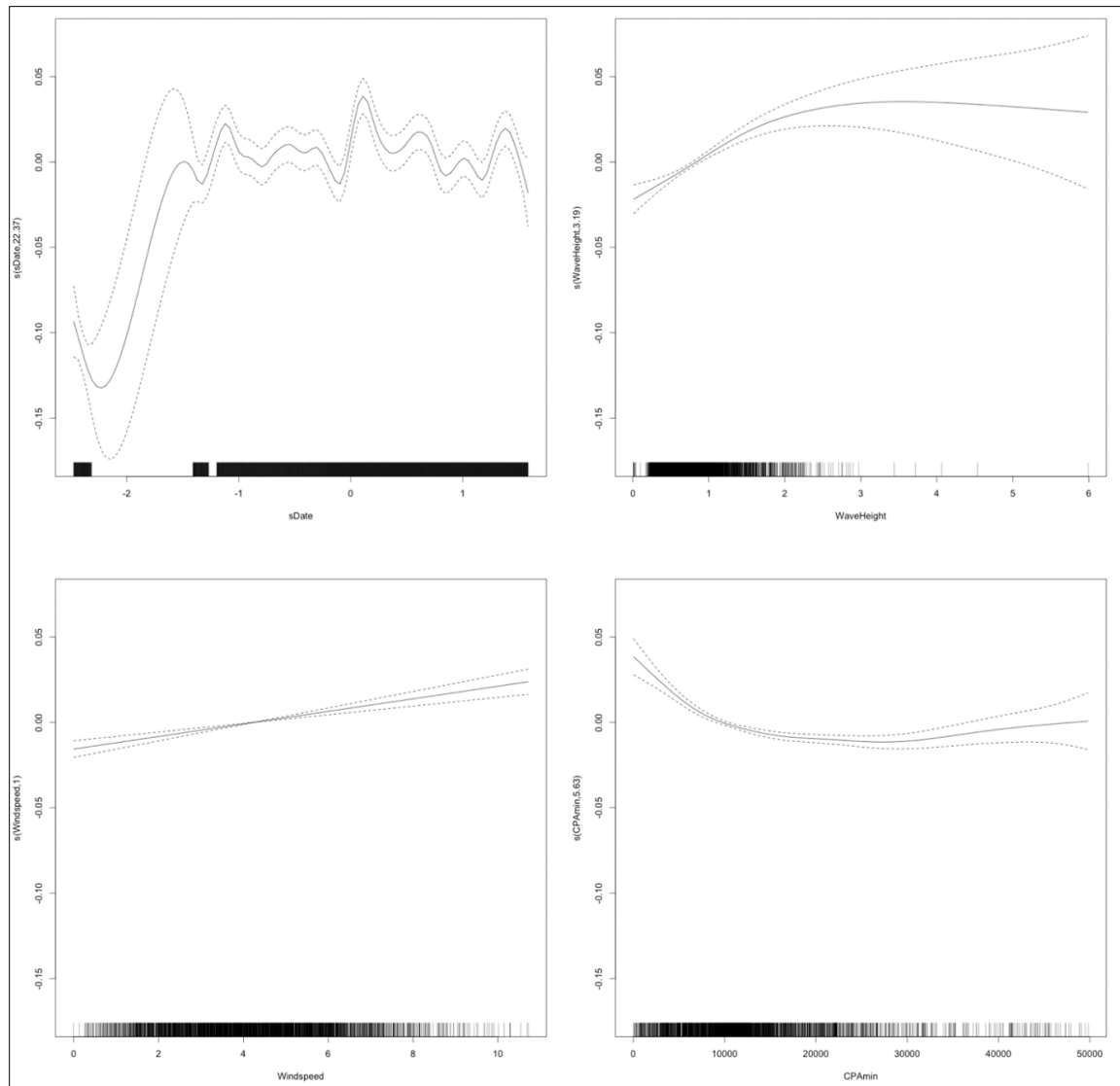
Figure D-B6. SA2 smoothing functions for Measured Vessel Band Noise as a function of Date, Wave Height, Windspeed, and CPA for Receiver 6, Deployment 2.

**Table D-B7. GAM output for Deployment 2, Receiver 7**

A. parametric coefficients	Estimate	Std. Error	t-value	p-value
(Intercept)	4.6444	0.0012	3772.6038	< 0.0001
km2	0.0090	0.0031	2.9288	0.0034
km4	0.0098	0.0011	8.7537	< 0.0001
km10	0.0081	0.0005	15.2436	< 0.0001
B. smooth terms	edf	Ref.df	F-value	p-value
s(sDate)	33.4126	49.0000	29.6004	< 0.0001
s(WaveHeight)	1.0000	1.0000	14.4946	0.0001
s(Windspeed)	1.0000	1.0000	113.9104	< 0.0001
s(CPAmin)	7.8582	7.8582	32.9471	< 0.0001
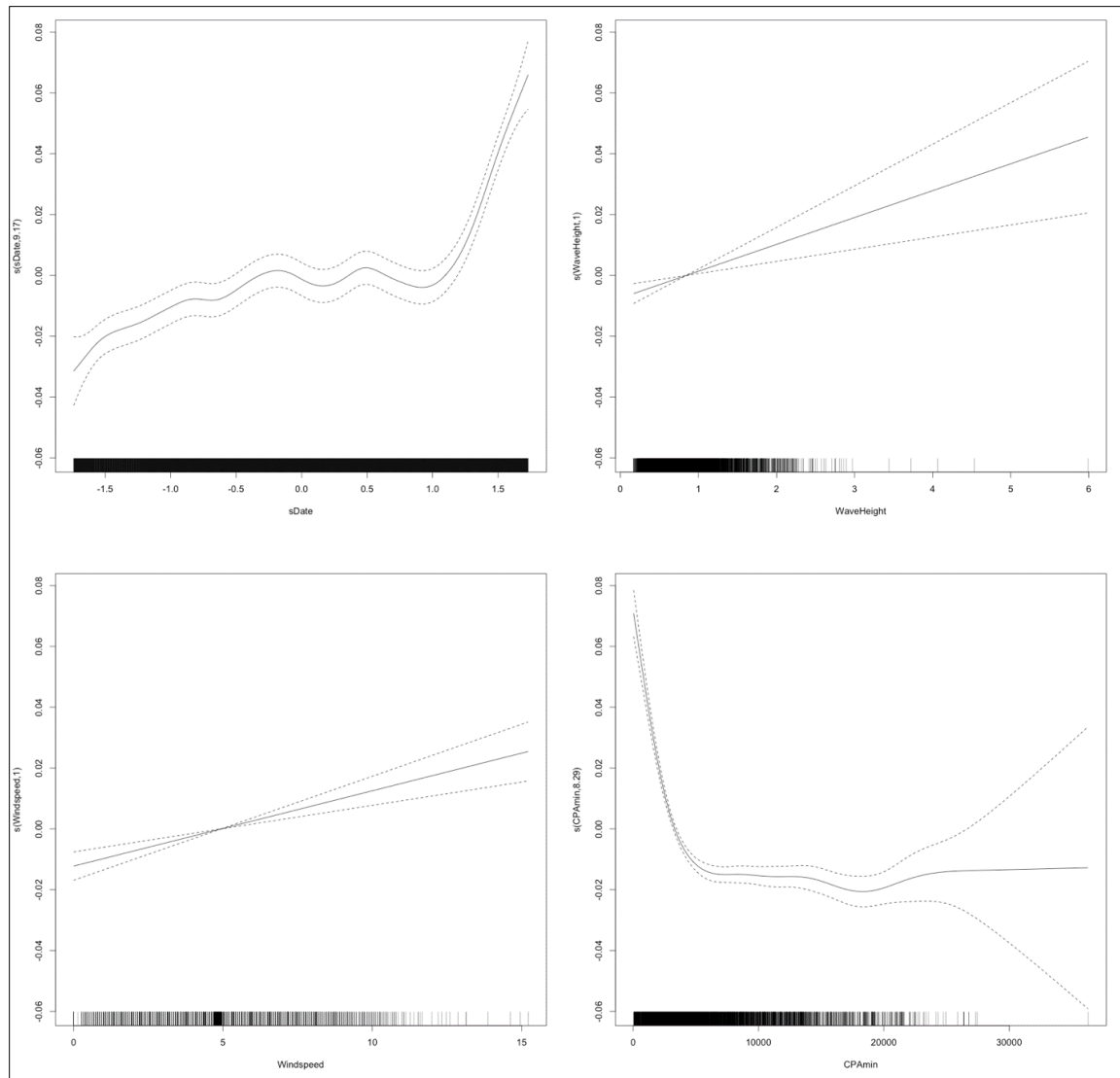
Figure D-B7. SA2 smoothing functions for Measured Vessel Band Noise as a function of Date, Wave Height, Windspeed, and CPA for Receiver 7, Deployment 2.

**Table D-B8. GAM output for Deployment 2, Receiver 8**

A. parametric coefficients	Estimate	Std. Error	t-value	p-value
(Intercept)	4.5371	0.0011	4005.3062	< 0.0001
km2	0.0181	0.0059	3.0607	0.0022
km4	0.0033	0.0040	0.8269	0.4084
km10	0.0028	0.0015	1.8543	0.0639
B. smooth terms	edf	Ref.df	F-value	p-value
s(sDate)	43.8914	49.0000	41.1393	< 0.0001
s(WaveHeight)	1.0000	1.0000	14.9270	0.0001
s(Windspeed)	1.0000	1.0000	29.0399	< 0.0001
s(CPAmin)	4.2942	4.2942	3.3612	0.0076
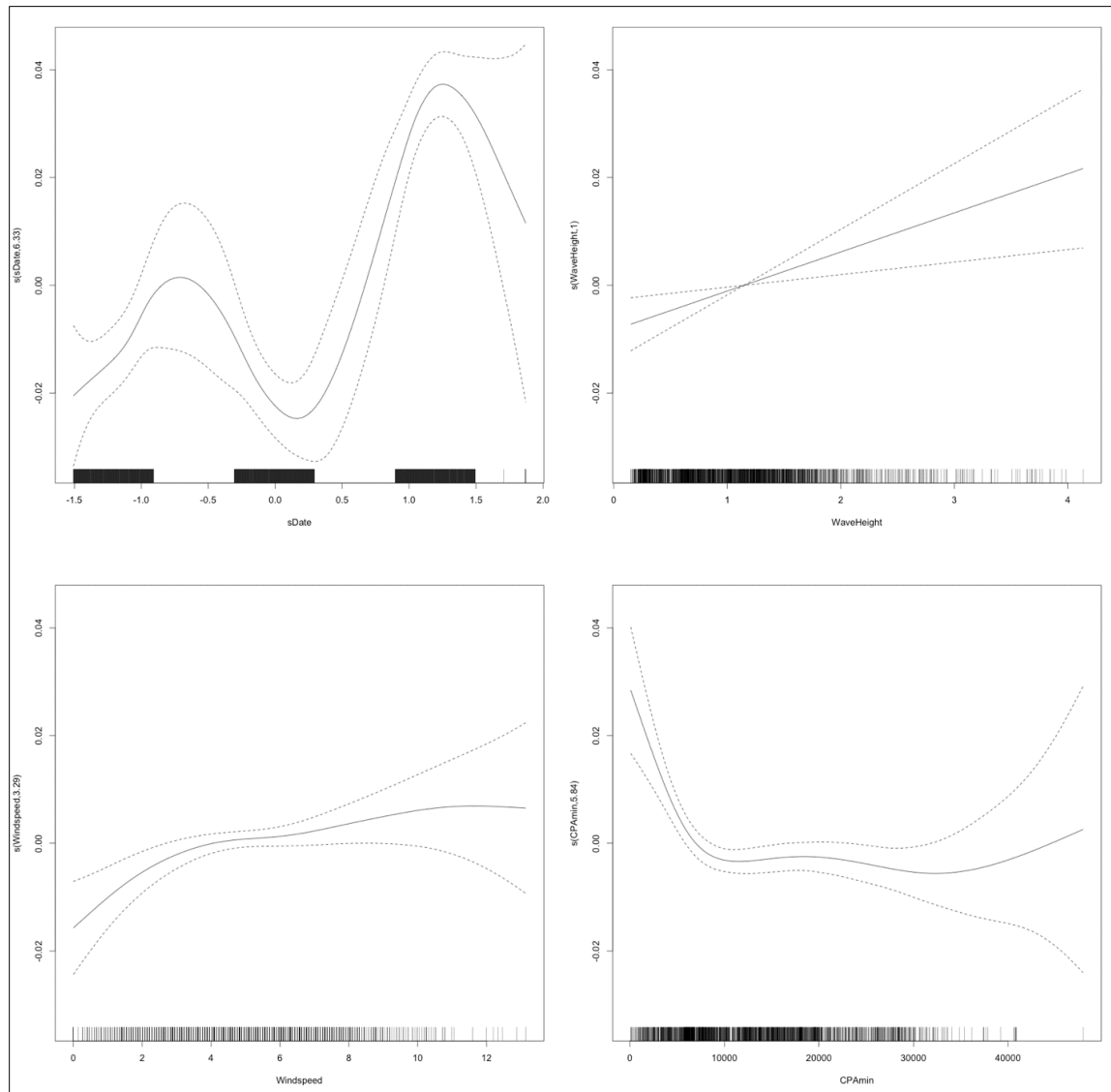
Figure D-B8. SA2 smoothing functions for Measured Vessel Band Noise as a function of Date, Wave Height, Windspeed, and CPA for Receiver 8, Deployment 2.

**Table D-B9. GAM output for Deployment 2, Receiver 9**

A. parametric coefficients	Estimate	Std. Error	t-value	p-value
(Intercept)	4.6645	0.0007	6926.7316	< 0.0001
km2	0.0184	0.0044	4.2264	< 0.0001
km4	0.0089	0.0023	3.9112	0.0001
km10	0.0021	0.0009	2.3536	0.0186
B. smooth terms	edf	Ref.df	F-value	p-value
s(sDate)	44.6442	49.0000	74.4437	< 0.0001
s(WaveHeight)	1.0000	1.0000	3.9165	0.0479
s(Windspeed)	3.8640	3.8640	58.4151	< 0.0001
s(CPAmin)	7.9599	7.9599	21.8303	< 0.0001
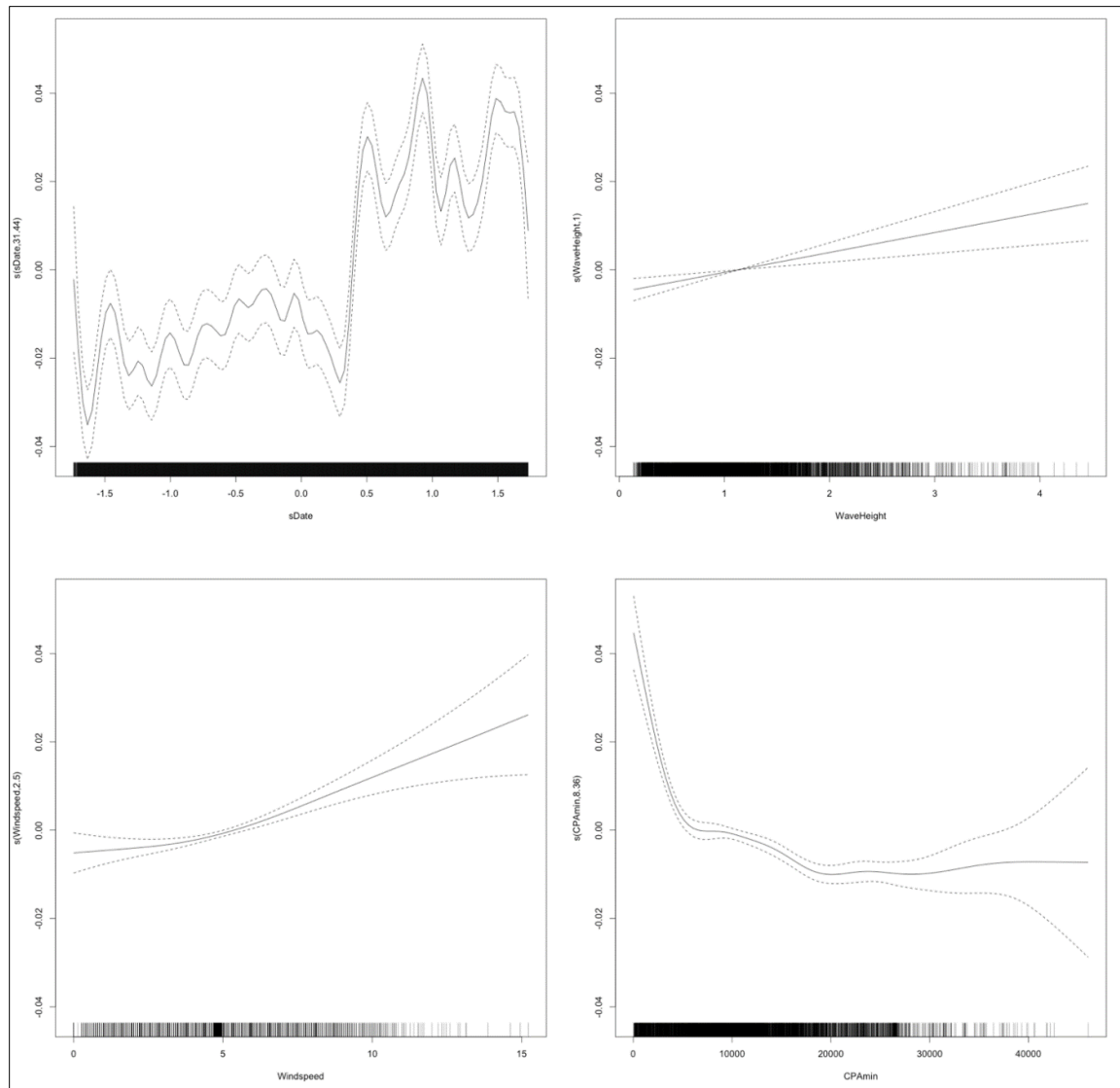
**Figure D-B9. SA2 smoothing functions for Measured Vessel Band Noise as a function of Date, Wave Height, Windspeed, and CPA for Receiver 9, Deployment 2.**

Table D-B10. GAM output for Deployment 2, Receiver 10

A. parametric coefficients	Estimate	Std. Error	t-value	p-value
(Intercept)	4.5866	0.0022	2131.0235	< 0.0001
km2	0.0093	0.0040	2.3409	0.0193
km4	0.0068	0.0020	3.4809	0.0005
km10	0.0006	0.0005	1.1033	0.2700
B. smooth terms	edf	Ref.df	F-value	p-value
s(sDate)	45.3898	49.0000	24.7921	< 0.0001
s(WaveHeight)	7.4772	7.4772	7.8193	< 0.0001
s(Windspeed)	4.3854	4.3854	8.6116	< 0.0001
s(CPAmin)	7.9034	7.9034	23.5431	< 0.0001
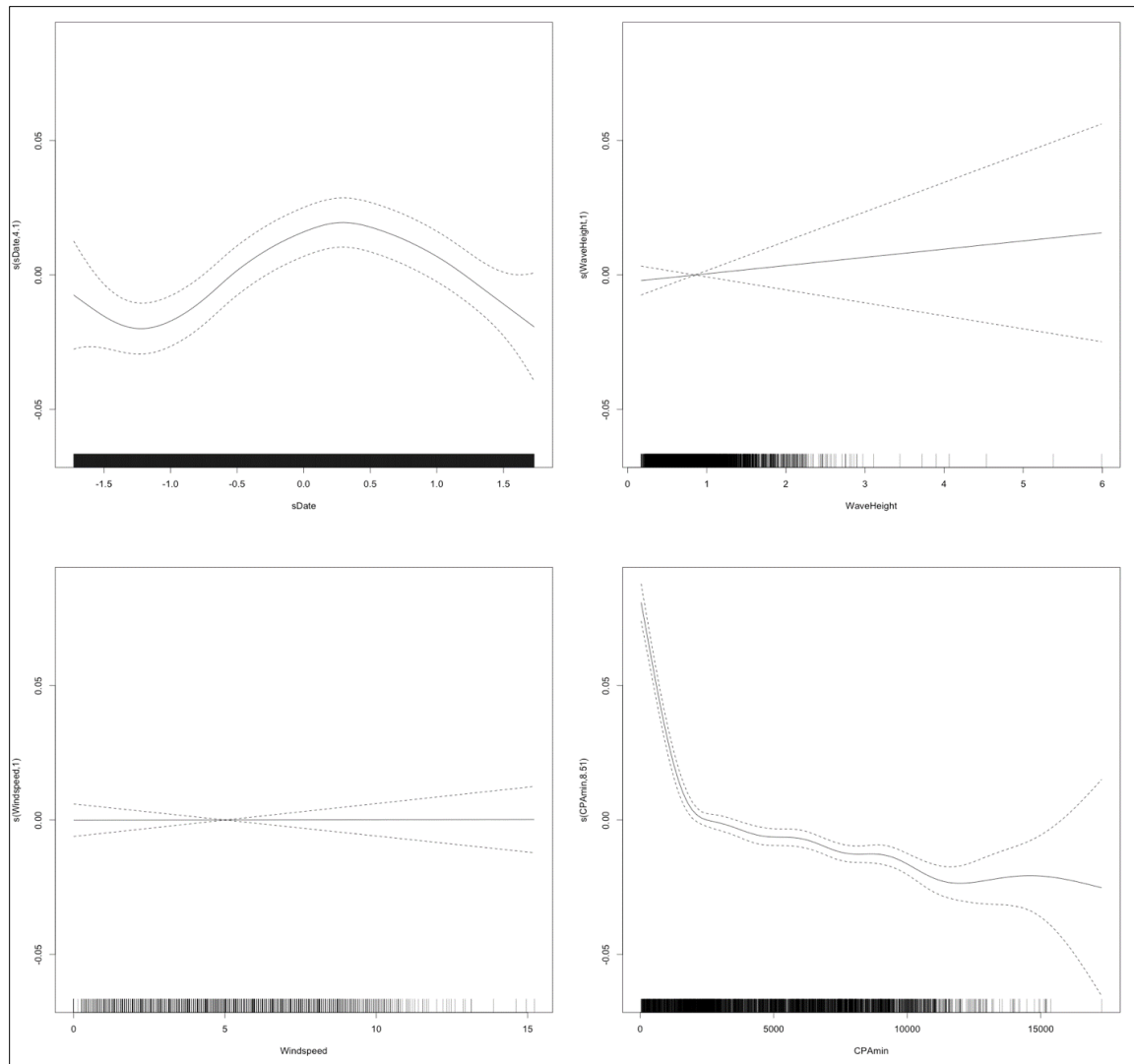
Figure D-B10. SA2 smoothing functions for Measured Vessel Band Noise as a function of Date, Wave Height, Windspeed, and CPA for Receiver 10, Deployment 2.

DEPLOYMENT 3

**Table D-B11. GAM output for Deployment 3, Receiver 1**

A. parametric coefficients	Estimate	Std. Error	t-value	p-value
(Intercept)	4.7106	0.0008	5583.3855	< 0.0001
km2	0.0392	0.0051	7.6588	< 0.0001
km4	0.0203	0.0036	5.6526	< 0.0001
km10	0.0205	0.0023	8.7221	< 0.0001
B. smooth terms	edf	Ref.df	F-value	p-value
s(sDate)	44.0524	49.0000	147.6610	< 0.0001
s(WaveHeight)	6.2418	6.2418	9.3809	< 0.0001
s(Windspeed)	1.0000	1.0000	10.5758	0.0012
s(CPAmin)	1.0000	1.0000	36.7337	< 0.0001
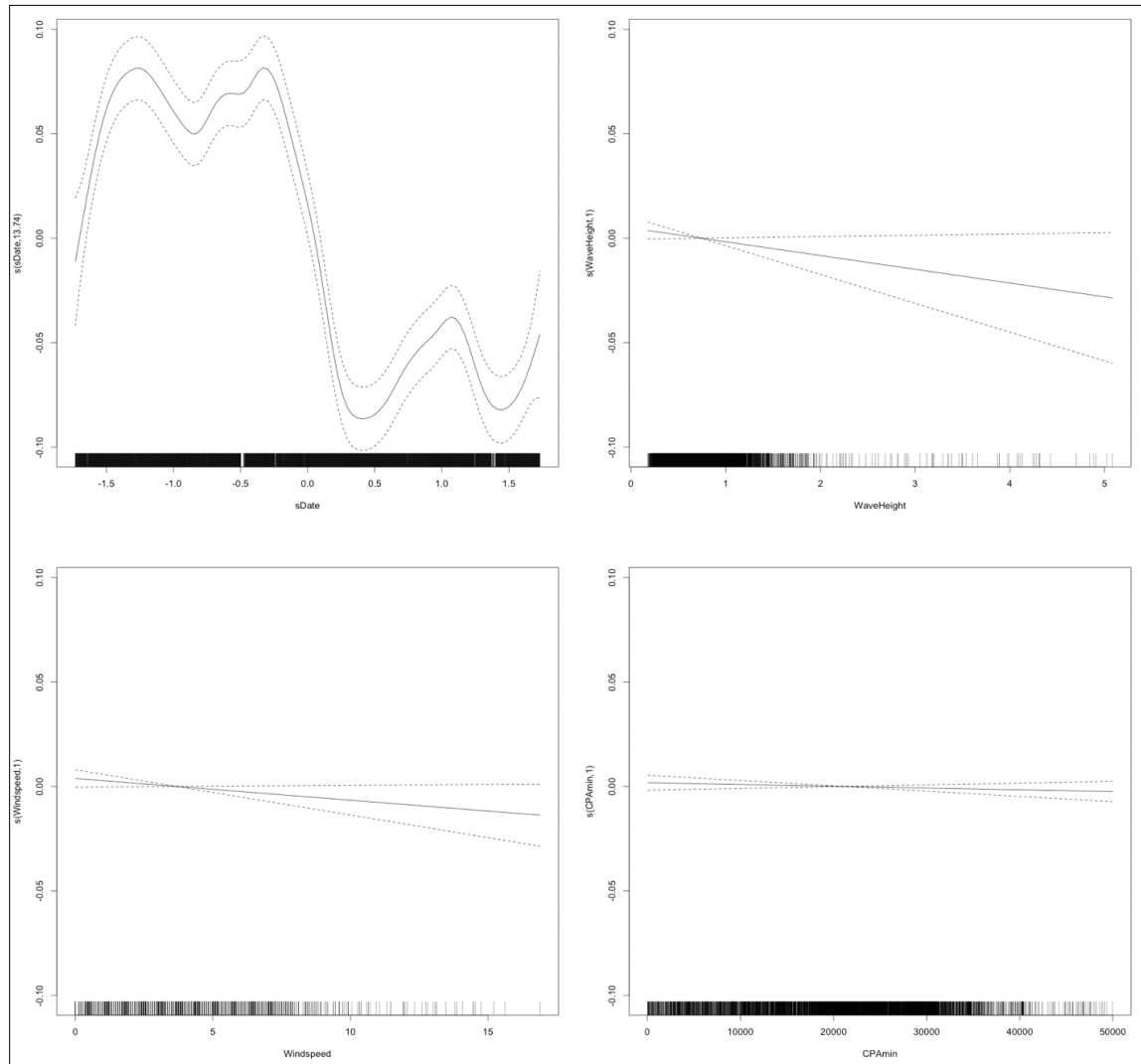
Figure D-B11. SA2 smoothing functions for Measured Vessel Band Noise as a function of Date, Wave Height, Windspeed, and CPA for Receiver 1, Deployment 3.

**Table D-B12. GAM output for Deployment 3, Receiver 2**

A. parametric coefficients	Estimate	Std. Error	t-value	p-value
(Intercept)	4.5523	0.0011	4004.1760	< 0.0001
km2	-0.0112	0.0103	-1.0841	0.2784
km4	-0.0312	0.0068	-4.5934	< 0.0001
km10	-0.0137	0.0028	-4.9573	< 0.0001
B. smooth terms	edf	Ref.df	F-value	p-value
s(sDate)	42.6704	49.0000	144.4241	< 0.0001
s(WaveHeight)	1.0000	1.0000	3.1564	0.0757
s(Windspeed)	1.0000	1.0000	32.8006	< 0.0001
s(CPAmin)	5.4551	5.4551	25.9581	< 0.0001
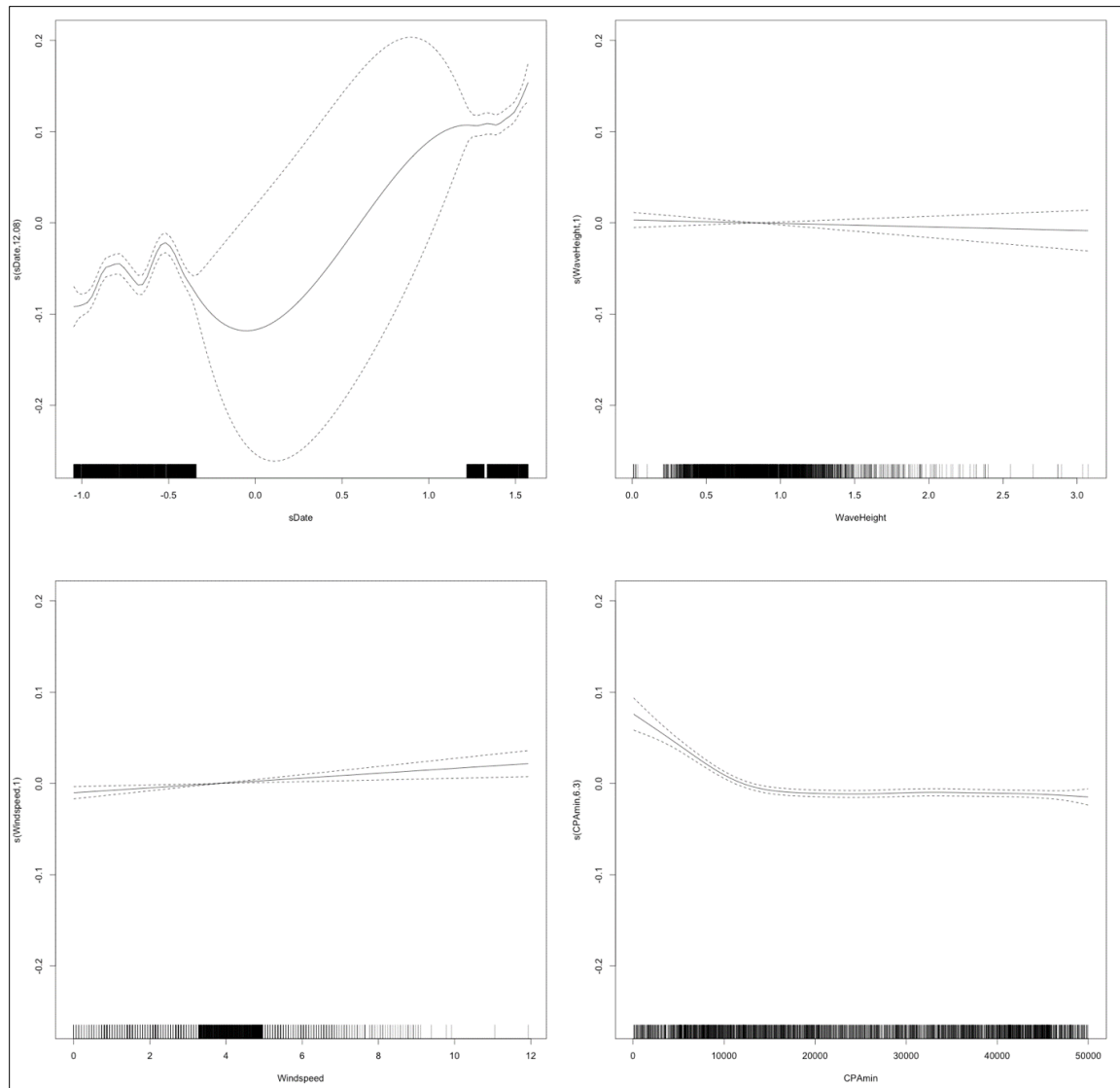
Figure D-B12. SA2 smoothing functions for Measured Vessel Band Noise as a function of Date, Wave Height, Windspeed, and CPA for Receiver 2, Deployment 3.

Table D-B13. GAM output for Deployment 3, Receiver 3

| A. parametric coefficients	Estimate	Std. Error	t-value	p-value
(Intercept)	4.6716	0.0012	4015.3891	< 0.0001
km2	0.0253	0.0120	2.1138	0.0346
km4	0.0303	0.0083	3.6505	0.0003
km10	0.0209	0.0039	5.4245	< 0.0001
B. smooth terms	edf	Ref.df	F-value	p-value
s(sDate)	43.0388	49.0000	86.1402	< 0.0001
s(WaveHeight)	1.8306	1.8306	1.4331	0.1646
s(Windspeed)	2.3699	2.3699	5.2449	0.0090
s(CPAmin)	7.0365	7.0365	23.1367	< 0.0001
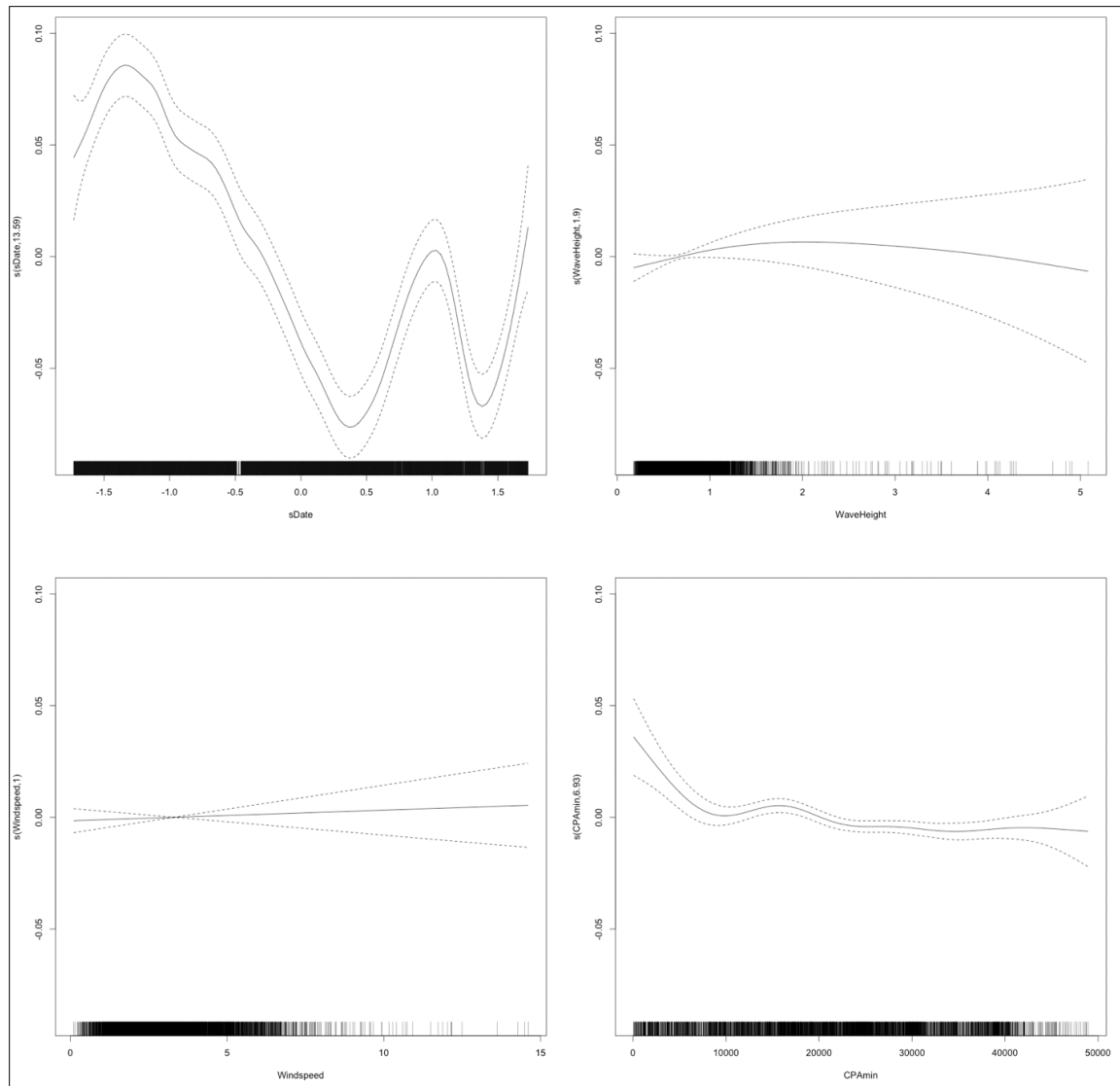
Figure D-B13. SA2 smoothing functions for Measured Vessel Band Noise as a function of Date, Wave Height, Windspeed, and CPA for Receiver 3, Deployment 3.

**Table D-B14. GAM output for Deployment 3, Receiver 4**

A. parametric coefficients	Estimate	Std. Error	t-value	p-value
(Intercept)	4.6399	0.0010	4692.0769	< 0.0001
km2	0.0271	0.0089	3.0515	0.0023
km4	0.0076	0.0044	1.7342	0.0830
km10	0.0078	0.0018	4.3025	< 0.0001
B. smooth terms	edf	Ref.df	F-value	p-value
s(sDate)	45.8327	49.0000	138.4059	< 0.0001
s(WaveHeight)	1.0000	1.0000	0.0533	0.8175
s(Windspeed)	1.9841	1.9841	4.1933	0.0216
s(CPAmin)	8.3865	8.3865	15.2919	< 0.0001
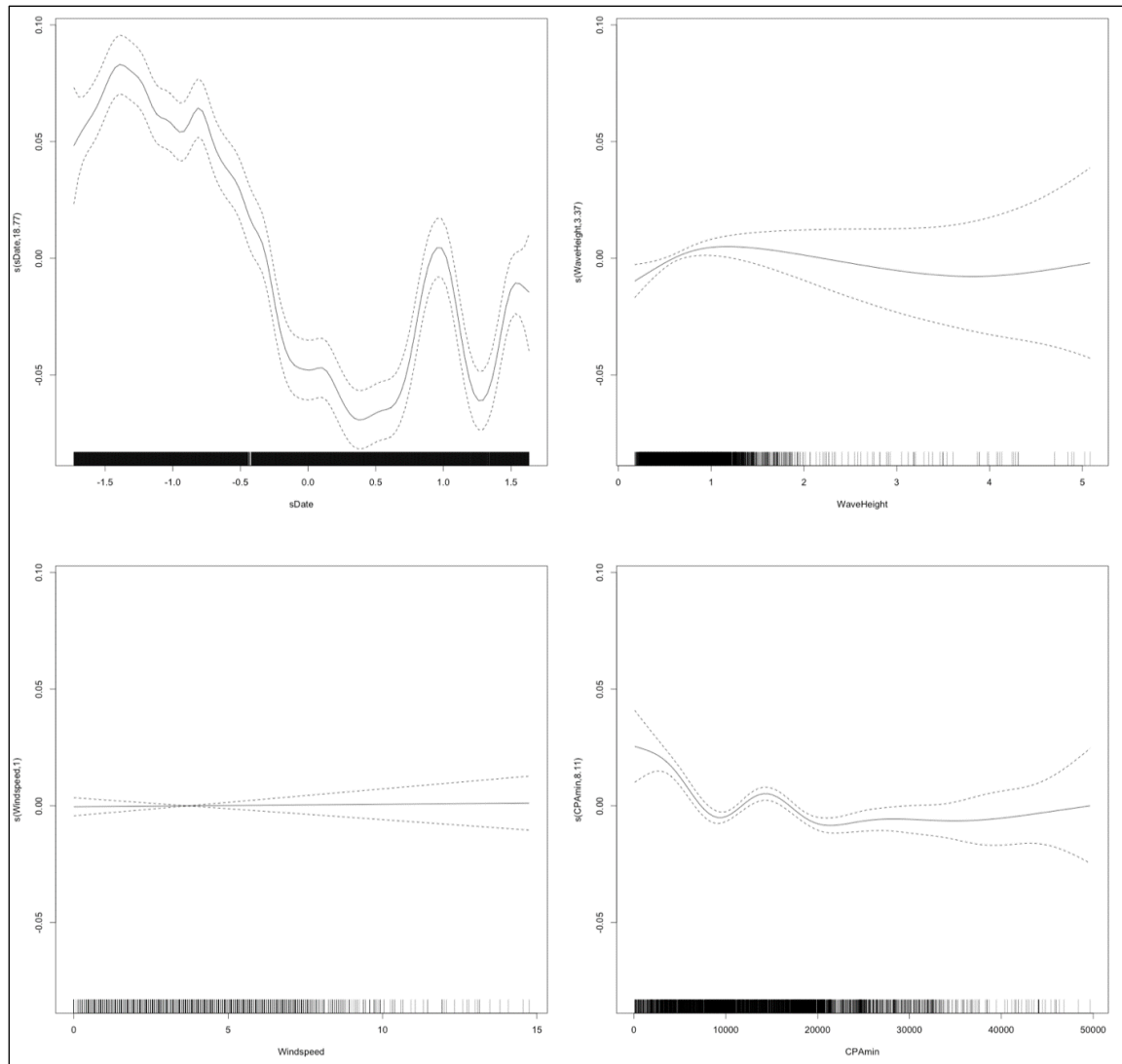
Figure D-B14. SA2 smoothing functions for Measured Vessel Band Noise as a function of Date, Wave Height, Windspeed, and CPA for Receiver 4, Deployment 3.

**Table D-B15. GAM output for Deployment 3, Receiver 5**

A. parametric coefficients	Estimate	Std. Error	t-value	p-value
(Intercept)	4.6514	0.0012	3788.2411	< 0.0001
km2	0.0149	0.0064	2.3187	0.0205
km4	0.0115	0.0041	2.7675	0.0057
km10	0.0059	0.0015	3.9861	0.0001
B. smooth terms	edf	Ref.df	F-value	p-value
s(sDate)	44.6340	49.0000	176.4041	< 0.0001
s(WaveHeight)	4.6557	4.6557	3.2043	0.0116
s(Windspeed)	1.0000	1.0000	0.0003	0.9874
s(CPAmin)	4.7100	4.7100	9.8872	< 0.0001
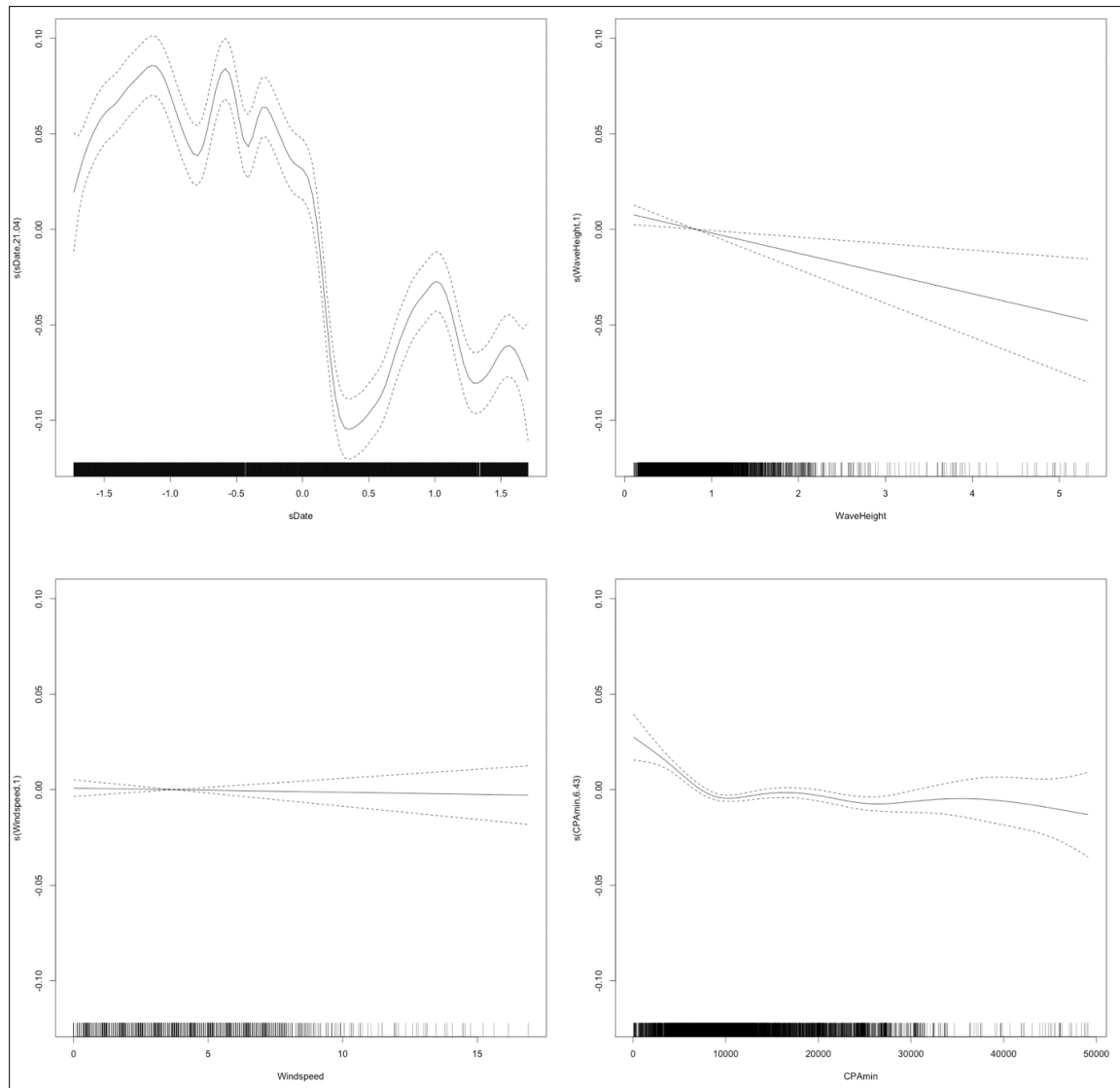
Figure D-B15. SA2 smoothing functions for Measured Vessel Band Noise as a function of Date, Wave Height, Windspeed, and CPA for Receiver 5, Deployment 3.

**Table D-B16. GAM output for Deployment 3, Receiver 6**

A. parametric coefficients	Estimate	Std. Error	t-value	p-value
(Intercept)	4.6818	0.0081	579.0495	< 0.0001
km2	-0.0034	0.0250	-0.1365	0.8917
km4	-0.0080	0.0187	-0.4276	0.6699
km10	-0.0000	0.0085	-0.0003	0.9997
B. smooth terms	**edf**	**Ref.df**	**F-value**	**p-value**
s(sDate)	0.0000	49.0000	0.0000	0.1608
s(WaveHeight)	1.0000	1.0000	4.6772	0.0331
s(Windspeed)	1.0000	1.0000	4.0072	0.0481
s(CPAmin)	1.0001	1.0001	0.7616	0.3850
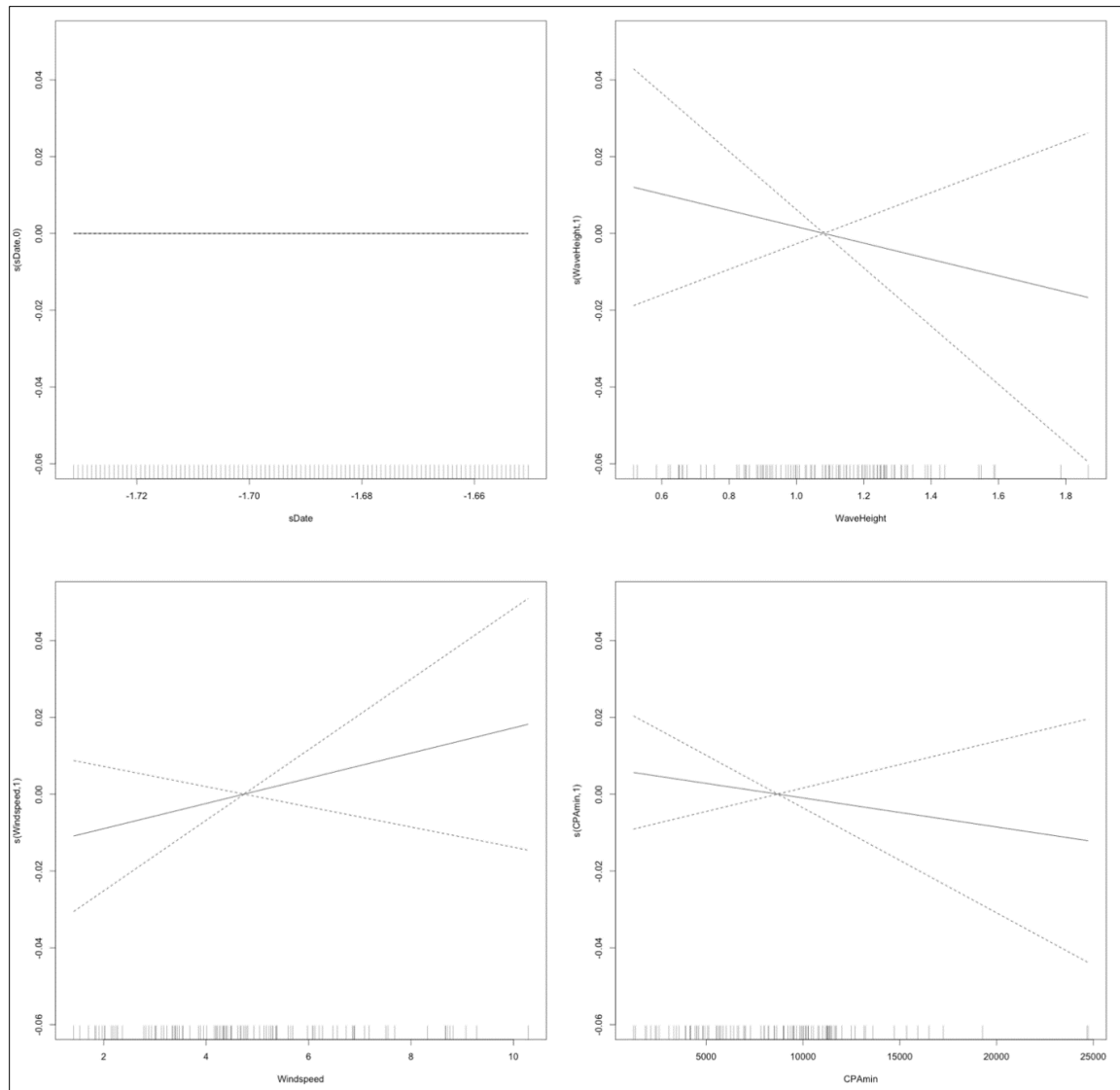
Figure D-B16. SA2 smoothing functions for Measured Vessel Band Noise as a function of Date, Wave Height, Windspeed, and CPA for Receiver 6, Deployment 3.

**Table D-B17. GAM output for Deployment 3, Receiver 7**

A. parametric coefficients	Estimate	Std. Error	t-value	p-value
(Intercept)	4.6113	0.0013	3561.7373	< 0.0001
km2	0.0051	0.0031	1.6183	0.1057
km4	0.0078	0.0013	6.0980	< 0.0001
km10	0.0048	0.0006	8.3078	< 0.0001
B. smooth terms	edf	Ref.df	F-value	p-value
s(sDate)	20.5795	49.0000	16.8289	< 0.0001
s(WaveHeight)	2.4064	2.4064	11.1277	< 0.0001
s(Windspeed)	4.0557	4.0557	22.8863	< 0.0001
s(CPAmin)	8.6301	8.6301	62.8541	< 0.0001
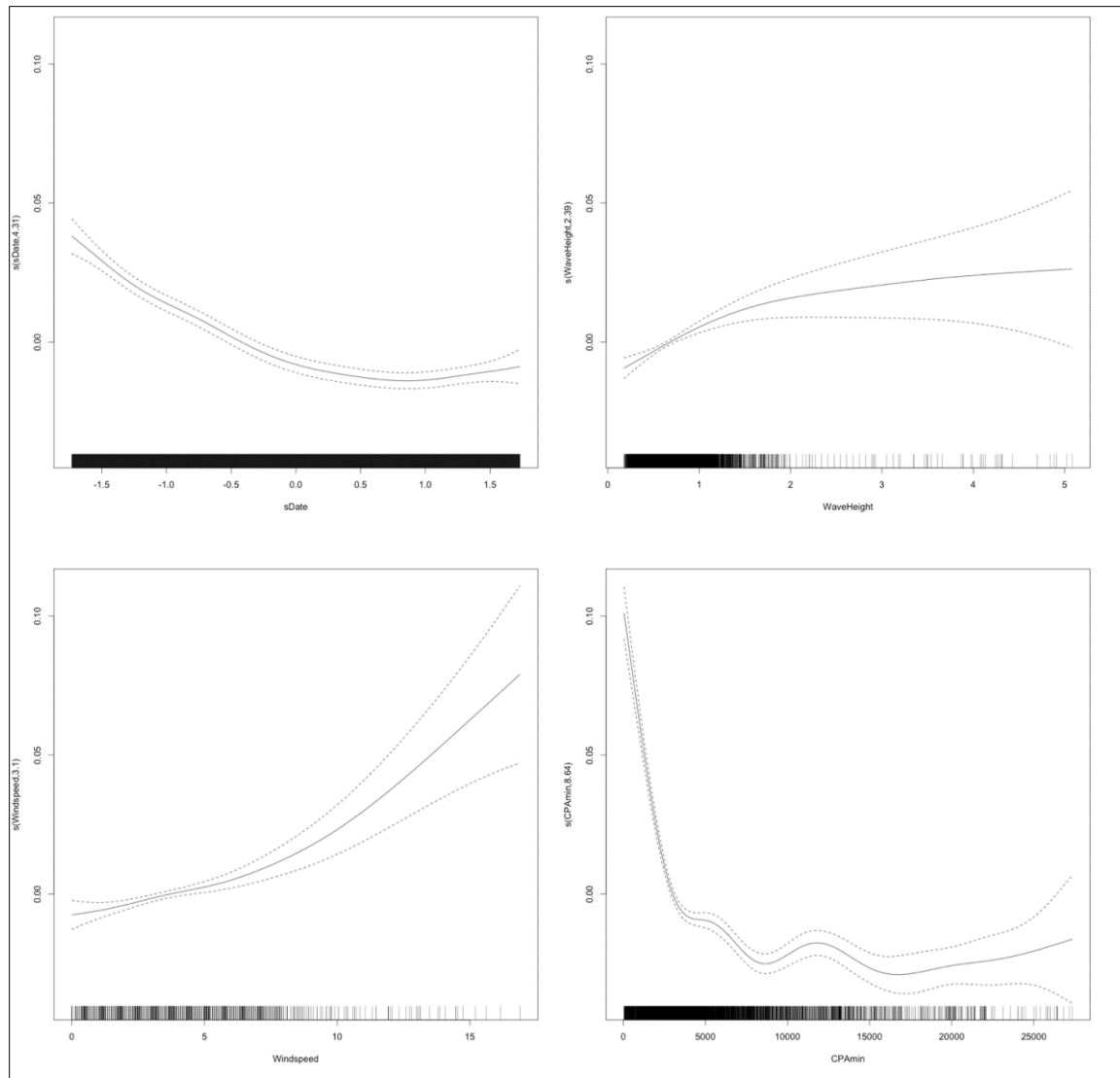
Figure D-B17. SA2 smoothing functions for Measured Vessel Band Noise as a function of Date, Wave Height, Windspeed, and CPA for Receiver 7, Deployment 3.

Table D-B18. GAM output for Deployment 3, Receiver 8

A. parametric coefficients	Estimate	Std. Error	t-value	p-value
(Intercept)	4.6536	0.0015	3025.7303	< 0.0001
km2	0.0241	0.0033	7.3836	< 0.0001
km4	0.0191	0.0026	7.3730	< 0.0001
km10	0.0081	0.0011	7.6352	< 0.0001
B. smooth terms	edf	Ref.df	F-value	p-value
s(sDate)	46.5480	49.0000	66.2399	< 0.0001
s(WaveHeight)	4.9890	4.9890	4.8216	0.0003
s(Windspeed)	3.4829	3.4829	10.4949	< 0.0001
s(CPAmin)	1.0000	1.0000	1.8984	0.1683
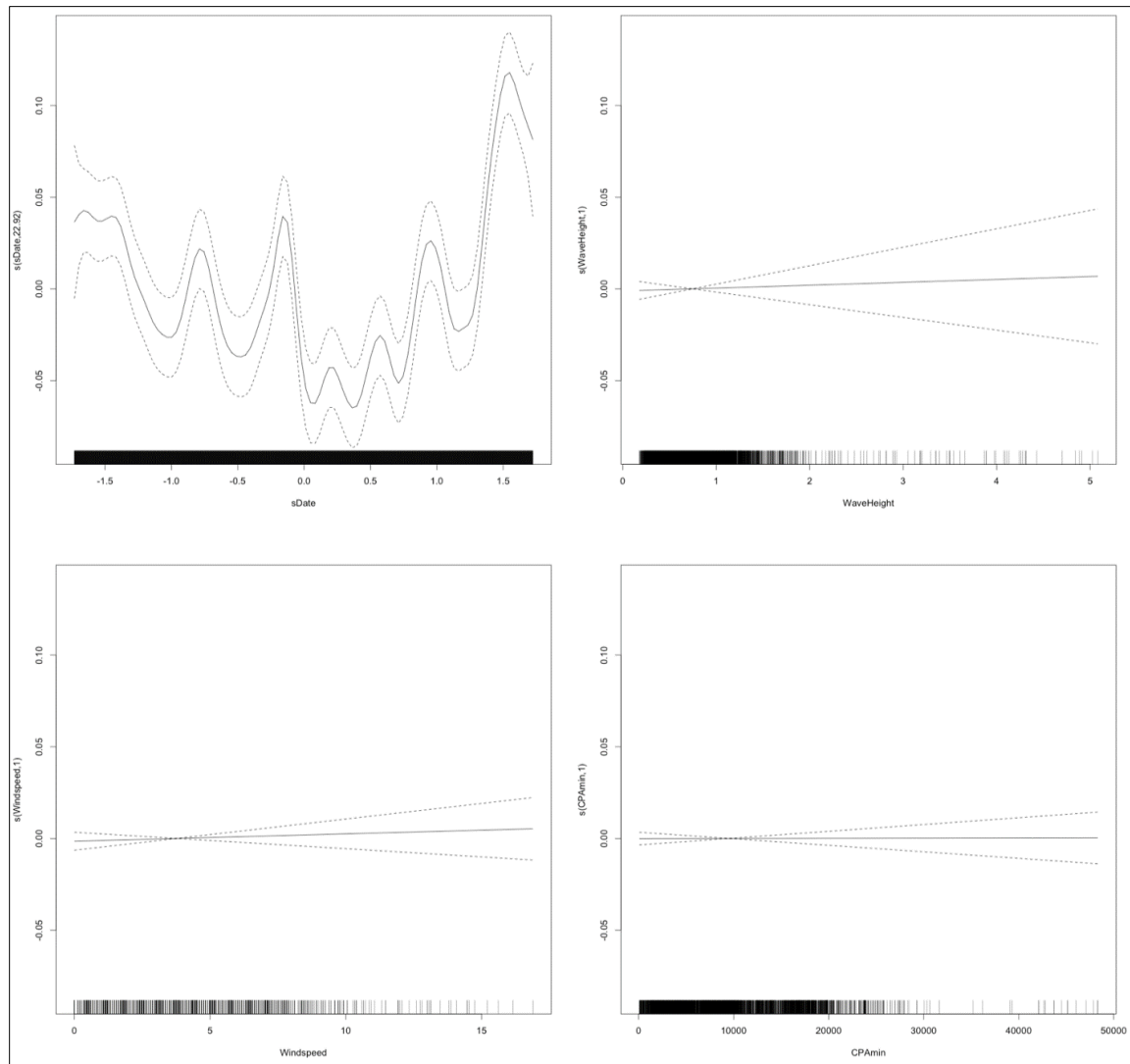
Figure D-B18. SA2 smoothing functions for Measured Vessel Band Noise as a function of Date, Wave Height, Windspeed, and CPA for Receiver 8, Deployment 3.

Table D-B19. GAM output for Deployment 3, Receiver 9

| A. parametric coefficients	Estimate	Std. Error	t-value	p-value
(Intercept)	4.7204	0.0013	3536.0458	< 0.0001
km2	0.0090	0.0059	1.5319	0.1256
km4	0.0150	0.0042	3.5468	0.0004
km10	0.0043	0.0011	3.9506	0.0001
B. smooth terms	edf	Ref.df	F-value	p-value
s(sDate)	43.2615	49.0000	147.6671	< 0.0001
s(WaveHeight)	4.8635	4.8635	4.1541	0.0019
s(Windspeed)	1.0000	1.0000	5.5435	0.0186
s(CPAmin)	4.3039	4.3039	2.8746	0.0155
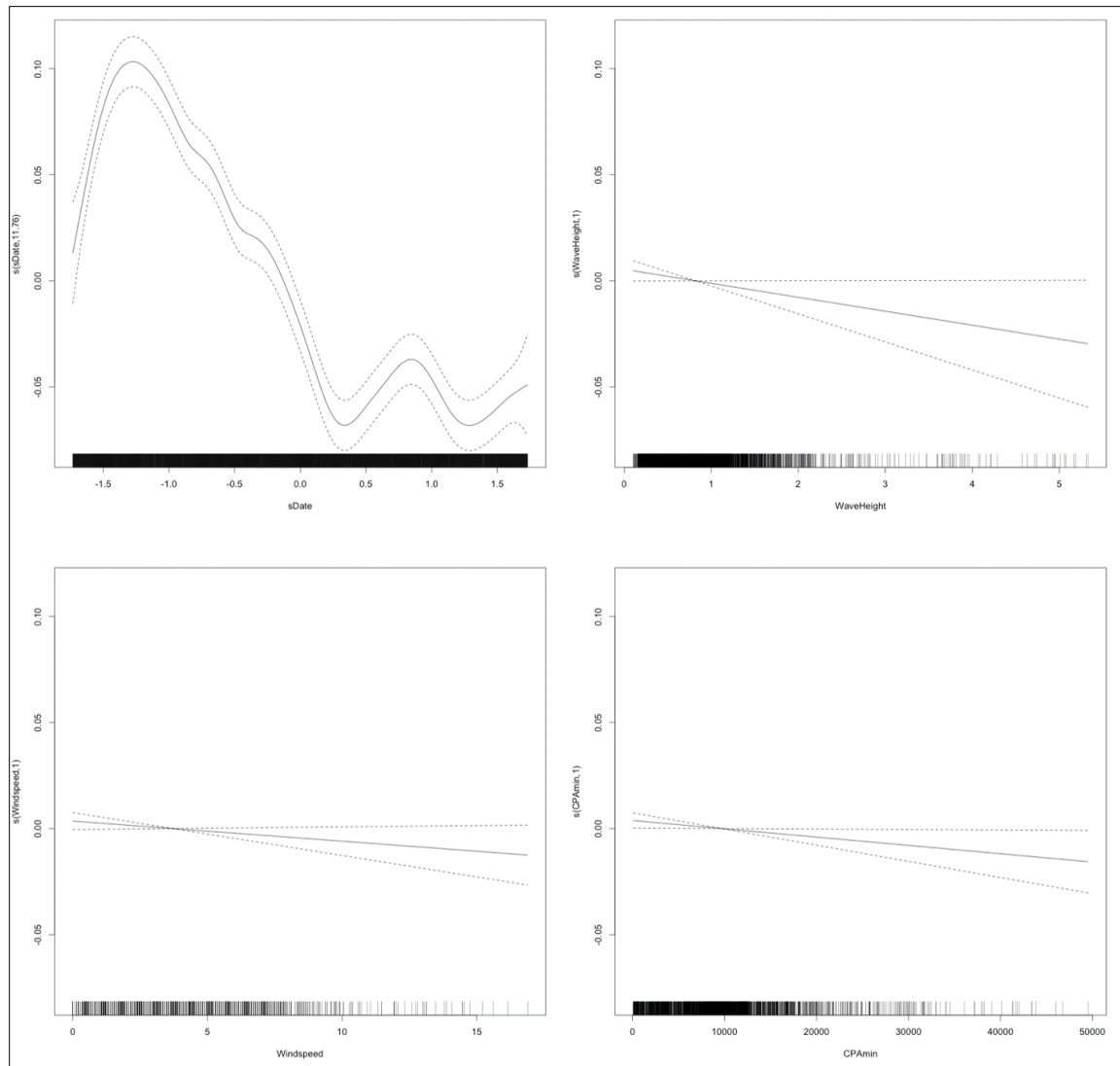
Figure D-B19. SA2 smoothing functions for Measured Vessel Band Noise as a function of Date, Wave Height, Windspeed, and CPA for Receiver 9, Deployment 3.

Table D-B20. GAM output for Deployment 3, Receiver 10

A. parametric coefficients	Estimate	Std. Error	t-value	p-value
(Intercept)	4.5806	0.0008	5402.7881	< 0.0001
km2	-0.0836	0.0221	-3.7799	0.0002
km4	-0.0666	0.0135	-4.9520	< 0.0001
km10	-0.0351	0.0069	-5.1095	< 0.0001
B. smooth terms	edf	Ref.df	F-value	p-value
s(sDate)	46.2455	49.0000	333.3361	< 0.0001
s(WaveHeight)	1.0000	1.0000	0.0866	0.7685
s(Windspeed)	1.0000	1.0000	18.6115	< 0.0001
s(CPAmin)	7.5534	7.5534	14.9459	< 0.0001
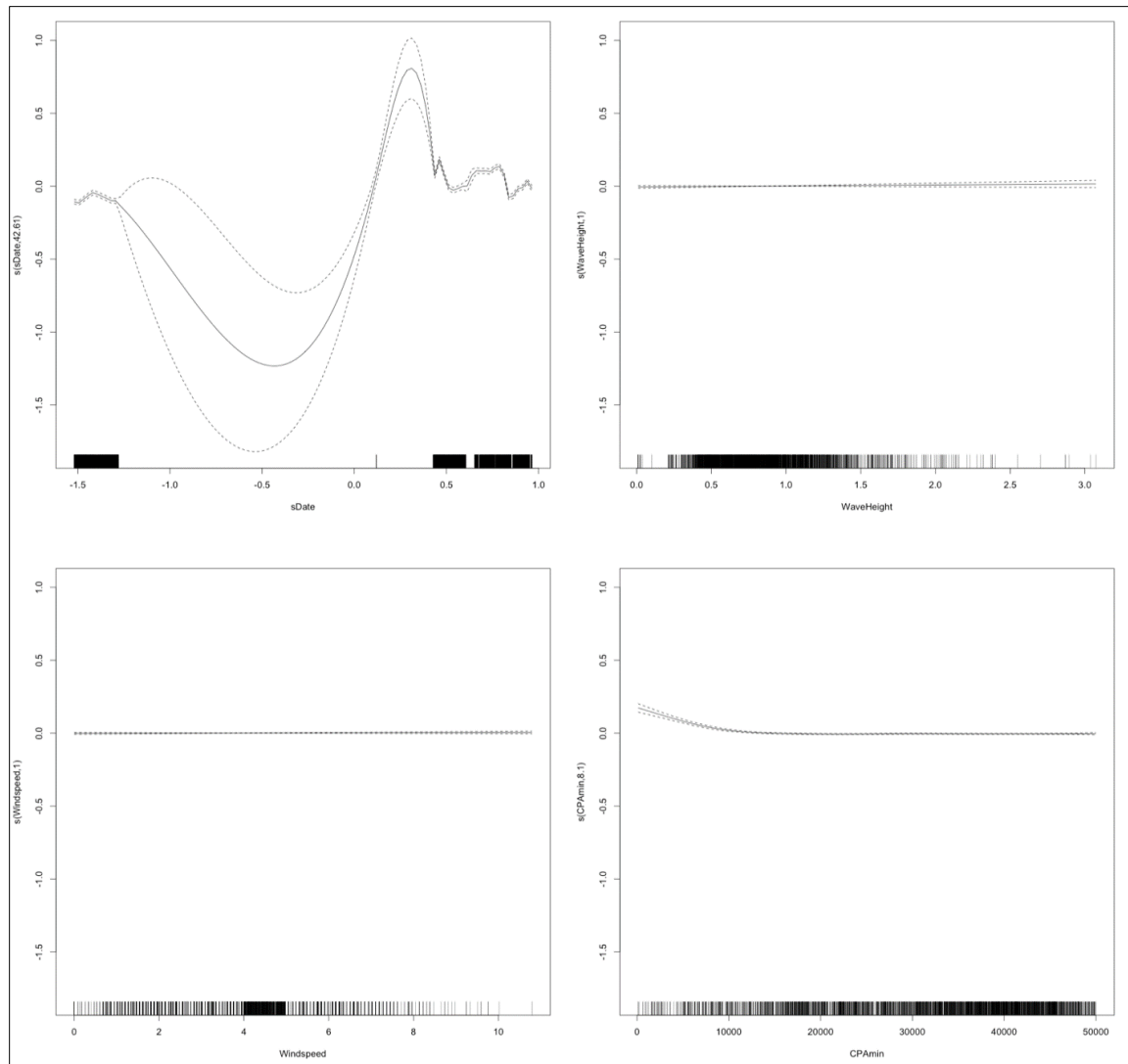
Figure D-B20. SA2 smoothing functions for Measured Vessel Band Noise as a function of Date, Wave Height, Windspeed, and CPA for Receiver 10, Deployment 3.

**Table D-B21. GAM output for Deployment 4, Receiver 1**

A. parametric coefficients	Estimate	Std. Error	t-value	p-value
(Intercept)	4.5883	0.0008	5444.7796	< 0.0001
km2	0.0072	0.0057	1.2568	0.2089
km4	0.0113	0.0033	3.4648	0.0005
km10	0.0076	0.0011	6.7575	< 0.0001
B. smooth terms	edf	Ref.df	F-value	p-value
s(sDate)	47.5477	49.0000	114.2021	< 0.0001
s(WaveHeight)	1.0000	1.0000	1.5406	0.2146
s(Windspeed)	4.2631	4.2631	25.2727	< 0.0001
s(CPAmin)	6.8045	6.8045	8.0060	< 0.0001
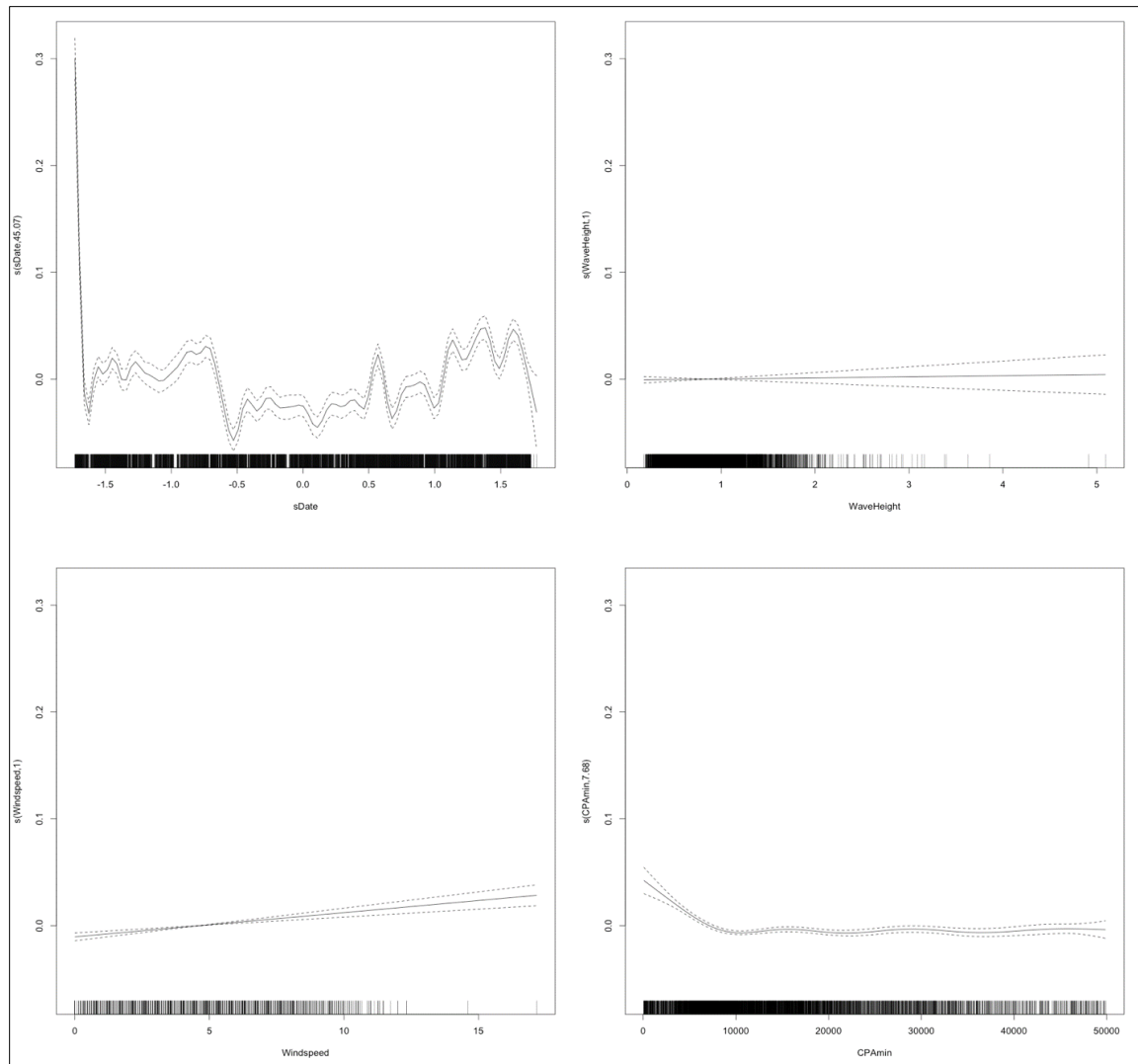
Figure D-B21. SA2 smoothing functions for Measured Vessel Band Noise as a function of Date, Wave Height, Windspeed, and CPA for Receiver 1, Deployment 4.

**Table D-B22. GAM output for Deployment 4, Receiver 2**

A. parametric coefficients	Estimate	Std. Error	t-value	p-value
(Intercept)	4.5883	0.0008	5444.7796	< 0.0001
km2	0.0072	0.0057	1.2568	0.2089
km4	0.0113	0.0033	3.4648	0.0005
km10	0.0076	0.0011	6.7575	< 0.0001
B. smooth terms	edf	Ref.df	F-value	p-value
s(sDate)	47.5477	49.0000	114.2021	< 0.0001
s(WaveHeight)	1.0000	1.0000	1.5406	0.2146
s(Windspeed)	4.2631	4.2631	25.2727	< 0.0001
s(CPAmin)	6.8045	6.8045	8.0060	< 0.0001
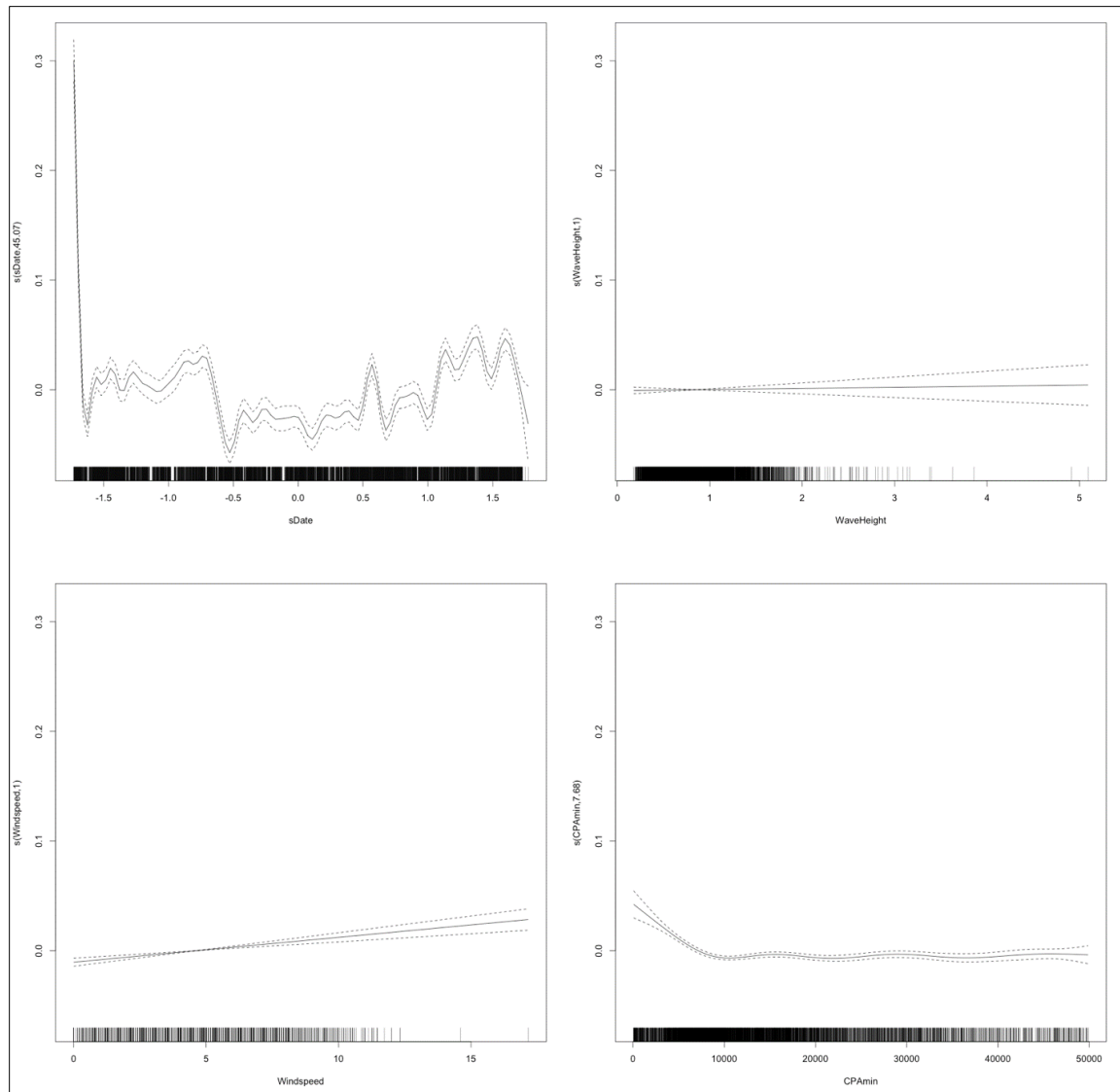
Figure D-B22. SA2 smoothing functions for Measured Vessel Band Noise as a function of Date, Wave Height, Windspeed, and CPA for Receiver 2, Deployment 4.

**Table D-B23. GAM output for Deployment 4, Receiver 3**

A. parametric coefficients	Estimate	Std. Error	t-value	p-value
(Intercept)	4.6453	0.0005	10197.2121	< 0.0001
km2	0.0536	0.0034	15.7011	< 0.0001
km4	0.0282	0.0034	8.2993	< 0.0001
km10	0.0071	0.0020	3.4685	0.0005
B. smooth terms	edf	Ref.df	F-value	p-value
s(sDate)	46.6381	49.0000	168.6880	< 0.0001
s(WaveHeight)	7.4054	7.4054	5.9423	< 0.0001
s(Windspeed)	7.2849	7.2849	28.8772	< 0.0001
s(CPAmin)	1.0000	1.0000	0.0007	0.9788
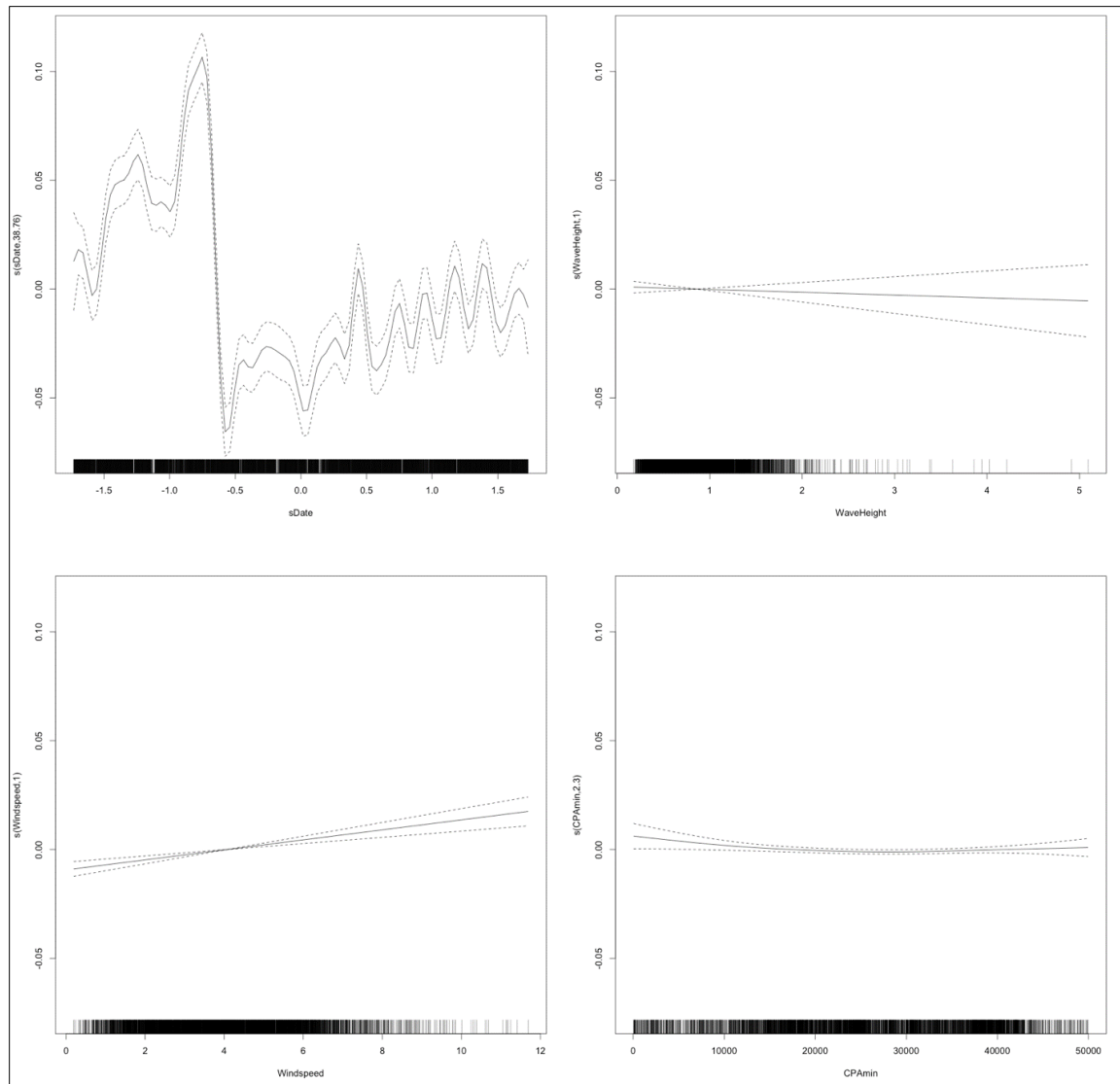
Figure D-B23. SA2 smoothing functions for Measured Vessel Band Noise as a function of Date, Wave Height, Windspeed, and CPA for Receiver 3, Deployment 4.

**Table D-B24. GAM output for Deployment 4, Receiver 4**

A. parametric coefficients	Estimate	Std. Error	t-value	p-value
(Intercept)	4.6076	0.0005	8797.6343	< 0.0001
km2	-0.0005	0.0047	-0.1152	0.9083
km4	-0.0036	0.0030	-1.2038	0.2287
km10	0.0024	0.0015	1.5669	0.1172
B. smooth terms	edf	Ref.df	F-value	p-value
s(sDate)	47.2705	49.0000	212.8172	< 0.0001
s(WaveHeight)	3.1221	3.1221	7.1035	0.0001
s(Windspeed)	7.3690	7.3690	12.5711	< 0.0001
s(CPAmin)	7.3001	7.3001	8.8686	< 0.0001
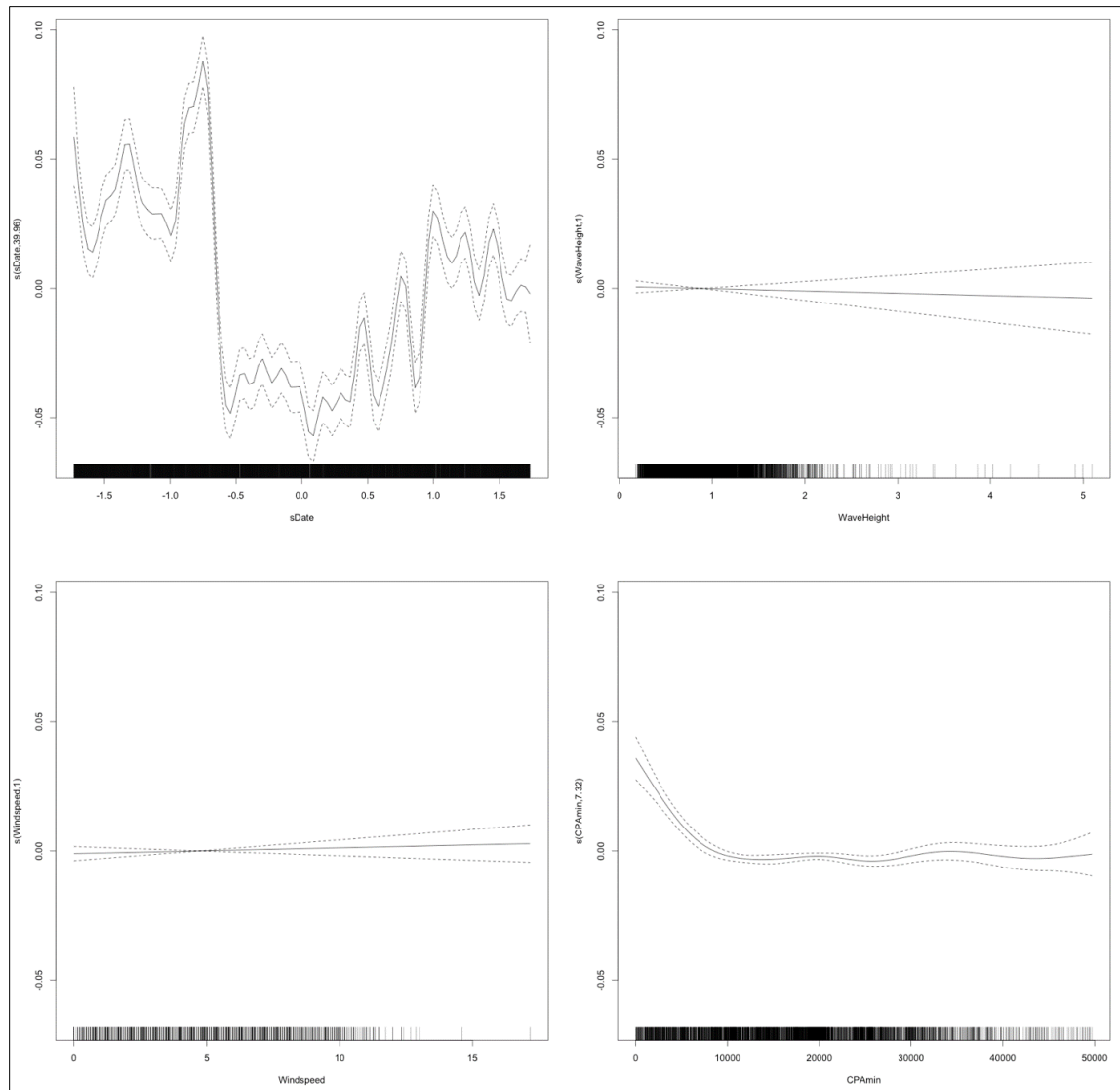
Figure D-B24. SA2 smoothing functions for Measured Vessel Band Noise as a function of Date, Wave Height, Windspeed, and CPA for Receiver 4, Deployment 4.

**Table D-B25. GAM output for Deployment 4, Receiver 5**

A. parametric coefficients	Estimate	Std. Error	t-value	p-value
(Intercept)	4.6397	0.0008	6059.5104	< 0.0001
km2	0.0037	0.0048	0.7645	0.4446
km4	0.0031	0.0032	0.9704	0.3319
km10	0.0034	0.0010	3.3206	0.0009
B. smooth terms	edf	Ref.df	F-value	p-value
s(sDate)	47.9023	49.0000	271.6773	< 0.0001
s(WaveHeight)	3.0305	3.0305	12.5542	< 0.0001
s(Windspeed)	2.7783	2.7783	12.3704	< 0.0001
s(CPAmin)	5.1568	5.1568	4.8082	0.0002
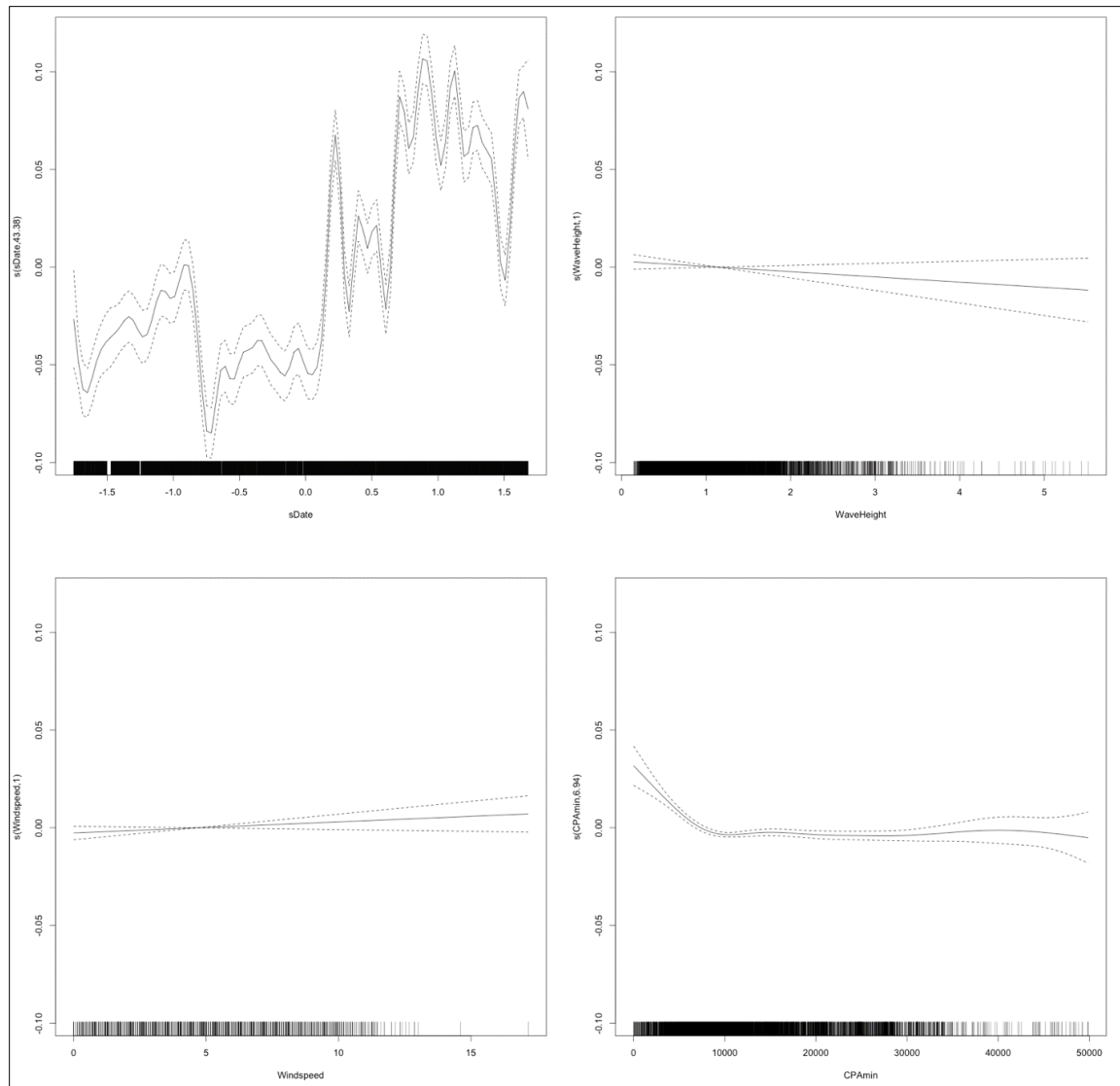
Figure D-B25. SA2 smoothing functions for Measured Vessel Band Noise as a function of Date, Wave Height, Windspeed, and CPA for Receiver 5, Deployment 4.

**Table D-B26. GAM output for Deployment 4, Receiver 6**

A. parametric coefficients	Estimate	Std. Error	t-value	p-value
(Intercept)	4.6020	0.0006	7347.5126	< 0.0001
km2	0.0220	0.0071	3.0808	0.0021
km4	0.0119	0.0032	3.7137	0.0002
km10	0.0032	0.0012	2.6970	0.0070
B. smooth terms	edf	Ref.df	F-value	p-value
s(sDate)	46.0139	49.0000	24.7882	< 0.0001
s(WaveHeight)	2.4235	2.4235	30.6503	< 0.0001
s(Windspeed)	2.5259	2.5259	300.8994	< 0.0001
s(CPAmin)	8.5607	8.5607	26.0196	< 0.0001
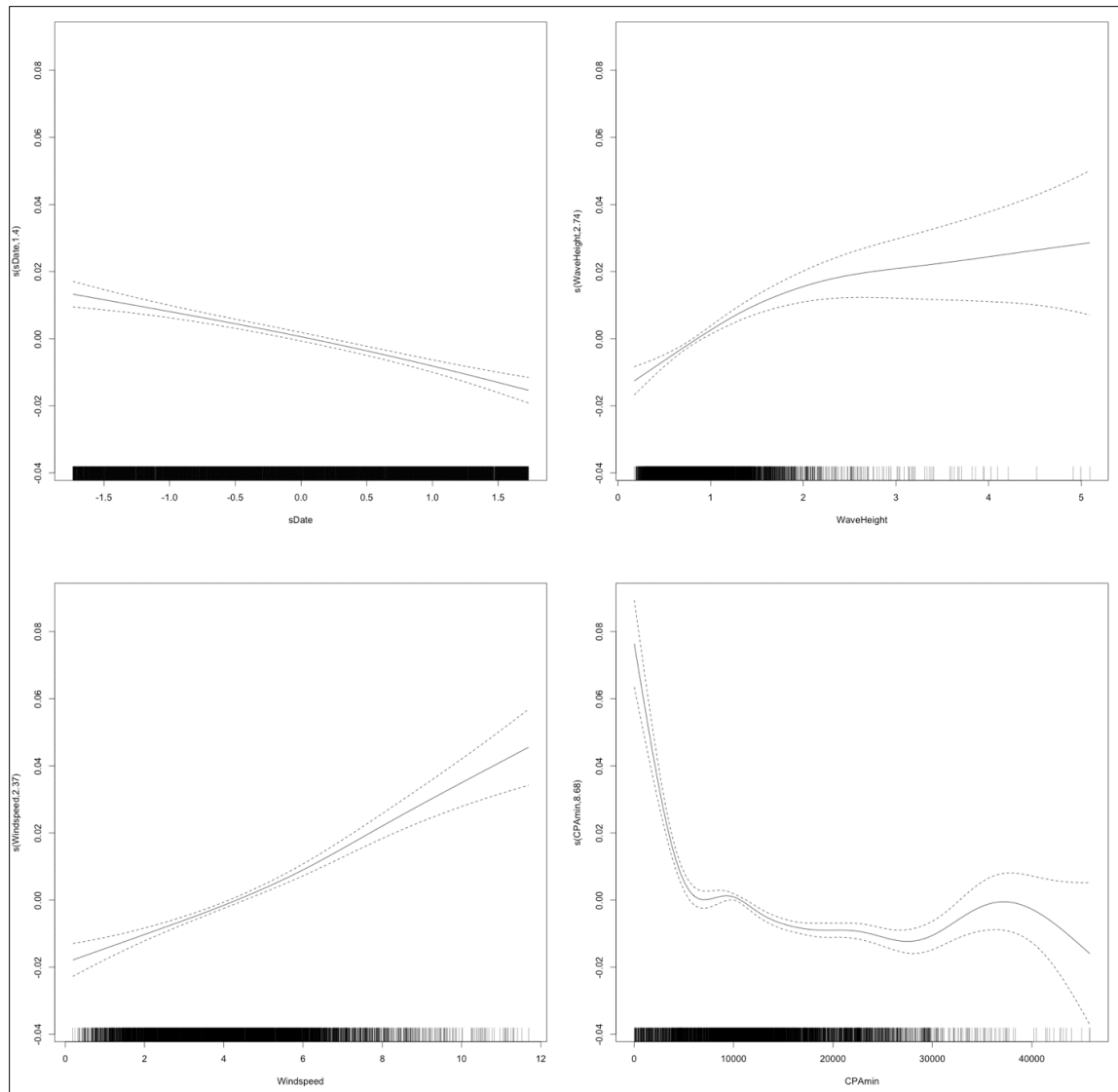
Figure D-B26. SA2 smoothing functions for Measured Vessel Band Noise as a function of Date, Wave Height, Windspeed, and CPA for Receiver 6, Deployment 4.

Table D-B27. GAM output for Deployment 4, Receiver 7

A. parametric coefficients	Estimate	Std. Error	t-value	p-value
(Intercept)	4.6381	0.0012	3768.9476	< 0.0001
km2	0.0031	0.0029	1.0720	0.2838
km4	0.0084	0.0012	7.1174	< 0.0001
km10	0.0051	0.0006	9.1537	< 0.0001
B. smooth terms	edf	Ref.df	F-value	p-value
s(sDate)	37.6492	49.0000	7.4021	< 0.0001
s(WaveHeight)	7.2361	7.2361	10.7915	< 0.0001
s(Windspeed)	1.0000	1.0000	166.2904	< 0.0001
s(CPAmin)	8.2418	8.2418	57.0747	< 0.0001
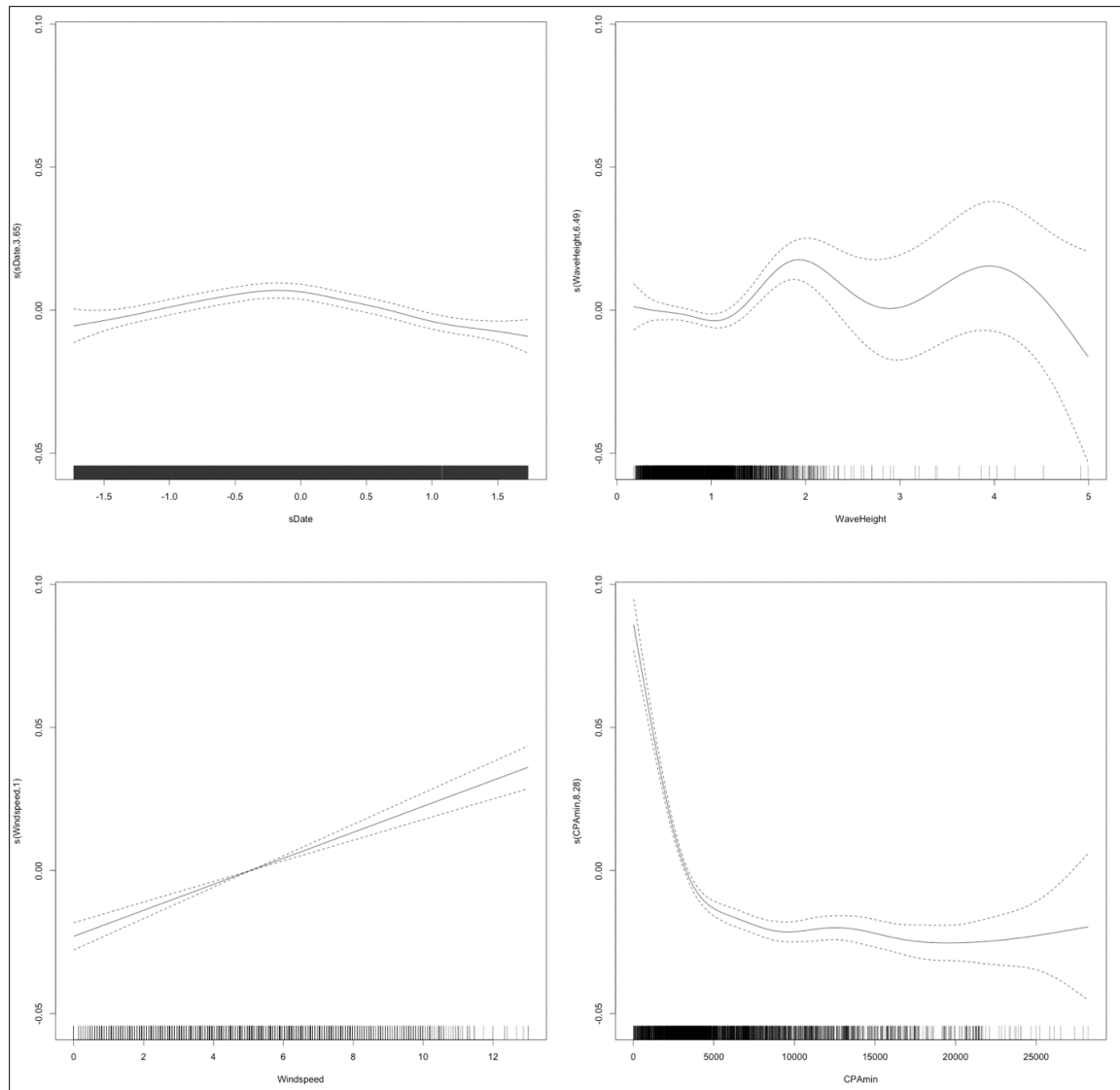
Figure D-B27. SA2 smoothing functions for Measured Vessel Band Noise as a function of Date, Wave Height, Windspeed, and CPA for Receiver 7, Deployment 4.

Table D-B28. GAM output for Deployment 4, Receiver 8

A. parametric coefficients	Estimate	Std. Error	t-value	p-value
(Intercept)	4.6186	0.0008	5639.2788	< 0.0001
km2	0.0018	0.0024	0.7633	0.4453
km4	0.0085	0.0017	4.8952	< 0.0001
km10	-0.0014	0.0006	-2.2015	0.0277
B. smooth terms	edf	Ref.df	F-value	p-value
s(sDate)	47.0673	49.0000	251.8503	< 0.0001
s(WaveHeight)	1.0000	1.0000	1.1667	0.2801
s(Windspeed)	5.2050	5.2050	16.3722	< 0.0001
s(CPAmin)	5.9901	5.9901	35.8062	< 0.0001
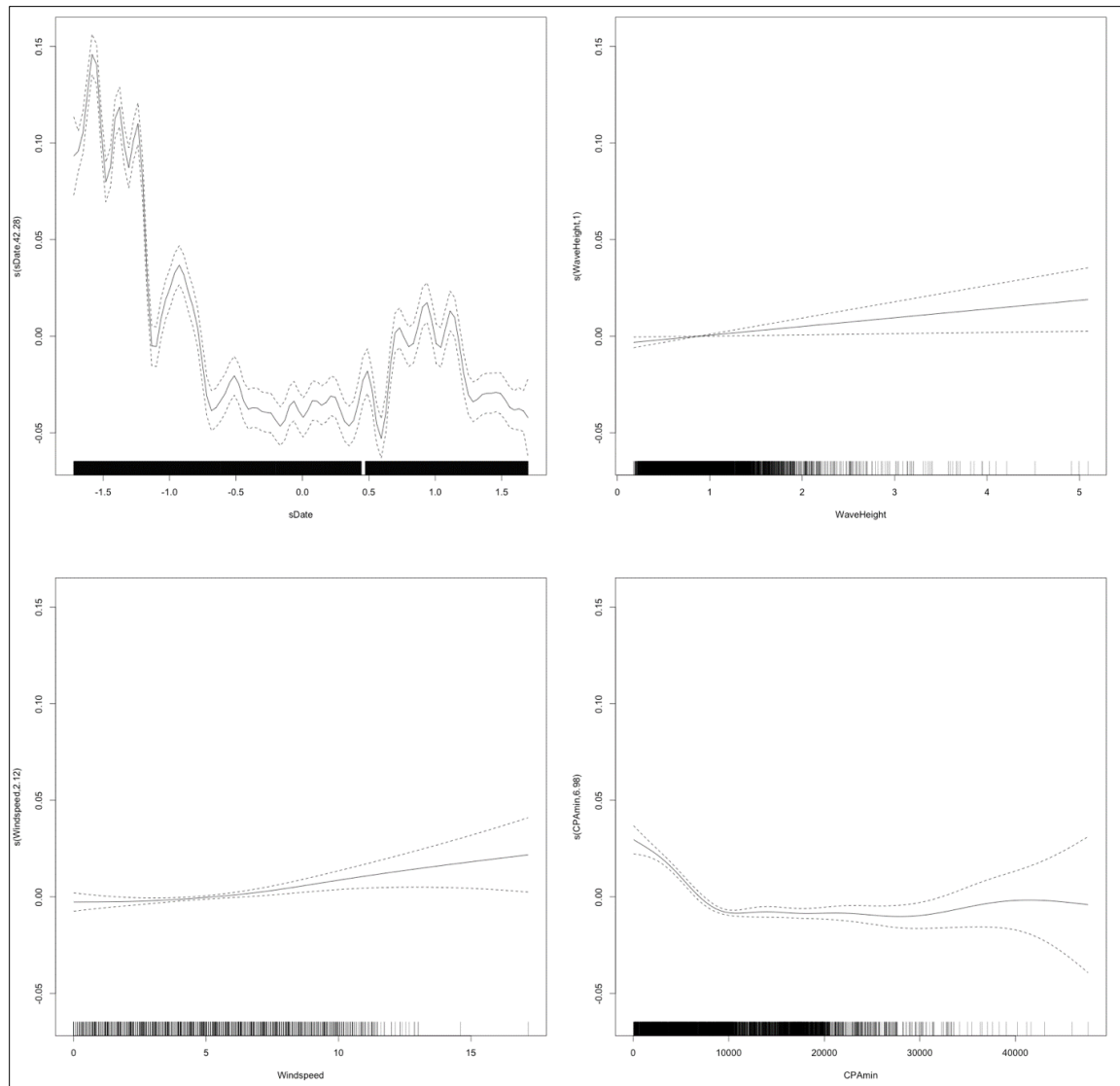
Figure D-B28. SA2 smoothing functions for Measured Vessel Band Noise as a function of Date, Wave Height, Windspeed, and CPA for Receiver 8, Deployment 4.

Table D-B29. GAM output for Deployment 4, Receiver 9

A. parametric coefficients	Estimate	Std. Error	t-value	p-value
(Intercept)	4.6668	0.0007	6413.5372	< 0.0001
km2	0.0138	0.0025	5.5763	< 0.0001
km4	0.0078	0.0023	3.3444	0.0008
km10	0.0011	0.0008	1.4499	0.1471
B. smooth terms	edf	Ref.df	F-value	p-value
s(sDate)	45.0765	49.0000	137.3508	< 0.0001
s(WaveHeight)	5.2936	5.2936	10.9832	< 0.0001
s(Windspeed)	1.0000	1.0000	7.0446	0.0080
s(CPAmin)	1.0000	1.0000	8.9335	0.0028
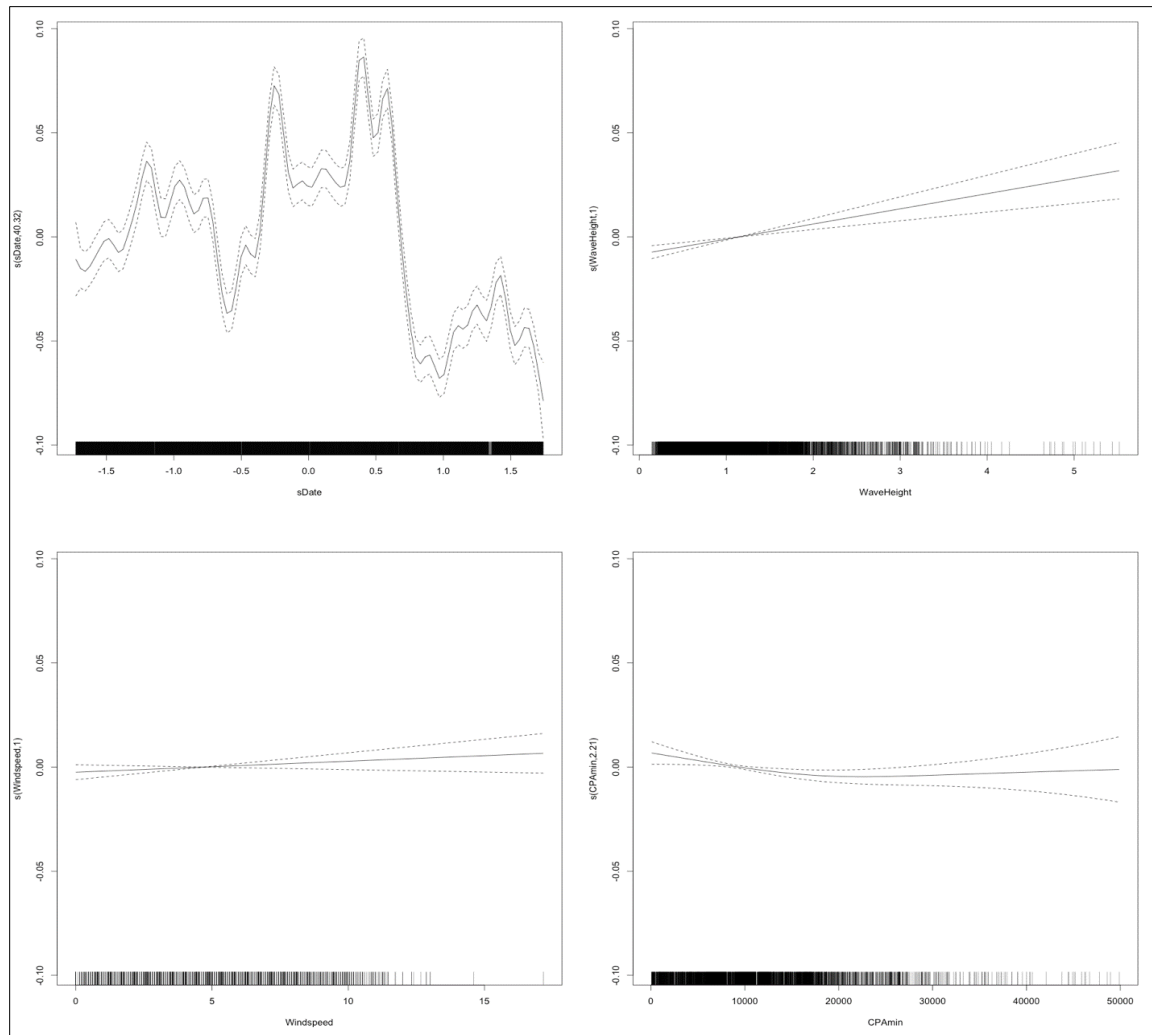
Figure D-B29. SA2 smoothing functions for Measured Vessel Band Noise as a function of Date, Wave Height, Windspeed, and CPA for Receiver 9, Deployment 4.

Table D-B30. GAM output for Deployment 4, Receiver 10

A. parametric coefficients	Estimate	Std. Error	t-value	p-value
(Intercept)	4.5756	0.0007	6719.7106	< 0.0001
km2	0.0333	0.0078	4.2686	< 0.0001
km4	0.0381	0.0074	5.1250	< 0.0001
km10	0.0143	0.0040	3.6062	0.0003
B. smooth terms	edf	Ref.df	F-value	p-value
s(sDate)	45.9727	49.0000	46.9735	< 0.0001
s(WaveHeight)	1.0000	1.0000	0.9119	0.3397
s(Windspeed)	1.6279	1.6279	1.9398	0.1033
s(CPAmin)	1.0000	1.0000	3.0621	0.0802
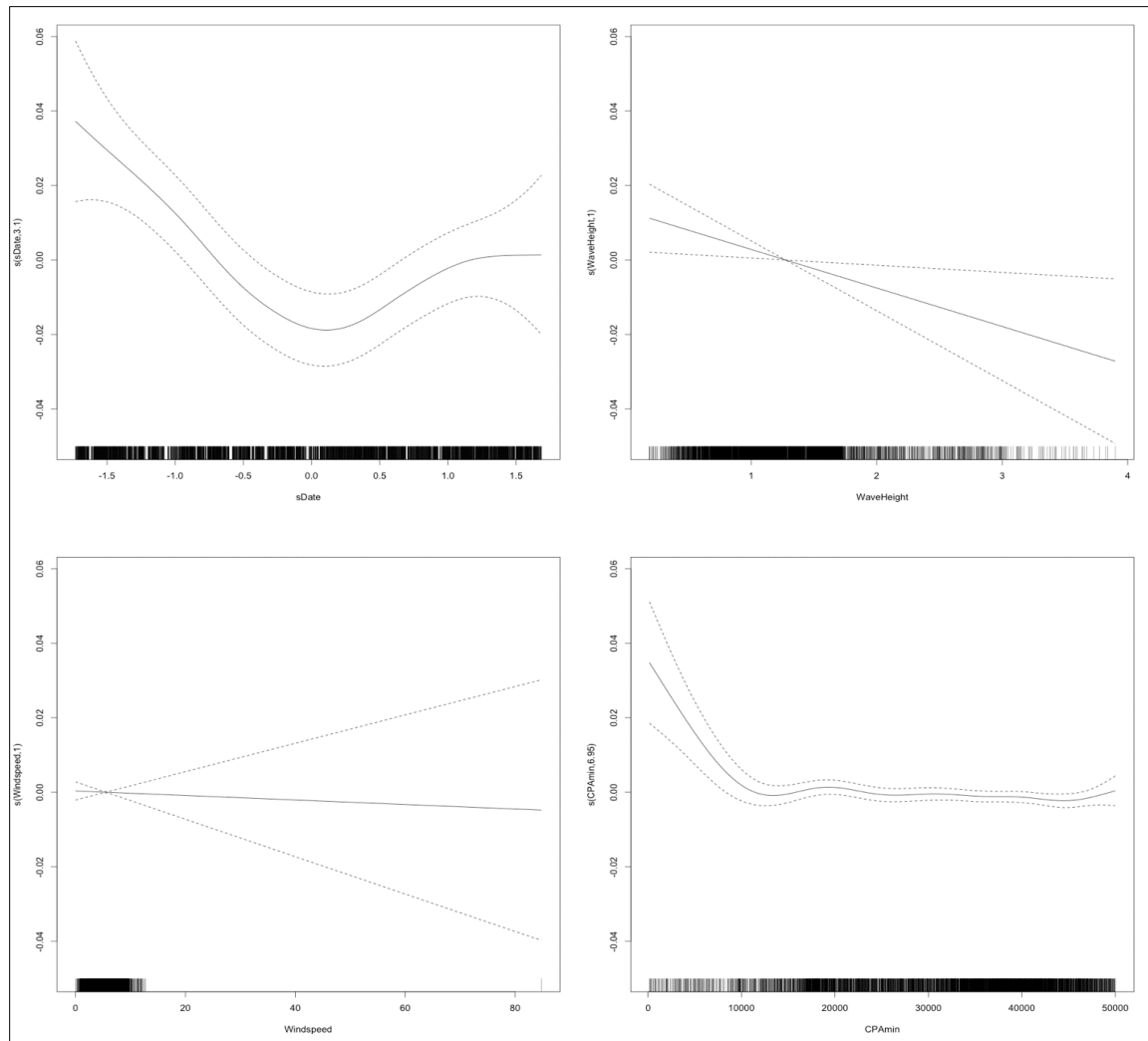
Figure D-B30. SA2 smoothing functions for Measured Vessel Band Noise as a function of Date, Wave Height, Windspeed, and CPA for Receiver 10, Deployment 4.

Appendix D-C: Spatial and Temporal Spectral Trends in RH and EARS Recorded Data

These **Appendix D-C** figures depict the temporal and spatial spectral levels recorded at the RH and EARS Sites 1 through 10 during the deployments that occurred from 2018 through early 2020. In each monthly figure, the solid lines represent the sites where RH recorders were deployed (Sites 1, 3, 6, 7, and 9), while the dashed lines represent the sites where EARS recorders were deployed (Sites 2, 4, 5, 8, and 10). The top spectrum in each of these **Appendix D-C** figures represents the entire frequency range, while the bottom panel presents the LF band (10 to 1,000 Hz) in more detail.
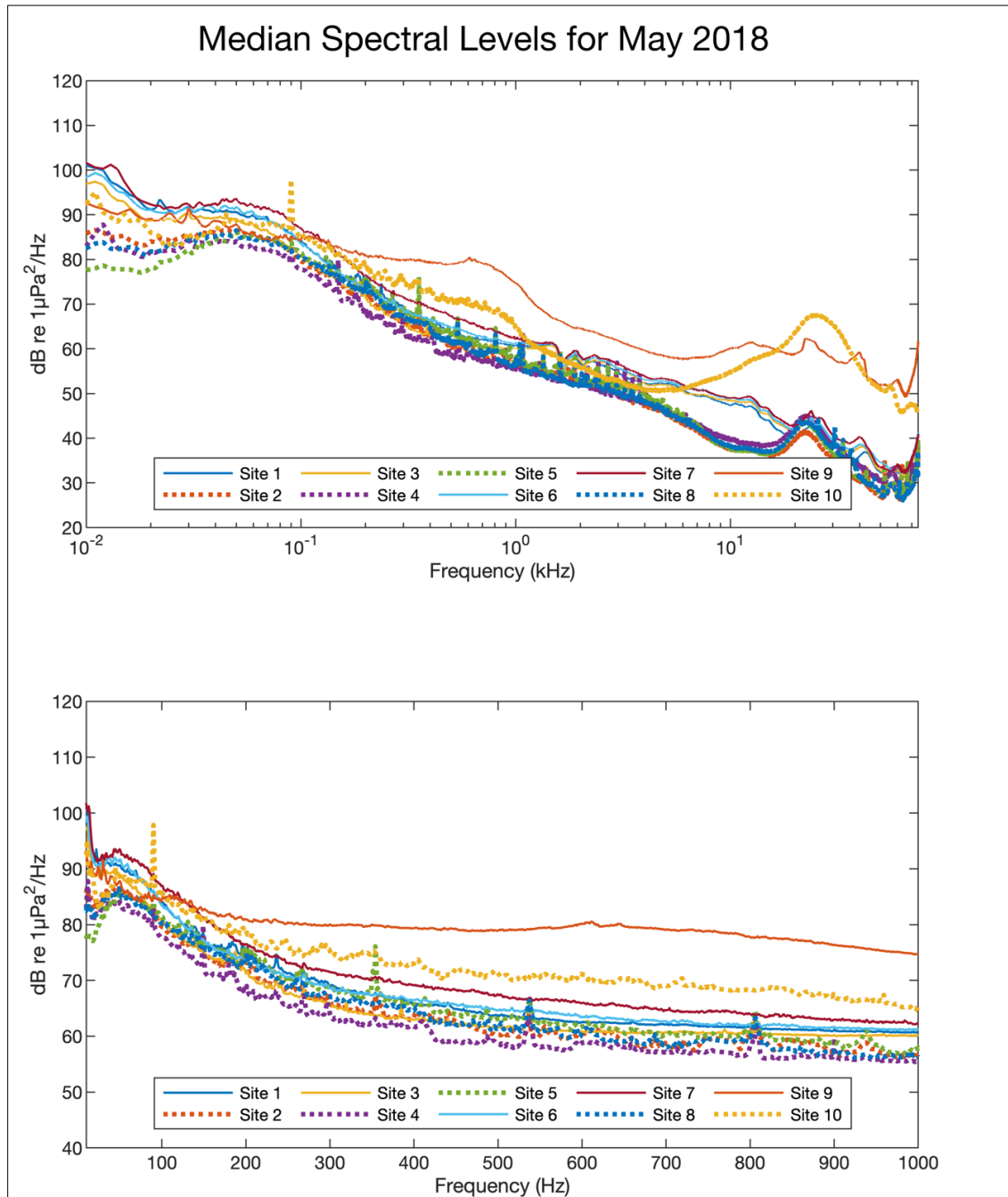

Figure D-C1. Median spectral values for May 2018.

313
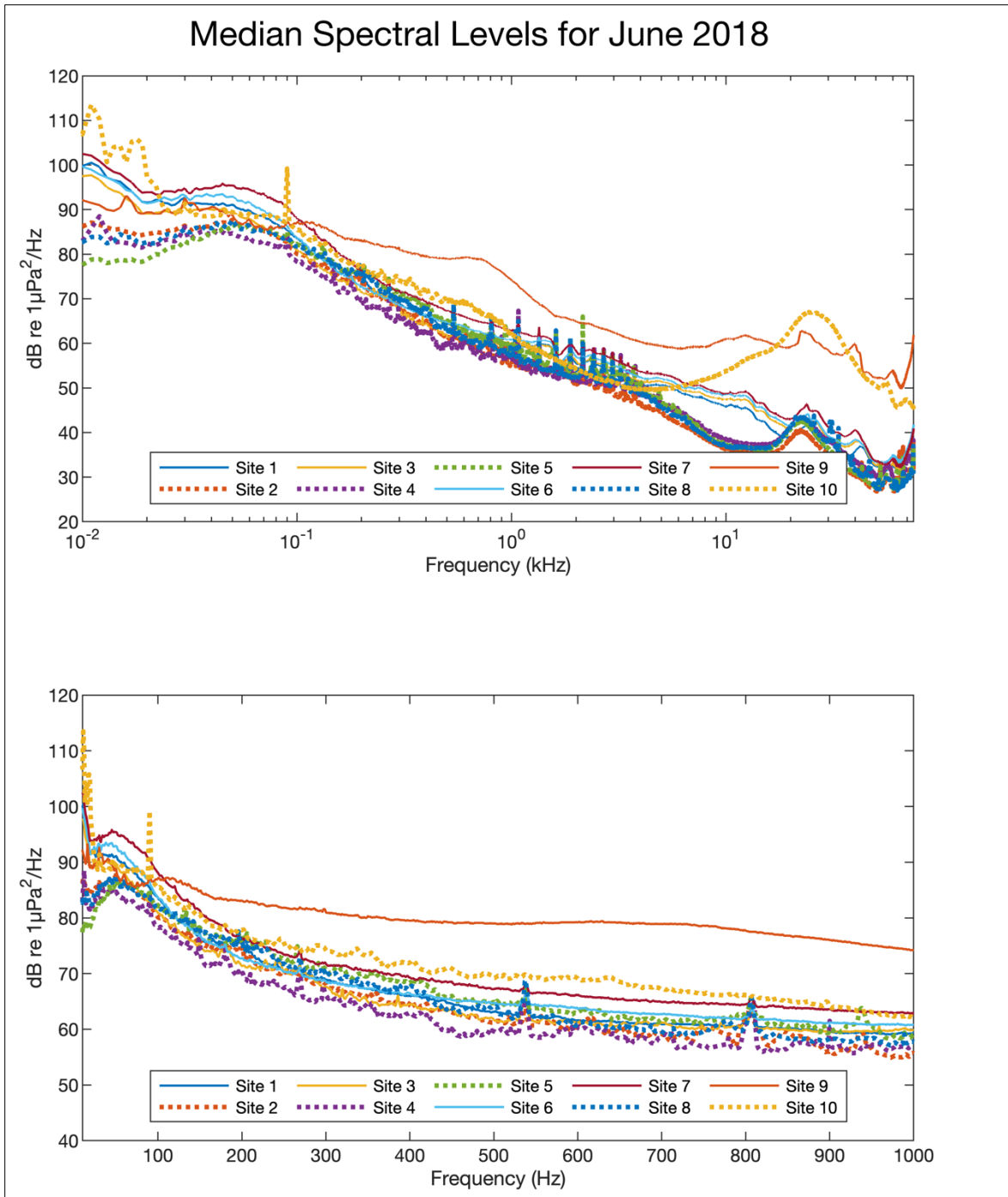
Figure D-C2. Median spectral values for June 2018.
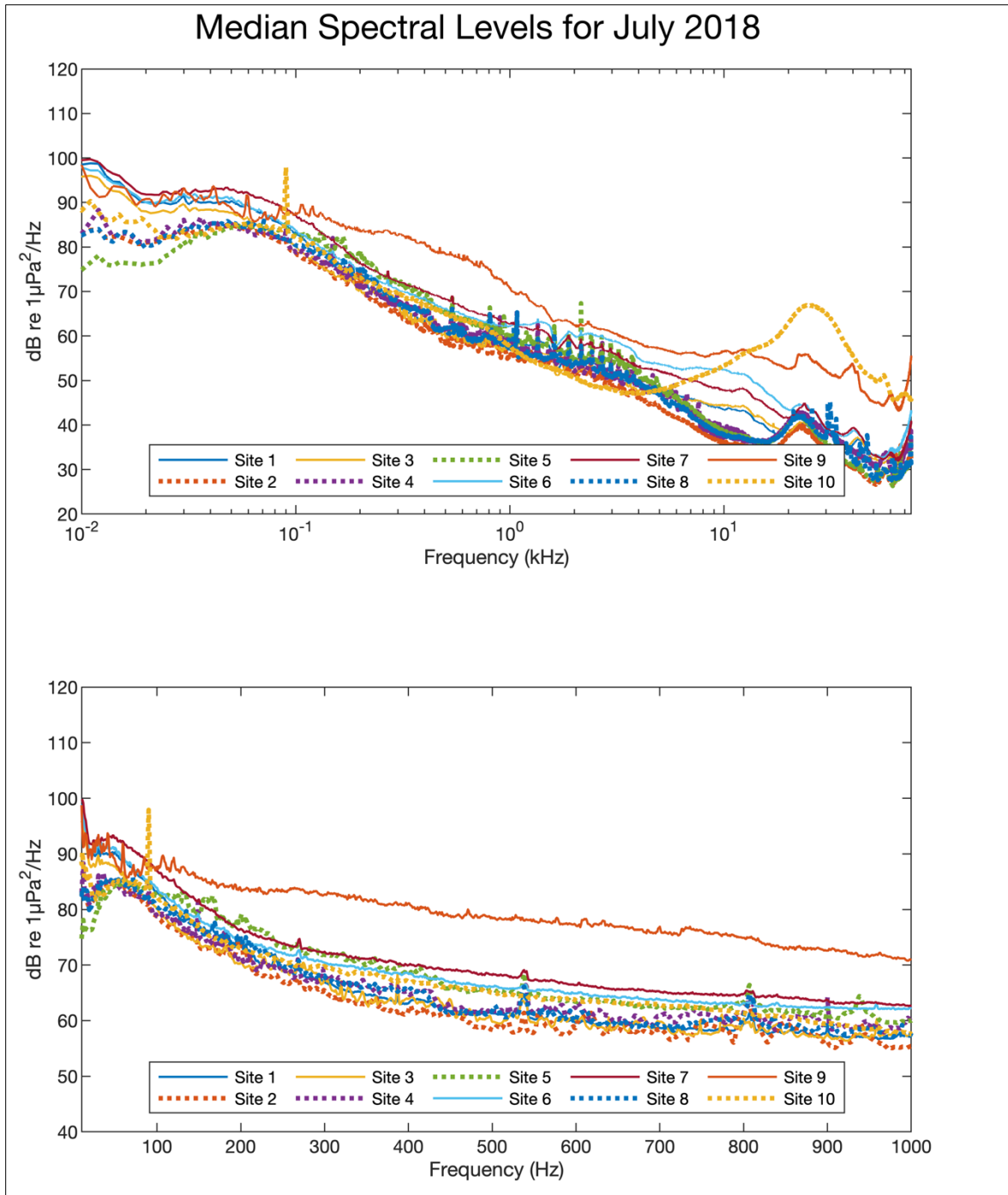
Figure D-C3. Median spectral values for July 2018.
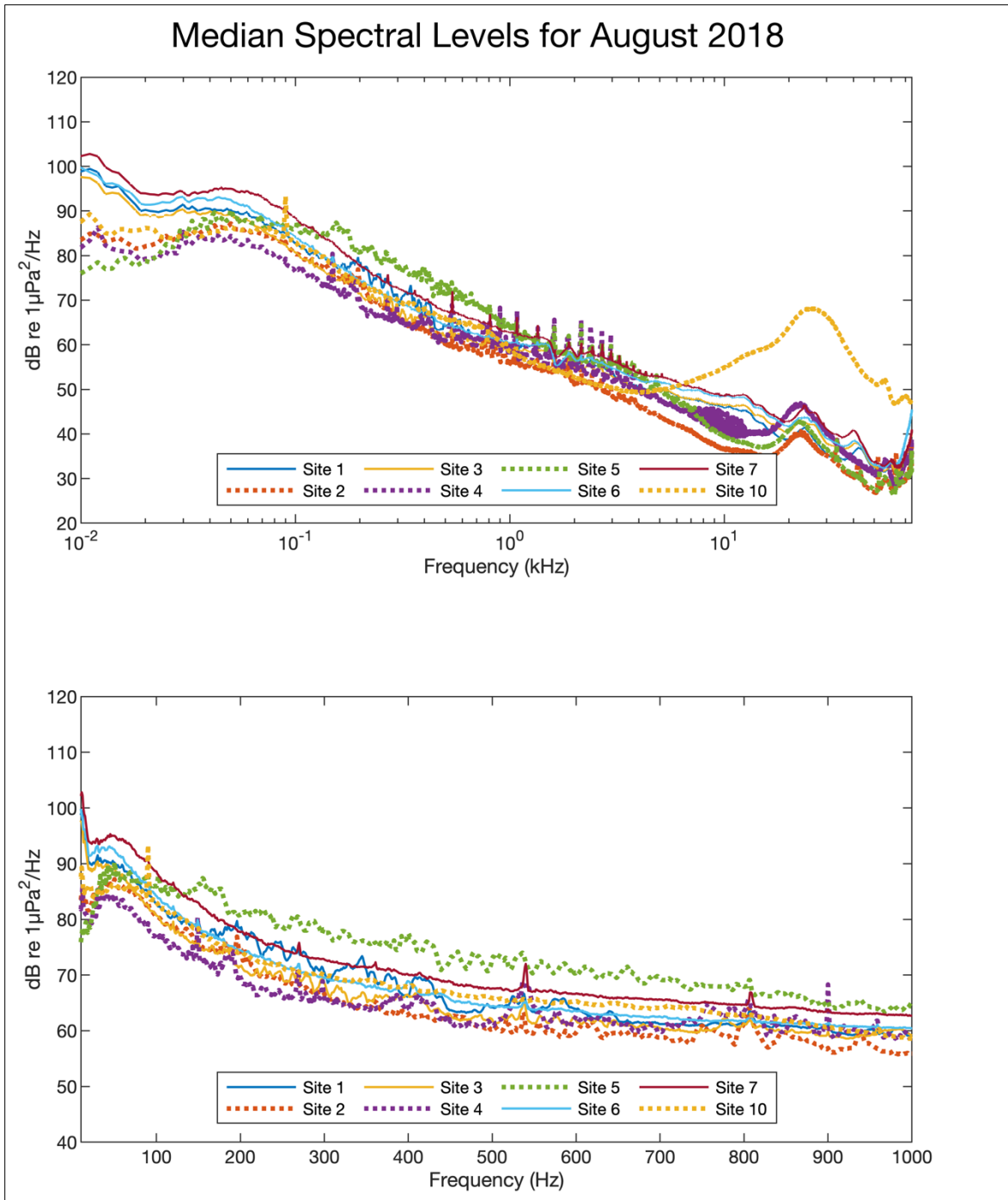
Figure D-C4. Median spectral values for August 2018.
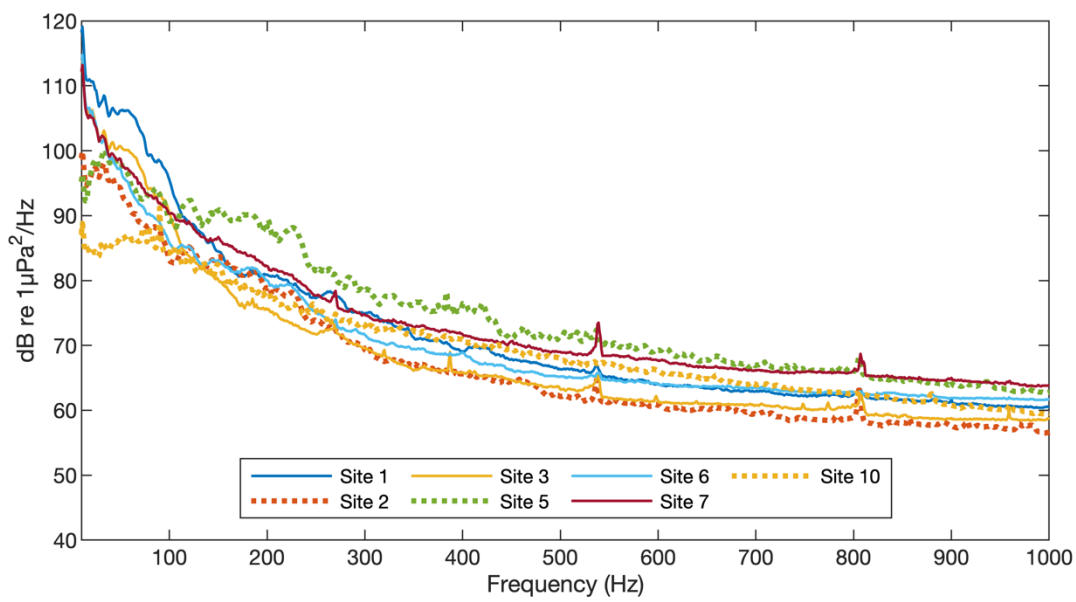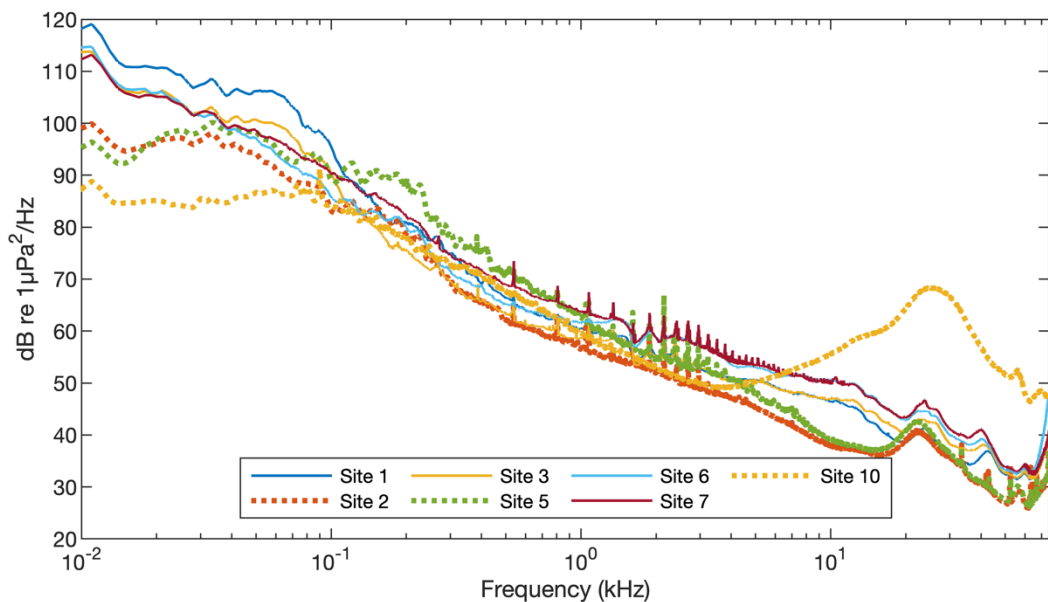
**Figure D-C5. Median spectral values for September 2018.**
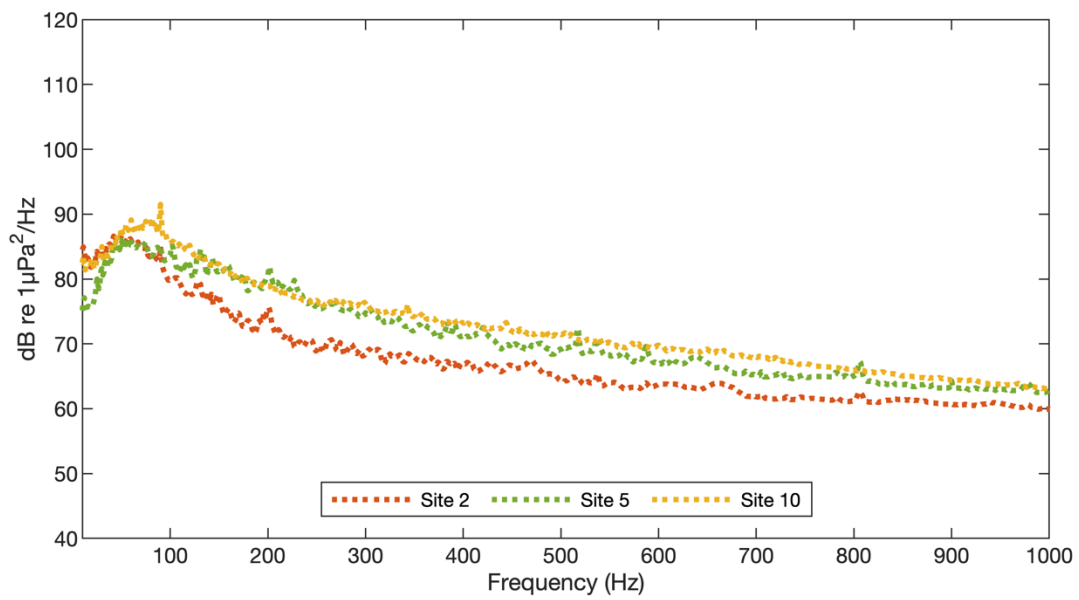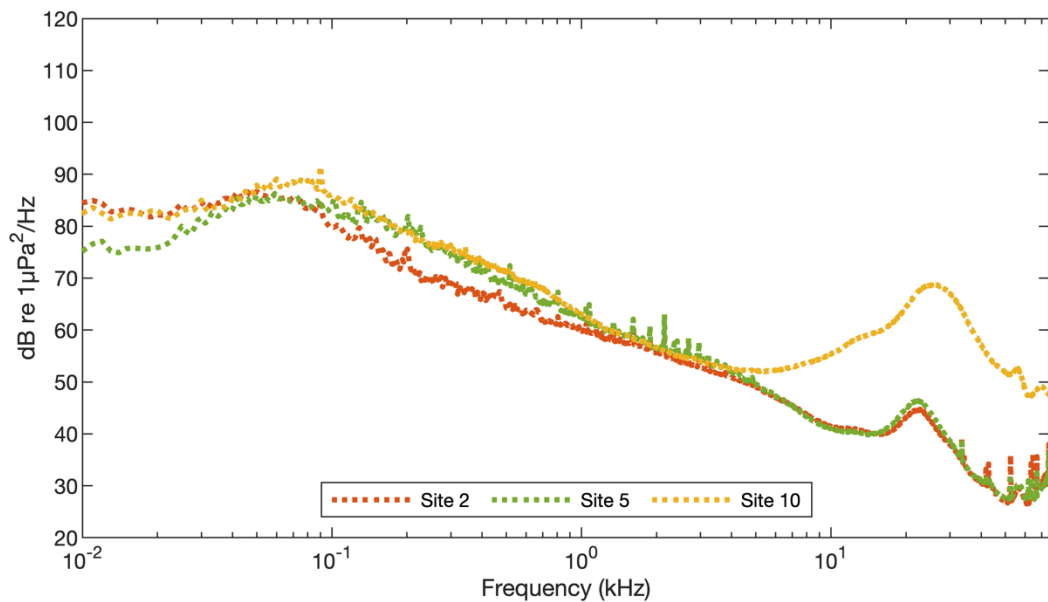
Figure D-C6. Median spectral values for October 2018.
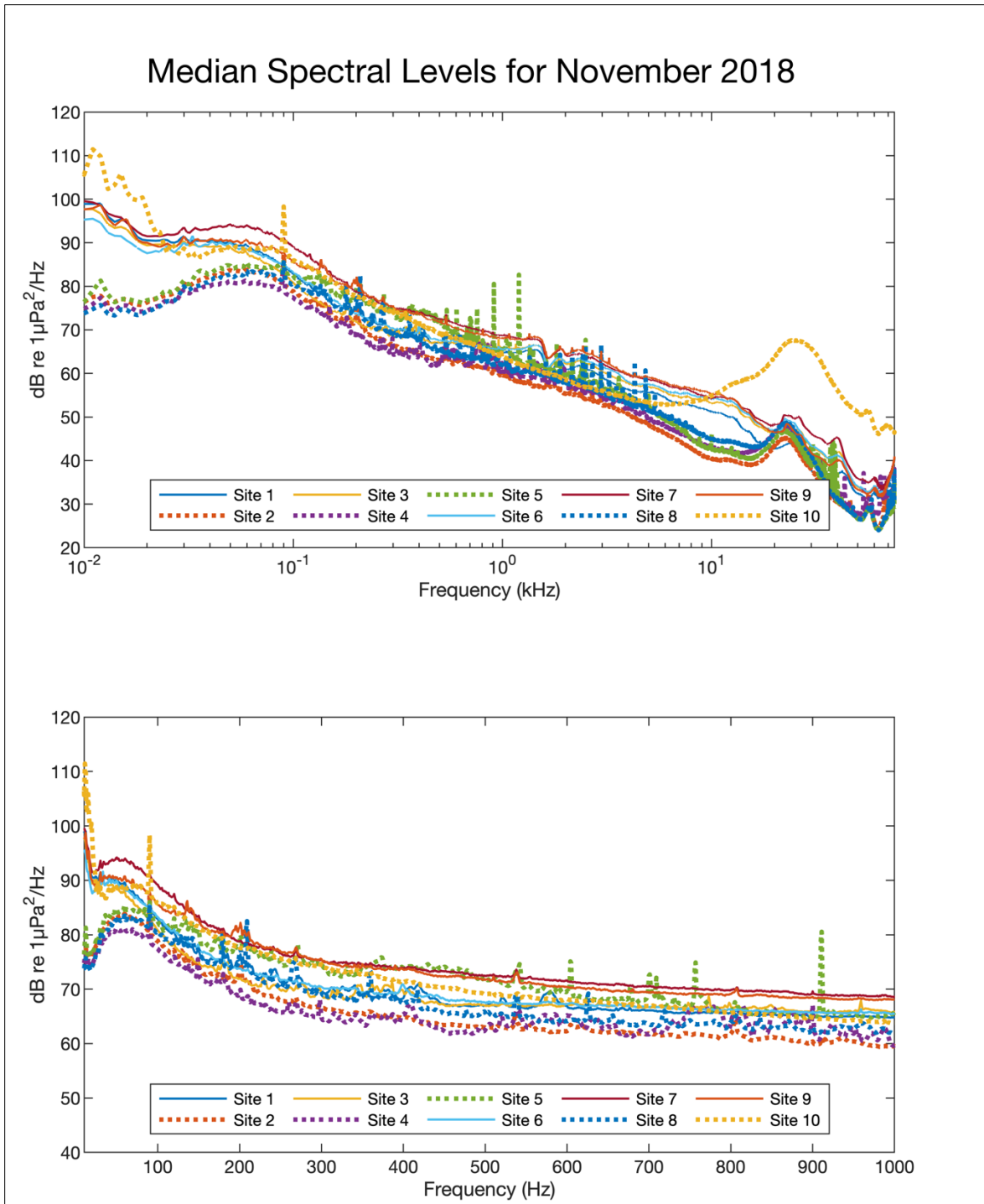
Figure D-C7. Median spectral values for November 2018.
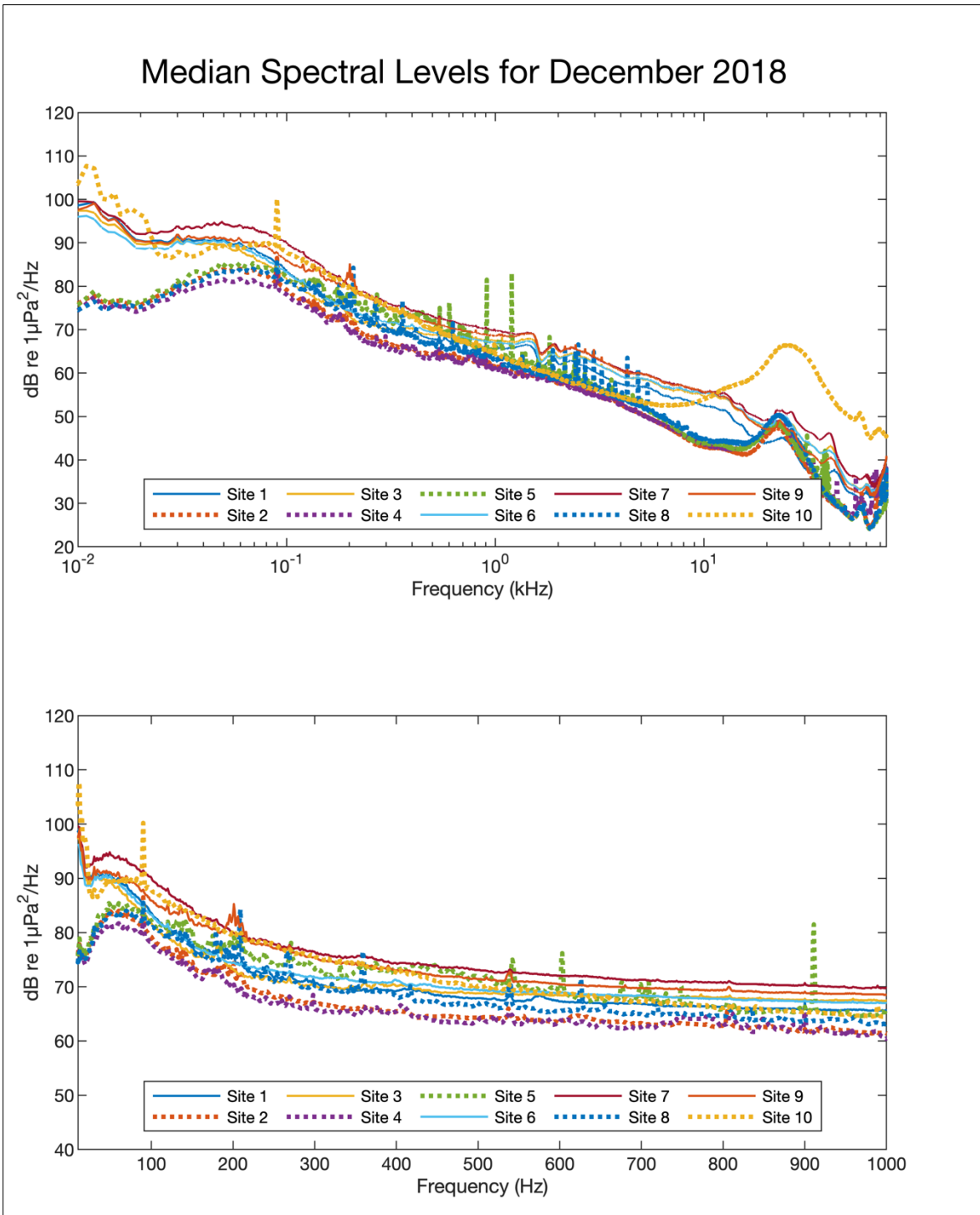
Figure D-C8. Median spectral values for December 2018.
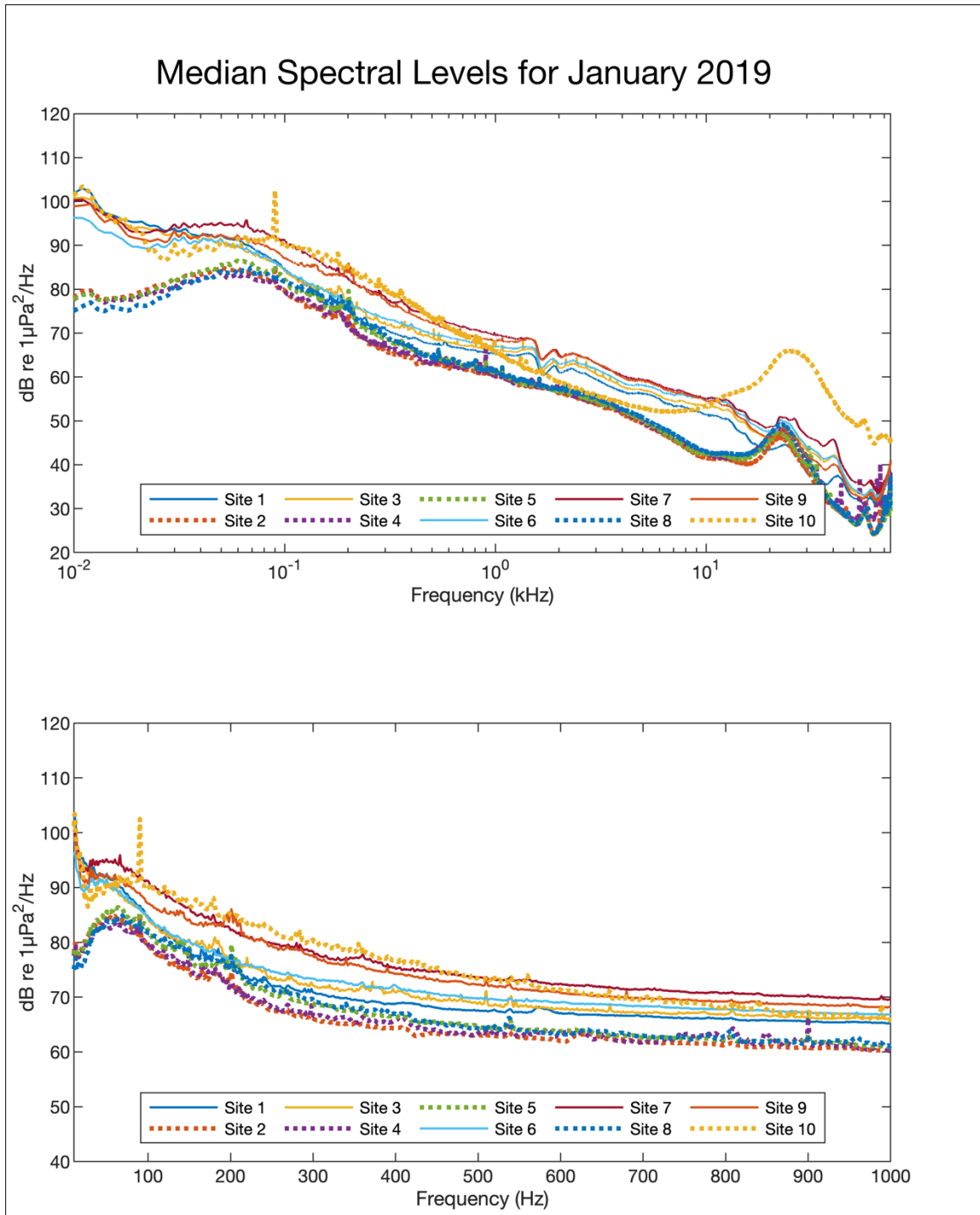
Figure D-C9. Median spectral values for January 2019.
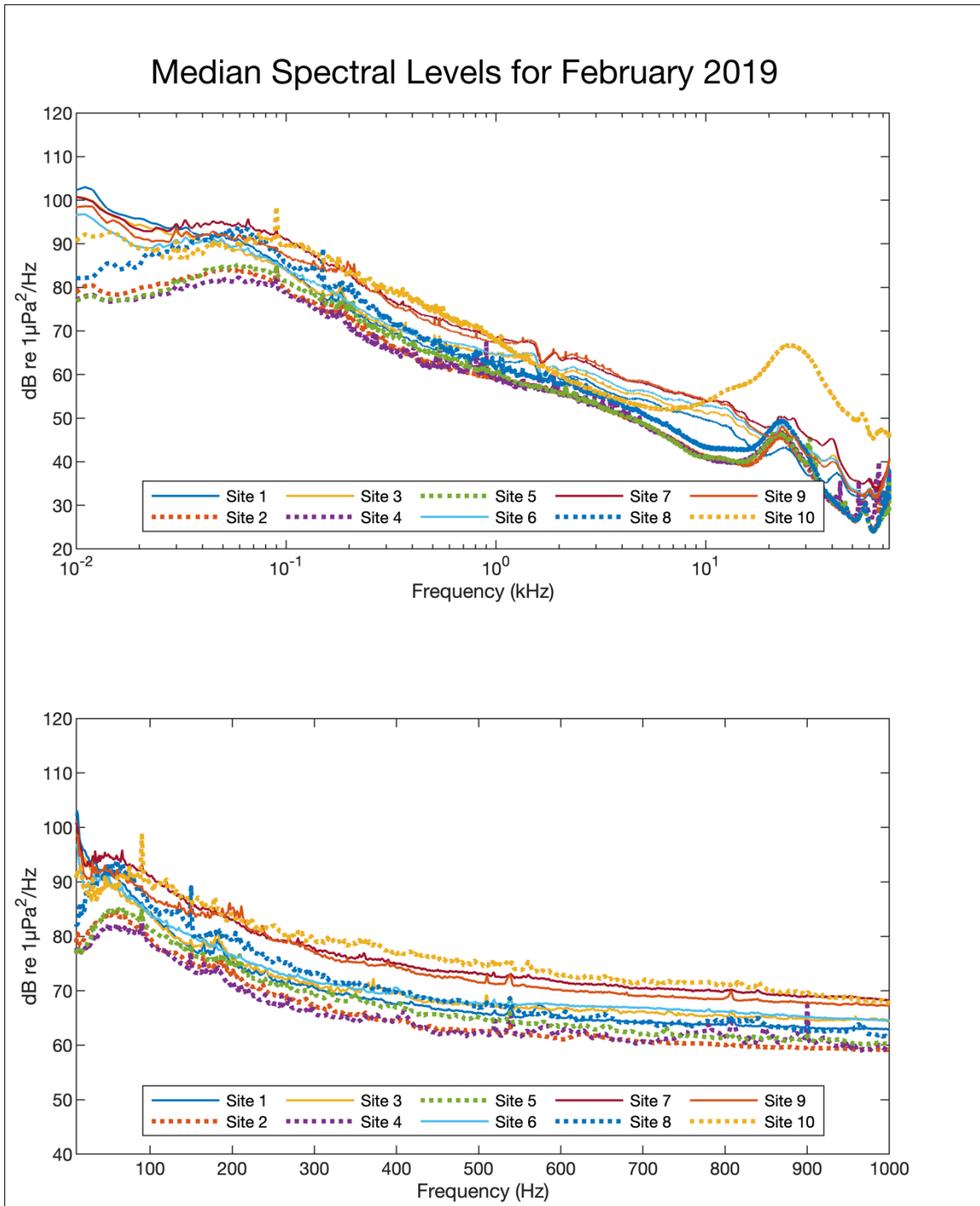
Figure D-C10. Median spectral values for February 2019.
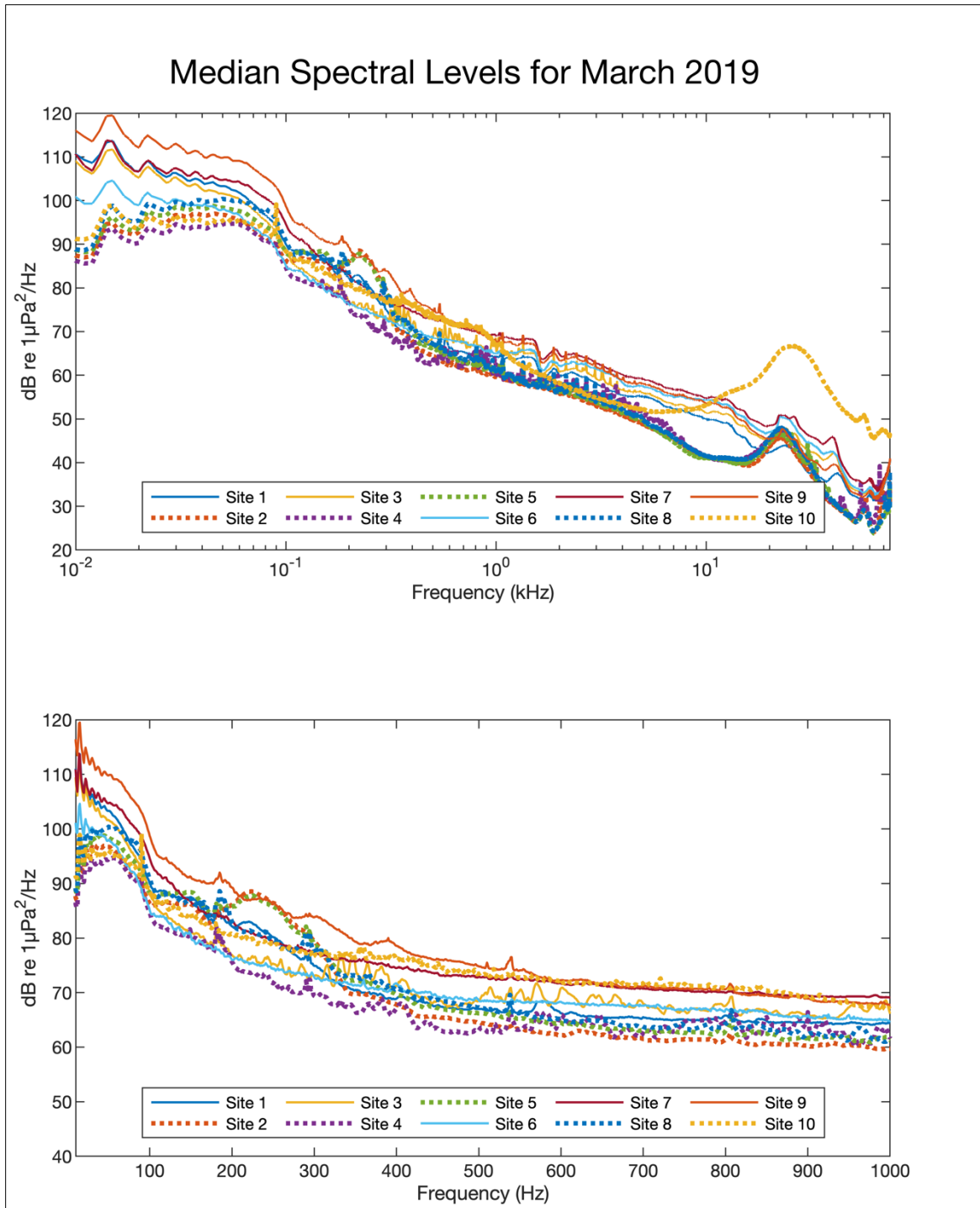
Figure D-C11. Median spectral values for March 2019.
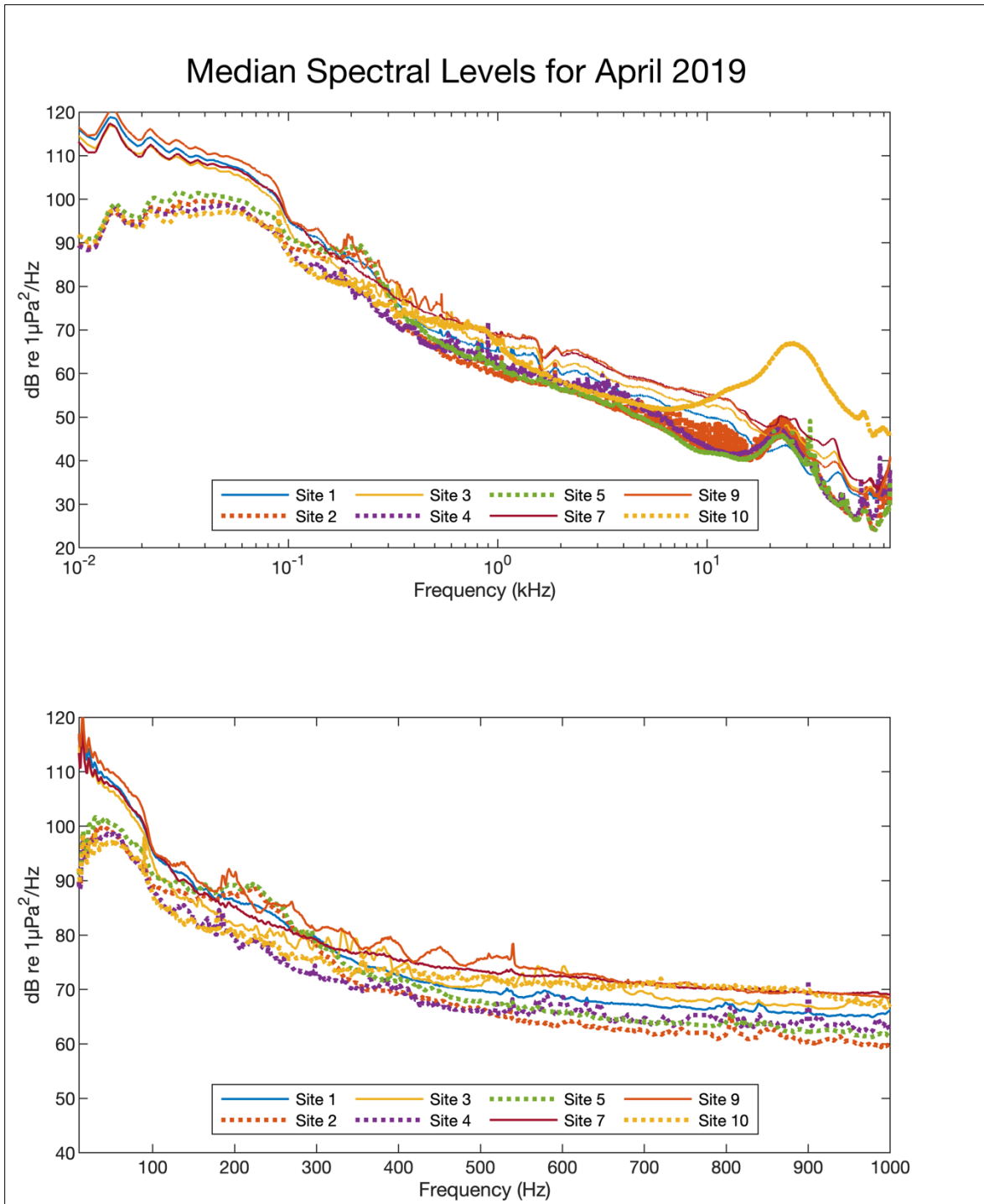
Figure D-C12. Median spectral values for April 2019.
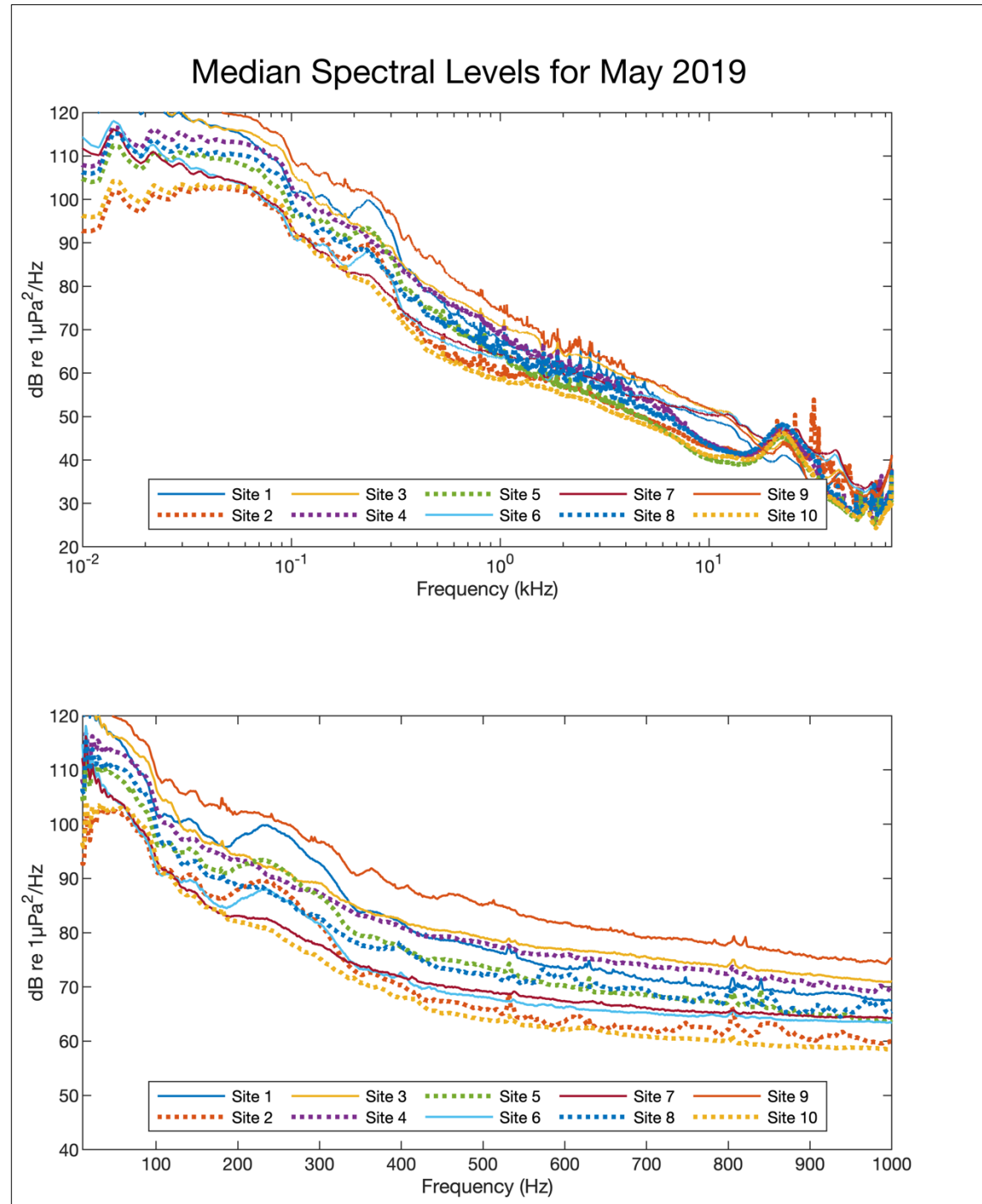
Figure D-C13. Median spectral values for May 2019.
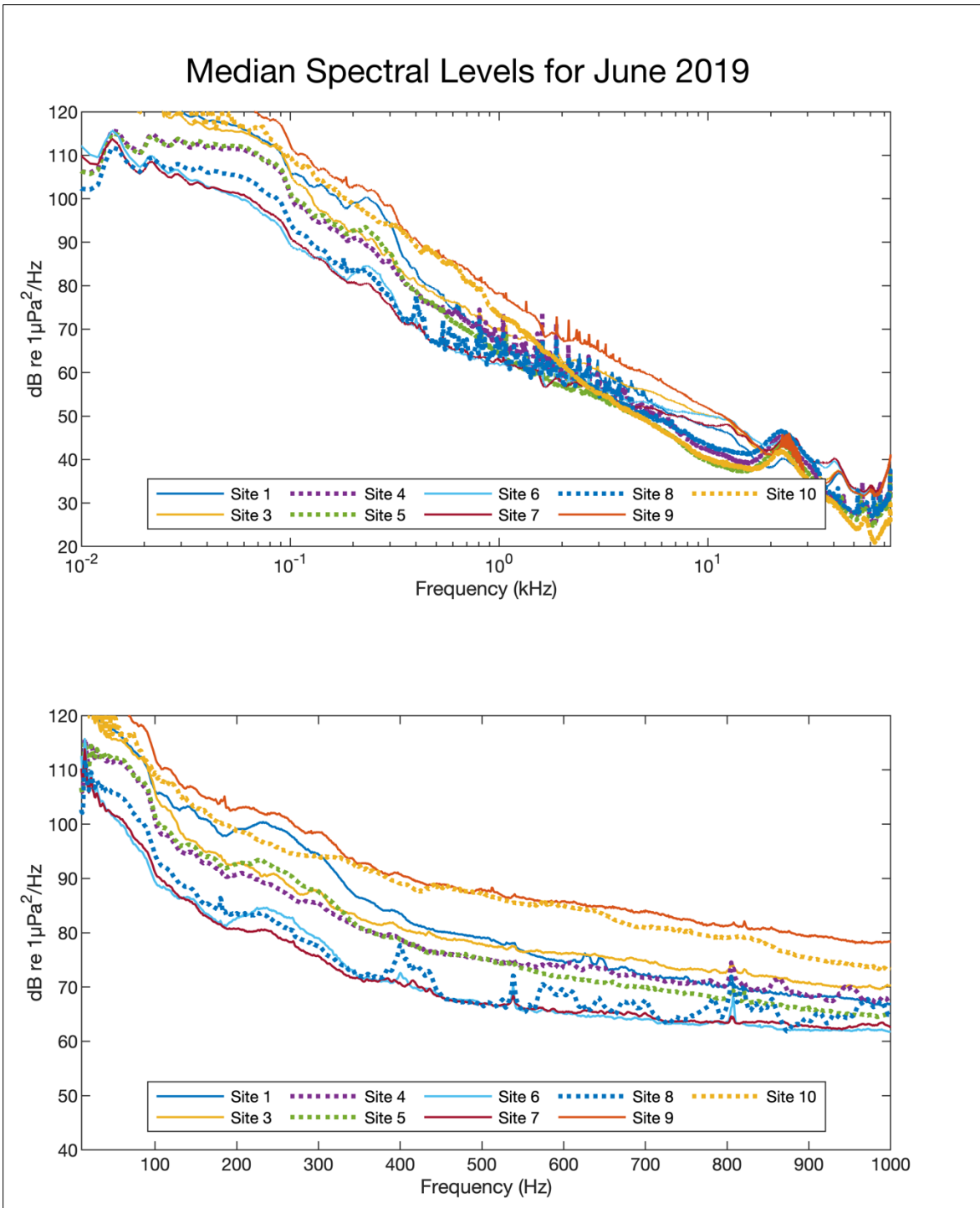
Figure D-C14. Median spectral values for June 2019.
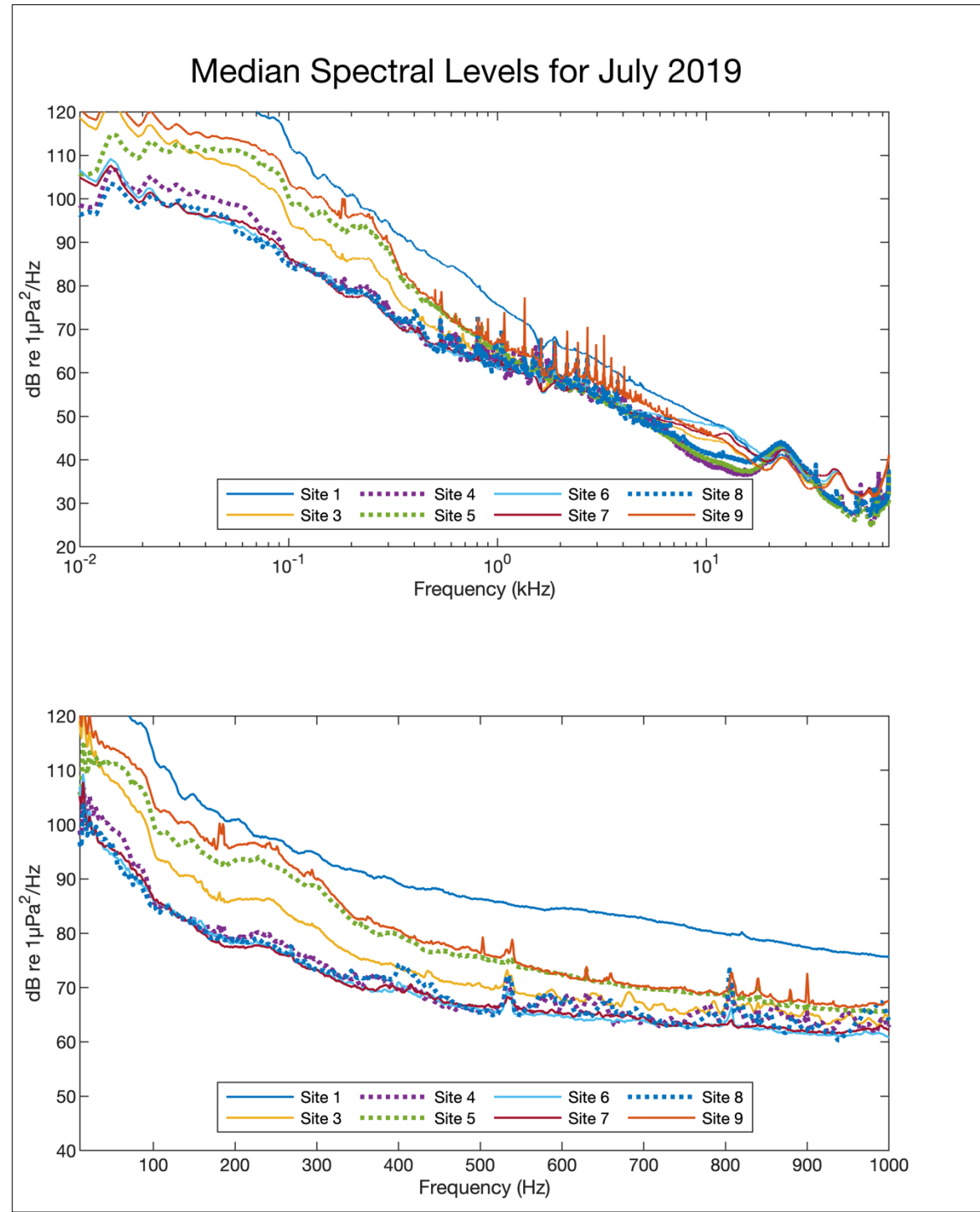
Figure D-C15. Median spectral values for July 2019.
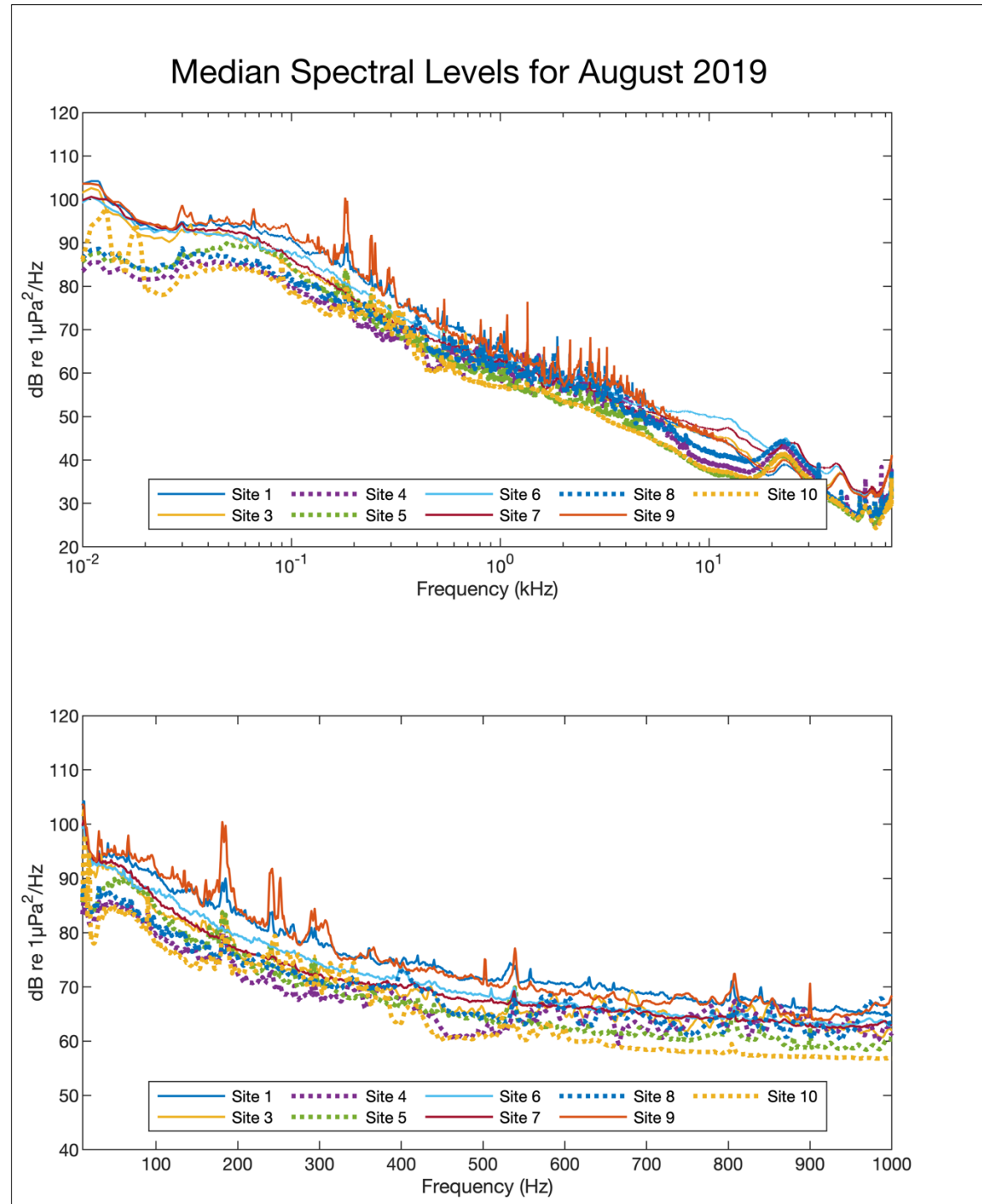
**Figure D-C16. Median spectral values for August 2019.**
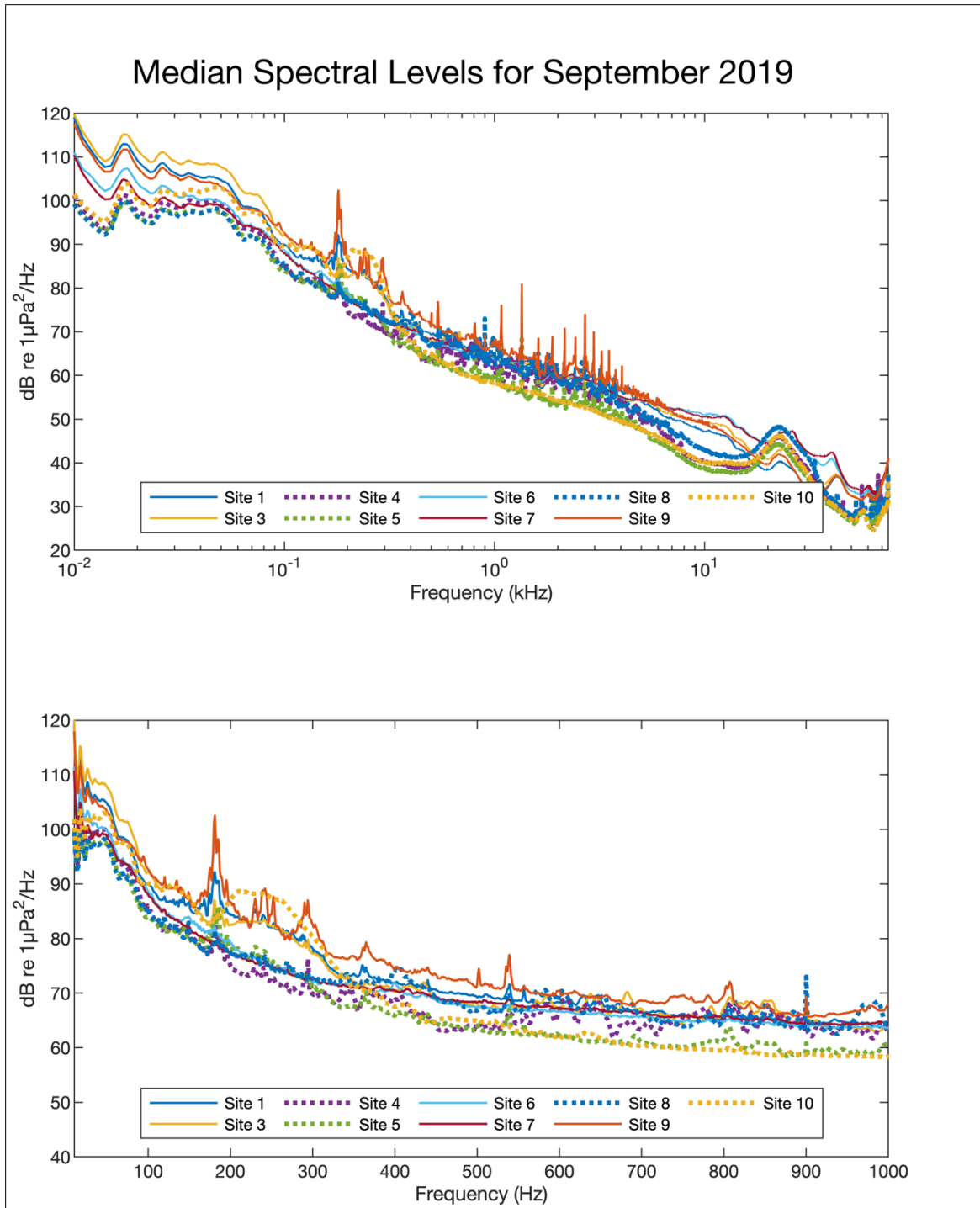
Figure D-C17. Median spectral values for September 2019.
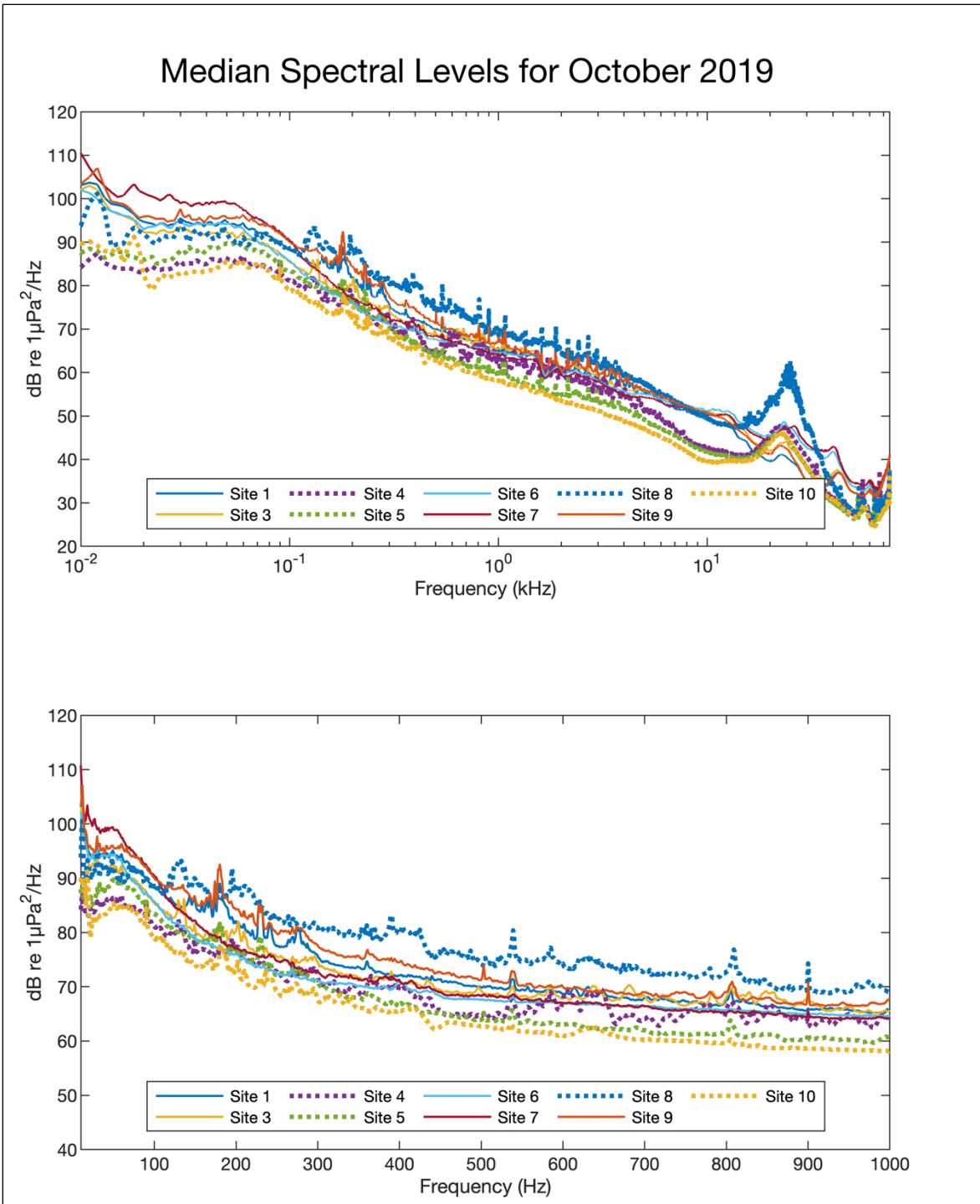
Figure D-C18. Median spectral values for October 2019.
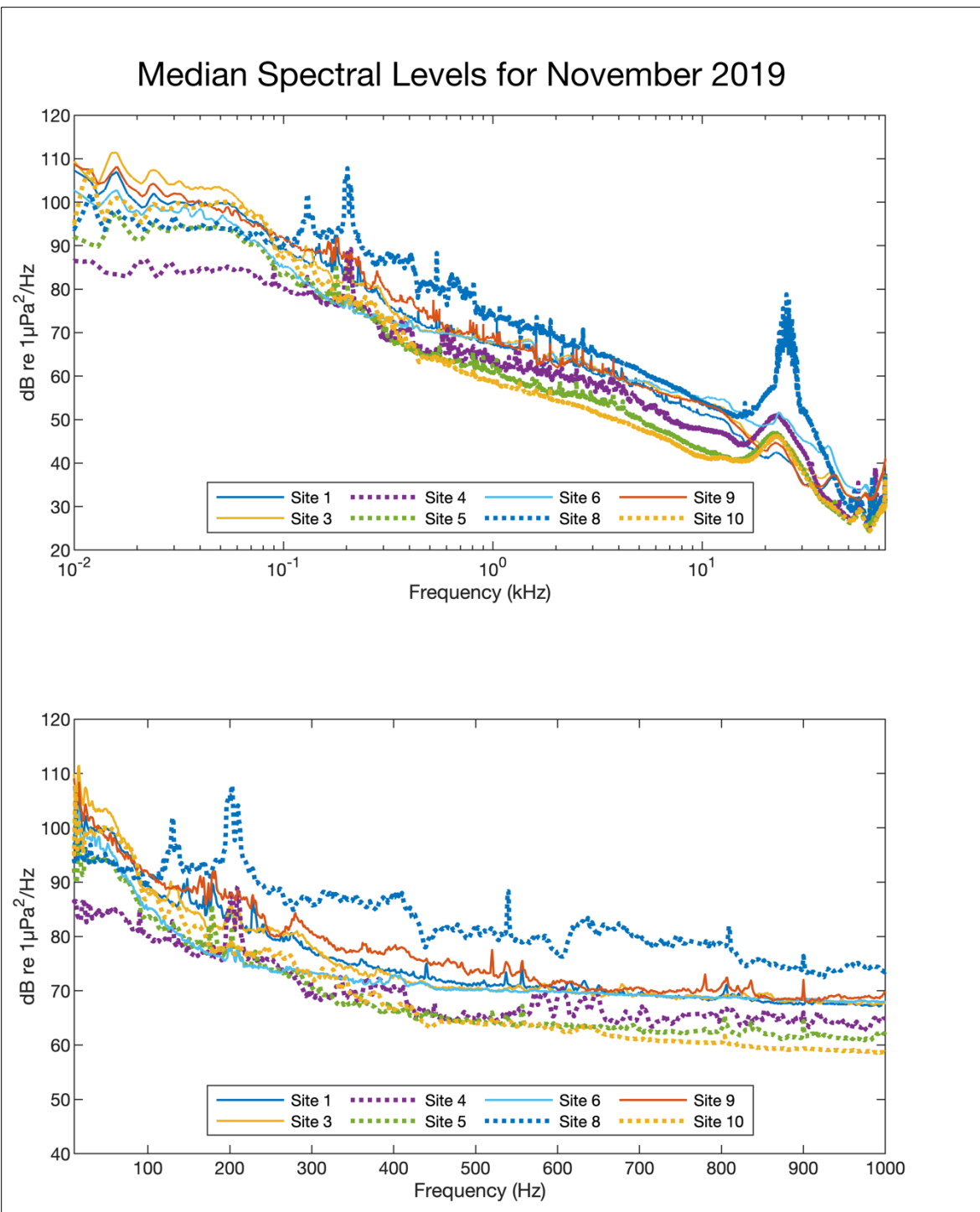
**Figure D-C19. Median spectral values for November 2019.**
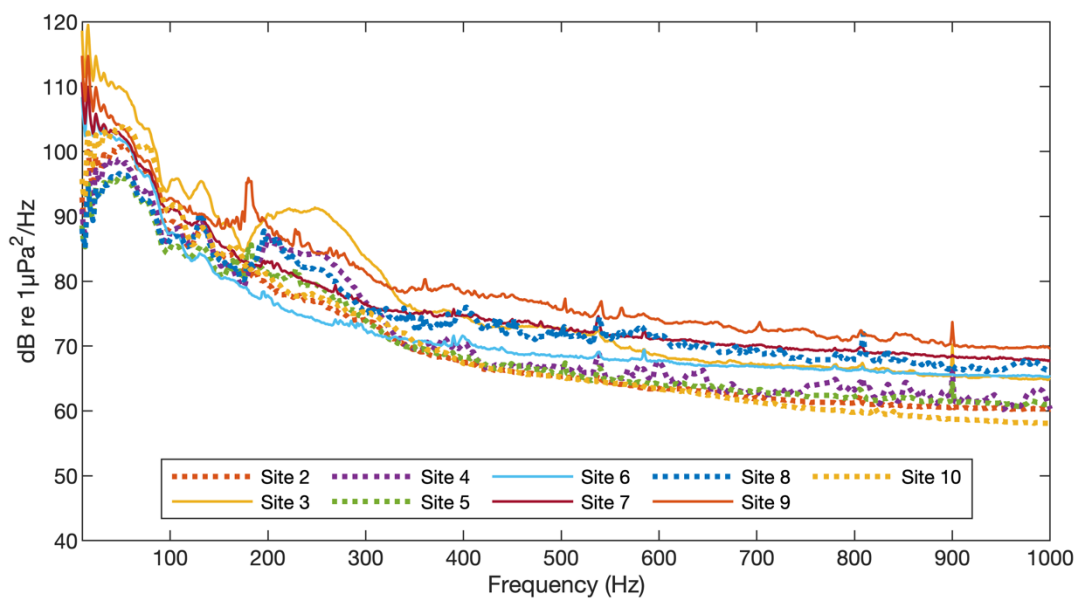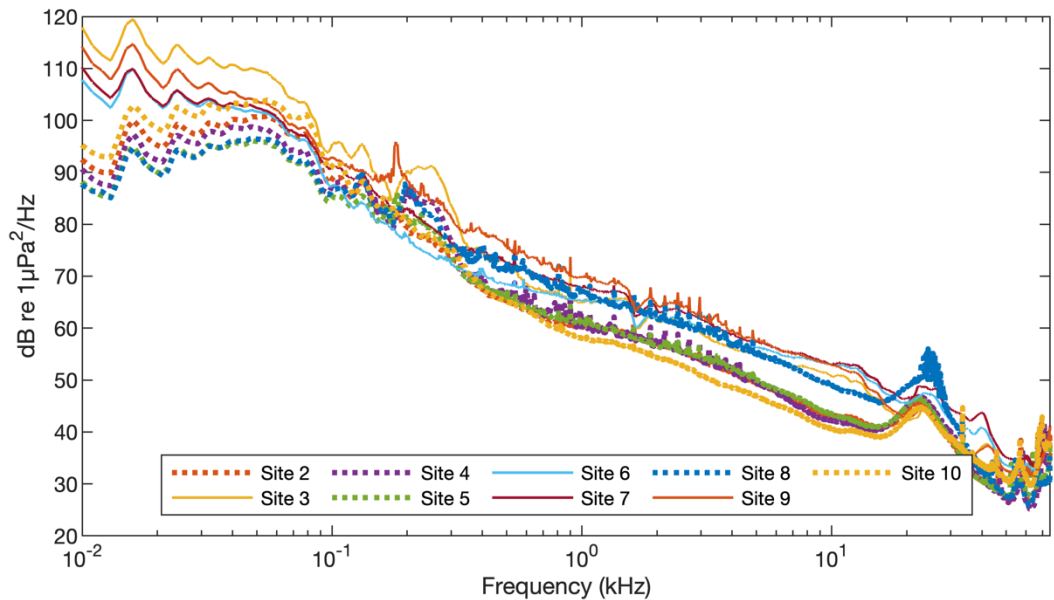
**Figure D-C20. Median spectral values for December 2019.**
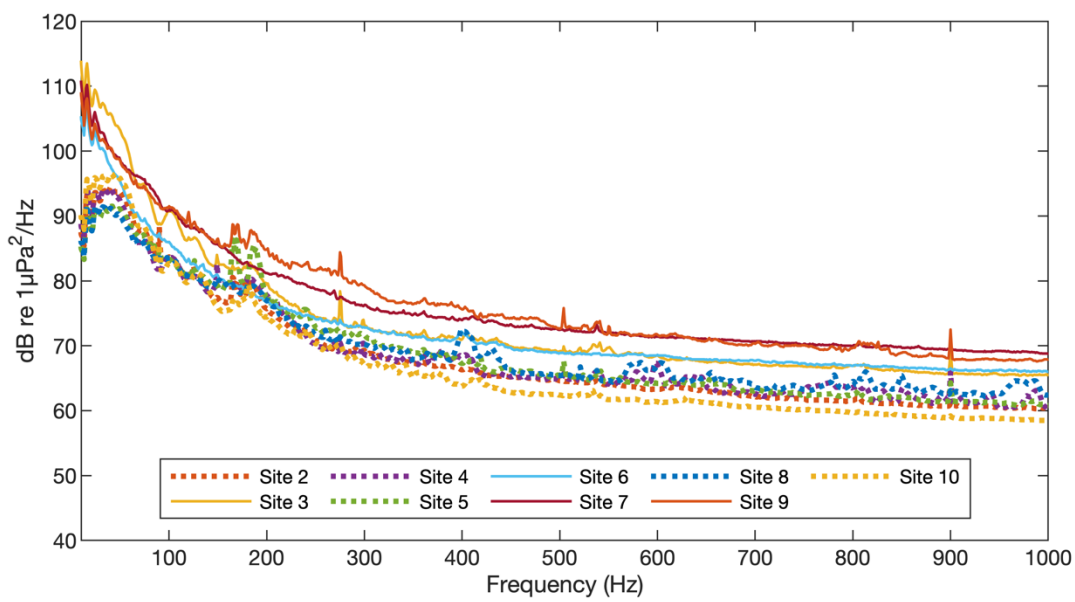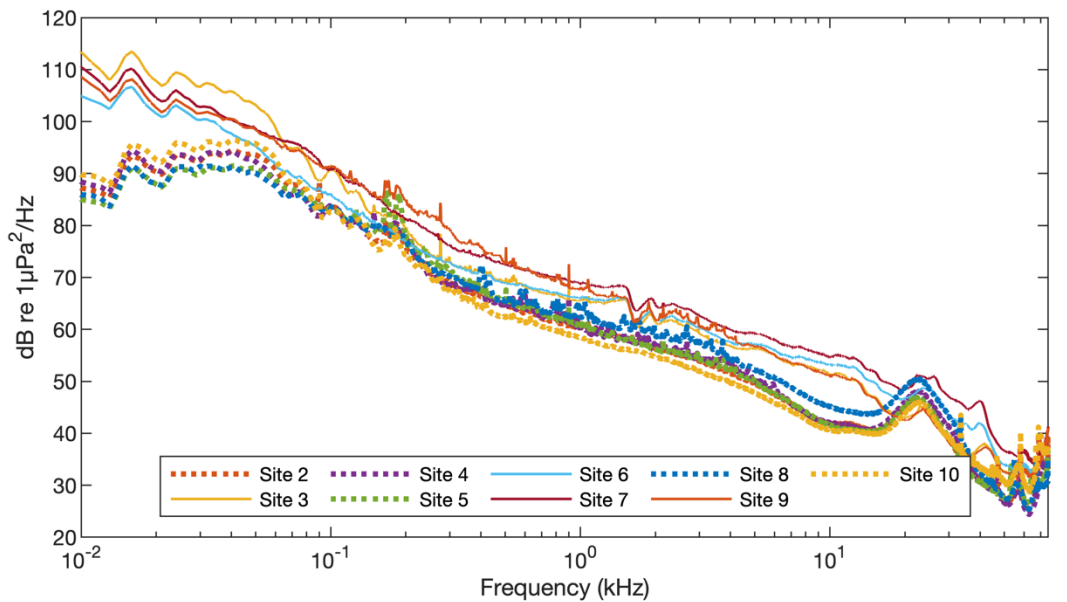
Figure D-C21. Median spectral values for January 2020.
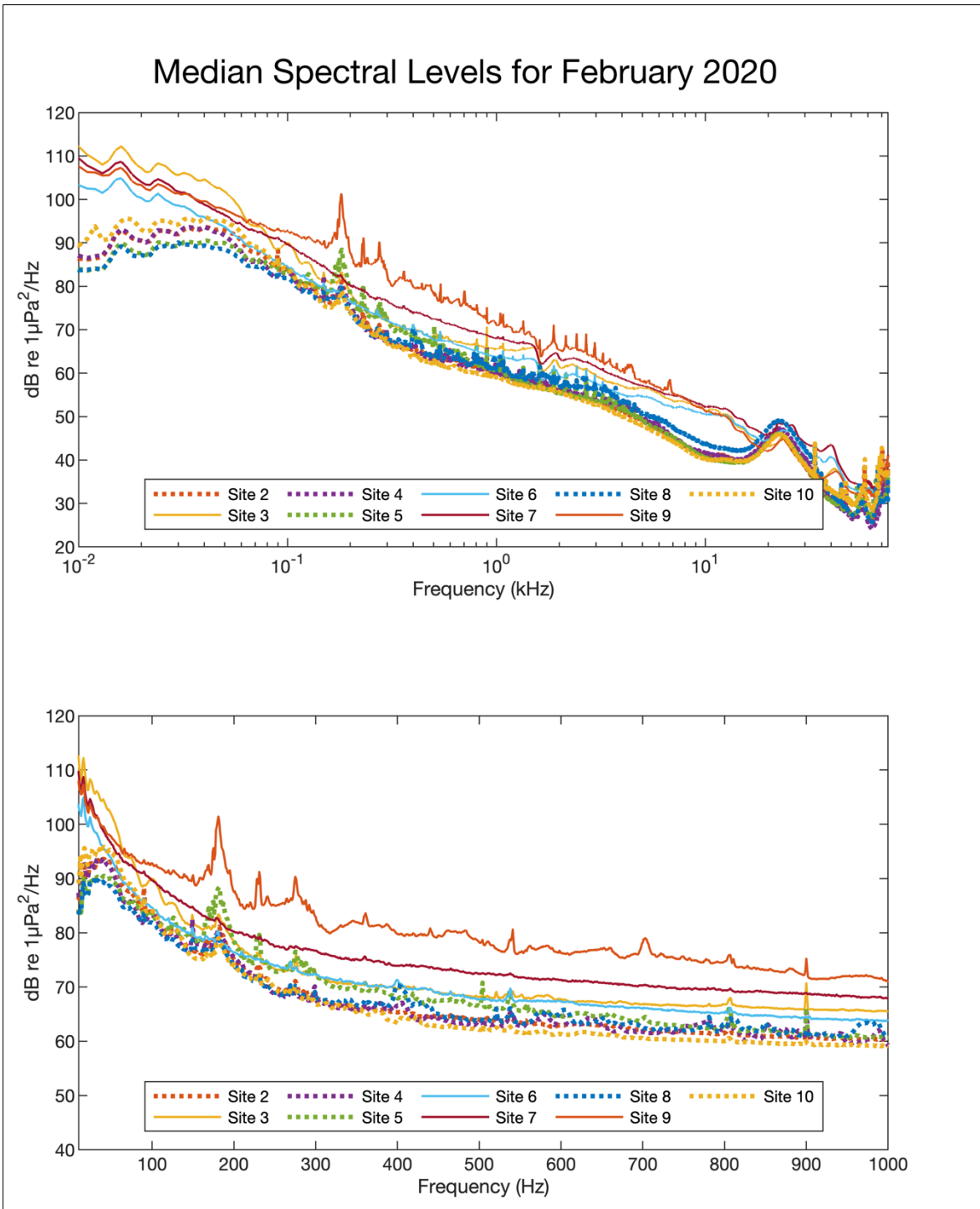
**Figure D-C22. Median spectral values for February 2020.**
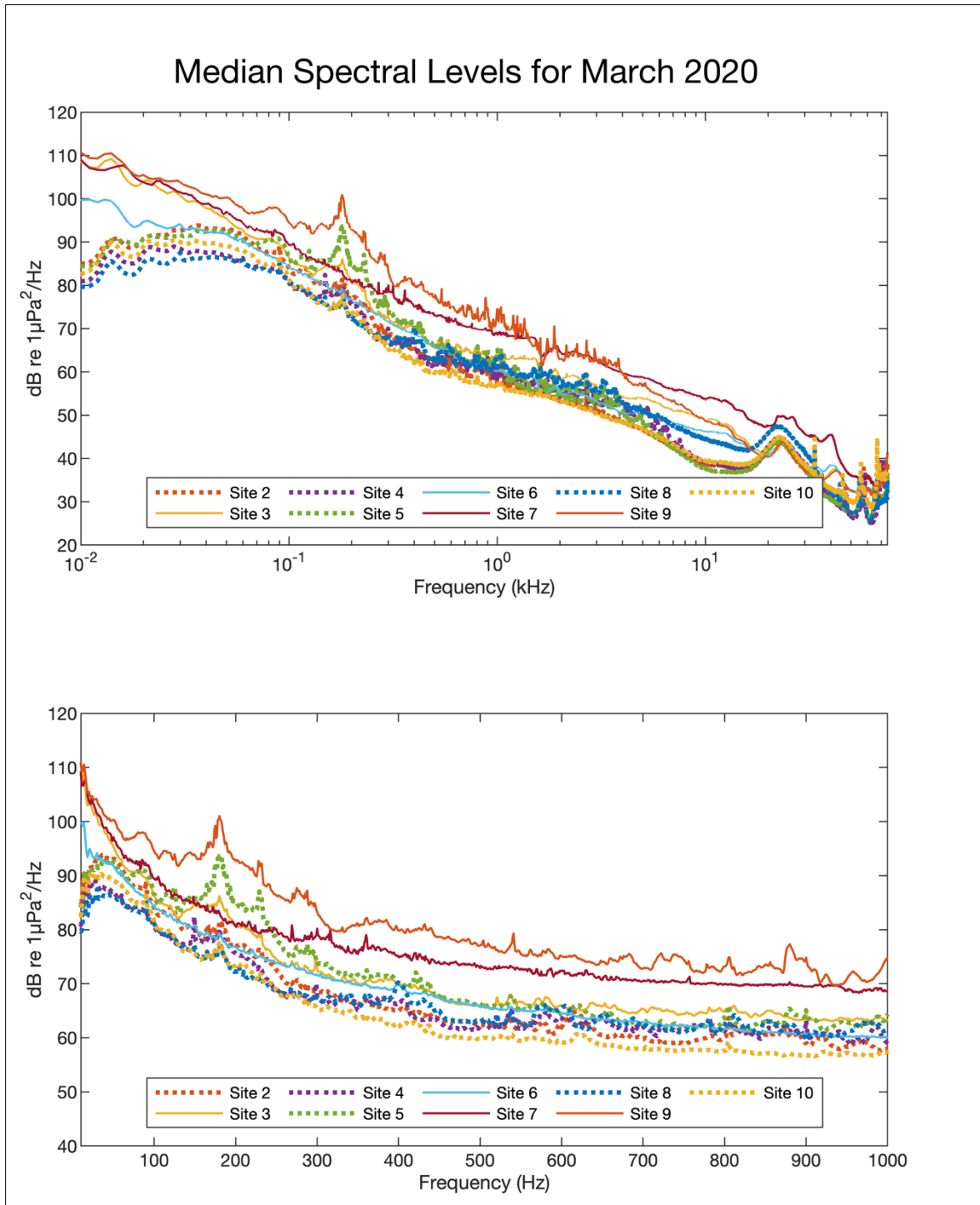
**Figure D-C23. Median spectral values for March 2020.**
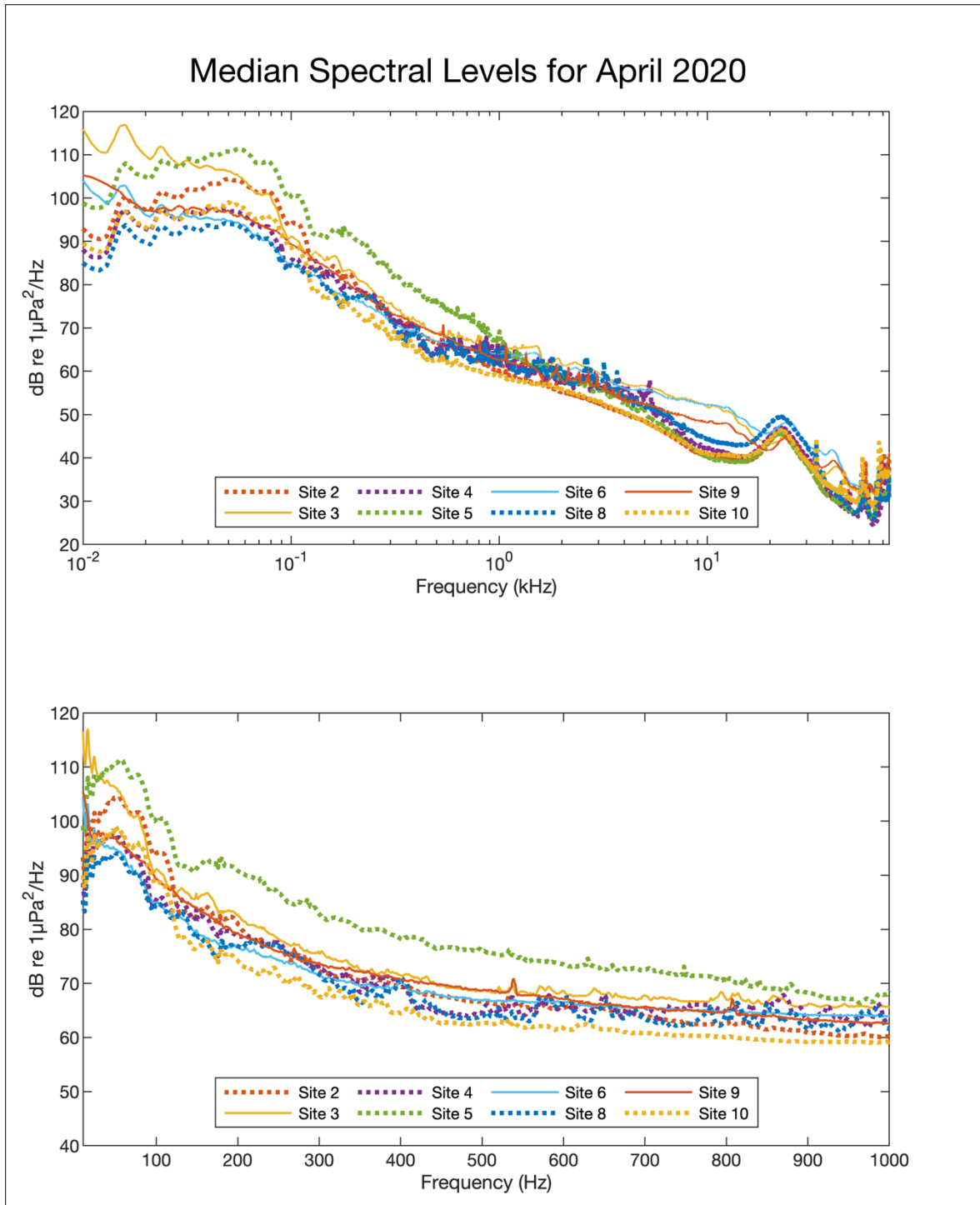
Figure D-C24. Median spectral values for April 2020.
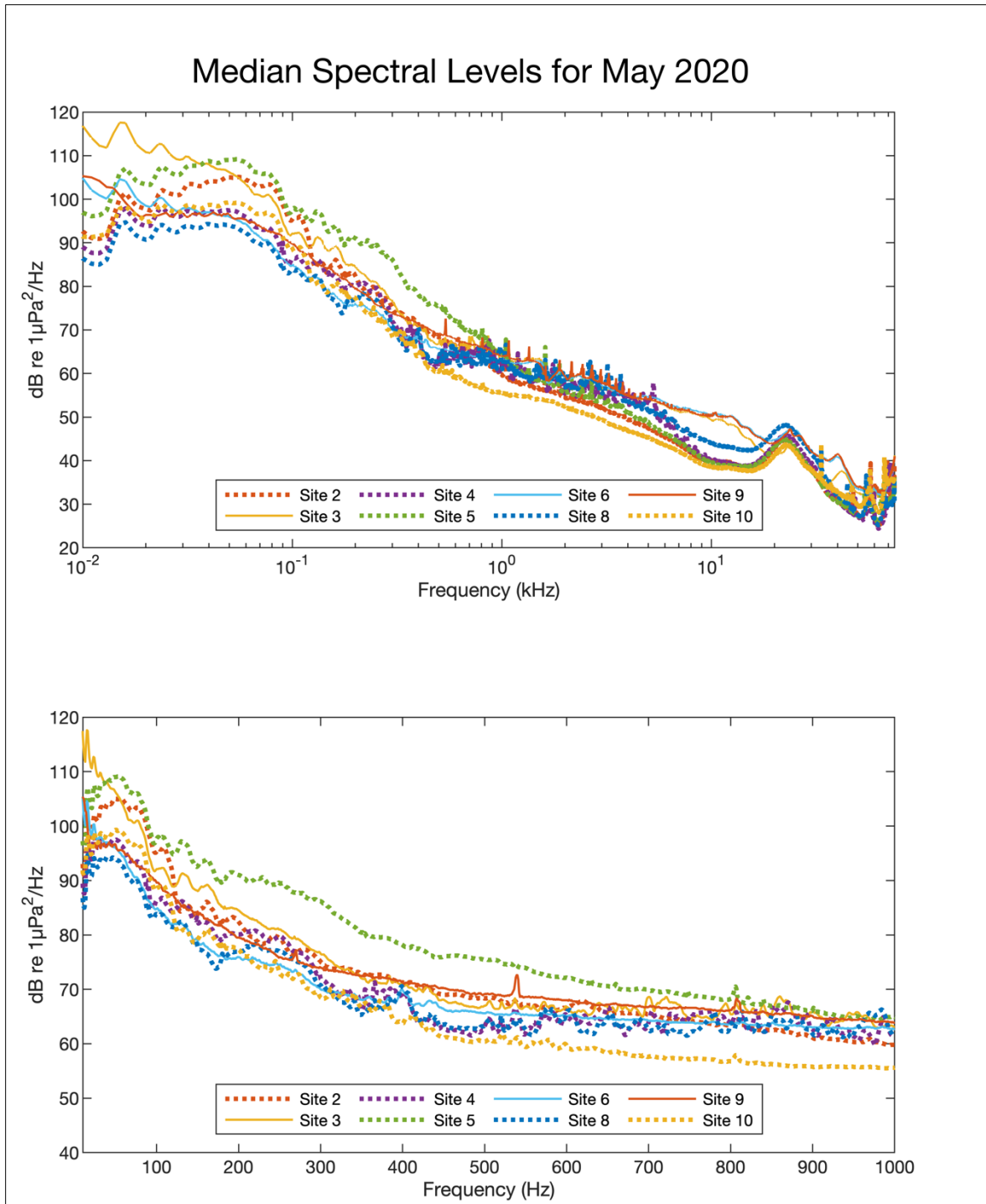
Figure D-C25. Median spectral values for May 2020.
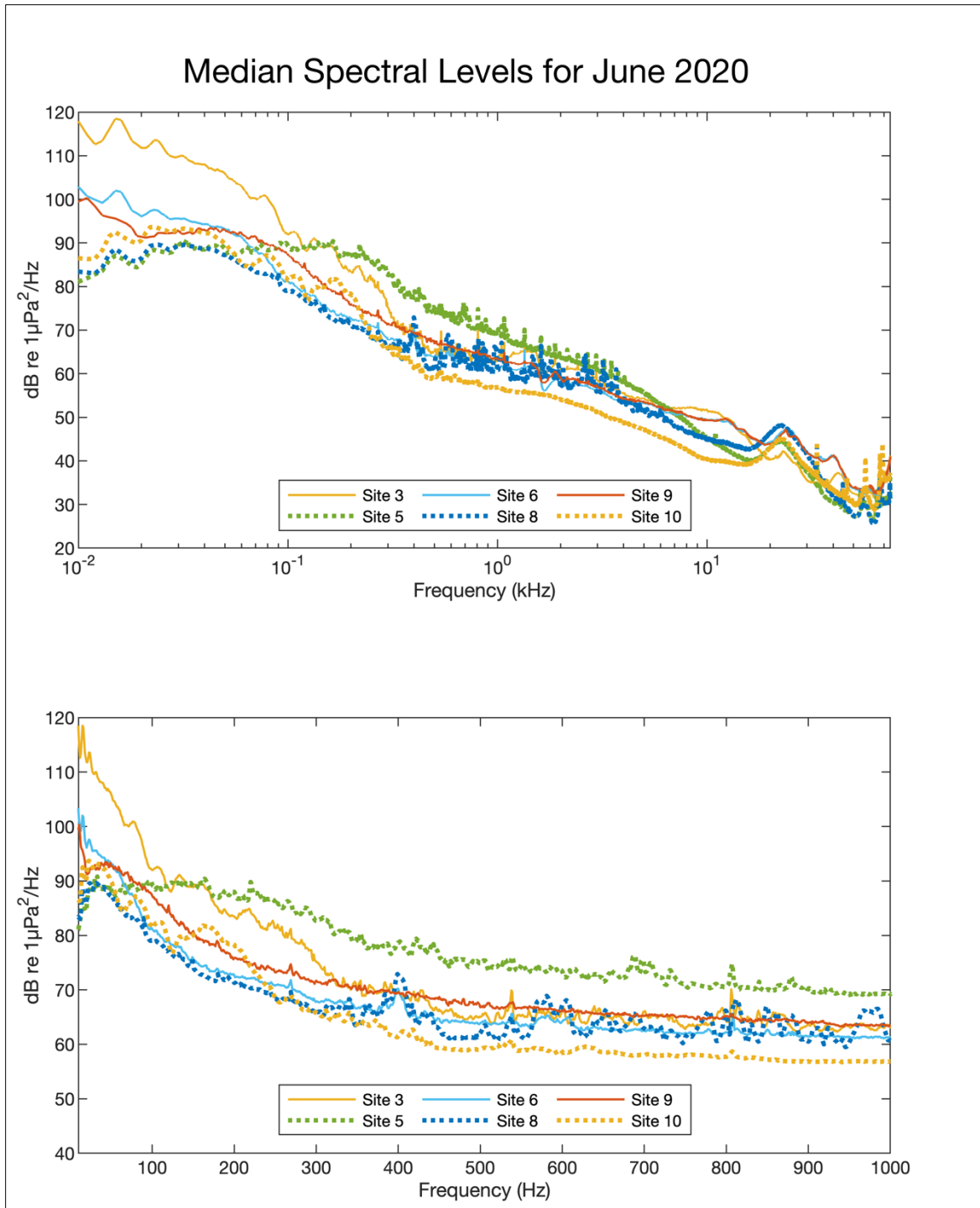
Figure D-C26. Median spectral values for June 2020.

Department of the Interior (DOI)
The Department of the Interior protects and manages the Nation's natural resources and cultural heritage; provides scientific and other information about those resources; and honors the Nation's trust responsibilities or special commitments to American Indians, Alaska Natives, and affiliated island communities.

Bureau of Ocean Energy Management (BOEM)
The mission of the Bureau of Ocean Energy Management is to manage development of U.S. Outer Continental Shelf energy and mineral resources in an environmentally and economically responsible way.

BOEM Environmental Studies Program
The mission of the Environmental Studies Program is to provide the information needed to predict, assess, and manage impacts from offshore energy and marine mineral exploration, development, and production activities on human, marine, and coastal environments. The proposal, selection, research, review, collaboration, production, and dissemination of each of BOEM's Environmental Studies follows the DOI Code of Scientific and Scholarly Conduct, in support of a culture of scientific and professional integrity, as set out in the DOI Departmental Manual (305 DM 3).